Shafiquzzaman Siddiquee
Melvin Gan Jet Hong
Md. Mizanur Rahman *Editors*

Composite Materials: Applications in Engineering, Biomedicine and Food Science

Springer

Composite Materials: Applications in Engineering, Biomedicine and Food Science

Shafiquzzaman Siddiquee
Melvin Gan Jet Hong • Md. Mizanur Rahman
Editors

Composite Materials: Applications in Engineering, Biomedicine and Food Science

Springer

Editors
Shafiquzzaman Siddiquee
Biotechnology Research Institute
Universiti Malaysia Sabah
Kota Kinabalu, Sabah, Malaysia

Md. Mizanur Rahman
Department of Mechatronics Engineering
World University of Bangladesh (WUB)
Dhaka, Bangladesh

Melvin Gan Jet Hong
Material and Mineral Research Unit
(MMRU), Faculty of Engineering
Universiti Malaysia Sabah
Kota Kinabalu, Sabah, Malaysia

ISBN 978-3-030-45488-3 ISBN 978-3-030-45489-0 (eBook)
https://doi.org/10.1007/978-3-030-45489-0

This Springer imprint is published by the registered company Springer Nature Switzerland AG
The registered company address is: Gewerbestrasse 11, 6330 Cham, Switzerland

Contents

Bibliography of Editors

Shafiquzzaman Siddiquee Assoc. Prof. Dr. was awarded his MSc (Molecular Microbiology) and PhD (Bioelectrochemistry) degrees in 2008 and 2010, respectively from University Putra Malaysia (UPM), Malaysia. First Dr. Siddiquee was appointed as a senior lecturer in 2011. Being trained as a Bioelectrochemist, he is a young, dedicated and highly motivated scientist, whose research main focus in the field of chemo- and bio- sensors, secondary metabolites, biofertilizers from waste substances, and fungal biodiversity. During tenure in UMS, he has taught 7 master and undergraduate courses, supervised 23 postgraduate students at the PhD and MSc level of which 12 have graduated while the rest are still on-going as well as 17 undergraduates and more than 10 internship students.

Dr. Siddiquee has published 79 research papers in peer reviewed journals (high impact factor (IF)-36, non-IF-24, non-index-19), 6 books, 18 book chapters, 37 proceeding papers in international and national conferences/symposiums/workshops, 21 research grants (international and national) of which two research grants are involved with community and industry. Currently his h-index is 22 h-index by Google scholar citation.

His findings have yielded in 4 Patents, 4 Trademarks, 8 Keynote Speakers and 60 Research Awards, including notable awards of the MOHE Entrepreneurial Project Award 2015, Gold Medals Winner from International Conference and Exposition on Inventions by Institutions of Higher Learning (PECIPTA) 2015 & 2019 and International Invention, Innovation & Technology Exhibition (ITEX) 2019.

Dr. Siddiquee was awarded a Young Scientists Award by the ProSPER.Net-Scopus 2014, in the order of Top 5 Penulis Prolifik Jurnal Berindeks ISI Dan Scopus, Memperoleh Sitasi Dalam Jurnal Berindeks, 2017 and Excellent Service Awards-2012/2013 by UMS.

For research outcomes, three (3) products (pet food; brand: Alphamate, Cosmetics (Vivify herbal soap, facial, body wash, tea,) out of ten (10) are officially in the process of commercialization. His several innovation had published daily newspaper,

for examples formalin in fish and fishery product detecting for 3 seconds and melamine in milk and dairy products for 30 seconds. He has also been appointed as consultant by 5 companies and editorial members of several reputed journals. His research findings had been broadcasted in several national TV stations (TV1, TV2 and TV7) as well as highlighted in various printed news agencies.

Melvin Gan Jet Hong received his Ph.D. from Shinshu University, Japan in 2015. Then, he joined Institute of Carbon Science and Technology, Japan for 1 year as a researcher. Now, he is a Senior Lecturer of Mechanical Engineering Program and a Research Fellow of Material & Mineral Research Unit at Faculty of Engineering, Universiti Malaysia Sabah, Malaysia.

His major field is related to materials science, which includes nanoparticles, hybrid nanomaterials, carbon-based nanomaterials, and composite materials. Some of his previous and currently active projects and works are related to polymer-based electroactive actuators, electromagnetic wave absorber, energy storage devices, and biomass derived carbon materials which are published in peer-reviewed journals, books including book chapters, conference proceedings, and abstracts. He is also an active reviewer for several material-related journals, a Graduate Member of Board of Engineers, Malaysia, and a Professional Technologist of Malaysia Board of Technologists

Md. Mizanur Rahman is working as an Associate Professor in the Mechatronics Engineering Department at World University of Bangladesh in Dhaka, Bangladesh. Dr. Rahman has more than nine years Teaching and Research experiences and his research interest lies in both fundamental and applied aspects of Energy Technologies, especially in new technologies to harvest electrical energy from solar, biomass and hydro sources. He has started my carrier at the Renewable Energy Technology in Asia (RETs in Asia) Phase -II Project in the year 1999 at Khulna Bangladesh and Bangkok, Thailand before joining as a Program Support Specialist in year 2005 at BRAC, Bangladesh. He was employed as an Assistant Manager (Technical) in the year 2006 in Rural Power Company Ltd (RPCL) at Dhaka, Bangladesh and later on in the year 2009 was started working as a Lecturer in the TAS Institute of Oil and Gas, at Kota Kinabalu, Sabah, Malaysia. Dr. Rahman moved to the Universiti Malaysia Sabah as Senior Lecturer in the year 2012 and continued until December 2018.

Dr. Rahman has received his Bachelor of Science in Engineering (Mechanical) in Mechanical Engineering from Bangladesh Institute of Technology (BIT) Khulna, Bangladesh, Masters of Science in Environmental Management from Joint degree programme offered by University of San Francisco, USA & Mahidol University,

Bangkok Thailand and Doctor of Philosophy (PhD) from Universiti Malaysia Sabah (UMS) respectively.

Dr. Rahman has published more than 55 research papers in the various journals and national & international conference proceedings, among then about 29 papers are SCOPUS indexed and hold a Patent on natural draft cooling tower. He is a chartered Energy Engineer and CEng Member of Institution of Mechanical Engineers (IMechE) and Energy Institute (EI), Fellow of Institute of Engineers Bangladesh (IEB), Member of Bangladesh Society of Mechanical Engineers (BSME) and American Society of Mechanical Engineering (ASME) and Professional Member of Institute of Materials Malaysia (IMM) and Society of Industrial Engineering and Operation Management (IEOM).

Part I
Engineering

Chapter 1
Carbon Materials From Various Sources for Composite Materials

Zhipeng Wang, Karen Wong Min Jin, and Gan Jet Hong Melvin

1.1 Introduction

Carbon material can be considered as a versatile material which is widely utilized in research development and industrial/commercial applications. Carbon materials can be in various forms; carbon nanotube (CNT), graphene, carbon black, activated carbon, graphite whisker, fullerene, and many more. Most of the carbon materials mentioned, possess significant mechanical, electrical, thermal, and chemical properties, which allow them to be utilized in diverse fields such as composite materials, energy storage/conversion, electronic, optical, sensor, and so on.

For decades the studies of macrocomposites such as reinforced polymers have been conducted intensively, where the length scale of polymer fillers is in micrometers. The reinforcement length scale is in micrometers, and the interface of fillers is close to the bulk polymer matrix (Koo 2006). Conversely, composites that are reinforced with nanometer scale fillers are considered as nanocomposites (Koo 2006; Young and Lovell 2011). Nanocomposites are composite materials in which the matrix material is reinforced by one or more separate nanomaterials in order to improve performance properties (Hu et al. 2010a). The nanocomposites have ultra large interfacial area per volume, and the distances between the polymer and filler components are extremely short. As a result, molecular interaction between the polymer and the nanoparticles (NPs) will give polymer nanocomposites outstanding

Z. Wang
Institute of Advanced Materials, Jiangxi Normal University,
Nanchang City, Jiangxi Province, China
e-mail: wangzhipeng@jxnu.edu.cn

K. W. M. Jin · G. J. H. Melvin (✉)
Material and Mineral Research Unit (MMRU), Faculty of Engineering,
Universiti Malaysia Sabah, Kota Kinabalu, Sabah, Malaysia
e-mail: melvin.gan@ums.edu.my

S. Siddiquee et al. (eds.), *Composite Materials: Applications in Engineering, Biomedicine and Food Science*, https://doi.org/10.1007/978-3-030-45489-0_1

material properties that conventional polymers do not possess (Koo 2006). Commonly, the matrix materials used for composites are polymers such as polyurethane, epoxy resin, synthetic/natural rubber, polyvinyl alcohol, polyvinyl chloride, paraffin wax, and so on.

Satisfactory range of mechanical, optical, electrical, and surface properties can be obtained from polymers alone (Ober and Müllen 2012). Over the last century, polymers have dynamically transformed technology more than any other materials. Their combination of light weight, low cost, molecular specificity, corrosion resistance, and the properties associated with their large molecular size have made them attractive replacements for metals and ceramics in their role as structural and functional materials (Ober and Müllen 2012). In recent years, the discovery of the electrical, electronic, and optical properties of polymers over the last decade has opened up a vast variety of new applications in enhancing and demanding technologies.

Nevertheless, there are often circumstances where even more specific or better performance is demanded from the polymers. Since the development of polymers, composite have been used to enhance properties or improve them. The formation of the composite involves incorporating filler, commonly an inorganic filler, to modify polymer performance. In recent years, very small scale fillers, some having dimensions of just a few nanometers, have been modulated to fabricate nanocomposites.

The development of composites has been driven by the need for materials with specific combinations of properties beyond those obtainable from a single material (Young and Lovell 2011). The incorporation of inorganic nanoparticles as the fillers into polymer systems has resulted in polymer nanocomposites showing multifunctional, high performance polymer characteristics further than those traditional filled polymeric materials possess (Koo 2006; Hu et al. 2010a; Schaefer and Justice 2007; Thostenson et al. 2005). Through control or alteration of the fillers at the nanoscale level, we will be able to maximize property enhancement of selected polymer systems to meet or exceed the requirements of current military, aerospace, commercial applications, and so on (Koo 2006). The technical approach involves the incorporation of nanoparticles into selected polymer systems whereby nanoparticles may be surface-treated to provide good dispersion and enhanced inclusion into polymer matrix.

1.2 Carbon-Based Composite Materials

1.2.1 Carbon Nanotube-Based Composite Materials

Huge numbers of research and development of CNTs, from history, synthesis, remarkable performances, and fabrication of CNT-based nanocomposites, are available. The enhancement and great attention to CNTs can be highlighted when Kroto et al. (1985) discovered fullerene (C_{60}, buckyball); Oberlin et al. (1976) synthesized

among the first CNTs; multi- (Iijima 1991) and single-walled (Iijima and Ichihashi 1993) CNTs were observed; which keep on developing up to today.

In general, CNTs can be categorized into single-walled CNT (SWCNT) and multi-walled CNT (MWCNT). A SWCNT can be considered as a rolled-up sheet of a graphene, which is a single layer of an allotrope of carbon called graphite, and the edges of the sheet are joined together to form a seamless tube (Young and Lovell 2011; Hierold et al. 2008). Few tubes of different diameters can be fitted into each other, which normally classified as MWCNT. Arc discharge, laser ablation, and chemical vapor deposition (CVD) are three major methods to produce CNTs. Each of these methods had its advantages and disadvantages and shortly explained below.

Arc discharge and laser ablation method depends on the evaporation of a graphite target to create gas phase carbon fragments that recombine to form CNTs. During the process, the temperature reached at 2000–3000 °C range, which allows the carbon atoms to rearrange into the tube structure. Normally, in order to promote the yield of CNTs, several different metals in concentrations about 1% are incorporated into the target materials that is evaporated (Hierold et al. 2008). In the case where large quantity of CNTs is necessary for composite materials, these methods would make the cost of CNTs unreasonable (Thostenson et al. 2001). Moreover, purification steps are also essential before the utilization of them, due to a large amount of non-tubular graphitic and amorphous carbon is also yielded during the process (Hierold et al. 2008; Thostenson et al. 2001).

One of the most broadly utilized methods to produce CNTs is CVD. Commonly, the CVD process includes catalyst-assisted decomposition of hydrocarbons, such as ethylene or acetylene, in a tube reactor within 400–1100 °C temperature range and the growth of CNTs over the catalyst upon cooling the system (Hierold et al. 2008; Hu et al. 2010b; Popov 2004). The growth temperature depends on the type of CNTs to be grown and the catalyst composition (Hierold et al. 2008). The advantages of this method are the ability to fabricate aligned arrays of CNTs with controlled diameter and length, and under the right condition only nanotubes can be yielded and no undesired graphitic material (Hierold et al. 2008; Thostenson et al. 2001).

CNTs also can be synthesized from various sources. For example, waste plastic such as polyethylene, polypropylene, and polyethylene terephthalate can be utilized as carbonaceous feed of CNT production (Bazargan A and McKay 2012; Mishra et al. 2012). Moreover, CNTs also can be obtained from coconut shell derived charcoal by using plasma enhanced CVD (Araga and Sharma 2017), and bamboo charcoal by CVD in the presence of ethanol vapor (Zhu et al. 2012). Many renewable carbon-based resources, especially biomasses, have high potential in CNTs production. Few examples are such as solid camphor, camphor oil, palm oil, chicken fat oil, honey, butter, and many more (Kumar et al. 2016; Titirici et al. 2015). The utilization of waste materials, renewable carbon resources, and low cost abundant materials will lead to the environmental friendly synthesis methods and the advancement of sustainable technologies.

Usually, CNTs are incorporated into polymer matrix to fabricate composite materials for various applications. In other cases, CNTs are combined with other

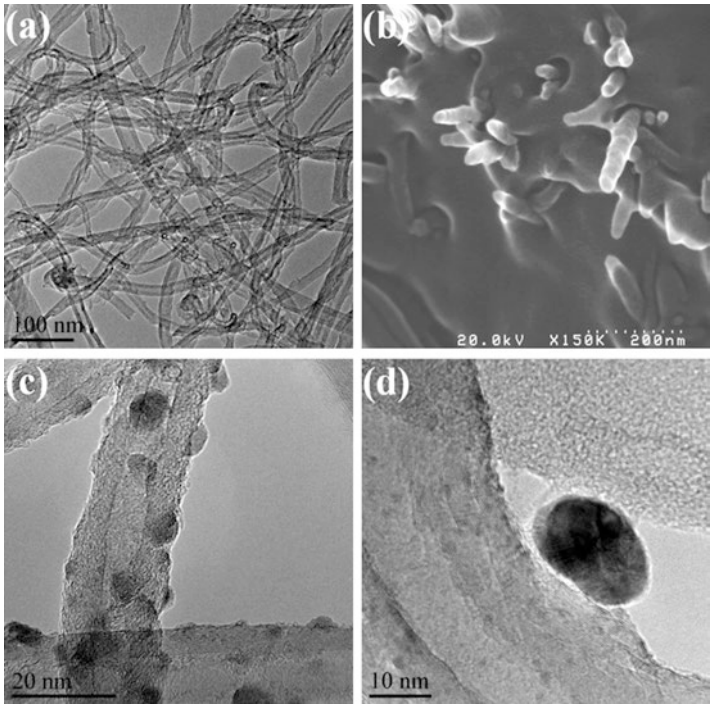

Fig. 1.1 (**a**) TEM image of MWCNT, (**b**) FE-SEM image of CNTs incorporated into polymer matrix, TEM images of (**c**) $BaTiO_3$/CNT, (**d**) Ag/CNT

materials to synthesize hybrid nanocomposites. Several CNT-based materials are depicted in Fig. 1.1. Ajayan et al. (1994) conducted one of the first fabrications of polymer nanocomposites using CNTs as fillers. Since then, the development of CNT-based composite materials is growing rapidly, for instance in electromagnetic (EM) wave absorber, electroactive actuator, energy storage devices, advanced materials, and many more applications.

CNTs are favorable candidate to be considered for EM wave absorber composite materials due to their the high electrical conductivity which enables strong polarization to occur, Ohmic losses, dissipation of electrostatic charges, or multiple scattering caused by the large specific area, which lead to enhanced complex permittivity (Melvin et al. 2019a). For example, Nwigboji et al. (2015) fabricated MWCNT-epoxy composites and evaluated their EM wave absorption performance. Significant EM wave absorption can be obtained for 8–10 wt.% samples within the frequency range of 1–26.5 GHz. In order to produce high performance EM wave absorber materials, combination of two/more materials or hybrid materials are desirable, where single material system unable to meet the demand. In this particular case, hybrid materials are referred as CNTs combined with magnetic, dielectric, or conductive particles for EM wave absorber applications. Qiu and Qiu (2015) fabricated magnetite nanoparticle – CNT – hollow carbon fiber composites and evaluated their

EM wave absorption capability. The minimum reflection loss achieved is −50.9 dB at 14.03 GHz for 2.5 mm thick sample layer. CNTs are also combined with dielectric ceramic such as barium titanate (BTO) nanoparticles through solvothermal method (Bi et al. 2011; Huang et al. 2013) and sol-gel method (Melvin et al. 2014a, 2017a), to enhance the absorption performance. It is worth noticing that the EM wave absorption performance can be improved not only by utilizing hybrid materials, but also by modulating the design, such as double-layer BTO/CNT composites (Ni et al. 2015). The double-layer BTO/CNT composites with total thickness of 1.3 mm, consist of BTO/CNT 30 wt.% (absorption layer) and BTO 30 wt.% (matching layer) exhibited minimum reflection loss of −63.7 dB (> 99.9999% absorption) at 13.7 GHz. Furthermore, CNTs are also integrated with conductive particles such as silver (Ag) nanoparticles, for single (Melvin et al. 2014b) or double-layer Ag/CNT (Melvin et al. 2015) EM wave absorber composite materials. The double-layer composites constructed from CNT 30 wt.% and Ag/CNT 30 wt.% with total thickness of 3.3 mm exhibited minimum reflection of −52.9 dB (> 99.999% absorption) at 6.3 GHz.

CNTs also can be incorporated into polymer matrix such as polyurethane (PU) to fabricate electroactive nanocomposite actuator. An electric field stimulated polymer-based materials are referred to as electroactive actuators (shape memory polymers) and have the advantages, such as light weight, flexible, tolerance against fracture, easy to fabricate, and they can convert electrical energy to mechanical energy and thus impart a force and produce large strain (Ali and Hirai 2011; Melvin et al. 2016). Moreover, through the inclusion of CNTs, mechanical and electrical properties can be improved significantly, which further make them suitable to be developed for actuator materials, sensors, artificial muscles, smart devices, and micro-switches (Sahoo et al. 2007; Melvin et al. 2014c, d, 2016). For instance, PU/CNT electroactive nanocomposite actuator film bents toward the cathode when an electric field was applied, and it reverted to its original position when the electric field was removed. Stable and similar bending displacement also observed upon voltage cycling (Melvin et al. 2014d). Furthermore, CNT/water-borne epoxy showed triple-shape memory effect when thermally actuated, where normally common epoxy or CNT/epoxy nanocomposites only possess dual-shape memory effect (Dong et al. 2015).

Not limited to those mentioned above, CNT-based composite materials are also widely used as the electrode materials in supercapacitor applications, due to their remarkable physiochemical properties such as high conductivity, high surface area, and electrochemical activity (Wang and Melvin 2019). For instance, CNTs constructed nitrogen-doped porous carbon monoliths for supercapacitor application (Wang et al. 2019c). Furthermore, CNTs are also incorporated into matrix material to fabricate functionally graded materials (FGM) and their fracture characteristics were evaluated (Kurd et al. 2017), protective coating (Zhang et al. 2011), CNT/rubber composites (Jiang et al. 2012), and many more. The inclusion of CNTs assisted in enhancement of mechanical, electrical, and thermal properties.

1.2.2 Graphene-Based Composite Materials

The attention towards graphene started since the isolation of graphene from bulk graphite (Novoselov et al. 2004), which then was recognized for Nobel Prize in Physics in 2010, accordingly. In that research, graphene sheets were obtained by using adhesive tape (Scotch tape) to remove flakes of graphite from a slab of highly ordered pyrolytic graphite into increasingly thinner pieces until individual atomic planes (monolayer of graphite) were gained (Randviir et al. 2014). Graphene is a one-atom-thick planar sheet of two-dimensional (2D) sheet sp^2 bonded carbon atoms that are densely packed in a honeycomb crystal lattice with remarkable properties such as high aspect ratio, large surface area, excellent electrical, thermal, mechanical properties, and so on (Dai et al. 2012; Pumera 2010; Randviir et al. 2014; Nasir et al. 2018). As the mother and components of all graphitic forms, graphene is a building block for carbon materials of all other dimensionalities, for instance 0D buckyballs, 1D nanotubes, and 3D graphite.

The preparation of graphene can be grouped into top-down and bottom-up methods. Few points such as such as cost effectiveness, scaled-up production, high electrochemical activity, conductivity, are to be considered in graphene preparation (Lv et al. 2016).

Top-down approach usually applies mechanical force or chemical intercalation to overcome the van der Waals forces between the graphene layers to achieve separation of graphene from bulk graphite, such as micromechanical cleavage (mechanical exfoliation), oxidation-exfoliation-reduction, intercalation exfoliation, solid exfoliation, and so on (Lv et al. 2016; Dong et al. 2017). In the case of mechanical exfoliation by Scotch tape, the process is less appropriate because of the low yield and lengthy process, even though the graphene produced possesses high quality (Randviir et al. 2014; Papageorgiou et al. 2015). The solvent-phase exfoliation process utilizes solvent, which can yield good quality graphene, but in quite small amount (Papageorgiou et al. 2015; Potts et al. 2011). Nevertheless, the graphene obtained through solvent-phase exfoliation is appropriate to be utilized for solution blending process in composite materials fabrication. For composite materials which needed high quantity of graphene as the filler materials, thermal exfoliation which utilizes thermal shock to obtain exfoliated graphene is considerable (Papageorgiou et al. 2015).

Bottom-up approach commonly uses a small molecule precursor to grow into graphene by CVD or chemical synthesis. For graphene prepared by CVD, they exhibit some excellent properties, due to their large crystal domains, monolayer structure and less defects in the graphene sheets, which are beneficial for boosting carrier mobility in electronic applications, and apparently in nanocomposites (Papageorgiou et al. 2015; Ke and Wang 2016). Furthermore, the layers and defects of graphene can be controlled by adjusting growth parameters such as temperature, time, catalyst, and so on.

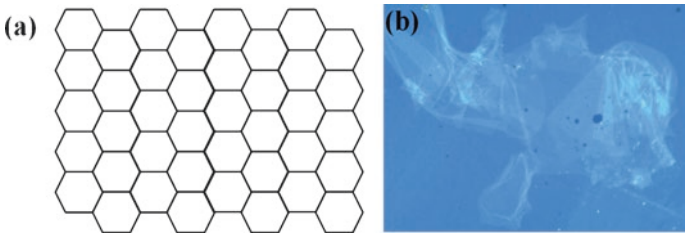

Fig. 1.2 (**a**) Graphene model, (**b**) few-layer GO on glass slide

Through the utilization of suitable physical or chemical method, production of porous graphene and doped graphene sheets can be accomplished, and high performance/functionality graphene can be further fabricated with the introduction of organic/inorganic materials. Furthermore, the production of graphene with low cost, high yield, and high quality is also a vital point. Usually, the chemical exfoliation of graphite into graphene oxides (GOs), followed by controllable reduction of GOs (with reduction agent such as hydrazine hydrate) into graphene can be considered as an efficient and low-cost method (Dong et al. 2017). Model of graphene and few-layer GO are shown in Fig. 1.2.

Similar with CNTs production, various low cost renewable carbon-based resources also can be utilized for graphene production. For instance, the growth of graphene on the surface of Cu foils under a H_2/Ar flowing atmosphere by using food, insects, and waste was reported (Ruan et al. 2011). Other materials such as paper cups, glucose, hemp, rice husk, cockroach legs, cookies, and grass also have been utilized for graphene production (Raghavan et al. 2017). Furthermore, uniform monolayer graphene film was also produced by using chicken fat oil through low pressure CVD process (Rosmi et al. 2016), and few layer graphene was also obtained from dead camphor leaves (Shams et al. 2015). Moreover, waste plastics which are rich in polyethylene and polystyrene also can be turned into high quality single crystal graphene by using ambient pressure CVD process (Sharma et al. 2014).

Graphene, derivative of graphene, and graphene hybrid materials are widely utilized in composite materials for numerous applications. For example, composite electrode with the combination of activated carbon and reduced graphene oxide (rGO) (Guardia et al. 2019), and rGO-Co_3O_4 composites (Zhang et al. 2019) exhibited enhanced supercapacitor performance. Not limited to energy storage applications, due to their excellent electrical properties, they are also used for high performance electromagnetic shielding application by using the composites consist of graphene and CNTs (Zhu et al. 2019). Graphene oxide-based composites also showed significant shape memory effect when thermally stimulated, which further reveal their potential to be utilized for actuator, biomedical device, sensor, or switches (Yan et al. 2019; Wang et al. 2019a).

1.3 Various Carbon Materials

1.3.1 Heat Treatment

Heat treatment is highly associated with pyrolysis, which is a process involves thermal decomposition of materials at certain temperature and in inert environment. Specifically, carbonization process can be further defined as a process where organic precursors are turned into carbon residues and volatile compounds during heating process in inert environment (Lin et al. 2018). Low crystalline carbon materials are usually obtained through carbonization process. At further higher temperature (>1200 °C), high crystalline carbon materials can be obtained through graphitization process (Lin et al. 2018).

Carbon materials are successfully derived from straw, corncob, and fallen leaves through carbonization at 800 °C for 0.5 h in nitrogen environment (Wu et al. 2016a). Furthermore, rice husks (RHs) are lignocellulosic materials, which is feasible to turn them into carbon materials (Wang et al. 2010). Generally, RHs are manipulated as low value energy resource, discarded, or simply burnt at the field, which will influence the air quality and threaten the environment. Through carbonization process, RHs and saw dusts can be derived into carbon materials, at 500–800 °C for 1-2 h under the presence of Argon gas (Melvin et al. 2017b; Melvin et al. 2019b). Additionally, the carbon materials produced from agro-based wastes are further utilized as activated carbon (AC) for adsorbents, electrochemical electrode composite materials, and many more. ACs can be majorly produced through chemical and physical activation, which enhanced their porosity and specific surface area. Usually, chemical activation involves mixing carbon precursor with chemical agents (KOH, H_3PO_4, H_2SO_4, K_2CO_3 etc) and the activation/carbonization takes place simultaneously when heat treated; meanwhile physical activation involves the introduction of oxidizing atmosphere (CO_2, steam, etc.) to carbonized materials (Wei and Yushin 2012). Few examples of AC utilized as adsorbents are; AC from RHs for nitrate removal from water (Satayeva et al. 2018), AC from date pits for lead ions removal (Krishnamoorthy et al. 2019), AC from pistachio wood for Pb(II) removal (Sajjadi et al. 2019). Moreover, high performance composite materials for supercapacitor electrodes are manipulated from AC derived from corn straws (Lu et al. 2017), oil palm shells (Abioye et al. 2017), etc. Interestingly, activated carbon fibers are obtained from sawdust (Huang et al. 2017), and large area activated few-layer graphene are obtained from peanut shell (Purkait et al. 2017), also for high performance supercapacitor applications.

Alternatively, ACs are also produced through microwave heating. Microwave heating, not limited to activation process, has been utilized in diverse fields due to its short time treatment and comparatively low energy consumption (Alslaibi et al. 2013). For example, carbonized saw dusts were activated through microwave heating by using K_2CO_3 (Foo and Hameed 2012). On the other hand, ACs obtained from microwave-assisted activation of petroleum coke by using KOH were used to fabricate electric double layer composite capacitors (He et al. 2010). Furthermore,

diverse types of carbon materials were also synthesized through microwave heating. Hollow carbon nanofibers were obtained from pine nut shell and palm kernel shell during microwave pyrolysis (Zhang et al. 2018; Omoriyekomwan et al. 2017). ACs which function as microwave receptor, were mixed with the biomasses during the microwave pyrolysis.

Furthermore, high crystallinity carbon materials can be obtained through heat treatment at high temperature. For instance, wrinkled few- and multi-layer graphene can be obtained from rice husks (RHs) treated at 2500 °C (Melvin et al. 2017b). Comparatively, they showed clean surface, clear edges, and relatively high crystallinity than RHs carbonized at low temperature. Composite materials consist of RHs treated at 2500 °C also exhibited significant electromagnetic wave absorption performance, over 98% absorption with thickness of 1.6 mm (Melvin et al. 2017c). Interestingly, RHs treated at 1500 °C produced a heterogeneous materials - mixture of carbon materials, silicon carbide (SiC) whiskers and SiC particles (Melvin et al. 2019c). Composite materials consist of RHs treated at 1500 °C showed over 99.9997% electromagnetic wave absorption. Furthermore, nanoparticles also can be attached onto their surface to fabricate nanocomposites (Melvin et al. 2017d). On the other hand, graphite whiskers also can be obtained when fullerene waste soot (Wang et al. 2015a), wood charcoal (Saito and Arima 2007), grounded graphite (Dong et al. 2001), and coffee grounds (Melvin et al. 2019d) are treated at various high temperatures. These graphite whiskers exhibited strong G' when investigated using Raman spectroscopy, which might be induced by the disclination of graphitized carbon layers. Vapor carbon that produced by the precursor can be assumed as the carbon source, when they are heat treated at high temperature. The high crystallinity of carbon materials obtained at high temperature might be attributed to realignment or restructure of vapor carbon. Few types of carbon materials obtained from agro-based waste materials heat treated at high temperature are shown in Fig. 1.3.

1.3.2 Plasma Enhanced Chemical Vapor Deposition (PECVD)

As mentioned above, CVD method was extensively employed for the synthesis of carbon materials including diamond, CNT, and graphene. For the sake of low-temperature synthesis of these carbon materials, plasma is involved in the CVD process, and it is regarded as plasma enhanced CVD (PECVD). In PECVD process, plasma which consists of electrons, ionized gas species (ions), and neutral species in both ground and excited states. The plasma is usually created and sustained by applying a high frequency voltage (e.g. radio frequency (rf), microwave) or direct current discharge between two electrodes to a low pressure gas. For the growth of carbon-based materials, plasma was initially utilized to fabricate diamond-like carbon (DLC) films. In 1983, Japanese researchers firstly obtained the crystalline diamond particles on silicon wafers using a gaseous mixture of H_2 and CH_4 under microwave glow discharge conditions (Kamo et al. 1983). Consequently, the

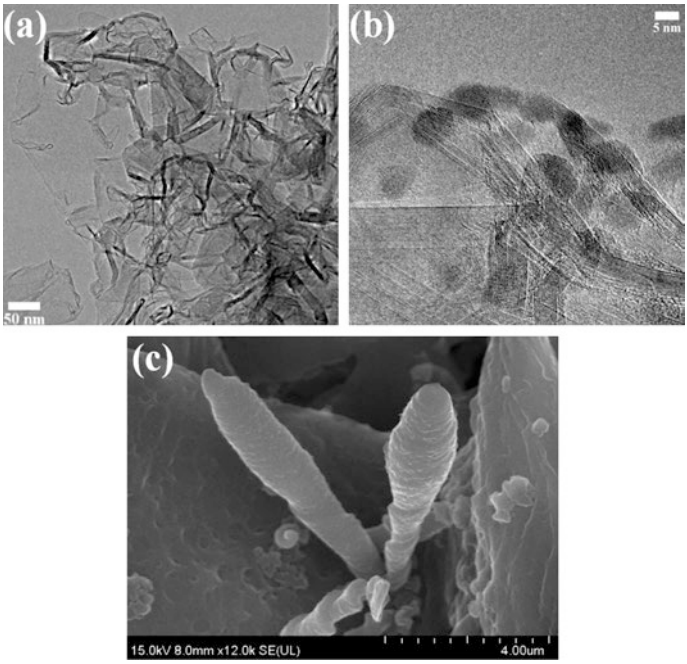

Fig. 1.3 TEM images of (**a**) corrugated few-layer graphene from RH treated at 2500 °C (Melvin et al. 2017b), (**b**) barium titanate nanoparticles immobilized onto the surface of RH treated at 2500 °C (Melvin et al. 2017d), FE-SEM image of (**c**) graphite whisker from waste coffee grounds treated at 2500 °C

microwave PECVD techniques with various designs have been extensively employed for diamond growth, and the resulting products with or without post treatment could be applied in the wide fields of electronic and optical devices, and electrochemical electrodes due to their excellent physical and chemical properties (Schwander and Partes 2011).

With the development of carbon materials, CNTs were firstly observed by Iijima (1991), and quickly attracted great attention in their fundamental research and applications at the beginning. The synthesis approaches of CNTs focus mainly on arc discharge, laser ablation, and CVD. In 1998, Ren et al. (1998) fabricated the CNTs on glass substrate with the decomposition of NH_3 and C_2H_2 by plasma-enhanced hot filament CVD. Compared to thermal CVD grown CNTs, the plasma-assisted CNTs not only grew at low temperatures (less than 666 °C) but also possessed vertical orientation to the substrate, thus, have a better performance in field emission emitters. The PECVD technique is most promising method, in which the decomposition and carbonization of the carbonaceous precursor have been done at low temperatures by the generation of plasma to synthesize multi- and single-walled CNTs (MWCNTs and SWCNTs). The CNT forest can be achieved even at 250–300 °C over large substrate areas under plasma condition (Kleinsorge et al. 2004; Boskovic et al. 2005), thus, they are more acceptable and applicable than

those obtained by conventional CVD. Until now, plasma grown CNTs can be used for lots of applications like energy storage and conversion, sensors, membranes, and field emission displays (Lone et al. 2017). For the application of field emission, plasma-assisted CNTs show some advantages, e.g., high electrical conductivity and low threshold field. However, there is a stable problem that the tallest CNT in the forest experiences the highest field and emits the entire current, which leads to burn it out (Zanin et al. 2013). Thus, some attempts have been employed to overcome it, e.g. combining CNTs with other materials to form composites. For example, the CNTs decorated with Er NPs (Shrestha et al. 2010), ZnO NPs (Ho et al. 2008), and nanodiamond (Guglielmotti et al. 2009) demonstrated the improved emission properties. Zanin et al. (2013) reported the vertically-aligned CNT (VACNT) and DLC composite (Fig. 1.4), in which they were synthesized in the system of N_2-H_2-CH_4 and C_6H_{14}-Ar using different PECVD techniques, respectively, like a honeycomb structure with significant enhancement in emission current, lifetime, stability, and flickering features. Due to higher conductivity and faster diffusion, the VACNTs on the metal substrates were more suitable as the electrodes of electrochemical devices,

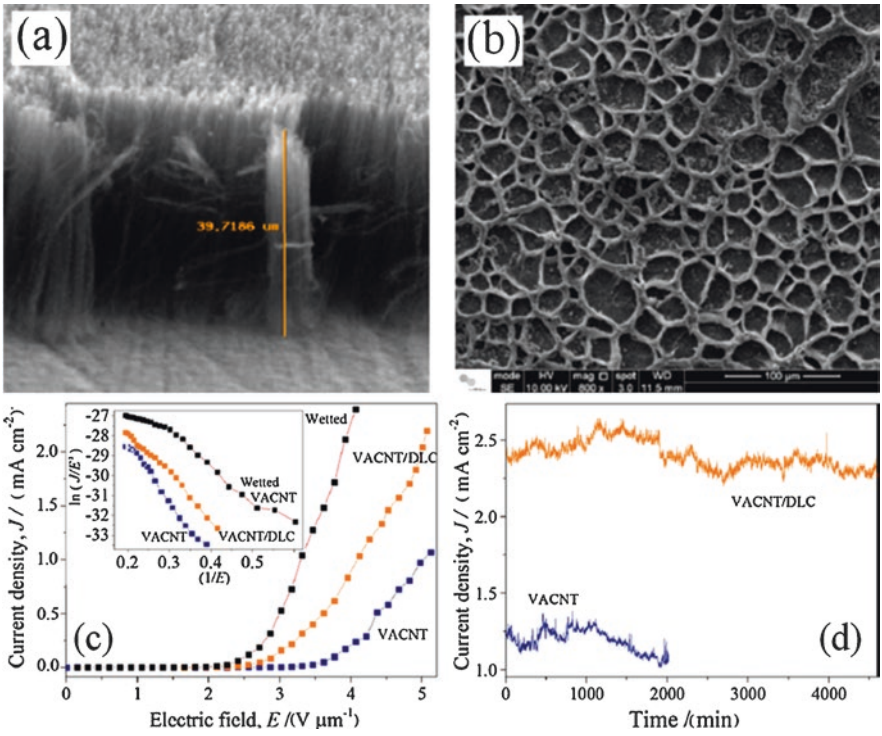

Fig. 1.4 SEM images of the VACNT films (**a**) without and (**b**) with the DLC coating, (**c**) Field-emission characteristics of the VACNT film, the DLC/VACNT film, and the wetted VACNT film. Inset: The corresponding Fowler-Nordheim plots from the three types of samples. (**d**) Field emission current-density stability test from the VACNT films with and without the DLC coating (Zanin et al. 2013)

e.g. supercapacitors and lithium ion batteries (LIBs), in comparison with the free-standing CNTs. The VACNTs composites can further improve the properties of LIBs and supercapacitors (Amade et al. 2011; Saghafi et al. 2014; Malik et al. 2017; Jiang et al. 2019).

Similar to CNTs, graphene-based materials can be also synthesized by various PECVD techniques since the first isolation of graphene using adhesive tape method (Nandamuri et al. 2010; Kim et al. 2011a; Kim et al. 2011b; Bo et al. 2013). In these plasma reactors, the carbonaceous gas was usually decomposed into carbon radicals to eventually form graphene materials on the substrate with the help of H_2 and/or Ar (other gases) as etching reagent. Among those graphene-based materials synthesized by PECVD, vertical graphene (VG), which grew perpendicularly to the substrate (Wang et al. 2011a), has demonstrated some unique characteristics (Fig. 1.5), e.g., nonagglomerated porous internetworked morphology, an abundant of open and sharp edges, and controllable structures. Thus, it makes VG possess more interesting properties, e.g., high electrical conductivity, high surface area, and high electrochemical activity, and many promising applications, e.g., field emission emitters, biosensors, catalysts or catalysts supports, and electrodes of electrochemical devices (Wang et al. 2011b, 2012a, 2012b). In addition, the VG films can be more easily formed on the different substrates including metals, semiconductors, and insulators with any shapes or sizes. It makes VG growth look like substrate-independent process that it attributes to the requirement of no catalyst and easy formation of nucleation sites under plasma conditions. Chen group utilized an atmospheric pressure PECVD to decompose CH_4 on the surface of the CNTs to form hybrid graphene-CNT composites, which have potential electronic and optoelectronic applications (Yu et al. 2011). More interestingly, the VG structures can be achieved from not only the carbonaceous gases but also liquid or solid precursors, including *Melaleuca alternifolia,* milk, honey, butter, sugar, cheese, solid carbon, and polymer (Seo et al. 2013a, 2013b, Wang et al. 2014a, 2014b, Jacob et al. 2015) under various plasma conditions though the resulting VG films exhibited different morphology and microstructure, as partially shown in Fig. 1.5.

The waste plant biomass, which was usually utilized as a source for activated carbon, has extensively been employed to synthesize other novel carbon structures including CNTs, graphene, and their derivatives (Wang et al. 2015b, 2015c), as

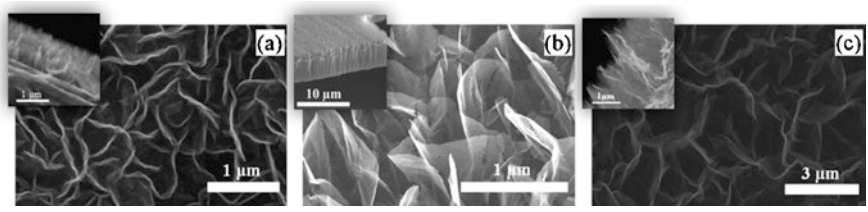

Fig. 1.5 Morphological structures of the VG films from different precursors: (**a**) CH_4 (Wang et al. 2011a), (**b**) Kapton polyimide (Wang et al. 2014a), (**c**) solid carbon (Wang et al. 2014b). Inset: the corresponding cross-sectional images

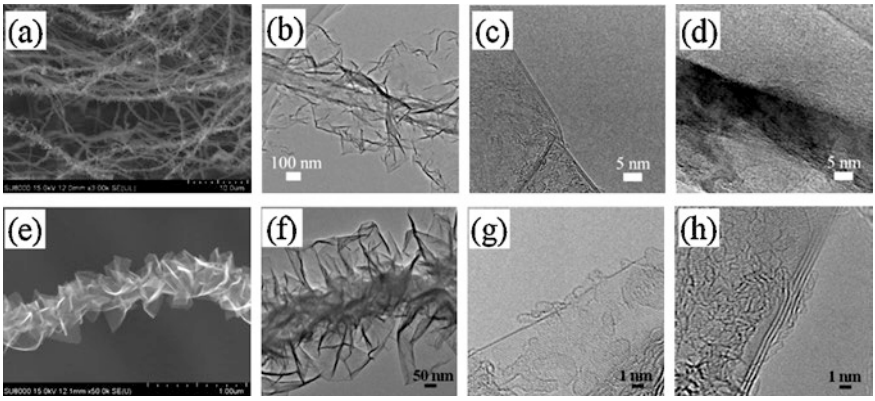

Fig. 1.6 Morphologies and microstructures of the g-CNTs and the GSF synthesized from RHs and coffee grounds, respectively, by microwave plasma irradiation technique: (**a**) SEM, and (**b-d**) TEM images of the g-CNTs, (**e**) SEM, and (**f-h**) TEM images of the GSF. (Wang et al. 2015b, 2015c)

depicted in Fig. 1.6. Microwave plasma irradiation technique was utilized to treat RHs, which located in the home-made Ni box, and found the graphene-CNT hybrid structures, in which graphene sheets grew on the walls of CNTs (named as graphenated CNTs, g-CNTs), on the Ni surface. The g-CNTs exhibited more excellent electrochemical properties than individual CNTs and graphene in the application of supercapacitors. In 2015, graphene-sheet fiber (GSF) were firstly synthesized when the coffee ground powders replaced the RHs. Differ from the g-CNTs, GSF consists of only graphene sheets without the CNT structure inside. The resulting GSFs have relatively excellent electrical conductivity and fantastic specific capacitance.

1.3.3 Hydrothermal Treatment

An aqueous solution of organic substances such as saccharides (glucose, sucrose or starch) or compounds (e.g., furfural) which was heat-treated at a range of temperatures of 150–350 °C for a certain time, the products including water-soluble organic substances and insoluble carbon-rich solids will be formed (Sevilla and Fuertes 2009a). The process, termed as hydrothermal carbonization (HTC), has attracted great interest in recent years. As was known, the HTC is not a new process, and has been utilized to treat various saccharides to investigate the mechanism information of natural coalification during the first decades of last century (Sevilla and Fuertes 2009a). Subsequently, the HTC of the cellulose was studied to obtain liquid chemicals or other solid products, which have the same composition of those obtained from the HTC of the glucose, suggesting that the hydrolysis products for both substances are similar (Van Krevelen 1950).

Wang et al. (2001) first reported the hydrothermal treatment of sucrose to produce carbon microspheres. Subsequently, Sun and Li (2004a) obtained similar

carbon spheres (CSs) by the HTC of the glucose, in which their sizes were adjustable through the experimental parameters and they can be loaded with metal NPs to form the hybrid carbon/metal materials (e.g., C/Ag, C/Cu, C/Au, C/Pd, C/Te). Studies have shown that the HTC-assisted CSs can be employed as sacrificial templates for fabricating hollow spherical structures of inorganic compounds (e.g., Ga_2O_3, GaN, WO_3, SnO_2) (Sun and Li 2004b; Li et al. 2004; Wang et al. 2007). The CSs synthesized from the HTC of different saccharides (glucose, sucrose or starch) can be used as precursors for the production of graphitic carbon nanocoils (Fig. 1.7(c)-(d)) with the help of Ni under nitrogen up to 900 °C for 3 h, and the products supported PtRu NPs for metal electrooxidation (Sevilla et al. 2007). Significantly, the glucose-derived CSs (Fig. 1.7(a)-(b)) were graphitized at extremely high temperatures in the range of 1200-2900 °C to achieve discrete fragments of curved graphitic planes (Wang et al. 2017), which are similar to heat-treated glassy carbon. But, they were different from the tetrahydrofuran-derived pyrolytic spheres (Zhang et al. 2006) and the hydrocarbon-derived carbon spheres by CVD technique (Wang et al. 2005) at extremely high temperatures, which demonstrated concentrically polyhedral graphitic shells. It implied that the microstructures of the resulting CSs after high temperature treatment were strongly dependent of the precursors.

Besides the saccharides (glucose, sucrose or starch), the cellulose can be converted into carbon microspheres (2–5 μm) by the HTC process at the temperatures in the range of 220–250 °C (Sevilla and Fuertes 2009b). The results confirmed that the formation of CSs involved into the path of a dehydration process, similar to the previous observation for the hydrothermal transformation of saccharides. Biomass is a biological matter that incorporates all living mater on earth, and mainly consists of cellulose, hemicellulose, and lignin. Thus, biomass is suitable substance for the formation hydrochar under HTC, which strongly depend on the process parameters including temperature, feed type, residence time, pressure, and catalyst (Nizamuddin et al. 2017).

In addition, hollow CSs with controllable size and morphology have been developed by the HTC of α-cyclodextrin in the presence of Pluronic F127 as a soft template (Yang et al. 2013), as illustrated in Fig. 1.7(e) and (f). Uniform carbon nanofibers (about 50 nm in diameter and some micrometers in length) with high aspect ratio could be produced using the HTC of the glucose in the present of Te nanowires (Qian et al. 2006), as shown in Fig. 1.7(g) and (h). The pure carbon nanofibers can be obtained by removal of the core of the product by treatment of with a mix aqueous solution of HCl and H_2O_2 at RT for 12 h.

HTC of biomass such as glucose and cellulose typically produces CSs with the diameter in micrometer size, which are insulating. When adding a certain amount of graphene oxide (GO) to glucose, the HTC products exhibit significant change in their morphologies and improve the conductivity of carbon materials with high degree of carbonization. At low mass loading of GO, HTC treatment can lead to dispersed carbon platelets with tens of nanometers in thickness, while at high mass loading, free-standing carbon monoliths can be obtained (Krishnan et al. 2014). GO, a two-dimensional single atomic sheet, is the chemical exfoliation product of graphite powders, and has rich oxygen-containing functional groups, e.g., epoxy

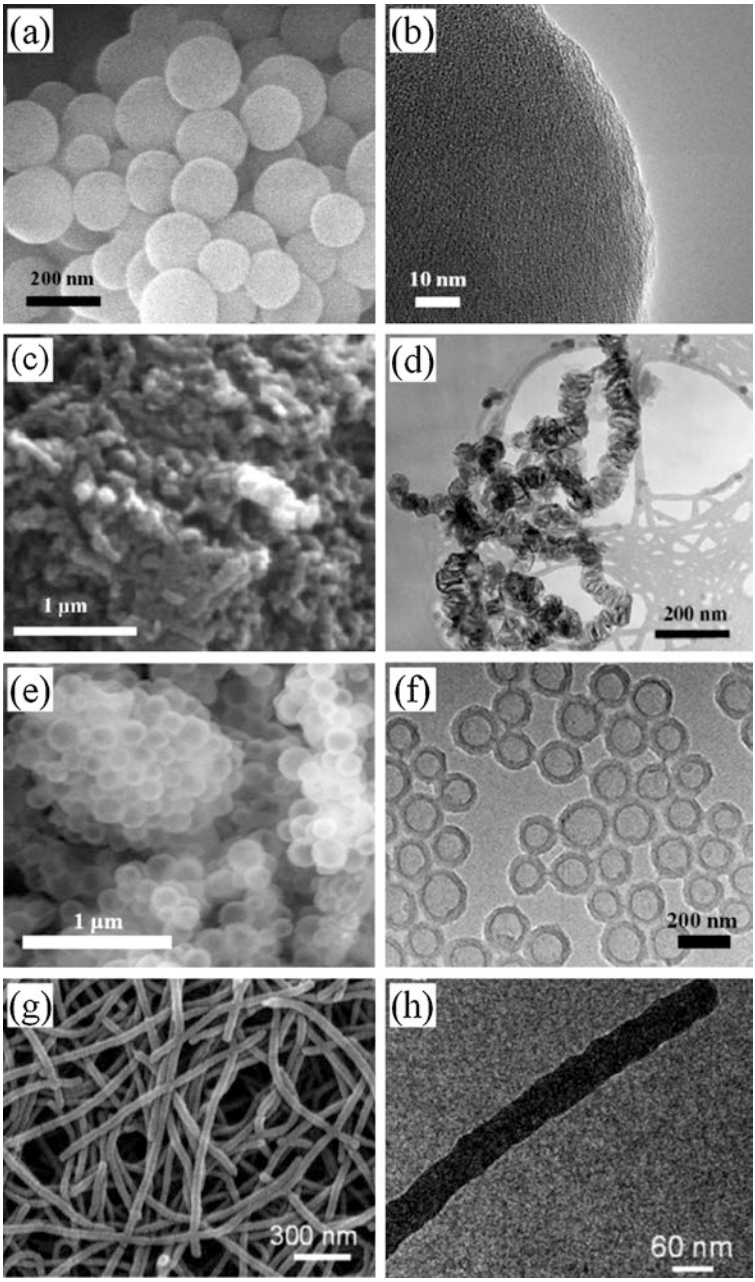

Fig. 1.7 SEM and TEM images of (**a-b**) glucose-derived carbon spheres (Wang et al. 2017), (**c-d**) saccharide-derived graphitic carbon nanocoils (Sevilla et al. 2007), (**e-f**) α-cyclodextrin-derived hollow carbon spheres (Yang et al. 2013), (**g-h**) glucose-derived carbon nanofibers under HTC conditions (Qian et al. 2006)

and hydroxyl groups, decorating the segregated nanographitic domains on their basal planes so that it is easily dispersed in water and many polar solvents. Compared with original GO sheets, reduced GO (rGO) sheets demonstrate the more outstanding physiochemical properties and promising applications. Thus, various attempts, e.g., chemical, thermal, solvothermal, and hydrothermal reductions (Zhou et al. 2009; Zhao et al. 2012; Huang et al. 2018), have been employed to reduce GO sheets into rGO sheets. Among them, hydrothermal reduction of GO is a simple, fast, and environmentally friendly route which involves water only without adding any toxic reducing agents. The graphene aerogel can be obtained from rGO using hydrothermal process, and demonstrated excellent elastic modulus, good electrical conductivity, high specific capacity, and thermal stability. The results confirmed that the properties of graphene aerogels strongly depend on GO concentration and hydrothermal reaction time (Xu et al. 2010). In order to achieve wider applications, graphene-containing composite materials have been extensively investigated. Researchers utilized one-step hydrothermal method to synthesize graphene-based composites, such as TiO_2-rGO, Co_3O_4-rGO, and doped rGO (Shen et al. 2011; Liu et al. 2013; Zhang et al. 2017), in which exhibited the improved properties and performances in supercapacitors and batteries.

During the HTC process, the GO as a template and catalyst can promote the polymerization of the fragments decomposed from egg proteins to form egg protein-derived carbon/rGO composite for supercapacitor electrode with high specific capacitance, good rate capability and excellent cycling stability (Ma et al. 2017). Hydrothermal approach was also employed to cut the thermally rGO sheets into surface-functionalized graphene quantum dots (GQDs) with 9.6 nm average diameter (Pan et al. 2010). The resulting GQDs exhibited bright blue photoluminescence due to their large edge effect.

1.3.4 Electro-Deposition Using Molten Salts

Over the course of years, the rapid growth of industrial sectors, the increase in human population, and open agricultural burning give rise to carbon dioxide gas emission into the atmosphere. The atmospheric concentration of carbon dioxide gas had reached an alarming level. According to National Oceanic and Atmospheric Administration (NOAA) and the American Meteorological Society report released in August 2018 entitled State of the Climate in 2017, the global atmospheric carbon dioxide concentration for the year 2017 was at 405.0 ± 0.1 ppm. The effort in reducing the level of carbon dioxide gas in the atmosphere had been one of the great concerns in this modern world. The awareness of the climate change gives way to researchers in utilizing carbon dioxide as the source of conversion to value-added product, therefore carbon capture and utilization (CCU) technologies (Alper and Yuksel Orhan 2017; Stuardi et al. 2019; Styring et al. 2011; Yan and Zhang 2019) was extensively studied either in industry or academically (Yuan et al. 2016). The conversion of carbon dioxide gas introduce the end products which contains the

carbon from the gas as a result of physical and chemical processes (Song 2002). Electrochemical conversion of carbon dioxide gas in molten salt electrolyte as one of the utilization method had progress rapidly due to the molten salt exceptional properties, for instance low vapor pressure, high electronic conductivity and low cost (Ge et al. 2016).

Electrolytic generated carbon in electrolysis of molten salts was accidentally discovered in the early 1900's where Haber and Bruner (1904) attained significant carbon deposition from barium chloride and barium carbonate mixture at 580 °C. While in the 1940's, Andrieux and Weiss (1944) unintentionally found carbon by utilizing carbonates and halides mixtures to synthesis inorganic carbides at 750 °C via electrochemical route. In 1960's, inspired by the previous accidental findings; Ingram et al. (1966) studied the occurrence of carbon deposition in electrolysis of molten carbonates with argon and carbon dioxide atmosphere, its characteristics and the properties of the deposited carbon, however limited interest was shown in this study throughout the years. Recently, researchers show interest in the electro-deposition of solid carbon using molten salts electrolyte with continuous supply of carbon dioxide gas. It is due to the discoveries of wide variation of interesting carbon microstructure and the utilization of carbon dioxide gas as carbonate source in the molten salt electrolysis process (Deng et al. 2018; Dimitrov et al. 2002; Gakim et al. 2015; Ge et al. 2016; Ijije et al. 2014a; Ingram et al. 1966; Karen et al. 2018; Le Van et al. 2009; Novoselova et al. 2008; Tang et al. 2013; Yin et al. 2013).

Wide variety of carbonaceous materials were discovered from electrolysis of molten salt electrolytes. The carbonaceous materials sizes ranging from micro- to nano- and was found to exhibit diverse microstructures depending on the electrolysis process parameters, *i.e.* electrolytes, substrates, temperatures, current densities and deposition potentials (Hughes et al. 2015; Kawamura and Ito 2000). There were various reasons and factors on the parameter selection, however some of the studies targeted selective electrolyte and electrode type due to the desired end product *i.e.* in the synthesis of carbon nanotubes or nanomaterials by using molten chloride salt. Molten chloride salt (LiCl, NaCl, KCl, and more) was utilized alongside graphite electrodes with carbon nanotubes as main product (Chen et al. 1998; Hsu et al. 1996). While Kamali et al. (2011) study the use of different type of graphite electrode to the carbon nanomaterial obtained by using LiCl electrolyte, further study by Kamali and Fray (2013) look into the corrosion of the electrode in mixture of LiCl salt with graphite powder. However, the selection of electrolyte should be considered carefully which could produce carbon materials as the end product. The molten salt electrolyte should be able to dissolve the O^{2-}ion which the ion is a product of carbon deposition and able to absorb CO_2 gas and convert it to CO_3^{2-} ions (Ijije et al. 2014b). Another important factor for successful carbon deposition is the presence of Li^+ ions in the electrolyte (Ingram et al. 1966; Delimarskii et al. 1968; Kawamura and Ito 2000; Massot et al. 2002; Ijije et al. 2014b). Based on the study on the role and effect of the alkali metal ions in electrolysis process, notable Na^+, K^+ and Li^+ ions, Ijije and Chen (2016) found that electrolyte containing Li^+ ion (Li_2CO_3) produced carbon material while electrolyte containing Na^+ (Na_2CO_3) and K^+

(K_2CO_3) produced alkali metal as the main cathodic reaction. Over the years, the selection of electrodes in the electrolysis process was not carefully explain by researchers, nonetheless, the use of silver, nickel, gold, tungsten, platinum or copper as electrodes have been reported (Ingram et al. 1966; Lantelme et al. 1999; Le Van et al. 2009; Tang et al. 2013; Yin et al. 2013; Ge et al. 2016; Deng et al. 2018). Likewise, the temperature, current densities and deposition potentials selection for the process were not vastly studied and limited information was available. Though, the process temperature often chosen while considering the melting temperature of the selected electrolyte.

Interesting microstructures was observed in the carbon materials obtained either in single-salt electrolyte of mixture of two or more salt. The electrolysis of single Li_2CO_3 yields micro-sized irregular shaped flakes under process temperature of 740 °C and voltage supply of 4 V by using stainless steel electrodes (Ijije and Chen 2016). Whereas nano-sized carbon nanofibers was produced under 730 °C with coiled galvanized steel wire cathode and Ni anode (Ren et al. 2015), and carbon nanotubes was observed in Wu et al. (2016b) study under the temperature of 770 °C and Ni as cathode with addition of ZnO additive (1 wt%). Figure 1.8 shows the findings of the studies respectively.

Diverse microstructures were observed in mixture of two or more salt electrolyte. Dimitrov (2009) observed nano-balls and flower-like sheets in electrolysis of binary LiCl-Li_2CO_3 using graphite electrodes at 700 °C, whereas Ge et al. (2015) found quasi-spherical microstructures with inert platinum anode and tungsten cathode at 700 °C of electrolysis temperature. On the other hand, Deng et al. (2018) obtained wide variety of carbon microstructures with the addition of salt additive ($CaCO_3$) into the binary LiCl-KCl. Crater-like, nanofibers, coral, quasi-spherical, spherical, carbon sheets, shell-like structure, flakes and aggregated nanoparticles was found in the study. While Kawamura and Ito (2000) and Song et al. (2012) observed aggregated quasi-spherical structure in electrolysis of ternary LiCl-KCl-K_2CO_3, at 450 °C with rectangular sheet of aluminum as cathode and glassy carbon

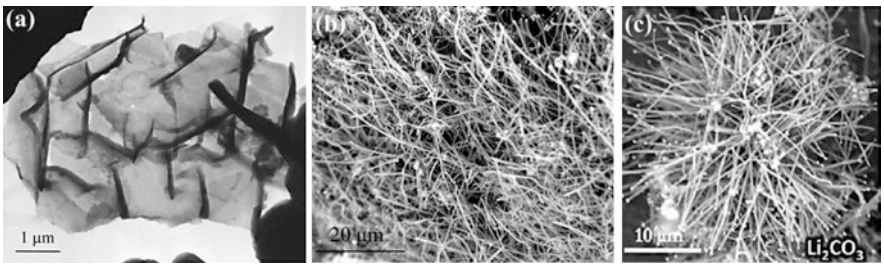

Fig. 1.8 The findings of carbon microstructures deposited in single Li_2CO_3 electrolyte, (**a**) TEM image of carbon deposited under 740 °C with 4 V in CO_2 atmosphere (Ijije and Chen 2016), (**b**) SEM image of nano-sized carbon nanofibers produced under 730 °C with coiled galvanized steel wire cathode and Ni anode (Ren et al. 2015), and (**c**) SEM image of carbon nanotubes obtained under the temperature of 770 °C and Ni as cathode with addition of 1 wt% ZnO additive (Wu et al. 2016b)

rod anode, and at 500 °C with graphite electrodes, respectively. Ternary mixture of Li_2CO_3-Na_2CO_3-K_2CO_3 was widely use as electrolyte since Ingram et al. (1966) successfully obtained carbon deposition. Groult et al. (2006) found nano-sized carbon particles in electrolysis of the ternary electrolyte at 450 °C with gold-sheet anode and Ni-sheet cathode, whereas Le Van et al. (2009) discover nano-sized quasi-spherical carbon with graphite anode and Ni cathode. While Yin et al. (2013) observed aggregated nano-sized carbon particles and flakes with SnO_2 rod anode and Ni-sheet cathode at 500 °C, Tang et al. (2013) obtained micro- and nano-sized flakes, nanowires, particles and thin sheets by using SnO_2 rod anode and U-shape Ni sheet cathode at process temperature of 450, 550, and 650 °C. Gakim et al. (2015) found micro-sized aggregated grape-like structure in electrolysis of $CaCO_3$-$CaCl_2$-KCl-LiCl quaternary mixture at temperature range between 575 and 585 °C. Study by Karen et al. (2018) in electrolysis of newly formulated ternary $CaCO_3$-Li_2CO_3-LiCl salt mixture at 550–650 °C and 4 – 6 V cell voltage using stainless steel as electrodes with CO_2 atmosphere showed five dominant microstructures: grape-like, tubes, thread-like, spheres, and flakes under the SEM analysis, as shown in Fig. 1.9(a) - (e) respectively.

Electrolysis involves the splitting of a particular substance when electrical energy was introduced into the system, and it is frequently applied to decompose a compound to its elements. The electrolyte in the electrolysis process could be the pure compound, for example H_2O or a molten salt, or a mixture of two or more molten salts (Silberberg 2006). The utilization of carbon dioxide gas as carbon source in the electrolysis of molten salt electrolyte produces carbonaceous materials.

Electro-deposition of solid carbon via electrolysis of molten salt in CO_2 atmosphere can be carried out in an electrolytic cell. The cell requires an electrolyte

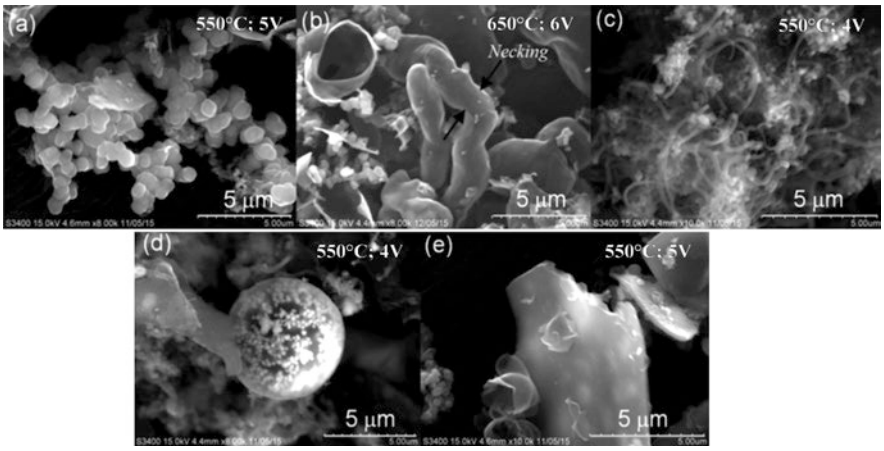

Fig. 1.9 The example of SEM images for (**a**) grape-like, (**b**) tubes, (**c**) thread-like, (**d**) sphere, and (**e**) flakes, as dominant microstructures found in the deposited solid carbon prepared at 550 and 650 °C with voltage supply of 4 – 6 V using ternary $CaCO_3$-Li_2CO_3-LiCl salt mixture (Karen et al., 2018)

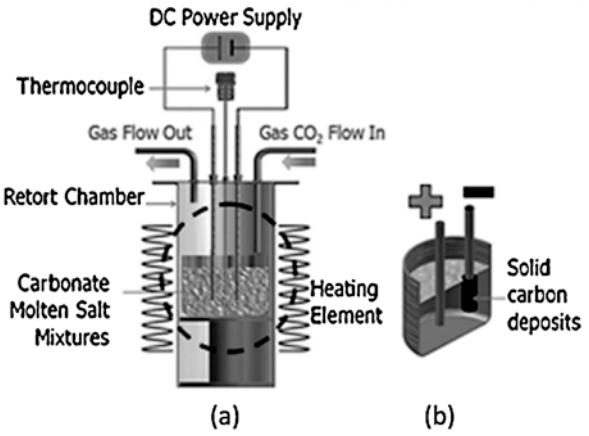

Fig. 1.10 The schematic diagram (not according to scale) of (**a**) experimental set-up for the electro-deposition of solid carbon via electrolysis process and (**b**) solid deposition on cathode surface for electrolysis in CO_2 gas environment (Karen et al. 2018)

which contains ions (cations and anions) and able to conduct electric when it is in liquid form. Electric current can be supplied to the electrolyte by the positive and negative electrodes which immersed in the electrolyte. CO_2 gas can be flowed into the system to replenish the carbonate ions (CO_3^{2-} as carbon source) in the electrolyte for continuous carbon deposition on the cathode surface. Fig. 1.10 displayed the example of experimental setup for electrolysis process and the deposition of solid carbon the cathode surface based on Karen et al. (2018) study.

The deposition of carbon occurred on the surface of cathode electrode as a result of the conversion reaction happened at the interface of cathode and the electrolyte (Ingram et al. 1966), as soon as the voltage was supplied to the system. The carbon source, carbonate ions (CO_3^{2-}), will be reduced to carbon in the electrolysis process in two steps of reaction as stated below (Ingram et al. 1966; Kawamura and Ito 2000; Kaplan et al. 2002; Massot et al. 2002; Le Van et al. 2009; Ijije et al. 2014c; Gakim et al. 2015).

Step 1:	$CO_3^{2-} + 4e^- \rightarrow C\ (s) + 3O^{2-}$	(1)
	$CO_3^{2-} + 2e^- \rightarrow CO_2^{2-} + O^{2-}$ then $CO_2^{2-} + 2e^- \rightarrow C\ (s) + 2O^{2-}$	(2 & 3)
Step 2:	$O^{2-} + CO_2\ (g) \rightleftharpoons CO_3^{2-}$	(4)

The CO_3^{2-} ions first reduced to carbon either by the single-step process based on reaction (1) (Ingram et al. 1966; Kaplan et al. 2002; Massot et al. 2002), or the two-step process based on reaction (2) and (3) (Delimarskii et al. 1968; Ito et al. 1992). Later, the molten salt electrolyte absorbs the CO_2 gas through reaction (4), and regenerates CO_3^{2-} ions in the electrolyte. The reactions cycle enables the continuous production of carbon on the cathode surface.

The application of carbon produced by electrolysis of molten salt electrolyte is not vastly studied. However, it has the potential to be utilized in various spectrum as the carbon obtained from the process exhibits a diverse microstructures and particle

sizes ranging from micro to nano sizes. For instance, composite materials for energy storage electrode (Ijije et al. 2014c). Moreover, the carbon could be further treated for attachment of desirable functional groups, *i.e.* carboxyl and hydroxyl groups, on the carbon surface which improved its dispersion ability, and later can be utilized as carbon filler in fabrication of composites or attachment of other particles onto their surface in fabrication of hybrid composites. Carbon fillers, *i.e.* carbon nanotubes (Anagappan et al. 2013), carbon nanofibers and carbon black, can be used as composites filler, and when mixing the carbon fillers with polymers, it could improve the overall mechanical, electrical and thermal stability.

1.4 Conclusions

In this chapter, carbon materials from various sources for composite materials are mainly described. Obviously, by using different material sources and methods, a great variety of carbon materials can be produced, such as carbon nanotube, graphene, carbon sphere, carbon flake, graphite whisker, and many more. Furthermore, the carbon materials also can be integrated with other materials, in order to achieve higher performance or specifically targeted properties. The carbon materials can be utilized for composite materials in vast fields and applications, such as energy storage devices, actuator, shape memory material, electromagnetic wave absorber, functionally graded material, and many more. Carbon-based composite materials is a prominent candidate to tackle our current or future demands to satisfy various necessities.

Acknowledgement This work was supported by Universiti Malaysia Sabah (Grant number GUG0386-2/2019), Malaysia.

References

Abioye AM, Noorden ZA, Ani FN (2017) Synthesis and characterizations of electroless oil palm shell based-activated carbon/nickel oxide nanocomposite electrodes for supercapacitor applications. Electrochim Acta 225:493–502. https://doi.org/10.1016/j.electacta.2016.12.101

Ajayan PM, Stephan O, Colliex C, Trauth D (1994) Aligned carbon nanotube arrays formed by cutting a polymer resin - nanotube composite. Science 265(5176):1212–1214. https://doi.org/10.1126/science.265.5176.1212

Ali M, Hirai T (2011) Characteristics of the creep-induced bending deformation of a PVC gel actuator by an electric field. J Mater Sci 46(24):7681–7688. https://doi.org/10.1007/s10853-011-5746-7

Alper E, Yuksel Orhan O (2017) CO_2 utilization: developments in conversion processes. Petroleum 3(1):109–126. https://doi.org/10.1016/j.petlm.2016.11.003

Alslaibi TM, Abustan I, Ahmad MA, Foul AA (2013) A review: production of activated carbon from agricultural byproducts via conventional and microwave heating. J Chem Technol Biotechnol 88(7):1183–1190. https://doi.org/10.1002/jctb.4028

Amade R, Jover E, Caglar B, Mutlu T, Bertran E (2011) Optimization of MnO2/vertically aligned carbon nanotube composite for supercapacitor application. J Power Source 196(1):5779–5783. https://doi.org/10.1016/j.jpowsour.2011.02.029

Anagappan S, Thirumal V, Ramkumar K, Visuvasam A (2013) Synthesis of carbon nanotubes by molten salt technique. Chem Sci Trans 2(2):575–583. https://doi.org/10.7598/cst2013.394

Andrieux L, Weiss G (1944) Productions of electrolysis of molten salts with an iron anode. Comptes Rendu 217:615

Araga R, Sharma CS (2017) One step direct synthesis of multiwalled carbon nanotubes from coconut shell derived charcoal. Mater Lett 188:205–207. https://doi.org/10.1016/j.matlet.2016.11.014

Bazargan A, McKay G (2012) A review – synthesis of carbon nanotubes from plastic wastes. Chem Eng J 195-196:377–391. https://doi.org/10.1016/j.cej.2012.03.077

Bi C, Zhu M, Zhang Q, Li Y, Wang H (2011) Synthesis and electromagnetic wave absorption properties of multi-walled carbon nanotubes decorated by $BaTiO_3$ nanoparticles. J Nanosci Nanotechnol 11(2):1030–1036. https://doi.org/10.1166/jnn.2011.3046

Bo Z, Yang Y, Chen J, Yu K, Yan J, Cen K (2013) Plasma-enhanced chemical vapor deposition synthesis of vertically oriented graphene nanosheets. Nanoscale 5:5180–5204. https://doi.org/10.1039/c3nr33449j

Boskovic BO, Golovko VB, Cantoro M, Kleinsorge B, Chuang AH, Ducati C, Hofmann S, Robertson J, Johnson BFG (2005) Low temperature synthesis of carbon nanofibres on carbon fibre matrices. Carbon 43:2643–2648. https://doi.org/10.1016/j.carbon.2005.04.034

Chen GZ, Fan X, Luget A, Shaffer MS, Fray DJ, Windle AH (1998) Electrolytic conversion of graphite to carbon nanotubes in fused salts. J Electroanal Chem 446(1–2):1–6. https://doi.org/10.1016/S0022-0728(97)00552-4

Dai L, Chang DW, Baek JB, Lu W (2012) Carbon nanomaterials for advanced energy conversion and storage. Small 8(8):1130–1166. https://doi.org/10.1002/smll.201101594

Delimarskii YK, Shapoval VI, Grishchenko VF, Vasilenko VA (1968) Peculiarities of the cathodic liberation of carbon in the electrolysis of molten carbonates. Dokl Akad Nauk SSSR 183(6):1332–1334

Deng B, Tang J, Gao M, Mao X, Zhu H, Xiao W, Wang D (2018) Electrolytic synthesis of carbon from the captured CO_2 in molten LiCl–KCl–$CaCO_3$: critical roles of electrode potential and temperature for hollow structure and lithium storage performance. Electrochim Acta 259:975–985. https://doi.org/10.1016/j.electacta.2017.11.025

Dimitrov AT, Chen GZ, Kinloch IA, Fray DJ (2002) A feasibility study of scaling-up the electrolytic production of carbon nanotubes in molten salts. Electrochim Acta 48(1):91–102. https://doi.org/10.1016/S0013-4686(02)00595-9

Dimitrov AT (2009) Study of molten Li_2CO_3 electrolysis as a method for production of carbon nanotubes. Maced J Chem Chem Eng 28(1):111–118. https://doi.org/10.20450/mjcce.2009.226

Dong J, Shen W, Zhang B, Liu X, Kang F, Gu J, Li D, Chen N (2001) New origin of spirals and new growth process of carbon whiskers. Carbon 39(15):2325–2333. https://doi.org/10.1016/S0008-6223(01)00064-1

Dong Y, Wu ZS, Ren W, Cheng HM, Bao X (2017) Graphene: a promising 2D material for electrochemical energy storage. Sci Bull 62(10):724–740. https://doi.org/10.1016/j.scib.2017.04.010

Dong Y, Xia H, Zhu Y, Ni QQ, Fu Y (2015) Effect of epoxy-graft-polyoxyethylene octyl phenyl ether on preparation, mechanical properties and triple-shape memory effect of carbon nanotube/water-borne epoxy nanocomposites. Compos Sci Technol 120:17–25. https://doi.org/10.1016/j.compscitech.2015.09.011

Foo KY, Hameed BH (2012) Mesoporous activated carbon from wood sawdust by K_2CO_3 activation using microwave heating. Bioresour Technol 111:425–432. https://doi.org/10.1016/j.biortech.2012.01.141

Gakim M, Khong LM, Janaun J, Liew WYH, Siambun NJ (2015) Production of carbon via electrochemical conversion of CO_2 in carbonates based molten salt. Adv Mater Res 1115:361–365. https://doi.org/10.4028/www.scientific.net/AMR.1115.361

Ge J, Hu L, Wang W, Jiao H, Jiao S (2015) Electrochemical conversion of CO_2 into negative electrode materials for Li-ion batteries. ChemElectroChem 2(2):224–230. https://doi.org/10.1002/celc.201402297

Ge J, Wang S, Hu L, Zhu J, Jiao S (2016) Electrochemical deposition of carbon in LiCl-NaCl-Na_2CO_3 melts. Carbon 98:649–657. https://doi.org/10.1016/j.carbon.2015.11.065

Groult H, Kaplan B, Lantelme F, Komaba S, Kumagai N, Yashiro H, Nakajima T, Simon B, Barhoun A (2006) Preparation of carbon nanoparticles from electrolysis of molten carbonates and use as anode materials in lithium-ion batteries. Solid State Ionics 177(9–10):869–875. https://doi.org/10.1016/j.ssi.2006.01.051

Guardia L, Suárez L, Querejeta N, Vretenár V, Kotrusz P, Skákalová V, Centeno TA (2019) Biomass waste-carbon/reduced graphene oxide composite electrodes for enhanced supercapacitors. Electrochim Acta 298:910–917. https://doi.org/10.1016/j.electacta.2018.12.160

Guglielmotti V, Chieppa S, Orlanducci S, Tamburri E, Toschi F, Terranova ML, Rossi M (2009) Carbon nanotube/nanodiamond structures: an innovative concept for stable and ready-to-start electron emitters. Appl Phys Lett 95:222113. https://doi.org/10.1063/1.3269929

Haber F, Bruner L (1904) Das Kohlenelement, eine Knallgaskette. Z Elektrochem Angew Phys Chem 10(37):697–713. https://doi.org/10.1002/bbpc.19040103702

He X, Geng Y, Qiu J, Zheng M, Long S, Zhang X (2010) Effect of activation time on the properties of activated carbons prepared by microwave-assisted activation for electric double layer capacitors. Carbon 48(5):1662–1669. https://doi.org/10.1016/j.carbon.2010.01.016

Hierold C, Brand O, Fedder GK, Korvink JG, Tabata O (2008) Carbon nanotube devices: properties, modeling, integration and applications, vol 8. Wiley, Chichester

Ho YM, Yang GM, Zheng WT, Wang X, Tian HW, Xu Q, Li HB, Liu JW, Qi JL, Jiang Q (2008) Synthesis and field electron emission properties of hybrid carbon nanotubes and nanoparticles. Nanotechnology 19(6):065710. https://doi.org/10.1088/0957-4484/19/6/065710

Hsu WK, Terrones M, Hare JP, Terrones H, Kroto HW, Walton DRM (1996) Electrolytic formation of carbon nanostructures. Chem Phys Lett 262(1–2):161–166. https://doi.org/10.1016/0009-2614(96)01041-X

Huang H-H, De Silva K, Kumara GRA, Yoshimura M (2018) Structural evolution of hydrothermally derived reduced graphene oxide. Sci Rep 8:6849. https://doi.org/10.1038/s41598-018-25194-1

Huang X, Chen Z, Tong L, Feng M, Pu Z, Liu X (2013) Preparation and microwave absorption properties of $BaTiO_3$@MWCNTs core/shell heterostructure. Mater Lett 111:24–27. https://doi.org/10.1016/j.matlet.2013.08.034

Huang Y, Liu Y, Zhao G, Chen JY (2017) Sustainable activated carbon fiber from sawdust by reactivation for high-performance supercapacitors. J Mater Sci 52(1):478–488. https://doi.org/10.1007/s10853-016-0347-0

Hu H, Onyebueke L, Abatan A (2010a) Characterizing and modeling mechanical properties of nanocomposites - review and evaluation. J Miner Mater Charact Eng 9(4):275–319

Hu L, Hecht DS, Gruner G (2010b) Carbon nanotube thin films: fabrication, properties, and applications. Chem Rev 110(10):5790–5844. https://doi.org/10.1021/cr9002962

Hughes MA, Allen JA, Donne SW (2015) Carbonate reduction and the properties and applications of carbon formed through electrochemical deposition in molten carbonates: a review. Electrochim Acta 176:1511–1521. https://doi.org/10.1016/j.electacta.2015.07.134

Iijima S (1991) Helical microtubules of graphitic carbon. Nature 354(6348):56–58. https://doi.org/10.1038/354056a0

Iijima S, Ichihashi T (1993) Single-shell carbon nanotubes of 1-nm diameter. Nature 363(6430):603–605. https://doi.org/10.1038/363603a0

Ijije HV, Sun C, Chen GZ (2014a) Indirect electrochemical reduction of carbon dioxide to carbon nanopowders in molten alkali carbonates: process variables and product properties. Carbon 73:163–174. https://doi.org/10.1016/j.carbon.2014.02.052

Ijije HV, Lawrence RC, Siambun NJ, Jeong SM, Jewell D, Hu D, Chen GZ (2014b) Electrodeposition and re-oxidation of carbon in carbonate-containing molten salts. Faraday Discuss 172:105–116. https://doi.org/10.1039/c4fd00046c

Ijije HV, Lawrence R, Chen G (2014c) Carbon electrodeposition in molten salts: electrode reactions and applications. RSC Adv 4:35808–35817. https://doi.org/10.1039/C4RA04629C
Ijije HV, Chen G (2016) Electrochemical manufacturing of nanocarbons from carbon dioxide in molten alkali metal carbonate salts: roles of alkali metal cations. Adv Manuf 4(1):23–32. https://doi.org/10.1007/s40436-015-0125-2
Ingram MD, Baron B, Janz GJ (1966) The electrolytic deposition of carbon from fused carbonates. Electrochim Acta 11(11):1629–1639. https://doi.org/10.1016/0013-4686(66)80076-2
Ito Y, Shimada T, Kawamura H (1992) Electrochemical formation of thin carbon film from molten chloride system. Proc – Electrochem Soc 1992-16:574–585. https://doi.org/. https://doi.org/10.1149/199216.0574PV
Jacob MV, Rawat RS, Ouyang B, Bazaka K, Kumar DS, Taguchi D, Iwamoto M, Neupane R, Varghese OK (2015) Catalyst-free plasma enhanced growth of graphene from sustainable sources. Nano Lett 15(9):5702–5708. https://doi.org/10.1021/acs.nanolett.5b01363
Jiang H, Ni QQ, Wang H, Liu J (2012) Fabrication and characterization of NBR/MWCNT composites by latex technology. Polym Compos 33(9):1586–1592. https://doi.org/10.1002/pc.22297
Jiang H, Wei Z, Cai X, Lai L, Ma J, Huang W (2019) A cathode for Li-ion batteries made of vanadium oxide on vertically aligned carbon nanotubes/graphene foam. Chem Eng J 359:1668–1696. https://doi.org/10.1016/j.cej.2018.10.223
Kamali AR, Schwandt C, Fray DJ (2011) Effect of the graphite electrode material on the characteristics of molten salt electrolytically produced carbon nanomaterials. Mater Charact 62(10):987–994. https://doi.org/10.1016/j.matchar.2011.06.010
Kamali AR, Fray DJ (2013) Molten salt corrosion of graphite as a possible way to make carbon nanostructures. Carbon 56:121–131. https://doi.org/10.1016/j.carbon.2012.12.076
Kamo M, Sato Y, Matsumoto S, Setaka N (1983) Diamond synthesis from gas phase in microwave plasma. J Cryst Growth 62:642–644. https://doi.org/10.1016/0022-0248(83)90411-6
Kaplan B, Groult H, Barhoun A, Lantelme F, Nakajima T, Gupta V, Komabe S, Kumagai N (2002) Synthesis and structural characterization of carbon powder by electrolytic reduction of molten $Li_2CO_3Na_2CO_3K_2CO_3$. J Electrochem Soc 149(5):D72–D78. https://doi.org/10.1149/1.1464884
Karen WMJ, Gakim M, Janaun JA, Liew WYH, Siambun NJ (2018) Effect of temperature and voltage on the preparation of solid carbon by electrolysis of a molten $CaCO_3$-Li_2CO_3-LiCl electrolyte. Int J Electrochem Sci 13:9771–9783. https://doi.org/10.20964/2018.10.43
Kawamura H, Ito Y (2000) Electrodeposition of cohesive carbon films on aluminum in a LiCl-KCl-K_2CO_3 melt. J Appl Electrochem 30:571–574. https://doi.org/10.1023/A:1003927100308
Ke Q, Wang J (2016) Graphene-based materials for supercapacitor electrodes - a review. J Mater 2(1):37–54. https://doi.org/10.1016/j.jmat.2016.01.001
Kim J, Ishihara M, Koga Y, Tsugawa K, Hasegawa M, Iijima S (2011a) Low-temperature synthesis of large-area graphene-based transparent conductive films using surface wave plasma chemical vapor deposition. Appl Phys Lett 98:091502. https://doi.org/10.1063/1.3561747
Kim Y, Song W, Lee SY, Jeon C, Jung W, Kim M, Park C-Y (2011b) Low-temperature synthesis of graphene on nickel foil by microwave plasma chemical vapor deposition. Appl Phys Lett 98:263106. https://doi.org/10.1063/1.3605560
Kleinsorge B, Golovko VB, Hofmann S, Geng J, Jefferson D, Robertson J, Johnson BFG (2004) Growth of aligned carbon nanofibres over large areas using colloidal catalysts at low temperatures. Chem Commun:1416–1417. https://doi.org/10.1039/B401785D
Koo JH (2006) Polymer nanocomposites: processing, characterization, and applications. McGraw-Hill, New York
Krishnamoorthy R, Govindan B, Banat F, Sagadevan V, Purushothaman M, Show PL (2019) Date pits activated carbon for divalent lead ions removal. J Biosci Bioeng. https://doi.org/10.1016/j.jbiosc.2018.12.011
Krishnan D, Raidongia K, Shao J, Huang J (2014) Graphene oxide assisted hydrothermal carbonization of carbon hydrates. ACS Nano 8(1):449–457. https://doi.org/10.1021/nn404805p
Kroto HW, Heath JR, O'Brien SC, Curl RF, Smalley RE (1985) C60: Buckminsterfullerene. Nature 318(6042):162–163. https://doi.org/10.1038/318162a0

Kumar R, Singh RK, Singh DP (2016) Natural and waste hydrocarbon precursors for the synthesis of carbon based nanomaterials: graphene and CNTs. Renew Sust Energ Rev 58:976–1006. https://doi.org/10.1016/j.rser.2015.12.120

Kurd SM, Hassanifard S, Hartmann S (2017) Fracture toughness of epoxy-based stepped functionally graded materials reinforced with carbon nanotubes. Iran Polym J 26(4):253–260. https://doi.org/10.1007/s13726-017-0512-6

Lantelme F, Kaplan B, Groult H, Devilliers D (1999) Mechanism for elemental carbon formation in molecular ionic liquids. J Mol Liq 83:255–269. https://doi.org/10.1016/S0167-7322(99)00090-2

Le Van K, Groult H, Lantelme F, Dubois M, Avignant D, Tressaud A, Komaba S, Kumagai N, Sigrist S (2009) Electrochemical formation of carbon nano-powders with various porosities in molten alkali carbonates. Electrochim Acta 54(19):4566–4573. https://doi.org/10.1016/j.electacta.2009.03.049

Li X-L, Lou T-J, Sun X-M, Li Y-D (2004) Highly sensitive WO_3 hollow sphere gas sensors. Inorg Chem 43(17):5442–5449. https://doi.org/10.1021/ic049522w

Lin L, Deng B, Sun J, Peng H, Liu Z (2018) Bridging the gap between reality and ideal in chemical vapor deposition growth of graphene. Chem Rev 118(18):9281–9343. https://doi.org/10.1021/acs.chemrev.8b00325

Liu G-J, Fan L-Q, Yu F-D, Wu J-H, Liu L, Qiu Z-Y, Liu Q (2013) Facile one-step hydrothermal synthesis of reduced graphene oxide/Co3O4 composites for supercapacitors. J Mater Sci 48:8463–8470. https://doi.org/10.1007/s10853-013-7663-4

Lone MY, Kumar A, Husain S, Zulfequar M, Husain M (2017) Growth of carbon nanotubes by PECVD and it applications: a review. Curr Nanosci 13:536–546. https://doi.org/10.2174/1573413713666170317150807

Lu Y, Zhang S, Yin J, Bai C, Zhang J, Li Y, Yang Y, Ge Z, Zhang M, Wei L, Ma M, Ma Y, Chen Y (2017) Mesoporous activated carbon materials with ultrahigh mesopore volume and effective specific surface area for high performance supercapacitors. Carbon 124:64–71. https://doi.org/10.1016/j.carbon.2017.08.044

Lv W, Li Z, Deng Y, Yang QH, Kang F (2016) Graphene-based materials for electrochemical energy storage devices: opportunities and challenges. Energy Storage Mater 2:107–138. https://doi.org/10.1016/j.ensm.2015.10.002

Ma H, Li C, Zhang M, Hong J-D, Shi G (2017) Graphene oxide induced hydrothermal carbonization of egg proteins for high-performance supercapacitors. J Mater Chem A 5:17040–17047. https://doi.org/10.1039/c7ta04771a

Malik R, Zhang L, McConnell C, Schott M, Hsieh Y-Y, Noga R, Alvarez NT, Shanov V (2017) Three-dimensional, free-standing polyaniline/carbon nanotube composite-based electrode for high-performance superecapacitors. Carbon 116:579–590. https://doi.org/10.1016/j.carbon.2017.02.036

Massot L, Chamelot P, Bouyer F, Taxil P (2002) Electrodeposition of carbon films from molten alkaline fluoride media. Electrochim Acta 47:1949–1957. https://doi.org/10.1016/S0013-4686(02)00047-6

Melvin GJH, Ni QQ, Natsuki T (2014a) Electromagnetic wave absorption properties of barium titanate/carbon nanotube hybrid nanocomposites. J Alloys Compd 615:84–90. https://doi.org/10.1016/j.jallcom.2014.06.191

Melvin GJH, Ni QQ, Suzuki Y, Natsuki T (2014b) Microwave-absorbing properties of silver nanoparticle/carbon nanotube hybrid nanocomposites. J Mater Sci 49(14):5199–5207. https://doi.org/10.1007/s10853-014-8229-9

Melvin GJH, Ni QQ, Natsuki T (2014c) Fabrication and characterization of polymer-based electroactive nanocomposite actuator. Microelectron Eng 126:9–12. https://doi.org/10.1016/j.mee.2014.04.001

Melvin GJH, Ni QQ, Natsuki T (2014d) Behavior of polymer-based electroactive actuator incorporated with mild hydrothermally treated CNTs. Appl Phys A Mater Sci Process 117(4):2043–2050. https://doi.org/10.1007/s00339-014-8616-8

Melvin GJH, Ni QQ, Natsuki T, Wang Z, Morimoto S, Fujishige M, Takeuchi K, Hashimoto Y, Endo M (2015) Ag/CNT nanocomposites and their single-and double-layer electromagnetic wave absorption properties. Synth Met 209:383–388. https://doi.org/10.1016/j.synthmet.2015.08.017

Melvin GJH, Ni QQ, Natsuki T (2016) Bending actuation and charge distribution behavior of polyurethane/carbon nanotube electroactive nanocomposites. Polym Compos 37(1):262–269. https://doi.org/10.1002/pc.23177

Melvin GJH, Ni QQ, Wang Z (2017a) Performance of barium titanate@carbon nanotube nanocomposite as an electromagnetic wave absorber. Phys Status Solidi A 214(2):1600541. https://doi.org/10.1002/pssa.201600541

Melvin GJH, Wang Z, Siambun NJ, Rahman MM (2017b) Carbon materials derived from rice husks at low and high temperatures. IOP Conf Ser: Mater Sci Eng 217:012017. https://doi.org/10.1088/1757-899X/217/1/012017

Melvin GJH, Wang Z, Ni Q-Q, Siambun NJ, Rahman MM (2017c) Electromagnetic wave absorption properties of rice husks carbonized at 2500°C. AIP Conf Proceed 1901(1):020002. https://doi.org/10.1063/1.5010439

Melvin GJH, Wang Z, Ni QQ, Siambun NJ, Rahman MM (2017d) Fabrication and characterization of carbonized rice husk/barium titanate nanocomposites. IOP Conf Ser: Mater Sci Eng 229:012024. https://doi.org/10.1088/1757-899X/229/1/012024

Melvin GJH, Zhu Y, Ni QQ (2019a) Nanomaterials: electromagnetic wave energy loss. In: Siddiquee S, Melvin GJH, Rahman MM (eds) Nanotechnology: applications in energy, drug and food. Springer, Cham, pp 73–97. https://doi.org/10.1007/978-3-319-99602-8_4

Melvin GJH, Chai KF, Tamiri FM (2019b) Characterization of carbonized waste materials: Rice husk and saw dust. IOP Conf Ser: Mater Sci Eng 606:012002. https://doi.org/10.1088/1757-899X/606/1/012002

Melvin GJH, Wang Z, Ni QQ (2019c) Electromagnetic wave absorption performance of carbonized rice husk obtained at various temperatures. Global Chall 3(11):1900045. https://doi.org/10.1002/gch2.201900045

Melvin GJH, Wang Z, Morimoto S, Fujishige M, Takeuchi K, Hashimoto Y, Endo M (2019d) Graphite whiskers derived from waste coffee grounds treated at high temperature. Global Chall 3(8):1800107. https://doi.org/10.1002/gch2.201800107

Mishra N, Das G, Ansaldo A, Genovese A, Malerba M, Povia M, Ricci D, Di Fabrizio E, Di Zitti E, Sharon M, Sharon M (2012) Pyrolysis of waste polypropylene for the synthesis of carbon nanotubes. J Anal Appl Pyrolysis 94:91–98. https://doi.org/10.1016/j.jaap.2011.11.012

Nandamuri G, Roumimov S, Solanki R (2010) Remote plasma assisted growth of graphene films. Appl Phys Lett 96:154101. https://doi.org/10.1063/1.3387812

Nasir S, Hussein M, Zainal Z, Yusof N (2018) Carbon-based nanomaterials/allotropes: a glimpse of their synthesis, properties and some applications. Materials 11(2):295. https://doi.org/10.3390/ma11020295

Ni QQ, Melvin GJH, Natsuki T (2015) Double-layer electromagnetic wave absorber based on barium titanate/carbon nanotube nanocomposites. Ceram Int 41(8):9885–9892. https://doi.org/10.1016/j.ceramint.2015.04.065

Nizamuddin S, Baloch HA, Griffin GJ, Mubarak NM, Bhutto AW, Abro R, Mazari SA, Ali BS (2017) An overview of effect of process parameters on hydrothermal carbonization of biomass. Renew Sust Energ Rev 73:1289–1299. https://doi.org/10.1016/j.rser.2016.12.122

Novoselov KS, Geim AK, Morozov SV, Jiang D, Zhang Y, Dubonos SV, Grigorieva IV, Firsov AA (2004) Electric field effect in atomically thin carbon films. Science 306(5696):666–669. https://doi.org/10.1126/science.1102896

Novoselova IA, Oliinyk NF, Volkov SV, Konchits AA, Yanchuk IB, Yefanov VS, Kolesnik SP, Karpets MV (2008) Electrolytic synthesis of carbon nanotubes from carbon dioxide in molten salts and their characterization. Phys E 40(7):2231–2237. https://doi.org/10.1016/j.physe.2007.10.069

Nwigboji IH, Ejembi JI, Wang Z, Bagayoko D, Zhao GL (2015) Microwave absorption properties of multi-walled carbon nanotube (outer diameter 20–30 nm)-epoxy composites from 1 to 26.5 GHz. Diam Relat Mater 52:66–71. https://doi.org/10.1016/j.diamond.2014.12.008

Ober CK, Müllen K (2012) Introduction – applications of polymers. In: Krzysztof Matyjaszewski K, Möller M (eds) Polymer science: a comprehensive reference. Elsevier, Amsterdam, pp 439–478

Oberlin A, Endo M, Koyama T (1976) Filamentous growth of carbon through benzene decomposition. J Cryst Growth 32(3):335–349. https://doi.org/10.1016/0022-0248(76)90115-9

Omoriyekomwan JE, Tahmasebi A, Zhang J, Yu J (2017) Formation of hollow carbon nanofibers on bio-char during microwave pyrolysis of palm kernel shell. Energy Convers Manag 148:583–592. https://doi.org/10.1016/j.enconman.2017.06.022

Pan D, Zhang J, Li Z, Wu M (2010) Hydrothermal route for cutting graphene sheets into blue-luminescent graphene quantum dots. Adv Mater 22:734–738. https://doi.org/10.1002/adma.200902825

Papageorgiou DG, Kinloch IA, Young RJ (2015) Graphene/elastomer nanocomposites. Carbon 95:460–484. https://doi.org/10.1016/j.carbon.2015.08.055

Popov VN (2004) Carbon nanotubes: properties and application. Mater Sci Eng R 43(3):61–102. https://doi.org/10.1016/j.mser.2003.10.001

Potts JR, Dreyer DR, Bielawski CW, Ruoff RS (2011) Graphene-based polymer nanocomposites. Polymer 52(1):5–25. https://doi.org/10.1016/j.polymer.2010.11.042

Pumera M (2010) Graphene-based nanomaterials and their electrochemistry. Chem Soc Rev 39(11):4146–4157. https://doi.org/10.1039/c002690p

Purkait T, Singh G, Singh M, Kumar D, Dey RS (2017) Large area few-layer graphene with scalable preparation from waste biomass for high-performance supercapacitor. Sci Rep 7(1):15239. https://doi.org/10.1038/s41598-017-15463-w

Qian H-S, Yu S-H, Luo L-B, Gong J-Y, Fei L-F, Liu X-M (2006) Synthesis of uniform Te@carbon-rich composite nanocables with photoluminescence properties and carbonaceous nanofibers by hydrothermal carbonization of glucose. Chem Mater 18:2102–2101. https://doi.org/10.1021/cm052848y

Qiu J, Qiu T (2015) Fabrication and microwave absorption properties of magnetite nanoparticle–carbon nanotube–hollow carbon fiber composites. Carbon 81:20–28. https://doi.org/10.1016/j.carbon.2014.09.011

Raghavan N, Thangavel S, Venugopal G (2017) A short review on preparation of graphene from waste and bioprecursors. Appl Mater Today 7:246–254. https://doi.org/10.1016/j.apmt.2017.04.005

Randviir EP, Brownson DA, Banks CE (2014) A decade of graphene research: production, applications and outlook. Mater Today 17(9):426–432. https://doi.org/10.1016/j.mattod.2014.06.001

Ren J, Li FF, Lau J, González-Urbina L, Licht S (2015) One-pot synthesis of carbon Nanofibers from CO_2. Nano Lett 15(9):6142–6148. https://doi.org/10.1021/acs.nanolett.5b02427

Ren ZF, Huang ZP, Xu JW, Wang JH, Bush P, Siegal MP, Provencio PN (1998) Synthesis of large arrays of well-aligned carbon nanotubes on glass. Science 282:1105–1107. https://doi.org/10.1126/science.282.5391.1105

Rosmi MS, Shinde SM, Rahman ND, Thangaraja A, Sharma S, Sharma KP, Yaakob Y, Vishwakarma RK, Bakar SA, Kalita G, Ohtani H, Tanemura M (2016) Synthesis of uniform monolayer graphene on re-solidified copper from waste chicken fat by low pressure chemical vapor deposition. Mater Res Bull 83:573–580. https://doi.org/10.1016/j.materresbull.2016.07.010

Ruan G, Sun Z, Peng Z, Tour JM (2011) Growth of graphene from food, insects, and waste. ACS Nano 5(9):7601–7607. https://doi.org/10.1021/nn202625c

Saghafi M, Mahboubi F, Mohajerzaden S, Holze R (2014) Preparation of vertically aligned carbon nanotubes and their electrochemical performance in supercapacitors. Synth Met 195:252–259. https://doi.org/10.1016/j.synthmet.2014.06.012

Sahoo NG, Jung YC, Yoo HJ, Cho JW (2007) Influence of carbon nanotubes and polypyrrole on the thermal, mechanical and electroactive shape-memory properties of polyurethane nanocomposites. Compos Sci Technol 67(9):1920–1929. https://doi.org/10.1016/j.compscitech.2006.10.013

Saito Y, Arima T (2007) Features of vapor-grown cone-shaped graphitic whiskers deposited in the cavities of wood cells. Carbon 45(2):248–255. https://doi.org/10.1016/j.carbon.2006.10.002

Sajjadi SA, Meknati A, Lima EC, Dotto GL, Mendoza-Castillo DI, Anastopoulos I, Alakhras F, Unuabonah EI, Singh P, Hosseini-Bandegharaei A (2019) A novel route for preparation of chemically activated carbon from pistachio wood for highly efficient Pb (II) sorption. J Environ Manag 236:34–44. https://doi.org/10.1016/j.jenvman.2019.01.087

Satayeva AR, Howell CA, Korobeinyk AV, Jandosov J, Inglezakis VJ, Mansurov ZA, Mikhalovsky SV (2018) Investigation of rice husk derived activated carbon for removal of nitrate contamination from water. Sci Total Environ 630:1237–1245. https://doi.org/10.1016/j.scitotenv.2018.02.329

Schaefer DW, Justice RS (2007) How nano are nanocomposites? Macromolecules 40(24):8501–8517. https://doi.org/10.1021/ma070356w

Schwander M, Partes K (2011) A review of diamond synthesis by CVD processes. Dia Relat Mater 20(9):1287–1301. https://doi.org/10.1016/j.diamond.2011.08.005

Seo DH, Han ZJ, Kumar S, Ostrikov K (2013a) Structure-controlled, vertical graphene-based, binder-free electrodes from plasma-reformed butter enhance supercapacitor performance. Adv Energy Mater 3(10):1316–1323. https://doi.org/10.1002/aenm.201300431

Seo DH, Rider AE, Han ZJ, Kumar S, Ostrikov K (2013b) Plasma break-down and re-bulid: same functional vertical graphenes from diverse natural precursors. Adv Mater 25(39):5638–5642. https://doi.org/10.1002/adma201301510

Sevilla M, Lota G, Fuertes AB (2007) Saccharide-based graphitic carbon nanocoils as supports for PtRu nanoparticles for methanol electrooxidation. J Power Sources 171:546–551. https://doi.org/10.1016/j.jpowsour.2007.05.096

Sevilla M, Fuertes AB (2009a) Chemical and structural properties of carbonaceous products obtained by hydrothermal carbonization of saccharides. Chem Eur J 15:4195–4203. https://doi.org/10.1002/chem.200802097

Sevilla M, Fuertes AB (2009b) The production of carbon materials by hydrothermal carbonization of cellulose. Carbon 47:2281–2289. https://doi.org/10.1016/j.carbon.2009.04.026

Shams SS, Zhang LS, Hu R, Zhang R, Zhu J (2015) Synthesis of graphene from biomass: a green chemistry approach. Mater Lett 161:476–479. https://doi.org/10.1016/j.matlet.2015.09.022

Sharma S, Kalita G, Hirano R, Shinde SM, Papon R, Ohtani H, Tanemura M (2014) Synthesis of graphene crystals from solid waste plastic by chemical vapor deposition. Carbon 72:66–73. https://doi.org/10.1016/j.carbon.2014.01.051

Shen J, Yan B, Shi M, Ma H, Li N, Ye M (2011) One step hydrothermal synthesis of TiO2-reduced graphene oxide sheets. J Mater Chem 21:3415–3421. https://doi.org/10.1039/C0JM03542D

Shrestha S, Choi WC, Song W, Kwon YT, Shrestha SP, Park C-Y (2010) Preparation and field emission properties of Er-decorated multiwalled carbon nanotubes. Carbon 48(1):54–59. https://doi.org/10.1016/j.carbon.2009.08.029

Silberberg MS (2006) Chemistry: the molecular nature of matter and change. McGraw Hill, Boston

Song C (2002) CO_2 conversion and utilization : an overview. In: Song C, Gaffney AF, Fujimoto K (eds) CO_2 conversion and utilization. ACS Symp Ser 809:2–30. https://doi.org/10.1021/bk-2002-0809.ch001

Song Q, Xu Q, Wang Y, Shang X, Li Z (2012) Electrochemical deposition of carbon films on titanium in molten LiCl–KCl–K_2CO_3. Thin Solid Films 520(23):6856–6863. https://doi.org/10.1016/j.tsf.2012.07.056

Styring P, Jansen D, De Coninck H, Reith H, Armstrong K (2011) Carbon capture and utilisation in the green economy. Centre for Low Carbon Futures

Stuardi FM, Macpherson F, Leclair J (2019) Integrated CO_2 capture and utilization : a priority research direction. Curr Opin Green Sustainable Chem 16:71–76. https://doi.org/10.1016/j.cogsc.2019.02.003

Sun X, Li Y (2004a) Colloidal carbon spheres and their core/shell structures with noble-metal nanoparticles. Angew Chem 116:607–611. https://doi.org/10.1002/ange.200352386

Sun X, Li Y (2004b) Ga_2O_3 and GaN semiconductor hollow spheres. Angew Chem Int Ed 43(29):3827–3831. https://doi.org/10.1002/anie.200353212

Tang D, Yin H, Mao X, Xiao W, Wang DH (2013) Effects of applied voltage and temperature on the electrochemical production of carbon powders from CO_2 in molten salt with an inert anode. Electrochim Acta 114:567–573. https://doi.org/10.1016/j.electacta.2013.10.109

Thostenson ET, Li C, Chou TW (2005) Nanocomposites in context. Compos Sci Technol 65:491–516. https://doi.org/10.1016/j.compscitech.2004.11.003

Thostenson ET, Ren Z, Chou TW (2001) Advances in the science and technology of carbon nanotubes and their composites: a review. Compos Sci Technol 61(13):1899–1912. https://doi.org/10.1016/S0266-3538(01)00094-X

Titirici MM, White RJ, Brun N, Budarin VL, Su DS, del Monte F, Clark JH, MacLachlan MJ (2015) Sustainable carbon materials. Chem Soc Rev 44(1):250–290. https://doi.org/10.1039/c4cs00232f

Van Krevelen DW (1950) Graphical-statistical method for the study of structure and reaction processes of coal. Fuel 29:269–228

Wang E, Dong Y, Islam MZ, Yu L, Liu F, Chen S, Qi X, Zhu Y, Fu Y, Xu Z, Hu N (2019a) Effect of graphene oxide-carbon nanotube hybrid filler on the mechanical property and thermal response speed of shape memory epoxy composites. Compos Sci Technol 169:209–216. https://doi.org/10.1016/j.compscitech.2018.11.022

Wang Z, Melvin GJH (2019) Carbon nanomaterials for energy storage devices. In: Siddiquee S, Melvin GJH, Rahman MM (eds) Nanotechnology: applications in energy, drug and food. Springer, Cham, pp 1–29. https://doi.org/10.1007/978-3-319-99602-8_1

Wang Y, Wang J, Morimoto S, Melvin GJH, Zhao R, Hashimoto Y, Terrones M (2019c) Nitrogen-doped porous carbon monoliths from molecular-level dispersion of carbon nanotubes into polyacrylonitrile (PAN) and the effect of carbonization process for supercapacitors. Carbon 143:776–785. https://doi.org/10.1016/j.carbon.2018.11.024

Wang Q, Li H, Chen L, Huang X (2001) Monodispersed hard carbon spherules with uniform nanopores. Carbon 39(14):2211–2214. https://doi.org/10.1016/S0008-6223(01)00040-9

Wang H, Abe T, Maruyama S, Iriyama Y, Ogumi Z, Yoshikawa K (2005) Graphitized carbon nanobeads with an onion texture as lithium-ion battery negative electrode for high-rate use. Adv Mater 17:2857–2860. https://doi.org/10.1002/adma.200500320

Wang C, Xiangfeng C, Mingmei W (2007) Highly sensitive gas sensors based on hollow SnO_2 spheres prepared by carbon sphere template method. Sens Actuators B: Chem 120(2):508–513. https://doi.org/10.1016/j.snb.2006.03.004

Wang L, Guo Y, Zhu Y, Li Y, Qu Y, Rong C, Ma X, Wang Z (2010) A new route for preparation of hydrochars from rice husk. Bioresour Technol 101(24):9807–9810. https://doi.org/10.1016/j.biortech.2010.07.031

Wang Z, Shoji M, Ogata H (2011a) Carbon nanosheets by microwave plasma enhanced chemical vapor deposition in CH_4-Ar system. Appl Surf Sci 257:9082–9085. https://doi.org/10.1016/j.apsusc.2011.05.104

Wang Z, Shoji M, Ogata H (2011b) Facile low-temperature growth of carbon nanosheets toward simultaneous determination of dopamine, ascorbic acid and uric acid. Analyst 136:4903–4905. https://doi.org/10.1039/c1an15630f

Wang Z, Shoji M, Ogata H (2012a) Electrochemical determination of NADH based on MPECVD carbon nanosheets. Talanta 99:487–491. https://doi.org/10.1016/j.talanta.2012.06.014

Wang Z, Shoji M, Ogata H (2012b) Synthesis and characterization of platinum nanoparticles on carbon nanosheets with enhanced electrocatalytic activity towards methanol oxidation. Appl Surf Sci 259:219–224. https://doi.org/10.1016/j.apsusc.2012.07.022

Wang Z, Ogata H, Morimoto S, Fujishige M, Takeuchi K, Hashimoto Y, Endo M (2014a) Synthesis of carbon nanosheets from Kapton polyimide by microwave plasma treatment. Carbon 72:421–424. https://doi.org/10.1016/j.carbon.2014.02.021

Wang Z, Shoji M, Baba K, Ito T, Ogata H (2014b) Microwave plasma-assisted regeneration of carbon nanosheets with bi- and trilayer of graphene and their application to photovoltaic cells. Carbon 67:326–335. https://doi.org/10.1016/j.carbon.2013.10.002

Wang Z, Ogata H, Morimoto S, Fujishige M, Takeuchi K, Hashimoto Y, Endo M (2015a) High-temperature-induced growth of graphite whiskers from fullerene waste soot. Carbon 90:154–159. https://doi.org/10.1016/j.carbon.2015.04.017

Wang Z, Ogata H, Morimoto S, Oritz-Medina J, Fujishige M, Takeuchi K, Muramatsu H, Hayashi T, Terrones M, Hashimoto Y, Endo M (2015b) Nanocarbons from rice husks by microwave plasma irradiation: from graphene and carbon nanotubes to graphenated carbon nanotube hybrids. Carbon 94:479–484. https://doi.org/10.1016/j.carbon.2015.07.037

Wang Z, Ogata H, Morimoto S, Fujishige M, Takeuchi K, Muramatsu H, Hayashi T, Oritz-Medina J, Yusop MZM, Tanemura M, Terrones M, Hashimoto Y, Endo M (2015c) Microwave plasma-induced graphene-sheet fibers from waste coffee grounds. J Mater Chem A 3:14545–14549. https://doi.org/10.1039/c5ta03833b

Wang Z, Ogata H, Melvin GJH, Obata M, Morimoto S, Ortiz-Medina J, Cruz-Silva R, Fujishige M, Takeuchi K, Muramatsu H, Kim TY, Kim YA, Hayashi T, Terrones M, Hashimoto Y, Endo M (2017) Structural evolution of hydrothermal carbon spheres induced by high temperatures and their electrical properties under compression. Carbon 121:426–433. https://doi.org/10.1016/j.carbon.2017.06.003

Wei L, Yushin G (2012) Nanostructured activated carbons from natural precursors for electrical double layer capacitors. Nano Energy 1(4):552–565. https://doi.org/10.1016/j.nanoen.2012.05.002

Wu A, Yan J, Xu W, Li X (2016a) Fabrication of waste biomass derived carbon by pyrolysis. Mat Lett 173:60–63. https://doi.org/10.1016/j.matlet.2016.03.025

Wu H, Li Z, Ji D, Liu Y, Li L, Yuan D, Zhang Z, Ren J, Lefler M, Wang B, Licht S (2016b) One-pot synthesis of nanostructured carbon materials from carbon dioxide via electrolysis in molten carbonate salts. Carbon 106:208–217. https://doi.org/10.1016/j.carbon.2016.05.031

Xu Y, Sheng K, Li C, Shi G (2010) Self-assembled graphene hydrogel via a one-step hydrothermal process. ACS Nano 4:4324–4330. https://doi.org/10.1021/nn101187z

Yan Y, Xia H, Qiu Y, Xu Z, Ni QQ (2019) Multi-layer graphene oxide coated shape memory polyurethane for adjustable smart switches. Compos Sci Technol 172:108–116. https://doi.org/10.1016/j.compscitech.2019.01.013

Yan J, Zhang Z (2019) Carbon capture, utilization and storage (CCUS). Appl Energy 235:1289–1299. https://doi.org/10.1016/j.apenergy.2018.11.019

Yang Z-C, Zhang Y, Kong J-H, Wong SY, Li X, Wang J (2013) Hollow carbon nanoparticles of tunable size and wall thickness by hydrothermal treatment of α-cyclodextrin template by F127 block copolymers. Chem Mater 25:704–710. https://doi.org/10.1021/cm303513y

Yin H, Mao X, Tang D, Xiao W, Xing L, Zhu H, Wang D, Sadoway DR (2013) Capture and electrochemical conversion of CO_2 to value-added carbon and oxygen by molten salt electrolysis. Energy Environ Sci 6(5):1538–1545. https://doi.org/10.1039/c3ee24132g

Young RJ, Lovell PA (2011) Introduction to polymers. CRC Press, Boca Raton

Yu K, Lu G, Bo Z, Mao S, Chen J (2011) Carbon nanotubes with chemically bonded graphene leaves for electronic and optoelectronic applications. J Phys Chem Lett 2:1556–1562. https://doi.org/10.1021/jz200641c

Yuan Z, Eden MR, Gani R (2016) Towards the development and deployment of large-scale carbon dioxide capture and conversion processes. Ind Eng Chem Res 55(12):3383–3419. https://doi.org/10.1021/acs.iecr.5b03277

Zanin H, May PW, Hamanaka MHMO, Corat EJ (2013) Field emission from hybrid diamond-like carbon and carbon nanotube composite structures. ACS Appl Mater Interfaces 5(23):12238–12243. https://doi.org/10.1021/am403386a

Zhang B, Bai S, Cheng H-M, Cai Q-K (2006) Graphitization-induced microstructural changes in tetrahydrofuran-derived pyrolytic carbon spheres. J Mater Res 21(9):2198–2203. https://doi.org/10.1557/jmr.2006.0292

Zhang J, Li C, Peng Z, Liu Y, Zhang J, Liu Z, Li D (2017) 3D free-standing nitrogen-doped reduced graphene oxide aerogel as anode material for sodium ion batteries with enhanced sodium storage. Sci Rep 7:4886. https://doi.org/10.1038/s41598-017-04958-1

Zhang J, Tahmasebi A, Omoriyekomwan JE, Yu J (2018) Direct synthesis of hollow carbon nanofibers on bio-char during microwave pyrolysis of pine nut shell. J Anal Appl Pyrolysis 130:142–148. https://doi.org/10.1016/j.jaap.2018.01.016

Zhang L, Ni QQ, Shiga A, Natsuki T, Fu Y (2011) Preparation of polybenzimidazole/functionalized carbon nanotube nanocomposite films for use as protective coatings. Polym Eng Sci 51(8):1525–1532. https://doi.org/10.1002/pen.21618

Zhang X, Zhang R, Xiang C, Liu Y, Zou Y, Chu H, Qiu S, Xu F, Sun L (2019) Polydopamine-assisted formation of Co_3O_4-nanocube-anchored reduced graphene oxide composite for high-performance supercapacitors. Ceram Int. https://doi.org/10.1016/j.ceramint.2019.04.087

Zhao B, Liu P, Jiang Y, Pan D, Tao H, Song J, Fang T, Xu W (2012) Supercapacitor performance of thermally reduced graphene oxide. J Power Sources 1998:423–427. https://doi.org/10.1016/j.jpowsour.2011.09.074

Zhou M, Zhai YM, Dong SJ (2009) Electrochemical sensing and biosensing platform based on chemically reduced graphene oxide. Anal Chem 81(14):5603–5613. https://doi.org/10.1021/ac900136z

Zhu J, Jia J, Kwong FL, Ng DH, Tjong SC (2012) Synthesis of multiwalled carbon nanotubes from bamboo charcoal and the roles of minerals on their growth. Biomass Bioenergy 36:12–19. https://doi.org/10.1016/j.biombioe.2011.08.023

Zhu S, Xing C, Wu F, Zuo X, Zhang Y, Yu C, Chen M, Li W, Li Q, Liu L (2019) Cake-like flexible carbon nanotubes/graphene composite prepared via a facile method for high-performance electromagnetic interference shielding. Carbon 145:259–265. https://doi.org/10.1016/j.carbon.2019.01.030

Chapter 2
Carbon Fibre Reinforced Polymer (CFRP) Composites: Machining Aspects and Opportunities for Manufacturing Industries

Sharizal Ahmad Sobri, Robert Heinemann, and David Whitehead

2.1 Introduction

Composite materials, or just composites, as they are often referred to, consist of two or more distinct constituents or phases made from engineered or naturally-occurring materials, where each material has significantly different physical or chemical properties, which remain separate and distinct within the finished/combined structure. According to Lau et al. (1995), Shanmugam et al. (2002), Hernandez et al. (2011) and Santhanakrishnan et al. (1988), composite materials will eventually become the most wanted type in industry and are already gaining wide acceptance in, for example, construction, furniture, packing, flooring, panelling and automotive. In addition, composites are applied in many high-tech industries, such as aerospace and defence (Shanmugam et al. 2002). Matthews and Rawlings (1999) predict that the demand for synthetic composites, i.e. fine fibres embedded in polymers, will continue to increase steadily as it has been with metal and ceramic-based composites. Moreover, as Brouwer (2019) states, during the last decade there has been a renewed interest in natural fibres as a substitute for glass, motivated by potential advantages in weight saving, reduced raw material price and 'thermal recycling', which refers to the ecological advantages of using resources that are renewable. Brouwer also points out that natural fibres used in composites, such as wood, cotton, silk, wool, jute, hemp and sisal, need to be cost-competitive with glass fibres.

S. A. Sobri (✉)
Faculty of Bioengineering & Technology, Universiti Malaysia Kelantan, Jeli Campus, Jeli, Kelantan, Malaysia
e-mail: sharizal.s@umk.edu.my

R. Heinemann · D. Whitehead
School of Mechanical, Aerospace, and Civil Engineering, the University of Manchester, Manchester, UK

S. Siddiquee et al. (eds.), *Composite Materials: Applications in Engineering, Biomedicine and Food Science*, https://doi.org/10.1007/978-3-030-45489-0_2

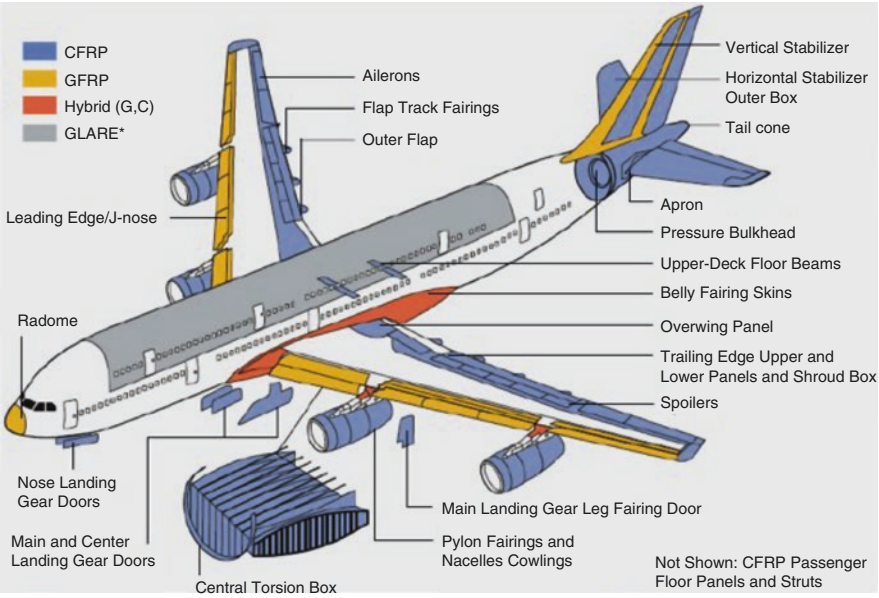

Fig. 2.1 Schematic illustration of the structure of 22% composite made Airbus A380 aeroplane (Reza 2010)

According to Caggiano (2018), Garrick (2007) and Mangalgiri (1999), fibre-reinforced plastics including carbon fibre reinforced plastic/polymer (CFRP) are the most prominent and sought-after materials for aircraft manufacturing today. The latest generation of large passenger/commercial aircrafts contains a large proportion of composite materials; for example the Airbus A350 and Boeing B787 have a composite contents of over 30% and 50%, respectively Reza (2010). Figure 2.1 shows the components that are made of composites with regards to the Airbus A380.

2.2 Composites Technology

The characteristics of composite materials are anisotropy, non-homogeneity and the fact that their reinforcing fibres are very abrasive; this make these materials more difficult to machine than metals (Abrate and Walton 1992). In modern manufacturing industries, common composite materials have different types of reinforcements and matrix compositions; in general they are divided into three major types: fibre reinforced polymers (FRP), metal matrix composites (MMC) and ceramic matrix composites (CMC). FRPs usually provide a higher specific strength and stiffness, and are lightweight compared to traditional steels. These characteristics make FRPs the favoured material for high performance applications, such as in Formula-1 cars and combat aircraft components, despite the fact that they are expensive to

manufacture (Komanduri 1997). The strength of FRPs is relatively low when they reach their maximum-use temperature, because this type of material is prone to chemical decomposition or degradation at even moderate temperatures. For example, carbon fibres can endure temperatures of up to 3000 °C until degradation of the structure is initiated (Pecat et al. 2012). MMCs are suitable for higher operating temperature applications compared to FRPs. Continuous fibres in MMC provide the highest stiffness and strength, whereas other types such discontinuous and particulate fibres have better dimensional stability compared to unreinforced alloys, which Fig. 2.2 shows specific strength versus specific stiffness for various MMC materials and each composite indicates the number for the reinforcement volume fraction. The main performance of using CMC is to improve fracture toughness during applications. For heavy cuts, or to avoid fracture during cutting, CMCs exhibit an increased toughness compared to ceramic cutting tools. CMCs are superior to metals due to higher specific modulus and mechanical properties at elevated temperatures. In many types of composites, FRPs count among the most high-performance materials in the field of light-weight design (Pecat et al. 2012). Aircraft and aerospace design in particular has benefitted from carbon-fibre-reinforced polymers (CFRPs), which today are the most popular composite in the aerospace industry (Caggiano et al. 2018, Brouwer 2019, Dandekar and Shin 2012, Garrick 2007, Askeland and Phulé 2006, Komanduri 1997, Santhanakrishnan et al. 1988).

Composites are categorized into two main groups, depending on the way the fibres are arranged within the matrix. Figure 2.3 shows the schematic illustration of reinforcing plastics; the first group is called fibre-reinforced composites, whereas the second group is called particle-reinforced composites. Each group of composites has a different reinforcement mechanism and strengths, depending on the application. FRPs consist of fibres (in discontinuous or dispersed phase) in a plastic matrix (the continuous phase) (Kalpakjian and Schmid 1999). In components manufactured from long - or even continuous - fibre reinforced composites, such as unidirectional or cross-ply laminates, anisotropy may be desirable as it can be

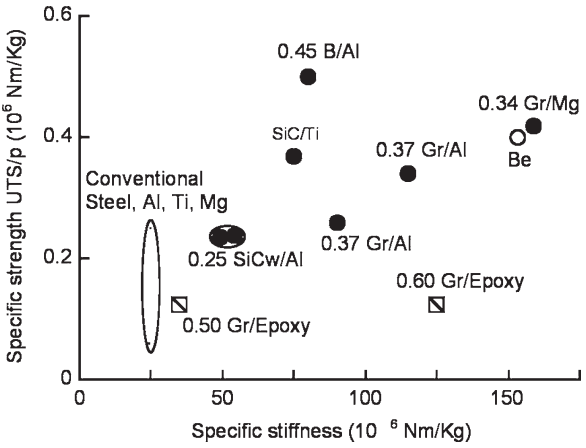

Fig. 2.2 Specific strength versus specific stiffness for various MMC materials (adapted from Teti 2002)

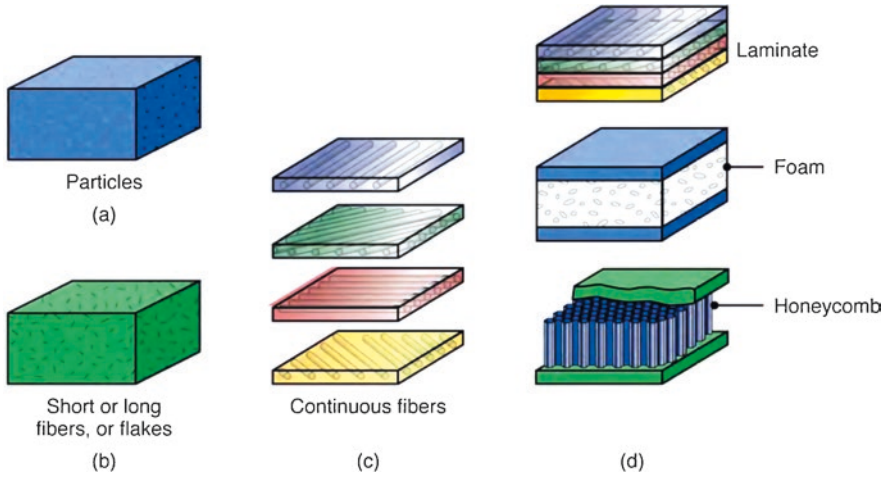

Fig. 2.3 Schematic illustration of methods of reinforcing plastics (matrix) with (**a**) particles; (**b**) short or long fibres or flakes; and (**c**) continuous fibres. The laminate structures in (**d**) can be manufactured from the layers of continuous fibres or sandwich structures using a foam or honeycomb core (Kalpakjian and Schmid 2016)

arranged so that the maximum service stress lies in the direction that has the highest strength (Matthew and Rawlings 1999). However, unidirectional orientations provide poor properties if the load is perpendicular to the fibres (Askeland and Phulé 2006). Most fibre-reinforced composites provide improved strength, fatigue resistance, Young's modulus, and strength-to-weight ratio, by incorporating strong and stiff but brittle fibres into a softer, more ductile matrix (Askeland and Phulé 2006). Boron, carbon, polymers (aramids) and ceramics provide exceptional reinforcement in advanced composites, based on matrices of polymers, metals, ceramics and even intermetallic compounds (Askeland and Phulé 2006, Matthew and Rawlings 1999). Epoxies comprise 80% of the matrix materials used in reinforced plastics, but polyesters are also used as they are less expensive (Kalpakjian and Schmid 1999). Moreover, as Askeland and Phulé (2006) pointed out, several directions of the matrix can be arranged in long continuous fibres; for example, orthogonal arrangements with 0°/90° plies which have good strength in two perpendicular directions. More complicated arrangements such as 0°/±45°/90° plies provide reinforcement in multiple directions. Figure 2.4 shows the different fibre orientation and fibre arrangement types. The most common types of FRPs are Aramid-Fibre Reinforced Plastics (ARFP), Glass-Fibre Reinforced Plastics (GFRP), Carbon-Fibre Reinforced Plastics (CFRP).In addition, another type of FRP composite called Kevlar-Fibre Reinforced Plastics (KFRP) initially introduced by du Pont in 1972 under the trade name Kevlar® and this type of composite is also categorised under Aramid fibres (Komanduri 1997). These three composites are very similar in their fabrication process, but each composite has a different machining behaviour due to its difference in physical and mechanical properties (Santhanakrishnan et al. 1988).

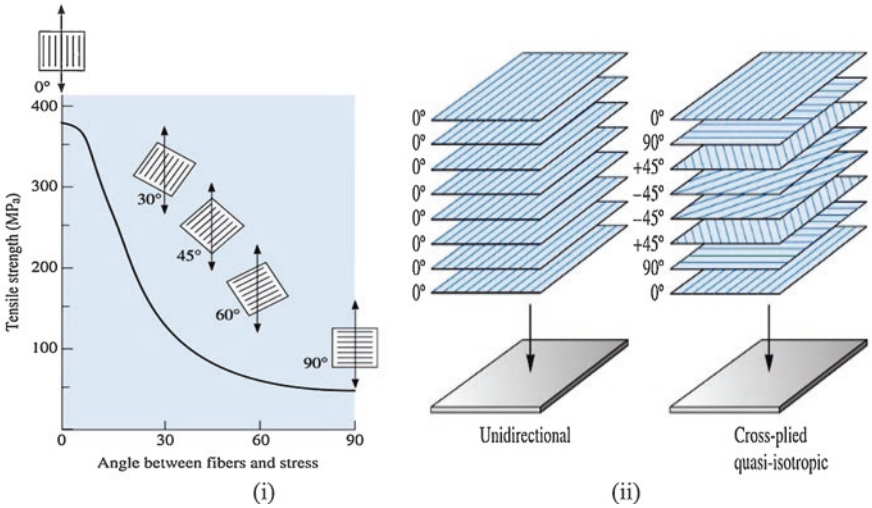

Fig. 2.4 (**i**) Effect of fibre orientation on the tensile strength of E-glass fibre-reinforced epoxy composites; (**ii**) Several directions within the matrix for long, continuous fibres) (Askeland and Phulé 2006)

2.3 Mechanical Machining of FRP

Good surface finish and integrity, long tool life, and low force and power requirements are important elements of good machinability (Kalpakjian and Schmid 1999). Drilling produces holes for mechanical joints such as rivets, bolts and screws, which it is one of the most frequent operations in manufacturing. Only an appropriate tool geometry using the correct process conditions, and ideal machining performance, will produce a level of damage that is acceptable (Reza 2010). In the case of components made from carbon fibre-reinforced polymers, it is often necessary to machine the components - for example to make holes or trim the edge - but the cutting of CFRPs is often associated with delamination of the composites and short tool life (Koplev et al. 1983). The machinability of composites depends on the fibre type, fibre volume content, fibre orientation, and the manufacturing process. It is difficult to analogize the surface formation and tool wear mechanisms seen in the machining of composites from the data obtained in the cutting of homogenous material such as steel (Pecat et al. 2012, Santhanakrishnan et al. 1988, Komanduri 1997). Furthermore, as Pecat et al. (2012) postulated, due to non-homogenous and anisotropic material properties, machining of CFRP presents specific difficulties like fibre pull-out, delamination and decomposition of matrix material, which leads to a degradation of surface quality and material properties.

2.3.1 Cutting Mechanisms

When a cutting tool advances into a metal workpiece, the metal in front of the tool is severely stressed; the cutting tool produces internal shearing action in the metal. The metal below the cutting edge yields and flows plastically in the form of chip. Compression of the metal under the tool takes place. When the ultimate stress of the metal is exceeded, separation of metal takes place, the plastic flow takes place in a localized area known as the shear plane, and the chip moves upward on the face of the tool.

There are two basic types of metal cutting by a single-point cutting tool: orthogonal and oblique cutting. Orthogonal cutting performed with the single cutting edge of the tool at right-angles to the direction of movement, and the surface cut parallel to the original. It is important to note how the forces are exerted from different directions; it is significant that the motion occurs relative to independent variables like workpiece material, condition and temperature, and cutting parameters such as tool speed and feed rate. Figure 2.5 shows how the forces exerted by the cutting tool; the tool exerts a force, R on the chip with a normal component, F_n and a friction component, F_f that opposes the flow of the chip up the tool face. For equilibrium to be reached, the chip must be subjected to a substantially equal and opposite reaction, R' from the workpiece at the shear plane, with a normal component, F_n and a shearing force, F_s along the shear plane. For convenience, the force, R applied to the tool, is resolved into a component F_c in the direction of tool movement, and a normal component, F_L. T_1 shows undeformed chip and T_2 shows deformedchip.

Figure 2.6 shows the difference between orthogonal and oblique cutting. In oblique cutting, the cutting edge is at an inclination angle *i,* as shown in Fig. 2.6(b). The chip in Fig. 2.6 (a) flows up the rake face of the tool at angle α_c (chip flow angle), which is measured in the plane of the tool face. Angle α_n is the normal rake angle, which is the basic geometric property of the tool. This is the angle between the normal *0z* to the workpiece surface and the line *0a* on the tool face. Figure 2.6(c) shows typical chips being produced by different inclination. Oblique cutting has

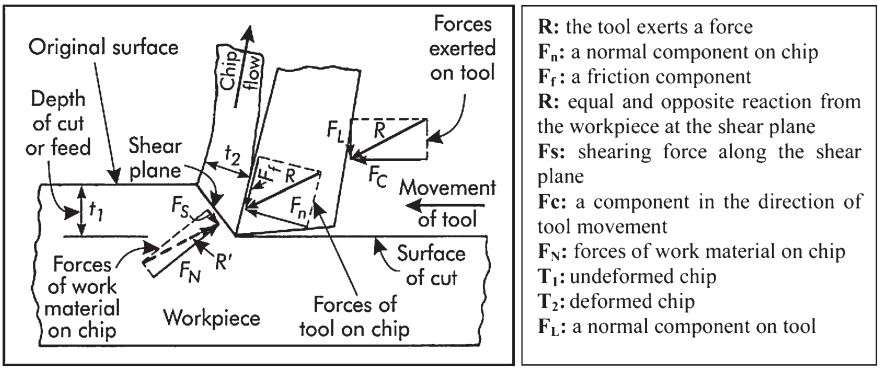

Fig. 2.5 Forces exerted by cutting tool – orthogonal cutting (Schrader and Elshennawy 2000)

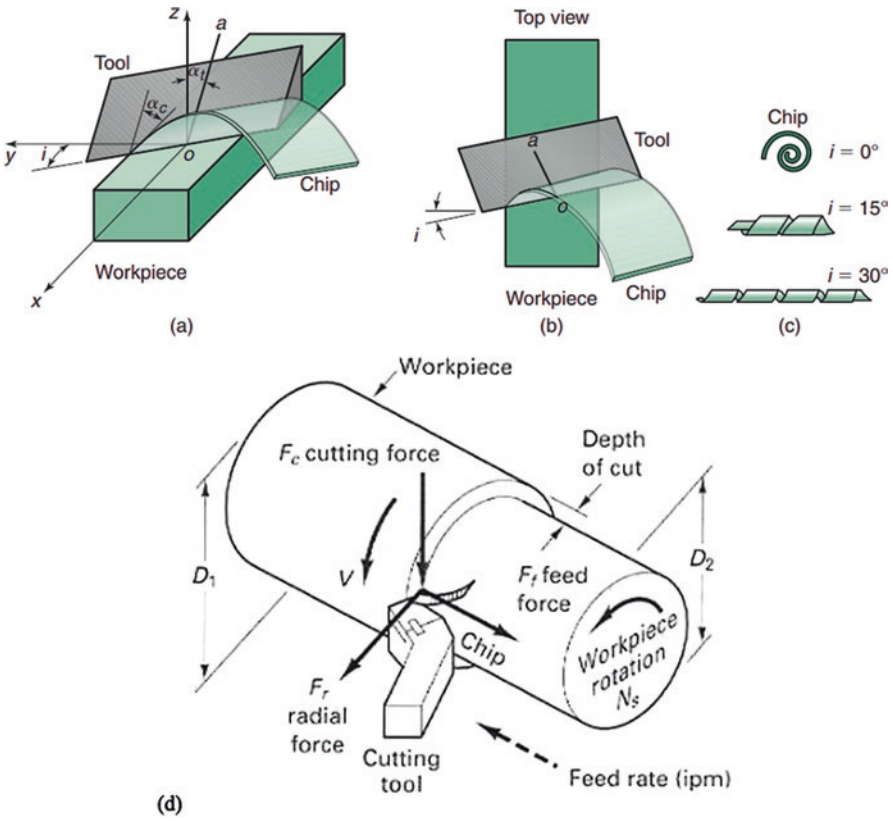

Fig. 2.6 (**a**) Schematic illustration of oblique cutting; (**b**) Inclination angle showing at the top view; (**c**) Types of chips being produced by different inclination; and (**d**) Oblique machining has three measurable components of forces (Kalpakjian and Schmid 1999)

three components as shown in Fig. 2.6(d). The first one is F_c which is a primary cutting force acting in the direction of the cutting velocity vector; it is the largest force geometry and accounts for 99% of the power required by the process. Next is F_f, which is a feed force acting in the direction of the tool used; it is usually about 50% of F_c, but it accounts for only a small percentage of the power required, because feed rates are usually small compared to cutting speeds. Finally, F_r is the radial or thrust force acting perpendicular to the machined surface; typically F_f contributes very little to the power requirements, because velocity in the radial direction is negligible. The main benefit of oblique cutting is that it is a means of controlling chip flow.

There are three most common types of chips (Askeland and Phulé 2006, Schrader and Elshennawy 2000, Kalpakjian and Schmid 1999). The first type are called continuous chips; the conditions that favour their production are small chip thickness, high cutting speed, sharp cutting edge, large rake angle in cutting tool and fine feed, smooth tool face and efficient lubricating system. Such chips are produced while

machining ductile materials like mild steel, copper and aluminium. Due to the plastic deformation of ductile material, long and continuous chips are produced; this is desirable because it produces good surface finish, low power consumption and longer tool life. These chips are difficult to handle and dispose of, furthermore they coil in a helix, and curl around the workpiece and tool. The tool face is in contact for a longer period, resulting in more frictional heat; however this problem could be rectified by the use of chip breakers, clamped onto the rake face of the cutting tool. During machining, long and continuous chips will affect machining. The chips should be broken into small pieces for easy removal, safety and to prevent damage to the machine tool and workpiece. The function of chip breakers is to reduce the radius of curvature of chips and thus break them. The upper side of continuous chips is notched, while the lower side which slides over the face tool is smooth and shiny. The chips have the same thickness throughout. The second type of chips are called discontinuous; these chips are produced when cutting more brittle materials like bronze, hard brass and gray cast iron. Since the chips break up into small segments, the friction between chip and tool reduces, resulting in a better surface finish. The smaller chip segments are more convenient to handle and dispose of. Discontinuous chips are also produced in ductile materials under conditions such as large chip thickness, low cutting speed, or small rake angle of tool. Brittle materials lack the ductility necessary for appreciable plastic chip deformation. The amount of deformation which the chip undergoes is limited by repeated fracturing. If these chips are produced from brittle materials, then the surface finish is fair, power consumption is low and tool life is reasonable; however, with ductile materials the surface finish is poor and tool wear is excessive.

Chips with built-up edges are the final type. The edges are simply small built-up areas sticking to the nose of the cutting tool, which occur with continuous chips (Schrader and Elshennawy 2000). When machining ductile materials, due to conditions of high local temperature and extreme pressure of the cutting zone, and also high friction in the tool chip interface, the possibility exists for the workpiece material to weld to the cutting edge of the tool, thus forming built-up edges. This weld metal is extremely hard and brittle, and the welding may affect the cutting action of the tool. Successive layers are added to the built-up edge; when it becomes large and unstable, it is broken and part of it is carried up the face of the tool along with chip, while the remainder is left in the surface being machined, contributing to the roughness of the surface. The size of the built-up edge varies during the machining operation - it increases, then decrease and again increases. This built-up edge protects the cutting edge of the tool, thus changing the geometry of the cutting tool. Low cutting speeds lead to the formation of a built-up edge, however, with the higher cutting speeds associated with sintered carbide tools, the built-up edge is negligible or does not exist. Conditions favouring the formation of built-up edges are low cutting speed, low rake angle, high feed and large depth of cut. This formation can be avoided by the use of coolants and taking light cuts at high speeds, which in turn leads to the formation of a crater on the surface of the tool.

This chapter focuses on drilling aspects because it is the most challenging machining process compared with sawing, planning, turning, milling and other

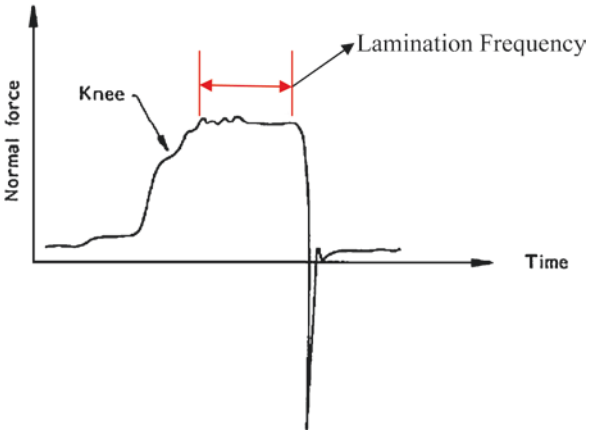

Fig. 2.7 Illustration of typical axial force during drilling of composite (Abrate and Walton 1992)

conventional machining process. The remaining sub-sections cover the experimental progress of drilling FRP composites. Drilling composite materials is more complex compared to drilling metal. When drilling metals, the forces which occur are fairly uniform over time, because the uncut chip thickness is constant (Sheikh-Ahmad 2009). The chip formation process in a drilling operation itself is considered as a complex mechanism, which occurs with multiple cutting edges of varied rake angles, tool wear, cutting speed and feed rate. There are two forces - thrust force (along the direction of the feed) and torque - which are generated from the tool during drilling operation. Previous experiments have shown that the thrust force increases steadily until a constant value when steady drilling through the thickness of laminate is reached (Sheikh-Ahmad 2009, Abrate and Walton 1992), this value is then followed by a sharp drop signal as the tool exits the opposite side and this scenario can be illustrated in Fig. 2.7. Furthermore, the sharp drop occurs when the tool acts like a punch separating the thin uncut layer fron the remainder of the laminate. This action introduced delaminations near the exit hole side, which is associated with an almost instantaneous drop in normal force from its steady state value down tremendously. The main point of interest for most researchers is looking at the steady portion of the drilling process, which is called the lamination frequency, as highlighted in Fig. 2.7. It is the main dynamic component of the thrust force, and is the most significant oscillation of normal forces. The lamination frequency is defined as the ratio of the number of plies per millimetre to the time taken by the drill to penetrate one millimetre of material (Abrate and Walton 1992). It is generally quite small compared to the frequency corresponding to tool rotation and the magnitude of the dynamic signal. Moreover, tool rotation and the magnitude of the dynamic signal show a good correlation with the waviness of the surface of the hole. Thus, the normal force signal is a very important piece of information concerning possible damage to the workpiece, and to tool wear; these can be monitored to determine when the tool should be replaced. In addition, it concerns about the surface quality of workpiece. Initial development by Hocheng and Dahran (1990) employed Linear Elastic Fracture Mechanics (LEFM) to understand the mechanism

of thrust force. They used this method to obtain the critical thrust force model for twist drill bits that are related to push-out delamination. A model that is simplified by them as a single concentrated load through a central point depends on the properties of the composite laminate workpiece (quasi-isotropic), and the uncut-ply thickness under the drill bit. However, there was a contradiction between this model and Zhang's model (Zhang et al. 2001) and experimental results by Sedlacek and Slany (2010), that thrust force is exerted by the drill bit, which is also contributed to by two major cutting edges (lips) in order to remove the bulk of the chip. Figure 2.8 shows the thrust and rotate action of cutting edges; when the bulge grows to a certain degree, the surface layer splits open, the chisel edge penetrates, then the cutting edges start to remove the chip by orthogonal cutting. The delamination damage initiated in the first phase further develops due to the continuous pushing and rotating of the cutting edge. The chisel edge also affects the drilling thrust force, and is considered as a major contributor (Zhang et al. 2001, Sheikh-Ahmad 2009, Sedlacek and Slany 2010). This is due to a blunt wedge with a large/highly-negative rake angle, which also removes a very thin chip by orthogonal cutting. At the centre of this small region (blunt wedge), an extrusion or smearing action is the mechanism of material removal.

Figure 2.9 shows the method of understanding the torque mechanism - based on the graph, it has been divided into three variations of torque during drilling (Abrate and Walton 1992). In the first phase, the torque rises slowly due to the smaller

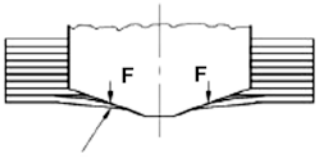

Thrust and rotate action of cutting edge

Fig. 2.8 Thrust and rotate action of cutting edge (Sedlacek and Slany 2010)

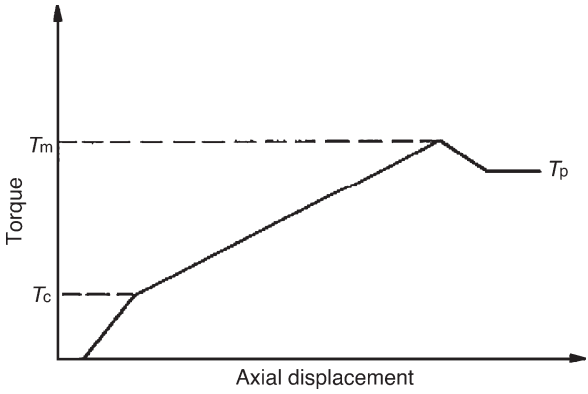

Fig. 2.9 Variations of torque mechanism (Abrate and Walton 1992)

cutting forces at the chisel edge, whereas the thrust force rises quickly. The torque then increases rapidly until the cutting edges of the tool are completely engaged; the cutting torque, $T_{c,}$ corresponds to the end of the engagement phase. Next is a phase where the torque increases linearly until a maximum value is reached (maximum torque, T_m). Finally, this is followed by a slight drop after hole completion (torque after penetration, T_p). According to this mechanism, the large difference between the cutting torque and maximum torque is attributable to high frictional forces between the lands of the drill (land width) and the wall of the hole. As drilling progresses, the tool is in contact with the side of the hole over an increasing area, where the frictional forces at the interface create increasing resistance torque. After completing the penetration, a small decrease in torque occurs due to friction, which is a major contribution to total torque. Furthermore, high temperatures and slightly negative coefficients of thermal expansion compound the problem by squeezing the drill (Di Ilio et al. 1991). The torque is further increased with increased feed rate, whereas an increase in the point angle of the drill leads to decreased torque (Gindy 1988, Lambert 1987). For the case of unidirectional composites, a variation of torque at a frequency corresponding to twice the drill rotation rate, which it reflects the variation of the stiffness of the workpiece with direction (Konig et al. 1985, Konig and GraS 1989). Thrust levels increase as feed rate, cutting speed or point of angle are increased (Gindy 1988, Lambert 1987), thus, maximum thrust force and torque are both increased significantly with the number of holes drilled, due to chipping and wear of cutting surfaces (Radkakrishnan and Wu 1981, Di Ilio et al. 1991, Sadat 1990, Konig et al. 1984, Sakuma et al. 1984). Some researchers have considered variation of peak thrust (at steady lamination frequency) as a function of the number of holes drilled. Thrust force increases due to tool wear have also been reported by researchers, who describe its greater importance when drilling graphite/epoxy than in glass/epoxy, due to the more abrasive nature of graphite fibres. Delaminations also occur due to higher thrust force, however maximum thrust force or torque does not correlate well with surface finish (Radkakrishnan and Wu 1981).

In machining of composites, the tool materials should be capable of withstanding the abrasiveness of fibres and debris resulting from machining. Based on this, the term is distinctively different in metal cutting theory, which the by-product is described as ‘chip’. However, majority of the researchers were used the by-product term as ‘chip’ for machining of composites (Sheikh-Ahmad 2009, Liu et al. 2012, Abrate and Walton 1992). Over the past century, a lot of research attempts have been conducted to investigate the mechanics of chip formation in metal machining. Due to this, metal machining is a well-established science and generally, most of the researchers have a better understanding as well as idea on how metal chips are formed and removed (Sheikh-Ahmad 2009). Furthermore, similar techniques to those used in studying metal machining have been transferred to the study of composites machining but only limited success have been reported (Liu et al. 2012, Sheikh-Ahmad 2009, Komanduri 1997, Abrate and Walton 1992). The chip formation process in metal machining is significantly different than machining of FRP. However, there are some common aspects in which the behaviour in machining both materials is to some extent similar. The wealth of information and expertise

in this field has allowed the advancement of metal cutting theory to the level of astounding predictive capabilities, and it can sometimes be applied in the study of composites machining, i.e. the by-product term called as 'chip' in the study of chip formation process for machining of composites, but with some caution (Sheikh-Ahmad 2009).

It is also essential to understand temperature distributions in the workpiece and the tool when drilling composites. Heat generated during drilling is distributed differently in each material. For metals, 75% of the thermal energy is eliminated with the chip material, 7% absorbed by the workpiece and 18% by the tool. For carbon/epoxy, approximately 50% of the energy is absorbed by the tool, the remainder is absorbed almost equally by the workpiece and the chips (Konig and GraS 1989). Thus, a larger fraction of the energy dissipated is absorbed by the workpiece and also by the tool - temperatures near the hole as high as 200 °C were reported. Spatial and temporal temperature gradients were strongly affected by the thermal conductivity of the material. For carbon/epoxy, smaller temperature gradients were observed than in glass/epoxy or aramid/epoxy materials under the same conditions. The upper cutting speed is limited by the risk of introducing thermal damage to the workpiece material (Konig et al. 1984, Konig et al. 1985), while the lower limit is governed by the surface quality, which becomes poor as the fibres recede in front of the cutting edge (Konig et al. 1984), therefore to avoid excessive forces which cause delamination, feed rates should be limited (Abrate and Walton 1992).

The damage when drilling composites is essential unavoidable. There are several types of damage, such as matrix cratering and thermal alterations, fibre pull-out and fuzzing, interlaminar cracks and delaminations, and geometrical defects which commonly occur in metal drilling as well. Based on the majority of research findings, delamination has been recognized as the major type of damage encountered in the drilling process, as an undesirable inter-ply failure phenomenon induced by drilling. Moreover, it drastically reduces assembly tolerance and bearing strength, including the potential for long term performance deterioration under fatigue loads (Mishra et al. 2010, Gaitonde et al. 2008, Jain and Yang 1994, Hocheng and Dahran 1990). Mechanisms of delamination can be explained in two ways, as observed by Ho-Cheng and Dharan (1990). The first phenomenon happens when peeling up of the top layer or 'peel-up' occurs around the drilled hole's entry periphery, as shown in Fig. 2.10(a). When the cutting edge of the drill bit makes contact with the composite laminate, a peeling force through the slope of the drill bit flutes results in separation of the plies, forming a delamination zone around the drilled hole's entry periphery. Another phenomenon occurs at the drill bit – the punching out of the uncut layer near to the exit, known as 'push-out'. Figure 2.10(b) illustrates the phenomenon of push-out delamination which occurs around the drilled hole's exit periphery. When the drill bit approaches the hole exit side, the uncut plies beneath the drill bit becomes more susceptible to deformation due to decreased thickness. Eventually, push-out appears at the drilled hole's exit periphery, if the thrust force applied to uncut plies exceeds the inter-ply bonding strength. The material removal process is primarily performed by the major cutting edge and fibre orientation in drilling; its consideration is essential to understand the cutting behaviour. However,

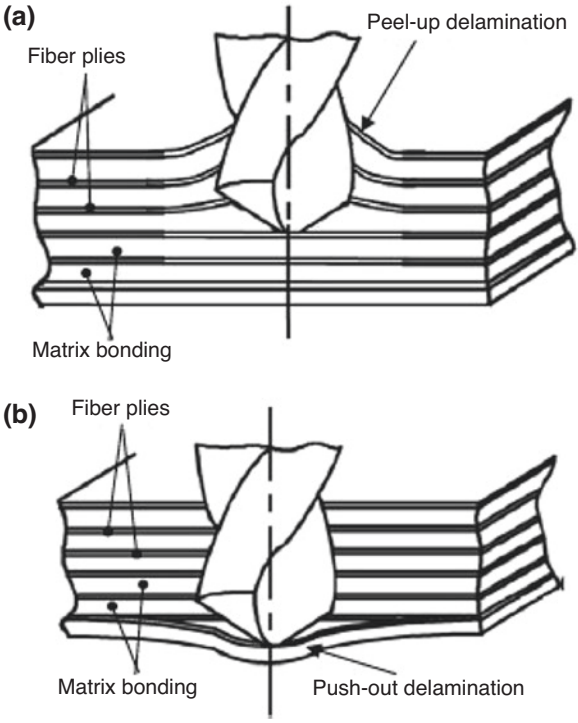

Fig. 2.10 Delamination mechanisms: (**a**) entrance or peel-up delamination (**b**) exit or push-out delamination (Hocheng and Dahran 1990)

it should be noted that the chisel edge contributes to a much lesser extent to material removal processes (Sheikh-Ahmad 2009, Abrate and Walton 1992).

In the case of unidirectional laminates or composites studied by previous researchers, the hole varies considerably around the circumference (Konig et al. 1985, Sheikh-Ahmad 2009, Abrate and Walton 1992). There are two most prominent effects of cutting directions; the first is with the cutting direction in parallel to fibre orientation 0°, where individual fibres are pulled out. Furthermore, it is also significant to understand that, when the angle of fibre orientation is increased, compression and bending occurs in the 20° – 45° range, where fibres are pulled out of the cut surface and diverted into the cut direction -this is considered as the worst surface quality range by previous researchers.

Another prominent cutting direction is perpendicular to fibre orientation, where fibres are subjected to shearing and bending. In this cutting direction, the surface quality is significantly better. Unlike milling, the chip thickness in drilling is independent of angular position, and the centre of rotation of the cutting tool is always fixed relative to the workpiece (Sheikh-Ahmad 2009). The strength of fibres is usually higher in tension, because the cutting forces are greater when the cutting direction is parallel to the fibre (Hickey 1987). Most of the researchers agree that angle-ply or quasi-isotropic laying-up sequences are easier to machine than unidirectional types.

The machining of FRP composites involves a combination of plastic deformation, shearing and bending rupture (Santhankrishnan et al. 1988). Santhankrishnan et al. (1988) conducted an experiment on machining of FRP composite surfaces by applying three mechanisms: abrasion, ploughing and cutting. The three different FRP composites under investigation - KFRP, CFRP and GFRP - exhibited different machined surfaces. In KFRP, the bending rupture was absent and plastic deformation and fibre elongation predominated, due to the flexibility of the Kevlar fibres. The Kevlar fibres were less brittle than the glass fibres in GFRP, which are less flexible, while for CFRP, the carbon fibres were the most brittle and the strain at failure the lowest. The authors also highlighted the fact that the carbon fibres experienced crushing and fractured sharply.

The research conducted by Koplev et al. (1983) explains the cutting mechanisms of FRP. The authors believe that the angle between fibre orientation and cutting velocity strongly contributes towards the chip formation. They describe the machined surfaces as a function of machining orientation, which depends on the fibre axis. In their experiments, they suggest two basic cutting mechanisms: cutting in a perpendicular direction (shearing), and cutting in a parallel direction (buckling). They examined the chips which plastic deformation mainly did not affect, but where a series of fractures occurred during the cutting process.

2.3.2 Typical Tools for Cutting FRP and Its Development to Support Machining of FRP

Drills made of High Speed Steel (HSS) fail to perform well with glass and carbon fibres due to the workpiece material's highly abrasive nature (Abrate and Walton 1992). Tungsten carbide possesses an adequate life particularly when submicron carbide is used. This submicron carbide has a resistance to rupture which is 50% higher than standard C2 grade (Mackey 1980). The tool materials recommended for use include cemented carbides (coated and uncoated), ceramics, cubic boron nitride (cBN), and diamond (single crystal or polycrystalline) since most fibers utilized in composites are hard and abrasive (Komanduri 1997). The primary tool used in the drilling of composites are twist drill bits made of HSS or carbides (Liu et al. 2012). Today, drilling tools used for cutting FRP come in many different geometries, and are made of different tool materials. Figure 2.11 shows the typical drill bits for machining of FRP composites. In some cases like graphite/epoxy or glass/epoxy, a tool geometry shape which has positive rake angles is able to generate the least amount of heat during cutting (Abrate and Walton 1992, Sheikh-Ahmad 2009). However, more positive rake angle may cause more fragile the cutting edges becomes. The second element of good tool geometry in order to improve the penetration rate is a small chisel edge.

Step drill bit has the tip ground down to a different diameter, which the transition between this ground diameter and the original diameter is either straight, to form a

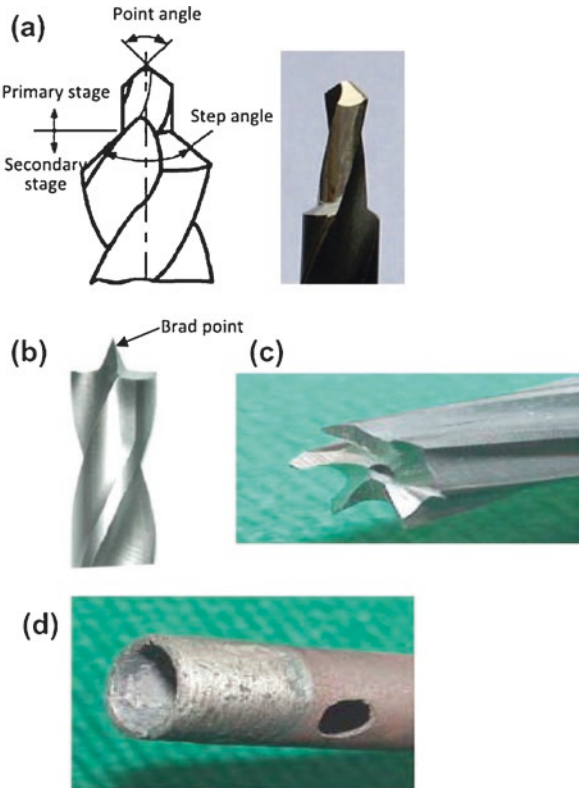

Fig. 2.11 Four examples of drill bit geometries; (**a**) step drill bit (Liu et al. 2012), (**b**) brad point drill bit (Liu et al. 2012), (**c**) saw drill bit (Hocheng and Tsao 2006), and (**d**) core drill bit (Hocheng and Tsao 2006)

counterbore, or angled, to form a countersink. It has the advantage that both diameters have same flute characteristics, which it keeps the bit from clogging when drilling soft material, i.e. aluminium. This drill bit usually is a custom-made for different application, which the tooling cost is quite expensive. A brad point drill bit is a tool designed to bore accurately and neatly through fibrous materials like wood and some composites. The sharp brad penetrates into the surface of the material and fixes the bit in place to ensure it bores a hole exactly to keep the drill bit in line. The brad point drill bit has a few advantages such as it can drill neat holes quickly, accurately, versatile and can be used on plastic and thin sheet metal or harder materials depending on the material from which the tool is made. However, this drill bit can be very difficult or even impossible to sharpen, as it can be easy to accidentally penetrate the wrong part of the tool and must be kept central to keep the bit from spinning irregularly when it contacts the workpiece. Saw drill bit can also acquire better machining quality that it is utilized the peripheral distribution of thrust for drilling composites. The tool-work contact for core drill bit is located in a circular area at bottom of drilling core and it removes the material to create cylindrical holes in a circular cross-section. All these special drill bits showed different level of the drilling thrust force varying with the feed rate and a distributed thrust towards the drill periphery rather than concentrated at hole center (twist drill) is advantageous.

However, the main issues for these drill bits are expensive tooling cost and difficult to regrind the tool.

For machining of CFRP, it is recommended to use diamond tooling in order to reduce tool wear (Komanduri 1997). Moreover, polycrystalline diamond (PCD) tool has been found to drill a much larger number of holes (Abrate and Walton 1992) and it also has long been the preferred method of drilling (Garrick 2007) PCD is formed in a large High Temperature-High Pressure (HT-HP) press, which it is either a diamond wafer on a backing carbide or forming a 'vein' of diamond within a carbide wafer or rod. The process of producing the diamond tool is quite complicated as it requires two elements (Kalpakjian and Schmid 1999, Schrader and Elshennawy 2000, Garrick 2007, Abrate and Walton 1992). The first element involves EDM or electrical discharge machining where wafers are polished to a mirror finish then cut by EDM into smaller, workable segments that are then brazed onto the sawblade, reamer, drill, or other tool. Often these wafers are EDM machined and/or ground, which it may required additional time to expose the vein of diamond along the tools, i.e. at the cutting edge, and these tools are mostly used for the machining of non-metallic and nonferrous materials. The second element is the grinding operation may apply by combining with EDM, which the combination allows a higher material removal rate and it is more cost effective in terms of providing a finer final surface after the EDM process. Thus, the process itself accomplished by combining the two elements, which it requires more time, stringent process to achieve fine shaping as well as surface geometry, the bonding in the PCD workpiece must be ample enough to provide the conductivity necessary for the combination of EDM and grinding operation to work, and lastly, the tooling cost is expensive.

It is essential to understand the thrust force and torque mechanisms applied in a drill bit. Cutting edges (lips) and chisel edges are the two most profound influences towards the surface quality. The main interest of this research is to identify the best combination of speed and feed in order to produce the best hole quality in thick CFRP composites, which have a highly abrasive nature and poor thermal conductivity. Moreover, the main purpose of conducting the experiments by using cutting tool parameters as inputs is to find the best tool geometry design, whereas this research aims to optimize the cutting operation parameters, by manipulating the thrust force and torque through drilling strategies and the capability of the machining centre. It is greatly beneficial to achieve the desired quality of drilled holes for thick composites, and to extend tool life.

2.3.3 Damage to FRP by Mechanical Machining

Machining of CFRP composites has been extensively studied experimentally. The influence of various input variables (feed rate, cutting speed, drill bit geometry and type of drill bit material) on the hole or surface quality (delamination and other damages) and drilling forces (thrust force and torque) are covered in this subsection. Shyha et al. (2009) focused on drilling 1.5 mm diameter holes in 3 mm

thick quasi-isotropic, unbacked CFRP laminate. This research was to establish the influence of machining parameters on tool life and workpiece damage, together with identifying the most preferred levels for process control factors. Conventional carbide drills with a diameter of 1.5 mm, and stepped carbide drills with a pilot diameter of 1 mm followed by a 1.5 sizing diameter were used. Tests were conducted in dry machining conditions. The authors' conclusions agreed with what Franke (2011) observed, so much so that the main factors for tool life and thrust force are drill type and feed rate, whereas cutting speed and feed rate have the most significant effect on torque. Stepped drill geometry, high feed rates and the use of uncoated tools increases tool life, while the step drill sequence reduces the thrust force, which the authors attribute to the higher feed rates and the drill's 140° point angle. Internal cracks, porosity (due to the absence of matrix material between layers), fibre/matrix cracking and resin loss were observed, but the change in helix angle between 24° and 30° did not appear to have any noticeable effect. Davim and Reis (2003) and Sardinas et al. (2006) observed that drilling woven-ply CFRP and unidirectional-ply CFRP (both were 3 mm thick) respectively, delamination expanded significantly in corresponding to high cutting speed settings. However, Gaitonde et al. (2008) inversely discovered that drilling thin woven-ply CFRP composites caused delamination increased due to the effect of feed rate. Drilling of CFRP composites experiment by Ramulu et al. (2001) had similar results like Shyha et al. (2009) and Franke (2011) where by increasing the feed rate caused the thrust force and feed rate increased. In comparison with high cutting speed settings, Ramulu et al. (2001) also experienced the same scenario like Davim and Reis (2003) and Sardinas et al. (2006) that by increasing the cutting speed, the tool wear increased, i.e. resulting in a short tool life and larger damage rings occurred. Based on these studies, only the work of Shyha et al. (2009) has a different drill bit geometry compared to others, which they used twist drill bits. The influence of feed rate and cutting speed settings on drilling forces is similar to what had occurred to the other research attempts except the reduction values on drilling forces and delamination were significantly better when using step drill bit. Thus, the most significant factor on hole quality based on these research attempts is feed rate, which it affects the drilling forces. Based on the cutting parameters used by the authors recently, the range for the cutting speed is between 11 and 200 m/min, while for feed rate is between 0.01 and 0.3 mm/rev.

Iliescu et al. (2010) studied the drilling of CFRP in order to extend tool life and improve hole quality. These tests involved both uncoated and coated carbide tool of 6 mm diameter, drilling through material 25 mm thick. Based on their observations, the authors pointed out the beneficial effect of a diamond drill bit as well a coated diamond drill bit on tool life, as the tool life of the tools was about 10 to 12 times the tool life of the uncoated carbide drill, for cutting speeds 3 times higher (170 m/min instead of 56 m/min). They also recommended a drill bit with two point angles, which has the region of 125° and the second with a 90° point angle. In addition to that,an helix angle in the range of 35–40° like a corkscrew is also recommended by them. By comparing with the work of Shyha et al. (2009), the drill bit used by Iliescu et al. (2010) almost like a step drill operation but each of drill bit geometry

serves a different purpose. Furthermore, a point angle of 125° is to ensure a proper balance of the drill bit and allowing if compatible with a very progressive output, which minimizes the thrust load near 90° point angle (Iliescu et al. 2010), whereas the drill bit geometry used by Shyha et al. (2009) that 140° point angle able to reduce the thrust force and the reduction was believed due to the lower chisel edge/workpiece material interaction when employed the step drill bit. Feed rate, cutting speed and tool wear are the most significant factors affecting the thrust force as stated in the work of Iliescu et al. (2010) and similar to other research attempts as highlighted in the first paragraph. They used 25 mm thick CFRP in this research attempt. Unfortunately, hole quality was not quantified, as the focus was clearly on tool wear. Research conducted by Santhanakrishnan et al. (1988) studied the machined surfaces of CFRP. In machining of CFRP, sintered carbide tools exhibit flank wear and secondary sides, combined with a predominant crater wear. Severe wear in the nose region and cobalt matrix pull out lead to the flow of the carbide skeleton due to the higher cutting temperature. In this experiment, two types of tool were used involving sintered carbides (P20, TiC coated, K20) and HSS. They found that K20 carbides performed better in machining of FRP composites compared to other types of sintered carbides and HSS. Based on the literature in the first as well as this paragraph, so far two types of tool material, i.e. diamond and carbide drill bits, are the most promising drill bits for drilling CFRP composites due to its machining results. Apart from the effect of tool wear, choosing the most suitable coating material, especially for drilling, is crucial due to the nature of removing material in a confined space, which this leads to a wide potential for damage. However, information regarding tool defects can be valuable for optimizing speed and feed. The recommended by the authors (Caggiano et al. 2018, Shyha et al. 2009, Franke 2011, Davim and Reis 2003, Sardiñas et al. 2006, Gaitonde et al. 2008, Ramulu et al. 2001, Iliescu et al. 2010, Santhankrishnan et al. 1988) that the range for point angle is between 80° and 140°, while for helix angle is between 23° and 43°.

One of the early orthogonal machining experiments in CFRP composites was conducted by Koplev et al. (1983), where the authors observed the chip formation, surface quality and cutting forces for two fibre orientations: perpendicular 90° and parallel 0° fibre orientations, relative to the cutting direction. They found that the surface was destroyed and cracks were formed that penetrated into the composite during machining at 90° fibre orientation, up to a depth of 0.3 mm. However, during machining of CFRP at 0° fibre orientation, the surface was smoother and the cracks in the composite reached a depth of only one or two fibre diameters. Another experiment was conducted in order to determine the horizontal cutting force, and it was found that horizontal force when the cutting direction was parallel to the fibres was dependent on the cutting depth and rake angle. The vertical force, in contrast, was dependent on the relief angle and the amount of wear the tool exhibited. Another experimental study, conducted by Pecat et al. (2012), investigated the circumferential up-cut milling process of unidirectional CFRP. In their paper, three relationships were discussed, and Fig. 2.12 shows the results achieved. The first result was the influence of the fibre orientation on the surface quality and process forces. They

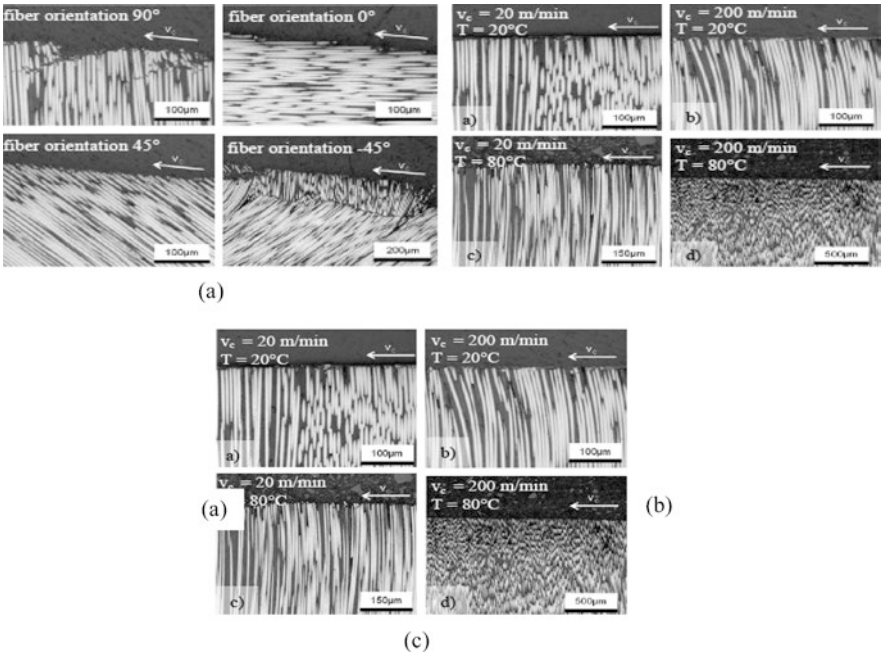

Fig. 2.12 Micrographs showing (**a**) specimens with different fibre orientations, (**b**) specimens machined with different cutting speeds and workpiece temperature, and (**c**) specimens machined with different cutting speeds and workpiece temperatures (Pecat et al. 2012)

pointed out that the fibre orientations under −45° and 90° showed serious damage in the form of cracks and segmentations. Based on their observation, they identified that the cutting mechanism was different for each fibre orientation. This is different compared to the findings by Koplev et al. (1983) that they reported only fibre orientation at 90° was experienced serious damages. Another relationship that they discovered was that between the influence of cutting speed on surface quality/damage, and process forces. They found out that high cutting speeds results in fibre bending in the cutting direction close to the machined surface. It was believed that this was caused by the thermo-mechanical load during the cutting process, therefore the level of damage rises when both cutting speed and workpiece temperature increase. The third relationship was the influence of the workpiece temperature on the surface and process forces. In this relationship, cracks were frequently formed when these were induced at low workpiece temperatures of −40 °C and 20 °C, but that they can be avoided at higher temperatures. In order to reach the specified workpiece temperatures, an in-process cooling and respectively heating was used. The cooling was done with a carbon dioxide nozzle while the heating was performed by a hot air stream. For a temperature of 120 °C, a severe alteration in the sub-surface region was found, which indicates thermal damage. They suggested that milling the CFRP at 80 °C led to the best results, i.e. the optimum condition can prevent crack formation leading to low cutting forces and to avoid thermal damage at the same time. These experiments indicated a good understanding of the relations between the

cutting speed, fibre orientation and workpiece temperature. Identifying where and how the defect occurs may lead to its consideration as a potential development for improving the machined surfaces. Understanding how the mechanisms work is crucial for tuning process parameters towards causing the least amount of damage to the workpiece material.

With respect to surface quality, both Pecat et al. (2012) and Koplev et al. (1983) observed similar levels of serious workpiece damage for cutting directions set at 90° to the fibre orientation. However, these research attempts are more concerned with the development of chip formation and the effects of tool shape design. Current research is primarily seeking information on the combined effects of speed and feed, but it is still considered as valuable information regarding the cutting forces mechanisms; understanding these may lead to the development of a good combination of speed and feed in order to reduce the compressive and radial forces during drilling operations. Apart from establishing relationships between surface damage and cutting parameters, the paper also provides an interesting way of minimizing the influence of vibrations during machining, by providing an adequate clamping of the specimens. These were embedded into aluminium shells, which were clamped on a multidirectional force measurement platform. This part emphasizes the importance of fixturing when conducting any machining trials, in order to avoid any workpiece movement during machining.

The study on delamination during the machining of CFRP conducted by Hintze et al. (2011) systematically investigated the occurrence of delamination of the top layers, with a focus on contour milling ("routing"). Two mechanisms are introduced to describe delamination: occurrence and propagation, as shown in Fig. 2.13. The authors found that the occurrence of delamination and fibre overhangs during the machining of CFRP generally depends on the condition of the tool wear and the fibre cutting angle on the top laminate layers. Neither delamination nor fibre overhangs were observed for angles of between $0° < X < 90°$, whereas for fibre cutting angles in the range of $90° \leq X < 180°$, delamination and fibre overhangs did occur. Delamination can propagate from the critical cutting angle range to the component edge, provided that the fibres are initially cut at a cutting angle of $90° \leq X < 180,°$ and at the component edge with a cutting angle of $0° < X < 90°$. The authors also conducted a drilling experiment, and found that a significant radial force component acts in addition to the axial feed force and cutting force, and corresponds to the passive force. Passive forces act on both major cutting edges. This paper provides a good explanation of delamination. A systematic scheme for describing the occurrence of delamination in milling is a good reference for understanding the nature of delamination and how it propagates. A critical angle range of $90° \leq X < 180°$ indicates serious damage, and similar results were obtained by other researchers (Pecat et al. 2012, Koplev et al. 1983). However, the experiment was carried out with a single value for each parameter, cutting speed and feed. Whether the use of different cutting parameters will make their findings obsolete is not known. It is reasonable to assume that the situation will be different, and the occurrence and propagation

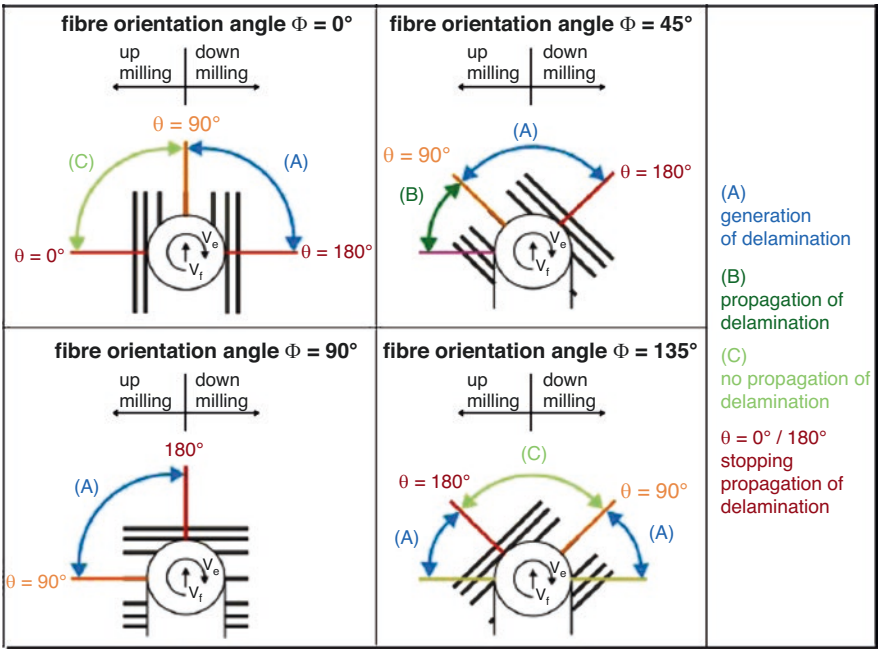

Fig. 2.13 Systematic scheme for describing the occurrence of delamination in milling (Hintze et al. 2011)

probably start at different points. The effect of each fibre orientation angle might also be changed.

The work of Sobri et al. (2018) emphasized the application of different drilling strategies on 25.4 mm thick CFRP in mechanical drilling experiments in order to determine whether the tools can actually drill through an entire stack in a single-step or whether the hole chip evacuation poses a serious problem, which it can ultimately fracture the tool. Experimental results showed that all strategies were able to penetrate the entire sample completely and only single-step drilling was capable of drilling 25.4 mm thick CFRP with minimum damages. It is practical for this strategy to manipulate the machining parameters in order to reduce hole damages in future work. Moreover, the first and final layer of the CFRP were covered by an additional surface or coating layer (i.e. peel-ply layer), which it works as a surface protection as discovered by Sobri et al. (2018). This could be due to a higher fibre density/concentration in the woven-ply structure compared to unidirectional configurations and led to increased interaction between abrasive fibres and the drill bit during drilling, which it results a significant delamination. This paper presented the results that are useful to define the relationships between machining parameters related to mechanical drilling and hole quality for future considerations and it is revealed that the 2-flute uncoated tungsten carbide (WC) drill bit produced the best holes so far.

2.4 Quality Assessment of Drilled Holes

It has been reported that, in the aircraft industry, up to 60% of parts containing composite materials are discarded during the final assembly process due to drilling-induced delamination damages (Caggiano et al. 2018, Wong et al. 1982, Stone and Krishnamurthy 1996). Other types of damage were also found in previous research, and efforts towards understanding drilling behaviour, particularly in drilling of CFRP, are still on-going. The quality of drilled holes is the important factor, and is complicated in nature due to the complexities of the material constituents, and the fact that examination of drilling effects is highly challenging during the evaluation process. Various techniques for evaluating drilled holes are currently available for researchers by using wide range of technology. The most favourable method in assessing drilled holes is non-destructive examination, which is commonly used by researchers; this method applies visual inspection through digital images extracted from optical microscope, stereomicroscope, ultrasonic C-scan, X-Ray computerized tomography (CT) and others. The following sub-sections explain all of the types of evaluation techniques which are applied commonly for quality assessment and evaluation purposes in drilling process.

2.4.1 Delamination Factor (F_d) and Relationships Between Forces and Delamination

The earliest metric for characterising delamination after a drilling process is the one-dimensional delamination factor, often abbreviated as F_d, which was introduced by Chen (Chen 1997). This method is based upon measurement of the maximum diameter of the damaged zone or delamination around a hole, with the centre point of the damage diameter located at the centre of the hole. It is one of the most commonly-used methods by researchers to quantify the amount of damage to a hole produced in fibre reinforced composite materials, by applying Eqs. (2.1),

$$F_d = \frac{D_{max}}{D_0} \tag{2.1}$$

where D*max* is the maximum diameter of the observed delamination zone and D*nom* or D*o* is the nominal diameter of the drilled hole. Figure 2.14 shows the measures used in calculating the delamination factor (F_d). This quantification method is mostly applied in measuring of holes drilled by mechanical operations. Moreover, this method can potentially be applied to laser-drilled holes; the ratio outcome may be significantly different due to thermal damage characteristics, as compared with mechanical drilling which is commonly affected by cutting operation parameters or cutting tool design.

The previous researchers believed that the relationship between delamination and thrust force has a significant correlation when drilling CFRP composites (Kim

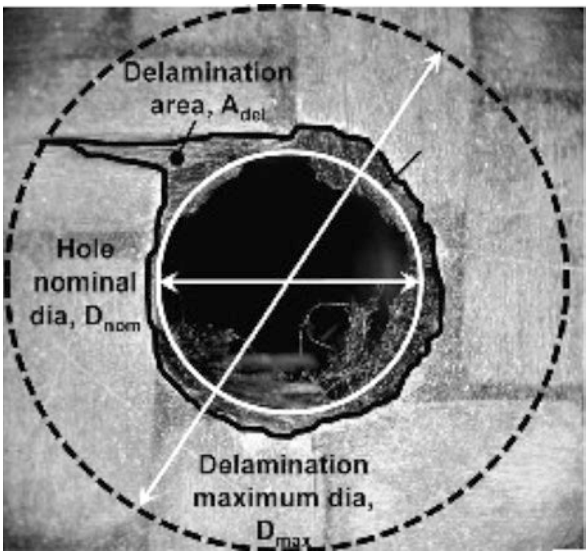

Fig. 2.14 Assessment of hole quality (adapted from Faraz et al. 2009)

and Lee 2005, Hocheng and Tsao 2006) and it is also believed that delamination can be identified by monitoring the force (Shyha et al. 2010). Feed rate, spindle speed, drill diameter, drill point angle and material configuration which the researchers pointed out that these process parameters affect the onset of delamination and the extent of delamination damage. Furthermore, the most influential parameter to control delamination is feed rate, and it is believed that this parameter has a direct influence on thrust force (Sheikh-Ahmad 2009). Apart from the thrust force, torque is also affected by the cutting speed, feed rate, and drill geometry. As explained in Sect. 2.3.1 (Cutting mechanisms of mechanical drilling), monitoring drilling thrust force and torque is essential for investigators or researchers to understand the evolution of the thrust force and torque, in order to see a detrimental effect on hole quality, in terms of workpiece delamination or damage. At the moment, this is the most common approach applied by researchers (Liu et al. 2012, Sheikh-Ahmad 2009). Moreover, researchers usually observe the trend or pattern of force signals which can use as an indicator of how the damage propagates, and which part of the revolution is most affected on the workpiece. Figure 2.15 shows a typical force diagram for a single hole, drilled using a stepped drill in this example. It can be seen that each section of the diagram shows a significant revolution generated by cutting action, and which part of the tool makes a major contribution to the damage. The main interest in observing the trend or pattern is on the maximum magnitude of the thrust force, which indicates the initiation of delamination (Sheikh-Ahmad 2009, Shyha et al. 2010, Caggiano et al. 2018). In spite of this, how certain a correlation between the course of thrust force and the amount of damage could not be found from any references (Caggiano et al. 2018, Liu et al. 2012, Sheikh-Ahmad 2009, Schrader and Elshennawy 2000, Shyha et al. 2010, Shyha et al. 2009, Chen 1997, Konig et al. 1985). However, the only possible way at the moment is to find the relationship between the amount of thrust force and the delamination factor, i.e. F_d

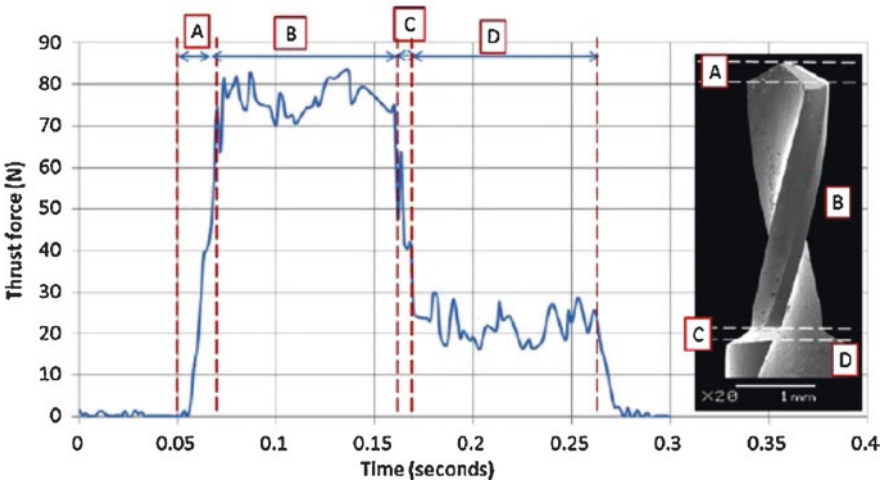

Fig. 2.15 Example of typical force diagram for a single hole drilled by using a stepped drill (Shyha et al. 2010)

ratio (Chen 1997) or F_{da} (Davim et al. 2007). Konig et al. (1985) and Chen (1997) revealed the relationship between the amount of thrust force and the width of damaged zone on the tool exit side at any cutting conditions by using conventional twist drill bit and suggested that as long as the thrust force is below a certain critical value, which depends upon the material composition, no damage occurs. If it is above the limit, the damage takes place and grows very rapidly.

2.4.2 Adjusted Delamination Factor (F_{da})

In cases where the damage is caused by a few fibres or fibre-bundles peeled up or pushed down result in a significant width, it will be difficult to assess the extent of the real, delamination characteristics across the entire hole periphery. Davim et al. 2007 suggest a two-dimensional delamination factor called the adjusted delamination factor, typically abbreviated as F_{da}; Fig. 2.16 illustrates a method to measure the F_{da}. An extension of this approach is to not only look at the diameter but at the amount of material left behind by the drilling process. One way of assessing this damage in a quantitative manner is by determining the area of workpiece material blocking off the hole entrance and exit, and by relating it to the size of the damage contribution, which represents the common establishment of delamination factor, F_d as shown in Eqs. (2.2).

$$F_{da} = \alpha \frac{D_{max}}{D_0} + \beta \frac{A_{max}}{A_0} \tag{2.2}$$

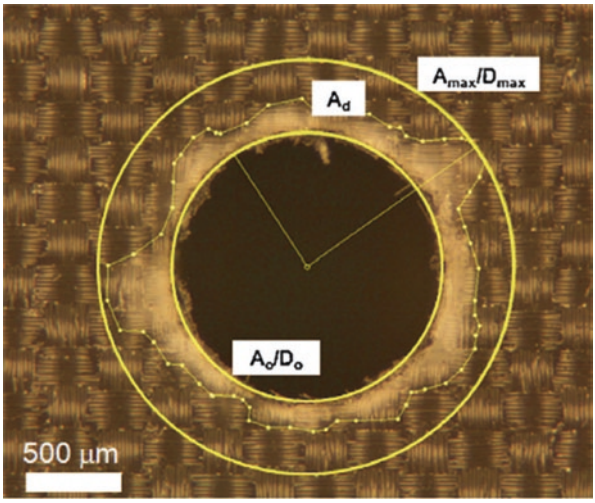

Fig. 2.16 Measuring elements in the adjusted delamination factor (F_{da}) (Shyha et al. 2010)

where A*max* is the cumulative peripheral damage area (the area marked by large yellow circle in Fig. 2.16), and A*o* is the nominal area of the hole drilled (marked by small yellow circle in Fig. 2.16). In Fig. 2.16, both measurement elements are shown in the same region for better understanding and comparison, i.e. A*max*/D*max* including A*o*/D*o* which are measured in the same region for both methods, F_{da} and F_d.

Davim et al. (2007) furthered the explanation of the parameters, α and β, which these are the weights in Eqs. (2.2). A*max* and A*o* are derived in Eqs. (2.3, 2.4):

$$A_{max} = \pi . \frac{D^2_{max}}{4} \tag{2.3}$$

$$A_0 = \pi . \frac{D^2_0}{4} \tag{2.4}$$

Substituting Eqs. (2.1, 2.3) and (2.4) into Eqs. (2.2), the simplified Eqs. is as follows:

$$F_{da} = \alpha . F_d + \beta . F^2_d \tag{2.5}$$

Based on the Eqs. above, parameter α is actually the accompaniment of parameter β, which is '$\alpha = 1 - \beta$'. Furthermore, parameter β is the ratio of the damage area (A*d*) to the area interrelated to D*max* (A*max*), and subtracts the nominal area of the hole (A*o*). Therefore, the Eqs. mentioned above can be equivalent to Eqs. (2.6, 2.7).

$$F_{da} = (1 \quad \beta) . F_d + \beta . F^2_d \tag{2.6}$$

$$F_{da} = F_d + \frac{A_d}{\left(A_{max} - A_0\right)}\left(F^2{}_d - F_d\right) \tag{2.7}$$

The criterion based on Eqs. (2.1) may generally have an inherent incoherence, because the extent of the delamination caused by just a few fibres peeled up or pushed down to a distinct and significant width does not truly depict the real delamination zone of the drilled hole periphery (Davim et al. 2007, Faraz et al. 2009, Shyha et al. 2010). Eqs. (2.2), in contrast, describes a two-dimensional delamination factor and might therefore be more appropriate for describing the damage caused to a hole or workpiece (Davim et al. 2007). In certain cases, Eqs. (2.2) provides a better discrimination of hole damage as compared to Eqs. (2.1). It may experience identical results, despite the big difference in damage during the analysis, and thus the adjusted delamination factor (F_{da}) gives more robust/characteristic measure for hole defects. A typical example of this scenario can be seen in Fig. 2.17, based on the experiments conducted by Shyha et al. (2010).

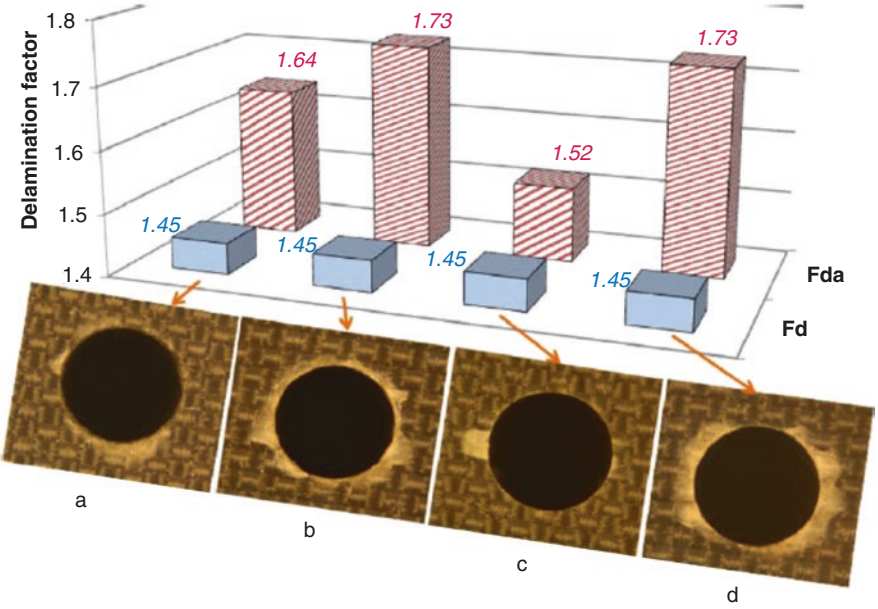

Fig. 2.17 An example of the application of conventional F_d and adjusted F_{da}: (**a**) final hole exit in Test 1; (**b**) final hole exit in Test 10; (**c**) first hole exit in Test 5; and (**d**) first hole entry in Test 10 (Adapted from (Shyha et al. 2010))

2.4.3 Assessment of Hole Geometry Accuracy

Circularity of hole and hole taper are some defects associated with mechanical drilling as well as laser drilling, due to the inherent nature of drilling difficult-to-cut materials such as high-strength metals, ceramics and composites. Excessive tool wear can affect the accuracy of drilled hole, thus, tool life assessment can be measured and correlated with measurement of the hole diameter. Shyha et al. (2010) found the drilled hole diameter to be undersized in all conditions tested, by between 36 to 73 µm at the maximum level of tool life performance. Moreover, they observed that all holes had a small taper, with slightly larger entry holes. It can be seen that a diametrical difference occurred between hole entry and exit which was 17 µm over a 2 mm height; however, further analysis was only considered at a 1.5 mm distance from hole entry or exit - the middle point reading. All tests were based on drilling of 3 mm-thick symmetric CFRP laminate specimens (unidirectional and woven arrangements), with various prepreg resin types provided by manufacturers. The machining used uncoated WC twin lipped stepped drills with a pilot diameter of 1 mm, incorporating a 1.5 mm sizing diameter section; the helix and point angles were 24° and 118° respectively. Figure 2.18 shows hole diameter measurement results in different prepreg resin type and prepreg form as well. They measured all holes by using 3-axis coordinate measuring machine, CMM equipped with a Renishaw head including a 1 mm ruby ball stylus. Three axial positions were measured as shown in Fig. 2.19, and twenty seven points taken for each axial position, repeated twice and averaged. The following sub-section explains the evaluation of hole geometry accuracy for a laser drilling operation.

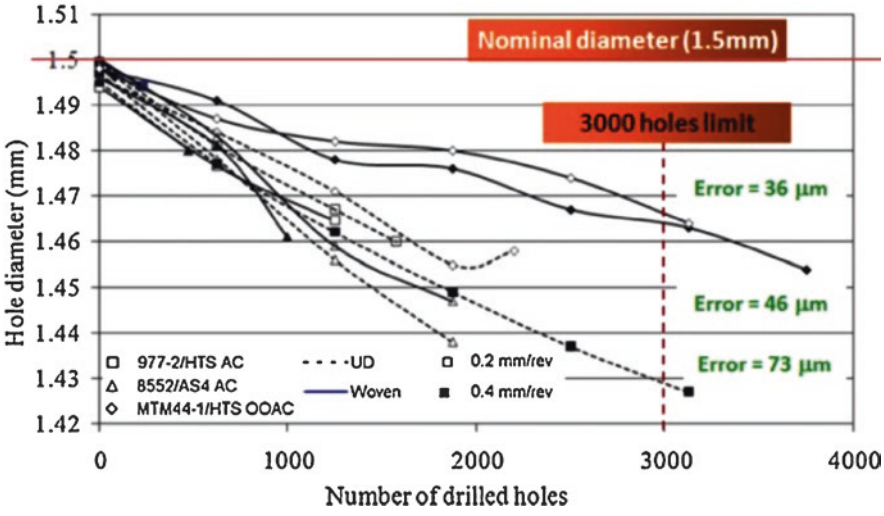

Fig. 2.18 Hole diameter measurement outcomes (Shyha et al. 2010)

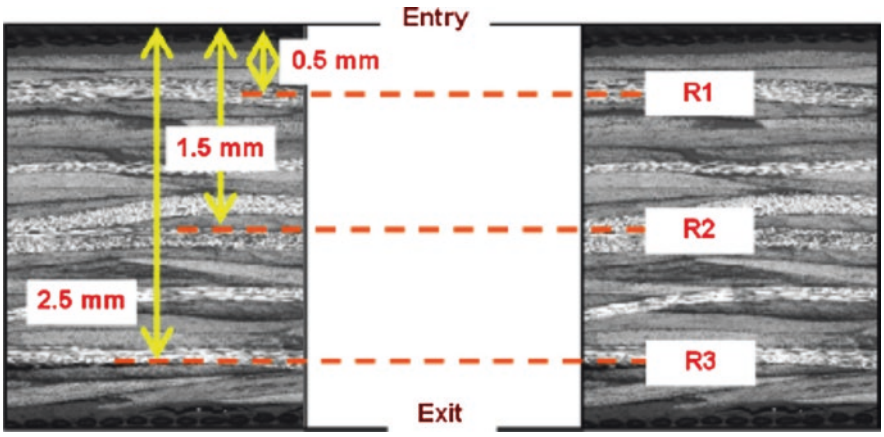

Fig. 2.19 Locations of hole diameter axial positions for 3 mm thick CFRP laminates (Adapted from (Shyha et al. 2010))

2.5 Summary

The physical properties of the fibre and matrix, fibre volume fraction, and fibre orientation primarily determine the properties of FRP materials. Owing to these properties, machining of FRP composites is a challenging task, which leads to some forms of material damage in any machining process. Drilling of composites, particularly CFRP, remains one of the most challenging machining operations, and among the key issues to be considered are thermal management, tool wear, delamination and other significant damage (Sheikh-Ahmad 2009); in drilling of CFRP composites, the optimum performance depends on the proper consideration of these factors (Caggiano et al. 2018, Sobri et al. 2018, Sheikh-Ahmad 2009, Kalpakjian and Schmid 1999). Mechanical drilling requires the selection of optimum cutting operation parameters - i.e. cutting speed (spindle speed) and feed rate - in order to avoid any excessive forces affecting the surface integrity of CFRP composites.

Although researchers or investigators have suggested some approaches to reducing the damage in mechanical drilling, such as the use of support plates, special drill bits and pre-drilled pilot holes, the optimization of cutting operation parameters (i.e. spindle speed and feed rate) is still considered as the best approach to enhance the hole quality without needing special equipment or tools which can be an expensive for future manufacturers. Some authors believe that optimizing cutting operation parameters leads to better quality, since the use of low feed rate and high spindle speed favour the minimum material damage and extend tool life. Many researchers have highlighted the optimum performance of spindle speed and feed rate in their experimental attempts, and they encourage others to refer to these results for future machining; however, these references may or may not be suitable for drilling a thick sample, e.g. a 25.4 mm CFRP workpiece. Previous drilling experiments were

attempted by researchers to drill material thickness ranging from 1 to 25 mm (mechanical: 1 to 25 mm); manipulating the machining parameters may produce different results due to the different thicknesses.

References

Abrate S, Walton DA (1992) Machining of composite materials, Part II: Non-traditional methods. Compos Manuf 3(2):85–94

Askeland DR, Phulé PP (2006) The science and engineering of materials (International Student Edition). Thomson Publishing

Brouwer WDR (2019) Natural Fibre Composites in Structural Components: Alternative Applications for Sisal? http://www.fao.org/DOCREP/004/Y1873E/y1873e0a.htm (Accessed on 16th April 2019)

Caggiano A, Nele L, Teti R (2018). Drilling of Fiber-Reinforced Composite Materials for Aeronautical Assembly Processes, Characterizations of Some Composite Materials, Hosam El-Din M. Saleh and Martin Koller, IntechOpen, DOI: https://doi.org/10.5772/intechopen.80466. Available from: https://www.intechopen.com/books/characterizations-of-some-composite-materials/drilling-of-fiber-reinforced-composite-materials-for-aeronautical-assembly-processes

Chen WC (1997) Some experimental investigation in the drilling of carbon fiber reinforced plastic (CFRP) composite laminates. Int J Mach Tools Manuf 37:1097–1108

Dandekar CR, Shin YC (2012) Modelling of machining of composite materials: a review. Int J Mach Tool Manu. https://doi.org/10.1016/j.ijmachtools.2012.01.006

Davim JP, Reis P (2003) Drilling carbon fibre reinforced plastics manufactured by autoclave – experimental and statistical study. Materials & Design 24(2003):315–324

Davim JP, Rubio JC, Abrao AM (2007) A novel approach based on digital image analysis to evaluate the delamination factor after drilling composite laminates. Compos Sci Technol 67:1939–1945

Di Ilio AM, Tagliaferri V, Veniali, F (1991) Tool life and hole quality in drilling aramid and fibrous composites, in Composite Material Technoloav 1991. Proc of 14th Annual Energv Sources Technology Conf. ahd Exhibition, Houston, TX, Jan 2{123,1991, ASME Publ. PD-Vol 37, pp 203–207

Faraz A, Biermann D, Weinert K (2009) Cutting edge rounding: an innovative tool wear criterion in drilling CFRP composite laminates. Int J Mach Tool Manu 49:1185–1196

Franke V (2011) Drilling of long fiber reinforced thermoplastics-influence of the cutting edge on the machining results. CIRP Ann Manuf Technol 60:65–68

Garrick R (2007) Drilling Advanced Aircraft Structures with PCD (Poly-Crystalline Diamond) Drills, SAE Technical Paper 2007-01-3893, https://doi.org/10.4271/2007-013893

Gaitonde vVN, Karnik SR, Campos RJ, Esteves CA, Abrao AM, Davim JP (2008) Analysis of parametric influence on delamination in high-speed drilling of carbon fiber reinforced plastic composites. J Mater Process Tech 203:431–438

Gindy NNZ (1988) Selection of drilling conditions for glass fibre reinforced plastics. Int J Research 25(8):1317–1327

Hernandez-Castaneda JC, Sezer HK, Li L (2011) The effect of moisture content in fibre laser cutting of pine wood. Opt Lasers Eng 49:1139–1152

Hickey J (1987) Drilling graphite composites. Modern Machine Shop 59:84–90

Hintze W, Hartmann D, Schutte C (2011) Occurence and propagation of delamination during the machining of carbon fibre reinforced plastics (CFRPs)-an experimental study. Compos Sci Tecnol 71:1719–1726

Hocheng H, Dahran CKH (1990) Delamination during drilling in composite laminates. J Eng of Indusry 112:236–239

Hocheng H, Tsao CC (2006) Effect of special drill bits on drilling-induced delamination of composite materials. J Mach Tools Manu 46:1403–1416
Iliescu D, Gehin D, Gutierrez ME, Girot F (2010) Modelling and tool wear in drilling CFRP. Int J Mach Tool Manu 50:204–213
Jain S, Yang DCH (1994) Delamination-free drilling of composite laminates. ASME J Eng Indust 116:475–481
Kalpakjian S, Schmid SR (1999) Manufacturing engineering and technology (international edition). Pearson Publishing, Fourth Edition
Kalpakjian S, Schmid SR (2016) Chapter 9 Composite materials: structure, general properties and applications https://www3.nd.edu/~manufact/MET_pdf_files/MET_Ch9.pdf (Accessed on 26th November 2016)
Kim GW, Lee KY (2005) Critical thrust at propagation of delamination zone due to drilling of FRP/metallic strips. Compos Struct 69:137–141
Komanduri R (1997) Machining fiber-reinforced composites. Mech Eng. (ISSN 0025–6501) 115(4):58–64
Konig W, Grass P, Heintze A, Okcy F, Schmitz-Justin C (1984) Developments in drilling & contouring composites containing Kevlar. Prod Eng 63(8):56–61
Konig W, Wulf Ch, Grass P, Willerscheid H (1985) Machining of fiber reinforced plastics. Ann CIRP 34(2):537–548
Konig W, GraS P (1989) Quality definition and assessment in drilling of fibre reinforced thermosets. Annals of the CIRP 38(1):119–124
Koplev A, Lystrup A, Vorm T (1983) The cutting process, chips, and cutting forces in machining CFRP. Composites 14(4):371–376
Lambert BK (1987) Cutting and drilling of composite materials. Carbide and Tool J 19(5):31–34
Lau WS, Yue TM, Lee TC, Lee WB (1995) Un-conventional machining of composite materials. J Mater Process Technol 48:199–205
Liu DF, Tang YJ, Gong WL (2012) A review of mechanical drilling for composite materials. Compos Struct 94:1265–1279
Mackey BA (1980) How to drill precision holes in reinforced plastics in a hurry. Plast Eng:22–24
Mangalgiri PD (1999) Composite materials for aerospace applications. Bull Mater Sci 22(3):657–664
Matthews FL, Rawlings RD (1999) Composite materials: engineering and science, vol 2000. CRC Press, Boca Raton, pp 1351–1366
Mishra R, Malik J, Singh I, Davim JP (2010) Neural network approach for estimate the residual tensile strength after drilling in uni-directional glass fiber reinforced plastic laminates. Mater Des 31:2790–2795
Pecat O, Rentsch R, Brinksmeier E (2012) Influence of milling process parameters on the surface integrity of CFRP. Procedia CIRP 2012(1):466–470
Radkakrishnan T, Wu SM (1981) On-line hole quality evaluation for drilling composite materials using dynamic data. Z Eng for Industry 103:119–125
Ramulu M, Branson T, Kim D (2001) A study on the drilling of composite and titanium stacks. Compos Struct 54:67–77
Reza N (2010) Laser cutting of carbon fibre-reinforced polymer composite materials. PhD thesis, the University of Manchester
Sadat AB (1990) Machining of composites. Encyclopedia of Composites 3(1990):95–102
Sakuma K, Yokoo Y, Seto M (1984) Study on drilling of reinforced plastics (GFRP and CFRP). Bulletin of JSME 27(228):1237–1244
Sardiñas RQ, Reis P, Davim JP (2006) Multi-objective optimization of cutting parameters for drilling laminate composite materials by using genetic algorithms. Compos Sci Technol 66(15). 1 December 2006:3083–3088
Shanmugam DK, Chen FL, Siores E, Brandt M (2002) Comparative study of jetting machining technologies over laser machining technology for cutting composite materials. Compos Struct 57(1–4):289–296

Santhanakrishnan G, Krishnamurthy R, Malhotra SK (1988) Machinability characteristics of fibre reinforced plastics composites. J Mech Work Technol 17:195–204

Schrader GF, Elshennawy AK (2000) Manufacturing processes & materials, Society of Manufacturing Engineers (SME), 4th Edition

Sedlacek J, Slany M (2010) Analysis of delamination in drilling of composite materials. MM Sci J

Sheikh-Ahmad JY (2009) Machining of polymer composites. Springer, New York

Shyha IS, Aspinwall DK, Loo SL, Bradley S (2009) Drill geometry and operating effects when cutting small diameter holes in CFRP. Int J Mach Tool Manu 49:1008–1014

Shyha IS, Soo SL, Aspinwall DK, Bradley S (2010) Effect of laminate configuration and feed rate on cutting performance when drilling holes in carbon fibre reinforced plastic composites. J Mater Process Technol 210(8):1023–1034

Sobri SA, Heinemann R, Whitehead D, Shuaib N (2018) Drilling strategy for thick carbon Fiber reinforced polymer composites (CFRP): a preliminary assessment. J Eng Tech Sci 50(1):21–39. https://doi.org/10.5614/j.eng.technol.sci.2018.50.1.2

Stone R, Krishnamurthy KA (1996) Neural network thrust force controller to minimize delamination during drilling of graphite-epoxy laminates. Int J Mach Tools Manuf 36:985–1003

Teti R (2002) Machining of composite materials. CIRP Ann-Manuf Techn 51(2):611–634

Wong TL, Wu SM, Croy GM (1982) An analysis of delamination in drilling composite materials. In: Proc 14th SAMPE tech Conf, pp 471–483

Zhang H, Chen W, Chen D, Zhang L (2001) Assessment of the exit defects in carbon fibre-reinforced plastic plates caused by drilling. Key Eng Mater 196:43–52. ISSN 1013-9826

Chapter 3
Surface Modification of Graphene Nanoplatelets (GNP) Towards Preparation of Natural/Synthetic Rubber Blend Nanocomposites

Ruey Shan Chen, Jeefferie Abd Razak, Noraiham Mohamad, and Sahrim Ahmad

3.1 Introduction

Inorganic materials are established for reinforcement in polymer composites. In the development of polymer nanocomposites (reinforced with nanofillers), nanoscopic inorganic particles (typically 1–10 nm in at least one dimension) are incorporated in a polymeric matrix with the ideal exfoliation level of nanofiller dispersion. Nanoparticles rubber composites play a vital role in rubber technology and material engineering (Konar et al. 2010). Lately, high-performance elastomer nanocomposites with the reinforcement of various kinds of inorganic nanofillers such as layered silicates, silica nanoparticles, multi-walled carbon nanotubes, etc. have been produced (Li et al. 2017). Graphene is well-known to have exceptional physical and chemical properties, and has been widely applied in electronic devices, adsorption, sensors, energy and conversion, and composites. In the field of composites, graphene serves as multifunctional nanofiller to enhance the mechanical performance, conductivity characteristics in terms of thermal and electrical aspects as well as barrier effect (for instance, gas impermeability) of composites (Bhattacharya 2016). The reinforcing (normalized modulus) mechanism of graphene in elastomers nanocomposite depends on the aspect ratio (filler geometry), volume fraction and orientation of the graphene filler (controlled by the processing methods) but it is independent of the filler modulus (Liu et al. 2018).

R. S. Chen (✉) · S. Ahmad
Materials Science Program, Department of Applied Physics, Faculty of Science and Technology, Universiti Kebangsaan Malaysia, Bangi, Selangor, Malaysia
e-mail: chen@ukm.edu.my

J. A. Razak · N. Mohamad
Advanced Manufacturing Centre, Fakulti Kejuruteraan Pembuatan, Universiti Teknikal Malaysia Melaka, Melaka, Malaysia

S. Siddiquee et al. (eds.), *Composite Materials: Applications in Engineering, Biomedicine and Food Science*, https://doi.org/10.1007/978-3-030-45489-0_3

In this chapter, a focus is made on the natural rubber/ ethylene-propylene-diene-monomer (NR/EDPM) blend matrix reinforced with graphene nanoplatelets (GNP) with different surface modification and nanofiller loading.

3.1.1 Graphene Nanoplatelets

Graphene nanoplatelets (GNP) is discs-shaped graphite particles in a nanometer-sized scale, which comprised of two-dimensional (2D) layers of sp2-hybridized carbon atoms in one-atom thickness that are arranged in a honeycomb hexagonal lattice structure (Chen et al. 2018). GNP made of multiple layers of graphene which corresponds to partially exfoliated graphite. In comparison to monolayer graphene, GNP with various particle sizes are commercially produced at a large scale through top-down methods at a relatively low cost (Zhang et al. 2016). Generally, GNP have an ultimate strength of 130 GPa, a high specific area of 2600 m^2/g as well as very high electric conductivity (6000 S/cm) and thermal conductivity above 5000 W m K^{-1} (Bhattacharya 2016). Therefore, the extraordinary properties of GNP as well as their ultrahigh aspect ratio (600–10,000) and large surface contact area with polymer have resulted this platelet nanomaterial as an ideal reinforcing and multi-functional fillers for polymer nanocomposites (PNC) (Kuan et al. 2018). The platelet's shape promotes higher tortuosity path for molecular transport which further provides the barrier effect to the resultant PNC (Abd Razak et al. 2015b).

The overall reinforcement of GNP in a polymeric matrix is strongly dependent upon its dispersion state and the nanofiller-matrix interfacial interaction. Nevertheless, GNP has a smooth, chemically inert and hydrophobic surface, which these inherent characteristic makes GNP not compatible with many polymers and a weak interfacial bonding is caused (Zhang et al. 2016). The dispersion of GNP in polymer matrices and interface quality control are very challenging because of their strong interlayer cohesive energy and surface inertia (Zhao et al. 2018). This renders GNP tends to easily agglomerate and re-stacking into graphite via van der Waals interactions as it is unable to repel the attractive forces between them as a result of the deficiency of intrinsic functional groups (Abd Razak et al. 2015a).

3.1.2 Surface Modification

Graphene based materials are difficult to achieve intercalation by huge species like polymer chains. In order to enhance the compatibility of GNP with various polymer matrices, the surface modification of GNP could be achieved through either covalent or noncovalent functionalization approaches (Mohamad et al. 2017). Covalent modification or treatment is critically susceptible to destroy the intrinsic properties of graphene, whereas non-covalent treatment ordinally preserves the pristine structure as well as the intrinsic electrical and thermal conductivities of graphene (Abd

Razak et al. 2015b). The covalent functionalization involves hybridization of one or more sp2 carbon atom to sp3 configuration, followed by simultaneous loss of electronic conjugations (Ijeomah et al. 2017). The covalent functionalization of graphene will not only increase the dispersion of GNP, but also increase the graphene-polymer interfacial interaction. GNP typically has a hydroxyl functional group on base and edge section where this hydroxyl group will be hydrated with silane coupling agents with the presence of certain catalyst (Wang et al. 2012). By applying this idea, the silane coupling agent, for instance, aminopropyltryetoxysilane (ATPS), can be act as a chemical bridge to link covalently with polymer matrices chains (Kuila et al. 2012). This covalent approach is proven to serve as an effective method in improving the filler-matrix interfacial interactions, and thus increasing the mechanical and thermal performances. However, the covalent bonding is still considered less than satisfactory as a result of the inadequate oxygen functional groups in GNP (Zhang et al. 2016).

On the other hand, non-covalent functionalization basically involves the van der Waals, electrostatic, π-π stacking, and hydrophobic forces, which require the physical adsorption of the corresponding molecules to the surface of GNP (Ijeomah et al. 2017). This approach has been exploited to tailor the interfaces between GNP and the organic media or to control interfaces within GNP network (Eleuteri et al. 2019). Poly(ethyleneimine) (PEI) is a polycationic polymer that is highly water soluble owing to ethylamine repeating units. The layers of GNP are able to gather the active amino groups in PEI for surface modification with some functional groups like carboxyl or epoxy groups (Abd Razak et al. 2015b).

3.1.3 Natural Rubber and Synthetic Rubber

A typical elastomer compound is mainly made from long chain molecules as known as the base polymer which contribute the basic physical and chemical properties. There is a small amount of free space which exists between the long chain molecules where this space permits the independent mobility of the elastomeric molecules, and causes the subsequent deformation (Mohamad et al. 2017). Due to the ease of deformation at ambient condition, good resistance to heat, superior flexibility and elongation before breaking, elastomers or rubbers are extensively used in various engineering industrial sectors such as packaging, aerospace, automotive and healthcare (Li et al. 2017). Rubbers possess good energy absorbing and mechanical (elasticity) properties which drive the commercial use of rubbers as polymeric matrices (La et al. 2018).

Natural rubber (NR) is the largest single type rubber which produced from latex, and NR has been extensively studied for practical applications in the field of automotive tires, footwear, gloves and condom (Mohamad et al. 2017; Srivastava and Mishra 2018). This is owing to biodegradability characteristic, and excellent mechanical properties such as high elasticity, cracking resistance and etc. However, for practical uses, the requirement of natural rubber is essential to enhance the

physical and mechanical properties, to promote processability and flexibility in product design, as well as to reduce the production cost (Mohamad et al. 2017). On the other hand, the most common important synthetic rubbers are ethylene-propylene-diene-monomer (EPDM), silicone rubber, acrylonitrile butadiene rubber, styrene butadiene rubber, ethylene vinyl acetate copolymer, and butyl rubber, etc. These synthetic elastomers are manufactured in the purpose to replace or to be combined with NR in making polymeric matrix with superior properties of NR (Srivastava and Mishra 2018).

In recent years, the elastomeric blends of NR and EPDM synthetic rubber have been extensively employed for investigation owing to their excellent heat and ozone resistance as well as superior performance in the tire application (Motaung et al. 2011). It is evident that the low environmental and ozone resistance of the NR can be improved by mixing highly unsaturated NR with the highly saturated and non-reactive EPDM (Alipour et al. 2013). Besides, the blending of high cost EPDM with the low cost NR could suit the economic aspects as the appreciable price difference can be balanced with outstanding performances.

3.2 Materials

The commercial grade of SMR 20 natural rubber (NR) obtained from Mentari Equipment and Project Sdn. Bhd., Malaysia was 0.16 wt.% dirty retained on 44 apertures, 1.00 wt.% ash content, 0.60 wt.% nitrogen, 0.80 wt.% volatile subject, 30 min Wallace rapid plasticity (Po) and 40 min. % of plasticity retention index (PFU). Ethylene propylene diene rubber (EPDM) grade BUNA EPT 9650 was supplied by LANXESS, Pittsburgh, USA with the Mooney viscosity UML (1 + 8) at 150 °C of 60 ± 6 MU, ethylene content of 53 ± 4 wt%, ENB content of 6.5 ± 1.1 wt% with volatile matter ≤0.75 wt%, specific gravity of 0.86 and total ash ≤0.50 wt% with non-staining stabilizer. Both rubbers were masticated with two-roll mill prior to their use. Other compounding ingredients such as stearic acid, sulphur and zinc oxide were purchased from Systerm/Classic Chemical Sdn. Bhd., and tetramethyl thiuram disulfide (TMTD) from the Aldrich Chemistry, whereas N-cyclohexylbenthiazyl sulphenamide (CBS) and N-(1,3-Dimethylbutyl)-N′-phenylp-phenylenediamine (6PPD) were supplied by Flexys America, USA. All ingredients were used as received. Graphene nanoplatelets (GNP) in black and gray powder form, grade KNG-150, was purchased from the Xiamen Graphene Technology Co. Ltd., China. It has a bulk density of 0.3 g/cm^3, a true density of 2.25 g/cm^3, a specific surface area of 40–60 m^2/g and a carbon content of >99.5. Aminopropyltryetoxysilane (ATPS) and poly(ethyleneimine) (PEI) were purchased from Sigma-Aldrich and were used without further purification. APTS has a linear formula of $H_2N(CH_2)_3Si(OC_2H_5)_3$, an average molecular weight (Mw) of 221.37 g mol^{-1} and a density of 0.946 g ml^{-1} at 25 °C. PEI, in the form of a viscous colorless liquid of branched polymer, has a linear formula of $H(NHCH_2CH_2)nNH_2$,

an average molecular weight (Mw) of 25,000 g mol^{-1} and a density of 1.030 g ml^{-1} at 25 °C.

3.3 Methods

3.3.1 ATPS-Dehydration and PEI-Adsorption of GNP

In this study, both surface treatment of GNP was performed via chemical modification of the exfoliated graphite flakes, which was adapted from Ganguli et al. (Ganguli et al. 2008). The mixture of solvent water: ethanol at the ratio of 25:75 was prepared for every treatment mixture of 2 g GNP and 3 g ATPS or PEI in the 1000 ml of solution mixture. The combination of mechanical stirring using high speed mixer (WiseStir HT50DX) at 1000 rpm and ultrasonication effect using ultrasonic bath set-up (JE10Tech UC-02) at 60 °C was performed for 5 hours. Next, the treated GNP was stirred using a hot-plate magnetic stirrer for 100 rpm, 100 °C for 45 min. Then, GNP was washed using distilled water as to remove the unreacted chemicals. Further oven heating at 150 °C was performed at 5 hrs for complete drying. The dried GNP product was grinded using agate mortar and placed in a close-sealed container.

3.3.2 Preparation of NR/EPDM Rubber Blend Filled GNP Nanocomposites

The compounding process was performed using a Haake Rheomix internal mixer with Banbury rotor type at 0.70 fill factor at 70 rpm of rotor speed and 70 °C of blending temperature for about 5 min mixing period. The formulations recipes used in the preparation of NR/EPDM blend were NR/EPDM blend (70,30 phr), EPDM-grafted-maleic anhydride 1.30 phr, 5.0 phr ZnO, 2.0 phr stearic acid, 2.0 phr 6-PPD, 1.0 phr CBS, 0.3 phr TMTD and 1.5 phr sulphur. The percentage of GNP was varied at a 0.00, 0.25, 0.50, 1.00, 3.00, 5.00 wt.%. On mixing procedure (Fig. 3.1), at first, NR, EPDM and EPDM-g-MAH compatibilizer were blended for 1 min before the

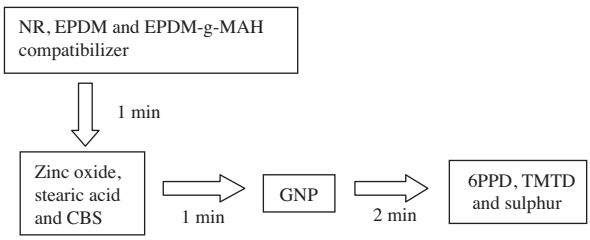

Fig. 3.1 Schematic flow of mixing sequence for nanocomposite preparation

first set of curatives consisted of zinc oxide, stearic acid and CBS were added into the internal mixer. After 2 min of mixing, the unmodified or modified GNP was compounded. Next, the second set of curatives consisted of accelerator (6PPD and TMTD) and sulphur were compounded at a minute before end of mixing period. The compound was left to stabilize for 24 hrs before characterization.

3.3.3 Characterization of Unmodified and APTS- and PEI-Modified GNP

Raman spectroscopy and Fourier-transform infra-red (FTIR) spectroscopy analysis were employed to evaluate the success of surface treatment done to the GNP. Raman spectrum was obtained using a Horiba JobinYvon model HR800 with a laser wavelength of 514.53 nm and a laser power at sample of 10 mW. The focal length used was 800 mm with drift amount of <0.015 nm sec^{-1}. FTIR analysis was performed using JASCO FT/IR 6100 setup at 0.5 cm^{-1} resolution at the range of 4000–400 cm^{-1}. The morphological evaluation was performed using Field Emission Scanning Electron Micrograph (FESEM, model Hitachi SU8000) at a magnification of 1000 x and a accelerating voltage of 2.0 kV to observe the transformation occurred on modified GNP due to the surface treatment.

3.3.4 Characterization of GNP Filled NR/EPDM Rubber Blend Nanocomposites

The cure characteristics of the blend were studied using MDR 2000 according to the ISO 3417 at 160 °C. Prior to testing, vulcanizate NR/EPDM based nanocomposites were conditioned for 24 h in a closed container at room temperature. The cure properties such as the scorch time (T_{S2}), maximum curing time (tc_{90}), minimum torque (ML), and maximum torque (MH) as well as cure rate index (CRI). CRI was calculated using the equation as: CRI = 100/ (tc90 - TS2) (Ahmed et al. 2012).

Tensile tests were conducted using a testometric tensometer Toyoseiki Strograph-R1 according to ASTM D1822. The dumbbell shaped specimens with the thickness of 2 mm were tested at a crosshead speed of 500 mm/min. At least 7 replicates of each formulation were taken for averaging purposes. The hardness measurements of the nanocomposites were carried out according to ISO 7691 -1 using a manual durometer type Shore A.

Dynamic mechanical thermal analysis was performed on the specimen with a rectangular dimension of 30 mm x 5 mm x 2 mm (length x width x thick) using TA Instruments DMA Q-800. Measurements were carried out from −100 °C to 100 °C at a frequency of 5 Hz, amplitude of 15 μm and heating rate of 5 °C/min.

3.4 Results and Discussion

3.4.1 Characterizations of GNP

Figure 3.2 portrays the Raman of unmodified, ATPS- and PEI-modified GNP. It is observed that there are three main characteristic peaks presented at around 1370–1375 cm^{-1}, around 1600–1610 cm^{-1} and around 2710–2740 cm^{-1} which are representing D band, G band and 2D band, respectively. It is found that the intensity of the G band and D band for the PEI–modified GNP becomes weaker than that of unmodified GNP. This phenomenon suggests that PEI-treatment results in a higher level of disorder and the formation of defects in the modified graphene layers. As reported in our previous study, G band indicates the intact nature of GNPs' graphitic domain, whereas the D band is a characteristic of defects and disorder (Abd Razak et al. 2015b). The analysis of 2D band peak could examine the arrangement and stacking of GNP layers (Kim et al. 2010). Comparing to unmodified GNP, the intensity of this band peak is lower for ATPS-modified GNP but is higher for PEI-modified GNP. Another strong vibration peak at 2081.11 cm^{-1} is only shown for ATPS-modified (covalent treatment) GNP which attributed to the formation of covalent bonds of C=C bond between the GNP and ATPS.

Besides, the ratio of D band and G band intensity (ID/IG) for ATPS-modified GNP (ID/IG = 0.379) is remarkably increased than those of unmodified GNP (ID/IG = 0.314) and PEI-modified GNP (ID/IG = 0.250). This indicates the transformation of some sp^3 carbon due to the covalent functionalization of GNP after the ATPS

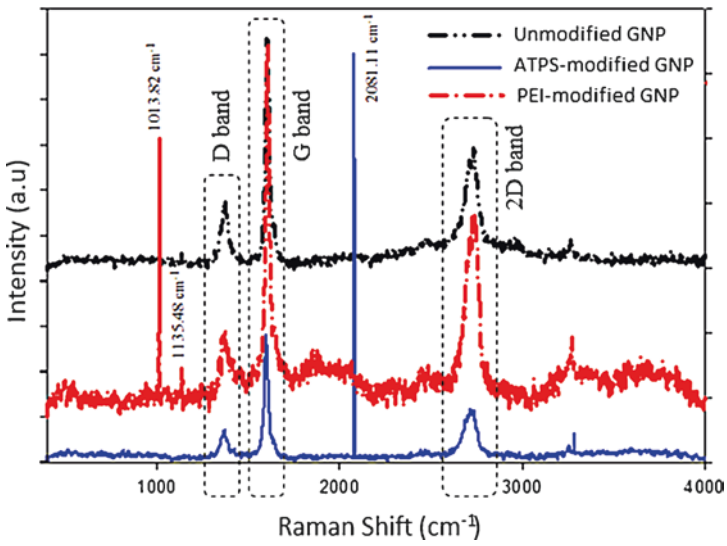

Fig. 3.2 Raman spectra of unmodified, ATPS- and PEI-modified GNP
(Part of the work published in (Abd Razak et al. 2015b))

treatment (Fang et al. 2009; Shen et al. 2010). Higher G mode of ATPS-modified GNP than that of untreated GNP confirmed the higher level of disorder for ATPS-modified GNP which relates to random arrangement of GNP layers. These situations might increase the possibilities for molecular chain of rubber into the interlayer space of the intercalated GNP and thus enhance the mechanical interlocking between the rubber blend and the surface of treated GNP for better interfacial interaction. In the case of PEI-modified GNP, the lower ID/IG ratio is corresponded to its high structural integrity caused from PEI treatment (Ma et al. 2014) where this non-covalent treatment done on GNP does not only promotes the disturbance on the arrangement and defects of platelets, but also improves the structure of GNP by physical adsorption.

The FTIR spectra of unmodified, ATPS- and PEI-modified GNP are shown in Fig. 3.3. The presence of absorption band at below ~1000 cm^{-1} for unmodified GNP refers to the presence of trace acid group that intercalates the graphite planes. In comparison to unmodified GNP, the absorption band of 821.08 cm^{-1} is disappeared for ATPS-modified GNP. This implies the possibility of covalent treatment by ATPS occurred through dehydration mechanisms which impedes the presence of minor functional group (C-O). Besides, for ATPS-modified GNP, the shift of C-C stretching of ethyl group ($–CH_2CH_3$) at 1060–1070 cm^{-1} suggests the asymmetric of Si-O-C doublet stretching vibration. These situations confirmed the success of

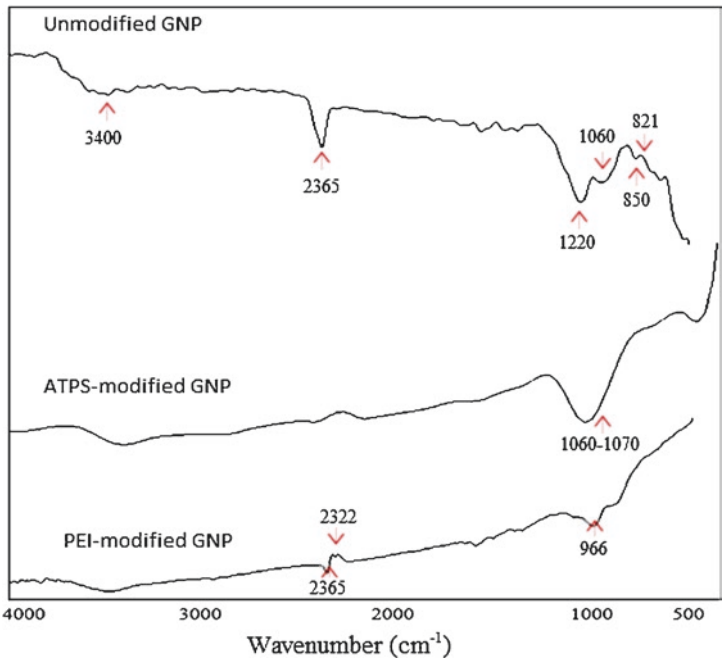

Fig. 3.3 FTIR spectra of unmodified, ATPS- and PEI-modified GNP (Abd Razak et al. 2015a)

covalent (ATPS) modifications on GNP. On the hand, for both unmodified GNP and PEI-modified GNP, there are two distinct peaks at 1069 cm^{-1} and 2365 cm^{-1} which corresponds to the skeletal C–C stretching of ethyl group (or C–O stretching) and the presence of hydroxyl group (–OH stretching), respectively. The FTIR spectrum of PEI-modified GNP displays a new weak band at 966.16 cm^{-1} which corresponds to the skeletal motion of the C–C backbone. This means that the PEI adsorption onto GNP's surface is probably to disturb the arrangement of atomic carbons in the GNP structure (hexagonal lattice) by vibrating to change the dipole moment (Stuart 2005). Also, a new peak at 2322.00 cm^{-1} is existed for PEI-modified GNP and this confirms the interaction between PEI and GNP's surface by forming the hydrogen bonding in the multiple structures of –OH related with the carboxylic acids. The presence of these two new peaks (966.16 cm^{-1} and 2322.00 cm^{-1}) confirms the success of non-covalent modification onto GNP's surface.

Figure 3.4 presents the morphological micrograph of (a) unmodified GNP, (b) ATPS-modified GNP, and (c) PEI-modified GNP. The untreated GNP is not completely exfoliated as the GNP comprises of more than monolayer (Fig. 3.4 (a)). In Fig. 3.4 (b) and (c), a clear separation (increased) interlayer spacing between GNP layers for modified GNP, either ATPS or PEI treatments, in which this confirms the exfoliation nature of modified GNP after undergone the ultrasonication and high-speed mechanical shearing treatment. In comparison to unmodified GNP (control sample), the FESEM micrographs clearly demonstrate the reduction of lateral size but inconsistency in lateral dimension that occurs in ATPS- and PEI-modified GNP. By reducing the dimension of GNP, the cohesive energy between the platelets is reduced and the dispersion of filler in the polymer matrix is improved (Sridhar et al. 2013), as demonstrated in FESEM micrographs.

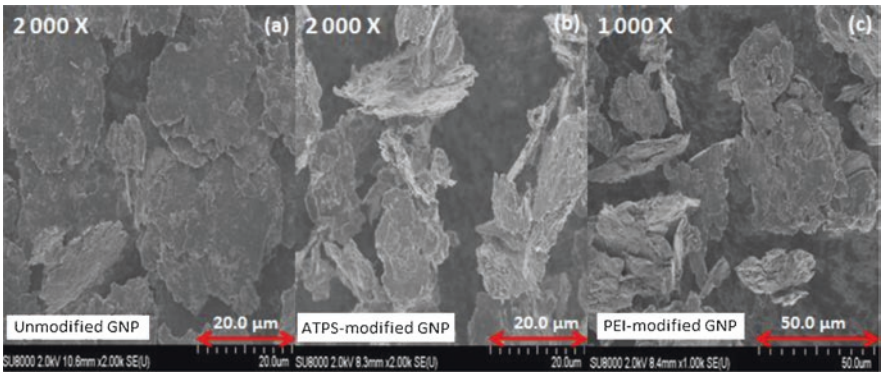

Fig. 3.4 FESEM micrograph of unmodified, ATPS- and PEI-modified GNP (Abd Razak et al. 2015a)

3.4.2 Cure Characterization Studies

The results of scorch time (T_{s2}) with respect of GNP loadings and GNP modifications are plotted in Fig. 3.5. T_{s2} is described as the time required for the state of cure to increase about two torque units higher than the minimum at a given temperature (Nabil et al. 2013). GNP-filled nanocomposites possess a lower scorch safety with an increase of GNP loading than that of the unfilled NR/EPDM blend. However, the NR/EPDM/PEI-modified GNP system has a higher value of T_{s2} than that of NR/EPDM/ATPS-modified GNP system. This means the functionalization of ATPS and the adsorption of PEI polymeric layer onto the surface of GNP tend to improve the interaction between rubber-filler interface, and thus promoting the fast curing of NR/EPDM blend. This phenomenon is due to the high thermal conductivity factor induced by GNP nanomaterial where this has aided in dissipating the heat efficiently and thereby promote the maturation reaction process (Abd Razak et al. 2015b).

Maximum curing time, tc_{90} is defined as the time needed to achieve 90% of full cure where most of the physical properties at this cure state reach their optimum. Figure 3.6 illustrates the tc_{90} of NR/EPDM filled with various loading of unmodified, ATPS-modified GNP, and PEI-modified GNP nanocomposites. It is found that the tc_{90} decreases with the increasing GNP loading for all NR/EPDM blend nanocomposite systems, due to the heat transfer in the nanocomposites is further enhanced by the presence of active GNP filler, thereby encouraging the fulfillment of molds during the vulcanization process. However, NR/EDPM blends incorporated with modified GNP exhibit lower tc_{90} values at all GNP loadings than that of the blends filled with unmodified GNP. This implies that the surface modifications

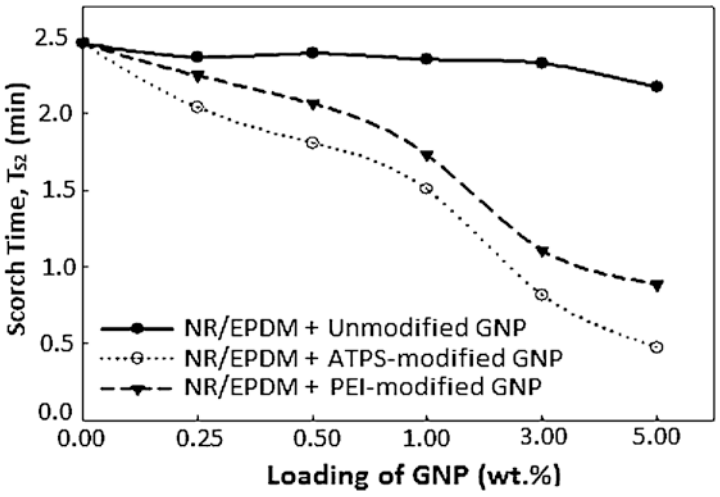

Fig. 3.5 Scorch time (T_{s2}) of NR/EPDM filled with various loading of unmodified, ATPS-modified GNP, and PEI-modified GNP nanocomposites

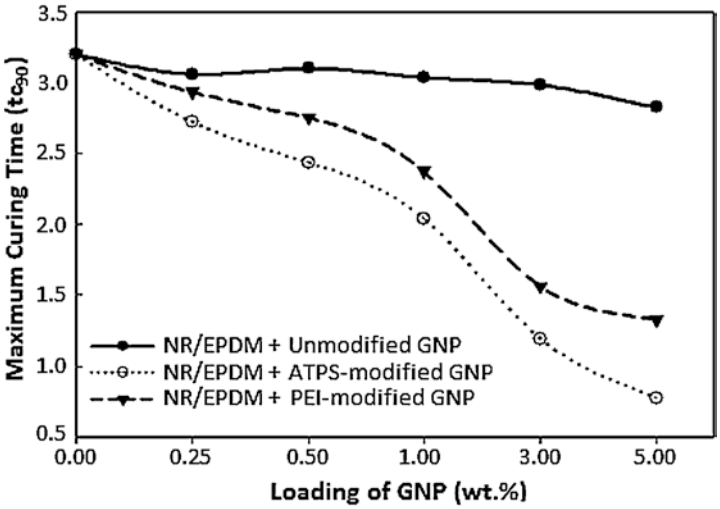

Fig. 3.6 Maximum curing time (tc_{90}) of NR/EPDM filled with various loading of unmodified, ATPS-modified GNP, and PEI-modified GNP nanocomposites

of GNP improve the solubility of GNP with the additional surface chemistry on GNP, and also induce a reduction in their lateral dimension size. These may assist the crosslinking during the vulcanization time for accelerated formation of polysulfide (Konar et al. 2010). Hence, the introduction of ATPS- and PEI-modified GNPs–PEI aids to efficiently cure the NR/EPDM blends with the acceleration of the vulcanization process, as evidence by the reduction of T_{s2} and tc_{90}.

Figure 3.7 and 3.8 show the maximum torque (MH) and maximum torque (ML) of NR/EPDM filled with various loading of GNP in the nanocomposites. MH is the maximum torque that is achieved during the curing time, and is a representative of the vulcanizated strength of rubber blend-based compounds or the crosslinking degree in the elastomer. Meanwhile, ML is the minimum torque measured in the rheometer that is oftenly correlated well with the Mooney viscosity of a compound, and ML is an indicator to the uncured stock's elastic modulus. A higher torque obtained indicates the higher number of crosslinks created (Abd Razak et al. 2015b). Overally, the incorporation of modified GNP increases the MH and ML with the increased filler loading. Unlike unmodified GNP, its NR/EPDM blend nanocomposites show a fluctuating pattern and static trend for both MH and ML, respectively, which indicating the less processability of the nancomposites. From another angle, nanocomposites containing ATPS- and PEI-modified GNP averagely exhibit higher MH and ML values as compared to the one with unmodified GNP. This is attributed to the sufficient filler wetting characteristics resulted from the enhanced filler interaction with NR/EPDM macromolecules network. The addition of modified GNP increases the processing load because of the increased flow resistance that caused by smaller sized GNP as well as the formation of percolation structures by the edge-to-edge and edge-to-face interactions between the dispersed layers. Therefore, this

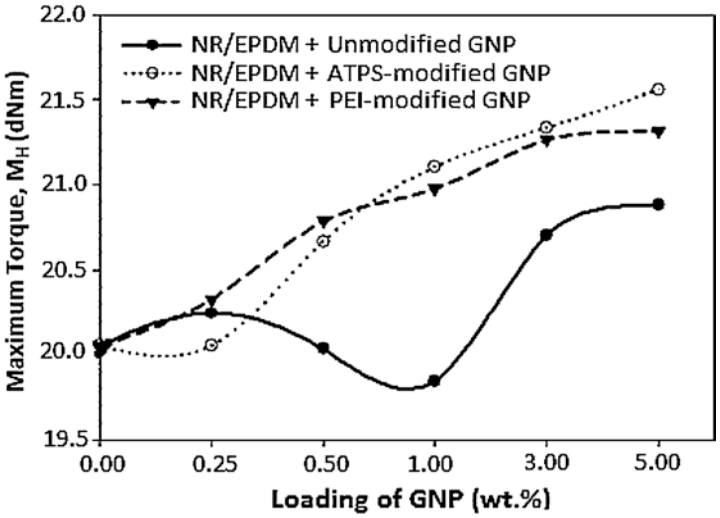

Fig. 3.7 Maximum torque (MH) of NR/EPDM filled with various loading of unmodified, ATPS-modified GNP, and PEI-modified GNP nanocomposites

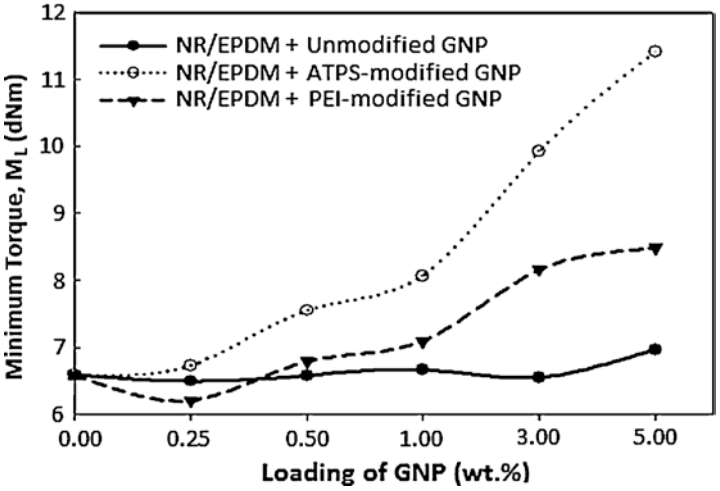

Fig. 3.8 Minimum torque (ML) of NR/EPDM filled with various loading of unmodified, ATPS-modified GNP, and PEI-modified GNP nanocomposites

factor strongly hinders the molecular movement of macromolecules and thus leading to an increase in the processing torque behavior (Konar et al. 2010).

The torque difference (MH – ML), a measurement of the vulcanization extent and accomplishment of a characteristic network chains (Konar et al. 2010), of NR/EPDM nanocomposites filled with various loading of GNP is portrayed in Fig. 3.9. The NR/EPDM nanocomposites filled with unmodified GNP show a uniform

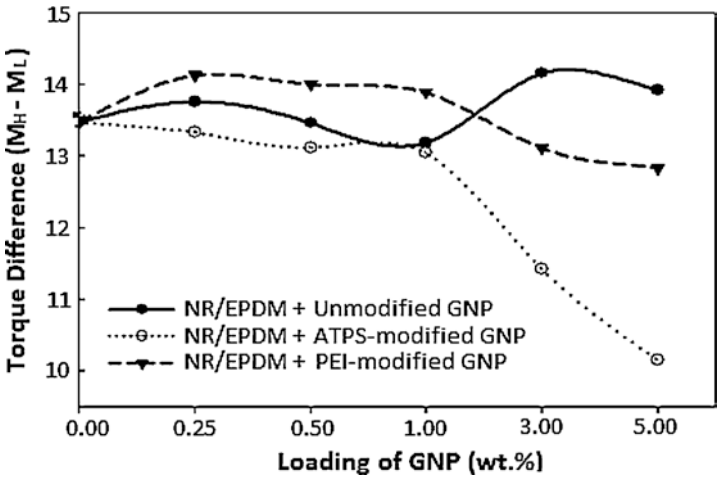

Fig. 3.9 Torque difference (MH – ML) of NR/EPDM filled with various loading of unmodified, ATPS-modified GNP, and PEI-modified GNP nanocomposites

fluctuating plot pattern for the torque difference with the increased loading of unmodified GNP. The fluctuation of MH - ML torque values indicates the possibility of a non-uniform cross-distribution phenomenon because of the incompatible maturation condition between the NR (highly unsaturated) and EPDM (highly saturated) rubber components, thereby resulting in an uneven distribution of crosslink density (Nabil et al. 2013) and inferior mechanical properties of the NR/EPDM filled unmodified GNP. Meanwhile, the nanocomposites filled with modified GNP present a decreasing trend of (MH - ML) values with the increase of GNP loading. The NR/EPDM filled ATPS-modified GNP seems to have a significantly reduced profile as compared to nanocomposites incorporated with PEI-modified GNP at all range of loadings. In the case of PEI-modified GNP nanocomposites, the presence of the PEI polymers absorbed on the surface of GNP has resulted in the disruption of the formation of continuous crosslinks and interactions between the rubber phases in the blends. This is ascribed to the uniform isolation and dispersion of PEI-modified GNP as compared to the unmodified GNP filled nanocomposites. The more the PEI-modified GNP presented, the lower the torque difference value, as a result of the reduced crosslinking formed in the NR/EPDM blend matrices. In contrast, the decline trend for ATPS-modified GNP nanocomposites is insignificant with the GNP loading.

The plot of cure rate index (CRI) versus the GNP loading for three nanocomposite systems is presented in Fig. 3.10. There is no considerable variation observed in the CRI for the unmodified GNP nanocomposite system. When approximately 0.50 wt.% of unmodified GNP was introduced into the NR/EPDM blend, the CRI is found to decrease slightly. This is attributed to cure incompatibility effects resulted from the decrease in reactive sites on the surface of rubber molecules that are available for crosslinking reactions (Nabil et al. 2013). On the other hand, the CRI value

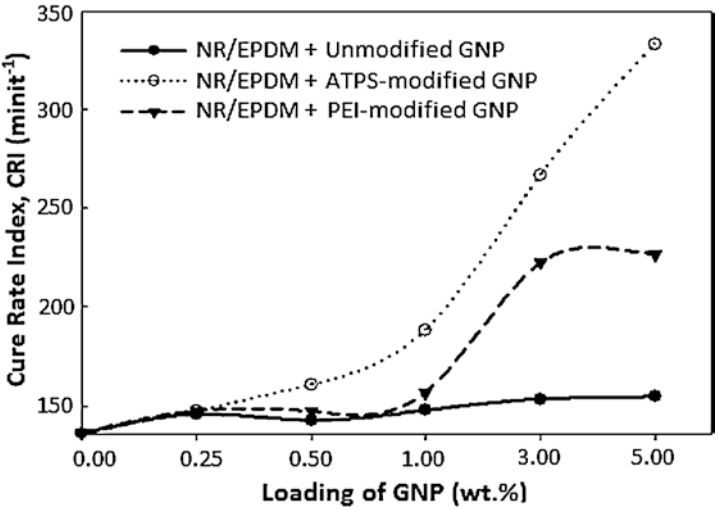

Fig. 3.10 Cure rate index (minit^{-1}) of NR/EPDM filled with various loading of unmodified, ATPS-modified GNP, and PEI-modified GNP nanocomposites

is in line with the increase in the loadings of ATPS- and PEI-modified GNP, which may be associated to the reduction of activation energy for crosslinking process (Tavakoli et al. 2011) and the increased interaction sites for vulcanization (Ahmed et al. 2012) with the presence of these two fillers.

Tensile strength, percentage of elongation, stiffness at 300% elongation (M300) and hardness Shore A of NR/EPDM nanocomposites filled with different loading and types of GNP are shown in Figs. 3.11, 3.12, 3.13, 3.14, respectively. Generally, the results clearly show that the tensile properties are significantly increased with the increase of GNP loading into the NR/EPDM matrices. However, surface modifications performed on GNP has caused the improvement in mechanical properties with the increasing filler loading, up to the certain filler loading, before the occurrence of decline of the improvement rate in tensile results at certain much of filler. By comparing the effect of surface modifications on GNP, nanocomposites filled with ATPS- and PEI-modified GNP experience a slightly improvement in tensile properties as compared to NR/EPDM nanocomposites filled with unmodified GNP at all loadings.

3.4.3 Mechanical Properties

As shown in Fig. 3.11, it is found that the tensile strength drastically increases up to 104–124% when 5.00 wt.% of ATPS- and PEI-modified GNP are added into NR/EPDM blend as compared to the unfilled blend. The maximum improvement of tensile strength obtained by ATPS-modified GNP nanocomposites indicates that the

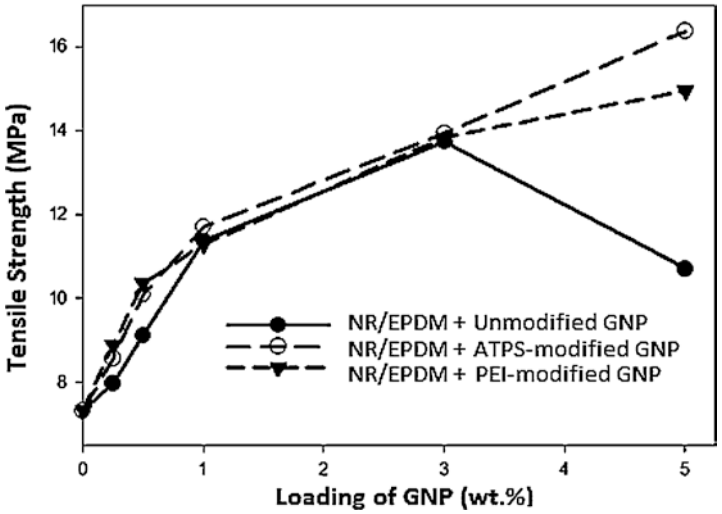

Fig. 3.11 Tensile strength of NR/EPDM filled with various loading of unmodified, ATPS-modified GNP, and PEI-modified GNP nanocomposites

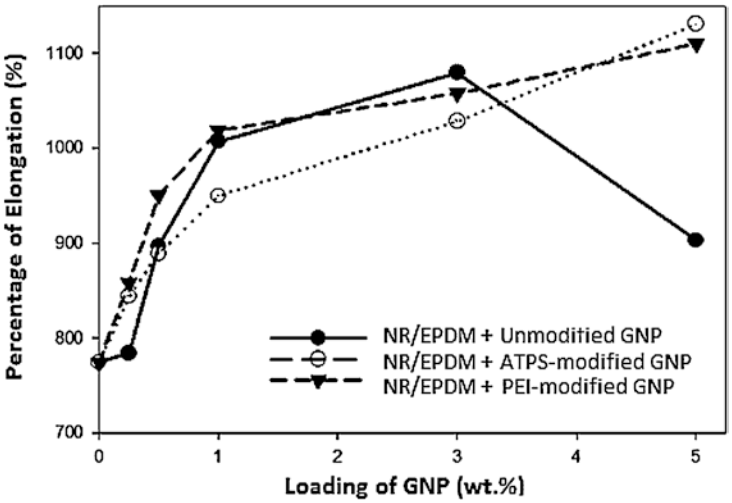

Fig. 3.12 Percentage of elongation of NR/EPDM filled with various loading of unmodified, ATPS-modified GNP, and PEI-modified GNP nanocomposites
(Razak et al. 2015; Razak et al. 2014)

covalent treatment aids the separation and intercalation between filler platelets as well as increases the surface wetting (Razak et al. 2014). Surface modification of GNP using PEI treatment succeeds in enhancing the mechanical performance of NR/EPDM blends by creating retention effects among GNP upon the adsorption of the polymeric layer of PEI, and the oxygen-containing groups in the GNP introduce

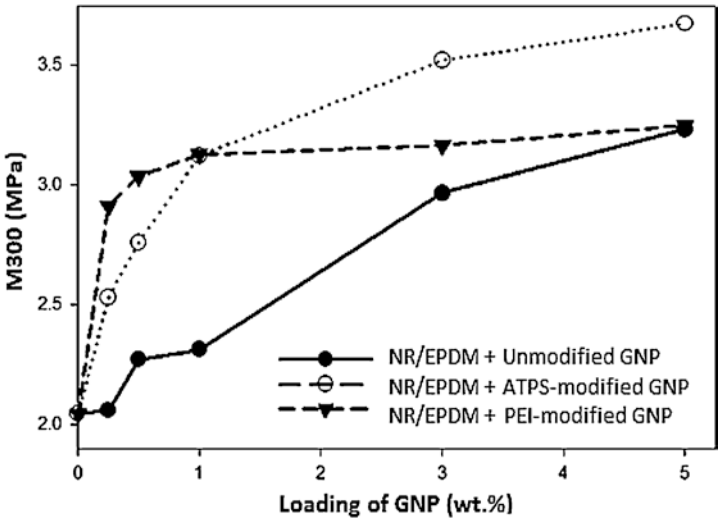

Fig. 3.13 Stiffness at 300% elongation (M300) of NR/EPDM filled with various loading of unmodified, ATPS-modified GNP, and PEI-modified GNP nanocomposites (Razak et al. 2015; Razak et al. 2014)

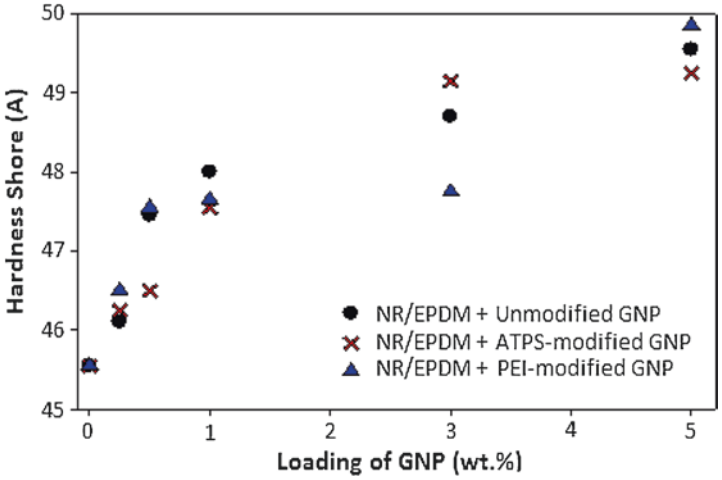

Fig. 3.14 Shore A hardness of NR/EPDM filled with various loading of unmodified, ATPS-modified GNP, and PEI-modified GNP nanocomposites

the polar interations between PEI-modified GNP sheets and polar polymer matrices, thereby results in the better filler dispersion within the NR/EPDM blend (Zhang et al. 2012). At the same filler loading of 5.00 wt.%, a reduction in tensile strength is encountered for nanocomposite system with unmodified GNP which is due to the agglomeration of GNP that allowing the pre-mature failure (Abd Razak et al. 2015b).

For percentage of elongation in Fig. 3.12, an overall increasing trend is clearly similar to tensile strength. The percentage of elongation increases dramatically with the increase of GNP loading in the NR/EPDM blend matrices. However, this phenomenon only applies to the nanocomposites filled with modified GNP, but not to the nanocomposites with unmodified GNP. Nanocomposites based on the unmodified GNP experience a major decrease in percentage of elongation value due to the induction of some weak points by the agglomeration of GNP in which this facilitates a pre-mature failure when the stress is applied. This suggests poor interfacial interactions and adherence between unmodified GNP and NR/EPDM matrices, and thus probably causes to reduction in the mechanical properties of filled rubber (Arayapranee and Rempel 2008). In the case of ATPS-modified GNP nanocomposites, the elongation values are slightly lower than those of other nanocomposite systems, at the loading of ATPS-modified GNP less than 5.00 wt.%. This situation shows that the interaction of rubber blend matrices with the ATPS-modified GNP is increasing because of the presence of the functional groups that forms the links between the nanofillers and matrices. In which this benefits the improvements of the stiffness properties. For PEI modification, this nanocomposite system has appreciably higher values of the percentage of elongation than the other two nanocomposite systems, for almost all loadings used. This can be ascribed to the even dispersion and distribution of PEI-modified GNP within the rubber blend matrices. Additionally, the physical adsorption of PEI on the GNP's surface is only bonded by the weak van Der Waals and this has increased the capability of GNP and rubber blend macromolecular for slippage. Therefore, the elongation ability is increased (Abd Razak et al. 2015b).

The stiffness at a specific elongation points of 300% (M300) for nanocomposites with various modifications and filler loadings are plotted as shown in Fig. 3.13. Generally, as the nanofillller (with and without surface modification) loading increases, the M300 values are noted to increases nonlinearly. This positive trend is the manifestation of the reinforcement effect imparted by GNP in the NR/EPDM rubber matrices. This finding was in agreement with the previous work reported on other rubber blend systems incorporated with various kinds of filler (Sae-oui et al. 2007; Shehata et al. 2006). In comparison of the surface modification strategies, it is noted that ATPS-modified GNP nanocomposites possesses the highest M300 values, followed by PEI-modified GNP nanocomposites and lastly for nanocomposites filled with unmodified GNP. The improvement for NR/EPDM blend nanocomposites filled with modified GNP is contributed to the lamellar structure of GNP which allowing a better wettability and rubber–nanofiller interactions induced by the hydrogen and van der Waals forces, and hence causing to a better stress transfer (Sridhar et al. 2013).

As observed in Fig. 3.14, Shore A hardness shows an increasing trend with the increase of GNP loading. The hardness value for unfilled NR/EPDM blend is 45.5 and the optimum value up to 49.8 for NR/EPDM blend nanocomposites filled with 5.00 wt.% PEI-modified GNP. The increase in hardness properties is related to the high strength of the resultant nanocomposites (Arroyo et al. 2007). As the value of hardness increases, the higher the amount of crosslinking content found in the blend

matrices, and the more effective reinforcement mechanism introduced by the presence of added GNP fillers. In the aspect of surface modification effects, it is found that at 3.00 wt.% GNP, the trend of Shore A hardness is as follows: NR/EPDM/APTS-modified GNP > NR/EPDM/unmodified GNP > NR/EPDM/ PEI-modified GNP.

3.4.4 Dynamic Mechanical Thermal Analysis

Storage modulus (E') refers to the energy stored elastically during deformation, which indicates the elasticity of a material (Chen et al. 2015). Figure 3.15 shows the storage modulus of NR/EPDM-based nanocomposites containing GNP with different surface modifications as a function of temperature. It can be observed that the E' values in the glassy region (around -50 °C) appeared in a sharp peak, following the descending trend as: NR/EPDM/APTS-modified GNP > NR/EDPM/unmodified GNP > NR/EDPM > NR/EDPM/PEI-modified GNP. This finding confirms the efficiency of APTS-modified GNP to act as active filler which provide the reinforcement effect to NR/EPDM (Karger-Kocsis et al. 2010). In the case of non-covalent treatment (with APTS), the addition of GNP had increased the energy stored in the NR/EDPM blend nanocomposites, thereby showing higher E' values. The improvement of E' implies the increased filler/matrix interfacial which thereby reducing the mobility of chains in which caused to the increased stability of nanocomposites with the increasing temperature. Therefore, the E' decreases with the temperature.

Loss modulus (E") is the energy being dissipated or replaced as heat during the deformation of a material, which is associated with the material's viscous behavior

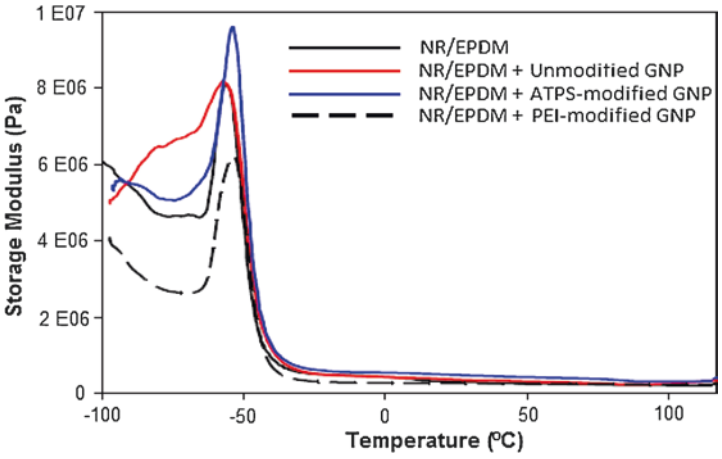

Fig. 3.15 Plots of storage modulus versus temperature for NR/EPDM nanocomposites filled with various modification of GNP
(Part of the work published in (Razak et al. 2017))

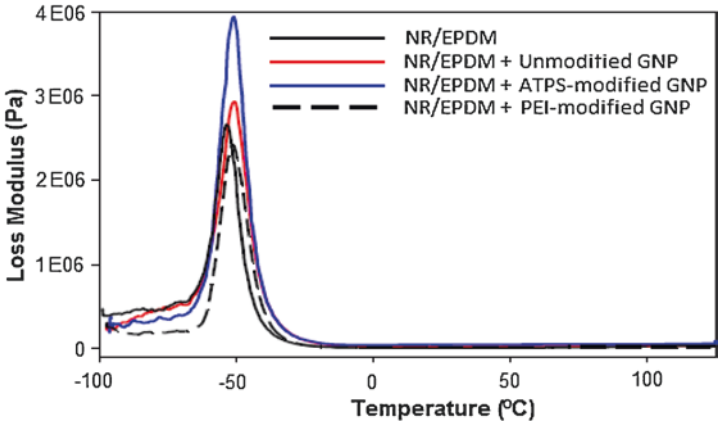

Fig. 3.16 Plots of loss modulus versus temperature for NR/EPDM nanocomposites filled with various modification of GNP
(Part of the work published in (Razak et al. 2017))

(Chen et al. 2015). The E" of NR/EPDM-based materials as a function of temperature is demonstrated in Fig. 3.16. At glass transition temperature, relaxation process allows the greater movement of individual chains in the NR/EPDM blends irrespective of GNP. This can be seen from the highest values of E" at around −50 °C in Fig. 3.16. Similarly, the E" peak for NR/EPDM nanocomposites filled with APTS-modified GNP is higher than that of unmodified GNP. This shows that covalent surface modification of GNP via APTS could increase the heat dissipation characteristics. The lesser heat entrapment in NR/EPDM reinforced with APTS-modified GNP has resulted in the consequent lacking of heat build-up in comparison to other investigated materials. Another reason for the improved E" in ATPS-modified GNP filled NR/EPDM nanocomposites is that APTS-modified GNP improved rubber-filler interface bond strength which is required to activate the immobilization of filler towards the stress transfer in the region of matrix-filler interface. There is another observation shown in Fig. 3.15, the broadening E" peak is as the following trend: NR/EDPM/APTS-modified GNP > NR/EDPM/unmodified GNP > NR/EDPM = NR/EDPM/PEI-modified GNP. The broaden modulus peak indicates the greater immobilization being introduced onto amorphous phase or molecular chains in NR/EDPM (induced by GNP particles) (Jayalatha and Kutty 2013).

3.4.5 Comparison of Mechanical Properties With Previous Studies

Table 3.1 describes the comparison of mechanical properties with previously reported work on NR/EDPM blend composite materials with different loadings of GNP. Generally, higher values of elongation at break (780–900% for untreated GNP

Table 3.1 Comparison of mechanical properties with previous studies

Matrix	GNP loading, (treatment)	Tensile Strength, MPa	Elongation at break, %	M300, MPa	Shore Hardness, A	Source
NR/ EDPM	0.25 wt.% (unmodified) (modified) 5 wt.% (unmodified) (modified)	 8 9 (PEI) 11 16 (APTS)	 780 850 (PEI) 900 1100 (APTS)	 2.1 2.9 (PEI) 3.1 3.6 (APTS)	 46 46.5 (PEI) 49.5 50 (APTS)	Current study
NR latex	3% (unmodified)	18–20	600	5	38–45	Charoenchai et al. (Charoenchai et al. 2019)
NR	5 phr 20 phr (unmodified)	18–24 14–23	–	–	56–58 68–72	Li et al. (Li et al. 2017)
Styrene butadiene rubber (S-SBR)	1 phr 25 phr (unmodified)	2.96 7.16	436 464	–	–	Das et al. (Das et al. 2012a; Das et al. 2012b)

and 850–1100% for APTS-modified GNP) are obtained from this study as compared with previous studies on natural rubber/GNP. However, the tensile strength and hardness are found to be comparable (or slightly lower) to the previously published works based on the similar content of GNP. This could be due to the use of NR/EDPM blend as matrix, instead of solely NR as used by previous research, which is likely to improve the elongation characteristic of rubber material.

3.5 Conclusion

This study has shown that covalent and non-covalent surface modifications of GNP with ATPS and PEI were successfully performed by a combination method of ultrasonication and high shear mechanical stirring procedure. The nanocomposites were prepared by dispersing the GNP in the NR/EPDM blend using the internal melt mixing procedure, and followed by curing under the semi-EV vulcanization system. A strong vibration band in Raman peak at 2081.11 cm^{-1} which corresponded to the formation of covalent bonds of C=C between the GNP and ATPS, as well as the disappearance of 821.08 cm^{-1} in FTIR spectrum confirmed the ATPS surface modification mechanism through dehydration. For PEI-modified GNP, the FTIR spectrum presented the presence of a new weak band at 966.16 cm^{-1} which referred to the skeletal motion of the C–C backbone, thus confirming an adsorption of the polymeric PEI into GNPs surface. The increasing GNP nanofiller loading in the NR/EPDM rubber blend promoted the processability of the blend by increasing the T_{s2} and CRI. By adding 5.00 wt.% ATPS- and PEI-modified GNP, approximately 124%

and 104% increments in tensile strength were obtained. In term of dynamic mechanical properties, the covalent modification (ATPS-modified GNP) appeared to be more suitable treatment for GNP than non-covalent method in giving the effective improvement. It can be concluded that the incorporation of GNP accelerated the curing process of rubber blend so to reduce the time and cost of the rubber blend vulcanization and product preparation cycle, as well as provided a remarkable improvement in mechanical properties of resultant nanocomposites.

Acknowledgments The authors would like to thank Universiti Kebangsaan Malaysia (UKM) and Universiti Teknikal Malaysia Melaka (UTEM) for financial support under the science fund GUP-2018-107 and PJP/2016/FKP/HI6/S01483.

References

Abd Razak J et al (2015a) Facile surface modification of Graphene Nanoplatelets (GNPs) using covalent ATPS-dehydration (GNPs-ATPS) and non-covalent Polyetherimide adsorption (GNPs-PEI) method. Appl Mech Mater 761:391–396. https://doi.org/10.4028/www.scientific.net/AMM.761.391

Abd Razak J, Haji Ahmad S, Ratnam CT, Mahamood MA, Mohamad N (2015b) Effects of poly(ethyleneimine) adsorption on graphene nanoplatelets to the properties of NR/EPDM rubber blend nanocomposites. J Mater Sci 50:6365–6381. https://doi.org/10.1007/s10853-015-9188-5

Ahmed K, Nizami SS, Raza NZ, Shirin K (2012) Cure characteristics, mechanical and swelling properties of marble sludge filled EPDM modified chloroprene rubber blends. Adv Mater Phys Chem 2:90. https://doi.org/10.4236/ampc.2012.22016

Alipour A, Naderi G, Ghoreishy MH (2013) Effect of nanoclay content and matrix composition on properties and stress–strain behavior of NR/EPDM nanocomposites. J Appl Polym Sci 127:1275–1284. https://doi.org/10.1002/app.37752

Arayapranee W, Rempel GL (2008) A comparative study of the cure characteristics, processability, mechanical properties, ageing, and morphology of rice husk ash, silica and carbon black filled 75: 25 NR/EPDM blends. J Appl Polym Sci 109:932–941. https://doi.org/10.1002/app.28111

Arroyo M, Lopez-Manchado M, Valentin J, Carretero J (2007) Morphology/behaviour relationship of nanocomposites based on natural rubber/epoxidized natural rubber blends. Compos Sci Technol 67:1330–1339. https://doi.org/10.1016/j.compscitech.2006.09.019

Bhattacharya M (2016) Polymer nanocomposites—a comparison between carbon nanotubes, graphene, and clay as nanofillers. Materials 9:262. https://doi.org/10.3390/ma9040262

Charoenchai M, Tangbunsuk S, Keawwattana W (2019) Influence of Graphene Nanoplatelets on silica-filled natural rubber composites: dispersion mixing and effect on thermal stability, rheological and mechanical properties. In: Materials science forum. Trans Tech Publ, pp 100–104. https://doi.org/10.4028/www.scientific.net/MSF.943.100

Chen RS, Ab Ghani MH, Ahmad S, Salleh MN, Tarawneh MA (2015) Rice husk flour biocomposites based on recycled high-density polyethylene/polyethylene terephthalate blend: effect of high filler loading on physical, mechanical and thermal properties. J Compos Mater 49:1241–1253. https://doi.org/10.1177/0021998314533361

Chen RS, Mohd Amran NA, Ahmad S (2018) Reinforcement effect of nanocomposites with single/hybrid graphene nanoplatelets and magnesium hydroxide. J Therm Anal Calorim. https://doi.org/10.1007/s10973-018-7935-y

Das A, Kasaliwal GR, Jurk R, Boldt R, Fischer D, Stöckelhuber KW, Heinrich G (2012a) Rubber composites based on graphene nanoplatelets, expanded graphite, carbon nanotubes

and their combination: a comparative study. Compos Sci Technol 72:1961–1967. https://doi.org/10.1016/j.compscitech.2012.09.005

Das A et al (2012b) Rubber composites based on graphene nanoplatelets, expanded graphite, carbon nanotubes and their combination: a comparative study. 72:1961–1967

Eleuteri M, Bernal M, Milanesio M, Monticelli O, Fina A (2019) Stereocomplexation of poly(lactic acid)s on graphite Nanoplatelets: from functionalized nanoparticles to self-assembled nanostructures. Front Chem 7:176–176. https://doi.org/10.3389/fchem.2019.00176

Fang M, Wang K, Lu H, Yang Y, Nutt S (2009) Covalent polymer functionalization of graphene nanosheets and mechanical properties of composites. J Mater Chem A 19:7098–7105. https://doi.org/10.1039/B908220D

Ganguli S, Roy AK, Anderson, DP (2008) Improved thermal conductivity for chemically functionalized exfoliated graphite/epoxycomposites. Carbon 46:806-817. https://doi.org/10.1016/j.carbon.2008.02.008

Ijeomah G, Samsuri F, Md Zawawi MA (2017) A review of surface engineering of Graphene for electrochemical sensing applications. J Eng Technol 8:1–31. https://doi.org/10.15282/ijets.8.2017.1.1.1076

Jayalatha G, Kutty SK (2013) Effect of short nylon-6 fibres on natural rubber-toughened polystyrene. Mater Des 43:291–298. https://doi.org/10.1016/j.matdes.2012.05.020

Karger-Kocsis J, Felhös D, Xu D (2010) Mechanical and tribological properties of rubber blends composed of HNBR and in situ produced polyurethane. Wear 268:464–472. https://doi.org/10.1016/j.wear.2009.08.037

Kim H, Abdala AA, Macosko CW (2010) Graphene/polymer nanocomposites. Macromolecules 43:6515–6530. https://doi.org/10.1021/ma100572e

Konar B, Roy S, Pariya T (2010) Study on the effect of nano and active particles of alumina on natural rubber–alumina composites in the presence of epoxidized natural rubber as compatibilizer. J Macromol Sci Part A Pure Appl Chem. 47:416–422. https://doi.org/10.1080/10601321003659531

Kuan C-F, Chiang C-L, Lin S-H, Huang W-G, Hsieh W-Y, Shen M-Y (2018) Characterization and properties of Graphene nanoplatelets/XnBr nanocomposites. Polym Polym Compos 26:59–68. https://doi.org/10.1177/096739111802600107

Kuila T, Bose S, Mishra AK, Khanra P, Kim NH, Lee JH (2012) Chemical functionalization of graphene and its applications. Prog Mater Sci 57:1061–1105. https://doi.org/10.1016/j.pmatsci.2012.03.002

La DD et al (2018) A new approach of fabricating Graphene Nanoplates@natural rubber latex composite and its characteristics and mechanical properties. J Carb Res 4:50. https://doi.org/10.3390/c4030050

Li S, Li Z, Burnett TL, Slater TJ, Hashimoto T, Young RJ (2017) Nanocomposites of graphene nanoplatelets in natural rubber: microstructure and mechanisms of reinforcement. J Mater Sci 52:9558–9572. https://doi.org/10.1007/s10853-017-1144-0

Liu M, Papageorgiou DG, Li S, Lin K, Kinloch IA, Young RJ (2018) Micromechanics of reinforcement of a graphene-based thermoplastic elastomer nanocomposite. Compos Part A Appl S 110:84–92. https://doi.org/10.1016/j.compositesa.2018.04.014

Ma J et al (2014) Development of polymer composites using modified, high-structural integrity graphene platelets. Compos Sci Technol 91:82–90. https://doi.org/10.1016/j.compscitech.2013.11.017

Mohamad N et al (2017) Vibrational damping behaviors of graphene nanoplatelets reinforced NR/EPDM nanocomposites. J Mech Eng Sci 11:3274–3287. https://doi.org/10.15282/jmes.11.4.2017.28.0294

Motaung TE, Luyt AS, Thomas S (2011) Morphology and properties of NR/EPDM rubber blends filled with small amounts of titania nanoparticles. Polym Compos 32:1289–1296. https://doi.org/10.1002/pc.21150

Nabil H, Ismail H, Azura A (2013) Compounding, mechanical and morphological properties of carbon-black-filled natural rubber/recycled ethylene-propylene-diene-monomer (NR/R--EPDM) blends. Polym Test 32:385–393. https://doi.org/10.1016/j.polymertesting.2012.11.003

Razak J et al (2017) Characterization on thermal and mechanical properties of non-covalent Polyethyleneimine wrapped on Graphene Nanoplatelets within NR/EPDM rubber blend Nanocomposites. J Ad Manuf Technol (JAMT) 11:85–100

Razak JA, Ahmad SH, Ratnam CT, Mahamood MA, Yaakub J, Mohamad N (2015) Graphene Nanoplatelets-filled NR/EPDM rubber blend: effects of GNPs loading on blend process ability, mechanical properties and fracture morphology. J Polymres 9:43

Razak JA et al (2014) The effects of covalent treated graphene nanoplatelets surface modification to cure characteristic, mechanical, physical and morphological properties of NR/EPDM rubber blend nanocomposites. Adv Environ Biol:3289–3299

Sae-oui P, Sirisinha C, Thepsuwan U, Thapthong P (2007) Influence of accelerator type on properties of NR/EPDM blends. Polym Test 26:1062–1067. https://doi.org/10.1016/j.polymertesting.2007.07.004

Shehata A, Afifi H, Darwish N, Mounir A (2006) Evaluation of the effect of polymeric compounds as compatibilizers for NR/EPDM blend. Polym-Plast Technol Eng 45:165–170. https://doi.org/10.1080/03602550500373964

Shen J, Li N, Shi M, Hu Y, Ye M (2010) Covalent synthesis of organophilic chemically functionalized graphene sheets. J Colloid Interface Sci 348:377–383. https://doi.org/10.1016/j.jcis.2010.04.055

Sridhar V, Lee I, Chun H, Park H (2013) Graphene reinforced biodegradable poly (3-hydroxybutyrate-co-4-hydroxybutyrate) nano-composites. Express Polym Lett 7

Srivastava S, Mishra Y (2018) Nanocarbon reinforced rubber Nanocomposites: detailed insights about mechanical, dynamical mechanical properties, Payne, and Mullin effects. J Nanomater 8:945. https://doi.org/10.3390/nano8110945

Stuart B (2005) Infrared spectroscopy. In: Kirk-Othmer encyclopedia of chemical technology. https://doi.org/10.1002/0471238961.0914061810151405.a01.pub2

Tavakoli M, Katbab AA, Nazockdast H (2011) Effectiveness of maleic anhydride grafted EPDM rubber (EPDM-g-MAH) as Compatibilizer in NR/Organoclay Nanocomposites prepared by melt compounding. J Macromol Sci Part B 50:1270–1284. https://doi.org/10.1080/00222348.2010.507439

Wang X, Xing W, Zhang P, Song L, Yang H, Hu Y (2012) Covalent functionalization of graphene with organosilane and its use as a reinforcement in epoxy composites. Compos Sci Technol 72:737–743. https://doi.org/10.1016/j.compscitech.2012.01.027

Zhang G, Wang F, Dai J, Huang Z (2016) Effect of functionalization of graphene nanoplatelets on the mechanical and thermal properties of silicone rubber composites. Materials 9:92. https://doi.org/10.3390/ma9020092

Zhang H-B, Zheng W-G, Yan Q, Jiang Z-G, Yu Z-Z (2012) The effect of surface chemistry of graphene on rheological and electrical properties of polymethylmethacrylate composites. Carbon 50:5117–5125. https://doi.org/10.1016/j.carbon.2012.06.052

Zhao S, Xie S, Liu X, Shao X, Zhao Z, Xin Z, Li L (2018) Covalent hybrid of graphene and silicon dioxide and reinforcing effect in rubber composites. J Polym Res 25:225. https://doi.org/10.1007/s10965-018-1616-1

Chapter 4
Mechanical Properties of Nanoclay Composite Materials

Lee Ching Hao, Lee Seng Hua, Lum Wei Chen, and Khalina Abdan

4.1 Introduction

Composite materials are very important in this modern world, credited to their remarkable versatility in many fields (Lee et al. 2018, 2014). Composite materials can be classified based on their type of matrix material (Ex: polymer matrix composites), form of dispersed phase (Ex: Continuous fiber-reinforced composite materials) and type of reinforcing fibers (Ex: organic fiber composite materials) (Wang et al. 2011). Among these, polymer-based composite is one of the important types of composite materials. In response to the call for replacing conventionally used metal alloys, the market for polymer-based composites is expanding with an upward tendency. Nowadays, the application of polymeric composite is very wide, including in the field of transportation, aerospace, sport, marine etc. (Koniuszewska and Kaczmar 2016; Ayu et al. 2018; Lee et al. 2016).

In addition to their excellence performance, the properties of the polymer composites could be further improved. One of the promising methods in improving the mechanical properties of polymer materials is by incorporation of nanoparticles. Nanoclay (nC) is among the favourite type of nanoparticles. Owing to their weak Van Der Waals bonding between layers, nC can disperse into individual layer. In addition, ion exchange reactions can also be conducted to alter the surface chemistry of nC in suiting for various applications, making nC one of the most sought-after nanoparticles (Ishida et al. 2000). nCs have been applied in many sectors, in order

L. C. Hao · L. S. Hua (✉) · K. Abdan
Institute of Tropical Forestry and Forest Products, Universiti Putra Malaysia, Serdang, Selangor, Malaysia
e-mail: lee_seng@upm.edu.my

L. W. Chen
Institute of Infrastructure Engineering and Sustainability Management, Universiti Teknologi MARA, Shah Alam, Selangor, Malaysia

S. Siddiquee et al. (eds.), *Composite Materials: Applications in Engineering, Biomedicine and Food Science*, https://doi.org/10.1007/978-3-030-45489-0_4

to enhance the performances to meet the requirements of product. Packaging materials that required low gasses permeability can be enhanced by nC (Gurses 2015). Besides, poly(e-caprolactone) (PCL)/nanoclay composite has successfully demonstrated significant low water vapor permeability and inhibited about 90% of the Escherichia coli growth (Yahiaoui et al. 2015). On the other hand, halloysite clay nanotube have been applied in drug delivery to allow for controllable sustained drug release for hours, days or even weeks (Lvov et al. 2016).

Clay represents the whole class of materials that consisting layered silicates with a small quantity of metal oxides and organic matter. Generally, clay minerals can be divided into four groups, namely kaolinite, montmorillonite/smectite, illite and chlorite according to difference in their layered structure (Uddin 2008). Among these clay minerals, montmorillonite (MMT) are the most prevalently used group as reinforcing agent for polymeric composites, attributed to their superior cationic exchange capacity, greater surface area and aspect ratio (Tjong 2006). The chapter discussed the factors that influence the mechanical properties of nC composite. In addition, types of nC and the processing methods of nanocomposites are also been reviewed. As pointed out by Rafiee and Shahzadi (2019), the term "nanocomposite" represents any polymeric composites that are reinforced with agents at scale of atomic level, or nano-scale. Therefore, in this chapter, polymeric composites that are reinforced with nC are referred as nC composite. Last but not least, modification of nC and type of matrix has also been described.

4.2 Factors of Influencing Mechanical Properties of nC Composites

NC is often incorporated into polymer in order to attain better mechanical properties of a composite material. The effects of the addition of nC is highly dependent on various factors such as size, dispersity and loading of the nC (Fu and Naguib 2006).

The size of the particles of nC played an important role in determining the properties of a composite material. NC with smaller distribution of particle size could led to better dispersion in the polymer matrix. Majdzadeh-Ardakani et al. (2014) investigated the degree of dispersion of commercial montmorillonite (MMT) and centrifuged clay (CMMT) in poly(ethylene terephthalate) (PET)/clay nanocomposites (Majdzadeh-Ardakani et al. 2014). Due to the removal of large particles using two-step centrifugation method, CMMT in water has smaller particle size compared to that of MMT. In comparison to MMT, X-ray diffraction results revealed that CMMT has larger gallery spacing. Through Transmission Electron Microscopy (TEM) analysis, CMMT was very dispersed in the polymer matrix while some aggregations were observed in the case of MMT. As a result of well dispersion, storage modulus (G') of the nanocomposite with the presence of CMMT increased.

Loading of nC in a polymer composite is a deciding factor in determine the properties of the material. Table 4.1 summarizes the effects of the loading of nC and the mechanical properties of the corresponding nC composite produced.

Based on the studies by various researchers, it is clear that the incorporation of nC into nC composite enhance its mechanical properties. However, different loading of the nC added have different degree of improvement. There are few proposed mechanisms on how nC enhances the properties of cement matrix. Rooj et al. (2011) suggested that nC with its tubular shape forms cross linkage with the cement matrix (Rooj et al. 2011). Hydroxyl group available on the surface of halloysite nC could also react chemically to the Ca^{2+} available in cement mixture and result in a denser microstructure compare to the samples without nC. As nanosized particles, the nC might also enter the void of the matrix and therefore function as fillers. Besides that, halloysite nC contains high amount of SiO_2 and its ultra-thin surface might have resulted in the increased activity of the nucleation of calcium hydrosilicate (C–S–H) due to the consumption of Portlandite in cement matrix (Rao et al. 2002). Furthermore, it was assumed that nC swells as it gradually absorbs and trap water within its layers. This cause the expansion of nC and the swelling improves the filling in capillary pores.

Often, there is a limit on the nC that one can be added. Beyond that limit, the properties of the nanocomposites would be diminished due to poor dispersion and agglomeration. Kord et al. (2011) fabricated polypropylene/wood flour composites with different content of glass fibers and nC (Kord et al. 2011). The concentration of nC used was 2, 4 and 6 per hundred compounds (phc) while the glass fiber content was 5, 10 and 15 wt%. The tensile properties of the composites were measured. Tensile modulus was found increased along with increasing glass fiber content at different loadings of nC. However, when the glass fiber content remained constant, it could be found that the tensile modulus of the composite enhanced with the increment of nC up to 4 phc. Beyond this limit, i.e. 6 phc, the tensile modulus reduced, mainly due to the agglomeration of nC at higher loading. Similar observation was recorded in impact strength, indicated that 4 phc of nC resulted in intercalation and better dispersion. Apart from nanocomposite, nC had also been added into coating to enhance the performance of water-based coating (Uyup et al. 2019). In the study, the authors reported that satisfied result in terms of abrasion resistance and impact strength of the nanocoating could be attained when 2% nC was used instead of higher loading of nC.

4.3 Type of nC

nCs are not a new composite filler for humankind, ceramists have been using them in various applications since prehistoric times. Clay are generally made from hydrous silicates and formed under sheet-like structure stacking over one and another. These sheet-structured silicates layers are composed by fine particle of aluminosilicates. Depends on the type of clay, every single layer could be constructed by two to four

Table 4.1 Effects of the loading of nC and the mechanical properties of the corresponding nC composite produced

Type of composite	NC type and loading	Findings	Reference
Bagasse flour/ reprocessed high density polyethylene (rHDPE)/ nC composites	montmorillonite clay modified with a quaternary ammonium salt (Cloisite-30B) -0%, 2%, and 4%	Tensile and flexural strength of the composite increased to 21.52 and 25.74 MPa, respectively, when 2% nC were added compared to that of control board with 0% nC (19.85 and 24.28 MPa, respectively). However, both tensile and flexural strength decreased when 4% nC were added (21.08 and 25.18 MPa, respectively)	Samariha et al. (2015)
Polylactide/ Poly[(butylene succinate)-co-adipate] blend composites	montmorillonite clay, Cloisite®C20A (C20A) - 0.5, 1, 2, 4, 6, and 9 wt %	Tensile modulus of the composite was improved up to addition of 6 wt% nC and started to decrease when 9 wt% nC was added	Ojijo et al. (2012)
Epoxy/3D orthogonal glass fiber woven composite	DK2 polymer-grade organic nC – 1, 2, 3 and 4 wt%	The highest tensile strength of the composite was recorded when 3 wt% nC was added	Wang et al. (2019))
Waste-glass powder (WGP) cement mortars	montmorillonite clay modified with a quaternary ammonium salt (Cloisite-30B)	Cement mortars were produced with WGP and the addition of nC. It was found that the introduction of nC can further enhance the bending and compressive strength of the samples. However, the compressive strength shows greater degree of improvement compared with bending strength	Aly et al. (2011)
Cement mortars	Halloysite nC	Four type of mortar cements containing 1, 2 and 3% halloysite nC of were produced and tested for compressive strength. The authors found out that the addition of nC in mortars improved the compressive strength by up to 24% in samples with 3% nC compared with samples without nC (control)	Farzadnia et al. (2013)
Autoclaved aerated concrete	halloysite powders	Halloysite of was 2%, 3.5%, 5.5% and 7.5% of cement was used as cement replacement. The results show that he incorporation of halloysite (≥3.5%) to the samples was able improved the compressive strength by at least 5% without negative impact on the samples' heat conduction coefficient	Owsiak et al. (2015)

(continued)

Table 4.1 (continued)

Type of composite	NC type and loading	Findings	Reference
Cement nanocomposites	NC (NC) and calcined nC (CNC)	Nanocomposite of cement samples was produced with the addition of CNC or NC into the cement matrix. Flexural strength of the samples with added CNC and NC showed significant improvement. Compared to the control specimens, the samples containing 1 wt%, 2 wt% and 3 wt % CNC increased the flexural performance by 42.9%, 34.8% and 30.6% respectively. On the other hand, the flexural performance of samples containing 1 wt%, 2 wt% and 3 wt% NC is increased by 32.1%, 29.3% and 24.7% respectively	Hakamy et al. (2015)
Low-clinker slag cement mortar	calcined halloysite nano-clay (CHNC)/ molecular weight of 294.19 g/mol	Ordinary Portland cement clinker produced was partially substituted with CHNC in ratios of 0%, 1%, 2%, 3%, 4%, 5% and 6% by weight. It was concluded that early age and long-term mechanical strengths of the samples were significantly enhanced with the addition of CHNC. The samples containing 5% of CHNC displays the highest improvement of the mechanical properties	Allalou et al. (2019)

sheets of octahedra and/or tetrahedra arrangement. The octahedral sheet (Fig. 4.1a) is comprised of closely packed oxygens and hydroxyls in which magnesium, iron or aluminium atoms are arranged in octahedral coordination. While tetrahedral sheet (Fig. 4.1b) in which the silicon atom is placed between four oxygens or hydroxyls. These tetrahedron arrangements are arranged to form a hexagonal network repeated infinitely in two horizontal directions to form what is called the tetrahedral sheet. The, these aluminosilicate layers were stacked on each other with a gap held by sharing the hydroxyls or oxygens and the gap known as interlayer. The interlayer possesses negatively charge due to the ionic substitutions in the sheets of clay minerals. It can be neutralized by adding exchangeable cations that have metal ions (Ca^{2+}, Mg^{2+}, K^{+} and Na^{+}) or water molecules. This intercalation modification weakens the force of attraction between layers and caused the lattice to expand.

Generally, the clays can be classified according to the octahedral and tetrahedral sheet's arrangement in the aluminosilicate layers (Lee and Tiwari 2012). Depending on numbers and the way that of the sheets stacking, the clay minerals can be

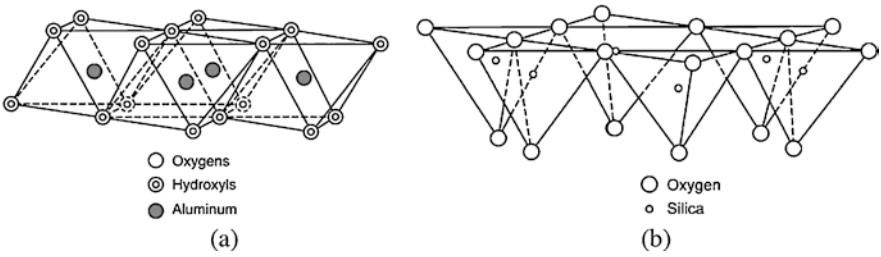

Fig. 4.1 Particles arrangement in (**a**) octahedral sheet and (**b**) tetrahedral sheet (Murray 2006)

Table 4.2 Grouping of clay fillers (Majeed et al. 2013)

Layer type	Sheet arrangement[a]	Interlayer material	Group	Species	Layer charge
1:1	T:O	H_2O or None	Kaolin–serpentine	Odinite, Halloysite, Nacrite, Dickite, Kaolinite, Brindleyite, Fraipontite, Kellyite, Nepouite, Cronstedtite, Amesite, Berthierine, Lizardite	<0.01
2:1	T:O:T	None	Pyrophyllite-Talc	Pyrophyllite, Pimelite, Kerolite, Talc, Willemseite, Ferripyrophyllite	0
		Hydrated exchangeable cations	Smectite	Volkonskoite, Nontronite, Beidellite, Montmorillonite, Swinefordite, Stevensite, Sauconite, Hetorite, Saponite	0.2–0.6
		Hydrated exchangeable cations	Vermiculite	Vermiculite	0.6–0.9
		Non-Hydrated exchangeable cations	True (flexible) mica	Paragonite, Celadonite, Glauconite, Illite, Muscovite, Lepidolite, Phlogopite, Biotite	0.6–1.0
		Non-Hydrated exchangeable cations	Brittle mica	Margarite, Anandite, Bityite, Kinoshitalite, Clintonite	1.8–2.0
2:1:1	(T:O:T):O	Variable	Chlorite	Nimite, Cookeite, Chamosite, Amesite	Variable

[a]T = tetrahedral, O = octahedral

classified into three classes which was listed in Table 4.2 and smectite group is the most widely research nC. However, chlorites (2:1:1) not considered a clay but a phyllosilicates group (Kotal and Bhowmick 2015).

Besides, the nC platelet undergoes a structural rearrangement to give different structures (fibrous- like, disc-like and tube-like) and shown in Fig. 4.2. Despite of

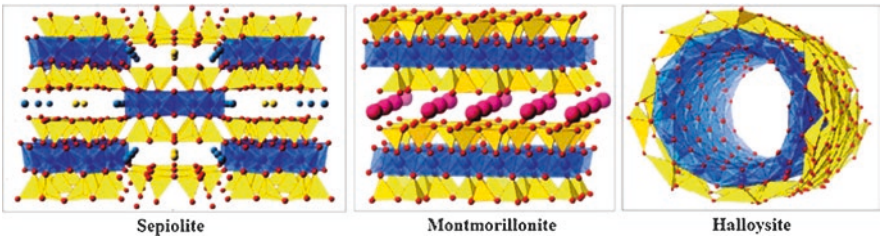

Fig. 4.2 Fibrous-like structure (Sepiolite), disc-like structure (Montmorillonite) and tube-like structure (Halloysite) (Raji et al. 2016)

the layer's arrangement differences, synthesis method, layer thickness, source of clay is reported to influence properties of nC, thereby varying the performances of nC reinforced composites.

Kaolin nC, from kalinite mineral, often used in building materials reinforcements. Fadzil (2017) has compared few types of nCs including kaolin clay and nano-kaolin clay (Fadzil et al. 2017). High percentage of silica contents in kaolin nC was expected to give high strength profiles when reinforced in cements. However, a 3 wt% of nC reinforcements was reported to be the most optimum contents in polyester composites. One study has investigated the effects of halloysite nC in carbon fibers reinforced epoxy composite (Lee et al. 2017). The interfacial bond energy increased up to 3 wt% of nC but decreased for specimens having more than 5 wt% of nC. This increased bond energy has synchronized with tensile value, which showing positive effect of halloysite nanotube clay reinforcements.

Yong et al. (2018) has studied three different types of nC (bentonite nanoplatelets, rod-like halloysite nanotube and sulfuric acid-etched halloysite nanotube) reinforcement into cellulose nanofibril biocomposites. Bentonite reinforced biocomposites has exhibited strong Young's Modulus and tensile strength due to higher amounts of hydroxyl groups compared to halloysites nC, resulted in better interaction with biocomposites. Furthermore, disc-like nCs (MMT and Laponite) has greater contact area to form bonding with matrix as better coverage on matrix surface which shown in SEM. Therefore it is being reported that forms strong electrostatic interaction and intermolecular force with cationic binder to the formation of hydrogel composites thereby increasing mechanical properties (Liao et al. 2019). On the other hand, rod-like nCs (Halloysite and Sepiolite) have small smaller charge density which leads to weak interaction with cationic binder, thereby disability to form aerogel composites.

Well-dispersed in composites is a key-factor of getting high strength performances. Agglomerations of nC will creates stress concentration spots, leading to crack failure before absorbing maximum load. Needle structured attapulgite nC which is hydrophilic found poor dispersion in polystyrene composite (Greesh et al. 2013). Yet, higher adhesive strength was observed by attapulgite and epoxy matrix

Table 4.3 Adhesive properties of the neat epoxy and attapulgite nC reinforced epoxy composites (Sun et al. 2018)

Attapulgite contents, wt%	Adhesive strength, MPa
0	6.05 ± 0.80
1	6.67 ± 0.89
3	7.49 ± 1.37
5	7.58 ± 0.59

up to 5 wt% of loadings and shown in Table 4.3. Therefore, it still provides limited thermal barrier to the nanocomposites. Disc-like MMT nCs which has strong bonding found homogenous dispersion in the polymer matrix. To provide the most optimum enhancement of mechanical properties by nC, suitable nC's layer or particle shapes are important to consider.

4.4 Nanocomposite Processing Methods

In the two distinct components system, low compatible bonding between inorganic and organic components leads to the poor mechanical properties. Moreover, agglomeration of particles created stress concentration spots, thereby reduce strength properties and produces weaker material (Giannelis 1996). Therefore, a phase-separation between nC sheets and polymer is often observed.

There are two types of nC composite structures can be obtained to provide promising interface between polymer and nCs (Fig. 4.3). The structure of intercalated is formed when extended polymer chains are intercalated between nC sheets. The alternating structure of polymeric and nC sheets resulted in about 20–30 Å separation (Dennis et al. 2001). On the other hand, exfoliated structure is construted when the clay sheets are well dispersed in polymer matrix with 80–100 Å separation distance (Alexandre and Dubois 2000).

The exfoliated structure of nanocomposites generally has better mechanical properties than interacted system since it maximizes the polymer-nC interactions. However, intercalated system nanocomposite is more widely reported in literature review. This is because of the highly anisotropic silicate layers with its length ranging from 100 to 1000 nm, it is not easy for nC to dispersed uniformly in melted polymer.

There are three main fabrication methods for producing nC/polymer composites (Solvent intercalation, in situ polymerization and melt intercalation). Melt intercalation and in situ polymerization are considered as potential methods to prepare polymer/clay nanocomposites in commercial scale. Rafiee and Shahzadi (2018) has studied a full stochastic multi-scare modelling to analysis Young' modulus of nC polymer composites (Rafiee and Shahzadi 2018). Exfoliated, intercalated and aggregated composite systems are factor of affecting mechanical properties.

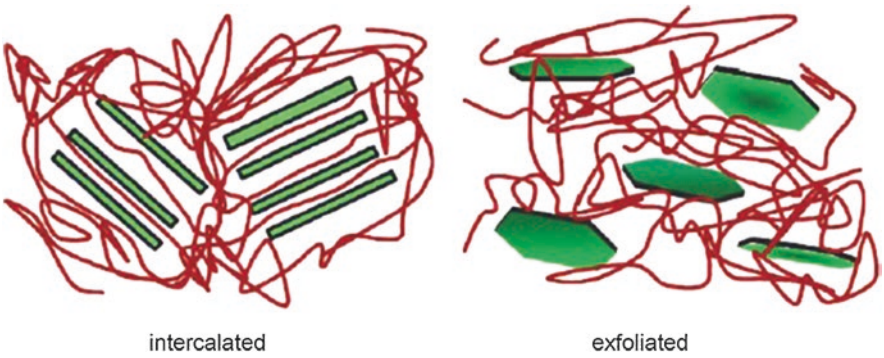

Fig. 4.3 Schematic graphic of two well-dispersed nCs reinforced polymer composites (Pavlidou and Papaspyrides 2008)

For solvent intercalation process, a solvent that compatible with matrix is used to exfoliates the layered silicate. This is because layered silicates are often bonded with a weak force and can be easily dispersed in an adequate solvent. After the nC has dissolved in the solvent, the polymer is then added to the solution. Precipitation or vaporization under vacuum was applied to removes the solvent. Non-polar polymers are suitable to apply by using this method in order to obtains intercalated structure. Yet, laboratory scale of fabrication was being done currently, the use of large quantities of solvents is one of the main issues faced by industrials (Alexandre and Dubois 2000).

Besides, in situ-polymerization was the pioneer method used to fabricates nC/polymer composites. A monomer solution is used to solutes the modified layered silicate by migrating into the galleries of the layered silicate, hence the polymerization can induce in between the intercalated sheets by producing long-chain polymers. There are several advantages of using this method, including ease of handling, short processing cycle, and promising properties of the final products (Ardanuy et al. 2008).

Thermoset polymer/nC composites generally prepared by in situ polymerization. The general methods for clay dispersion in the epoxy resin are slurry process, high pressure mixing, ball milling high shear mixing, ultrasonication and mechanical stirring (Zabihi et al. 2018). Table 4.4 listed a comparison of mechanical properties of some epoxy/MMT composites. Direct nC insertion into resin is the simplest methodology can be found in research studies (Shettar et al. 2017). Calculated portions of nC and thermoset resins have been mixed, stirred physically and cured in room temperature. Chan (2011) has studied the most optimum nC direct mixing parameters to produce homogenous nC/epoxy composites with evident of better mechanical properties (Chan et al. 2011). Figure 4.4 shows the principal of direct mixing. Sometimes external ice bath was used to prevent the heating of the mixture during stirring process (Binu et al. 2016).

Table 4.4 Comparison of mechanical properties of some epoxy/MMT composites by different methods of mixing (Zabihi et al. 2018)

Method of mixing	Structure	MMT loading, wt%	Tensile strength[a], %	Tensile modulus[a], %
High shear mixing	Exfoliated/ Intercalated	2–8	-31.14 to -2.5	+11.39 to +31.21
Hand stirring	Intercalated	2	+16.56	+1.41
Slurry process	Highly exfoliated	1–5	-30.19 to +17.86	+9.1 to +28.36
Mechanical stirring	Intercalated	2–10	-25.73 to +2.89	-46.97 to +52.46
	Exfoliated/ Intercalated	2.5–3	-36.56 to +19.67	+62.29
	Exfoliated	1–10	-31.04 to +48	+2.29 to +54
Sonication	Exfoliated/ intercalated	0.1–6	-33.85 to +68.38	+14.53 to +29.31

[a]Percentage value compared with their pure epoxy counterparts

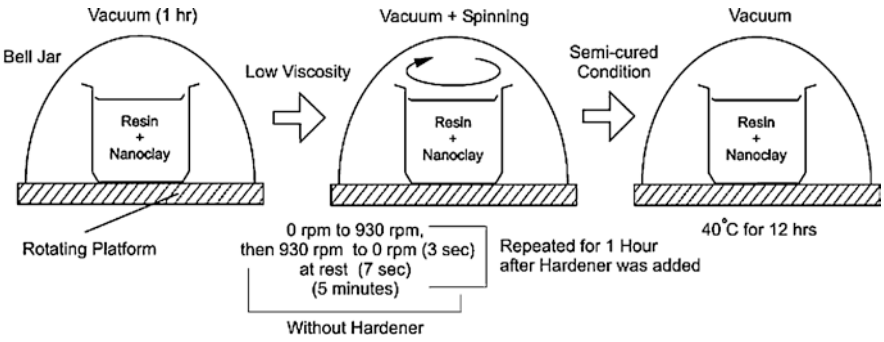

Fig. 4.4 Principal of direct mixing (Chan et al. 2011)

On the other hand, melted intercalation process is simply blending the nC with the molten polymer matrix. If the polymer are sufficiently compatible with the nC's surface, the polymer can flow into the interlayer space and form either an intercalated or an exfoliated structure (Beyer 2002). Melt intercalation is the most commonly used process. It can be carried out by using a single or twin-screw extruder. Twin screws extruder is more preferred as it has more advantage over single screw extruder. Well dispersion of nCs being reported up to 3 wt% of nC insertion by melt intercalation and the nC loading is found synchronized with highest mechanical properties composite (Daniel and Panneerselvam 2017).

4.5 Organically Modified nCs

Modification of nC shall lead to better dispersion in a polymer and provides an enhancement of thermal and physic-mechanical properties of the composite. The dimension of nanoplatelet is about 1 nm in thickness with 30–100 nm or longer,

depending on the type of nC and its aluminosilicates layers (Nguyen and Baird 2006). The most widely research MMT nC, was produced by partially substituting trivalent Al-cation by divalent Mg-cation in the octahedral layer, which giving a net negative charge at each layer due to the difference of electron valence (Paul and Robeson 2008).

The net negative charge is then can be balanced by alkali or alkaline earth metal (calcium or sodium ions). Interstitial water and other polar molecules may fill the spaces to cause swelling of silicate and replace by organic cations with cationic-exchange reaction, to change its hydrophilic behaviour as organophilic (Taxiarchou and Douni 2014). The organic cations lower the surface energy of the silicate surface and improve wetting with the polymer matrix (Kornmann et al. 2001). Therefore, modified organically of nC leads to better adhesion degree with polymers. In addition, increased distance between clay layers reported to have better composite strength as easier penetration of nC into hydrophobic polymeric chains (Zerda and Lesser 2001). Figure 4.5 shown schematic for catalytic initiation of ring opening reaction by clay modifier in epoxy-amine curing reaction, representing better interface bonding can be achieved by organo-nCs.

Martino (2017) has studied the effects of processing methods on organically modified nC reinforced biopolymer composites (Martino et al. 2017). Organically modified sepiolite (OSEP) reinforcements increases the molecular weight of polymer nanocomposites due to the formation of strong covalent bonding with polymer, which found same scenario with PLA polymer (Chen et al. 2005). On the other hand, organically MMT nC (OMMT) has found twice molecular weight reduction compared to net polymer. This is because high hydrolysis activities were found in OMMT. Hydroxyl groups on the edge of clay platelets and acidic sites have produced during alkyl-ammonium modification on MMT have accelerated polymer degradation under high temperature (Xie et al. 2001; Xu et al. 2009). Therefore, OMMT (Cloisite 20A, C20A) reinforcements found insignificant influences on tensile strength yet better hardness for rubber nanocomposites (Kumar et al. 2015). Cloisite commercial OMMT products are famous low cost nC materials as it improving the performances of nanocomposite in term of barrier, mechanical, crystallinity and thermal stability (Bracho et al. 2012).

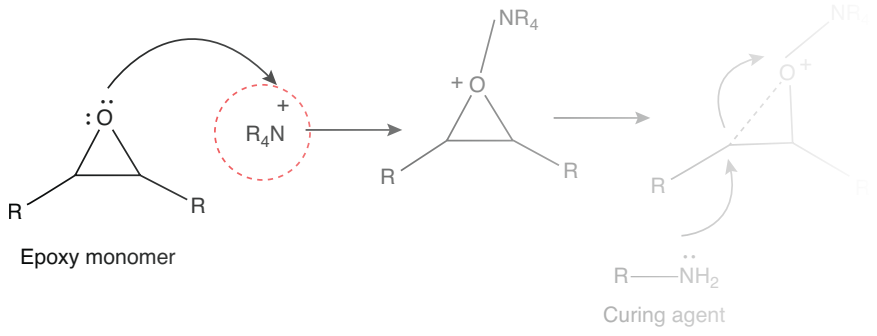

Fig. 4.5 Schematic for catalytic initiation of ring opening reaction by clay modifier in epoxy-amine curing reaction (Surendran et al. 2018)

Table 4.5 Mechanical properties of 5 wt% nC reinforced polyamide-6 (PA6) nanocomposites (Mohanty and Nayak 2007)

	PA6	NaMMT/PA6	C30B/PA6	OMMT/PA6	C16MMT/PA6
Tensile strength, MPa	70.00	77.23	90.45	86.23	88.76
Tensile modulus, MPa	3400	4348	4897	4371	4562
Elongation, %	20.00	5.61	6.45	5.60	5.61
Flexural strength, MPa	115.00	121.60	146.52	143.89	144.71
Flexural modulus, MPa	2600	2799	3254	3143	3201
Impact strength, J/m	90.00	83.21	90.91	89.76	90.32

The mechanical properties of virgin poly-amide-6 and 5 wt% nC reinforcement in nanocomposites are enumerated in Table 4.5 (Mohanty and Nayak 2007). The lowest tensile and flexural increment from sodium-montmorillonite, Na-MMT reinforcements possibly due to partial delamination of clay galleries. The nanocomposites prepared by using organically modified clays C30B, OMMT, and C16MMT have showed higher tensile modulus and strength. This is because of great polymer chains interaction with organic modification nCs and creating largely exfoliated nanocomposites. It is also likely to concludes that the molecular as well as silicate layer orientation along the flow direction have significantly contributed to the observed reinforcement effects [26]. Merah and Mohamed (2019) has compared three types of OMMT nCs (Cloisites 10A, Cloisites 20A and Nanomer L30E) in unsaturated polyester matrix with 3 wt% nC loadings (Merah and Mohamed 2019). It is clearly found that nanocomposite containing L30E nC outperforms other nC fillers in mechanical strength, shown in Fig. 4.6. About 75% of tensile strength improvement over pure matrix observed on L30E contented nanocomposite. This is because high aspect ratio of L30E nC and to better dispersion in matrix as evident in SEM micrographic. This is agreed by other author who found L30E nC reinforcements having positive effect on nanocomposite's mechanical properties (Rafiq et al. 2017).

The MMT modified with octadecyl amine has been used to reinforced rubber nanocomposites. Higher modulus properties have found regardless of organoclay contents (Zachariah et al. 2019). The reinforcing mechanism of OMMT can be referred to several modelling, like particle-particle interaction effects, geometry effects and shape factors. The Na-MMT also being applied to reinforces rubber nanocomposites (He et al. 2019). The author has confirmed promising mechanical performances have done by a well-dispersed of organophilic nC in rubber matrix, where clay gel or clay aqueous is obtained (Fig. 4.7). Pristine clay and swollen clay will be found be normal clay reinforcement composite system. Hydrophilic clay and strong ionic interaction between neighbouring clays in hydrophobic matrix, easily cause the clay to aggregate (Chiu et al. 2014). the incorporation of Na-MMT nC into the epoxy nanocomposites resulted in significant increase of the maximal applied stress and elongation (Tomić et al. 2019). The flexible chain of polymeric modifier existing on the clay-epoxy interface and the good adhesion were attributed to the enhanced stress transfer, which restricted the epoxy matrix from cracking.

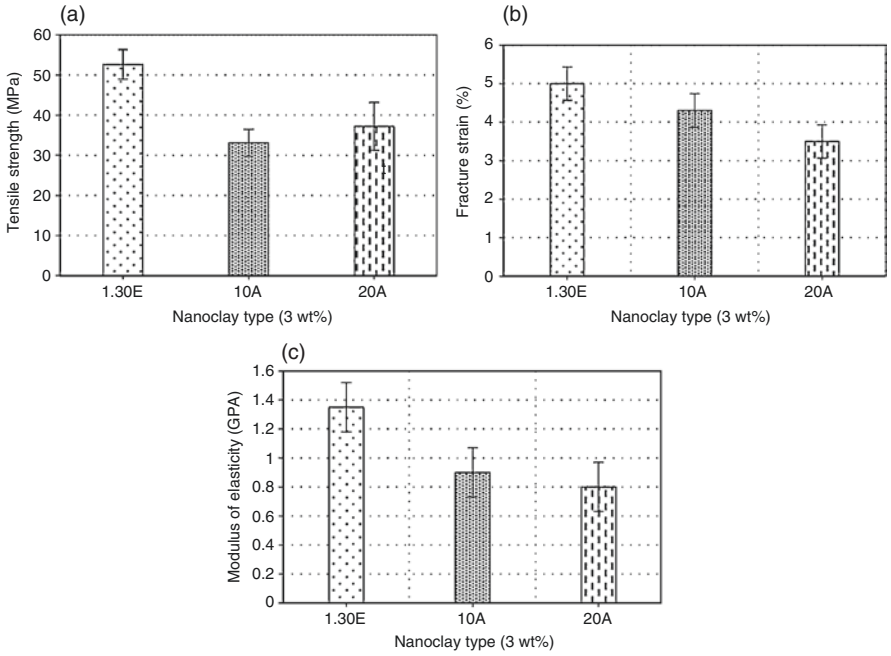

Fig. 4.6 The effect of nC type on (**a**) the tensile strength, (**b**) fracture strain, and (**c**) modulus of elasticity of nC reinforced unsaturaed polyester nanocomposites (Merah and Mohamed 2019)

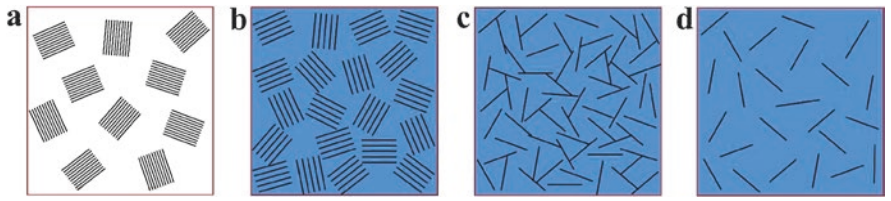

Fig. 4.7 Graphical structure of (**a**) pristine clay, (**b**) swollen clay, (**c**) clay gel and (**d**) clay aqueous suspension (He et al. 2019)

Halloysite nC reinforcements in cement shows impressive compressive and flexural strengths. It acts as an activator for pozzolanic reaction as well as nucleating sites to filling up the voids between cement particles and thereby formed a more compact structure (Allalou et al. 2019). Besides, it also reduced the initial and final setting time of cement pastes significantly.

Four times of Indole-3-carbaldehyde and indole-3-acetic acid was added into 200 cc deionized water containing 1.5CC HCI under stirring and 70 °C for an hour (Ashhari and Sarabi 2017). The modified nC fillers have reported better force at break and elongation at break. A hybrid organo modified montmorillonite nC (OMMT),

aluminum hydroxide flame retardant reinforced in Jute woven fiber in forced polylactic acid composites. The use of OMMT or flame retardant in jute composites were found deteriorated strength profile. Yet synergic effect between OMMT and flame retardant provides a strong interaction between all composite components, giving highest flexural strength values (114.4–117.4 MPa) (Malik et al. 2018).

4.6 Type of Matrix

A study has found insertion of nCs into banana reinforced epoxy composite has increase two- and seven-fold of flexural strength and modulus, respectively (Mohan and Kanny 2019). Hard, brittle and high strength ceramic phase of nC induces higher energy absorption characteristics (Sivasaravanan et al. 2014). Besides, nCs provide a denser microstructure with reduced porosity thereby enhances adhesion bond between matrix and fibres (Assaedi et al. 2016). On the other hand, Shettar (2017) has compared the nC reinforcement in epoxy and polyester composites (Shettar et al. 2017). The results showed epoxy-based nanocomposites have higher mechanical properties than polyester based specimens regardless of nC filler loadings. Figure 4.8 shows 3% nC contents in epoxy composite.

Organically modified nC can be "modified" to make more compatible to polymer. One study has run elemental analysis on cloisite nCs (Gómez et al. 2016). Cloisite 20A has lower inorganic content compared to Cloisite 30B nC, due to higher alkyl groups (two and one alkyl groups for 20A and 30B, respectively). Therefore, 20A nC is more compatible to hydrophobic polymers while hydrophilic polymers are more preferred from 30B reinforcements. On other hand, Cloisite 30B has higher specific area which turns into better polymer-particle interactions (Zou et al. 2008). Bandyopadhyay (2017) has successfully improve nucleation process on

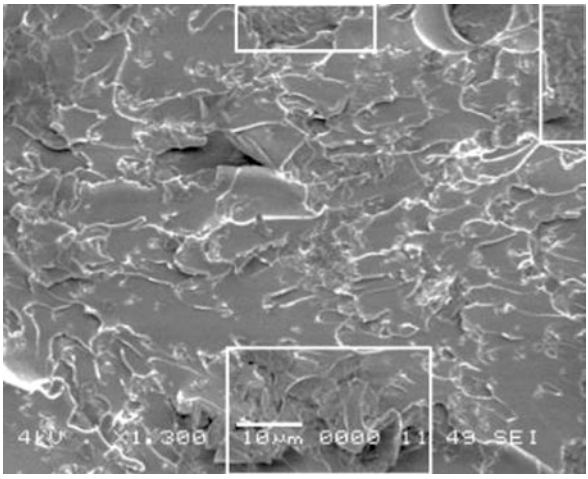

Fig. 4.8 3% nC contents in epoxy composite (Rafiq et al. 2017)

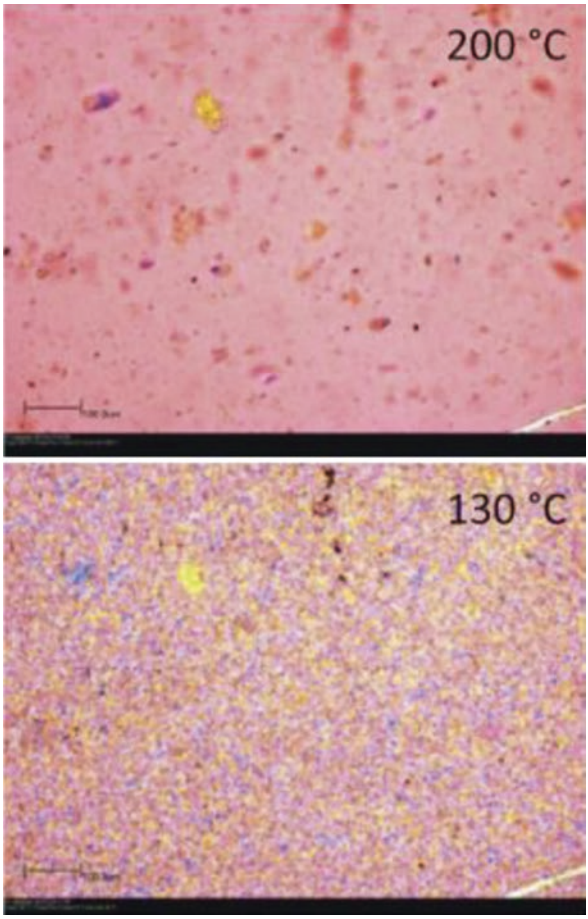

Fig. 4.9 Polarized optical microscopic images of organoclay contented composites (Bandyopadhyay et al. 2017)

polypropylene polymer by dispersed organoclay fillers (Bandyopadhyay et al. 2017). Highly nucleated composite provides higher crystallinity content which turns into better mechanical properties. Figure 4.9 shows the polarized optical microscopic images of organoclay contented composites. The crystallization process is almost complete in 130 °C.

Waste polymer treatment always needed to work out to increase their efficiency. In the year 2015, less than 9.1% of plastic wastes being transformed into recycled plastics, which is relatively insignificant. Besides, recycled plastics always have lower properties than virgin plastic products. Insertion of nCs into recycled plastic polymers found improvement of mechanical properties of composites. Cloisite 15A found fits well in recycled polypropylene in achieving promising mechanical properties and it is only about 5.28% of tensile strength value reduction was found when compared to virgin polypropylene/nC composites (Cengiz 2008). On the other hand, insertion of Cloisite 15A fillers help to maintains impact strength, regardless of number of polypropylene reuse cycle, successfully illustrated the effects of nCs

Table 4.6 nC composites with different polymer matrix

Matrix	nC	nC Content, %	Tensile strength, MPa	References
Acrylonitrile-butadiene rubber	Na-MMT	0–10	5.9–12.1	He et al. (2019)
Natural and chlorobutyl rubber	Montmorillonite modified with an organic modifier octadecyl amine	0–10	–	Zachariah et al. (2019)
Hydroxyapatite-zinc oxide	Cetyl trimethyl ammonium bromide and montmorillonite (k-10)	0–15	16.16–30.13	Bhowmick et al. (2018)
Hydrogel	Na-MMT and Laponite XLG	0.7–3.5	–	Liao et al. (2019)
Unsaturated isophthalic acid based unsaturated polyester	Cloisite 30B	5	60.3	Bagheri et al. (2018)
Chitosan	Halloysite	7.5	54.2	Liu et al. (2012)
Sodium carboxymethyl cellulose	Acid treated Halloysite with metallic salts	2	44.2–48.9	Wang and Rhim (2017)
Alginate	Naoh-Halloysite with zinc oxide	1–7	62.0–67.5	Shankar et al. (2018)
Bisphenol epoxy based vinylester resin	Silicon carbide	5–15	–	Bharath Kumar et al. (2018)
Natural rubber	Cloisite	2.5	16.71	Roy et al. (2018)

insertion (Othman et al. 2017). Zdiri (2018) has reviewed the application of several nC fillers into recycled polypropylene composites (Zdiri et al. 2018). Generally, insertion of nCs induced better composite's mechanical properties until it reaches 3 wt% contents where unexfoliated agglomerations and structural voids effects are significant (Zhao et al. 2005). Therefore, the type of matrix used in nC contented composites is one of the influencing factors in order to predicts composite's mechanical properties. Table 4.6 shows some studies being done by previous researchers on nC composites with different polymer matrix.

4.7 Conclusions

Incorporation of nC could led to significantly improvement in performance of the polymeric composites, particularly mechanical properties. NC composites showed a promising future as it can be applied in a wide range of application. Nevertheless, it should be noted that the preparation technology of nC composites exert direct effects to its development and utilization. Therefore, in order to improve and innovate the current preparation methods, focus shall be emphasizing on looking for an

economically viable method to produce a more uniform dispersion system. Apart from that, the main research direction and further efforts should be put on exploring the practical application technology and realizing industrial production.

References

Alexandre M, Dubois P (2000) Polymer-layered silicate nanocomposites: preparation, properties and uses of a new class of materials. Mater Sci Eng R Rep 28(1):1–63. https://doi.org/10.1016/S0927-796X(00)00012-7

Allalou S, Kheribet R, Benmounah A (2019) Effects of calcined halloysite nano-clay on the mechanical properties and microstructure of low-clinker cement mortar. Case Studies in Const Mater 10:e00213. https://doi.org/10.1016/j.cscm.2018.e00213

Aly M, Hashmi MSJ, Olabi AG, Messeiry M, Hussain AI (2011) Effect of nano clay particles on mechanical, thermal and physical behaviours of waste-glass cement mortars. Mater Sci Eng A 528(27):7991–7998. https://doi.org/10.1016/j.msea.2011.07.058

Ardanuy M, Velasco JI, Realinho V, Arencón D, Martínez AB (2008) Non-isothermal crystallization kinetics and activity of filler in polypropylene/Mg–Al layered double hydroxide nanocomposites. Thermochim Acta 479(1):45–52. https://doi.org/10.1016/j.tca.2008.09.016

Ashhari S, Sarabi AA (2017) Effects of organically modified nanoclay particles on the mechanical properties of aliphatic polyurethane/clay nanocomposite coatings. Polym Compos 38(6):1167–1174. https://doi.org/10.1002/pc.23680

Assaedi H, Shaikh FUA, Low IM (2016) Characterizations of flax fabric reinforced nanoclay-geopolymer composites. Compos Part B 95:412–422. https://doi.org/10.1016/j.compositesb.2016.04.007

Ayu RS, Khalina A, Harmaen AS, Zaman K, Jawaid M, Lee CH (2018) Effect of modified tapioca starch on mechanical, thermal, and morphological properties of PBS blends for food packaging. Polymers 10(11):1187

Bagheri K, Razavi SM, Ahmadi SJ, Kosari M, Abolghasemi H (2018) Thermal resistance, tensile properties, and gamma radiation shielding performance of unsaturated polyester/nanoclay/PbO composites. Radiat Phys Chem 146:5–10. https://doi.org/10.1016/j.radphyschem.2017.12.024

Bandyopadhyay J, Ray SS, Ojijo V, Khoza M (2017) Development of a highly nucleated and dimensionally stable isotactic polypropylene/nanoclay composite using reactive blending. Polymer 117:37–47. https://doi.org/10.1016/j.polymer.2017.04.013

Beyer G (2002) Nanocomposites: a new class of flame retardants for polymers. Plastics, Additives and Compounding 4(10):22–28. https://doi.org/10.1016/S1464-391X(02)80151-9

Bharath Kumar T, Haseebuddin MR, Raghavendra N, Vishnu Mahesh KR (2018) Influence of sic on mechanical, thermal, fire and wear studies of vinylester/glass fibre composites. Materials Today: Proceedings 5(10, Part 3):22675–22686. https://doi.org/10.1016/j.matpr.2018.06.644

Bhowmick A, Banerjee SL, Pramanik N, Jana P, Mitra T, Gnanamani A, Das M, Kundu PP (2018) Organically modified clay supported chitosan/hydroxyapatite-zinc oxide nanocomposites with enhanced mechanical and biological properties for the application in bone tissue engineering. Int J Biol Macromol 106:11–19. https://doi.org/10.1016/j.ijbiomac.2017.07.168

Binu PP, George KE, Vinodkumar MN (2016) Effect of Nanoclay, Cloisite15A on the mechanical properties and thermal behavior of glass Fiber reinforced polyester. Procedia Technol 25:846–853. https://doi.org/10.1016/j.protcy.2016.08.191

Bracho D, Dougnac VN, Palza H, Quijada R (2012) Functionalization of silica nanoparticles for polypropylene Nanocomposite applications. J Nanomater 2012:8. https://doi.org/10.1155/2012/263915

Cengiz F (2008) Preparation and characterization of recycled polypropylene based Nanocomposites. Middle East Technical University

Chan M-l, Lau K-t, Wong T-t, Ho M-p, Hui D (2011) Mechanism of reinforcement in a nanoclay/polymer composite. Compos Part B 42(6):1708–1712. https://doi.org/10.1016/j.compositesb.2011.03.011

Chen G-X, Choi JB, Yoon JS (2005) The role of functional group on the exfoliation of clay in poly(L-lactide). Macromol Rapid Commun 26(3):183–187. https://doi.org/10.1002/marc.200400452

Chiu CW, Huang TK, Wang YC, Alamani BG, Lin JJ (2014) Intercalation strategies in clay/polymer hybrids. Prog Polym Sci 39(3):443–485. https://doi.org/10.1016/j.progpolymsci.2013.07.002

Daniel DJ, Panneerselvam K (2017) Manufacturing issues of polypropylene nanocomposite by melt intercalation process. Materials Today: Proceedings 4(2, Part A):4032–4041. https://doi.org/10.1016/j.matpr.2017.02.305

Dennis HR, Hunter DL, Chang D, Kim S, White JL, Cho JW, Paul DR (2001) Effect of melt processing conditions on the extent of exfoliation in organoclay-based nanocomposites. Polymer 42(23):9513–9522. https://doi.org/10.1016/S0032-3861(01)00473-6

Fadzil MA, Muhd Nurhasr MS, Norliyati MA, Hamidah MS, Wan Ibrahim MH (2017) Assrul RZ Characterization of Kaolin as Nano Material for High Quality Construction. In: MATEC Web of Conferences

Farzadnia N, Ali A, Demirboga R, Parvez A (2013) Effect of halloysite nanoclay on mechanical properties, thermal behavior and microstructure of cement mortars. Cem Concr Res 48:97–104. https://doi.org/10.1016/j.cemconres.2013.03.005

Fu J, Naguib HE (2006) Effect of nanoclay on the mechanical properties of PMMA/Clay nanocomposite foams. J Cell Plast 42(4):325–342. https://doi.org/10.1177/0021955x06063517

Giannelis EP (1996) Polymer layered silicate Nanocomposites. Adv Mater 8(1):29–35. https://doi.org/10.1002/adma.19960080104

Gómez M, Palza H, Quijada R (2016) Influence of organically-modified montmorillonite and synthesized layered silica nanoparticles on the properties of polypropylene and polyamide-6 nanocomposites. Polymers 8(11):386

Greesh N, Sinha Ray S, Bandyopadhyay J (2013) Role of nanoclay shape and surface characteristics on the morphology and thermal properties of polystyrene nanocomposites synthesized via emulsion polymerization. Ind Eng Chem Res 52(46):16220–16231. https://doi.org/10.1021/ie4024929

Gurses A (2015) Introduction to polymer-clay Nanocomposites. Jenny Stanford Publishing, New York

Hakamy A, Shaikh FUA, Low IM (2015) Characteristics of nanoclay and calcined nanoclay-cement nanocomposites. Compos Part B 78:174–184. https://doi.org/10.1016/j.compositesb.2015.03.074

He S, He T, Wang J, Wu X, Xue Y, Zhang L, Lin J (2019) A novel method to prepare acrylonitrile-butadiene rubber/clay nanocomposites by compounding with clay gel. Compos Part B 167:356–361. https://doi.org/10.1016/j.compositesb.2019.03.013

Ishida H, Campbell S, Blackwell J (2000) General approach to nanocomposite preparation. Chem Mater 12(5):1260–1267. https://doi.org/10.1021/cm990479y

Koniuszewska AG, Kaczmar JW (2016) Application of polymer based composite materials in transportation. Prog Rubber Plast Recycl Technol 32(1):1–24. https://doi.org/10.1177/147776061603200101

Kord B, Mohsen S, Kiakojouri H (2011) Effect of nanoclay dispersion on physical and mechanical properties of wood flour/polypropylene/glass fiber hybrid composites. Bioresources 6

Kornmann X, Lindberg H, Berglund LA (2001) Synthesis of epoxy–clay nanocomposites. Influence of the nature of the curing agent on structure. Polymer 42(10):4493–4499. https://doi.org/10.1016/S0032-3861(00)00801-6

Kotal M, Bhowmick AK (2015) Polymer nanocomposites from modified clays: recent advances and challenges. Prog Polym Sci 51:127–187. https://doi.org/10.1016/j.progpolymsci.2015.10.001

Kumar S, Nando GB, Nair S, Unnikrishnan G, Sreejesh A, Chattopadhyay S (2015) Effect of organically modified montmorillonite clay on morphological, physicomechanical, thermal stability, and water vapor transmission rate properties of BIIR-co rubber nanocomposite. Rubber Chem Technol 88(1):176–196. https://doi.org/10.5254/rct.14.85996

Lee CH, Salit MS, Hassan MR (2014) A review of the flammability factors of kenaf and allied fibre reinforced polymer composites. Adv Mater Sci Eng 2014:8. https://doi.org/10.1155/2014/514036

Lee CH, Sapuan SM, Hassan MR (2018) Thermal analysis of kenaf fiber reinforced floreon biocomposites with magnesium hydroxide flame retardant filler. Polym Compos 39(3):869–875. https://doi.org/10.1002/pc.24010

Lee CH, Sapuan SM, Lee JH, Hassan MR (2016) Melt volume flow rate and melt flow rate of kenaf fibre reinforced floreon/magnesium hydroxide biocomposites. Springerplus 5(1):1680. https://doi.org/10.1186/s40064-016-3044-1

Lee J-W, Park S-J, Kim Y-H (2017) Improvement of interfacial adhesion of incorporated Halloysite-nanotubes in fiber-reinforced epoxy-based composites. Appl Sci 7(5):441

Lee SM, Tiwari D (2012) Organo and inorgano-organo-modified clays in the remediation of aqueous solutions: an overview. Appl Clay Sci 59-60:84–102. https://doi.org/10.1016/j.clay.2012.02.006

Liao W, Wang G, Liu Z, Xu S, Wang Y-Z (2019) Rheological premonitory of nanoclay morphology on the mechanical characteristics of composite aerogels. Compos Part B 173:106889. https://doi.org/10.1016/j.compositesb.2019.05.100

Liu M, Zhang Y, Wu C, Xiong S, Zhou C (2012) Chitosan/halloysite nanotubes bionanocomposites: structure, mechanical properties and biocompatibility. Int J Biol Macromol 51(4):566–575. https://doi.org/10.1016/j.ijbiomac.2012.06.022

Lvov YM, DeVilliers MM, Fakhrullin RF (2016) The application of halloysite tubule nanoclay in drug delivery. Expert Opin Drug Deliv 13(7):977–986. https://doi.org/10.1517/17425247.2016.1169271

Majdzadeh-Ardakani K, Lofgren EA, Jabarin SA (2014) The effect of particle size distribution on the dispersion of nanoclays in poly(ethylene terephthalate)/clay nanocomposites. J Reinf Plast Compos 33(4):358–368. https://doi.org/10.1177/0731684413512229

Majeed K, Jawaid M, Hassan A, Abu Bakar A, Abdul Khalil HPS, Salema AA, Inuwa I (2013) Potential materials for food packaging from nanoclay/natural fibres filled hybrid composites. Mater Des 46:391–410. https://doi.org/10.1016/j.matdes.2012.10.044

Malik N, Kumar P, Ghosh SB, Shrivastava S (2018) Organically modified nanoclay and aluminum hydroxide incorporated bionanocomposites towards enhancement of physico-mechanical and thermal properties of lignocellulosic structural reinforcement. J Polym Environ 26(8):3243–3249. https://doi.org/10.1007/s10924-018-1184-9

Martino L, Guigo N, van Berkel JG, Sbirrazzuoli N (2017) Influence of organically modified montmorillonite and sepiolite clays on the physical properties of bio-based poly(ethylene 2,5-furandicarboxylate). Compos Part B 110:96–105. https://doi.org/10.1016/j.compositesb.2016.11.008

Merah N, Mohamed O (2019) Nanoclay and water uptake effects on mechanical properties of unsaturated polyester. J Nanomater 2019:11. https://doi.org/10.1155/2019/8130419

Mohan TP, Kanny K (2019) Compressive characteristics of unmodified and nanoclay treated banana fiber reinforced epoxy composite cylinders. Compos Part B 169:118–125. https://doi.org/10.1016/j.compositesb.2019.03.071

Mohanty S, Nayak SK (2007) Effect of clay exfoliation and organic modification on morphological, dynamic mechanical, and thermal behavior of melt-compounded polyamide-6 nanocomposites. Polym Compos 28(2):153–162. https://doi.org/10.1002/pc.20284

Murray HH (2006) Chapter 2 structure and composition of the clay minerals and their physical and chemical properties. In: Murray HH (ed) Developments in clay science, vol 2. Elsevier, pp 7–31. https://doi.org/10.1016/S1572-4352(06)02002-2

Nguyen QT, Baird DG (2006) Preparation of polymer–clay nanocomposites and their properties. Adv Polym Technol 25(4):270–285. https://doi.org/10.1002/adv.20079

Ojijo V, Sinha Ray S, Sadiku R (2012) Effect of nanoclay loading on the thermal and mechanical properties of biodegradable polylactide/poly[(butylene succinate)-co-adipate] blend composites. ACS Appl Mater Interfaces 4(5):2395–2405. https://doi.org/10.1021/am201850m

Othman MH, Aisha MM, Khamis SZ (2017) Injection moulding reprocessing cycles effect towards mechanical properties of polypropylene-Nanoclay. International Journal of Advances in Mechanical & Automobile Engineering 4(1)

Owsiak Z, Sołtys A, Sztąboroski P, Mazur M (2015) Properties of autoclaved aerated concrete with Halloysite under industrial conditions. Procedia Engineering 108:214–219. https://doi.org/10.1016/j.proeng.2015.06.140

Paul DR, Robeson LM (2008) Polymer nanotechnology: Nanocomposites. Polymer 49(15):3187–3204. https://doi.org/10.1016/j.polymer.2008.04.017

Pavlidou S, Papaspyrides CD (2008) A review on polymer–layered silicate nanocomposites. Prog Polym Sci 33(12):1119–1198. https://doi.org/10.1016/j.progpolymsci.2008.07.008

Rafiee R, Shahzadi R (2018) Predicting mechanical properties of nanoclay/polymer composites using stochastic approach. Compos Part B 152:31–42. https://doi.org/10.1016/j.compositesb.2018.06.033

Rafiee R, Shahzadi R (2019) Mechanical properties of nanoclay and nanoclay reinforced polymers: a review. Polym Compos 40(2):431–445. https://doi.org/10.1002/pc.24725

Rafiq A, Merah N, Boukhili R, Al-Qadhi M (2017) Impact resistance of hybrid glass fiber reinforced epoxy/nanoclay composite. Polym Test 57:1–11. https://doi.org/10.1016/j.polymertesting.2016.11.005

Raji M, Mekhzoum MEM, Qaiss AK, Bouhfid R (2016) Nanoclay modification and functionalization for nanocomposites development: effect on the structural, morphological, mechanical and rheological properties. In: Jawaid M, AeK Q, Bouhfid R (eds) Nanoclay reinforced polymer composites: Nanocomposites and Bionanocomposites. Springer, Singapore, pp 1–34. https://doi.org/10.1007/978-981-10-1953-1_1

Rao CNR, Kulkarni GU, Thomas PJ, Edwards PP (2002) Size-dependent chemistry: properties of nanocrystals. Chem Eur J 8(1):28–35. https://doi.org/10.1002/1521-3765(20020104)8:1<28::Aid-chem28>3.0.Co;2-b

Rooj S, Das A, Heinrich G (2011) Tube-like natural halloysite/fluoroelastomer nanocomposites with simultaneous enhanced mechanical, dynamic mechanical and thermal properties. Eur Polym J 47(9):1746–1755. https://doi.org/10.1016/j.eurpolymj.2011.06.007

Roy K, Chandra Debnath S, Das A, Heinrich G, Potiyaraj P (2018) Exploring the synergistic effect of short jute fiber and nanoclay on the mechanical, dynamic mechanical and thermal properties of natural rubber composites. Polym Test 67:487–493. https://doi.org/10.1016/j.polymertesting.2018.03.032

Samariha A, Hooman Hemmasi A, Ghasemi I, Bazyar B, Nemati M (2015) Effect of nanoclay contents on properties, of bagasse flour/reprocessed high density polyethylene/nanoclay composites (AOP Paper). MADERAS-CIENC TECNOL. https://doi.org/10.4067/S0718-221X2015005000056

Shankar S, Kasapis S, Rhim J-W (2018) Alginate-based nanocomposite films reinforced with halloysite nanotubes functionalized by alkali treatment and zinc oxide nanoparticles. Int J Biol Macromol 118:1824–1832. https://doi.org/10.1016/j.ijbiomac.2018.07.026

Shettar M, Achutha Kini U, Sharma SS, Hiremath P (2017) Study on mechanical characteristics of nanoclay reinforced polymer composites. Materials Today: Proceedings 4(10):11158–11162. https://doi.org/10.1016/j.matpr.2017.08.081

Sivasaravanan S, Raja VKB, Manikandan (2014) Impact characterization of epoxy LY556/E-glass fibre/Nano clay hybrid Nano composite materials. Procedia Engineering 97:968–974. https://doi.org/10.1016/j.proeng.2014.12.373

Sun Y, Liu Y, Jiang Y, Xu K, Xi Z, Xie H (2018) Thermal and mechanical properties of natural fibrous nanoclay reinforced epoxy asphalt adhesives. Int J Adhes Adhes 85:308–314. https://doi.org/10.1016/j.ijadhadh.2018.07.005

Surendran A, Pionteck J, Vogel R, Kalarikkal N, V G G, Thomas S (2018) Effect of organically modified clay on the morphology, rheology and viscoelasticity of epoxy –thermoplastic nanocomposites. Polym Test 70:18–29. https://doi.org/10.1016/j.polymertesting.2018.06.023

Taxiarchou M, Douni I (2014) The effect of oxalic acid activation on the bleaching properties of a bentonite from Milos Island, Greece. Clay Miner 49(4):541–549. https://doi.org/10.1180/claymin.2014.049.4.04

Tjong CS (2006) Tjong, S.C.: Structural and mechanical properties of polymer nanocomposites. Mater. Sci. Eng. R Rep 53:73–197. https://doi.org/10.1016/j.mser.2006.06.001

Tomić M, Dunjić B, Nikolić MS, Trifković K, Stanković N, Pavlović VB, Bajat J, Djonlagić J (2019) Polyamidoamine as a clay modifier and curing agent in preparation of epoxy nanocomposites. Prog Org Coat 131:311–321. https://doi.org/10.1016/j.porgcoat.2019.02.037

Uddin F (2008) Clays, Nanoclays, and Montmorillonite minerals. Metall Mater Trans A 39(12):2804–2814. https://doi.org/10.1007/s11661-008-9603-5

Uyup MKA, Khadiran T, Husain H, Lee SH (2019) Effects of nanoclay contents on the properties of water-based coating. J Trop For Sci 31:353–361. https://doi.org/10.26525/jtfs2019.31.3.353

Wang C, Gao X, Li Y (2019) Mechanical properties improvement of nanoclay addition epoxy 3D orthogonal woven composite material. Fibers Polym. 20(7):1495–1503. https://doi.org/10.1007/s12221-019-9116-4

Wang L-F, Rhim J-W (2017) Functionalization of halloysite nanotubes for the preparation of carboxymethyl cellulose-based nanocomposite films. Appl Clay Sci 150:138–146. https://doi.org/10.1016/j.clay.2017.09.023

Wang R-M, Zheng S-R, Zheng Y-P (2011) 1 – Introduction to polymer matrix composites. In: Wang R-M, Zheng S-R, Zheng Y-P (eds) Polymer matrix composites and technology. Woodhead Publishing, pp 1–548. https://doi.org/10.1533/9780857092229.1

Xie W, Gao Z, Pan W-P, Hunter D, Singh A, Vaia R (2001) Thermal degradation chemistry of alkyl quaternary ammonium Montmorillonite. Chem Mater 13(9):2979–2990. https://doi.org/10.1021/cm010305s

Xu X, Ding Y, Qian Z, Wang F, Wen B, Zhou H, Zhang S, Yang M (2009) Degradation of poly(ethylene terephthalate)/clay nanocomposites during melt extrusion: effect of clay catalysis and chain extension. Polym Degrad Stab 94(1):113–123. https://doi.org/10.1016/j.polymdegradstab.2008.09.009

Yahiaoui F, Benhacine F, Ferfera-Harrar H, Habi A, Hadj-Hamou AS, Grohens Y (2015) Development of antimicrobial PCL/nanoclay nanocomposite films with enhanced mechanical and water vapor barrier properties for packaging applications. Polym Bull 72(2):235–254. https://doi.org/10.1007/s00289-014-1269-0

Yong C, Mei C, Guan M, Wu Q, Han J, Sun X (2018) A comparative study of different nanoclay-reinforced cellulose nanofibril biocomposites with enhanced thermal and mechanical properties. Compos Interface 25(4):301–315. https://doi.org/10.1080/09276440.2018.1400271

Zabihi O, Ahmadi M, Nikafshar S, Chandrakumar Preyeswary K, Naebe M (2018) A technical review on epoxy-clay nanocomposites: structure, properties, and their applications in fiber reinforced composites. Compos Part B 135:1–24. https://doi.org/10.1016/j.compositesb.2017.09.066

Zachariah AK, Chandra AK, Mohammed PK, Thomas S (2019) Vulcanization kinetics and mechanical properties of organically modified nanoclay incorporated natural and chlorobutyl rubber nanocomposites. Polym Test 76:154–165. https://doi.org/10.1016/j.polymertesting.2019.02.003

Zdiri K, Elamri A, Hamdaoui M, Harzallah O, Khenoussi N, Brendlé J (2018) Reinforcement of recycled PP polymers by nanoparticles incorporation. Green Chem Lett Rev 11(3):296–311. https://doi.org/10.1080/17518253.2018.1491645

Zerda AS, Lesser AJ (2001) Intercalated clay nanocomposites: morphology, mechanics, and fracture behavior. J Polym Sci B Polym Phys 39(11):1137–1146. https://doi.org/10.1002/polb.1090

Zhao C, Qin H, Gong F, Feng M, Zhang S, Yang M (2005) Mechanical, thermal and flammability properties of polyethylene/clay nanocomposites. Polym Degrad Stab 87(1):183–189. https://doi.org/10.1016/j.polymdegradstab.2004.08.005

Zou H, Wu S, Shen J (2008) Polymer/silica Nanocomposites: preparation, characterization, properties, and applications. Chem Rev 108(9):3893–3957. https://doi.org/10.1021/cr068035q

Chapter 5
Fireproof Capability of Rigid Polyurethane Foam Based Composite Materials

Nazim Usta, Recep Yurtseven, Erkin Akdoğan, and Fatih Demiryuğuran

5.1 Introduction

Polyurethane foams are used in thermal insulation, automotive and furniture industries due to the best combination of performance and cost. There are mainly three different polyurethane foams used in different industries, namely rigid, semi rigid/integral and flexible polyurethane foams. The rigid polyurethane foams (PUR) that have closed cell structures and low thermal conductivity coefficients are preferred for thermal insulation applications. Semi rigid – integral polyurethane foams are used for production of some parts for automotive and furniture industries. The flexible polyurethane foams that have open cell structure are suitable for seating and bed applications in all kinds of industries.

The polyurethane foams are widely preferred because of their superior properties such as lightweight, thermal and electrical insulating, design flexibility, easy production, corrosion resistance etc. Nevertheless, the foams are flammable materials and this is an important disadvantage of the foams. During the ignition and the combustion of the foams, smoke, heat, toxic and corrosive compounds are released at different rates depending on the generic nature of the polyurethanes and the environmental conditions. The release rate of heat, smoke, toxic and corrosive compounds are responsible for generating both thermal and non-thermal hazards in fires. These hazards can be reduced by increasing fire resistance of the polyurethanes. Thus, the polyurethanes are modified by variety of techniques to increase their fire resistance. The most common technique is to use flame retardant materials and inorganic fillers (Gao et al. 2013, Jin et al. 2014, Kirpluks et al. 2014, Xu and Wang 2015, Lu et al. 2018, Qu et al. 2017, Kairytė et al. 2018, Shi et al. 2018,

N. Usta (✉) · R. Yurtseven · E. Akdoğan · F. Demiryuğuran
Mechanical Engineering Department, Pamukkale University, Denizli, Turkey
e-mail: n_usta@pau.edu.tr; ryurtseven@pau.edu.tr; eakdogan@pau.edu.tr; fdemiryuguran@pau.edu.tr

S. Siddiquee et al. (eds.), *Composite Materials: Applications in Engineering, Biomedicine and Food Science*, https://doi.org/10.1007/978-3-030-45489-0_5

Chen et al. 2018). It should be taken in account the compatibilities of fillers and flame retardants with the polyol and the isocyanate components of the polyurethane foams and negative effects on the thermal and the mechanical properties (Usta 2012, Luo et al. 2015, Li et al. 2017). Furthermore, there are different studies related to the usage of glass fiber in rigid polyurethane foams (Latere Dwanisa et al. 2004, Kim et al. 2010, Han et al. 2010, Kumar and Kaur 2017) and in other polymers (Jiang et al. 2015, Hu et al. 2016).

In this chapter, the thermal, the combustion and the mechanical behaviors of the rigid polyurethane foams commonly used in thermal insulation, automotive and furniture industries were examined. New and effective fire-resistant polyurethane based composite foams were developed and tested in terms of the thermal, the combustion and the mechanical properties.

5.2 Rigid Polyurethane Foam (PUR)

Rigid polyurethane foams are produced by mixing of polyol and isocyanate components at certain ratios. After the mixing process, the foam rises, reaches a maximum point, and then slightly drops. Meanwhile some additives such as blowing agents, catalysts, surfactants, flame retardants and fillers are incorporated into the polyol component before mixing the isocyanate. Figure 5.1 shows an example for the foam formation and Fig. 5.2 shows the foam rising with respect to the time. The foam rising can be measured by using a special laser beam (Usta et al. 2011).

In general, low and high-pressure injection machines are used for mixing processes in industrial applications. The mixture is poured into special heated molds. The mixture expands and fills the inside of the mold. Figure 5.3 show a low-pressure polyurethane injection machine and process.

Rigid polyurethane foams have closed cell structure and low thermal conductivity coefficients. Figure 5.4 shows an example view of the cell structure that was taken by a microscope. In addition, they should withstand certain loads. The rigid polyurethane foams are mainly used in all thermal insulation applications. Density and thermal conductivity of the foams may change depending on the raw materials, the polyol/the isocyanate ratio and the production applications.

Fig. 5.1 The isocyanate, the polyol and the foam formation after mixing of them

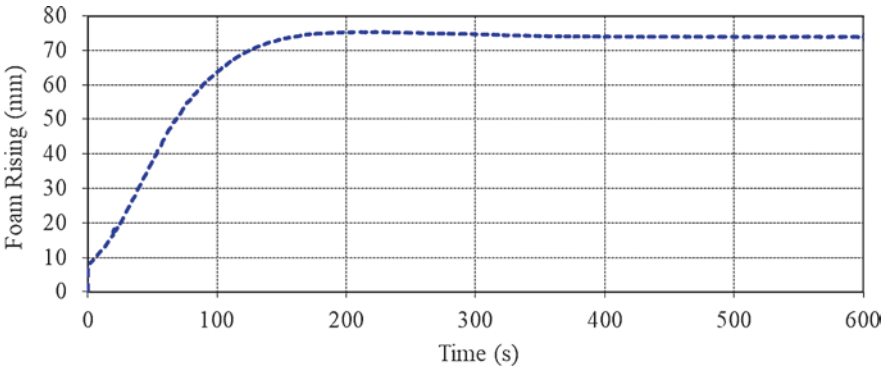

Fig. 5.2 Foam rising versus time after after mixing of the polyol and the isocyanate

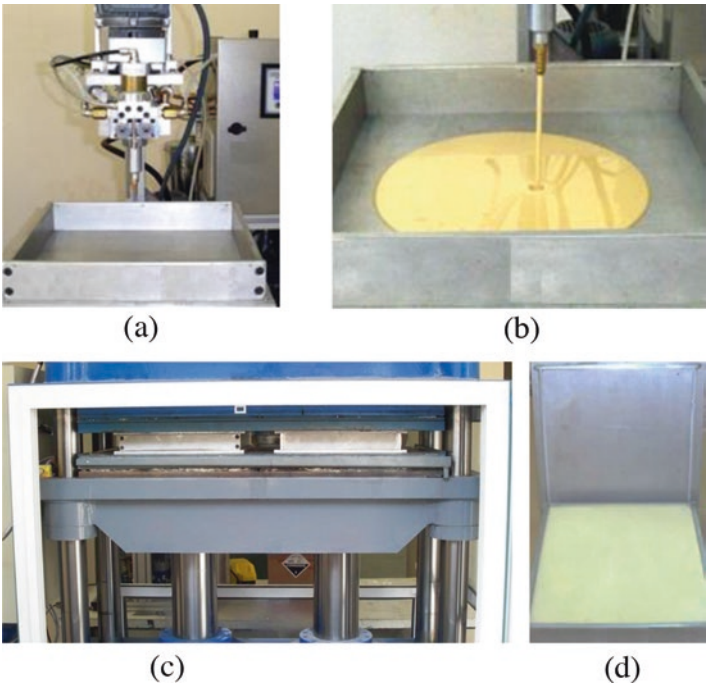

Fig. 5.3 (**a**) Low pressure injection machine, (**b**) Pouring of the polyol and the isocyanate mixture into the mold, (**c**) Curing process inside a heated press, (**d**) The rigid polyurethane foam

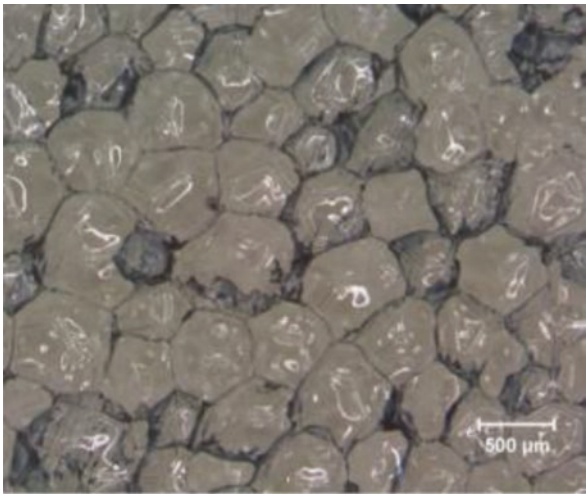

Fig. 5.4 Cell structure of PUR

5.3 Flame Retardancy and Intumescent Flame Retardant Systems

5.3.1 Flame Retardancy

Many studies have been performed to obtain fireproof rigid polyurethane foams. In general, different flame retardant materials and fillers are added into the polyol component and the doped polyol is mixed with the isocyanate component. Meanwhile it should be pointed out that the other properties of the foams should not be worsen. Otherwise, the foams cannot be used in the real life applications.

There are different studies related to the thermal decomposition, the combustion and the fire resistance of polyurethane foams in the literature. The thermal decomposition is very important step before start of combustion. Because solid materials do not burn directly. When a matter is exposed to a heat or a fire, some gases initially decompose from the solid matters and combustible gases can be ignited and burned easily. Meanwhile some liquid may appear before gasification. Then, the liquid / solid matters start to burn due to the generated heat. In general, the thermal decomposition of polyurethanes begins at thermally weakest links, namely allophanate and biuret, and the decomposition continue at ureas, urethanes, and isocyanurate group (Levchik and Weil 2004). In addition, the combustion of polyurethane foams were separated into two stages, namely solid and liquid pool combustions. In the solid phase combustion, the isocyanate component burns and yellow smoke is generated. Then the yellow smoke may decompose organic compounds and hydrogen cyanide, which partially results in nitrogen oxides. In the liquid pool phase combustion, the polyol component burns and heat, carbon monoxide and carbon dioxide are generated.

Flame retardants may be divided into two different groups as reactive and non-reactive (Singh and Jain 2009). It should be pointed out that the non-reactive flame retardants can be physically filled into the polyurethane foams and the reactive flame retardants can be incorporated chemically into the foams. Although the reactive flame retardants take part in the foaming reaction, the non-reactive flame reactants do not. Moreover, the reactive flame retardants essentially consist of phosphorus, nitrogen and halogen materials and they try to maintain the fire resistance of the foam by slowing down the decomposition of the foam (Tashev et al. 1992, Modesti and Simioni 1994, Prociak et al. 1997, Usta 2012). However, the flame retardants including the halogen produce hazardous poisonous gases and dense smoke during burning of the foam. Therefore, the flame retardants including halogens are not preferred and permitted in most of countries and many studies have been focused on halogen-free flame retardants. Flame retardants which consist of phosphorus and nitrogen can form char layer and decrease the generation of hazardous poisonous gases and dense smoke (Singh et al. 2008, Usta 2012).

Yang et al. (2015) studied on synthesis, mechanical properties and fire behaviors of rigid polyurethane foams with a reactive flame retardant including phosphazene and phosphate. They synthesized reactive flame retardant hexa-(phosphite-hydroxyl-methyl-phenoxyl)-cyclotriphosphazene (HPHPCP) by using hexachlorocyclotriphosphazene, diethyl phosphite and p-hydroxybenzaldehyde. It was reported that HPHPCP as a flame retardant inhibits foam collapse, pool-fire formation and restricted flame spread during burning.

The non-reactive flame retardants which may contain aluminum, boron, antimony, carbon, sulphur, phosphorus, nitrogen, halogens, and silicones etc., may be either compatible with the raw materials of the polyurethane foams acting as plasticizers, or not. The non-reactive flame retardants that are not compatible with the raw materials are evaluated as filler materials. The non-reactive flame retardants enhance fire resistance of the foam on weight basis. In general, the amounts of raw materials are decreased as the amounts of the fillers and this causes decreasing of the combustible decomposed gases (Lu and Hamerton 2002, Thirumal et al. 2009).

When the metal hydroxides as a part of the non-reactive flame retardants are added into the foams in high amount, namely more than 60 phr, the fire resistance of the foams may be significantly enhanced (Levchik and Weil 2004, Thirumal et al. 2010a, Lv et al. 2005, Zhang et al. 2004). However, the mechanical properties and the thermal insulation of the foams may be deteriorated (Bahattab et al. 2010, Liu et al. 2010). The deteriorations can be explained with inadequate interactions between the metal hydroxides and the foam materials (Thirumal et al. 2010b). In addition, the usage of the non-reactive and the reactive flame retardants together is also advised to generate synergistic effects for enhancing fire resistance of the foams (Zatorski et al. 2008, Bastin et al. 2003).

Akdogan et al. (2019) investigated the effects of triphenyl phosphate (TPhP), aluminum trihydrate (ATH), and zinc borate (ZnB) alone, as well as their binary blends on the thermal conductivity, the compressive strength and the flame retardancy of rigid polyurethane foams. The amounts of flame retardants were changed from 10 to 50% by polyol weight percentage. It was reported that there were no any

negative effects on the thermal insulation and the compressive strength. The fire retardancy of the foams that were determined with limited oxygen index (LOI) and cone calorimeter tests were enhanced by the flame retardant additions.

Flame retardants may act either in the condensed phase or in the vapor phase of the combustion through physical and/or chemical mechanisms to delay and/or stop the combustion process consisting of heating, pyrolysis, ignition and flame spread stages. Jia et al. (2019) used imide and oxazolidinone, which were synthesized by using 3, 30, 4, 40-biphenyltetracarboxylic dianhydride (PTDA) and 9, 10-dihydro-9-oxa-(10-glycidoxypropylene)-10-phosphap-henanthrene-10-oxide (e-DOPO) as reactive flame retardants. They reported that the compressive strength and the thermal conductivity of the foams were improved with the flame retardant additions. The fire behaviors of the foams were investigated by using the limited oxygen index, cone calorimetry test, and smoke density test. They pointed out that the char layer of the foam including PTDA and e-DOPO achieved a stronger barrier to burning in the condensed-phase.

Red phosphorus (RP) and the coated RP with melamine formaldehyde resin (MFcP) were used in production of rigid polyurethane foam by Cao et al. (2017). The enhancement of fire resistance of the doped foam was determined with limiting oxygen index and UL 94 test. In addition, the results of the cone calorimeter test indicate that MFcP100 addition causes less heat, smoke and toxic gases than RP. In addition, it was reported that MFcP primarily takes effect in the condensed phase of the burning while RP is effective in the gaseous phase. This was explained with the wrap effect of graphitic carbon nitride generated from melamine.

Meanwhile, some flame retardants may act in the both condensed and the vapor phases (Weil and Levchik 2004, Lu and Hamerton 2002). Wang et al. (2018a) synthesized a novel reactive flame retardant triol (TDHTPP) based on a triazine and a phosphate structure for rigid polyurethane foams and the triol was chemically merged in the main chains of the foam as a chain-extender. They reported that TDHTPP retain both vapor phase and condensed phase flame retardant behaviors and only 5 wt % of TDHTPP addition results in V-0 rating (UL 94) for the foam.

Liu and Wang (2018) introduced a novel phosphorus and nitrogen-based flame retardant, zinc amino-tris-(methylenephosphonate) (Zn- AMP), into rigid polyurethane foam to improve the flame retardancy, the mechanical and the thermal properties. It was reported that 20 wt % Zn-AMP considerably increases the thermal stability of the foam and Zn-AMP acts in both the condensed and the gas phases of the burning. Zn-AMP can result in formation a stable char residue and releases of non-combustible nitrogen-containing gases diluting oxygen and flammable gases in the gas phase.

Xu et al. (2018) produced fire resistive rigid polyurethane foams by using tris (1-chloro-2-propyl) phosphate (TCPP) and modified aramid fiber (MAF). It was found that using TCPP and MAF together could decrease smoke and toxic emissions such as hydrogen cyanide and increase char residue compared to the using TCPP alone. In addition, nonflammable gases carbon dioxide and water were also decreased. It was reported that TCPP and MAF could generate the quench effect in the gaseous phase and barrier effect in the condensed phase.

In another study, effects of functionalized graphene oxide (fGO) on thermal degradation and the flame retardant mechanism of the rigid polyurethane foams were investigated by Chen et al. (2019). It was pointed out that only 0.25 g fGO addition could achieve 28.1% (LOI) and V-0 rating (UL 94) for the rigid polyurethane foam. In other words, the fGO can be considered effective flame retardant, which can increase the thermal stability and decrease the flammability of the foams.

Michałowski and Pielichowski (2018) physically modified polyurethane foams by two additive phosphorous flame retardants - phenol isobutylenated phosphate or phenol isopropylated phosphate, and chemically reinforced by functionalized 1, 2-propanediolizobutyl POSS (PHI-POSS). The analysis of micro calorimetry test revealed an enhancement of fire resistance of the foams including hybrid reactive (POSS)/additive (phosphate) flame retardant systems resulting reduced heat release rates.

Effect of environmentally-friendly flame retardants, such as ammonium polyphosphate, melamine pyrophosphate, triethyl phosphate, bentonite and expanded graphite on the fire resistance and the mechanical properties of rigid polyurethane foams were investigated by Czech-Polak et al. (2016). They classified the doped foams with flammability class V-0 (UL 94). It was reported that the addition of the flame retardants resulting V-0 rating does not considerably deteriorated the mechanical properties of the foams. Norzali and Badri (2016) developed palm-based polyurethane containing phosphate ester (PE) as a fire retardant. It was found that the lowest burning rate could be achieved with loading of 15 wt % PE.

In general, the researchers focused on intumescent flame retardant systems which form a char layer acting as an insulator/mass transfer barrier and enhance the fire resistance (Lv et al. 2005, Tuzcu 2010, Usta 2012, Hu and Wang 2013, Luo et al. 2017, Chen et al. 2017, Hu and Wang 2013, Xu et al. 2013, Wu et al. 2013a, Wu et al. 2013b, Wu et al. 2014, Gao et al. 2014, Li et al. 2019b, Sykam et al. 2019).

Effects of different size-modified expandable graphite (EG) and ammonium polyphosphate (APP) on the flame retardancy, the thermal stability, the physical and the mechanical properties of rigid polyurethane foams were investigated by Pang et al. (2019). It was reported that APP is more effective matter for forming the chemical char than EG. In addition, the size of EG is an important parameter for better thermal and fire resistance. As the size of EG increases, the heat release rate and the total heat released decrease.

Some fillers such as calcite, clay and fly ash are used in polyurethane foams for decreasing production costs (Alavi Nikje et al. 2006, Zatorski et al. 2008, Akdogan 2011, Yurtseven et al. 2013). In addition, the fillers may strengthen the char layer produced by the intumescent flame retardants. The uniform dispersion of the small sized fillers in the foam are very important for enhancement of all the properties (Gürü et al. 2009a, Gürü et al. 2009b, Mishra et al. 2005, Mishra and Shimpi 2007, Shimpi and Mishra 2010, Mishra et al. 2009).

Peng et al. (2018) investigated effects of hydrotalcite on different properties of rigid polyurethane foam including 10 wt % organic phosphate mixture as a commercial flame retardant. It was concluded that the hydrotalcite increases the char residue, retards the decomposition temperatures, improve the thermal stability, and

enhance the sound absorption. In addition, it was reported that a small amount of hydrotalcite increases the compressive strength; however, excessive hydrotalcite negatively affects it. The optimum amount of hydrotalcite was mentioned as 5 wt % for most of the properties.

The effects of multi-walled carbon nanotubes and nanoscale titanium dioxide on the flammability and smoke emission of rigid polyurethane foams containing halogen-free fire retardants were examined by Salasinska et al. (2017). They reported a synergistic effect between the nano fillers and halogen-free flame retardants in terms of fire resistance of the foam. It was informed that generation of the carbonized coating on the surface of the foams restricting the access of fire into the unburned parts of the foam and inhibiting the formation of radicals enhanced the fire resistance of the foam.

Peng et al. (2019) investigated the effects of magnesium hydroxide and aluminum hydroxide additions on the flame retardancy, the thermal stability, the sound absorption and the mechanical properties of rigid polyurethane foam including an organic phosphate mixture as a commercial flame retardant. It was determined that aluminum hydroxide is more effective filler than magnesium hydroxide in terms of the flame retardancy of the foam.

Kuznia et al. (2019) reported that the incorporation of fluidized bed combustion fly ash as a filler enhances the thermal stability of rigid polyurethane foams due to the barrier effect of the fly ash preventing the release of gases from the foam. Furthermore, it was determined that the addition of the fly ash into the foam, up to 10 wt %, improves the mechanical performance of the foams. Cheng et al. (2018) investigated effects of flax fiber on improving performance of rigid polyurethane foams. Their results reveal that the fiber can enhance the mechanical properties and fire resistance of the foam.

As a different approach, Li et al. (2019a) decorated silica aerogels onto surfaces of rigid polyurethane foam to produce porous silica aerogel/polyurethane foam composites. It was reported that the introduction of silica aerogel increased the compressive strength and decreased the thermal conductivity of the foam. In addition, the fire resistance of the foam was enhanced with a compact silica-rich hybrid barrier preventing the thermal decomposition products and the heat transfer during burning. In addition, there are some studies, which are related to the fire protective coating on the surface of the foam (Liu et al. 2019).

5.3.2 Intumescent Flame Retardant (IFR) Systems

The intumescent flame retardant system is composed of mainly three components, namely acid source, blowing agent and carbonizing agent. There are different chemical matters for these components. In this study, ammonium polyphosphate (APP) as an acid source and blowing agent and pentaerythritol (PER) as a carbonizing agent were used to synthesize the intumescent flame retardant (Usta et al. 2011). APP and PER are generally mixed into the polyol component by using a mechanical

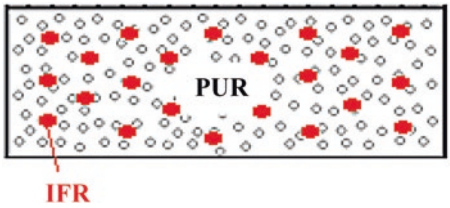

Fig. 5.5 PUR with IFR

mixer and a homogenizer. Then the doped polyol and the isocyanate are mixed by using a mechanical mixer. IFR (APP/PER) should be homogeneously distributed in the foam as shown in Fig. 5.5.

Since the thermal decomposition is an important step before the ignition of the foam, thermogravimetric analyses should be examined to investigate the fire retardant mechanism of IFR. The thermogravimetric analyses of ammonium polyphosphate (APP, Clariant - Exolit AP 423, n > 1000, Phase II, d_{50} = 8 μm) and pentaerythritol (PER, MKS Marmara Chemistry Company d < 75 below 75 μm) are shown in Fig. 5.6. The analyses were performed between 40 °C and 800 °C at a rate of 20 °C/min under nitrogen by using Perkin–Elmer Diamond thermogravimetric analysis (TG/DTA) equipment. Ceramic pans were used in the experiments. The decomposition of PER begins around 175 °C and ends completely around 345 °C. PER has only one decomposition process in which the maximum degradation temperature and the maximum rate of degradation were 334.9 °C and 53.3%/min, respectively. APP starts to decompose around 250 °C and there are three decomposition steps between 40 °C and 785 °C. The residual weight of APP is approximately 12%. Ammonia, water and polyphosphoric acid are evaluated between 300 °C and 450 °C and the polyphosphoric acid is evaporated and/or dehydrated to phosphorus oxides between 500 °C – 700 °C (Duquesne et al. 2000, Wu et al. 2008).

When the rigid polyurethane foam composed of the intumescent flame retardant is exposed to heat or fire, it swells, IFR decomposes and a char layer acting as an insulator and mass transfer barrier slowing down the escape of the combustible volatiles and enhancing the fire resistance of the foam is generated (Lu and Hamerton 2002, Wang and Chen 2005, Bian et al. 2008, Ni et al. 2009, Ni et al. 2010, Barikani et al. 2010, Wang et al. 2018b, Wang et al. 2018c). Figure 5.7 shows a simple view of the char layer.

The ratio of APP to PER is an important factor for effectiveness of IFR system. Four different ratios (APP/PER) which are 1:0, 3:1, 2:1 and 1:2 were investigated for the rigid polyurethane foam. In general, addition of additives and flame retardants may deteriorate the foam process and negatively affect the rising. The effects of IFR systems additions on the foam rising are shown in Fig. 5.8. It was determined that 10% IFR additions resulted in decreasing of foam rising between 7.2% and 9.1%.

There are different kinds of tests used for investigation of fire resistance of polymeric materials, like UL 94, LOI and cone calorimeter (Usta 2012, Gao et al. 2013, Luo et al. 2017). The fire resistance of PUR with and without IFR system, which was determined by using UL 94 test, are shown in Fig. 5.9. Although the flame

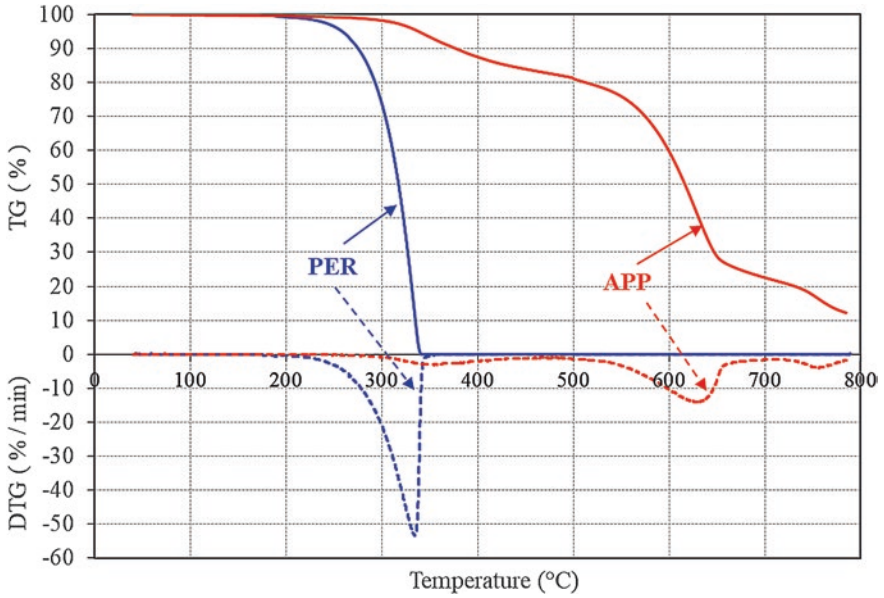

Fig. 5.6 Thermogravimetric analysis of APP and PER

Fig. 5.7 Simple view of intumescent flame retardant mechanism

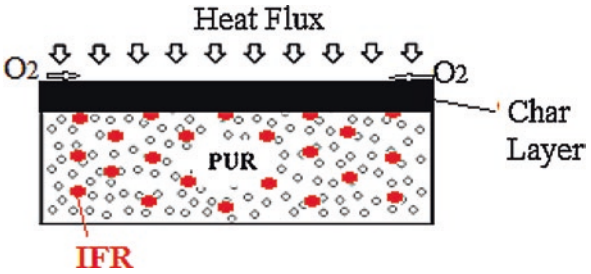

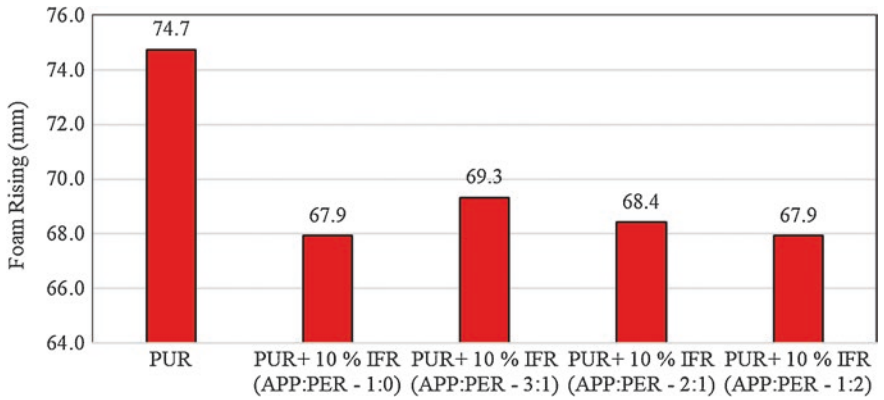

Fig. 5.8 The effects of IFR systems additions on the foam rising

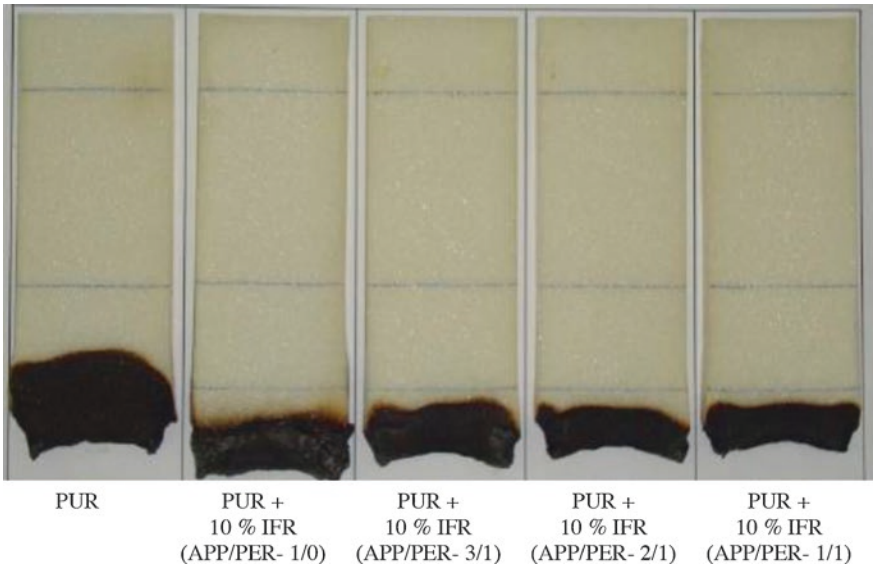

Fig. 5.9 The foam pictures after UL 94 tests

passed the first gauge mark in the pure PUR foam at the burning speed of 40 mm/min, IFR additions obviously enhanced the flammability resistance of the foams. All of the systems show similar effects, and the flame did not pass the first reference line.

In addition, the effects of IFR systems additions on the compressive strength are shown in Fig. 5.10. The compressive tests were performed using an Instron 8801 computer controlled testing machine (model 8801) in accordance with the ASTM D1621- 04a (2004b) standard. As it is expected that IFR additions decreased the compressive strength of the foam. 10% IFR addition causes decreasing of the compressive strength in the range of 15.8 to 29.6%. However, it should be pointed out that all of them have the compressive strength more than 100 kPa, which is an acceptable value for most of the rigid polyurethane foam applications.

Thermal conductivity is an important property for rigid polyurethane foams. The effects of different IFR systems on the thermal conductivity that was measured using Kyoto QTM-500 are shown in Fig. 5.11. The addition of IFR system caused increasing of thermal conductivity of the foams in the range of 4.3 to 9.0%. The smallest increase was obtained with IFR (APP:PER – 2:1) as 4.3%.

In general, these results imply that effective fire resistance of the rigid polyurethane foam can be obtained by using the intumescent flame retardant including APP:PER in the mass ratio of 2:1 without significant increasing of thermal conductivity. Demir et al. (2005) also found the same ratio for fireproof polypropylene.

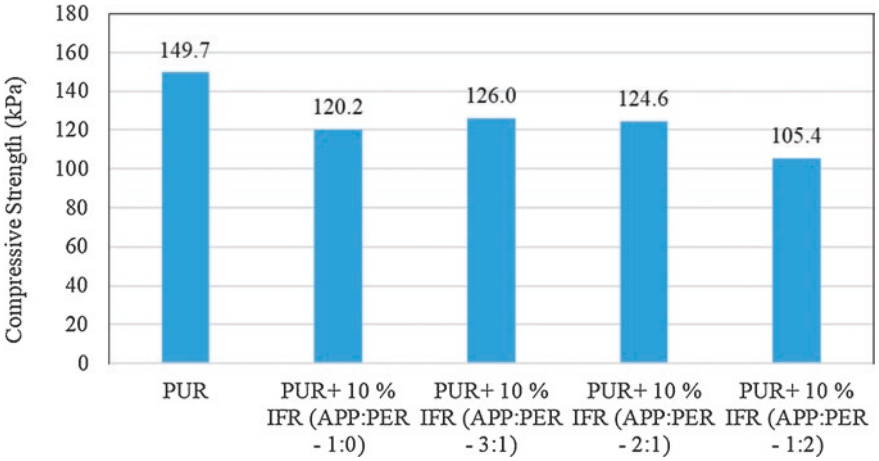

Fig. 5.10 Effects of different IFR systems on the Compressive Strength of the foams

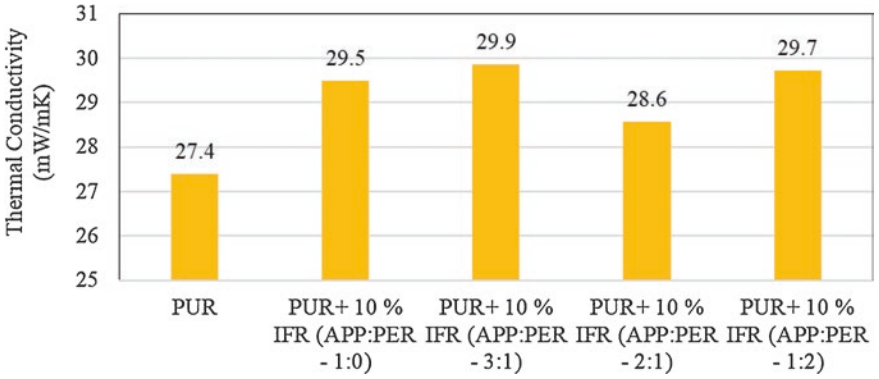

Fig. 5.11 Effects of different IFR systems on the thermal conductivity of the foams

5.4 Fireproof Rigid Polyurethane Foams

In this section, two different applications were presented for fireproof rigid polyurethane foams. The first one is halogen-free intumescent flame retardant (IFR) addition into the PUR and the second one is covering of the PUR with glass fiber fabric (GFf). In addition, these two approaches are compared at two different fire scenarios, namely medium sized and small sized fire scenarios.

5.4.1 Intumescent Flame Retardant (IFR) Application

The intumescent flame retardant containing ammonium polyphosphate (APP, 2 unit) as an acid source/blowing agent and pentaerythritol (PER, 1 unit) as a carbonific agent was used as a flame retardant for rigid polyurethane foams (Usta et al. 2011). "IFR" notation implies this combination of the intumescent flame retardant in the rest of the chapter. A laboratory-scale batch process was used to produce the rigid polyurethane foams (PUR) with and without IFR. The ratio of polyol and isocyanate was 1/1.18 and the amounts of the components were determined to get foams of 40 ± 0.5 kg/m^3 density. IFR was incorporated into the polyol in 5, 10, 15 and 20 wt % by using a mechanical homogenizer. The polyol/IFR and the isocyanate are mixed with a mechanical stirrer. Then the mixture was poured into a preheated aluminum mold. The samples were removed from the mold, which was kept under a press after the curing process completion. Effects of different amounts of IFR on the rising of the foam are shown in Fig. 5.12. IFR addition results in decreasing of the foam rising. However, the foam rising of PUR with 20% IFR addition is acceptable level. In addition, the density of the foam increases with IFR (Fig. 5.13).

In addition, the compressive strength and the thermal conductivity are very important properties for thermal insulation applications. The effects of IFR additions on these properties are shown in Figs. 5.14 and 5.15. IFR additions slightly enhanced the compressive strength of the foam. However, there was a slight increase in thermal conductivity. 20% IFR addition caused less than 5% increase in the thermal conductivity. Different factors, which are the cell size and orientation, the foam

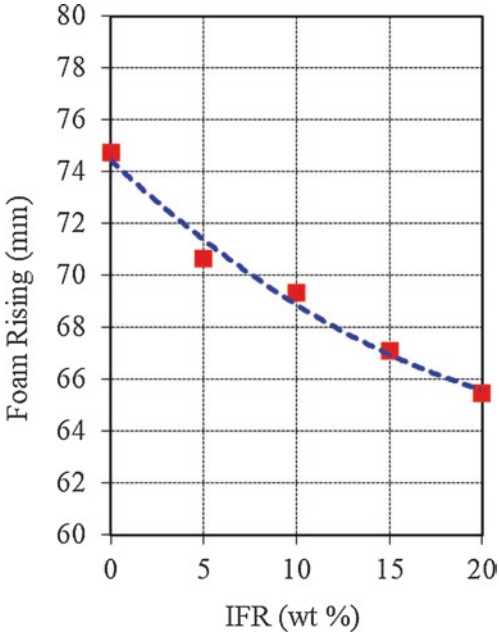

Fig. 5.12 Effects of different amounts of IFR systems on the rising of foam

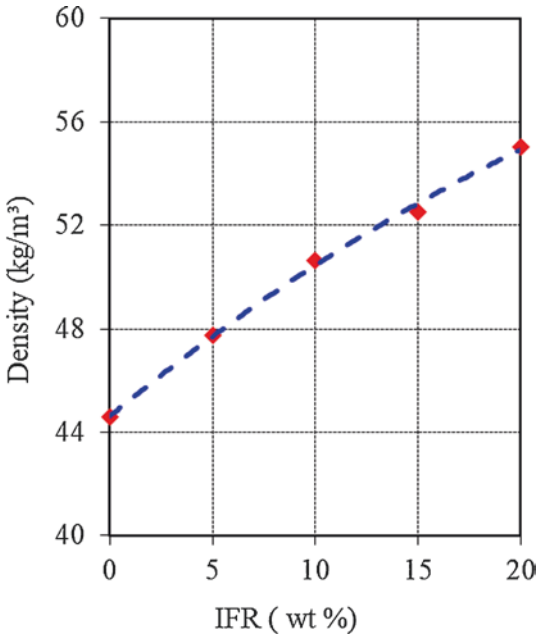

Fig. 5.13 Effects of different amounts of IFR systems on the density of foam

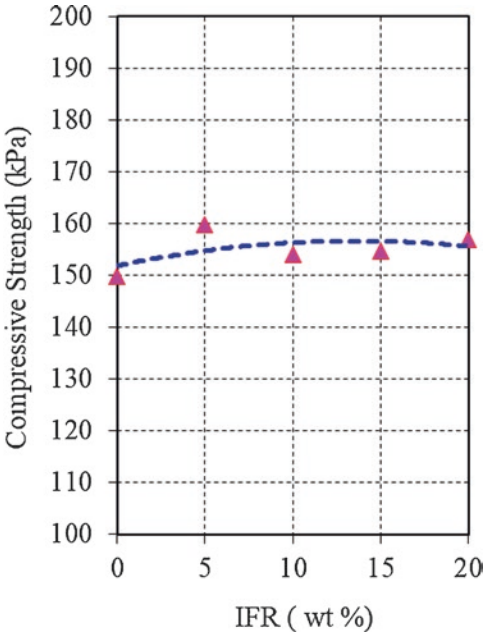

Fig. 5.14 Effects of different amounts of IFR systems on the compressive strength

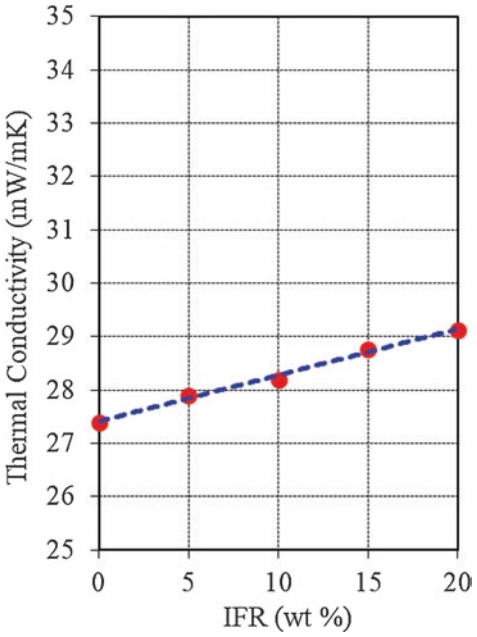

Fig. 5.15 Effects of different amounts of IFR systems on the thermal conductivity

density, the ratio of close to open cell and the thermal conductivity of the gases in the cells and the filling materials, affects the thermal conductivity of rigid polyurethane foam (Thirumal et al. 2010a). As a different description, the thermal conductivity of the foam is affected by three different parameters, namely, thermal conductivity of the gas inside the cells, thermal conductivity of the solid phase and the radiation across the cells (Modesti and Simioni 1994).

Scanning Electron Microscope (SEM) views of the foams are shown in Fig. 5.16. The shape of cells in PUR was approximately polyhedron. However, the addition of IFR into PUR slightly changed the shapes of the cells. There was slightly increasing in the mean diameters of the cells.

As it is known that investigation of the thermal degradation is very important to investigate the flammability, the burning, and the flame retardancy of polymer materials. The thermogravimetric analyses of the foams are shown in Fig. 5.17. The foams exhibited similar three decomposition processes. The thermal decomposition starts with evolving water (over 100 °C) and continued with the dissociation of the thermally weakest links, namely allophanate and biuret (Levchik and Weil 2004).

The incorporation of IFR accelerated the main decomposition processes and decreased the maximum degradation temperature (Duquesne et al. 2001). The early decomposition of PUR including IFR can be explained with the intumescent flame retardant. Because IFR quickly decomposes and produces a char layer. This char layer can partially slow down the decomposition of the foam. This results in enhancing of the thermal stability at high temperatures (Kulesza et al. 2006, Wu et al. 2008). Figure 5.18 shows the results of UL 94 flammability tests of the foams. As it is shown that 20% IFR addition provided the best fire resistance.

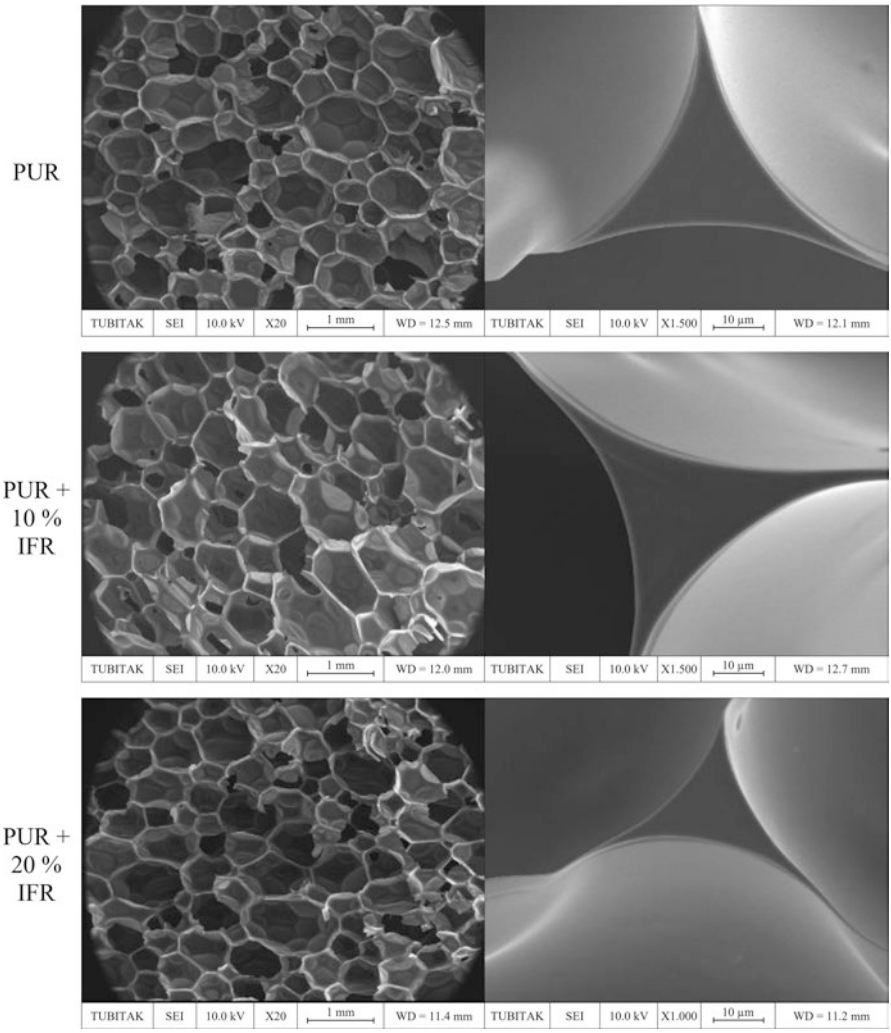

Fig. 5.16 SEM views of PUR and IFR added PUR

Cone calorimeter is a bench-scale equipment that can simulate real-world fire conditions (Morgan and Bundy 2007, Usta 2012). In addition, cone calorimeter test which is a combustion test for investigation of fire resistance of polymeric materials (Wu et al. 2008, Beyer 2007) can generate important parameters such as time to ignition (TTI), heat release rate (HRR), total heat released (THR), residual mass, smoke and CO/CO_2 release rates (Chung et al. 2009).

The fire behaviors of PUR, PUR+ 10% IFR and PUR+ 20% IFR were examined by a cone calorimeter according to ASTM E-1354 (2004a) and ISO-5660 (2002) standards. Figure 5.19 shows the pictures of the cone calorimeter. The foams (100 x

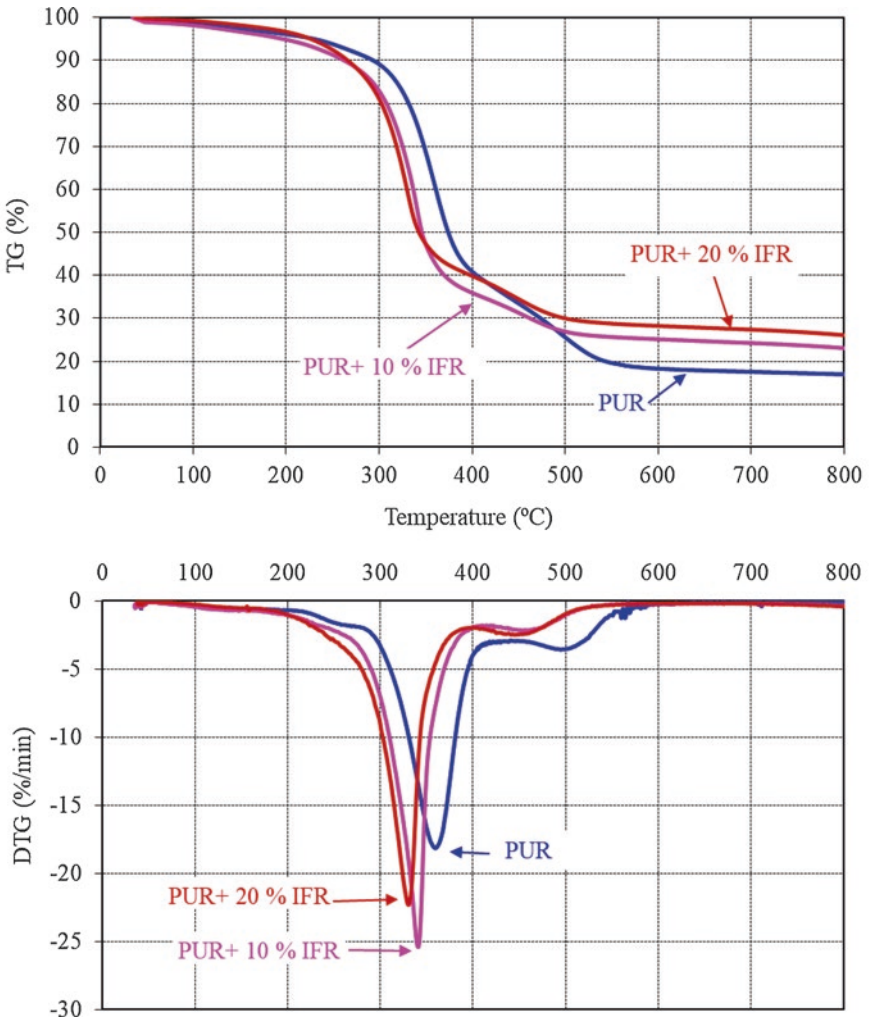

Fig. 5.17 Thermogravimetric analysis of PUR, PUR + 10% IFR and PUR + 20% IFR

100 x 50 mm) were exposed horizontally to a heat flux of 35 ± 1 kW/m^2 as shown in Fig. 5.20.

Heat release rate (HRR) is an important parameter to investigate fire resistance of polymer materials (Zhang et al. 2004). The heat release rates of PUR, PUR+ 10% IFR and PUR+ 20% IFR foams are given in Fig. 5.21. All of the foams presented similar characteristics of thermally thick charring samples. In other words, when the foams are exposed a heat flux, the heat release rate increases and then a char layer is generated, after that the thickness of the char layer increases resulting in decreases in the heat release rates (Schartel and Hull 2007, Lu et al. 2015, Wang et al. 2011, Usta 2012). However, IFR additions resulted in decreasing of peak heat release rates

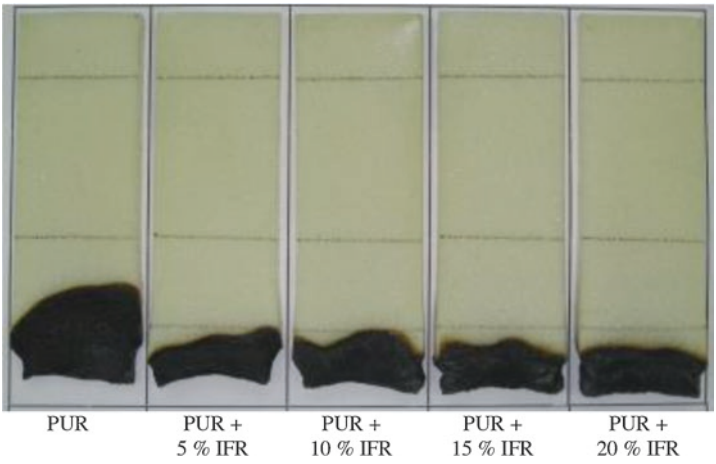

Fig. 5.18 Pictures of the foams after UL 94 Flammability Tests

Fig. 5.19 Pictures of the cone calorimeter

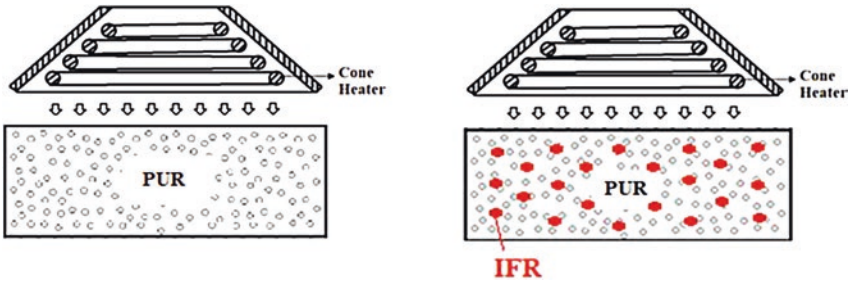

Fig. 5.20 Heat flux applications

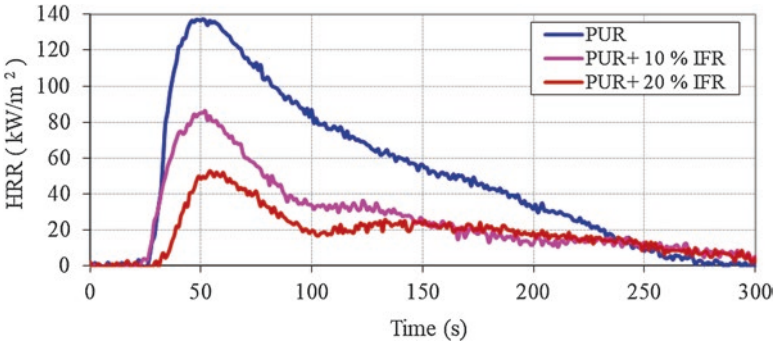

Fig. 5.21 The HRR variations of PUR, PUR+ 10% IFR and PUR+ 20% IFR

and extended the time to reach peak heat release rates. Furthermore, it should be pointed out that peak heat release rate (PHRR) is an important parameter indicating the intensity of fires (Chung et al. 2009). IFR decomposition accelerates the formation of a better char layer. This char layer slows down the decomposition of the foam and reduces the heat release rate (Usta 2012). Although 10% IFR did not increase the time to ignition significantly, 20% IFR delayed the ignition. It is desirable to have a long ignition time for the foams (Checchin et al. 1999). It can be said that PUR+ 20% IFR present better performance in terms of the fire resistance.

Figure 5.22 shows total heat released (THR) curves of PUR, PUR+ 10% IFR and PUR+ 20% IFR. It is obviously seen that IFR significantly reduced the THR values. The reductions are explained with the barrier effect of the char layer (Zhao et al. 2005, Konig et al. 2009). It is thought that 20% IFR addition results in a stronger and more effective char layer with respect to 10%IFR addition.

Smoke and carbon monoxide (CO) emissions are the most important toxic substances in fires of rigid polyurethane foams (Checchin et al. 1999). Smoke and CO emissions of PUR, PUR+ 10% IFR and PUR+ 20% IFR are given in Fig. 5.23 and Fig. 5.24, respectively. The strength of fire and the material properties affect the generation of smoke and CO, which are formed due to the incomplete combustion of the foam. The smoke and CO changes are similar. IFR additions considerably decreased the peak values of the smoke and CO. In addition, the effects of IFR continue, and smoke/CO generations decrease during the rest of burning times. Although the heat release rates reduced to nearly zero and there was no flame at the end of the burning time of 300 s, there were still some smoke and CO emissions because of the smoldering combustion of the foams at low intensity (Price et al. 2000).

The carbon dioxide (CO_2) emissions are shown in Fig. 5.25. CO_2 emissions of PUR+ 10% IFR and PUR+ 20% IFR were lower than that of PUR. The CO_2 emissions of the foams revealed similar changes with the HRR curves (Bustamante Valencia et al. 2009). The CO_2 emissions of PUR+ 10% IFR and PUR+ 20% IFR decreased because of the char layer formation generated by IFR. It is thought that

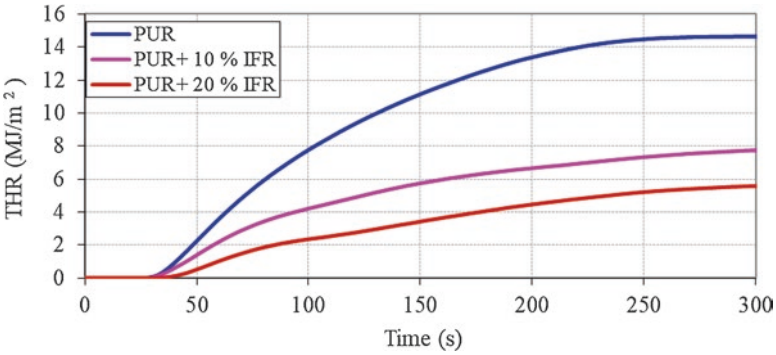

Fig. 5.22 The THR variations of PUR, PUR+ 10% IFR and PUR+ 20% IFR

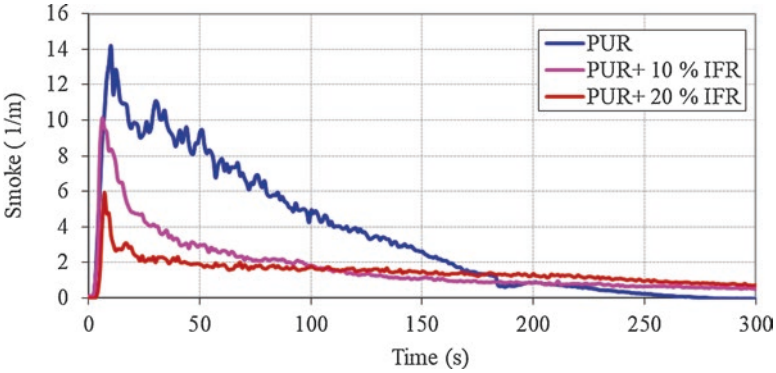

Fig. 5.23 Smoke emissions of PUR, PUR+ 10% IFR and PUR+ 20% IFR

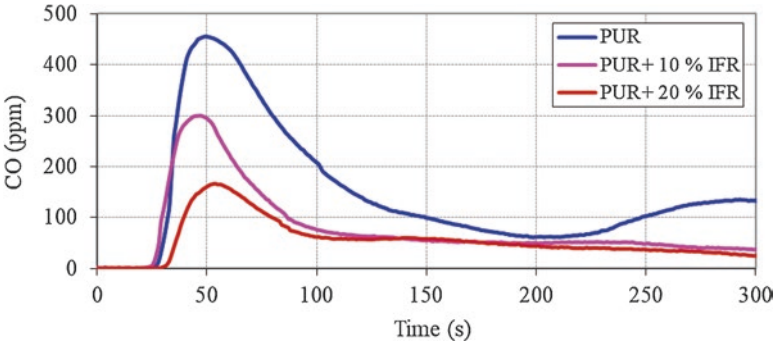

Fig. 5.24 CO emissions of PUR, PUR+ 10% IFR and PUR+ 20% IFR

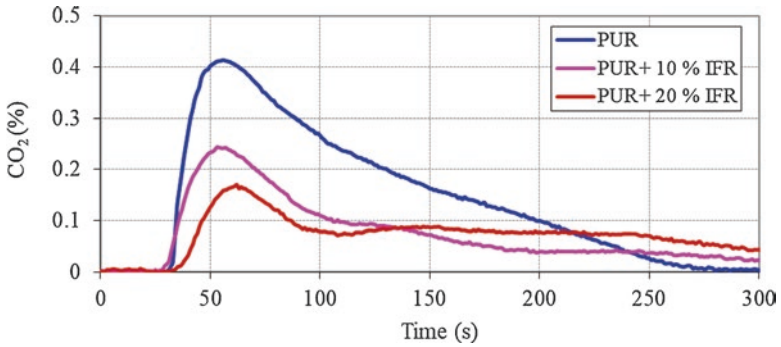

Fig. 5.25 CO_2 emissions of PUR, PUR+ 10% IFR and PUR+ 20% IFR

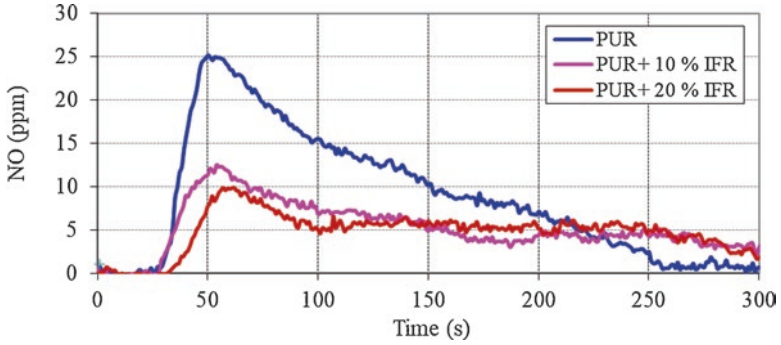

Fig. 5.26 Nitrogen oxides of PUR, PUR + 10% IFR and PUR + 20% IFR

the char layer protects the underlying foam from further burning (Duquesne et al. 2000, Wu et al. 2008).

Bustamante Valencia et al. (2009) reported that the quantities of nitrogen gas species (NO_2, HCN, N_2O, NH_3) are less than 2 ppm in gas products emitted during burning of the polyurethane foams at different heat applications. Since even the small amount of NO emission is considerably harmful, it is useful to examine NO emission. There are mainly two reasons for the formation of NO emission from the polyurethane foam burning, namely the high temperature and the nitrogen in the foam. Figure 5.26 shows NO emissions of PUR, PUR+ 10% IFR and PUR+ 20% IFR. IFR additions decreased NO emissions. This situation can be explained with the lower HRR values of PUR+ 10% IFR and PUR+ 20% IFR. Twenty percent IFR addition reduced NO emission below 10 ppm.

The char structure may reveal the burning behavior of the foams. The effective char layer formation prevents the heat transfer and the oxygen between the burning foam and the flame zone. Meantime the layer retards the decomposition of the foam

and retains the underlying foam from further burning (Lv et al. 2005). Pictures of PUR, PUR+ 10% IFR and PUR+ 20% IFR after cone calorimeter tests are shown in Fig. 5.27. It is obviously seen that the char layer of PUR + 20% IFR is better than that of PUR+ 10% IFR. In addition, the residual mass of PUR+ 20% IFR is more than that of PUR + 10% IFR.

5.4.2 *Glass Fiber Fabric (GFf) Application*

A laboratory-scale batch process is used to produce the rigid polyurethane foams (PUR) as mentioned previous section. Similar procedure was applied to produce the rigid polyurethane foam covered with glass fiber fabric (PUR + GFf) (Demiryuguran 2015). However, the glass fiber fabric, which was supplied from Cam Elyaf Corporation (Turkey), was placed at the bottom of the mold and under the cover of the mold as shown in Fig. 5.28. The schematic of PUR with GFf is shown in Fig. 5.29.

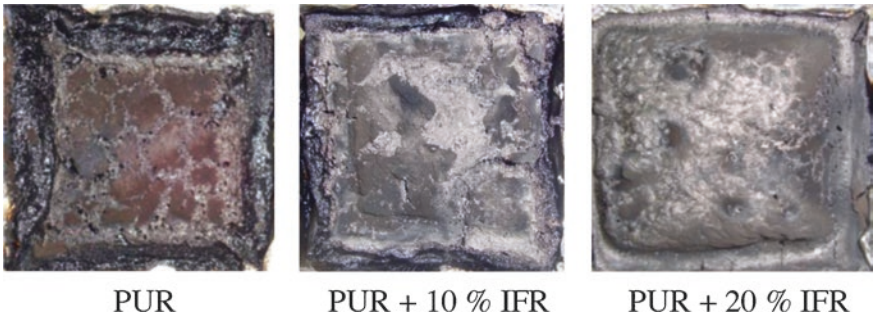

Fig. 5.27 Pictures of PUR, PUR+ 10% IFR and PUR+ 20% IFR after cone calorimeter tests

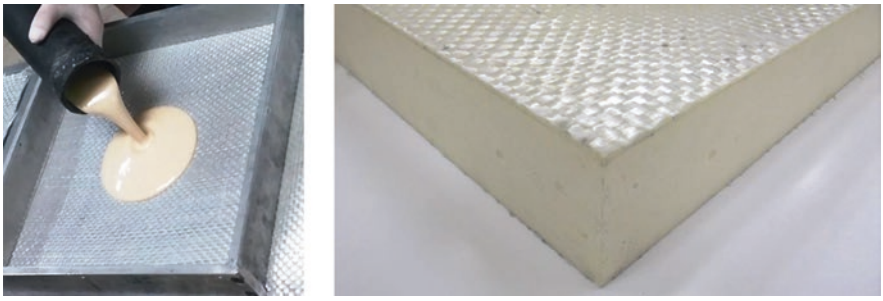

Fig. 5.28 Pouring of polyol and isocyanate mixture over GFf and PUR with GFf

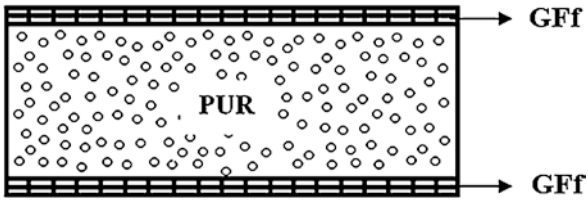

Fig. 5.29 Schematic of PUR with GFf

The thermogravimetric analysis of the glass fiber fabric, which is an E-glass woven fabric (0°/90°) with areal weight of 500 g/m^2, is shown in Fig. 5.30. As it is shown that GFf does not decompose up to 950 °C.

PUR and PUR+GFf were tested in the cone calorimeter at different heat fluxes, namely 15 kW/m^2 and 35 kW/m^2 in the horizontal position as shown in Fig. 5.31 to simulate small and medium sized fires, respectively.

5.4.2.1 Medium-Sized Fire Simulation (35 kW/m^2)

The HRR values of PUR+ GFf are compared with those of PUR and PUR+ 20% IFR at heat flux of 35 kW/m^2 in Fig. 5.32. Although GFf does not considerably affect the ignition behavior of the foam, the peak heat release rate was slightly decreased with GFf. However, PUR+ GFf cannot satisfy the fire resistance as much as PUR + 20% IFR addition. Meanwhile, the effect of GFf on the total heat released (THR) is shown in Fig. 5.33. There is only 26% reduction was occurred in 300 s with GFf.

Figures 5.34 and 5.35 show smoke and CO generations of PUR, PUR+ GFf and PUR+ 20% IFR, respectively. GFf retards the smoke generation and results in lower smoke than that of PUR. However, GFf cannot decrease the smoke as much as 20% IFR addition. Meanwhile, GFf causes reduction in CO emissions and the general trend of PUR+ GFf is very similar to that of PUR+ 20% IFR. CO emission of PUR foam increases after approximately 230 s implying smoldering combustion of the foam. Again, GFf and 20% IFR reduces the smoldering combustion intensity of the foam. CO_2 emissions of PUR, PUR+ 20% IFR and PUR+ GFf are shown in Fig. 5.36. Since the CO_2 formation is directly related to burning mass of the foam, CO_2 emissions are very similar to the HRR values. NO emissions of the foams are compared in Fig. 5.37. GFf coverage does not change NO emission of PUR. Figure 5.38 shows the pictures of the foams after cone calorimeter test. The glass fiber fabric can be seen clearly, but the foam under the glass fiber fabric was burned.

5.4.2.2 Small-Sized Fire Simulation (15 kW/m^2)

When the foams were exposed to the heat flux of 15 kW/m^2, there were obvious differences in burning characteristics and the fire resistances of the foams. Although PUR+ 20% IFR shows similar trend with PUR, PUR+ GFf shows different characteristics

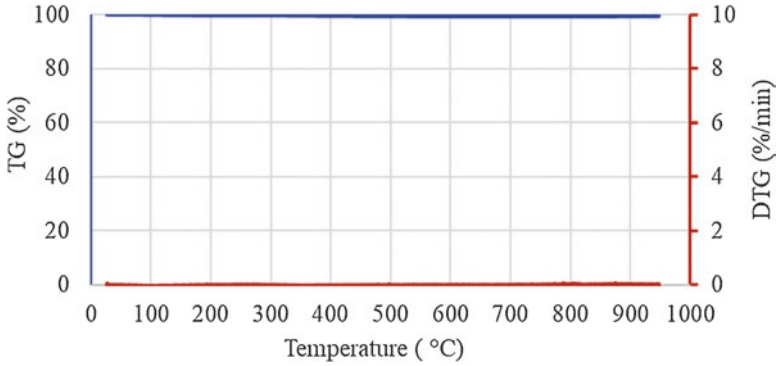

Fig. 5.30 Thermogravimetric analysis of GFf

Fig. 5.31 Heat Flux application on PUR + GFf

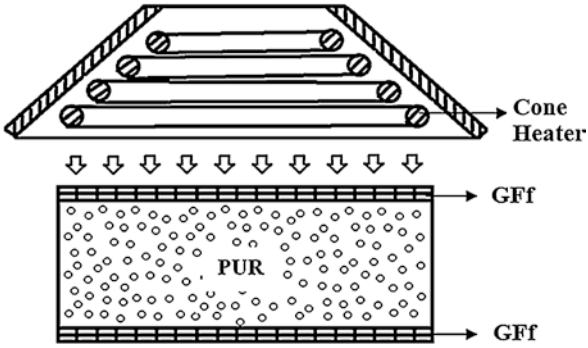

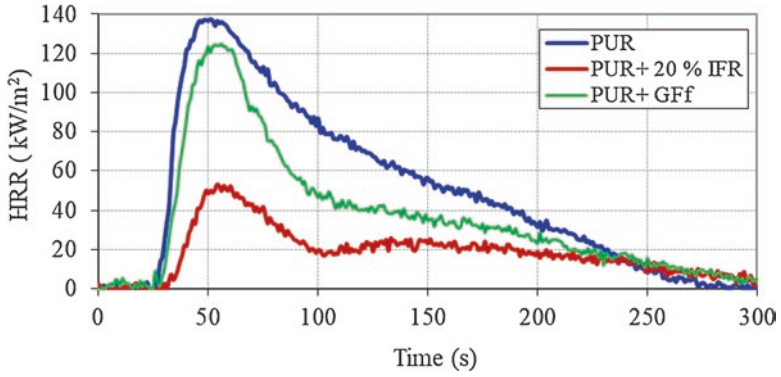

Fig. 5.32 HRR variations of PUR, PUR+ 20% IFR and PUR+ GFf at heat flux of 35 kW/m^2

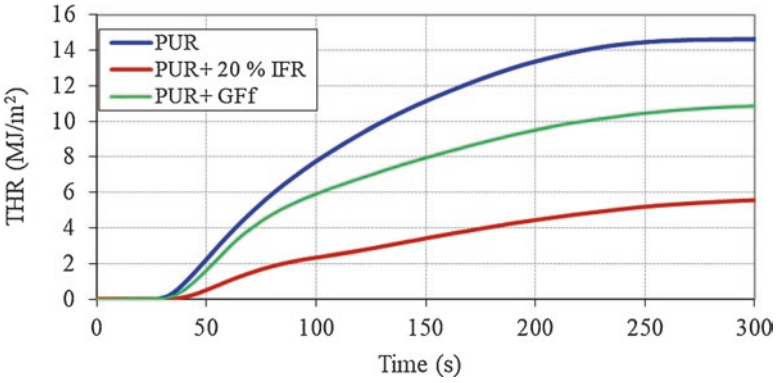

Fig. 5.33 THR variations of PUR, PUR+ 20% IFR and PUR+ GFf at heat flux of 35 kW/m^2

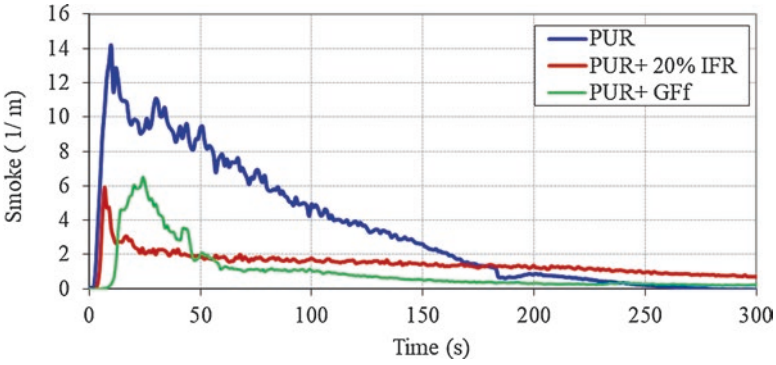

Fig. 5.34 Smoke emissions of PUR, PUR+ 20% IFR and PUR+ GFf at heat flux of 35 kW/m^2

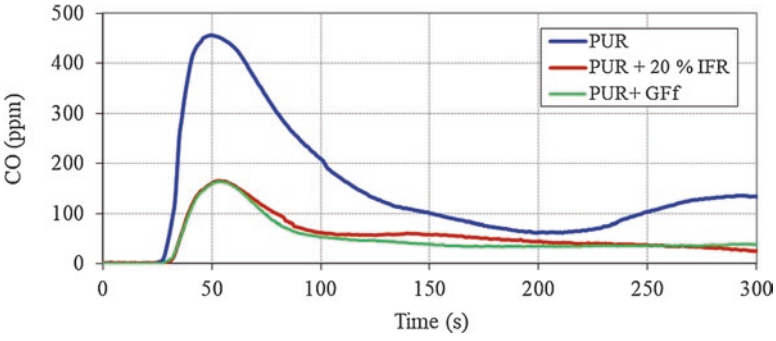

Fig. 5.35 CO emissions of PUR, PUR + 20% IFR and PUR + GFf at heat flux of 35 kW/m^2

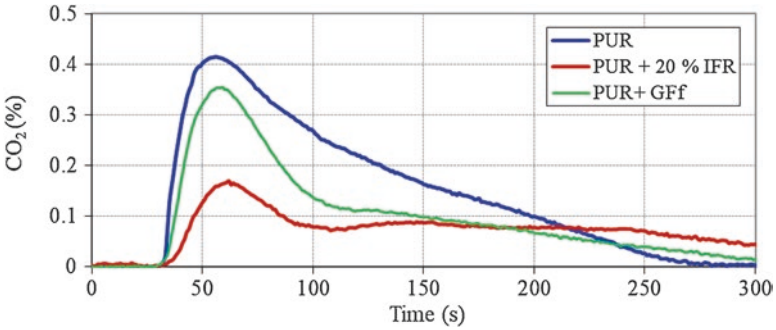

Fig. 5.36 CO_2 emissions of PUR, PUR + 20% IFR and PUR+ GFf at heat flux of 35 kW/m^2

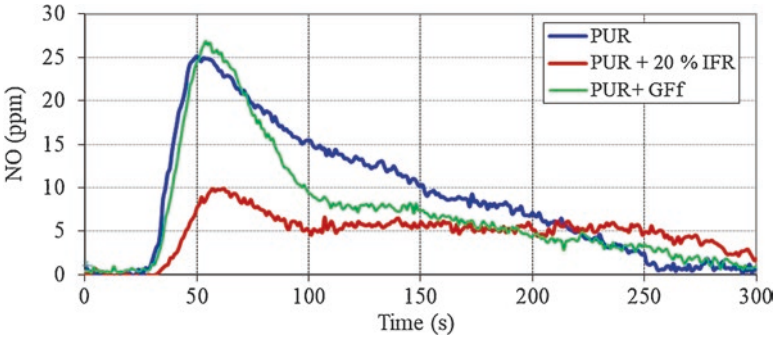

Fig. 5.37 NO emissions of PUR, PUR+ 20% IFR and PUR+ GFf at heat flux of 35 kW/m^2

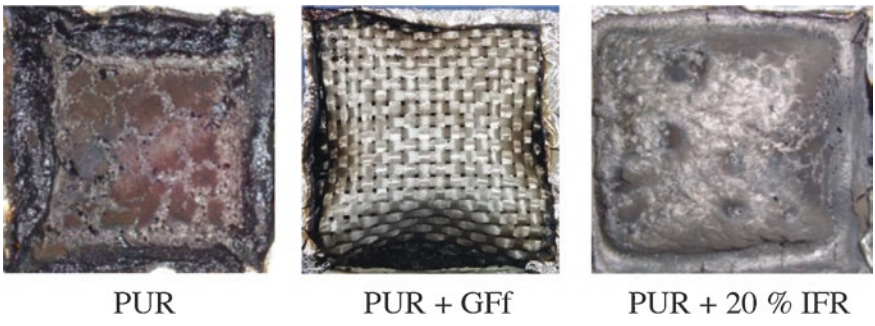

Fig. 5.38 Pictures of PUR, PUR+ 20% IFR and PUR+ GFf after cone calorimeter tests (35 kW/m^2)

(Fig. 5.39). The time to ignition increased with GFf and the peak heat release rate increased sharply, but it decreased quickly. The flame diminished early than others. In addition, the difference can be seen clearly in THR values shown in Fig. 5.40. GFf can achieve better fire resistance than 20% IFR addition at the heat flux of 15 kW/m^2.

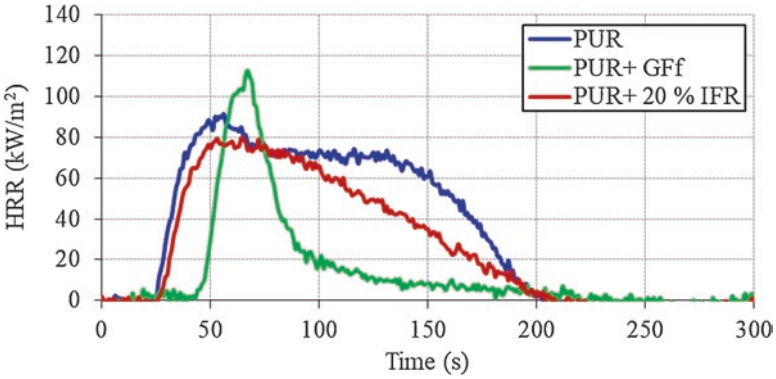

Fig. 5.39 HRR variations of PUR, PUR+ 20% IFR and PUR+ GFf at heat flux of 15 kW/m^2

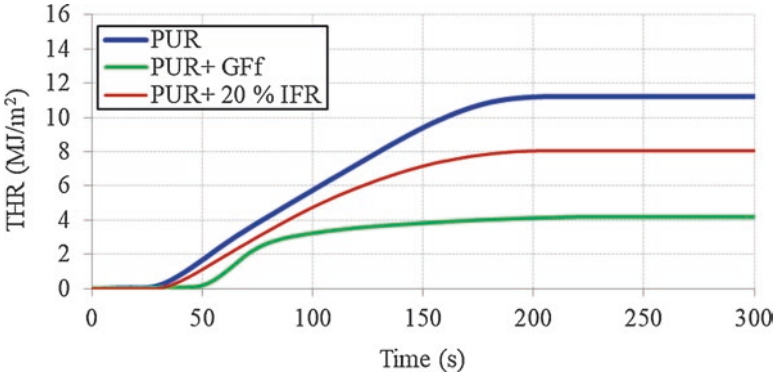

Fig. 5.40 THR variations of PUR, PUR+ 20% IFR and PUR + GFf at heat flux of 15 kW/m^2

Smoke emissions are shown in Fig. 5.41. The smoke generations were reduced with decreasing of the heat flux. The smoke generations of PUR and PUR+ 20% IFR are very close each other. However, GFf retarded the smoke emissions and again resulted in lower smoke emissions in shorter time range.

CO emissions are presented in Fig. 5.42. There is a strange changing at the heat flux of 15 kW/m^2. PUR+ 20% IFR generate more CO emissions than PUR. However, GFf retarded CO emissions and resulted in lower CO emissions.

CO_2 emissions of PUR, PUR+ 20% IFR and PUR+ GFf at heat flux of 15 kW/m^2 are shown in Fig. 5.43. Since the CO_2 formation is directly related to burning mass of the foam, CO_2 emissions are very similar to the HRR values. NO emissions of the foams are compared in Fig. 5.44. GFf retarded NO emission and generation of NO occurred in a short time. Figure 5.45 shows the pictures of the foams after cone calorimeter test. The positive effect of the glass fiber fabric can be seen clearly.

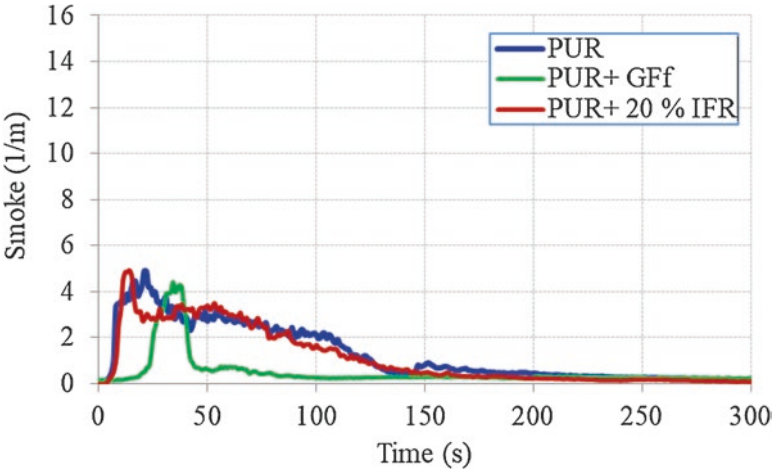

Fig. 5.41 Smoke emissions of PUR, PUR+ 20% IFR and PUR+ GFf at heat flux of 15 kW/m^2

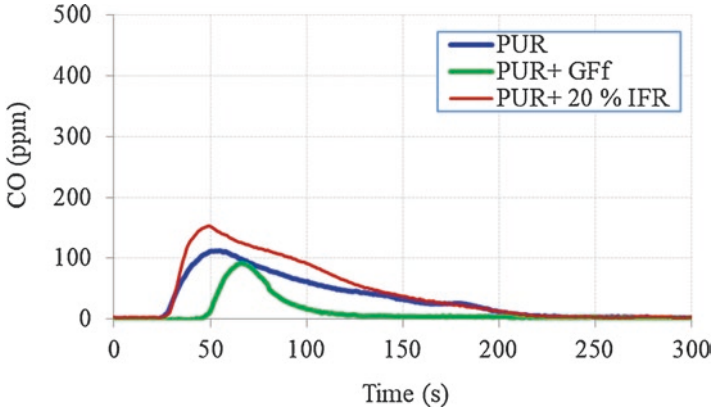

Fig. 5.42 CO emissions of PUR, PUR+ 20% IFR and PUR+ GFf at heat flux of 15 kW/m^2

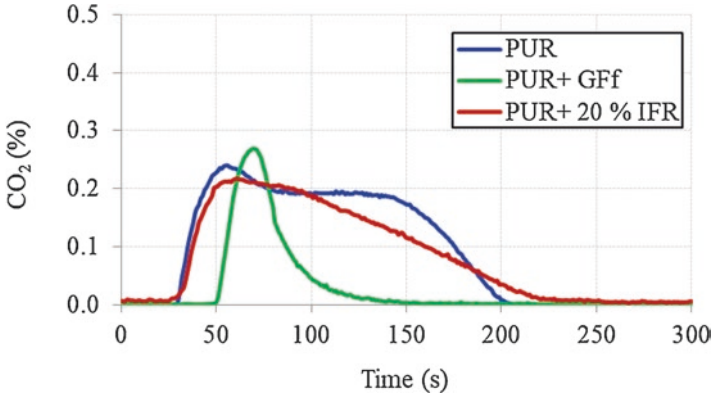

Fig. 5.43 CO_2 emissions of PUR, PUR+ 20% IFR and PUR+ GFf at heat flux of 15 kW/m^2

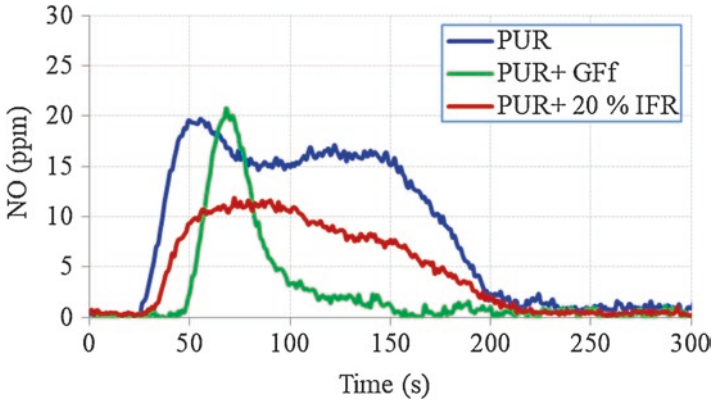

Fig. 5.44 NO emissions of PUR, PUR+ 20% IFR and PUR+ GFf at heat flux of 15 kW/m^2

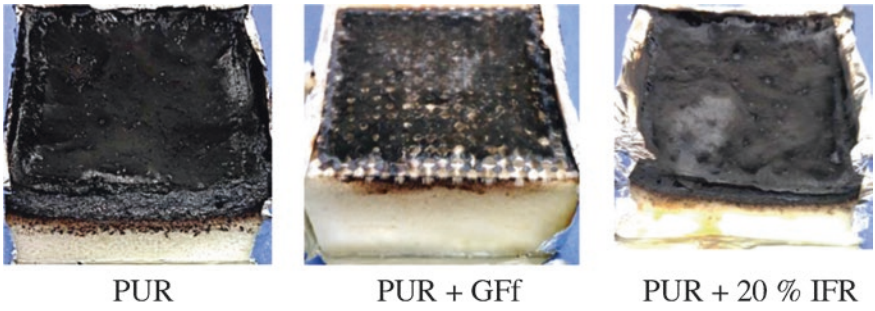

Fig. 5.45 Pictures of PUR, PUR+ 20% IFR and PUR+ GFf after cone calorimeter tests (15 kW/m^2)

5.5 Conclusions

In this chapter, the information about different studies that were performed to enhance the fireproof capability of rigid polyurethane foams are presented briefly. In this context, the flame retardants and their effects on the fire resistance of the foams are introduced. Among them, the intumescent flame retardants as halogen-free flame retardants have been found to stand out because of better performance. Therefore, extensive studies were conducted on the intumescent flame retardants for providing fireproof rigid polyurethane foams.

The effects of intumescent flame retardant (IFR) systems which are composed of ammonium polyphosphate (APP) as an acid source/blowing agent and pentaerythritol (PER) as a carbonific agent on the fire resistance, the thermal stability, the thermal conductivity and the mechanical properties of the rigid polyurethane foams were investigated. 20 wt % IFR (APP:PER – 2:1) addition into the rigid polyurethane foam can effectively enhance the fire resistance of the foam at medium sized fire condition (heat flux of 35 kW/m^2) without deterioration of the mechanical

properties, the thermal stability and the thermal conductivity. Furthermore, it was determined that IFR additions can decrease toxic emissions namely CO, smoke and NO, during the burning.

Additionally, a different approach, which is the coverage of rigid polyurethane foams with glass fiber fabric (GFf), is introduced to enhance the fireproof capability of the foams in this chapter. Although the coverage of the foam with GFf can provide limited fire resistance at the medium sized fires (heat flux of 35 kW/m^2), it can achieve very good fire resistance at small sized fire conditions (heat flux of 15 kW/m^2), even better than 20 wt % IFR addition. Moreover, GFf can significantly inhibit CO, smoke and NO emissions at the small sized fire conditions.

Acknowledgments The authors would like to thank TÜBİTAK (The Scientific and Technological Research Council of Turkey) supporting this study under project contract no. 108T246. In addition, the authors would like to Pamukkale University for providing necessary facilities to complete this study.

References

Akdogan E (2011) Farklı Katkı Maddelerinin Poliüretan Malzemelerin Mekanik Özellikleri Üzerine Etkileri (in Turkish)., MSc Thesis. Pamukkale University

Akdogan E, Erdem M, Ureyen ME, Kaya M (2019) Rigid polyurethane foams with halogen-free flame retardants: thermal insulation, mechanical, and flame retardant properties. J Appl Polym Sci 47611:47611. https://doi.org/10.1002/app.47611

Alavi Nikje MM, Garmarudi AB, Haghshenas M (2006) Effect of talc filler on physical properties of polyurethane rigid foams. Polym Plast Technol Eng 45:1213–1217. https://doi.org/10.1080/03602550600887541

ASTM (2004a) E-1354-04a standard test method for heat and visible smoke release rates for materials and products using an oxygen consumption calorimeter. An American National Standard. https://doi.org/10.1520/E1354-04A

ASTM (2004b) D-1621-04a, standard test method for compressive properties of rigid cellular plastics, ASTM international. An American National Standard. https://doi.org/10.1520/D1621-04A

Bahattab MA, Mosnáček J, Basfar AA, Shukri TM (2010) Cross-linked poly(ethylene vinyl acetate) (EVA)/lowdensity polyethylene (LDPE)/metal hydroxides composites for wire and cable applications. Polym Bull 64:569–580. https://doi.org/10.1007/s00289-009-0194-0

Barikani M, Askari F, Barmar M (2010) A comparison of the effect of different flame retardants on the compressive strength and fire behaviour of rigid polyurethane foams. Cell Polym 29:343–358. https://doi.org/10.1177/026248931002900602

Bastin B, Paleja R, Lefebvre J (2003) Fire behavior of polyurethane foams. J Cell Plast 39:323–340. https://doi.org/10.1177/0021955X03039004005

Beyer G (2007) Flame Retardancy of thermoplastic polyurethane and polyvinyl chloride by organoclays. J Fire Sci 25:65–78. https://doi.org/10.1177/0734904107064602

Bian X-C, Tang J-H, Li Z-M (2008) Flame retardancy of hollow glass microsphere/rigid polyurethane foams in the presence of expandable graphite. J Appl Polym Sci 109:1935–1943. https://doi.org/10.1002/app.27786

Bustamante Valencia L, Rogaume T, Guillaume E et al (2009) Analysis of principal gas products during combustion of polyether polyurethane foam at different irradiance levels. Fire Saf J 44:933–940. https://doi.org/10.1016/j.firesaf.2009.05.003

Cao ZJ, Dong X, Fu T et al (2017) Coated vs. naked red phosphorus: a comparative study on their fire retardancy and smoke suppression for rigid polyurethane foams. Polym Degrad Stab 136:103–111. https://doi.org/10.1016/j.polymdegradstab.2016.12.004

Checchin M, Cecchini C, Cellarosi B, Sam F (1999) Use of cone calorimeter for evaluating fire performances of polyurethane foams. Polym Degrad Stab 64:573–576. https://doi.org/10.1016/S0141-3910(98)00131-1

Chen X, Li J, Gao M (2019) Thermal degradation and flame retardant mechanism of the rigid polyurethane foam including functionalized graphene oxide. Polymers (Basel):11. https://doi.org/10.3390/polym11010078

Chen Y, Li L, Qian L (2018) The pyrolysis behaviors of phosphorus-containing organosilicon compound modified ammonium polyphosphate with different phosphorus-containing groups, and their different flame-retardant mechanisms in polyurethane foam. RSC Adv 8:27470–27480. https://doi.org/10.1039/c8ra04439b

Chen Y, Li L, Wang W, Qian L (2017) Preparation and characterization of surface-modified ammonium polyphosphate and its effect on the flame retardancy of rigid polyurethane foam. J Appl Polym Sci 134:1–9. https://doi.org/10.1002/app.45369

Cheng JJ, Qu WJ, Sun SH (2018) Effects of flame-retardant flax-fiber on enhancing performance of the rigid polyurethane foams. J Appl Polym Sci 135:1–10. https://doi.org/10.1002/app.46436

Chung YJ, Kim Y, Kim S (2009) Flame retardant properties of polyurethane produced by the addition of phosphorous containing polyurethane oligomers (II). J Ind Eng Chem 15:888–893. https://doi.org/10.1016/j.jiec.2009.09.018

Czech-Polak J, Przybyszewski B, Heneczkowski M et al (2016) Effect of environmentally-friendly flame retardants on fire resistance and mechanical properties of rigid polyurethane foams. Polimery/Polymers 61:113–116. https://doi.org/10.14314/polimery.2016.113

Demir H, Arkış E, Balköse D, Ülkü S (2005) Synergistic effect of natural zeolites on flame retardant additives. Polym Degrad Stab 89:478–483. https://doi.org/10.1016/j.polymdegradstab.2005.01.028

Demiryuğuran F (2015) Cam Elyaf, Karbon Elyaf ve Organik Madde Takviyeli Kompozit Poliüretan Köpük Malzemelerin Isıl Bozunma ve Yanma Davranışlarının İncelenmesi (in Turkish)., MSc Thesis. Pamukkale University

Duquesne S, Le Bras M, Bourbigot S et al (2000) Analysis of fire gases released from polyurethane and fire-retarded polyurethane coatings. J Fire Sci 18:456–482. https://doi.org/10.1106/6CRG-Q8VD-PV3G-ELDD

Duquesne S, Le Bras M, Bourbigot S et al (2001) Mechanism of fire retardancy of polyurethanes using ammonium polyphosphate. J Appl Polym Sci 82:3262–3274. https://doi.org/10.1002/app.2185

Gao L, Zheng G, Zhou Y et al (2013) Synergistic effect of expandable graphite, melamine polyphosphate and layered double hydroxide on improving the fire behavior of rosin-based rigid polyurethane foam. Ind Crop Prod 50:638–647. https://doi.org/10.1016/j.indcrop.2013.07.050

Gao M, Wu W, Liu S et al (2014) Thermal degradation and flame retardancy of rigid polyurethane foams containing a novel intumescent flame retardant. J Therm Anal Calorim 117:1419–1425. https://doi.org/10.1007/s10973-014-3856-6

Gürü M, Aruntaş Y, Tüzün FN, Bilici I (2009a) Processing of urea-formaldehyde-based particleboard from hazelnut shell and improvement of its fire and water resistance. Fire Mater 33:413–419. https://doi.org/10.1002/fam.1011

Gürü M, Şahin M, Tekeli S, Tokgöz H (2009b) Production of polymer matrix composite particleboard from pistachio shells and improvement of its fire resistance by Fly ash. High Temp Mater Process 28:191–195. https://doi.org/10.1515/HTMP.2009.28.3.191

Han DS, Park IB, Kim MH et al (2010) The effects of glass fiber reinforcement on the mechanical behavior of polyurethane foam. J Mech Sci Technol 24:263–266. https://doi.org/10.1007/s12206-009-1136-3

Hu X, Cheng W, Nie W, Wang D (2016) Flame retardant, thermal, and mechanical properties of glass fiber/nanoclay reinforced phenol–urea–formaldehyde foam. Polym Compos 37:2323–2332. https://doi.org/10.1002/pc.23411

Hu XM, Wang DM (2013) Enhanced fire behavior of rigid polyurethane foam by intumescent flame retardants. J Appl Polym Sci 129:238–246. https://doi.org/10.1002/app.38722

ISO (2002) ISO 5660-1 Reaction-to-fire tests — Heat release, smoke production and mass loss rate - Part 1: Heat release rate (cone calorimeter method). International Standard. 1–8

Jia D, Hu J, He J, Yang R (2019) Properties of a novel inherently flame-retardant rigid polyurethane foam composite bearing imide and oxazolidinone. J Appl Polym Sci 136:1–12. https://doi.org/10.1002/app.47943

Jiang J, Cheng Y, Liu Y et al (2015) Intergrowth charring for flame-retardant glass fabric-reinforced epoxy resin composites. J Mater Chem A 3:4284–4290. https://doi.org/10.1039/c4ta06486k

Jin J, Dong QX, Shu ZJ et al (2014) Flame retardant properties of polyurethane/expandable graphite composites. Procedia Eng 71:304–309. https://doi.org/10.1016/j.proeng.2014.04.044

Kairytė A, Kirpluks M, Ivdre A et al (2018) Cleaner production of polyurethane foam: replacement of conventional raw materials, assessment of fire resistance and environmental impact. J Clean Prod 183:760–771. https://doi.org/10.1016/j.jclepro.2018.02.164

Kim SH, Park HC, Jeong HM, Kim BK (2010) Glass fiber reinforced rigid polyurethane foams. J Mater Sci 45:2675–2680. https://doi.org/10.1007/s10853-010-4248-3

Kirpluks M, Cabulis U, Zeltins V et al (2014) Rigid polyurethane foam thermal insulation protected with mineral intumescent mat. Autex Res J 14:259–269. https://doi.org/10.2478/aut-2014-0026

König A, Fehrenbacher U, Kroke E, Hirth T (2009) Thermal decomposition behavior of the flame retardant melamine in slabstock flexible polyurethane foams. J Fire Sci 27:187–211. https://doi.org/10.1177/0734904108099329

Kulesza K, Pielichowski K, German K (2006) Thermal decomposition of bisphenol A-based polyetherurethanes blown with pentane: Part i - Thermal and pyrolytical studies. J Anal Appl Pyrolysis 76:243–248. https://doi.org/10.1016/j.jaap.2005.12.002

Kumar M, Kaur R (2017) Glass fiber reinforced rigid polyurethane foam: synthesis and characterization. E-Polymers 17:517–521. https://doi.org/10.1515/epoly-2017-0072

Kuźnia M, Magiera A, Pielichowska K et al (2019) Fluidized bed combustion fly ash as filler in composite polyurethane materials. Waste Manag 92:115–123. https://doi.org/10.1016/j.wasman.2019.05.012

Latere Dwan'isa JP, Mohanty AK, Misra M et al (2004) Biobased polyurethane and its composite with glass fiber. J Mater Sci 39:2081–2087. https://doi.org/10.1023/B:JMSC.0000017770.55430.fb

Levchik SV, Weil ED (2004) Thermal decomposition, combustion and fire-retardancy of polyurethanes - a review of the recent literature. Polym Int 53:1585–1610. https://doi.org/10.1002/pi.1314

Li J, Mo X, Li Y et al (2017) Effect of zeolites on morphology and properties of water-blown semi-rigid ammonium polyphosphate intumescent flame-retarding polyurethane foam. J Polym Res 24:1–10. https://doi.org/10.1007/s10965-017-1306-4

Li ME, Wang SX, Han LX et al (2019a) Hierarchically porous SiO_2/polyurethane foam composites towards excellent thermal insulating, flame-retardant and smoke-suppressant performances. J Hazard Mater 375:61–69. https://doi.org/10.1016/j.jhazmat.2019.04.065

Li Q, Wang J, Chen L et al (2019b) Ammonium polyphosphate modified with β-cyclodextrin cross-linking rigid polyurethane foam: enhancing thermal stability and suppressing flame spread. Polym Degrad Stab 161:166–174. https://doi.org/10.1016/j.polymdegradstab.2019.01.024

Liu H, Yang H, Chen M et al (2019) An effective approach to reducing fire hazards of rigid polyurethane foam: fire protective coating. J Coatings Technol Res 16:257–261. https://doi.org/10.1007/s11998-018-0149-1

Liu L, Wang Z (2018) High performance nano-zinc amino-tris-(methylenephosphonate) in rigid polyurethane foam with improved mechanical strength, thermal stability and flame retardancy. Polym Degrad Stab 154:62–72. https://doi.org/10.1016/j.polymdegradstab.2018.05.023

Liu SM, Huang JY, Jiang ZJ et al (2010) Flame retardance and mechanical properties of a polyamide 6/polyethylene/surface-modified metal hydroxide ternary composite via a master-batch method. J Appl Polym Sci 117:3370–3378. https://doi.org/10.1002/app.32086

Lu C, Liu L, Chen N et al (2015) Influence of clay dispersion on flame retardancy of ABS/PA6/APP blends. Polym Degrad Stab 114:16–29. https://doi.org/10.1016/j.polymdegradstab.2015.01.024

Lu S-Y, Hamerton I (2002) Recent developments in the chemistry of halogen-free flame retardant polymers. Prog Polym Sci 27:1661–1712. https://doi.org/10.1016/S0079-6700(02)00018-7

Lu W, Li Q, Zhang Y et al (2018) Lignosulfonate/APP IFR and its flame retardancy in lignosulfonate-based rigid polyurethane foams. J Wood Sci 64:287–293. https://doi.org/10.1007/s10086-018-1701-4

Luo F, Wu K, Guo H et al (2015) Effect of cellulose whisker and ammonium polyphosphate on thermal properties and flammability performance of rigid polyurethane foam. J Therm Anal Calorim 122:717–723. https://doi.org/10.1007/s10973-015-4766-y

Luo F, Wu K, Li D et al (2017) A novel intumescent flame retardant with nanocellulose as charring agent and its flame retardancy in polyurethane foam. Polym Compos 38:2762–2770. https://doi.org/10.1002/pc.23874

Lv P, Wang Z, Hu K, Fan W (2005) Flammability and thermal degradation of flame retarded polypropylene composites containing melamine phosphate and pentaerythritol derivatives. Polym Degrad Stab 90:523–534. https://doi.org/10.1016/j.polymdegradstab.2005.04.003

Michałowski S, Pielichowski K (2018) 1,2-Propanediolizobutyl POSS as a co-flame retardant for rigid polyurethane foams. J Therm Anal Calorim 134:1351–1358. https://doi.org/10.1007/s10973-018-7537-8

Mishra S, Patil UD, Shimpi NG (2009) Synthesis of mineral nanofiller using solution spray method and its influence on mechanical and thermal properties of EPDM nanocomposites. Polym Plast Technol Eng 48:1078–1083. https://doi.org/10.1080/03602550903092492

Mishra S, Shimpi NG (2007) Studies on mechanical, thermal, and flame retarding properties of Polybutadiene rubber (PBR) Nanocomposites. Polym Plast Technol Eng 47:72–81. https://doi.org/10.1080/03602550701580987

Mishra S, Sonawane SH, Badgujar N et al (2005) Comparative study of the mechanical and flame-retarding properties of polybutadiene rubber filled with nanoparticles and fly ash. J Appl Polym Sci 96:6–9. https://doi.org/10.1002/app.21114

Morgan AB, Bundy M (2007) Cone calorimeter analysis of UL-94 V-rated plastics. Fire Mater 31:257–283. https://doi.org/10.1002/fam.937

Modesti M, Simioni F (1994) Effect of phospho-halogenated polyether polyol on fire behavior of rigid polyurethane foams blown with various agents. Cell Polym 13:277–291

Ni J, Song L, Hu Y et al (2009) Preparation and characterization of microencapsulated ammonium polyphosphate with polyurethane shell by in situ polymerization and its flame retardance in polyurethane. Polym Adv Technol 20:999–1005. https://doi.org/10.1002/pat.1354

Ni J, Tai Q, Lu H et al (2010) Microencapsulated ammonium polyphosphate with polyurethane shell: preparation, characterization, and its flame retardance in polyurethane. Polym Adv Technol 21:392–400. https://doi.org/10.1002/pat.1441

Norzali NRA, Badri KH (2016) The role of phosphate ester as a fire retardant in the palm-based rigid polyurethane foam. Polym Polym Compos 24:711–718. https://doi.org/10.1177/096739111602400906

Pang XY, Xin YP, Shi XZ, Xu JZ (2019) Effect of different size-modified expandable graphite and ammonium polyphosphate on the flame retardancy, thermal stability, physical, and mechanical properties of rigid polyurethane foam. Polym Eng Sci. https://doi.org/10.1002/pen.25123

Peng HK, Wang XX, Li TT et al (2018) Effects of hydrotalcite on rigid polyurethane foam composites containing a fire retarding agent: compressive stress, combustion resistance, sound absorption, and electromagnetic shielding effectiveness. RSC Adv 8:33542–33550. https://doi.org/10.1039/C8RA06361C

Peng HK, Wang XX, Li TT et al (2019) Mechanical properties, thermal stability, sound absorption, and flame retardancy of rigid PU foam composites containing a fire-retarding agent: effect of magnesium hydroxide and aluminum hydroxide. Polym Adv Technol:2045–2055. https://doi.org/10.1002/pat.4637

Price D, Liu Y, Hull TR et al (2000) Burning behaviour of fabric/polyurethane foam combinations in the cone calorimeter. Polym Int 49:1153–1157. https://doi.org/10.1002/1097-0126(200010)49:10<1153::AID-PI551>3.0.CO;2-S

Prociak A, Pielichowski J, Modesti M, Simioni F (1997) Influence of different flame retardants on fire behaviour of rigid polyurethane foams blown with n-pentane. Cell Polym 16:284–295

Qu H, Fan R, Yuan J et al (2017) Preparation and performance of a P–N containing intumescent flame retardant based on hydrolyzed starch. Polym Plast Technol Eng 56:1760–1771. https://doi.org/10.1080/03602559.2017.1289405

Salasinska K, Borucka M, Leszczyńska M et al (2017) Analysis of flammability and smoke emission of rigid polyurethane foams modified with nanoparticles and halogen-free fire retardants. J Therm Anal Calorim 130:131–141. https://doi.org/10.1007/s10973-017-6294-4

Schartel B, Hull TR (2007) Development of fire-retarded materials—interpretation of cone calorimeter data. Fire Mater 31:327–354. https://doi.org/10.1002/fam.949

Shi X, Jiang S, Zhu J et al (2018) Establishment of a highly efficient flame-retardant system for rigid polyurethane foams based on bi-phase flame-retardant actions. RSC Adv 8:9985–9995. https://doi.org/10.1039/c7ra13315d

Shimpi NG, Mishra S (2010) Synthesis of nanoparticles and its effect on properties of elastomeric nanocomposites. J Nanopart Res 12:2093–2099. https://doi.org/10.1007/s11051-009-9768-x

Singh H, Jain AK (2009) Ignition, combustion, toxicity, and fire retardancy of polyurethane foams: a comprehensive review. J Appl Polym Sci 111:1115–1143. https://doi.org/10.1002/app.29131

Singh H, Jain AK, Sharma TP (2008) Effect of phosphorus-nitrogen additives on fire retardancy of rigid polyurethane foams. J Appl Polym Sci 109:2718–2728. https://doi.org/10.1002/app.28324

Sykam K, Meka KKR, Donempudi S (2019) Intumescent phosphorus and triazole-based flame-retardant polyurethane foams from castor oil. ACS Omega 4:1086–1094. https://doi.org/10.1021/acsomega.8b02968

Tashev E, Zabski L, Shenkov S, Borissov G (1992) Phosphorus-containing rigid polyurethane foams-II. Modifiers based on trimethyl phosphate. Eur Polym J 28:689–693. https://doi.org/10.1016/0014-3057(92)90044-3

Thirumal M, Khastgir D, Nando GB et al (2010a) Halogen-free flame retardant PUF: effect of melamine compounds on mechanical, thermal and flame retardant properties. Polym Degrad Stab 95:1138–1145. https://doi.org/10.1016/j.polymdegradstab.2010.01.035

Thirumal M, Khastgir D, Singha NK et al (2009) Effect of a nanoclay on the mechanical, thermal and flame retardant properties of rigid polyurethane foam. J Macromol Sci Part A 46:704–712. https://doi.org/10.1080/10601320902939101

Thirumal M, Singha NK, Khastgir D et al (2010b) Halogen-free flame-retardant rigid polyurethane foams: effect of alumina trihydrate and triphenylphosphate on the properties of polyurethane foams. J Appl Polym Sci 116:2260–2268. https://doi.org/10.1002/app.31626

Tuzcu H (2010) Isı yalıtımı ve otomotiv endüstrilerinde kullanılan yanmaya dirençli poliüretan esaslı malzemelerin tutuşma ve yanma karakteristiklerinin deneysel incelenmesi (in Turkish)., MSc Thesis. Pamukkale University

Usta N (2012) Investigation of fire behavior of rigid polyurethane foams containing fly ash and intumescent flame retardant by using a cone calorimeter. J Appl Polym Sci 124:3372–3382. https://doi.org/10.1002/app.35352

Usta N, Deda Altan B, Yurtseven R, Akdogan E, Tuzcu H (2011) Otomotiv ve Isı Yalıtım Endüstrileri İçin Yeni Yanmaya Dirençli Poliüretan Esaslı Malzeme Geliştirilmesi ve Bu Malzemelerin Isıl Bozulma ve Yanma Davranışlarının Deneysel ve Teorik İncelenmesi (in Turkish). Report 108T246, The Scientific and Technological Research Council of Turkey

Wang C, Wu Y, Li Y et al (2018c) Flame-retardant rigid polyurethane foam with a phosphorus-nitrogen single intumescent flame retardant. Polym Adv Technol 29:668–676. https://doi.org/10.1002/pat.4105

Wang J, Chen Y (2005) Flame-retardant mechanism resulting from an intumescent system. J Fire Sci 23:55–74. https://doi.org/10.1177/0734904105044266

Wang L, Wu X, Wu C et al (2011) Study on the flame retardancy of EVM/magnesium hydroxide composites optimized with a flame retardant containing phosphorus and silicon. J Appl Polym Sci 121:68–77. https://doi.org/10.1002/app.33226

Wang SX, Zhao HB, Rao WH et al (2018a) Inherently flame-retardant rigid polyurethane foams with excellent thermal insulation and mechanical properties. Polymer (Guildf) 153:616–625. https://doi.org/10.1016/j.polymer.2018.08.068

Wang Y, Wang F, Dong Q et al (2018b) Expandable graphite encapsulated by magnesium hydroxide nanosheets as an intumescent flame retardant for rigid polyurethane foams. J Appl Polym Sci 135:1–9. https://doi.org/10.1002/app.46749

Weil ED, Levchik SV (2004) Commercial flame retardancy of polyurethanes. J Fire Sci 22:183–210. https://doi.org/10.1177/0734904104040259

Wu K, Wang Z, Hu Y (2008) Microencapsulated ammonium polyphosphate with urea-melamine-formaldehyde shell: preparation, characterization, and its flame retardance in polypropylene. Polym Adv Technol 19:1118–1125. https://doi.org/10.1002/pat.1095

Wu D, Zhao P, Liu Y (2013a) Flame retardant property of novel intumescent flame retardant rigid polyurethane foams. Polym Eng Sci 53:2478–2485. https://doi.org/10.1002/pen.23710

Wu D, Zhao P, Zhang M, Liu Y (2013b) Preparation and properties of flame retardant rigid polyurethane foam with phosphorus-nitrogen intumescent flame retardant. High Perform Polym 25:868–875. https://doi.org/10.1177/0954008313489997

Wu DH, Zhao PH, Liu YQ et al (2014) Halogen free flame retardant rigid polyurethane foam with a novel phosphorus-nitrogen intumescent flame retardant. J Appl Polym Sci 131. https://doi.org/10.1002/app.39581

Xu D, Yu K, Qian K (2018) Thermal degradation study of rigid polyurethane foams containing tris(1-chloro-2-propyl)phosphate and modified aramid fiber. Polym Test 67:159–168. https://doi.org/10.1016/j.polymertesting.2018.01.034

Xu D-M, Hao J-W, Liu G-S, Xie S-M (2013) Thermal degradation and smoke production during combustion for intumescent flame retardant rigid polyurethane foams. Acta Polym Sin:832–840. https://doi.org/10.3724/SP.J.1105.2013.12264

Xu W, Wang G (2015) Synthesis of polyhydric alcohol/ethanol phosphate flame retardant and its application in PU rigid foams. J Appl Polym Sci 132:1–9. https://doi.org/10.1002/app.42298

Yang R, Hu W, Xu L et al (2015) Synthesis, mechanical properties and fire behaviors of rigid polyurethane foam with a reactive flame retardant containing phosphazene and phosphate. Polym Degrad Stab 122:102–109. https://doi.org/10.1016/j.polymdegradstab.2015.10.007

Yurtseven R, Tarakcılar AR, Topcu M (2013) Dolgu Maddesi Olarak Kullanılan Farklı Uçucu Küllerin Sert Poliüretan Köpük Malzemelerin Mekanik Özellikleri İle Isıl Ve Yanma Davranışları Üzerine Etkileri (in Turkish). J Fac Eng Archit Gazi Univ 28:841–853

Zatorski W, Brzozowski ZK, Kolbrecki A (2008) New developments in chemical modification of fire-safe rigid polyurethane foams. Polym Degrad Stab 93:2071–2076. https://doi.org/10.1016/j.polymdegradstab.2008.05.032

Zhang J, Wang X, Zhang F, Richard Horrocks A (2004) Estimation of heat release rate for polymer-filler composites by cone calorimetry. Polym Test 23:225–230. https://doi.org/10.1016/S0142-9418(03)00098-9

Zhao C, Qin H, Gong F et al (2005) Mechanical, thermal and flammability properties of polyethylene/clay nanocomposites. Polym Degrad Stab 87:183–189. https://doi.org/10.1016/j.polymdegradstab.2004.08.005

Chapter 6
Structural Behaviour of Composite Materials in Fire

Aslina Anjang Ab Rahman

6.1 Introduction

Fire is a serious safety issue when it comes to a structural component of a civilian building, offshore platform, naval ships or an aircraft that carries high numbers of passengers. At present, many structural components mentioned above is being replaced from a conventional material to an advanced material such as fibre reinforced polymer composites that exhibit superior performance compared to traditional materials. Some common type of high-temperature resin used in composite structures are polyimides, bezoxazines, bismaleimides and cyanate esters. In aerospace application, the combination of carbon fibre and bismaleimide matrix is material of choice for jet engines due to the excellent fire performance. Fire performance is considered as one of the most significant factors in restricting the broader use of composite materials for structural applications. Despite their superior performance compared to other materials such as steel, aluminium or reinforced concrete, composite materials are reactive at high temperatures, particularly for organic matrix and fibres. Composite materials decompose and release heat and smoke when exposed to high temperature and fire environment. The exposure of composite material structures to high temperatures leads to decomposition, associated with thermal and mechanical properties degradation. The degradation causes a reduction in mechanical performances, which is the primary concern in safety aspects.

When a composite material is exposed to fire or heat at a temperature around 300 to 400 °C, the organic matrix decomposes and releasing heat, smoke, soot and toxic volatiles (Mouritz and Gibson 2006). Similar to an organic matrix, organic fibres will also decompose and generate heat, fumes and smoke. Fire scenarios are very complex and different depending on many factors. Figure 6.1 gives an overview of

A. A. Ab Rahman (✉)
School of Aerospace Engineering, Universiti Sains, Nibong Tebal, Pulau Pinang, Malaysia
e-mail: aeaslina@usm.my

S. Siddiquee et al. (eds.), *Composite Materials: Applications in Engineering, Biomedicine and Food Science*, https://doi.org/10.1007/978-3-030-45489-0_6

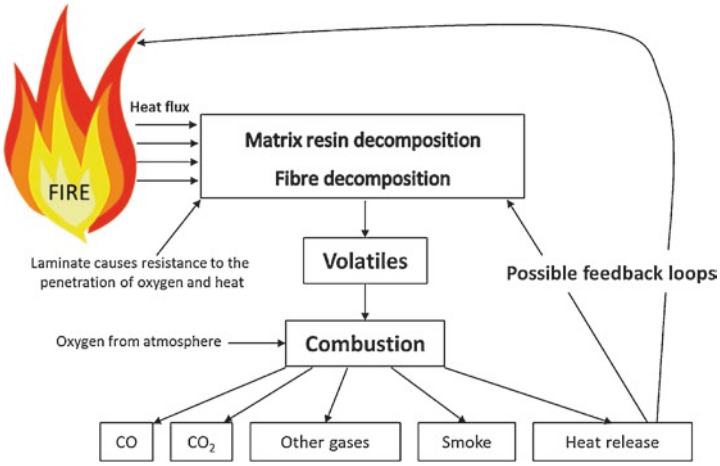

Fig. 6.1 Processes in a fire scenario (A.P. Mouritz and Gibson 2006)

the fire scenario and the mechanism involved in the thermal decomposition of composite materials with possible additional feedback into the composites due to the local burning of decomposition products. The product of decomposition gives feedback into the centre of the fire and will affect the burning intensity.

Figure 6.2 shows the processes occurring in a composite laminate subjected to fire. The process involved when composite laminates receive heat/fire are thermal, chemical, physical as well as the influence in failure modes (Mouritz et al. 2009). The thermal process involved heat conduction, heat generation or absorption by decomposition reaction and convective heat loss from the egress of hot reaction gases and moisture vapours from the composite into the fire. The chemical processes include thermal softening, melting, pyrolysis and volatilisation of the polymer matrix, organic fibres and core material together with the formation, growth and oxidation of char. The physical processes involve thermal expansion and contraction, internal pressure build-up due to the formation of volatile gases and vaporisation of moisture; thermally-induced strains; delamination damage; matrix cracking; surface ablation; and softening, melting and fusion of fibres. The failure modes depend on the temperature, heat flux and duration of the fire; magnitude and type of load (e.g. tension, compression, bending, torsion); and geometry of the structure. Some of the failure modes experienced by composite laminates include matrix decomposition, pore formation, delamination cracking, matrix cracking, fibre–matrix debonding, and char formation.

The reduction to the structural properties of composite materials due to heat and fire requires an in-depth understanding of the thermal, chemical, physical, softening and failure mechanism. It is crucial to understand the process involved as well as their interactions in analysing the structural behaviour of composites in a fire. The fire reaction properties that define the flammability and fire hazard of polymer composites are described in the next section. Some of the reaction properties include

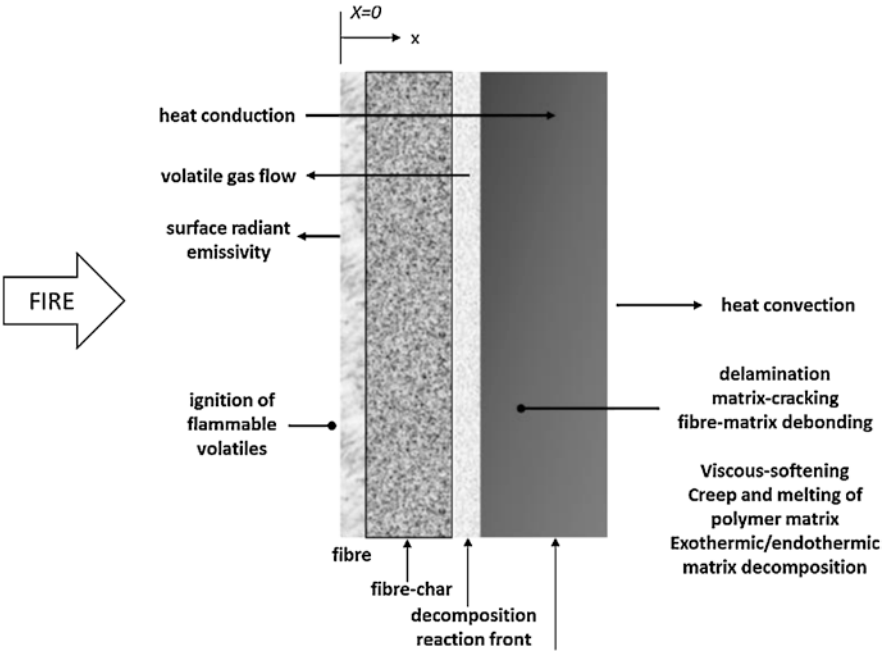

Fig. 6.2 Reaction processes of laminates exposed to fire (Mouritz et al. 2009)

time-to-ignition, heat release rate, flame spread, smoke and gaseous combustion products. The fire resistive properties of composites, such as burn-through rate and mechanical integrity during and after fire, are also described in the next section of this chapter. Overall, this chapter summarises the understanding and key issues on the structural behaviour of composite materials at high temperature and in fire environment. It is envisaged that the understanding of the fire behaviour and mechanisms will increase the fire safety criteria of existing and future application of composite structures.

6.2 Fire Reaction and Resistance Properties of Composites

Fire reaction and fire resistance capability of a material play a significant role in the safety of the structures and personnel in case of fire. Fire reaction properties influence the initiation, growth and spread of fire and determine the survival of humans exposed to fire. Fire resistance measures the ability of a structure to prevent heat transmission and determine structural integrity. In this section, both fire reaction and fire resistance properties are adequately presented.

In the field of fire sciences, fire reaction is a general term that defines the flammability and combustion properties of composite materials. Some of the most

critical fire reaction properties are time-to-ignition, heat release rate, peak heat release rate, smoke density, limiting oxygen index, and flame spread rate (Anjang et al. 2014). The heat release rate is being classified as the most critical fire reaction property because it indicates the fire hazard of combustible material (Mouritz et al. 2006). The heat release rate is a quantitative measure of the amount of thermal energy released by a material per unit area when exposed to a fire that radiates a constant heat flux or temperature. The heat release rate value of composite material is not constant but varies with fire exposure times. The value of the heat release rate is determined by the thermal energy released in thermo-chemical decomposition processes. Time-to-ignition is the minimum period required for a combustible material to promote ignition and continuos flaming due to a constant radiant heat flux. The ignition time is used as an approximate measure of the flammability resistance of a material. In high fire risk application, it is very sensible to use materials with longer ignition times. The flame spread rate describes the speed of propagation at which the flame front travels over the surface of combustible material. The flame spread rate is an experimentally measured value and cannot be directly determined. Oxygen index is defined as the minimum oxygen content in the fire environment required to sustain flaming combustion of a material. Materials with high oxygen index values are used in high fire risk applications due to the potential behaviour for self-extinguishing. Two other crucial fire reaction properties are smoke density and gas toxicity. Both properties exhibit a significant impact on the ability of humans to survive in a fire incident. Most fatalities are not triggered by heat and flame but are due to smoke that caused confusion and disorientation that has slow the escape process from the fire incident. As the exposure time to toxic fumes increases, the fire incident may lead to incapacitation and fatalities. The fire reaction properties of composite materials have been characterised, and a wealth of reaction data for different fire or heat flux conditions has been published (Allison et al. 1991; Mouritz et al. 2006; Scudamore 1994; Tewarson and Macaione 1993; Egglestone and Turley (1994); Grenier et al. (1998); Mouritz et al. (2009)).

Fire resistance describes the burn-through resistance and mechanical integrity of a loaded material or structure during and after fire exposure. Resistance to fire also defines the ability of a material or structure to limit the spread of fire from room to room. These fire parameters can be evaluated using small, intermediate or full-scale test methods. These tests can provide information on the mechanical integrity and burn-through resistance of the composites design for a specific fire test condition. However, the tests are complicated to perform, time-consuming, involved high cost and only provide information on the specific case of fire test condition. Fire resistance also describes the physical and mechanical resistance of materials to fire attack. Fire resistance is critical to the safe use of load-bearing composites in aircraft, ships and buildings as their structures may collapse or fail due to losses in strength, stiffness and creep resistance. Several tests are used to determine fire resistance properties, where the furnace and burn-through fire tests are the most notable test. When evaluating the fire resistance of composite structures by using furnace method, controlled heating and realistic fire conditions can easily be achieved. However, the method has some deficiencies that can affect the reliability of the test

results; variable results between different furnaces and testing organisations, even though all technically comply with the requirements of the standards. It is also compelling to note that only a relatively small number of tests are suitable for determining the fire reaction properties of composite materials or structures (Mouritz, 2003a; Mouritz and Gibson 2006). When discussing the fire resistance capability, it is interesting to contemplate on the effect of simultaneous heating and loading that is exposed to a composites material or structure. A large amount of experimental data on the fire resistance of composite laminates has been obtained, particularly for fibreglass reinforced polymer laminates and sandwich composites (Allison et al. 1991; Anjang et al. 2014; Bai and Keller 2009; Feih et al. 2007b; Feih and Mouritz 2012; Gibson et al. 2012; Gibson et al. 2010; Luo et al. 2012; Marquis et al. 2013; Summers et al. 2012a). More information on the behaviour of the materials under simultaneous heating and loading is thoroughly discussed in the next sections of the chapter.

At present, there is no single test or experimental method that are adequate in evaluating all the fire properties of a composite. Two or more methods is necessary to obtain a complete understanding of the fire reaction and resistance behaviour of a composite.

6.3 Thermal Response of Composite Materials

Composite materials that are exposed to sufficiently high heat flux radiated from the fire or due to the high temperature environment will thermally decompose and yield gaseous, chars and smokes. The thermal response of composite materials due to heat exposure or fire environment is a temperature-dependent process (Mouritz et al. 2009). Figure 6.3 summarised the approximate temperatures on the different processes that occurred in a composite material. The first event that occurs when composite material is exposed to high temperature and fire is heat conduction. The heat conduction is governed by the incident heat flux and thermal diffusivity of the virgin composite material. The heat conduction through composite material is complicated due to the highly anisotropic nature of the thermal properties. The rate of heat conduction along the fibre direction is much faster compared to the through-thickness direction. The situation is further complicated as the thermal conductivity, and the specific heat of composite materials vary with temperature.

The heat conduction will expand and contract the composite materials specimen or structure depending on the temperature. The amount of contraction and expansion on the polymer matrix below the glass transition temperature, T_g is determined by the thermal expansion linear coefficient of the virgin material. Thermal gradient in the through-thickness direction is non-uniform; highest at the hot surface and lowest at the cold face (Pei Gu and Chen 2012). Some types of fibre display anisotropic thermal conductivity behaviour, where when the material is heated, both contraction and expansion coincided. As an example, carbon fibre will expand in the

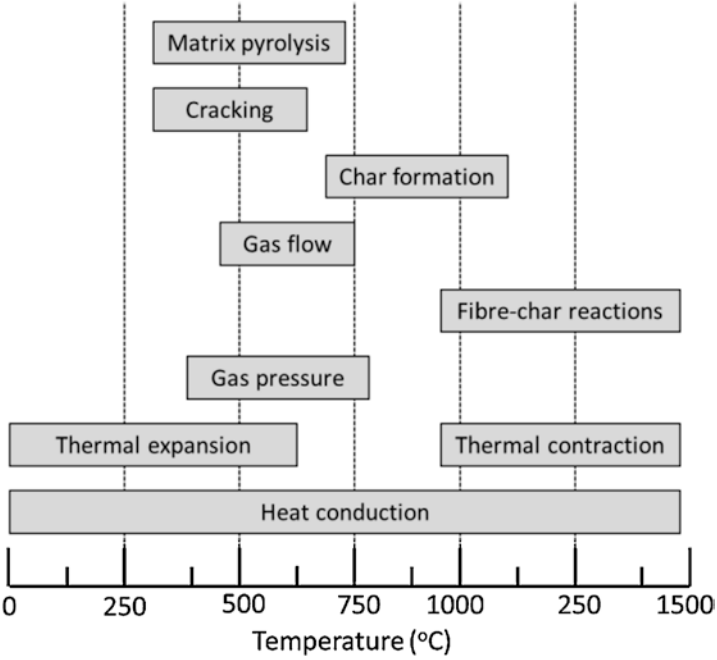

Fig. 6.3 Different processes and temperature (Mouritz et al. 2009)

through-thickness direction and contract slightly in the axial (or fibre) direction when heated.

Below the decomposition temperature of a polymer matrix, heat energy is transferred via conduction, where a small amount of energy is absorbed in the thermal expansion. Composite materials begin to decompose at sufficiently high temperature. Typically, the decomposition temperature of a polymer matrix is in the range of 250° to 350 °C depending on the composition and chemical stability of the organic material, heating rate as well as the fire atmosphere (Rahman and Kumarasamy 2017). In the physical process where contraction and expansion involved, internal pressure rise and build-up due to the formation of volatile gases; vaporisation of moisture; thermally-induced strains; delamination damage; matrix cracking; surface ablation; and softening, melting and fusion of fibres. These processes occur concurrently, and this enumerates to the complexity of fire behaviour. The pressure exerted by the gas culminates pores formation, delamination and matrix cracking. When the matrix has becomes sufficiently porous, and crack is noticeable, the volatile gases and water vapour flow through the degraded region into the heat or fire environment. This has a convective cooling effect which reduced the heat conduction. The pyrolysis gas will also cool the composite depending on the heat capacity of the gases.

For the organic matrix and fibre, the endothermic decomposition process continues until the reaction zone reaches to the back face of the composite laminates. The

combustible matrix and fibre are then finally degraded to volatiles and chars. At this phase, the decomposition process ends unless a sufficiently high temperature that instigates pyrolysis reactions between the fibres and char. In the case of glass fibres where the temperature exceeds ~1000 °C, the char retaliate with the silica network resulting in a substantial mass loss. For carbon fibre composites, the fibres and chars were oxidised due to the oxygen-rich environment during fire (Feih and Mouritz 2012).

In summary, many processes involved when composite materials are exposed to fire. The overall process is very complex depending on the fire scenarios as well as due to the different types of composite materials involved in the scenario. The processes also do not occur in separation from each other. The complexity of the process is further cumbersome due to the anisotropic properties and the temperature-dependent properties of composites. It is also essential to understand the sequence of events that occur when composite material is exposed to high temperature and fire environment.

6.4 Fire Structural Behaviour Under Loading

The mechanical responses such as strength, stress, strain and displacement of composites under elevated temperatures and fire environments are significantly affected by their thermal exposure (Bai and Keller 2009). Contrarily, mechanical responses have almost no influence on the thermal responses of these materials. As a result, the mechanical and thermal responses can be dissociated from each other. Structural fire behaviour under loading considers both thermal and mechanical response. Significant advances have been made in the modelling and testing of the structural response of composite materials in fire. Thermal-mechanical models have been developed to predict temperature rise, softening rate, residual stiffness and strength, and failure stress and failure time of composites at elevated temperature or in fire (Asaro et al. 2009; Bai and Keller 2009; Yu Bai et al. 2008; Birman et al. 2006; Dimitrienko 1997; Gu 2012; Liu et al. 2011; Luo et al. 2012; Mouritz et al. 2009; Nguyen et al. 2019; Sullivan 1993; Summers et al. 2012b; Tran et al. 2018). A large amount of experimental data on the fire resistance of composites has also been obtained, particularly for fibreglass reinforced polymer laminates (Anjang et al. 2014; Anjang et al. 2017; Elmughrabi et al. 2008; Feih et al. 2007a,b; Feih et al. 2007; Gibson et al. 2010; Wang et al. 2014). This section provides a review of the structural fire behaviour under tensile and compressive loading.

Substantial progress has been made in the development of finite element and analytical models to investigate the compressive structural integrity of composites in fire (Bhat et al. 2017; Birman et al. 2006; Pei Gu and Asaro 2008; Pei Gu and Chen 2012; Krysl et al. 2004; Looyeh and P. Bettess 2001). Modelling the structural response of composites in predicting their fire behaviour under compression loading is less complicated because the fibre reinforcement is not significant in controlling softening and failure. The initial step in analysing the compression properties is the

calculation of the temperature distribution through the composite with increasing time using the thermal model. By using the through-thickness temperature distribution, the reduction to the mechanical properties can be calculated. Currently, the reduction to the mechanical properties with increasing temperature must be measured experimentally at elevated temperature under isothermal conditions. The compression model assumes that the mechanical properties of the composites decrease via a single-stage (rigid-to-rubbery) glass transition of the polymer matrix with increasing temperature. The compression strength of most composite laminates decreases with increasing temperature, as depicted in Fig. 6.4.

The simplest method to assess the fire structural behaviour under loading is by performing a small-scale test set up (stress-rupture test). Although the full-scale fire test is generally required in displaying the realistic condition, the small-scale fire test is adequate to predict the fire resistance capability of a structure under loading (Mouritz and Gibson 2006). Many researchers have investigated the fire structural survivability of composites under combined compressive loading and one-sided heating (Bhat et al. 2017; Boyd et al. 2007; Feih et al. 2008; Pei Gu and Asaro 2012; Liu et al. 2011). Studies on the reduction to the mechanical properties of composite materials due to combined heating and compressive loading have unveiled that compressive creep failure occurs at temperatures around the glass transition temperature of the polymer matrix, within the range of 100–180 °C (Boyd et al. 2007; Feih et al. 2007a). At higher temperatures, failure is also dependent on the decomposition and the matrix delamination cracking (Gibson et al. 2006; Liu et al. 2011). The experiment revealed that time-to-failure values decreased with increasing heat flux (temperature) and applied compressive stress (Feih et al. 2007a; Feih et al. 2008; Kim et al. 2007). The thermo-mechanical model used in calculating the

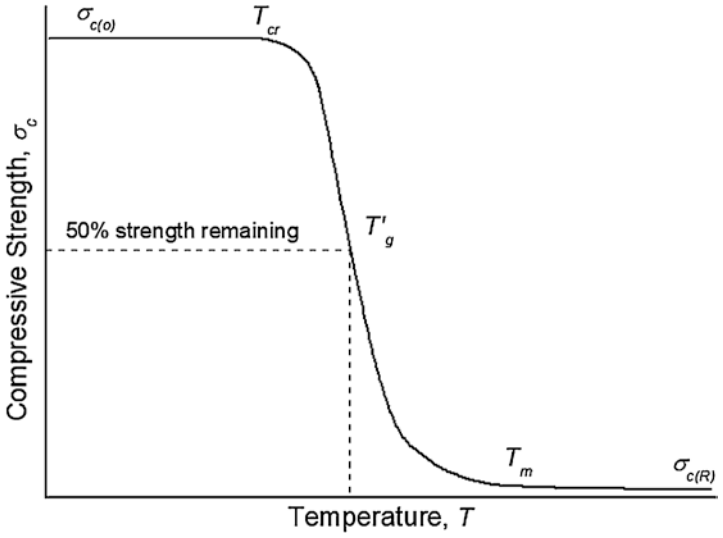

Fig. 6.4 Typical relationship between temperature and compressive strength (Feih et al. 2008)

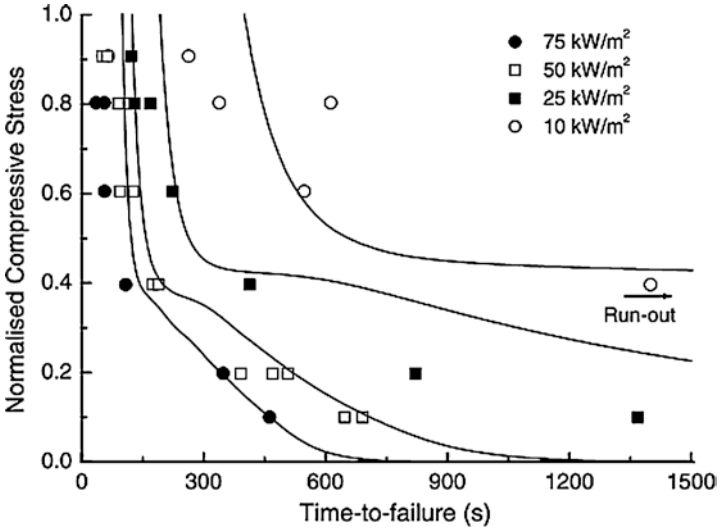

Fig. 6.5 Failure times of the composite laminate tested at different heat fluxes (Feih et al. 2007a)

time-to-failure of laminates supporting a static compressive stress during one-sided heating able to predict the experiment with reasonable accuracy as depicted in Fig. 6.5.

The thermal-mechanical model developed by Feih (Feih et al. 2008) also able to calculate with reasonable accuracy the failure times of sandwich composites consisting of E-glass/vinyl ester and balsa core. The model predicts that the time-to-failure increases with the skin thickness and when the applied compressive stress or heat flux is reduced as depicted in Fig. 6.6. Nevertheless, the model was not able to accurately predict the failure time for all heat flux conditions due to the complexity of the failure process of the face skins of the sandwich. The model is accurate when all plies in the front skin fail at the same time due to microbuckling, which occurs under high heat flux and high stress conditions. Extensive amounts of research on the development of thermal-mechanical models for calculating the fire structural response and failure of composites under compression load models only assume that the weakening of the composite is solely due to matrix softening (Boyd et al. 2007; Pei Gu and Asaro 2008, 2012; Lattimer et al. 2004; Lua et al. 2006). Other softening processes such as pore formation and delamination are not considered into their mechanical models. Further analysis and validation are needed to incorporate damage and failure processes into the thermal-compressive mechanical models. The accuracy of the newly developed model also needs to be determined against experimental data for a wide variety of composite materials.

The behaviour of composites in fire under tensile loading is different and more complicated than compression loading. In analysing the tensile response, both matrix and fibre softening effects need to be considered and analysed. Several models have been developed to calculate the tensile softening and failure of composites

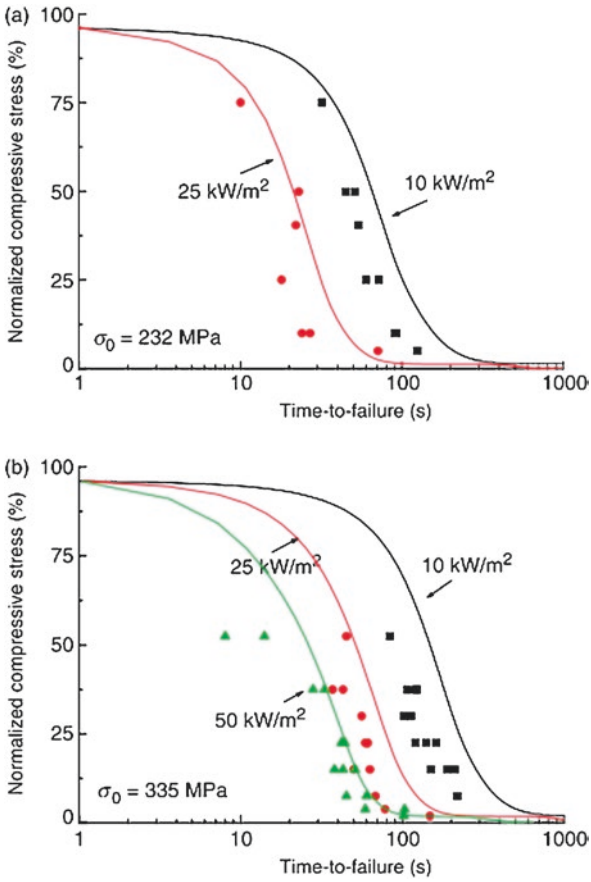

Fig. 6.6 Failure times of sandwich composites under combined compression and one-sided heating at different heat fluxes (**a**) 2 mm skin thickness and (**b**) 5 mm skin thickness (solid curve: prediction, data points: experimental) (Feih et al. 2008)

in fire (Anjang et al. 2014, 2017; Bhat et al. 2015; Elmughrabi et al. 2008; Feih et al. 2007; Pering et al. 1985). Similar to the compression model, tension model takes into account both thermal-mechanical response into the fire behaviour (stress rupture) analysis. The loss in tensile strength of the fibreglass with increasing temperature is much more gradual than the loss in compressive strength of the polymer matrix, and this accounts for the laminate having longer failure times under tensile loading. Figure 6.7 gives the time-to-failure of a woven glass/vinyl ester composite under tension and compression loading when being exposed with similar heat flux level. The failure times for tension loading is about an order of magnitude longer than for a compression loading. Failure of the laminate under tension loading involved the decomposition of the polymer matrix and is later controlled by creep rupture of the fibres, whereas under compression the process is strongly influenced by thermal softening of the polymer matrix.

Similar to compression, the tensile strength of most polymer laminate decrease with increasing temperature as depicted in Fig. 6.8. In analysing fire under tensile loading, fibre strength loss is regarded as both time and temperature-dependent.

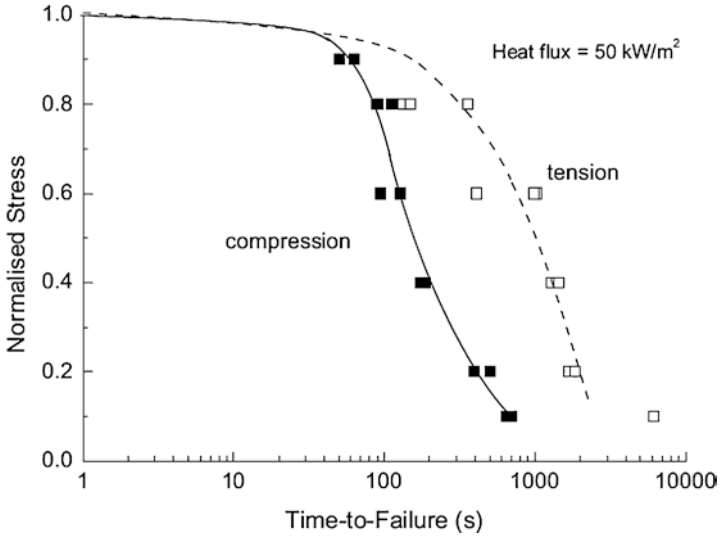

Fig. 6.7 Comparison of the time-to-failure of a glass/vinyl ester laminate under tension and compression at a heat flux of 50 kW/m^2 (Feih et al. 2007b)

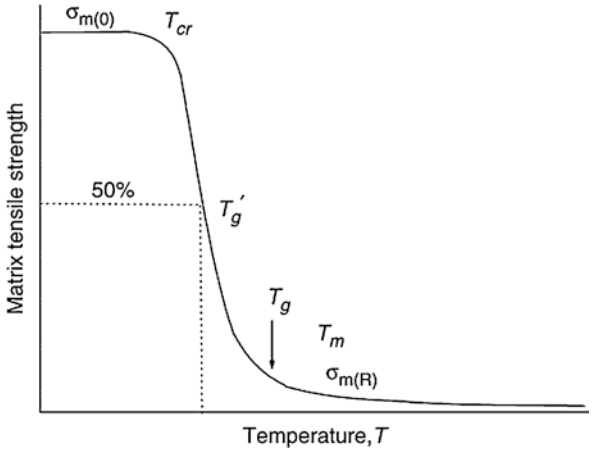

Fig. 6.8 Relationship between temperature and tensile strength of a polymer (Feih et al. 2007)

Figure 6.9 shows the effect of temperature and heating time on the normalised tensile strength of E-glass bundles. The tensile strength of the fibre bundles decreases with increasing temperature and heating time. Details on the equation used to model the thermal-mechanical response will not be discussed in this chapter. A comprehensive explanation of the model can be found written by Feih et al. (2007). Only types of fire model to predict the failure behaviour will be discussed and the validation with experimental fire test are shown.

The average strength model developed by Feih et al. (2007) and Gibson et al. (2006) as shown in Fig. 6.10 can predict the failure stresses and times of fibreglass

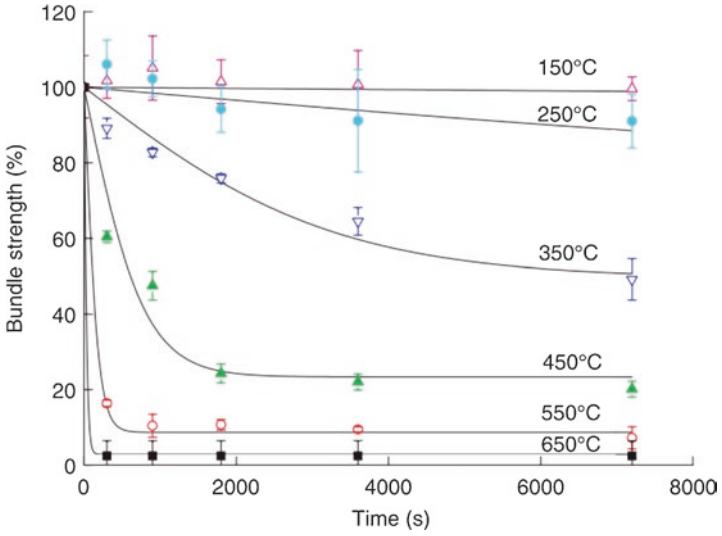

Fig. 6.9 Fibre strength as a function of time and temperature (Feih et al. 2007)

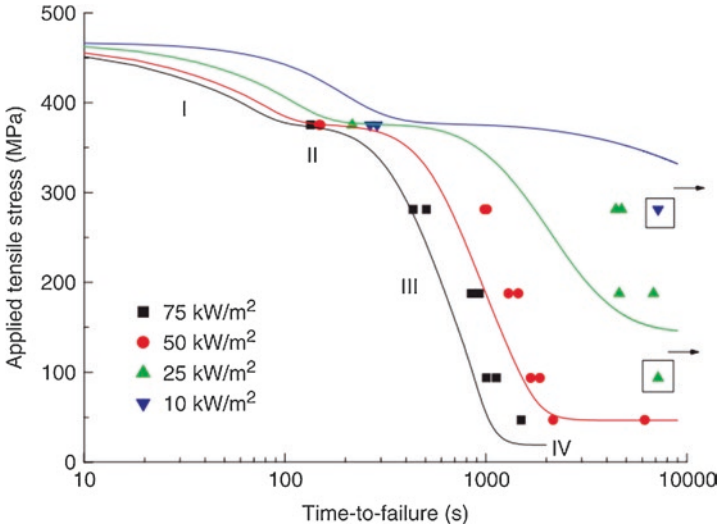

Fig. 6.10 Comparison of failure times calculated using average strength model for a glass-vinyl ester laminate at different heat fluxes (Feih et al. 2007)

laminates with good accuracy. This tension model does not analyse all the damage processes which control the mechanical properties and failure such as thermal strain, pore formation, delamination and fibre-matrix debonding however the model gives a good estimation of tensile strength and failure time of E-glass/vinyl ester composite. Another model by Gibson et al. (Gibson et al. 2006) has shown that the

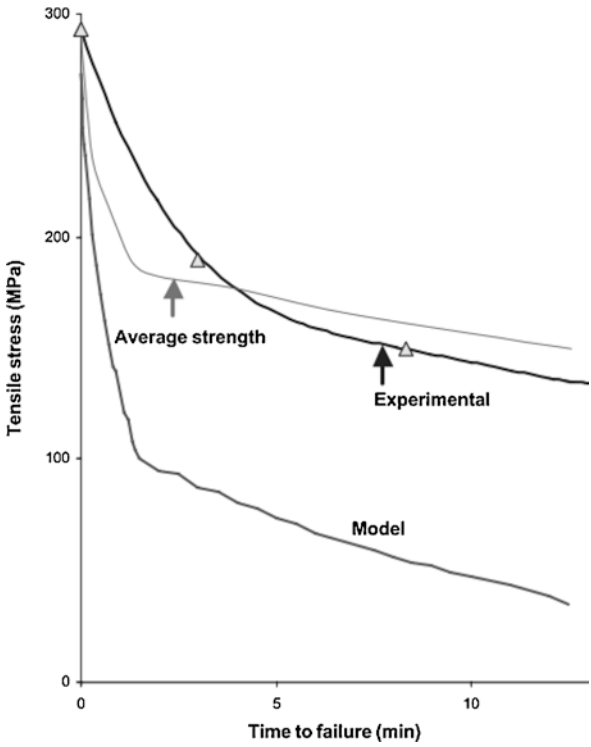

Fig. 6.11 Time-to-failure prediction for glass/polyester laminate (Gibson et al. 2006)

thermal model, coupled to laminate theory, can give reasonable predictions for mechanical behaviour under load. The thermal model, coupled to this laminate theory is from previous analysis that predicts the evolution of temperature and resin decomposition with time through-the-thickness of the laminate. Figure 6.11 gives the failure curve calculated using the average strength model on a glass/polyester composite. Model to analyse the tensile response of sandwich composites exposed to fire is also capable to determine the temperature rise, tensile failure stress and failure mechanism of the sandwich (Anjang et al. 2014; Anjang et al. 2017). Although the above mentioned model able to calculate with reasonable accuracy of the fire structural behaviour, further development is required to incorporate damage modelling (cracks and other damage) into the thermal–mechanical model.

6.5 Post-Fire Behaviour of Composite Materials

The post-fire behaviour is essential to evaluate the structural integrity and safety of heat-affected composite materials following a fire. The polymer matrix used in the composite materials will decompose, ignite and burn due to the exposure to high

temperature or fire. Inadequate fire protection will result in rapid ignition to the composite structures that release large amounts of heat, smoke and potentially toxic fumes (Anjang et al. 2015; Gardiner et al. 2004; Mouritz and Gardiner 2002; Sorathia et al. 1993). After a fire is extinguished, it is vital to analyse the post-fire properties in order to assess the residual integrity and safety of the composite structures. The residual mechanical properties of composite following fire can be significantly reduced due to the decomposition and damage of the polymer matrix (Mouritz and Mathys 1999, 2000, 2001). Mouritz and Mathys suggested that when a burnt composite is loaded in uniaxial tension at room temperature, the residual tensile properties can be approximated using a rule-of-mixtures model. In the model, the post-fire properties are determined by combining the tensile properties of the unburnt and char regions using a rule-of-mixture formulation to give the bulk post-fire strength and stiffness of the fire-damaged composite. Figure 6.12 shows a schematic of fire damage in a laminate which forms the basis of the model.

The post-fire models have been validated for several types of laminates and sandwich composites (Gardiner et al. 2004; Gibson et al. 2004; Mouritz, 2002; Mouritz and Gardiner 2002; Z Mathys et al. 2002). Figure 6.13 shows one example of a successful validation of the post-fire tensile strength and stiffness of a woven glass/polyester laminate. The post-fire properties decrease with increasing heating time, and the agreement between the calculated and measured post-fire properties is excellent. The reduction is due to the thermal degradation of the polymer matrix that forms a weak char region. Figure 6.14 gives the validation of the post-fire properties for sandwich composites. The model reveals that the post-fire tension properties are controlled by char damage to the entire sandwich. Different from post-fire tension, post-fire compression shows more significant degradation. This difference occurs because softening and failure of the composite materials under compression loading are dominated by the front skin (Anjang et al. 2015). The post-fire models are capable of predicting the temperature rise in the composite materials and the resultant reduction to the mechanical properties. The post-fire model also had shown that

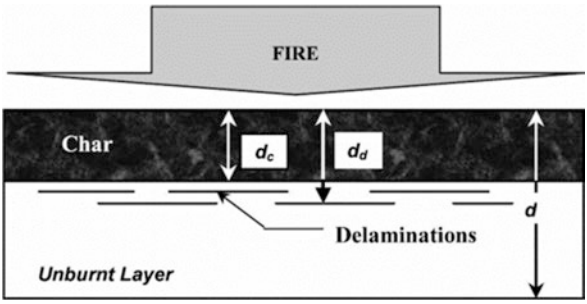

Fig. 6.12 Schematic of fire damage (Mouritz 2002)

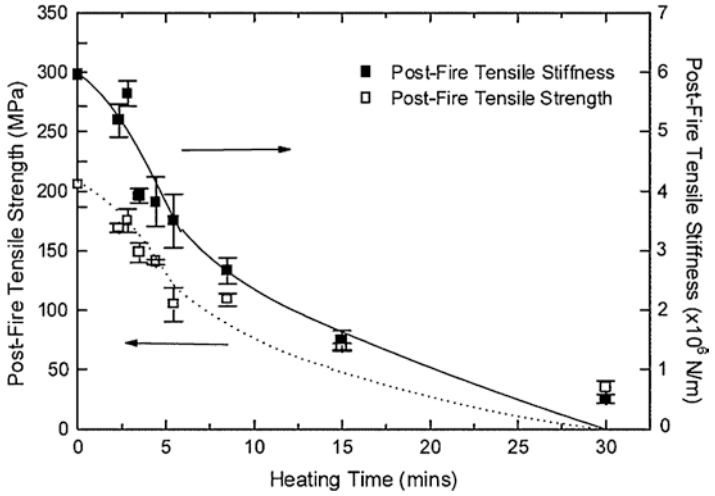

Fig. 6.13 Post-fire tensile strength and stiffness (Mouritz 2003b)

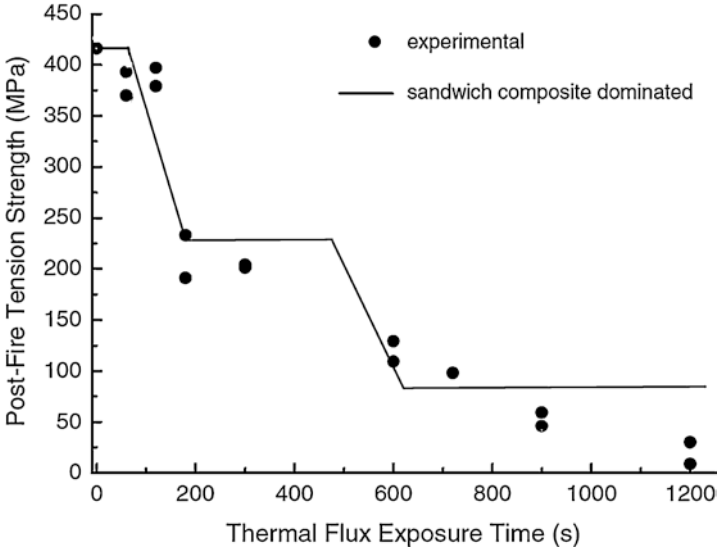

Fig. 6.14 Post-fire tensile properties of sandwich composites (Anjang et al. 2015)

other types of fire-induced damage, such as delamination cracking and overheating of the resin within the unburnt region of the composite, do not have a considerable influence on the post-fire properties (Mouritz et al. 2004).

6.6 Fire Protection for Composite Materials

It has been demonstrated that structural survivability of composite structures depends on the capability of the material in resisting deformation and failure, rather than on eluding from flaming combustion (Mouritz et al. 2009). The protection system is crucial in reducing the risk of fire on composite materials. There are two types of fire protection for composite materials; namely passive and active fire protection. As the thermal softening of the polymer matrix is the dominant process controlling the structural behaviour of composites in high temperature and fire environments; thermal insulation protection is vital to be incorporated into the composite structure. Passive insulation involves fire protecting the composite with a surface coating which has very low thermal conductivity and is thermally inert. Examples of passive insulation materials are cement-based coatings, aggregate gypsum containing cellulosic particulates or glass fibre reinforcement, mineral fibres, and insulations board.

Reactive insulation is different from passive insulation. In reactive insulation, the coatings react when exposed to the fire, which increases their thermal insulation properties. Some reactive coatings release volatiles into the fire, which then reacts against the combustion process. The most common type of reactive insulation is intumescent coating, which is commonly applied onto the substrate as an organic-based paint. Intumescent coatings provide fire protection by undergoing an endothermic decomposition reaction process at an elevated temperature that causes the material to swell and foam into a highly porous, thick and thermally stable char layer (Camino et al. 1989). In recent years, there has been an increasing interest in the application of intumescent coatings due to their advantages, including their ability to form foamed char and produce less smoke and toxic gases during combustion (Jeencham et al. 2014; Rajaei et al. 2017; Wu and Yang 2011).

In summary, whenever fire resistance is required, better fire performance can be obtained by adding the selected protection system in the composites. By having the fire protection system, flame retardancy is enhanced and will reduce the incident that may occur due to fire.

6.7 Conclusion

Studying and understanding the fire behaviour of composite materials is essential in preventing accidents in the many industries that utilising composite materials as the structure or component. This chapter has reviewed the fire reaction and fire resistance properties of composite materials. The thermal response, as well as the effect of loading on the fire behaviour, is also adequately explained. The thermal and mechanical model is essential in predicting the behaviour of the composites at elevated temperature and due to fire exposure. Advancement on the models still needs to be enhanced for better prediction of the fire behaviour. Fire testing; although

expensive and cumbersome; also needs to be performed to validate the model further on various types of composites. It is envisaged that by understanding the fire behaviour and mechanisms, the fire safety criteria of existing and future application of composite structures will be surpassed and enhanced.

References

Allison DM, Marchand AJ, Morchat RM (1991) Fire performance of composite materials in ships and offshore structures. Mar Struct 4(2):129–140. https://doi.org/10.1016/0951-8339(91)90017-6

Anjang A, Chevali VS, Kandare E, Mouritz AP, Feih S (2014) Tension modelling and testing of sandwich composites in fire. Compos Struct 113(1):437–445. https://doi.org/10.1016/j.compstruct.2014.03.016

Anjang A, Chevali VS, Lattimer BY, Case SW, Feih S, Mouritz AP (2015) Post-fire mechanical properties of sandwich composite structures. Compos Struct 132:1019–1028. https://doi.org/10.1016/j.compstruct.2015.07.009

Anjang A, Mouritz AP, Feih S (2017) Influence of fibre orientation on the tensile performance of sandwich composites in fire. Compos A: Appl Sci Manuf 100:342–351. https://doi.org/10.1016/j.compositesa.2017.05.028

Asaro RJ, Lattimer B, Ramroth W (2009) Structural response of FRP composites during fire. Compos Struct 87(4):382–393. https://doi.org/10.1016/j.compstruct.2008.02.018

Bai Y, Keller T (2009) Modeling of mechanical response of FRP composites in fire. Compos A: Appl Sci Manuf 40(6–7):731–738

Bai Y, Vallée T, Keller T (2008) Modeling of thermal responses for FRP composites under elevated and high temperatures. Compos Sci Technol 68(1):47–56. https://doi.org/10.1016/j.compscitech.2007.05.039

Bhat T, Chevali V, Liu X, Feih S, Mouritz AP (2015) Fire structural resistance of basalt fibre composite. Compos A: Appl Sci Manuf 71:107–115. https://doi.org/10.1016/j.compositesa.2015.01.006

Bhat T, Kandare E, Gibson AG, Di Modica P, Mouritz AP (2017) Compressive softening and failure of basalt fibre composites in fire: modelling and experimentation. Compos Struct 165:15–24. https://doi.org/10.1016/j.compstruct.2017.01.003

Birman V, Kardomateas GA, Simitses GJ, Li R (2006) Response of a sandwich panel subject to fire or elevated temperature on one of the surfaces. Compos A: Appl Sci Manuf 37(7):981–988. https://doi.org/10.1016/j.compositesa.2005.03.014

Boyd SE, Case SW, Lesko JJ (2007) Compression creep rupture behavior of a glass/vinyl ester composite subject to isothermal and one-sided heat flux conditions. Compos A: Appl Sci Manuf 38(6):1462–1472. https://doi.org/10.1016/j.compositesa.2007.01.006

Camino G, Costa L, Martinasso G (1989) Intumescent fire-retardant systems. Polym Degrad Stab 23(4):359–376. https://doi.org/10.1016/0141-3910(89)90058-X

Dimitrienko YI (1997) Thermomechanical behaviour of composite materials and structures under high temperatures: 1. Materials Composites Part A: Applied Science and Manufacturing 28(5):453–461. https://doi.org/10.1016/S1359-835X(96)00144-3

Egglestone GT, Turley DM (1994) Flammability of GRP for use in ship superstructures. Fire Mater 18(4):255–260. https://doi.org/10.1002/fam.810180408

Elmughrabi AE, Robinson M, Gibson AG (2008) Effect of stress on the fire reaction properties of polymer composite laminates. Polym Degrad Stab 93(10):1877–1883. https://doi.org/10.1016/j.polymdegradstab.2008.07.004

Feih S, Mouritz AP (2012) Tensile properties of carbon fibres and carbon fibre–polymer composites in fire. Compos A: Appl Sci Manuf 43(5):765–772. https://doi.org/10.1016/j.compositesa.2011.06.016

Feih S, Mouritz AP, Mathys Z, Gibson AG (2007) Tensile strength modeling of glass fiber—polymer composites in fire. J Compos Mater 41(19):2387–2410. https://doi.org/10.1177/0021998307075461

Feih S, Mathys Z, Gibson AG, Mouritz AP (2007a) Modelling the compression strength of polymer laminates in fire. Compos A: Appl Sci Manuf 38(11):2354–2365. https://doi.org/10.1016/j.compositesa.2007.04.013

Feih S, Mathys Z, Gibson AG, Mouritz AP (2007b) Modelling the tension and compression strengths of polymer laminates in fire. Compos Sci Technol 67(3–4):551–564. https://doi.org/10.1016/j.compscitech.2006.07.038

Feih S, Mathys Z, Gibson AG, Mouritz AP (2008) Modeling compressive skin failure of Sandwich composites in fire. J Sandw Struct Mater 10(3):217–245. https://doi.org/10.1177/1099636207082307

Gardiner CP, Mathys Z, Mouritz AP (2004) Post-fire structural properties of burnt GRP plates. Mar Struct 17(1):53–73. https://doi.org/10.1016/j.marstruc.2004.03.003

Gibson AG, Wright PNH, Wu YS, Mouritz AP, Mathys Z, Gardiner CP (2004) The integrity of polymer composites during and after fire. J Compos Mater 38(15):1283–1307

Gibson AG, Wu Y-S, Evans JT, Mouritz AP (2006) Laminate theory analysis of composites under load in fire. J Compos Mater 40(7):639–658. https://doi.org/10.1177/0021998305055543

Gibson AG, Torres MEO, Browne TNA, Feih S, Mouritz AP (2010) High temperature and fire behaviour of continuous glass fibre/polypropylene laminates. Compos A: Appl Sci Manuf 41(9):1219–1231. https://doi.org/10.1016/j.compositesa.2010.05.004

Gibson A, Browne T, Feih S, Mouritz A (2012) Modeling composite high temperature behavior and fire response under load. J Compos Mater 46(16):2005–2022. https://doi.org/10.1177/0021998311429383

Grenier AT, Dembsey NA, Barnett JR (1998) Fire characteristics of cored composite materials for marine use. Fire Saf J 30(2):137–159. https://doi.org/10.1016/S0379-7112(97)00059-3

Gu P (2012) 4 – structural integrity of polymer matrix composite panels in fire. In: Robinson P, Greenhalgh E, Pinho S (eds) Failure mechanisms in polymer matrix composites. Woodhead Publishing, pp 79–109

Gu P, Asaro RJ (2008) Designing polymer matrix composite panels for structural integrity in fire. Compos Struct 84(4):300–309. https://doi.org/10.1016/j.compstruct.2007.08.006

Gu P, Asaro RJ (2012) Skin wrinkling of sandwich polymer matrix composite panels subjected to fire exposure. Thin-Walled Struct 51(0):139–146. https://doi.org/10.1016/j.tws.2011.10.008

Gu P, Chen W (2012) Influence of thermal distortion to compression failure of polymer matrix composite panels in fire. Compos Struct 94(7):2174–2180. https://doi.org/10.1016/j.compstruct.2012.02.014

Jeencham R, Suppakarn N, Jarukumjorn K (2014) Effect of flame retardants on flame retardant, mechanical, and thermal properties of sisal fiber/polypropylene composites. Compos Part B 56:249–253. https://doi.org/10.1016/j.compositesb.2013.08.012

Kim J, Lee SW, Kwon S (2007) Time-to-failure of compressively loaded composite structures exposed to fire. J Compos Mater 41(22):2715–2735. https://doi.org/10.1177/0021998307078731

Krysl P, Ramroth WT, Stewart LK, Asaro RJ (2004) Finite element modelling of fibre reinforced polymer sandwich panels exposed to heat. Int J Numer Methods Eng 61(1):49–68. https://doi.org/10.1002/nme.1055

Lattimer BY, Ouellette J, Sorathia U (2004) Large scale fire resistance tests on sandwich composite materials. In: Proceedings of SAMPE 04(Long Beach, CA, May 16–20)

Liu L, Holmes J, Kardomateas G, Birman V (2011) Compressive response of composites under combined fire and compression loading. Fire Technol 47(4):985–1016. https://doi.org/10.1007/s10694-009-0123-7

Looyeh MRE, P. Bettess RK (2001) Thermomechanical response of sandwich panels to fire. Finite Element Anal & Design 37:913–927

Lua J, O'Brien J, Key CT, Wu Y, Lattimer BY (2006) A temperature and mass dependent thermal model for fire response prediction of marine composites. Compos A: Appl Sci Manuf 37(7):1024–1039. https://doi.org/10.1016/j.compositesa.2005.01.034

Luo C, Lua J, DesJardin PE (2012) Thermo-mechanical damage modeling of polymer matrix sandwich composites in fire. Compos A: Appl Sci Manuf 43(5):814–821. https://doi.org/10.1016/j.compositesa.2011.03.006

Marquis DM, Pavageau M, Guillaume E, Chivas-Joly C (2013) Modelling decomposition and fire behaviour of small samples of a glass-fibre-reinforced polyester/balsa-cored sandwich material. Fire Mater 37(6):413–439. https://doi.org/10.1002/fam.2136

Mouritz AP (2002) Post-fire flexural properties of fibre-reinforced polyester, epoxy and phenolic composites. J Mater Sci 37(7):1377–1386. https://doi.org/10.1023/A:1014520628915

Mouritz AP (2003a) Fire resistance of aircraft composite laminates. J Mater Sci Lett 22(21):1507–1509. https://doi.org/10.1023/A:1026103231041

Mouritz AP (2003b) Simple models for determining the mechanical properties of burnt FRP composites. Mater Sci Eng A 359(1–2):237–246. https://doi.org/10.1016/S0921-5093(03)00351-4

Mouritz AP (2009) Review of smoke toxicity of Fiber-polymer composites used in aircraft. J Aircr 46(3):737–745. https://doi.org/10.2514/1.36472

Mouritz AP, Gardiner CP (2002) Compression properties of fire-damaged polymer sandwich composites. Compos A: Appl Sci Manuf 33(5):609–620. https://doi.org/10.1016/S1359-835X(02)00022-2

Mouritz AP, Gibson AG (2006) Fire properties of polymer composite materials. Springer

Mouritz AP, Mathys Z (1999) Post-fire mechanical properties of marine polymer composites. Compos Struct 47(1–4):643–653. https://doi.org/10.1016/S0263-8223(00)00043-X

Mouritz AP, Mathys Z (2000) Mechanical properties of fire-damaged glass-reinforced phenolic composites. Fire Mater 24(2):67–75. https://doi.org/10.1002/1099-1018(200003/04)24:2<67::AID-FAM720>3.0.CO;2-0

Mouritz AP, Mathys Z (2001) Post-fire mechanical properties of glass-reinforced polyester composites. Compos Sci Technol 61(4):475–490. https://doi.org/10.1016/S0266-3538(00)00204-9

Mouritz AP, Mathys Z, Gardiner CP (2004) Thermomechanical modelling the fire properties of fibre–polymer composites. Compos Part B 35(6–8):467–474. https://doi.org/10.1016/j.compositesb.2003.09.005

Mouritz AP, Mathys Z, Gibson AG (2006) Heat release of polymer composites in fire. Compos A: Appl Sci Manuf 37(7):1040–1054. https://doi.org/10.1016/j.compositesa.2005.01.030

Mouritz AP, Feih S, Kandare E, Mathys Z, Gibson AG, Des Jardin PE et al (2009) Review of fire structural modelling of polymer composites. Compos A: Appl Sci Manuf 40(12):1800–1814. https://doi.org/10.1016/j.compositesa.2009.09.001

Nguyen PL, Hong Vu X, Ferrier E (2019) Thermo-mechanical performance of Carbon Fiber Reinforced Polymer (CFRP), with and without fire protection material, under combined elevated temperature and mechanical loading conditions. Compos Part B 169:164–173. https://doi.org/10.1016/j.compositesb.2019.03.075

Pering GA, Farrell PV, Springer GS (1985) Degradation of tensile and shear properties of composites exposed to fire or high temperature. J Compos Mater 14:54–66

Rahman AAA, Kumarasamy S (2017) Fire structural behavior of aerospace composites. Adv Aerosp Sci Technol:51–80

Rajaei M, Wang D-Y, Bhattacharyya D (2017) Combined effects of ammonium polyphosphate and talc on the fire and mechanical properties of epoxy/glass fabric composites. Compos Part B 113:381–390. https://doi.org/10.1016/j.compositesb.2017.01.039

Scudamore MJ (1994) Fire performance studies on glass-reinforced plastic laminates. Fire Mater 18(5):313–325. https://doi.org/10.1002/fam.810180507

Sorathia U, Beck C, Dapp T (1993) Residual strength of composites during and after fire exposure. J Fire Sci 11(3):255–270. https://doi.org/10.1177/073490419301100305

Sullivan RM (1993) A coupled solution method for predicting the Thermostructural response of decomposing, expanding polymeric composites. J Compos Mater 27(4):408–434. https://doi.org/10.1177/002199839302700404

Summers PT, Lattimer BY, Case S, Feih S (2012a) Predicting compression failure of composite laminates in fire. Compos A: Appl Sci Manuf 43(5):773–782. https://doi.org/10.1016/j.compositesa.2012.02.003

Summers PT, Lattimer BY, Case S, Feih S (2012b) Sensitivity of thermo-structural model for composite laminates in fire. Compos A: Appl Sci Manuf 43(5):783–792. https://doi.org/10.1016/j.compositesa.2012.01.006

Tewarson A, Macaione DP (1993) Polymers and composites- an examination of fire spread and generation of heat and fire products. J Fire Sci 11(5):421–441. https://doi.org/10.1177/073490419301100504

Tran P, Nguyen QT, Lau KT (2018) Fire performance of polymer-based composites for maritime infrastructure. Compos Part B 155:31–48. https://doi.org/10.1016/j.compositesb.2018.06.037

Wang HW, Zhou HW, Gui LL, Ji HW, Zhang XC (2014) Analysis of effect of fiber orientation on Young's modulus for unidirectional fiber reinforced composites. Compos Part B 56(0):733–739. https://doi.org/10.1016/j.compositesb.2013.09.020

Wu N, Yang R (2011) Effects of metal oxides on intumescent flame-retardant polypropylene. Polym Adv Technol 22(5):495–501. https://doi.org/10.1002/pat.1539

Z Mathys CPG, Mouritz AP, Townsend CR (2002) Mechanical properties of GRP composites with localised thermal damage. Int J Mater Prod Technol 17(1/2):134–142

Chapter 7
Natural Resources Based Green Composite Materials

M. R. Mansor, M. J. Taufiq, and A. F. Ab Ghani

7.1 Introduction

Green composites materials can be described as composite materials made from the natural resources, either as the reinforcement material, the matrix or both reinforcement and matrix. They are also known as natural fibre composites, wood plastic composites and fibre reinforced plastics. Nowadays, there have been huge efforts and accomplishment in the development of green composite materials from natural resources, especially to replace and reduce the use of synthetic composites. Green composites materials offer many advantages compared to synthetic composites for many applications. In term of material properties, the natural fibre used as the reinforcement materials for the green composites has low density property, which further contributes to a higher specific strength and specific modulus compared to synthetic composites. The low density physical property is also one of the key advantages for green composites because it helps to reduce the overall final composite weight. Furthermore, natural based fibres are also more environmentally friendly, whereby there are obtained from renewable, recyclable and biodegradable resources, as compared to synthetic based fibres which are made from non-renewable petroleum based resource. Green composite materials also offer similar product development advantages as compared to synthetic composites, such as a high degree of flexibility where the product final form with complex geometrical shape can be customized. Green composite materials are also able to be produced in varying sizes

M. R. Mansor (✉) · M. J. Taufiq
Faculty of Mechanical Engineering, Universiti Teknikal Malaysia Melaka, Durian Tunggal, Melaka, Malaysia
e-mail: muhd.ridzuan@utem.edu.my

A. F. Ab Ghani (co-author)
Faculty of Mechanical and Manufacturing Engineering Technology, Universiti Teknikal Malaysia Melaka, Durian Tunggal, Melaka, Malaysia

S. Siddiquee et al. (eds.), *Composite Materials: Applications in Engineering, Biomedicine and Food Science*, https://doi.org/10.1007/978-3-030-45489-0_7

by using a similar manufacturing process. Besides, they are also known to have minimal impacts on users' health issues such as skin irritation, as well as encompassed fewer abrasive properties which help to reduce tool wear and prolong tool life. Another distinct advantage of green composites is lower final composite cost; due to the cheap and renewable source of constituents that making up the final composite material.

Despite the advantages, green composites also inherit several limitations that challenges further development of these materials, especially for higher load bearing applications. Among the most notable limitation is due to the hydrophilic nature of the reinforcement materials (which is derived from plant based natural resources). The hydrophilic nature caused dimensional instability to the final composites as well as poor fibre-matrix adhesion performance which strongly affect the structural strength of the material. Moreover, uneven fibre size also affects the structural properties due to varying load distribution along the fibre length, which causes larger stress concentration at a certain location in the final composites. These factors are currently limiting green composites application to low load bearing application.

In this chapter, an overview of green composite materials is discussed. The discussion is focused on green composites reinforced polymer matrix, as it is the most applied type of green composites made from natural resources being developed currently. Among the topics included are types of green composites, application of green composites, their mechanical properties and processing methods. This chapter also highlights the latest development of green composite materials such as hybrid green composites; green composites reinforced recycled polymer matrix and green composites with nanomaterials. The chapter is concluded with brief remarks on the opportunities which can be ventured both by researchers and practitioners, to address existing limitation such as regarding the material properties, processing and design method.

7.2 Overview of Natural Resources Based Green Composites Materials

In general, the basic structure for the formulation of green composites from natural resources comprised of the reinforcement and the matrix. The main function of the reinforcement (or the fibre) is to absorb the applied load, while the matrix acts as to hold all the fibres together to form the shape of the final composites as well as evenly distribute the load applied across the composites structure. In addition, new class of advanced green composites also encompassed nanoparticle fillers (such as nanoclays, graphene, carbon nanotubes (CNT) and cellulose crystals) to further enhance the materials existing mechanical, thermal, physical and other functional properties. Figure 7.1 shows the basic structure in green composites formulation from natural resources.

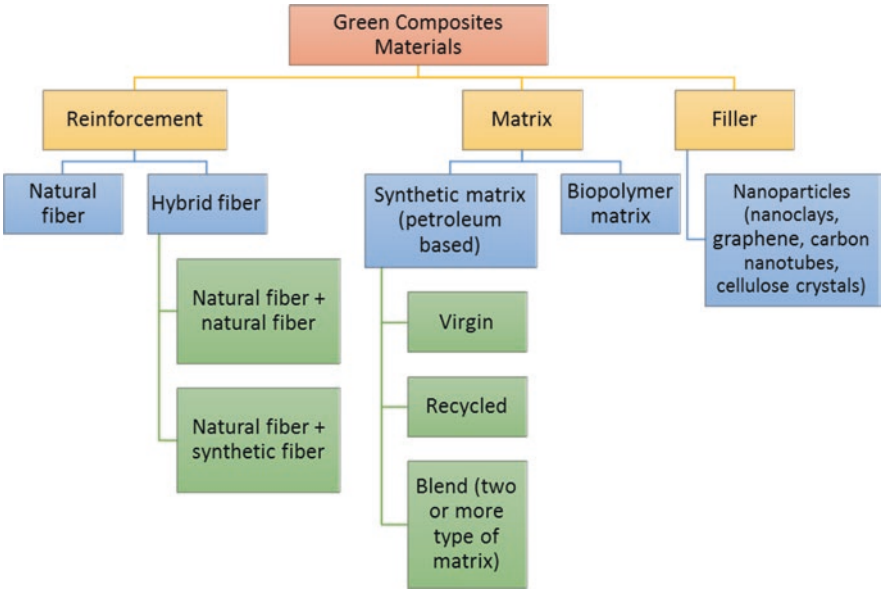

Fig. 7.1 Basic structure in green composites formulation from natural resources

Based on Fig. 7.1, there are multiple combinations on the type of reinforcement and matrices from natural resources developed for green composites. Green composites can be formulated from single fibre/single matrix up to hybrid fibre/blend of matrix. Green composites can also be formulated to become fully green composites (both reinforcement and matrix are made from natural resources) or partially green composites (either the reinforcement or matrix are made from natural resources).

7.2.1 Green Composites Reinforcement Material

Pecas et al. (2018) published a very comprehensive review on the characteristics of green composites reinforcement and matrix materials. They stated that as the main load bearing element for the green composites, the reinforcement or fibre performance depends on several factors such as fibre volume (amount of fibre used), aspect ratio, shape, orientation, arrangement and also the interfacial adhesion with the matrix. Green composites reinforcement is available in the form of particle or fibre and is characterized as continuous or discontinuous (i.e., chopped) depending on its length-to-diameter (l/d) ratio. Commonly, the fibre-reinforced phase arrangement is classed as woven or non-woven. A woven fabric is characterized by continuous interlacing of perpendicular yarns, in a regular pattern. Yarns are structures consisting of several interlocked fibres. The twist angle is responsible for the cohesion of the fibres and yarn strength up to a certain point, beyond which, the

maximum fibre strength decreases due to the increase in obliquity. Moreover, the increase of the fibre twist angle is correlated with a decrease of fibre-resin bond strength, lower permeability and consequently poor mechanical properties. When continuous fibres are used, the fibre architecture can be one-dimensional and two-dimensional, or often termed as unidirectional or bidirectional. In the one-dimensional architecture, the twist angle and the level of alignment of continuous-filament yarns play a significant role in determining the maximum applied load. The reinforcement is able to hold the highest applied load in the fibre direction compared to transverse fibre directions. Pecas et al. (2018) also further explained that a non-woven arrangement consists of a flat structure without interwoven strands, with randomly oriented or unidirectional fibre orientation. Furthermore, the mat or woven can either be composed of continuous or chopped unidirectional fibres, randomly chopped fibres or suspended particles. In particular, mat composed with randomly chopped fibres does not have any preferential stress direction, but they are the preferable choice for large-scale production due to the high availability, ease and cost-effectiveness when manufacturing complex parts of isotropic nature.

Reinforcement from natural resources can be classified based on their origin into the following groups: animal, mineral and plant. Plant originated natural fibres are the most commonly accepted fibres by the industry and the most analysed by the research community due to the short growth period, renewability and wider availability (Cristaldi et al. 2010). As shown in Fig. 7.2, plant fibres are composed of cellulose, hemicellulose and lignin, which can be extracted from bast, leaf, seed, fruit, wood, stalk and grass/reed (Shah 2014). Among the types of commodity plant fibres used to manufacture green composites are kenaf, jute, flax, wood and hemp.

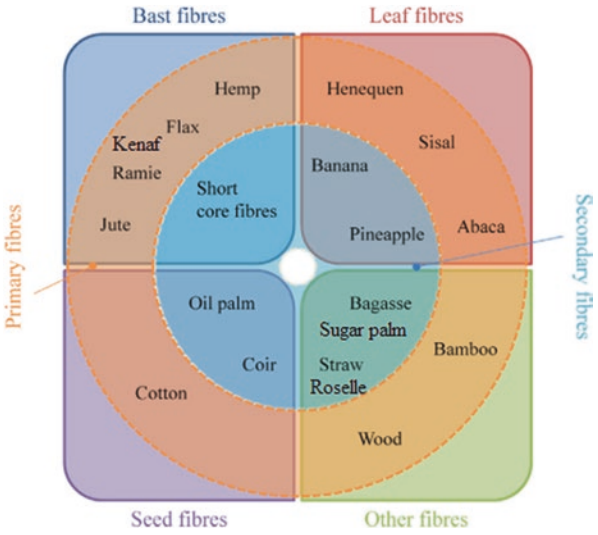

Fig. 7.2 Type of natural fibres resources (Shah 2014; Aji et al. 2009, Radzi et al. 2019a; Ishak et al. 2013)

Natural fibres offer many advantages compared to synthetic fibres such as good specific strength and modulus, low density, low manufacturing energy consumption, low cost, high acoustic damping, low carbon footprint, renewable and biodegradable (Faruk et al. 2014). However, natural fibres have negative aspects due to their low consistency of properties and quality. These fibres have higher variability of physical and mechanical properties, higher moisture absorption, lower durability, lower strength and lower processing temperature (Pickering et al. 2016). The large varieties of properties are mainly dependent upon plant species, growth conditions and methods of fibre extraction (Sanjay et al. 2016). Moreover, the related properties are also depending on the fibre cell geometry of each type of cellulose and its degree of polymerization (Ho et al. 2012; Shah 2013).

There have been many publications summarizing the important properties of plant fibres for green composites application. One of them was by Gurunathan et al. (2015) who have listed major type of plant fibres according to their physical and mechanical properties as shown in Fig. 7.3. It can be observed that among the fibres with the highest tensile strength and modulus properties available are pineapple, kenaf, flax and hemp fibres; while among the lightest fibres are bamboo, kenaf, coir and sisal fibres. Hence, consideration on the appropriate type of fibres can also be a challenge for producing green composites products, which needs to be based on the weight of importance for the selected properties to be used for the intended product. Another important information which need to be alerted for selection of suitable plant fibres are the range of values within the similar fibre itself, due to varying factors such as type of growth conditions and method of fibre extractions as stated previously.

7.2.2 Green Composites Matrices

Matrix is a vital component in the formulation of polymer based green composites. As described earlier, matrix acts as to hold all the fibres together to form the shape of the final composites as well as to distribute the load applied evenly across the composites structure. In general, there are two categories of matrix applied for

Fibre	Density (g/cm^3) [a]	Diameter (μm) [a]	Length (mm) [a]	Tensile Strength (MPa) [a]	Young's Modulus (GPa) [a]	Elongation at Break (%) [a]	Moisture Content (%) [a]
Abaca	1.5	10–30 (20)	4.6–5.2 (4.9)	430–813 (621.5)	31.1–33.6 (32.35)	2.9	14
Bamboo	0.6–1.1 (0.85)	25–88 (56.5)	1.5–4 (2.75)	270–862 (566)	17–89 (53)	1.3–8 (4.65)	11–17 (14)
Banana	1.35	12–30 (21)	0.4–0.9 (0.65)	529–914 (721.5)	27–32 (29.5)	5–6 (5.5)	10–11 (10.5)
Coir	1.2	7–30 (18.5)	0.3–3 (1.65)	175	6	15–25 (20)	10
Cotton	1.21	12–35 (23.5)	15–56 (35.5)	287–597 (442)	6–10 (8)	2–10 (6)	33–34 (33.5)
Flax	1.38	5–38 (21.5)	10–65 (37.5)	343–1035 (689)	50–70 (60)	1.2–3 (2.1)	7
Hemp	1.47	10–51 (30.5)	5–55 (30)	580–1110 (845)	30–60 (45)	1.6–4.5 (3.05)	8
Jute	1.23	5–25 (15)	0.8–6 (3.4)	187–773 (480)	20–55 (37.5)	1.5–3.1 (2.3)	12
Kenaf	1.2	12–36 (24)	1.4–11 (6.2)	295–930 (612.5)	22–60 (41)	2.7–6.9 (4.8)	6.2–12 (9.1)
Pineapple	1.5	8–41 (24.5)	3–8 (5.5)	170–1627 (898.5)	60–82 (71)	1–3 (2)	14
Ramie	1.44	18–80 (49)	40–250 (145)	400–938 (669)	61.4–128 (94.7)	2–4 (3)	12–17 (14.5)
Sisal	1.2	7–47 (27)	0.8–8 (4.4)	507–855 (681)	9–22 (15.5)	1.9–3 (2.45)	11

Fig. 7.3 Selected physical and mechanical properties of natural fibres for green composites (Gurunathan et al. 2015)

green composites, which are thermoset and thermoplastic. They are originally derived from petroleum based resources, but as the need for more environmentally friendly alternatives arise, a new class of matrix which is fully biodegradable (often term as biopolymer) are extensively developed to construct fully biodegradable green composites. This new class of biopolymer is an important solution to reduce plastics wastes issues related to petroleum based plastics nowadays.

In overall, thermoplastic materials that currently dominate as matrices for green composites are polypropylene (PP), polyethylene (PE), and polyvinyl chloride (PVC) while thermosets, such as phenolics and polyesters, are common matrices (Malkapuram et al. 2009). Elsewhere, it is also reported that PE and PP are the most widely used plastics and account for 61% of the U.S. plastics market. PE and PP have glass transition temperatures (T_g) much lower than ambient temperature, which makes them tough, and are semi-crystalline, which makes them rigid, with moderate melting temperatures (T_m), which makes them easy to process. The combination of toughness, rigidity, and processing ease along with a density of 0.93–0.96 g/cm^3 makes them useful for a wide variety of applications from bottles to automotive parts. While the semi-crystallinity gives them exceptional properties for a wide range of applications, PE and PP also exhibit the challenge in generating the largest shrinkage after molding compared to other commodity polymers, which is a direct result of the semi-crystallinity. This results in large warpage of the part while in use (Davis et al. 2019). Moreover, polystyrene, and polyamides (nylon 6 and 6, 6) are also common types of thermoplastic used especially in the automotive application. Holbery and Houston (2006) reported that the development of thermoplastic green composites is constrained by two primary physical limits: the upper temperature at which the fibre can be processed and the significant difference between the surface energy of the wood and the polymer matrix. Process temperature is a limiting factor in green composites applications. The generally perceived upper limit before fibre degradation occurs is on the order of 150 °C for long processing durations, although plant fibres may withstand short-term exposures to 220 °C. The result of prolonged high-temperature exposure may be discoloration, volatile release, poor interfacial adhesion, or embrittlement of the cellulose components. Therefore, it is important to obtain as rapid a reaction rate as possible during both surface treatment and polymer processing to limit exposure to cell wall components preventing degradation. The development of low-process-temperature surface treatments with high service capabilities is viewed as an enabling technology for the application of plant fibres in green composite materials.

Holbery and Houston (2006) also reported that among the primary thermoset resins used for green composites especially in automotive applications are polyester, vinylester, and epoxy resins. Polyester resins are widely used, particularly the "unsaturated" type capable of cure from a liquid to a solid under a variety of conditions. A range of polyesters is made from different glycols (polyethylene glycol, ethylene glycol, etc.), acids (malaeic, anhydride), and monomers, all having various properties. Orthophthalic polyester is the standard economic resin commonly used, and it yields highly rigid products with low heat resistance. Isophthalic polyester is now more common when moisture resistance is needed. Epoxy resins offer high

performance and resistance to environmental degradation. On the other hand, vinylester resins have excellent chemical resistance, good thermal and mechanical properties, and the relative ease of processing and rapid cure characteristics of polyester resins. These have better moisture resistance than epoxies when cured at room temperature. Vinylester resins are similar in their molecular structure to polyesters, but differ in that the reactive sites are positioned at the ends of the molecular chains, allowing for the chain to absorb energy. This results in a tougher material when compared to polyesters.

Biopolymer is an emerging and highly potential alternative for the formulation of green composites, especially in the future. Biopolymer is made from natural resources such as plants. Sahari and Sapuan (2011) summarized several important types of biopolymer, which are further categorized into biodegradable natural based polymer and biodegradable petroleum based polymer. Among the types of biodegradable petroleum based polymer are aliphatic polyester, aliphatic-aromatic polyester, polyester amide, polyalkynene succinates and polyvinyl alchohol (PVA). On the other hand, examples of the biodegradable natural based polymer are polylactide acid (PLA), thermoplastic starch, cellulose and polyhydroxyalkanoate (PHAs). PLA is an environmentally and commercially interesting biopolymer as it has many exclusive qualities, such as good transparency, glossy appearance, high rigidity, and good processability. However, PLA also draws some limitation in term of its inherent brittleness and poor toughness (Siakeng et al. 2019a, b). Thermoplastic starch (TPS) is derived from renewable and cheap raw material feedstock such as sugar palm starch and agar (seaweed), cassava, corn, wheat, and potatoes. Starch is composed of two polymers namely amylose and amylopectin. The linear structure of amylose makes it closely resembled the behaviour of conventional synthetic thermoplastic, hence, enabled TPS to be used in various fabrication machines for its production; that is, extrusion, compression moulding, injection moulding, etc. Nevertheless, pure TPS also possesses several disadvantages such as poor mechanical strength and weak water resistance (Jumaidin et al. 2017). In overall, due to the low mechanical properties of biopolymer as compared to synthetic matrices, their application in green composite materials is limited to low load bearing conditions.

7.3 Hybrid Green Composites Materials

Single fibre/matrix green composites have been extensively studied over the years, using various types of plant fibres as the reinforcement material. However, single fibre/matrix green composites are still facing the challenges in term of low mechanical properties as compared to single fibre/matrix synthetic composites such as glass fibre reinforced composites and carbon fibre reinforced composites. To address the issue, researchers have ~~has~~ come out with a solution to use hybridization method for alleviating the properties of the green composites. The hybridization method combines two or more types of fibres in a single matrix, to form hybrid green composites. As shown in Fig. 7.1 previously, hybrid green composites may be formed using

either the combination of natural based fibre-synthetic fibre or natural based fibre-natural based fibre type of reinforcements. The goal of hybridization is to improve the overall performance of the final green composites, by combining initially less strong natural fibres with stronger fibre counterparts within the same matrix. The synergetic combination enables improvement for the final green composite properties. Moreover, the hybridization method also allowed obtaining a balance between performance and cost for the final green composites, which is very beneficial for optimum use such as in application with medium load bearing requirement (Mukhtar et al. 2018).

Up to date, many efforts have been reported on the development of hybrid green composites using fully natural fibre/natural fibre type of reinforcements. This is due to the increasing drive towards formulating better eco-friendly green composite material (higher use of renewable and biodegradable contents) as well as having a lower overall raw material cost. Cavalcanti et al. (2019) have developed a novel intralaminar hybrid green composite using jute, sisal and curaua fibres. The fibres were woven together to produce hybrid jute/sisal and hybrid jute/curaua mat. The hybrid mats were later reinforced with epoxy matrix at 70 wt%. In their study, the fibres were also subjected to alkalization and mixed alkalization and silanization chemical treatments. Characterization was performed on the intralaminar hybrid green composites to determine their density, tensile, flexural impact properties. Navaneethakrishnan et al. (2019) also developed new hybrid green composites using sisal and luffa fibres. Sisal fibre was extracted from sisal leaf, whereas luffa fibres were extracted from cucumber (after its cellulose was removed). Unsaturated vinyl ester resin was used as the matrix for the green composites. They studied three hybrid sisal:luffa fibre loadings which were 10:20, 15:15, 20:10, and the hybrid green composites were fabricated using compression moulding process. In another study, Chee et al. (2019) developed hybrid green composites using bamboo and kenaf fibres. The bamboo fibre used was in the form of non-woven mat while the kenaf fibre was in the form of woven mat. Total hybrid fibre loading of 40 wt% was used to formulate the hybrid green composites, while the bamboo and kenaf fibre ratio was fixed at 30:70, 50:50 and 70:30 wt%. The hybrid composites were characterized in term of their coefficient of thermal expansion (CTE) and dynamic mechanical properties. Furthermore, Premnath (2019) also developed hybrid jute/sisal reinforced epoxy green composites. The green composites were fabricated using hand lay-up process. The jute fibre loadings were also varied. His study also involved the assessment of chemically treated (using NaOH) and untreated jute/sisal hybrid fibres in term of the mechanical properties (tensile, flexural, impact and hardness).

Other types of natural fibres were also reported as reinforcement materials for hybrid green composites. Zin et al. (2019) produced hybrid green composites by combining banana-pineapple leaf (PALF)-glass woven fibres, using epoxy matrix. Ninampure et al. (2019) developed hybrid sisal fibrils/kenaf fibres unsaturated polyester green composites. The novel hybrid fibres were targeted as an environmentally friendly alternative material for high strength electrical insulation applications. The hybrid reinforcement was varied from 10 to 40 wt%. The hybrid green composites

were later characterized in term of the mechanical, thermal and electrical insulating properties. Apart from that, Asim et al. (2019) produced hybrid pineapple leaf fibre/ kenaf reinforced phenolic green composites and studied their thermomechanical properties at varying hybrid fibre loadings. Elsewhere, Arulmurugan et al. (2019) also developed new aloe vera /hemp/flax natural fibre sandwich laminate hybrid green composites with the addition of barium sulfate as the filler. The hybrid green composites performance was investigated in term of their nonlinear viscoelastic behaviour, tensile and flexural strength properties.

Kumar et al. (2019) further developed hybrid Grewia optiva/Bauhinia vahlii fibre reinforced epoxy composites. This new class of natural fibres is mostly found around Himalayan region. A similar type of Bauhinia vahlii fibre was also developed as hybrid green composites, by combining the fibre with Nettle fibre (which also originated around Himalayan region). The hybrid Nettle fibre/ Bauhinia vahlii fibre was developed using epoxy matrix (Kumar et al. 2019a). In addition, Bauhinia-vahlii-weight/sisal (BVWS) fibres reinforced epoxy composites was also developed as green composites. The hybrid BVWS green composites were also added with risk husk as filler at varying filler loadings and characterized in term of the final composites physical, mechanical and sliding wear properties (Kumar et al. 2019b). The use of new and unique species of plant fibres by the aforementioned researchers showcased positive research growth towards identifying more alternative to produce high performance natural fibre for green composites application.

There are also reported studies about the effect of varying laminate stacking sequence on hybrid green composites material properties. Kumar et al. (2019) studied on the effect of different stacking sequence to the tensile, compressive, interlaminar shear strengths (ILSS) and hardness material properties for hybrid hemp/ sisal reinforced epoxy green composites. The hybrid green composites were fabricated using hand lay-up and hot press method. Sanjay et al. (2019) performed a similar study using jute/kenaf reinforced epoxy and jute/kenaf/e-glass reinforced epoxy composites. They found that the addition of e-glass fibre to the jute/kenaf hybrid fibres further help to enhanced the mechanical properties. The laminates were developed using vacuum bagging method by utilizing woven fabric shape. Jothibasu et al. (2018) studied the effect of stacking sequence on the mechanical properties of areca sheath fibre/jute fibre/glass-woven fabric reinforced epoxy green composites. The natural fibres were also subjected to alkali-treatment process and the samples were fabricated using hand lay-up method. Similarly, Mohamad Hamdan et al. (2019) developed various stacking sequence for hybrid woven jute–roselle green composites to investigate its performance. They used hand lay-up method to produce the green composites. Furthermore, Khan et al. (2019) also investigated the similar effect using kenaf/jute reinforced epoxy green composites. They compared two type of stacking sequences for the hybrid fibres in the study, which are kenaf/jute/kenaf (K/J/K) and jute/kenaf/jute (J/K/J). The hybrid green composites were also fabricated using hand lay-up method.

Apart from thermoset matrix, hybrid green composites were also developed using thermoplastic matrix. For example, Radzi et al. (2019a) developed of roselle (RF)/sugar palm (SP) fibre reinforced thermoplastic polyurethane (TPU) hybrid

green composites using hot compression moulding process. The fibres used were in short fibre form. They also further investigated the roselle (RF)/sugar palm (SP) fibre reinforced thermoplastic polyurethane (TPU) hybrid green composites properties when subjected to alkali treatment process (Radzi et al. 2019b). Moreover, Siakeng et al. (2019a, b) developed pineapple leaf fibres (PALF)/coir reinforced polylactic acid (PLA) green composites in short fibre form, which is targeted for food packaging application. The hybrid green composites were produced with different fibre ratios and manufactured using internal mixer plasticizer and hot press machine. In addition, Rahman et al. (2019) developed short fibre hybrid composites using the combination of kenaf and jute fibres, and bound together using polyethylene matrix. The hybrid natural fibres were also subjected to alkaline-treated and compared with untreated hybrid fibres for their physical, mechanical and thermal properties. Table 7.1 summarized the recent works available from literature on the development of hybrid green composites from natural resources.

7.4 Green Composites Materials Using Recycled Polymer Matrix

Synthetic polymer is a man-made material, containing organic or semi organic material which is malleable and can be moulded into almost any simple and complex shapes. With regards to this fact, the synthetic polymer has been used in varieties of applications in human daily life including in technical used or household appliances. The special characteristics of low density, possibly adjustable properties, easy workability, and resistance to moisture and chemicals have made the synthetic polymer can take over the conventional materials such as metal (Worsfold et al. 2019). However, the broad applications of synthetic polymer have caused another problem, faced by many countries, which is the rising of plastic waste abundance. The rising of plastic waste abundance also could reduce the landfill area. Ritchie and Roser (2018) reported that high-income country tends to produce more plastic waste. This was supported by the data collected by Dorger (2019) where it shows that China has produced the most plastic waste (59.8 million tons/year), followed by United States (37.83 million tons/year) and Germany (14.48 million tons/year). In addition, the polymer waste might be produced from the post-consumer use or even from the industrial sector. Hence, the polymer wastes need to be recycled ~~as~~ to reduce the waste abundance as well as extending the life cycle of the synthetic polymer.

The growing awareness of eco-friendly materials must be paralleled with environmental regulations and conservation. Green composite is said as an eco-friendly material, since it is made by the combination of synthetic polymer (as matrix) and natural fibre (reinforcement). For some application, the green composite can replace the conventional material, because of its characteristics of low cost, low density, nonabrasive, noncorrosive, inherent biodegradability, acceptable specific strength

Table 7.1 Summary of recent works on the development of hybrid green composites from natural resources

Year	Type of hybrid green composites	Authors
2019	Jute/sisal and jute/curaua reinforced epoxy composites	Cavalcanti et al. (2019)
2019	Sisal-luffa reinforced unsaturated vinyl ester composites	Navaneethakrishnan et al. (2019)
2019	Bamboo/kenaf composites	Chee et al. (2019)
2019	Jute/sisal reinforced epoxy composites	Premnath (2019)
2019	Grewia optiva/Bauhinia vahlii fibre reinforced epoxy composites	Kumar et al. (2019)
2019	Nettle fibre/Bauhinia vahlii reinforced epoxy composites	Kumar et al. (2019a)
2019	Bauhinia-vahlii-weight/sisal reinforced epoxy composites	Kumar et al. (2019b)
2019	Banana/pineapple leaf (PALF)/glass reinforced epoxy composites	Zin et al. (2019)
2019	Roselle (RF)/sugar palm (SP) fibre reinforced thermoplastic polyurethane (TPU) composites	Radzi et al. (2019a); Radzi et al. (2019b)
2019	Hemp/sisal reinforced epoxy composites	Kumar et al. (2019)
2019	Jute/kenaf reinforced epoxy and jute/kenaf/e-glass reinforced epoxy composites	Sanjay et al. (2019)
2019	Areca sheath fibre/jute fibre/glass-woven fabric reinforced epoxy composites	Jothibasu et al. (2018)
2019	Woven jute/roselle composites	Mohamad Hamdan et al. (2019)
2019	Kenaf/jute reinforced epoxy composites	Khan et al. (2019)
2019	Pineapple leaf fibres (PALF)/coir reinforced polylactic acid (PLA) composites	Siakeng et al. (2019)
2019	Kenaf/jute reinforced polyethylene composites	Rahman et al. (2019)
2019	Sisal fibrils/kenaf fibres unsaturated polyester composites	Ninampure et al. (2019)
2019	Pineapple leaf fibre/kenaf reinforced phenolic green composites	Asim et al. (2019)
2019	Aloevera /hemp/flax natural fibre sandwich laminate composites	Arulmurugan et al. (2019)

and stiffness, easily available, and recyclable (Naveen et al. 2019). Moreover, the current development on green composite can be seen on the using of recycled synthetic polymers as the matrix. The using of a recycled synthetic polymer may reduce the material cost and abundance plastic waste, and support sustainable product development (Taufiq et al. 2017).

In the 2018, Taufiq et al. discovered the mechanical and thermal properties of kenaf fibre reinforced recycled polymer blend composite. The recycled polymers were received from rejected unused disposable diapers, obtained from a disposable diaper manufacturer. Mainly in disposable diapers, the plastic parts were made by polyethylene, polypropylene, polystyrene, super absorbent material, and colouring materials (Espinosa-Valdemar et al. 2011). Those materials are synthetic polymer,

thus suitable to be used for green composite matrix. Through electron microscopy examination on the fractured samples, it can be seen the using of recycled polymers and kenaf fibre are compatible within the range of 30–40 wt.% of fibre. The flexural strength also proved the maximum strength can be found on the point of 30 wt.% and started to decrease at 40 wt.%. On the Izod strength characteristic, the addition of kenaf fibre does not improved the impact strength. The deterioration of impact strength may due to fibre-to-fibre contact, causing the fibre breakage to be dominant. In addition, the increases of fibre content have affected the insufficient matrix to hold the reinforcement. The absence of coupling agent also induced the fibre pull-out, poor adhesion, and failure on matrix and reinforcement interfaces. Figure 7.4 showed the failure mode on the tested samples.

Similar work was done by Turku et al. (2018), on the using recycled synthetic polymer that received from municipal and construction wastes. Their work was comparing the durability towards manipulated weathering of the green composite made by two types of recycled polymer matrix. As reported in their earlier studies, the recycled polymer that obtained from construction contained the packaging and non-packaging plastics (Turku et al. 2017). Meanwhile, the municipal recycled polymers were made of household packaging and appliances. These construction and municipal polymer waste generally made by polyethylene, polypropylene, polystyrene, poly vinyl chloride (PVC) and other polyolefin materials, thus essential for green composite production. The freeze-thaw cycling method was used to examine the irreversible effect of water absorption on the mechanical properties of the composites made by two different matrices. The thickness swelling and water absorption more in composite made by recycled municipal plastic rather than recycled construction plastic, showing higher wettability. This caused the fibre swelling that leads to stress in matrix, inducing microcracking formation. In addition, the water absorbed also weakened the fibre and matrix interfacial interaction, which later support the reason for composites made by recycled municipal plastic have lower in mechanical strength and modulus. Figure 7.5 showed the SEM images of the microcracks that occurred in the matrix.

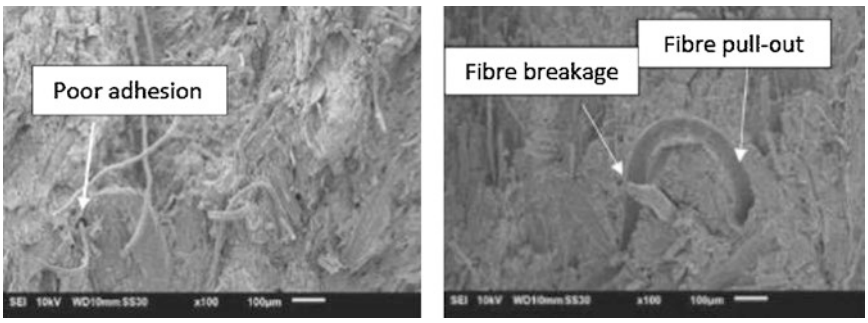

Fig. 7.4 Some of the detected failures on the Izod impact fractured samples (Taufiq et al. 2018)

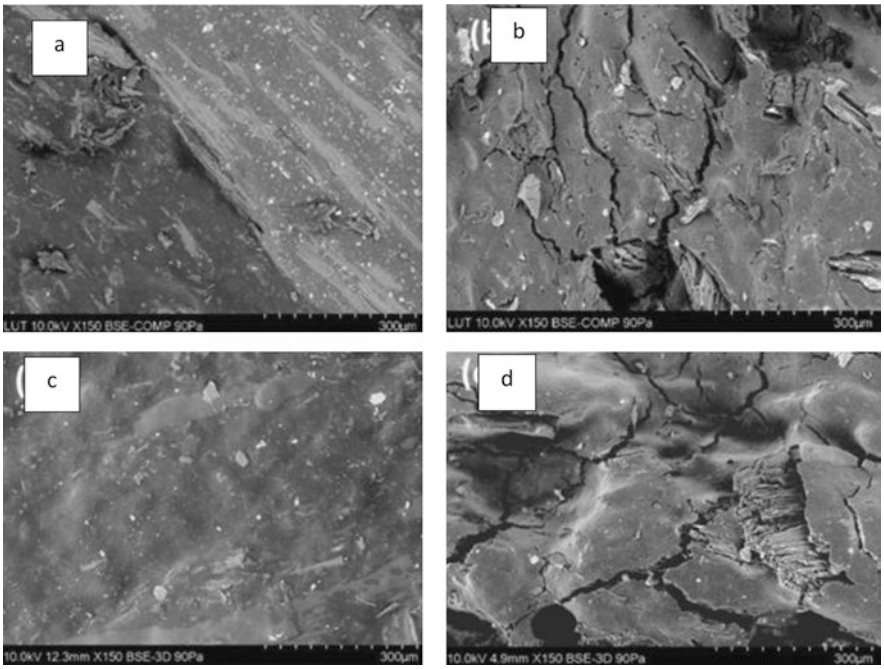

Fig. 7.5 SEM images of the microcrack on the matrix; (**a**) before, (**b**) after water absorption of recycled construction plastic, (**c**) before (**b**) after water absorption of recycled municipal plastic (Turku et al. 2018)

7.5 Green Composites Materials Using Nanomaterials

In the pursue to address the existing limitation of green composites, efforts have also been made by researchers to incorporate nanomaterials as filler material. These new classes of advanced green composites encompassed nanomaterial fillers such as nanoclays, graphene, carbon nanotubes (CNT) and cellulose crystals to enhance the materials existing mechanical, thermal, physical and other functional properties. Among the nanomaterials, nanoclays are leading the development of advanced green composites. Nanoclays play a significant role to improve composite performance by enhancing their properties such as thermal stability, mechanical strength, and barrier properties. Some of the important parameters which contribute the most in modifying the properties of various composites include the content, shape, size, and the affinity towards matrix material (Cheng et al. 2016).

Among several examples on the application of nanoclays in green composites was by Rajesh et al. (2019) who developed short madar fibre reinforced polyester composite using nanoclay to increase its mechanical properties. The composite specimens were prepared with the addition of 1 wt.% nanoclay at varying weight proportions of short madar fibre in the polyester matrix from 2.5 to 15 wt.%. Meanwhile, Mohan and Kanny (2019) developed banana reinforced epoxy green

composites with the addition of Na + montmorillonite (MMT) nanoclay to enhance the unmodified composites mechanical properties (tensile, flexural and compressive strength). Shahroze et al. (2018) also used MMT nanoclay to enhance the mechanical properties of sugar palm reinforced polyester composites. They stated that, MMT nanoclay is the most widely applied constituent in composites manufacturing applications due to its good tendency for cation exchange, high aspect ratio and good swelling properties as compared to other nanoclay materials such as saponite, hectorite, stevensite, beidellite and nontronite.

Apart from nanoclays, enhancement of green composites is also performed by the addition of graphene nanomaterials. Graphene is regarded as the future materials due to its superior mechanical, thermal and electrical properties. Among the many recent works on the use of graphene in green composites is by Sarker et al. (2019). They used graphene oxide (GO) and graphene flakes in the preparation of jute reinforced epoxy composites using hot press method to improve the unmodified composites tensile strength and tensile modulus properties, tailored for various stiffness-driven applications. Naveen et al. (2019) also used varying graphene nanoplatelets loadings in improving the mechanical and moisture resistant properties of Kevlar (K)/cocos nucifera sheath (CS)/epoxy hybrid green composites. Elsewhere, Dang et al. (2019) employed GO in the formulation of ramie fibre reinforced polypropylene green composites, to enhance the materials interlaminar shear strength. The GO-ramie fibre reinforced polypropylene green composite was prepared by hot press method.

There are also many recent positive improvements regarding the green composites modified with carbon nanotubes (CNT) and cellulose nanocrystals which have been reported by the related research works. Nor et al. (2019) demonstrated the improvement of impact properties for hybrid bamboo/glass fibre polymer composites filled with CNT as nanofillers. Meanwhile, Wang et al. (2019) applied multi-walled carbon nanotubes (MWCNTs) to modify the mechanical and thermodynamic properties of flex reinforced epoxy composites. On the other hand, among the research works reported on cellulose nanocrystal for green composites was by Chang et al. (2019) who developed sisal reinforced starch composites using starch nanocrystals (SNCs). In their study, the SNCs were obtained by the hydrolysis of waxy starch. It was shown that the addition of SNC helped to improve the interfacial adhesion of the sisal reinforced starch composites. Whereas, Zhang et al. (2017) reported the development of new sisal reinforced epoxy composites with the addition of cellulose nanocrystal. In their study, sisal fibres were first treated with alkali before the cellulose nanocrystal were deposited onto the fibre surface using electrophoretic deposition (EPD) method.

7.6 Application of Green Composites Materials

Up to date, there are many reports on the application of green composites, which provide clear evidence on its positive growth for both research and development (R&D) and commercialization purpose. Grand View Research (2018), one of the leading market research and consulting firm published a forecast report on the green composites commercialization for year 2018 until 2024, stating that the global green composites market size was valued at USD 4.46 billion in 2016, and expected to steadily increase with cumulative annual growth rate (CAGR) of 11.8% from the year 2016 to 2024 (Market Research Report 2018). The company also reported that major types of natural fibres used in the current application are wood, flax, kenaf, cotton, and hemp. Wood fibres top the list with 59.3% of the overall natural fibre market revenue in 2015. Meanwhile in term of market application, green composites are widely used by building and construction, automotive, electronics and sporting goods industry. Product examples are decking, railing, window, building frames, mobile cases, laptop cases, tennis racket, bicycle, and snowboards. The highest market application of green composites is recorded by building and construction industry, followed by the automotive industry based on 2016 data from similar report. Among the major factors contributing to the rapid growth of green composites, especially from natural resources are spiralling demand for lightweight products from the automotive industry, rising awareness about green products, growing inclination towards eco-friendly products, and urging uptake of recyclable products mainly by consumers and industrial players.

There are two major factors that drive the rapid progress of green composites in automotive application; (1) vehicle light-weighting and (2) end-of-life performance. It is estimated that a 25% reduction in car weight would be equivalent to saving 250 million barrels of crude oil. Thus, the utilization of low-density natural fibres towards the formulation of green composite materials could lead to a weight reduction of 10–30%, which significantly contribute to achieving lightweight vehicle target. Moreover, the recycling concerns being driven by EU regulations (ELV) are forcing automotive manufacturers to consider the environmental impacts of their production and possibly shift from petroleum-based to agro-based materials. Agro based materials such as green composites derived from natural resources provide better end of life performance in term biodegradability and recyclability as compared to synthetic composites and other conventional engineering materials. Furthermore, green composites also provide advantages in term of low raw materials cost for vehicle production as they are renewable resources with high availability (Mansor et al. 2014a, b). Pecas et al. (2018) listed a very extensive list of existing green composites used in vehicle interior application such as door panels, panels and other trim components. Green composites are also reported to be used as fillers in automotive friction components (brake and clutch pads) such as areca sheath fibre (Krishnan et al. 2019), banana fibres (Zhen-Yu et al. 2019) and kenaf fibres (Abdollah et al. 2015).

However, despite the advantages, the use of green composites from natural resources are still dominated for low load bearing applications due to the relatively low structural strength of the composites as compared to synthetic composites and metals. Nevertheless, steady progress has been reported by researchers to venture into medium load bearing application using green composites. Mastura et al. (2017) have developed a conceptual design of automotive anti-roll bar using hybrid sugar palm/glass fibre composites while Ishak et al. (2018) proposed a new design of automotive car front hood using kenaf fibre-metal-laminates (FML). Furthermore, Mansor et al. (2014b) developed a new conceptual design of automotive parking brake lever using hybrid kenaf/glass reinforced polypropylene composites and while Shahruzaman et al. (2019) proposed a new concept of vehicle side door impact beam using kenaf reinforced thermoplastic composites. In addition, Mansor et al. (2015) also proposed a new design of automotive rear spoiler using kenaf reinforced thermoplastic composites, utilizing sandwich construction solution to gain higher product rigidity. The use of innovative design approach such as Theory of Inventive Problem Solving (TRIZ), biomimetics and multicriteria design making tools (such as Analytic Hierarchy Process (AHP) and Vlse Kriterijumska Optimizacija Kompromisno Resenje (VIKOR)) as demonstrated by the aforementioned researchers are spearheading new solutions for green composites to be used in higher load bearing applications.

Green composites are also reported to be applied for new application such as aerospace and military industries, particularly due to their lightweight, impact resistance and vibration damping properties. Mansor et al. (2019) summarized the recent application of green composites in the aerospace industry such as for the development of aircraft radome, aircraft interior cabin component and aircraft honeycomb structure. Furthermore, Strohrmann et al. (2019) also reported the use of hybrid flax/carbon fibre polymer composites to develop lightweight helicopter cockpit door component. On the other hand, several researchers have also reported the use of green composites in the military industry. Kumar et al. (2019) developed armour component using conch seashells/chopped banana fibres/aluminium layer reinforced epoxy composites. The hybrid green composites were later subjected to ballistic test with the short hand gun, and results obtained showed that composite successfully fit for ballistic protection application. Braga et al. (2017) constructed lightweight and efficient Multilayered Armor Systems (MAS) component using laminate shape. The MAS laminate consists of three layers, whereby the front layer was made from ceramic, followed by sisal reinforced polyester composite for the second layer, and ductile metal for the third layer. Results from ballistic tests performed using class III 7.62x51 mm ammunition showed that 30 vol.% sisal reinforced polyester composite and the conventional aramid laminates were equally efficient in terms of MAS second layer due to similar capacity of the different composites to retain the fragments generated by the interaction of the projectile with the front ceramic. Meanwhile, Yahaya et al. (2016) developed a new military vehicle spall liner component using hybrid kenaf/aramid reinforced epoxy composites. The hybrid composites were produced in laminate form using woven kenaf mat from unidirectional kenaf yarn of 800 tex at 0°/90° ply orientation.

7.7 Mechanical Properties of Green Composites Materials

Mechanical properties of the final material depend on many different parameters. The main parameters are the fibre and matrix material properties and the compatibility of matrix and the fibre bundle. Many investigations have been carried out on the potential of natural fibres as reinforcement for composites, and in several cases, the results have shown that natural fibre composites reached a good stiffness, but their final strength was not improved (Oksman et al. 2002; Mathew et al. 2005). In addition, mechanical properties were also useful in the identification and classification of materials for different applications. The considerable properties of mechanical tests are tensile strength, modulus, impact resistance, compression, hardness, and toughness. These properties also depend on the orientation of the reinforcements and atmospheric conditions.

Starch-based plastic mixtures possess poor mechanical properties such as low tensile strength, stiffness, low elongation at break, low humidity stability and release small amounts of plasticizing molecules from a starch matrix. Modification of starch, with the use of compatibilizer, reinforcement, and improvement of process conditions, are likely to make starch as a practical plastic substitution material (Zhang et al. 2007).

Elongation, thermal stability, and water resistance of PU/PDSP films increase with the addition of PU (Liu et al. 2008). Lu et al. (2005) developed PU from rapeseed oil-based polyols, and then used it to modify glycerol plasticized starch (PS) to overcome the disadvantages of starch, namely poor mechanical properties and water sensitivity. The results exhibited that plasticized glycerol starch could be combined with rapeseed oil-based PU at PU content below 20% and phase separation ascended when PU content increased. Incremental of PU into the starch matrix also intensify film resistance to water (Lu et al. 2005).

Kumar and Siddaramaiah (2005) studied the effect of coating bamboo fibres with Polyurethane (PU) and Polyurethane/Polystyrene Interpenetrating Network (PU/PSIPN) on the tensile property of the composites. Both the untreated / alkali treated bamboo fibres were coated with polyethylene glycol based PU and its semi interpenetrating network (SIPN) with PS. It was found that the tensile strength of bamboo has increased after coating with PU and PU/PS system. PU/PS coating on alkali treated bamboo fibres have shown a rise (74%) in the tensile load at break than PU (11%) coating on alkali treated fibre. Lee and Ohkita (2004) have fabricated biocomposites of poly (lactic acid) (PLA)/bamboo fibre (BF) and poly (butylene succinate) (PBS)/bamboo fibre (BF). They have investigated the effect of lysine based diisocynate (LDI) as coupling agent on properties of bio composites. They have reported that tensile properties and water resistance were improved by the addition of LDI. These improvements were due to enhanced interfacial adhesion between polymer matrix and bamboo fibre.

Chen et al. (1998) have fabricated bamboo reinforced polypropylene (PP) composites. Polypropylene was modified with maleic anhydride. Modified polypropylene was prepared by solution grafting method. They have investigated the effect of

bamboo fraction, MAPP content and bamboo sizes on mechanical properties of unmodified and modified Bamboo Fibre/PP composite. Tensile modulus of modified composite increased with bamboo content up to 65 wt%, but modulus of unmodified composite was not affected by changing bamboo fraction. Tensile strength of modified composite has increased about 50 wt% bamboo fibre, but for unmodified composite, tensile strength has decreased slightly. This effect was also studied by Tran et al. (2011) using a compatibilizer of maleic anhydride polypropylene (MAPP), it enhances the flexural strength compared to pure PP, and this resultant material becomes stronger and less flexible. A similar effect was observed by Lee et al. (2009) while adding 3-glycidoxypropyltrimethoxysilane (GPS) as a coupling agent in the PLA/kenaf fibre biocomposites. The flexural strength and flexural modulus of the composites increased with increasing the content of GPS, while compared with pure PLA. This coupling agent significantly increases the interfacial strength between resin and fibres.

Thwe and Liao (2002, 2003) have fabricated the bamboo reinforced polypropylene (BFRP) and bamboo-glass reinforced Polypropylene (BGRP) composites. They have studied the effect of fibre content, fibre length, bamboo to glass ratio, coupling agent (maleated polypropylene) on tensile and flexural properties of these composites. It was reported that moisture absorption of BFRP during aging can be reduced by replacing bamboo fibre with glass fibre and by using Compatilizers. Mechanical properties of BFRP and BGRP have degraded after aging in water. Rozman et al. (2004) studied the effect of isocyanate (MDI and toluene diisocyanate-TDI) treatment on the mechanical properties of EFB composites with polyethylene (PE) as the matrix. The composite with fibre treated with MDI showed higher tensile and flexural strengths than those treated with TDI. It is well known that to achieve optimum mechanical strength and stiffness in a composite, the reinforcement fibres should be continuous and aligned in the direction of the applied load. The same is true for natural fibres.

Moreover, there are also studies which reported on the use of physical treatments such as plasma and corona discharge to improve the functional properties of natural fibres. Plasma treatment in oxygen can roughen the surface. Low-temperature plasma treatments improve the surface of natural fibres by causing chemical implantation, etching, polymerisation, free radical formation and crystallisation (Mohanty et al. 2005). For example, the wettability of wood fibres has been found to improve significantly with an increased level of corona treatment (Wallace 2005). Also, there are some methods that combine the physical and chemical methods and called physico-chemical methods such as hydrothermal and steam explosion (Jawaid and Khalil 2011; LI et al. 2007). Badri et al. (2001) prepared medium-density fibreboard (MDF) with palm-based PU as the binder. Various sizes of refined EFB ranging from 53 ∝m to 500 ∝m and fixed blending ratio of PU to EFB at 20:80 were used. The smallest size of EFB fibres gave higher impact strength and better water resistivity due to the lesser voidage between the EFB particles.

Apart from physical treatment, alkali treatment is also a common method to clean and modify the surface of natural fibres to promote enhanced fibre-polymer adhesion. Mercerization is a traditional alkali treatment based on sodium hydroxide

(NaOH, caustic soda), which improves the take up of dye in textile processing. Several studies have found that alkali treatments can improve the properties of natural fibres and the interfacial adhesion to polymers (Liu et al. 2004; Bachtiar et al. 2008). In addition, acetylation is also a treatment of particular interest in natural fibres. In this treatment, acetic anhydrides substitute the cell wall hydroxyl groups of a natural fibre with acetyl groups, rendering the surface more hydrophobic and thus less susceptible to moisture uptake and biological attack and more compatible with polymer matrices (Tserki et al. 2005). Isocyanates can be used as coupling agents to improve the bonding of natural fibres to polymers. For example, the strength and stiffness of wood-polypropylene (PP) composites can be increased by treating the fibres with polymethylene-polyphenyl-isocyanate (Wallace 2005). For example, lysine diisocyanate has been successfully used to improve the mechanical properties and water resistance of bamboo fibre-polylactide composites through enhanced fibre-matrix interfacial adhesion (Lee and Wang 2006).

There are a few epoxy resins on the market which contain a proportion of bio-based material. It is also possible to use bio-based products to improve the performance of synthetic resins. For example, the impact strength of petroleum-based epoxies can be significantly improved by blending with epoxidised vegetable oils (Mohanty et al. 2005). However, if natural fibres were to be used in combination with plastic polymers, the resulting composites would have low tensile strength values and poor interfacial adhesion because of incompatibility between the kenaf fibres and plastics (Yussuf et al. 2010; Nishino et al. 2003; Akil et al. 2011; Alayudeen et al. 2015). In order to compensate for these disadvantages, various chemical treatments have been studied. Among the chemical modifications, acetylation is one of the most commonly used methods, where the –OH groups that are responsible for hydrophilic properties of lignocellulose are modified by hydrophobic acetyl groups (Hu et al. 2011). For example, acetylation can be used to control hygroscopic properties, dimensional stability, durability, and the physical properties of plant-based materials and composites. This chemical modification strategy is regarded as an inexpensive, simple method for lowering the surface energy characteristics of natural fibres to make them more compatible with common polymers (Ismail et al. 2011; Ifuku et al. 2010). If kenaf fibres were made less hydrophilic, their compatibility with PLA would be improved, leading to an enhancement in adhesion, and thus also the strength of the resulting composites.

The flexural and tensile strengths of the kenaf–PLA composites were enhanced when the introduced acetyl constituted over 25% of the mass of fibres. With respect to the lower acetylation levels that were examined in this study, there was no improvement in the mechanical properties as compared with the untreated kenaf–PLA composites. The detrimental surface smoothening of kenaf upon brief acetylation, as evidenced by morphology studies, was a possible explanation for such mechanical performance (Chung et al. 2018).

On the other hand, modifying the composites architecture through alignment of fibre orientation could also alter the mechanical properties of the green composite produced from natural resources. Aligned natural fibres can be combined with thermoplastic polymers in a number of ways. Woven or stitched fabrics can be

interleaved with thermoplastic sheets or films, often referred to as film stacking, then heated and consolidated in a press or by vacuum bagging (Arnold et al. 2007). Natural fibre-thermoplastic pultrusion is also possible (Van and Kiekens 2001), although the natural fibre materials must have sufficient strength to resist breaking during the process. Thermoplastic polymers are highly viscous so do not flow readily and care must be taken during processing, as with all thermoplastic composites, to ensure good impregnation and consolidation. By using aligned natural fibres, the mechanical properties of these biocomposites are significantly higher than non-woven mat composites (Hoydonckx et al. 2009). Compatibilizers are often used to improve fibre-matrix bonding, such as maleicanhydride for PP. In particular, the development of aligned, natural fibre fabrics suitable for composite reinforcement will provide significantly enhanced properties and will open the door to a range of semi-structural applications. Compatibilization is necessary to obtain a composite with tailored mechanical properties and good efficiency in the transferring of the stress from the matrix to the fibres.

7.8 Manufacturing Process of Green Composite Materials

A polymer is a material made by macromolecule, built of many repeated monomer subunits, which have a significant and broad role in human daily life. Either can be synthetic or natural polymer, the synthetic polymers are petroleum-based material which falls into four major divisions, namely thermosets, thermoplastic, elastomer, and synthetic fibre. Meanwhile, the natural fibre can be found from plant, wood, or even from animal protein. The monomer can chemically react with another monomer with the same or different molecules that occurred naturally is called ~~as~~ natural polymer, where the derived or man-made polymers are known as a synthetic polymer. The broad application of polymer nowadays in human daily life including for medication, nutrition, communication, transportation, irrigation, container, clothing, recording history, buildings, highways, and so on, made the polymer industry the rapidly developed and wider than the copper, steel, aluminium and some other industries (Namazi 2017).

Although the polymer has played a significant role in our daily life, there is no perfect material that currently found. As mentioned earlier, the polymer is created by the chemical reaction of a monomer with another monomer. This can be supported by applying the heat during the chemical reaction, so that the polymer chains can break up and combined with other polymer chains. However, too much heat could cause thermal degradation which later reduces the mechanical properties of the desired material. During production, heat can be intentionally applied (by the heat of mould, or extruder) or unintentionally applied (speed or revolution of extruder or mixer). The thermal degradation could occur when the strained or entangled sections of the polymer chains to be free. The rearrangement of these freed macromolecules segments were changed from the previous arrangement polymer chains, thus affecting the crystallinity of the material. The variation of ordered

molecular chains or known as the degree of crystallinity is later affecting the mechanical properties of the polymer material (Costa et al. 2007; Madi 2013). In conclusion, the temperature selected for the production process is vital so that we can minimise the thermal degradation.

Various manufacturing methods can be used for green composite production, either the injection moulding, hand layup, or rapid prototyping. The selection of manufacturing process is depending on the type of polymer used. Injection moulding is one of the manufacturing processes that involved with the using of polymer. According to Todd et al. (1994), the injection moulding commonly used for thermoplastic material, where the molten polymer is injected into the mould cavity at a certain temperature and speed. As can be observed in Fig. 7.6 below, the material in granule shape is fed into the barrel that containing the heater and forced out into the mould cavity by screw plunger. The molten polymer is left cooled inside the cavity that has been taken out. In green composite, the using injection moulding is not a new thing. Various researchers have reported the production of green composite by using this method. Montanes et al. (2019) studied the potential to use conventional injection moulding method for the green composite made by a biobased high density poly(ethylene) matrix and a high lignocellulosic filler from industrial thyme wastes. The modelling works were done with parallel with experimental validation. By using 100:0, 90:10, 80:20, 70:30, 60:40, and 50:50 HDPE:thyme wt.% ratio, the best formulation was found up to 20 wt.%, as can be found in Fig. 7.7. The process temperature and shear speed are the important parameters in this process. The higher temperature will provide lower viscosity, but it would induce thermal degradation onto the filler and the matrix. Furthermore, as the thyme fibre wt.% increases, it requires higher pressure to absolutely fill the mould cavity, which later may damage the pressure transmission. In overall, the green composites were successfully produced by using SLS method, with the optimum matrix to filler ratio not more than 20 wt.%. In addition, the simulation tools are useful in predicting and validating the rheological behaviour of high lignocellulosic content polymer systems.

In order to maintain the lower production costs at a high volume of the green composite, the hand layup method was commonly used which it requires the manual laying down the individual layers or plies of reinforcement (natural fibre). The plies can be in the form of single unidirectional or woven, which involves the

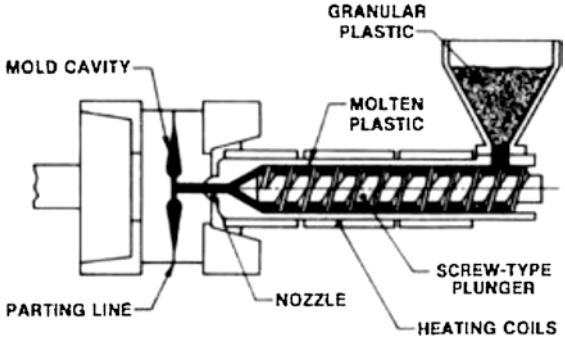

Fig. 7.6 The schematic diagram of typical injection moulding machine (Todd et al. 1994)

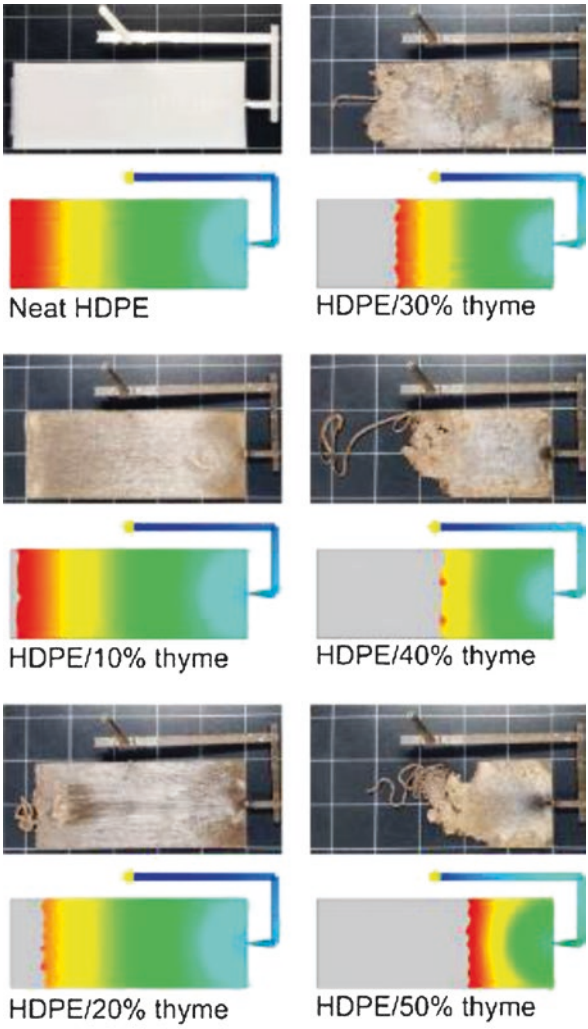

Fig. 7.7 Comparison on the injected green composite with the variation of thyme fibre ratio (wt.%) (Montanes et al. 2019)

manipulating each ply into shape by hand, and then firmly pressed with or without mould by ensuring there is no air pocket between plies (Elkington et al. 2015). Normally, thermoset polymers were chosen as the matrix as it is a liquid resin which suitable for the hand layup method. One of the modifications in hand layup method is by using two or more reinforcement plies, called as a hybrid green composite. As reported by Yahaya et al. (2015), hybridisation of the two types of reinforcement could be one of the solutions on the natural polymer limitations. Combining two types of reinforcement could obtain the full advantage of the properties of the constituents, and become an optimal, superior but economical step in improving green composites. In their research, the kenaf fibre was hybrid with Kevlar and pressed with epoxy resin. As expected, the hybridisation of kenaf fibre with Kevlar does

improved the mechanical properties (tensile, flexural, and impact) of the green composites. In addition, the hybrid with the Kevlar as the outer part (Kevlar/kenaf/Kevlar) also produced better mechanical properties compared to (kenaf/Kevlar/kenaf). The layering sequences are portrayed in Fig. 7.8 below.

The rapid prototyping or so-called 3D printing is one of advanced manufacturing which has been available in late 1980s by using layered method and using laser light for fusing the metal powder in solid prototypes (Bagaria et al. 2011). In addition, the rapid prototyping can be used to produce a product that meeting the requirements of the shape and precision, shortening the design and evaluation cycle of a new product, and providing the actual and observable look of the model (Jiang et al. 2010). The application of rapid prototyping can be seen in automotive, aerospace, electronics, medical, and green composite. Although the usage of rapid prototyping is a fast production, there are required studies towards the effectiveness ~~on~~ of using rapid prototyping for green composite production. This is because the natural polymers are vulnerable to oxidative degradation when exposed to the ultraviolet radiation and they were which later may lead to degradation of the mechanical properties. Due to that matter, Jiang et al. (2010) reported the production of green composite containing aspen wood flour by using selective laser sintering (SLS) method. Based on their study, the green composite can be manufactured by using the rapid prototyping method if supported by the presence of additive and coupling agent. The fibre treatment with sodium hydroxide (NaOH) solution also proved in improving the binding between matrix and reinforcement which later may provide better surface roughness and mechanical properties (see Fig. 7.9). Figure 7.10 below shows the part that produced by using SLS method. In conclusion, the green composite can be produced either using conventional hand layup method, or via advanced rapid prototyping. The only matters are the production cost, the production volume, and type of materials used for the products.

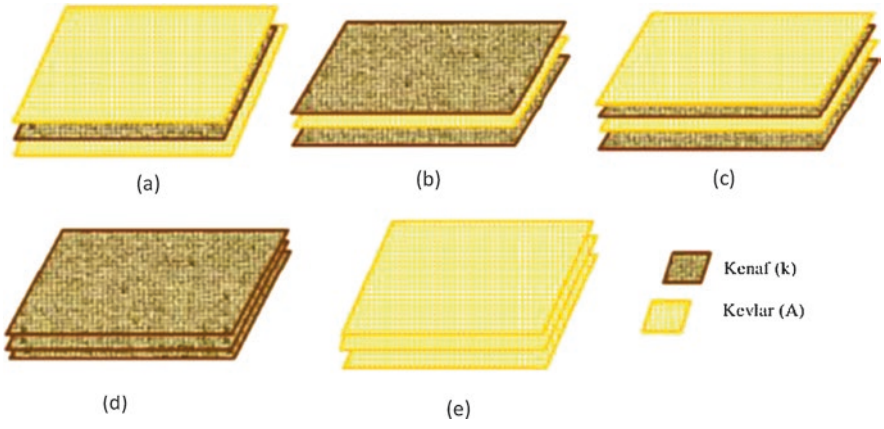

Fig. 7.8 The illustration of the layering sequences of kenaf fibre and Kevlar (Yahaya et al. 2015)

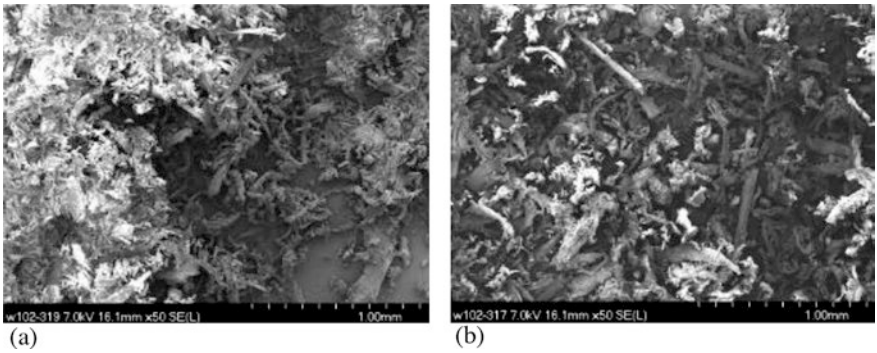

Fig. 7.9 SEM images presenting the comparison of; (**a**) untreated and (**b**) treated aspen wood flour (Jiang et al. 2010)

Fig. 7.10 The part produced by SLS method (Jiang et al. 2010)

7.9 Conclusion

Green composites in overall have shown a rapid growth both in term of research and development, as well as industrial application. At the present moment, its application is focused on low load bearing application, due to its lower mechanical properties as compared to synthetic composites and metals. However, as explained in the previous section within this chapter, many efforts have been carried out to improve the properties of the green composites.

With regards to that, many other opportunities, especially in research, are available to be pursued. Development on the new class of single fibre/matrix and hybrid composites with better material properties can be carried out by increasing the works to discover a new type of natural fibres from unique plant species and polymer matrices, especially biopolymer matrix. The development of more alternative materials could support the goal of creating many fully biodegradable green composites, which will be very beneficial in term of environmental friendly aspect. This will also help to reduce the current problem in managing plastic waste issue around the world.

Furthermore, research opportunity is also vastly opened in enhancing the material properties of natural-based green composites by utilizing the advantages of advanced nanomaterials as the filler to formulate the material. It is shown that various type of nanomaterials significantly improved the performance of the green composites. Further works can be carried out to characterize the nanomaterials effect to as many as possible green composites, as well as to fully understand how the enhancement mechanism is obtained.

It is also briefly described in the previous section how the use of innovative product development and processing method could address the material property limitation in producing an end product with higher load bearing capability. This is also an exciting area to be explored by researchers as well as composite practitioners. Clever modification of the geometrical parameters of product could reduce the maximum stress generated when a load is applied, hence enabling the use of green composites as raw material to construct it without compromising the required structural performance. In addition, the use of advanced rapid manufacturing process such as additive manufacturing should also be incorporated more aggressively to develop a product from green composites. Among the works which could be carried out is enabling the use of fibres with higher aspect ratio, improving the fibre-matrix adhesion properties, as well as creating new filament material using various type of natural fibres and matrices.

In conclusion, the future is bright for green composites, especially made from natural resources to expand its presence in more demanding applications. It is expected based on the accumulating attention and positive progress made so far, green composites from natural resources will take over the domination of synthetic composites as a commercially viable solution in many applications.

Acknowledgement The authors wish to thank all members from Faculty of Mechanical Engineering (FKM), Universiti Teknikal Malaysia Melaka and Faculty of Mechanical and Manufacturing Engineering (FTKMP), Universiti Teknikal Malaysia Melaka for the warm and continuous support provided throughout the completion of this publication.

References

Abdollah MFB, Shuhimi FF, Ismail N, Amiruddin H, Umehara N (2015) Selection and verification of kenaf fibres as an alternative friction material using weighted decision matrix method. Mater Des 67:577–582

Aji IS, Sapuan SM, Zainudin ES, Abdan K (2009) Kenaf fibres as reinforcement for polymeric composites: a review. Int J Mech Mater Des 4(3):239–248

Akil H, Omar MF, Mazuki AAM, Safiee SZAM, Ishak ZM, Bakar AA (2011) Kenaf fiber reinforced composites: a review. Mater Des 32(8–9):4107–4121

Alavudeen A, Rajini N, Karthikeyan S, Thiruchitrambalam M, Venkateshwaren N (2015) Mechanical properties of banana/kenaf fiber-reinforced hybrid polyester composites: effect of woven fabric and random orientation. Mater Des (1980–2015) 66:246–257

Arnold E, Weager B, Bishop G (2007) Development of high performance bio-derived composite materials, in Proceedings of Composites Innovation, Barcelona, Spain, 4–5 October 2007.

Arulmurugan M, Prabu K, Rajamurugan G, Selvakumar AS (2019) Viscoelastic behavior of aloevera/hemp/flax sandwich laminate composite reinforced with BaSO4: dynamic mechanical analysis. J Ind Text. 1528083719852312

Asim M, Jawaid M, Paridah MT, Saba N, Nasir M, Shahroze RM (2019) Dynamic and thermo-mechanical properties of hybridized Kenaf/PALF reinforced phenolic composites. Polym Compos

Bachtiar D, Sapuan SM, Hamdan MM (2008) The effect of alkaline treatment on tensile properties of sugar palm fibre reinforced epoxy composites. Mater Des 29(7):1285–1290

Badri KH, Ahmad SH, Zakaria S (2001) Production of a high-functionality RBD palm kernel oil-based polyester polyol. J Appl Polym Sci 81(2):384–389

Bagaria V, Rasalkar D, Bagaria SJ, Ilyas J (2011) Medical applications of rapid prototyping-A new horizon. Advanced Applications of Rapid Prototyping Technology in Modern Engineering, 1–21

Braga FDO, Bolzan LT, Ramos FJHTV, Monteiro SN, Lima ÉP Jr, Silva LCD (2017) Ballistic efficiency of multilayered armor systems with sisal fiber polyester composites. Mater Res 20:767–774

Cavalcanti DKK, Banea MD, Neto JSS, Lima RAA, da Silva LFM, Carbas RJC (2019) Mechanical characterization of intralaminar natural fibre-reinforced hybrid composites. Compos Part B 175:107149

Chang Y, Li JJ, Sun TS, Zhou XD (2019) Grafting starch nanocrystals onto the surface of sisal fibers and consequent improvement of interfacial adhesion in sisal reinforced starch composite. J Appl Polym Sci 136(11):47202

Chee SS, Jawaid M, Sultan MTH, Alothman OY, Abdullah LC (2019) Thermomechanical and dynamic mechanical properties of bamboo/woven kenaf mat reinforced epoxy hybrid composites. Compos Part B 163:165–174

Chen X, Guo Q, Mi Y (1998) Bamboo fiber-reinforced polypropylene composites: a study of the mechanical properties. J Appl Polym Sci 69(10):1891–1899

Chen Z, Kuang T, Yang Z, Ren X (2016) Effect of Nanoclay on natural Fiber/Polymer composites. In: Jawaid M, Qaiss AK, Bouhfid R (eds) Nanoclay reinforced polymer composites. Springer, Singapore, pp 175–207

Chung TJ, Park JW, Lee HJ, Kwon HJ, Kim HJ, Lee YK, Tai Yin Tze W (2018) The improvement of mechanical properties, thermal stability, and water absorption resistance of an eco-friendly PLA/kenaf biocomposite using acetylation. Appl Sci 8(3):376

Costa HM, Ramos VD, de Oliveira MG (2007) Degradation of polypropylene (PP) during multiple extrusions: thermal analysis, mechanical properties and analysis of variance. Polym Test 26(5):676–684

Cristaldi G, Latteri A, Recca G, Cicala G (2010) Composites based on natural fibre fabrics. In: Dubrovski P (ed) Woven fabric engineering. InTech, London, pp 317–342

Dang CY, Shen XJ, Nie HJ, Yang S, Shen JX, Yang XH, Fu SY (2019) Enhanced interlaminar shear strength of ramie fiber/polypropylene composites by optimal combination of graphene oxide size and content. Compos Part B 168:488–495

Davis AM, Hanzly LE, DeButts BL, Barone JR (2019) Characterization of dimensional stability in flax fiber reinforced polypropylene composites. Polym Compos 40(1):132–140

Dorger S (2019) These Countries Produce the Most Plastic Waste. In: TheStreet. retrieved online from https://www.thestreet.com/world/countries-most-plastic-waste-14878534. on 23 July 2019

Elkington M, Bloom D, Ward C, Chatzimichali A, Potter K (2015) Hand layup: understanding the manual process. Adv Manuf Polymer Compos Sci 1(3):138–151

Espinosa-Valdemar RM, Turpin-Marion S, Delfín-Alcalá I, Vázquez-Morillas A (2011) Disposable diapers biodegradation by the fungus Pleurotus ostreatus. Waste Manag 31(8):1683–1688

Faruk O, Bledzki AK, Fink HP, Sain M (2014) Progress report on natural fiber reinforced composites. Macromol Mater Eng 299(1):9–26

Gurunathan T, Mohanty S, Nayak SK (2015) A review of the recent developments in biocomposites based on natural fibres and their application perspectives. Compos A: Appl Sci Manuf 77:1–25
Ho MP, Wang H, Lee JH, Ho CK, Lau KT, Leng J, Hui D (2012) Critical factors on manufacturing processes of natural fibre composites. Compos Part B 43(8):3549–3562
Holbery J, Houston D (2006) Natural-fiber-reinforced polymer composites in automotive applications. J Miner Met Mater Soc (JOM) 58(11):80–86
Hoydonckx HE, Switsers G, Weager BM, Arnold EL (2009) A novel prepreg material combining natural fibres with a furan resin, JEC Magazine, Issue 46, January/February 2009.
Hu W, Chen S, Xu Q, Wang H (2011) Solvent-free acetylation of bacterial cellulose under moderate conditions. Carbohydr Polym 83(4):1575–1581
Ifuku S, Morooka S, Morimoto M, Saimoto H (2010) Acetylation of chitin nanofibers and their transparent nanocomposite films. Biomacromolecules 11(5):1326–1330
Ishak MR, Sapuan SM, Leman Z, Rahman MZA, Anwar UMK, Siregar JP (2013) Sugar palm (Arenga pinnata): its fibres, polymers and composites. Carbohydr Polym 91(2):699–710
Ishak NM, Sivakumar D, Mansor MR (2018) The application of TRIZ on natural fibre metal laminate to reduce the weight of the car front hood. J Braz Soc Mech Sci Eng 40(2):105
Ismail H, Abdullah AH, Bakar AA (2011) Influence of acetylation on the tensile properties, water absorption, and thermal stability of (high-density polyethylene)/(soya powder)/(kenaf core) composites. J Vinyl Addit Tech 17(2):132–137
Jawaid MHPS, Khalil HA (2011) Cellulosic/synthetic fibre reinforced polymer hybrid composites: a review. Carbohydr Polym 86(1):1–18
Jiang KY, Guo YL, Zeng WL, Xin ZS (2010) The preparation of WPC for SLS rapid prototyping and manufacturing. In: Advanced materials research, vol 113. Trans Tech Publications, pp 1722–1725
Jothibasu S, Mohanamurugan S, Vijay R, Lenin Singaravelu D, Vinod A, Sanjay MR (2018) Investigation on the mechanical behavior of areca sheath fibers/jute fibers/glass fabrics reinforced hybrid composite for light weight applications. J Ind Text. https://doi.org/10.1177/1528083718804207
Jumaidin R, Sapuan SM, Jawaid M, Ishak MR, Sahari J (2017) Thermal, mechanical, and physical properties of seaweed/sugar palm fibre reinforced thermoplastic sugar palm starch/agar hybrid composites. Int J Biol Macromol 97:606–615
Khan T, Sultan MTH, Shah AUM, Ariffin AH, Jawaid M (2019) The effects of stacking sequence on the tensile and flexural properties of Kenaf/Jute fibre hybrid composites. J Nat Fibers:1–12
Krishnan GS, Jayakumari LS, Babu LG, Suresh G (2019) Investigation on the physical, mechanical and tribological properties of areca sheath fibers for brake pad applications. Mater Res Express 6(8):085109
Kumar H, Siddaramaiah (2005) Study of chemical and tensile properties of PU and PU/PS coated bamboo fibers. Polym-Plast Technol Eng 44(7):1369–1377
Kumar GA, Kumar MR, Babu AR, Kumar RR, Kumar GS, Parameswaran P (2019a) Experimental analysis on ballistic performance of newly developed sandwich hybrid natural composites. Materials Today: Proceedings
Kumar S, Patel VK, Mer KKS, Gangil B, Singh T, Fekete G (2019b) Himalayan natural fiber-reinforced epoxy composites: effect of Grewia optiva/Bauhinia Vahlii fibers on physico-mechanical and dry sliding wear behavior. J Nat Fibers:1–11
Lee SH, Ohkita T (2004) Bamboo fiber (BF)-filled poly(butylenes Succinate) biocomposites - effect of BF-e-MA on the properties and crystallization kinetics. Holzforschung 58:537–543
Lee SH, Wang S (2006) Biodegradable polymers/bamboo fiber biocomposite with bio-based coupling agent. Compos A: Appl Sci Manuf 37(1):80–91
Lee BH, Kim HS, Lee S, Kim HJ, Dorgan JR (2009) Bio-composites of kenaf fibers in polylactide: role of improved interfacial adhesion in the carding process. Compos Sci Technol 69(15–16):2573–2579
Li X, Tabil LG, Panigrahi S (2007) Chemical treatments of natural fiber for use in natural fiber-reinforced composites: a review. J Polym Environ 15(1):25–33

Liu W, Mohanty AK, Askeland P, Drzal LT, Misra M (2004) Influence of fiber surface treatment on properties of Indian grass fiber reinforced soy protein based biocomposites. Polymer 45(22):7589–7596

Liu D, Tian H, Zhang L, Chang PR (2008) Structure and properties of blend films prepared from castor oil-based polyurethane/soy protein derivative. Ind Eng Chem Res 47(23):9330–9336

Lu Y, Tighzert L, Berzin F, Rondot S (2005) Innovative plasticized starch films modified with waterborne polyurethane from renewable resources. Carbohydr Polym 61(2):174–182

Madi NK (2013) Thermal and mechanical properties of injection molded recycled high density polyethylene blends with virgin isotactic polypropylene. Mater Des 46:435–441

Malkapuram R, Kumar V, Negi YS (2009) Recent development in natural fiber reinforced polypropylene composites. J Reinf Plast Compos 28(10):1169–1189

Mansor MR, Sapuan SM, Hambali A, Zainudin ES, Nuraini AA (2014a) Materials selection of hybrid bio-composites thermoset matrix for automotive bumper beam application using TOPSIS method. Adv Environ Biol:3138–3143

Mansor MR, Sapuan SM, Zainudin ES, Nuraini AA, Hambali A (2014b) Conceptual design of kenaf fiber polymer composite automotive parking brake lever using integrated TRIZ-morphological chart-analytic hierarchy process method. Mater Des 54:473–482

Mansor MR, Sapuan SM, Hambali A, Zainudin ES, Nuraini AA (2015) Conceptual design of kenaf polymer composites automotive spoiler using TRIZ and morphology chart methods. Appl Mech Mater 761:63–67

Mansor MR, Nurfaizey AH, Tamaldin N, Nordin MNA (2019) Natural fiber polymer composites: utilization in aerospace engineering. In: Verma D, Fortunati E, Jain S, Zhang X (eds) Biomass, biopolymer-based materials, and bioenergy. Woodhead Publishing, pp 203–224

Market Research Report (2018) Natural Fiber Composites (NFC) Market Size, Share & Trends Analysis Report by Raw Material, By Matrix, By Technology, By Application, And Segment Forecasts, 2018–2024, retrieved online from https://www.grandviewresearch.com/industry-analysis/natural-fiber-composites-market on 21 August 2019.

Mastura MT, Sapuan SM, Mansor MR, Nuraini AA (2017) Conceptual design of a natural fibre-reinforced composite automotive anti-roll bar using a hybrid approach. Int J Adv Manuf Technol 91(5–8):2031–2048

Mathew AP, Oksman K, Sain M (2005) Mechanical properties of biodegradable composites from poly lactic acid (PLA) and microcrystalline cellulose (MCC). J Appl Polym Sci 97(5):2014–2025

Mohamad Hamdan MH, Siregar JP, Thomas S, Jacob MJ, Jaafar J, Tezara C (2019) Mechanical performance of hybrid woven jute–roselle-reinforced polyester composites. Polym Polym Compos:0967391119847552

Mohan TP, Kanny K (2019) Compressive characteristics of unmodified and nanoclay treated banana fiber reinforced epoxy composite cylinders. Compos Part B 169:118–125

Mohanty AK, Misra M, Drzal LT (eds) (2005) Natural fibers, biopolymers, and biocomposites. CRC Press, Boca Raton

Montanes N, Quiles-Carrillo L, Ferrandiz S, Fenollar O, Boronat T (2019) Effects of lignocellulosic fillers from waste thyme on melt flow behavior and processability of wood plastic composites (WPC) with biobased poly (ethylene) by injection molding. J Polym Environ 27(4):747–756

Mukhtar I, Leman Z, Ishak MR, Zainudin ES (2018) Sugar palm fiber–reinforced polymer hybrid composites: an overview. In: Sapuan SM, Sahari J, Ishak MR, Sanyang ML (eds) Sugar palm biofibers, biopolymers, and biocomposites. CRC Press, Boca Raton, pp 145–164

Namazi H (2017) Polymers in our daily life. Bioimpacts 7:73–74

Navaneethakrishnan G, Karthikeyan T, Saravanan S, Selvam V, Parkunam N, Sathishkumar G, Jayakrishnan S (2019) Structural analysis of natural fiber reinforced polymer matrix composite. Materials today: proceedings.

Naveen J, Jawaid M, Zainudin ES, Thariq Hameed Sultan M, Yahaya R (2019) Improved mechanical and moisture-resistant properties of woven hybrid epoxy composites by graphene nanoplatelets (GNP). Materials 12(8):1249

Nimanpure S, Hashmi SAR, Kumar R, Bhargaw HN, Kumar R, Nair P, Naik A (2019) Mechanical, electrical, and thermal analysis of sisal fibril/kenaf fiber hybrid polyester composites. Polym Compos 40(2):664–676

Nishino T, Hirao K, Kotera M, Nakamae K, Inagaki H (2003) Kenaf reinforced biodegradable composite. Compos Sci Technol 63(9):1281–1286

Nor AFM, Sultan MTH, Jawaid M, Azmi AMR, Shah AUM (2019) Analysing impact properties of CNT filled bamboo/glass hybrid nanocomposites through drop-weight impact testing, UWPI and compression-after-impact behaviour. Compos Part B 168:166–174

Oksman K, Wallström L, Berglund LA, Filho RDT (2002) Morphology and mechanical properties of unidirectional sisal–epoxy composites. J Appl Polym Sci 84(13):2358–2365

Peças P, Carvalho H, Salman H, Leite M (2018) Natural fibre composites and their applications: a review. J Compos Sci Technol 2(4):66

Pickering KL, Efendy MA, Le TM (2016) A review of recent developments in natural fibre composites and their mechanical performance. Compos A: Appl Sci Manuf 83:98–112

Premnath AA (2019) Impact of surface treatment on the mechanical properties of sisal and jute reinforced with epoxy resin natural fiber hybrid composites. J Nat Fibers 16(5):718–728

Radzi AM, Sapuan SM, Jawaid M, Mansor MR (2019a) Water absorption, thickness swelling and thermal properties of roselle/sugar palm fibre reinforced thermoplastic polyurethane hybrid composites. J Mater Res Technol

Radzi AM, Sapuan SM, Jawaid M, Mansor MR (2019b) Effect of alkaline treatment on mechanical, physical and thermal properties of Roselle/sugar palm Fiber reinforced thermoplastic polyurethane hybrid composites. Fibers Polym 20(4):847–855

Rahman MR, Hamdan S, Jayamani E, Kakar A, Bakri MKB, Yusof FABM (2019) Tert-butyl catechol/alkaline-treated kenaf/jute polyethylene hybrid composites: impact on physico-mechanical, thermal and morphological properties. Polym Bull 76(2):763–784

Rajesh G, Rao MR, Vijay K, Gopinath S (2019) Evaluation of tensile properties of Nanoclay-Filled Madar Fiber-Reinforced polyester hybrid composites. In: Hiremath SS, Shanmugam NS, Bapu BRR (eds) Advances in manufacturing technology. Springer, Singapore, pp 1–8

Ritchie H, Roser M (2018) Plastic Pollution. In: Our World Data. Retrieved online from https://ourworldindata.org/plastic-pollution on 23 July 2019

Rozman HD, Ahmadhilmi KR, Abubakar A (2004) Polyurethane (PU)—oil palm empty fruit bunch (EFB) composites: the effect of EFBG reinforcement in mat form and isocyanate treatment on the mechanical properties. Polym Test 23(5):559–565

Sahari J, Sapuan SM (2011) Natural fibre reinforced biodegradable polymer composites. Rev Adv Mater Sci 30(2):166–174

Sanjay MR, Arpitha GR, Naik LL, Gopalakrishna K, Yogesha B (2016) Applications of natural fibers and its composites: an overview. Nat Resour 7(03):108

Sanjay MR, Arpitha GR, Senthamaraikannan P, Kathiresan M, Saibalaji MA, Yogesha B (2019) The hybrid effect of Jute/Kenaf/E-glass woven fabric epoxy composites for medium load applications: impact, inter-laminar strength, and failure surface characterization. J Nat Fibers 16(4):600–612

Sarker F, Potluri P, Afroj S, Koncherry V, Novoselov KS, Karim N (2019) Ultra-high performance of nano-engineered graphene-based natural jute fiber composites. ACS Appl Mater Interfaces

Shah DU (2013) Developing plant fibre composites for structural applications by optimising composite parameters: a critical review. J Mater Sci 48(18):6083–6107

Shah DU (2014) Natural fibre composites: comprehensive Ashby-type materials selection charts. Mater Des (1980–2015) 62:21–31

Shaharuzaman MA, Sapuan SM, Mansor MR, Zuhri MYM (2019) The weighting of product design specification for a composite side-door impact beam using the analytic hierarchy process method. Int J Mater Prod Technol 59(1):63–80

Shahroze RM, Ishak MR, Salit MS, Leman Z, Asim M, Chandrasekar M (2018) Effect of organo-modified nanoclay on the mechanical properties of sugar palm fiber-reinforced polyester composites. Bioresources 13(4):7430–7444

Siakeng R, Jawaid M, Ariffin H, Sapuan SM (2019a) Mechanical, dynamic, and thermomechanical properties of coir/pineapple leaf fiber reinforced polylactic acid hybrid biocomposites. Polym Compos 40(5):2000–2011

Siakeng R, Jawaid M, Ariffin H, Sapuan SM, Asim M, Saba N (2019b) Natural fiber reinforced polylactic acid composites: a review. Polym Compos 40(2):446–463

Strohrmann K, André N, Hajek M (2019) Hybrid Natural Fiber Composites in a Helicopter Cabin Door–Mechanical Properties and Ecological Efficiency. In 75th Annual Forum of the Vertical Flight Society, Philadelphia, Indiana, USA, May 13–16, 2019.

Taufiq MJ, Mustafa Z, Mansor MR (2017) Utilisation of recycled thermoplastics sourced from rejected-unused disposable diapers as polymer blends. J Mech Eng Sci 11(4):3137–3143

Taufiq MJ, Mansor MR, Mustafa Z (2018) Characterisation of wood plastic composite manufactured from kenaf fibre reinforced recycled-unused plastic blend. Compos Struct 189:510–515

Thwe MM, Liao K (2002) Effects of environmental aging on the mechanical properties of bamboo–glass fiber reinforced polymer matrix hybrid composites. Compos A: Appl Sci Manuf 33(1):43–52

Thwe MM, Liao K (2003) Durability of bamboo-glass fiber reinforced polymer matrix hybrid composites. Compos Sci Technol 63(3–4):375–387

Todd RH, Allen DK, Alting L (1994) Injection Molding. In: Manufacturing processes reference guide. Industrial Press Inc, New York, p 240

Tran T, Lee BH, Yang HS, Chotineeranat S, Sriroth K, Kim HJ (2011) Use of starch granules melting to control the properties of bio-flour filled polypropylene and poly (butylene succinate) composites: mechanical properties. Starch-Stärke 63(10):637–648

Tserki V, Zafeiropoulos NE, Simon F, Panayiotou C (2005) A study of the effect of acetylation and propionylation surface treatments on natural fibres. Compos A: Appl Sci Manuf 36(8):1110–1118

Turku I, Kärki T, Rinne K, Puurtinen A (2017) Characterization of plastic blends made from mixed plastics waste of different sources. Waste Manag Res 35(2):200–206

Turku I, Kärki T, Puurtinen A (2018) Durability of wood plastic composites manufactured from recycled plastic. Heliyon 4(3):e00559

Van de Velde K, Kiekens P (2001) Thermoplastic pultrusion of natural fibre reinforced composites. Compos Struct 54(2–3):355–360

Wallace S (2005) Review of potential surface modifications and fibre treatments to aid compatibility of hydrophilic natural fibres with hydrophobic matrix polymers. RAPRA Report 45170

Wang H, Yang L, Guo H, Zhao Y, Zhao J (2019) Mechanical and thermodynamic properties of unidirectional flax fiber reinforced CNT modified epoxy composites. Fibers Polym 20(6):1266–1276

Worsfold P, Townshend A, Poole CF, Miró M (2019) Encyclopedia of analytical science. Elsevier

Yahaya R, Sapuan SM, Jawaid M, Leman Z, Zainudin ES (2015) Effect of layering sequence and chemical treatment on the mechanical properties of woven kenaf–aramid hybrid laminated composites. Mater Des 67:173–179

Yahaya R, Sapuan SM, Jawaid M, Leman Z, Zainudin ES (2016) Effect of fibre orientations on the mechanical properties of kenaf–aramid hybrid composites for spall-liner application. Def Technol 12(1):52–58

Yussuf AA, Massoumi I, Hassan A (2010) Comparison of polylactic acid/kenaf and polylactic acid/rise husk composites: the influence of the natural fibers on the mechanical, thermal and biodegradability properties. J Polym Environ 18(3):422–429

Zhang QX, Yu ZZ, Xie XL, Naito K, Kagawa Y (2007) Preparation and crystalline morphology of biodegradable starch/clay nanocomposites. Polymer 48(24):7193–7200

Zhang Z, Li Y, Chen C (2017) Synergic effects of cellulose nanocrystals and alkali on the mechanical properties of sisal fibers and their bonding properties with epoxy. Compos A: Appl Sci Manuf 101:480–489

Zhen-Yu W, Jie W, Feng-Hong C, Yun-Hai M, Singh T, Fekete G (2019) Influence of banana fiber on physicomechanical and tribological properties of phenolic based friction composites. Mater Res Express 6(7):075103

Zin MH, Abdan K, Norizan MN (2019) The effect of different fiber loading on flexural and thermal properties of banana/pineapple leaf (PALF)/glass hybrid composite. In: Structural health monitoring of biocomposites, fibre-reinforced composites and hybrid composites. Woodhead Publishing, pp 1–17

Chapter 8
Composite Materials for Wind Turbine Structure

Mizanur Rahman, Molla Rashied Hussein, Abu Salman Shaikat, and Rumana Tasnim

8.1 Introduction

Fast advancements in material technology have resulted in varieties of structure of wind turbines. In wind structures, blades are one of the most significant components. Different shapes and dimensions of blades are used based on the strength of turbine. Previously, materials used in turbine blade design were limited to clothing, wood and sheet metal. However, in past few decades, composite materials have been used by all wind turbine manufacturing companies (Eker et al. 2005). In wind turbine structures, a vast range of materials is being used. Nevertheless, some aspects, namely weight, firmness, fatigue, mechanical component corrosion, breaking toughness, overall appearance etc. have impact on turbine materials. (Eker et al. 2006) These factors have led towards using composite materials in wind turbine structures. This chapter presents a review on different choice of composite materials for wind turbine.

8.2 Wind Energy

Wind energy is a promising renewable energy source. It is a type of solar energy. Although a little segment of solar radiation is captured by the earth, it gives nearly all of earth's energy requirements. It has been anticipated that the entire world receives nearly 1.8×10^{11} MW in which only 2% (i.e. 3.6×10^{9} MW) is transformed

M. Rahman (✉) · A. S. Shaikat · R. Tasnim
World University of Bangladesh, Dhaka, Bangladesh
e-mail: mizanur.rahman@mte.wub.edu.bd

M. R. Hussein
University of Asia Pacific, Dhaka, Bangladesh

S. Siddiquee et al. (eds.), *Composite Materials: Applications in Engineering, Biomedicine and Food Science*, https://doi.org/10.1007/978-3-030-45489-0_8

into wind energy and about 35% of wind energy is used within 1000 m of the earth (Tong 2009). Hence, the free wind power that has a possibility of converting into other forms of energy is nearly 1.26×10^9 MW (Nelson 2009). In this rate, wind energy can possibly fulfil almost majority of the energy requirements of the earth. Wind energy is a clean and eco-friendly energy source. Fossil fuels release harmful gases and nuclear power producing radioactive wastes. The ever-increasing use of wind energy will decrease the demands for fossil fuels which may finish within this century. Moreover, comparatively the wind power costs much lesser than that of solar power (El-Ali et al. 2007).Over 240,000 wind turbines are currently being operated all over the world covering 4% of world's total electricity.

8.3 Wind Generation

Wind is generated when earth's surface is unevenly heated by the sun. Atmospheric pressure gradients make air movements which result in Wind. Wind flows from more pressured regions to lesser pressured regions. The more the atmospheric pressure gradient increases, the wind speed gets higher and produce more wind power. Which means wind energy-converting machinery can absorb more wind power from the wind. Several factors make wind generation and movement complex, which include but not limited to inequality in solar heating, the Coriolis effect because of self-revolving Earth, and regional geographical circumstances.

8.4 Historical Development of Wind Turbine

At seventeenth century B.C, the Babylonian emperor Hammurabi used wind power for the first time for an irrigation project. Later in the first century AD, the very first wind driven wheel was used by Greek Engineer Heron of Alexandria to power a machine. The very old Tibet and China started using such wheel from the fourth century. In majority of Europe grain crushing mills became well-known within thirteenth century. French and English people approved of this technology and started using it within 1105 A.D. and 1191 A.D respectively. Figure 8.1 shows a picture of ancient wind mill.

Wind turbine based electricity generation embarked on its journey at nearly 1900's. In 1890, the very first wind driven electricity generation came into reality in Denmark. In 1931, the earliest utility-scale scheme was mounted in Russia. Later in 1941, Palmer C. Putman designed and developed a noteworthy1.25 MW wind turbine in large-scale which became known as Smith–Putnam wind turbine. The turbine was connected to local electrical distribution system at Castleton, Vermont, US. The turbine remained the biggest wind turbine ever constructed until 1979. It ran for hours and continued generating electricity. However, the blades suddenly failed operating after continuously operating for 1100 hours (Fig. 8.2) (Carlin et al.

Fig. 8.1 Ancient wind mill (Carlin et al. 2003)

Fig. 8.2 World's first megawatt size wind turbine (Carlin et al. 2003)

2003). Hence, appropriate selection of materials as a blade material for wind turbine has proven to be of utmost significance in the early history of wind turbine development. Later on Johannes Juul designed the first successful wind turbine, namely Gedser wind turbine (Fig. 8.3), using three different composite blades from steel spars, with Aluminium shells supported by wooden ribs. During 1956–1957 this was mounted at Gedser coast in Denmark. The 200 kW Gedser turbine contained three blades with 24 m rotor and operated smoothly for 11 years without having any maintenance. The first wind turbine having steel blades could not successfully operate for long. On the contrary, the second one having composite blades ran for a long time (The Wind Energy Pioneers 2000).Thus, a direct connection has been established between smooth operation of wind turbine and use of appropriate composite materials as blade material. Ever since 1970s, wind turbines have been being made using composite blades (Brøndsted et al. 2005a).

During the past three decades, remarkable advancement in wind power has been happening all over the world. In 2009, the globally constructed wind generation capacity reached 37 GW annually, making the world total wind capacity to 158 GW

Fig. 8.3 Gedser wind turbine (The Wind Energy Pioneers 2000)

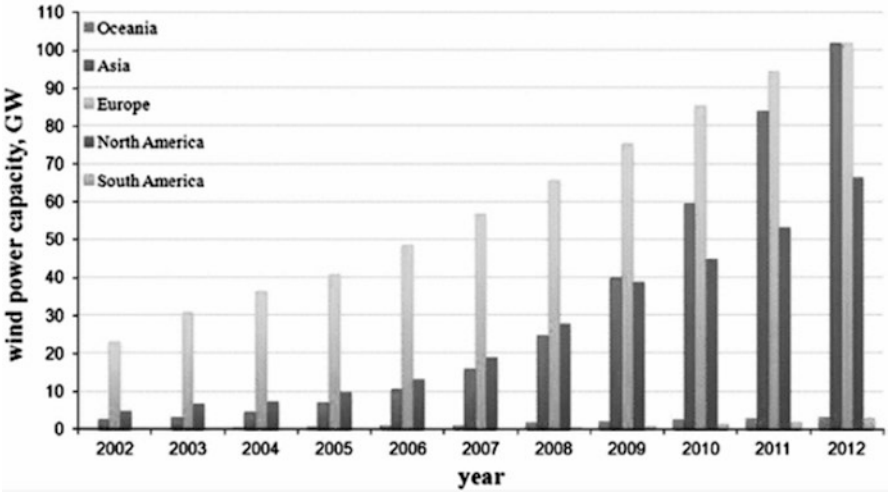

Fig. 8.4 Wind power capacity of 5 Continents' shares from 2002 to 2012 (Goudarzi and Zhu 2013)

(Tong 2009). As one of the cleanest, and reliable renewable energy sources, wind power is anticipated to fulfill a major requirement on power generation in future decades. Figure 8.4 illustrates five continents' share in the total installed wind power capacity from 2002 to 2012 progressively (Goudarzi and Zhu 2013; Solyali and Redfern 2009).

Modern advancement of wind-energy technology and applications is extensive. Over the past three decades, research and development has taken wind energy technology to a much expected level.

8.5 Structure of Wind Turbine

Wind turbine utilizes wind energy and produces electricity. Wind turbine operates in a contrary manner of a fan. That means, a fan consumes electricity for producing wind, while wind turbine makes use of wind for producing electricity. The blades of a wind turbine are rotated by wind, which revolves a shaft, which sequentially turns a generator for producing electricity. Wind turbine transforms wind's kinetic energy to mechanical energy. This transformed mechanical energy can be utilized for carrying out precise jobs, for example: refining grains or pumping water from the surface below. Moreover, a generator can transform the aforementioned mechanical energy for producing electricity to power homes, enterprises, schools, universities and more to name. In the Fig. 8.5 shows the block diagram of different component of a wind turbine.

Wind energy helps to rotate the turbine blade that connects with rotor of the wind turbine. The rotor is connected with gearbox before it connected with generator. In the wind turbine, low speed shaft is used to connect rotor with gearbox and high speed shaft is used to connect gearbox with generator. A control system is used to control generation of electricity from wind turbine. Wind turbine power generation system can be off grid or on grid. The difference between off grid and on grid system is mainly the connection of wind turbine with national grid system. Although different type of wind turbines are available in the market but the details of the structure of a wind turbine are same as shown in the Fig. 8.6:

Foundation The foundation is the connection between the wind turbine tower and the terrain underneath. It carries all the static and dynamic loads generating from the wind turbine.

Tower The tower construction not only bears the nacelle's and the rotor blades' weight, but also soaks the enormous static loads generated by the varying wind power. It is constructed from materials such as: tubular steel, concrete, or steel lattice. It carries the foremost turbine structure. Since wind speed elevates as height increases, taller towers facilitate turbines to consume more wind energy and produce electricity more.

Nacelle The nacelle is situated at the top of the tower. It resides the entire machine set that a wind turbine needs to operate successfully. It comprises the gear box, shafts having low-speed and high-speed, generator, brake and controller. Some nacelles are so gigantic that even a helicopter can land on it in case of emergency.

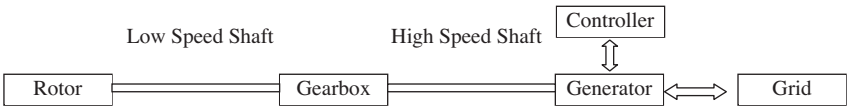

Fig. 8.5 Block diagram of wind turbine power generation system

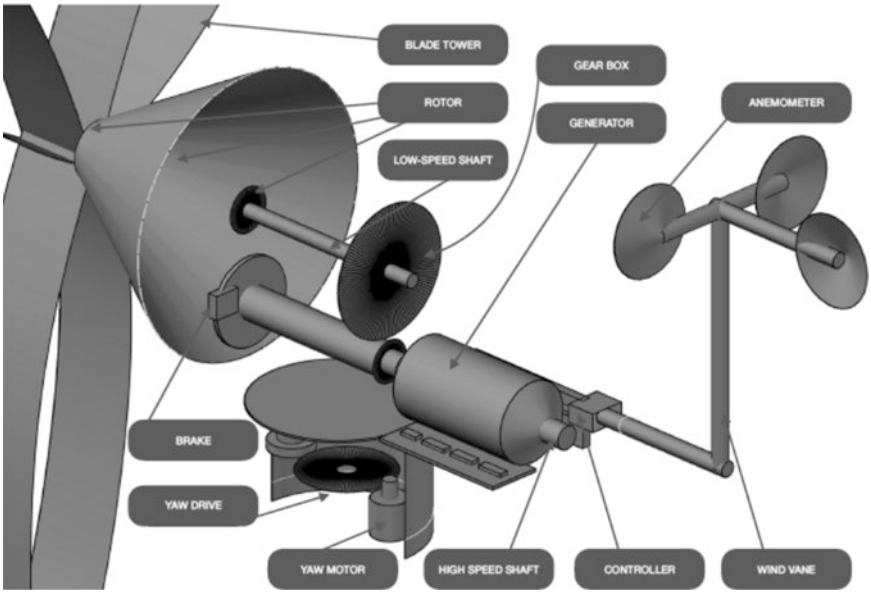

Fig. 8.6 Structure of wind turbine (Guzzeta et al. 2007)

Blades The majority of wind turbines consist of either two or three blades. Blades elevate and revolve whenever wind blows over them, making the rotor to rotate.

Rotor Blades and hub collectively make the structure of the rotor. The rotor blades absorb the wind power and transport the power to the rotor hub.

Anemometer Anemometer is a tool to measure the wind speed. It transmits data regarding wind speed to the controller. The electronic controller of a wind turbine utilizes the electronic signals from the anemometer for initiating the turbine.

Brake Brake is used to stop the rotor's operation mechanically, or electrically, or even hydraulically in case of emergencies.

Controller Controller starts the machine when the wind speed is around 8 to 16 miles per hour (mph). It stops the machine when the wind speed crosses more than 55 mph, because high wind can damage turbines.

Gear Box For achieving the potential as convincing alternative contributor of energy, wind turbine systems utilize highly efficient, dependable and robust components. Amid the components, most essential are the gearboxes. Particularly, planetary gearboxes are especially significant. It attaches the low-speed shaft with the high-speed shaft. It amplifies the rotational speed from around 30 to 60 rotations per minute (rpm) to around 1000 to 1800 rpm as this is the required rotational speed

for majority of generators to create electricity. The gear box is an expensive and overweight component of the wind turbine. For that reason, Engineers these days are looking at alternate options, such as: “direct-drive” generators, which operate at comparatively lower rotational speeds and do not need any gear box.

Generator The purpose of a generator in a wind turbine is to transform the mechanical energy into the electrical energy. Doubly-fed asynchronous generators are most commonly used in case of high power wind turbines.

High-Speed Shaft High-speed shaft connects to and drives the generator at around 1000 to 1800 rpm for producing electricity.

Low-Speed Shaft Low-speed shaft is turned at around 30–60 rpm by the gear box.

Pitch Pitch is the component for pitching or turning rotor blades out of the wind for controlling the rotor speed. It also keeps the rotor from turning in the wind whenever wind speed is too high or too low for creating electricity.

Wind Direction Wind direction decides the design of a turbine. Upwind turbines face itself into the wind. On the other hand, downwind turbines face itself away from the wind.

Wind Vane Wind vane is the component for measuring wind direction and for communicating with the yaw drive for adjusting the turbine appropriately with respect to the wind.

Yaw Drive Yaw drive adjusts upwind turbines so that they keep themselves facing the wind whenever the wind direction alters. However, downwind turbines do not need a yaw drive, since the wind is manually blown to the rotor in an away manner.

Yaw Motor Yaw motor powers the yaw drive for adjusting upwind turbines.

8.6 Composite Materials

A composite material, also known as a composition material, commonly acknowledged as composite in short, is a material comprises two or more composing materials. These composing materials have distinct physical or chemical properties from each other. When they are mixed, they develop a diversified character material dissimilar from themselves. However, unlike composites in mixtures and solid solutions, each composing materials are isolated and discrete within the completed structure.

8.7 Composite Materials for Wind Turbine Blades

Rotor blades are crafted from composite materials, mixing either fiber glass with polyester, or fiber glass with epoxy, even mixing wood with carbon at times. The most frequently used kinds of composite material in wind turbine manufacturing are glass fiber-reinforced plastics, commonly known as GRP in short. (Mishnaevsky et al. 2017)

8.7.1 Fibers

Glass and Carbon Fiber The toughness of composites is determined by the toughness of fiber and its volume substance. Normally, e-glass fibers, that are borosilicate glass, which is called "electric glass" or "e-glass" for its resistance against high electricity, are utilized as a foremost reinforcement in the composites.

As the volume substance of fibers in UD composites elevates, the toughness, flexibility and compression strength grow correspondingly. However, high volume substance of fibers, specifically after crossing 65%, dry areas might arise which show lack of bondage between fibers. It also decreases the fatigue strength of the composites (Mishnaevsky et al. 2009a).

Usually, the glass and epoxy composites made for wind blades comprise up to 75% weight per glass. Numerous cases regarding the development of fibers, which could be tougher than the typical E-glass fibers, have been studied. Glass fibers with altered composites (S-glass, R-glass and so on), Carbon Fibers, Basalt and Aramid fibers are known to be high strength fibers. S-glass, where S stands for "Strength", is a high strength glass which was developed back in 1960s, exhibits 40% more ductile and flexural strengths. It shows 10% to 20% more compressive strength and flexural modulus contrasting with E-glass. The S-glass is also costlier than E-glass. S2 glass was developed in the year 1968 as a marketable variety of S-glass. S glass and S2 glass fibers contain identical composition, that is Magnesium Alumino-Silicate. However, the prime variances are in sizing, which means fiber coating, and certification process. The S2-glass is about 10 times expensive than E-glass.

Carbon Fibres Carbon fibers are regarded as a capable alternative to glass fibers. They display more toughness and lesser density than the glass fibers. It produces thinner, tougher and lightweight rotor blades for wind turbine. But their damage tolerance, compressive strength and eventual strain are comparatively low. Also, they are costlier than the E glass fibers (Grande 2008; Carbon Fiber vs. Fiberglass 2019).

Aramid and Basalt Fibers A remarkable alternative could be non-glass, high strength fibers, such as: Aramid(Aromatic Polyamide). Such fibers show great mechanical strength. Also, they are tough and less prone to damage. However, as

they possess low compressive strength, low bond to polymer resins, get moisturized, and show degradation because of ultraviolet radiation. In recent works, the Basalt fibers were utilized in fusion with Carbon fibers. (Mengal et al. 2014; Abashidze et al. 2015)

Hybrid Composites E-glass/carbon and E-glass/aramid are remarkable hybrid composites. The lengthiest wind turbine rotor blades of the world are manufactured using Carbon with glass hybrid composites. Many research works are being carried out based on strength of hybrid composites (Mishnaevsky et al. 2014; Dai et al. 2014; Prabhakaran et al. 2013). Report shows that incorporating glass fibers and Carbon fiber composites improves their impact properties and ductile strain. Some researchers exhibited that the composite strength depends on the ratio of material mixtures(Mishnaevsky et al. 2014). Even though hybrid composites have a huge potential for designing wind turbine blades, advanced studies and research are required for making better composition of the materials.

Natural Fibre The benefits of natural fibers include Sisal, Flax, Hemp, Jute, are that they are less expensive, available all year long and environment friendly. The drawbacks are that they vary in quality, highly moisturized and thermally unstable in case of the raw fibers (Kalagi et al. 2016). Holmes et al. (Holmes et al. 2007; Holmes et al. 2009) examined a unique Bamboo-Poplar Epoxy Laminate for wind turbine blades, and showed that this material has strong and stiff, and can be utilized in wind blades rather using common composites. The more strength and durability of bamboo and its rapid growth and wide availability allow it to be a remarkable material for the wind energy applications. A fascinating alternative for developing countries is small turbines. They are producible on-site, and manufactured from natural composites, that is from local and available timber. Some researchers investigated the application of timbers for producing wind turbines. They showed that the turbines made with wooden blades could be a dependable and less expensive alternate for the developing countries (Mishnaevsky et al. 2011; Mishnaevsky et al. 2009b).

8.7.2 Matrix

Usually, matrices in wind turbine's blade composites are made of thermosets (epoxies, polyesters and vinyl-esthers) or thermoplastics.

Thermosets 80% of the reinforced polymers are based on thermosets (Joncas 2010). Thermosets offer lower viscosity. Previously, polyester resins were used for producing composite blades. However, since the large and extra-large wind turbines begin to be developed, polyester is replaced by epoxy resins. They are now mostly used as matrices for producing wind blade composites (Joncas 2010).Researchers

are working on further development of matrix materials which could be cured faster and at lesser temperatures.

Thermoplastics Thermoplastics could be a potential alternate of thermoset matrices. A significant benefit of using thermoplastic composites is that they are recyclable. However, their drawbacks are the need for high processing temperatures, which consumes more energy and affect fiber properties probably. Also, it is quite difficult to produce large, which is more than 2 meters, and thick, which is more than 5 millimeters segment. Fatigue performance of thermoplastics is usually not satisfactory compared to thermosets, even coupled with carbon or glass fibers. However, thermoplastics are superior to thermosets in term of fracture toughness and inferior to thermosets in term of fatigue.

Nano-Engineered Polymers and Composites In some recent works, it was shown that adding nano-reinforcement in matrix could possibly enhance composites properties. Adding very small amount of nano-reinforcement, which could be either carbon nanotubes or nanoclay in the polymer matrix of composites, fiber sizing can raise the fatigue resistance, shear strength and fracture stiffness of the composites (Zhou et al. 2016; Ma and Zhang 2014). Some researchers designed and developed various wind turbine blades with secondary carbon nanoparticles reinforcement, namely, Vinyl-ester, Thermoplasts, Epoxy composites comprising CNTs. It was revealed from the research that incorporating small amount of Carbon Nanotubes (CNT) can boost the lifetime up to 15 times better (Loos et al. 2012).

Besides, Graphene was investigated as a secondary reinforcement for the nano-modification of wind turbine composites. Graphene reinforcement makes it possible to develop tougher and longer-lasting wind turbine blades (Yavari et al. 2010). It was theoretically approximated that adding 1% to 5% of Carbon Nanofibers, or CNF in short, to the interfaces of glass fiber reinforced epoxy composites for wind turbine blades used in 2 MW and 5 MW turbines improves ductile stress and modulus, and reduces 20% weight in the blades, thus increases lifespan(Merugula et al. 2010). Using nano-modified polymers as matrix improves property values intrinsically in areas like glass transition temperature and limits the processing or applying nano-modified polymers (Khare and Khare 2013). However, the implementation of nano-engineered wind turbines faces numerous practical and economic challenges (Loos and Schulte 2011).

8.8 Summary

For decreasing the dependence on fossil fuel, wind driven electricity generation should be enhanced in upcoming future. This can be obtained by installing more large and extra-large wind turbines. The most crucial parts of a wind turbine, namely rotor blades are made from composite materials. Wind turbine can perform better

when its blades can be made lightweight; fatigue resistant, damage tolerant and also designed with long-lasting and rigid composite materials. Thorough implementation of such materials on turbine blades will ensure a controlled wind turbine structure with smooth operation.

References

Abashidze S et al (2015) Hybrid fiber and nanopowder reinforced composites for wind turbine blades. J Mater Res Technol 4:60–67

Brøndsted P et al (2005a) Composite materials for wind power turbine blades. Annu Rev Mater Res 35:505–538

Brøndsted P et al (2005b) Composite materials for wind power turbine blades. Annu Rev Mater Res 35:505–538

Carbon Fiber vs. Fiberglass (2019): A Comparison between the Two Materials Which Material Is Superior? Available at: https://infogr.am/carbon-fiber-vs-fiberglassAccessed 8 Nov 2019

Carlin P W et al (2003)The History and State of the Art of Variable-Speed wind turbine Technology in WIND ENERGY

Dai GM et al (2014) Fatigue of hybrid carbon/glass composites: 3D computational modelling. Compos Sci Technol 94:71–79. https://doi.org/10.1016/j.compscitech.2014.01.014

Eker B et al (2005) Mathematical modeling of wind turbine blades through volumetric view. Proceedings of the 6th Asia-Pacific Conference on Wind Engineering, Sept. 12–14, 2005, Sheraton Walker Hill Hotel, Seoul, Korea, pp 1–21

Eker B et al (2006) Using of composite material in wind turbine blades. J Appl Sci 6(14):2917–2921

El-Ali A et al (2007) Comparison between solar and wind energy in Lebanon. Proc. of 9th Int. Conf. on Electrical Power Quality and Utilisation, Barcelona

Goudarzi N, Zhu WD (2013) A review on the development of wind turbine generators across the world. International Journal of Dynamics and Control 1(2):192–202

Grande JA (2008) Wind power blades energize composites manufacturing. Plast Technol 54:68–75

Guzzeta A et al (2007) Types Of Wind Turbines And Associated Advantages. Available at:http://me1065.wikidot.com/types-of-wind-turbines-and-associated-advantages Accessed 12 Nov 2019

Holmes JW et al (2007) Reliability of Wind Turbine Blades: An Overview of Materials Testing; Proceedings of the Wind Power Shanghai, 1–3 November 2007. Shanghai, China

Holmes JW et al (2009) Development of a bamboo-based composite as a sustainable green material for wind turbine blades. J Wind Eng 33:197–210. https://doi.org/10.1260/030952409789141053

Joncas S (2010) Ph.D. Thesis. TU Delft; Delft, The Netherlands. Thermoplastic Composite Wind Turbine Blades: An Integrated Design Approach. p 273

Kalagi G et al (2016) Natural Fiber reinforced polymer composite materials for wind turbine blade applications. Int J Sci Dev Res 1:28–37

Khare KS, Khare R (2013) Effect of carbon nanotube dispersion on glass transition in cross-linked epoxy-carbon nanotube nanocomposites: role of interfacial interactions. J Phys Chem B 117:7444–7454. https://doi.org/10.1021/jp401614p

Loos MR, Schulte K (2011) Is it worth the effort to reinforce polymers with carbon nanotubes? Macromol Theory Simul 20:350–362. https://doi.org/10.1002/mats.201100007

Loos M et al (2012) Carbon nanotube-reinforced epoxy composites for wind turbine blades. Plast Res Online. https://doi.org/10.1002/spepro.004276

Ma PC, Zhang Y (2014) Perspectives of carbon nanotubes/polymer nanocomposites for wind blade materials. Renew Sust Energ Rev 30:651–660. https://doi.org/10.1016/j.rser.2013.11.008

Mengal AN et al (2014) Basalt carbon hybrid composite for wind turbine rotor blades: a short review. Adv Mater Res 970:67–73. https://doi.org/10.4028/www.scientific.net/AMR.970.67

Merugula LV, Khanna V, Bakshi BR (2010) Comparative life cycle assessment: Reinforcing wind turbine blades with carbon nanofibres; Proceedings of the 2010 IEEE Symposium on Sustainable Systems and Technology (ISSST); Washington, DC, USA. 17–19 May 2010; pp. 1–6

Mishnaevsky L et al (2009a) Statistical modelling of compression and fatigue damage of unidirectional fiber reinforced composites. Compos Sci Technol 69:477–484

Mishnaevsky L et al (2009b) Strength and reliability of wood for the components of low-cost wind turbines: computational and experimental analysis and applications. J Wind Eng 33:183–196. https://doi.org/10.1260/030952409789141062

Mishnaevsky L et al (2011) Small wind turbines with timber blades for developing countries: materials choice, development, installation and experiences. Renew Energy 36:2128–2138. https://doi.org/10.1016/j.renene.2011.01.034

Mishnaevsky L et al (2014) Hybrid carbon/glass fiber composites: micromechanical analysis of structure-damage resistance relationship. Comput Mater Sci 81:630–640. https://doi.org/10.1016/j.commatsci.2013.08.024

Mishnaevsky L et al (2017)Materials for wind turbine blades: an overview', Materials (Basel). 10(11): 1285. Available at: https://www.ncbi.nlm.nih.gov/pmc/articles/PMC5706232/#sec2-materials-10-01285title Accessed 14 Nov 2019

Nelson V (2009) Wind energy – renewable energy and the environment. CRC Press

Prabhakaran D et al (2013) Tensile and compression properties of hybrid composites—A comparative study; Proceedings of the 19th International Conference on Composite Materials (ICCM19); Montreal, QC, Canada. 28 July–2 August 2013. pp. 1029–1035

Solyali D, Redfern MA (2009) Have wind turbines stop maturing? In: IEEE 44th International Universities, Power Engineering Conference (UPEC)

The Wind Energy Pioneers (2000) The Gedser wind turbine. Frederiksberg, Denmark, Danish Wind Industry Association

Tong W (2009) Fundamentals of wind energy. Wind power generation and wind turbine design, vol 23. WIT Press

Yavari F et al (2010) Dramatic increase in fatigue life in hierarchical Graphene composites. ACS Appl Mater Interfaces 2:2738–2743. https://doi.org/10.1021/am100728r

Zhou HW et al (2016) Carbon fiber/carbon nanotube based hierarchical composites: effect of CNT distribution on shearing strength. Compos B 88:201–211. https://doi.org/10.1016/j.compositesb.2015.10.035

Chapter 9
Electrochromic Smart Windows: An Energy-Efficient Technology

Xing Yan Tan, Hao Wang, and Tae Gyu Kim

9.1 Introduction

Sustainable and renewable energies have gain increased attention as people are more aware toward environment protection. While finding alternative energy to replace fossil fuels may be the ultimate solution to keep carbon footprint at minimum, the existing solution available are yet to replace fossil fuel, which is far more cost efficient (Sims et al. 2003). But a different approach such as reducing energy consumption from our daily life can be taken instead to reduce emission of greenhouse gases. One way to achieve this is through implementation of energy-efficient technologies such as "smart windows". Smart window is one of the applications of electrochromic (EC) devices and it stand out to be the most striking and potentially most important application. This is because building with smart windows capable of varying throughput of visible light and solar energy; avoid overheating while achieve good indoor lighting conditions; reduce energy consumption for air conditioning and lighting (Granqvist 1995; Gillaspie et al. 2010).

Statistical analysis shown that global population had bloom dramatically from just 2.5 billion in 1950 to about 7.9 billion in present year (2019). The number is forecasted to continue growth and level off at a magnitude of nearly eleven billion in around year 2100 (UNDESA 2019). Change in qualities of life is happening simultaneously with the explosion of population; countries that are under

X. Y. Tan (✉) · H. Wang
Department of Nano Fusion Technology, College of Nanoscience & Nanotechnology, Pusan National University, Busan, Republic of Korea
e-mail: txy511@pusan.ac.kr

T. G. Kim
Department of Nanomechatronics Engineering, College of Nanoscience & Nanotechnology, Pusan National University, Busan, Republic of Korea
e-mail: tgkim@pusan.ac.kr

S. Siddiquee et al. (eds.), *Composite Materials: Applications in Engineering, Biomedicine and Food Science*, https://doi.org/10.1007/978-3-030-45489-0_9

developing have progressed in improving overall living standards of their citizens by providing various amenities. One of dire the consequences is, however, putting strain on the limited resources globally especially on energy, which is derived mainly from unsustainable resources – fossil fuels with ensuing injection of carbon dioxide into air. More carbon dioxides are released into the atmosphere when more energies are demanded; the cycle continues as population growth, causing global warming, sea level rising, and other chain reactions (Houghton et al. 1990).

From the total energy production, fossil fuels remained the dominant energy source since industrial era, albeit they are environmentally intensive and contributing to global warming. This situation is not expected to change soon without proper policy interventions and technological improvements. About 30 to 40% of worldwide primary energy has been spent in buildings for heating, cooling, lighting, etc. (Huovila 2007). Huge potential for saving tremendous amount of energy in buildings sector, however, a detailed study conducted in USA states that a large fraction of the energy delivered to buildings is wasted because of inefficient building technologies (Richter et al. 2008). Energy savings must be made without reducing the standard of living, but by utilizing more efficient technologies to provide the same or better performance.

Windows are the weak links in the buildings' energy system that frequently let in or let out too much energy, then temperature is balanced by energy guzzling of cooling or heating. Windows are very important in both architecture design and connection to outdoor. Without eliminating or making the window apertures smaller, the solution to this conundrum is implementing an energy efficient window. Clearly an energy efficient window must harmonize with nature and make good use of what nature offers in term of light and energy. To further elaborate this, sunlight is an electromagnetic radiation mainly composed of visible and infrared spectrum. An energy efficient "smart window" is capable of providing daylight to the rooms while blocking near-infrared radiation from heating (Kim et al. 2015).

Near-infrared (NIR) radiation is accounted for about half of the solar energy that is incident upon a windows but does not contribute to daylighting within a building (Runnerstrom et al. 2014). Smart window can manipulate the amount of transmission of visible and NIR transmission separately so that to save energy from lighting and air conditioning of the buildings. Motivated by the potential for significant energy savings from reduced loads of lighting, cooling and heating, many researches have been conducted in EC smart windows that dynamically control sunlight entering a building (Deb 2008; Mortimer 2011). The focus on improved energy efficiency and the development of advanced buildings drives the majority of current EC research.

In the modern society today, people are get used to the idea of building automation. Robot vacuum, dishwasher, washing machine and much more are already became part of our life. Traditionally, windows are fitted with curtains or blinds to shelter from sunlight (or heat) and provide privacy. The intuitive of energy-saving and automation lead to the development of smart window that can change from clear to dark and vice versa. To realize this, a phenomenon known as electrochromism, where the colour, transparency or other optical property of a material changes

when voltage is applied, is integrated into the design of windows. In other words, electrochromism is the basis for operation of smart window that can block or unblock the sunlight with a push of a button.

Conventionally, EC smart windows are prepared by sputtering of transition metal oxide thin films as the active material (Mortimer 2011; Granqvist 2014). Unfortunately, conventional materials suffer significant drawbacks from material degradation associated with repeated ion intercalation, and adopt dark, distinct colours in their tinted states, simultaneously blocking both visible and NIR light (Granqvist 2014). For these reasons and also the cost of expenses, conventional electrochromic windows struggled to achieve widespread adoption (Gillaspie et al. 2010). A newly developed and fundamentally different class of EC device based on plasmonic electrochromism is designed to overcome those limitations and ultimately minimize the cost-performance ratio.

One of the unique features of plasmonic electrochromism that standout from conventional electrochromism is the ability to selectively control NIR absorption. Figure 9.1 shows the plasmonic EC nanocrystal smart window operates at different states; in 'bright' state, the smart window is transparent, allowing both NIR and visible rays to pass through freely; in 'cool' state, the smart window is transparent, allowing visible lights to pass through but blocking NIR rays, providing daylight to the room while keeping away from heat; in 'dark' state, the smart window is translucent that block both NIR and visible rays. Details of spectral selectivity will be further discussed in Sect. 9.4. Figure 9.2 below is the breakdown of various EC windows classes. EC performance is evaluated in terms of coloration efficiency, durability, and switching time, whereby performance of EC window depends on material structure and composition.

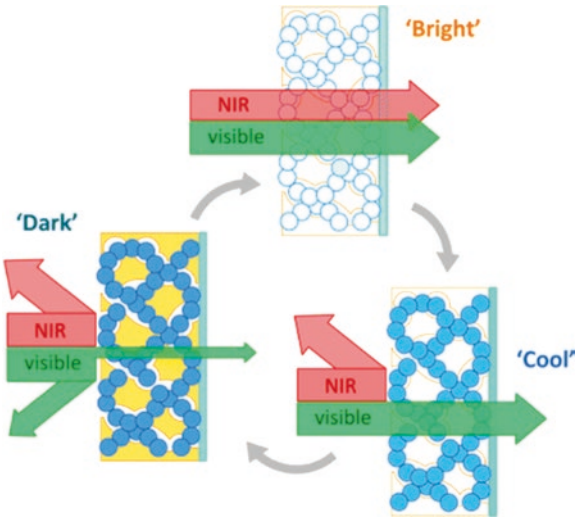

Fig. 9.1 Schematic diagram of solar radiation passes through smart windows at different states (Kim et al. 2015)

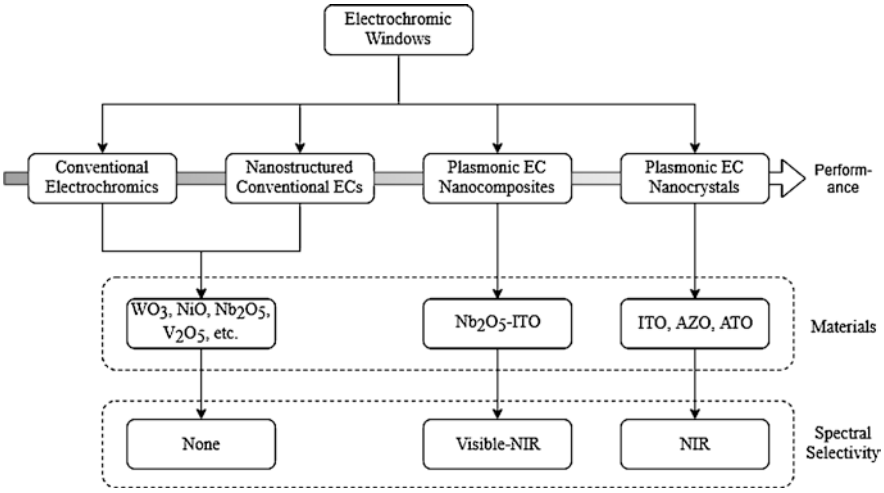

Fig. 9.2 Classification of various electrochromic windows

9.2 Fundamentals of Electrochromic Device Operation and Preparation

Figure 9.3 presents a generic EC device coating with five superimposed layers – an active electrochromic electrode layer, an ion storage layer acts as counter electrode, an ion conductor layer separating the two electrodes, and two transparent conducting layers serve as electrical leads, on a single transparent substrate or positioned between 2 transparent substrates. This EC device structure is referred as thin film electrical battery whose charging state corresponds to a certain level of optical absorption and this is the most common geometry for EC devices (Niklasson and Granqvist 2007; Granqvist 2014). The working principles of EC devices are similar to electrochemical reaction in battery. Small ions such as protons (H^+) or lithium ions (Li^+) are often used as charge carrier in majority of EC devices because of good ion mobility.

During off or bleached state, the cations are residing in the electrolyte and the ion storage layer. When the device is switched on, electric field is generated in between cathode and anode due to potential difference in which driven the cations to migrate from ion storage layer (anode), through the electrolyte, into the electrochromic layer (cathode). Ions insertion and extraction occur during the charge transfer contribute to the variability of the optical transmittance of EC film(s). This is because electrochromic materials are made up from transition metal oxides that consist of multiple oxidation states with different optical properties (Chernova et al. 2009; Wang et al. 2010). Transparent conductor layers play an important role here in conducting electricity through external circuit. Indium tin oxide (ITO) is well-known for its superior optical and electrical properties and is commonly used as transparent conductor.

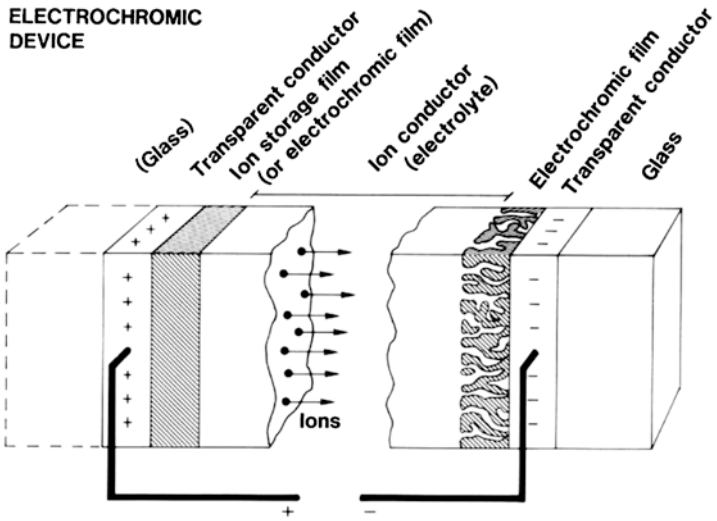

Fig. 9.3 Generic five-layer EC device design. Arrows indicate the movement of ions in an applied electric field (Granqvist 2014)

In previous section, we mentioned that EC device performance is evaluated from material structure and composition which in turn determined by coating technique. Thanks to the emergence of nanotechnology, conventional inorganic EC compounds in nanostructure form opens up possibilities of enhanced properties, such as improved switching times, higher colouration efficiency, and improved stability against electrochemical cycling (Runnerstrom et al. 2014). There are numerous numbers of techniques to coat films of EC device. For example, traditional thin film preparation such as physical and chemical vapour deposition, a plethora of chemical methods (chemical bath deposition, sol-gel deposition, spin coating, Langmuir-Blodgett technique, etc.), electrochemical methods (plating, anodization) and others, and sometimes employing nanoparticles as intermediate steps as well as templating. Sputtering from physical vapour deposition is suitable for the EC films preparation because sputtering process is well understood in manufacturing. Hence, suggest that sputtering will likely be the most practical production method for smart windows in foreseeable future (Gillaspie et al. 2010). This topic mainly surrounds EC devices based on conventional materials and nanostructured of it.

On the other hand, EC device shown in Fig. 9.1 utilizes plasmonic nanomaterials which enable it to absorb NIR light at same time allow visible light to pass through. Plasmonic nanoparticles that support localized surface plasmon resonances (LSPR) have been in academic pursuit over the past decade for signal transduction and efficiency in both energy and space, as well as sensitive and specific, through miniaturization to the nanoscale (Pastoriza-Santos et al. 2018). Plasmon resonance is the phenomenon of collective oscillations of charge carriers in solids. The excess charge carriers (impurity holes or electrons) in semiconductor plasmonic nanocrystals allow themselves as intense absorption bands in the NIR region of the spectrum. In

contrast to metal nanocrystal, the LSPR lies in the visible region of the spectrum and able to absorb light (Litvin et al. 2018). There are two general approaches for the preparation of nanoparticle: (1) colloidal chemistry and (2) epitaxial growth and/or nanoscale patterning through lithography-based technology (Drbohlavova et al. 2009).

9.2.1 Electrochromic Oxides

Perhaps EC films are the most important component inside an EC device. The unique ability to change colour and thus the transmittivity, enable the applications of EC device such as smart windows. All elements that show electrochromism with their respective oxides are transition metals. In principal, EC oxides can be categorised into two kinds, one that referred as "cathodic" that colouring under ion insertion, and the other referred as "anodic" that colouring under ion extraction. Figure 9.4 indicates the location of transition metals capable of forming oxides of these two particular categories, and interestingly, vanadium oxides are classified as intermediate or "hybrid" which are class of its own (Granqvist 1995). From Fig. 9.4, one can clearly distinguish oxides with cathodic or anodic colouration in transition metal region because electrochromism is closely related to the electronic structure of the oxides. Electrochromism can also be found in binary and ternary mixed oxide and in oxyfluorides. Also, transition metal hexacyanometallates are non-oxide with anodic electrochromism.

Cathodic colouration is found in oxides of Ti, Nb, Mo, Ta, and W, with tungsten oxide (WO_3) being by far the most extensively studied one (Granqvist 2000). Take tungsten oxide (WO_3) as example, upon ion injection, WO_3 changes colour from a clear, transparent state to a dark blue, translucent state as tungsten ions are reduced (Granqvist 1995). Protons or cations in the electrolyte compensate the injected electrons through insertion into WO_3 octahedral sites, as shown in Eq. (9.1). The injected

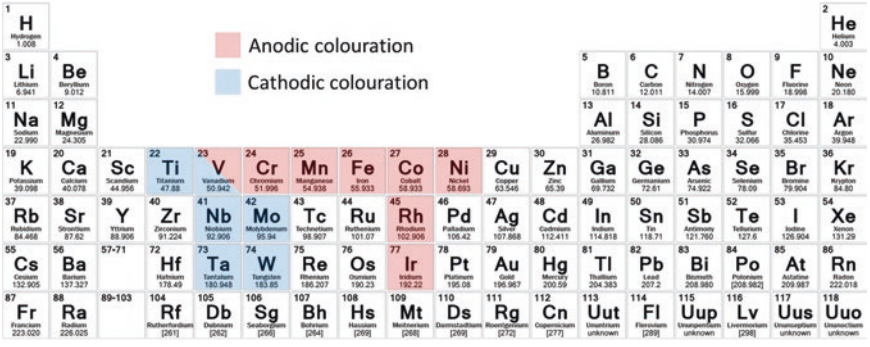

Fig. 9.4 Location of transition metal oxides in periodic table that are anodic (red) or cathodic (blue) colouration

electrons occupy the previously empty d band, giving rise to new electronic transitions. In crystalline WO_3, the added electrons occupy delocalized states, whereas in amorphous WO_3 electrons are localized at metal sites, resulting in polaronic absorption that can be described as an electronic charge-transfer transition between adjacent metal sites with different valency (Runnerstrom et al. 2014).

$$\left[\mathrm{WO_3} + \mathrm{H^+} + \mathrm{e}\right]_{\text{bleach}} \rightleftharpoons \left[\mathrm{HWO_3}\right]_{\text{coloured}} \tag{9.1}$$

Anodic colouration is found in oxides of Cr, Mn, Fe, Co, Ni, Rh, and Ir, with nickel oxide and iridium oxide being the ones investigated in most detail (Granqvist 1995). Anodic colouration mechanism is in reverse manner compared to cathodic colouration. Take nickel oxide (NiO) as example, the electrochromic reaction can proceed via the exchange of H^+ and OH^- depending on the nature of the films as well on the electrolyte (Wen et al. 2014). The situation become more complicated when the films evolve during electrochemical cycling (Estrada et al. 1988; Ren et al. 2013). The electrochromic effect in NiO involves several phases and is pointed at the general applicability of the Bode reaction scheme (Wen et al. 2014); specifically the reactions in alkali electrolyte associate with $Ni(OH)_2$ and NiOOH as shown in Eq. (9.2) in a simplified manner (Avendaño et al. 2005; Avendaño et al. 2009).

$$\left[\mathrm{Ni(OH)_2}\right]_{\text{bleach}} \rightleftharpoons \left[\mathrm{NiOOH} + \mathrm{H^+} + \mathrm{e}\right]_{\text{coloured}} \tag{9.2}$$

Both cathodic oxide and anodic oxide are usually employed in a typical smart window with two respective EC films; one can adjust the optical transmittance and achieve better colour neutrality than with one single EC film (Granqvist 2014). Take combination of tungsten oxide and nickel oxide as illustrated in Eqs. (9.1) and (9.2) for example, applying voltage in one direction between these two EC films will transport the ions from one to another makes both of these films coloured, while reversing the potential polarity makes both of the films bleached by return to their original properties. When there is no move of charges, the EC device shows memory effect by retaining the current state (coloured or bleached respectively). The terminology "rocking chair" has been used describe operation in smart windows as well as rechargeable battery applications (Goldner et al. 1993).

$$\mathrm{CE}(\lambda) = \frac{\Delta OD}{\mathrm{Q}} = \frac{\log\left[\mathrm{T_{bleached}}(\lambda) / \mathrm{T_{coloured}}(\lambda)\right]}{\mathrm{Q}} \tag{9.3}$$

Furthermore, performance of each individual EC materials and devices is merited by colouration efficiency (CE) given in Eq. (9.3) (Gillaspie et al. 2010; Thakur et al. 2012), where Q is the electronic charge injected into the EC material per unit area, T_{bleached} is the transmittance in the bleached state, and T_{coloured} is the transmittance in the coloured state. The CE therefore gives the change in optical density (OD) achieved by the injection of unit charge over unit area. In general, materials

with higher CEs will have better durability and faster switching times, since less charge is required to produce a given optical response (Gillaspie et al. 2010).

9.2.2 Ion Conductor

At the central of the EC device resides the ion conductor layer which is the key component for ions transportation between cathode and anode during EC reaction. To ensure proper operation of the device, the ion conductivity of electrolyte should be larger than 10^{-4} S/cm (Granqvist 1995). Other requirement of electrolyte is high thermal and UV stability on top of not cause any degradations toward EC layers (Marszalek et al. 2012). Ion conductor can be generalized into two – liquid and solid electrolyte. Figure 9.5 shows the schematic diagram EC devices with different type of electrolytes.

Transparent liquid electrolytes and ion-containing thin oxide films were used in early studies on EC and later the interest has switched toward polymer (solid) electrolyte mainly following the development of electrical battery technology (Granqvist 2014). Undoubtedly, the main advantages of liquid electrolyte are easy to synthesize, high ion conductivity (response time) and good stability (cycle life) (Girotto and Paoli 1999), which make it the popular candidate over the years when researching EC device. Regardless, efforts in sealing to prevent the potential of leakage and evaporation are the biggest flaws of liquid electrolyte as ion conductor in application like smart window. But the problems can be overcome by opting solid electrolyte, and it opens up the doors to all plastic and flexible EC devices too. Ionic charge transports as well as the diffusing species that enter the EC layers via electrolyte are the only major drawback in comparison to liquid electrolyte.

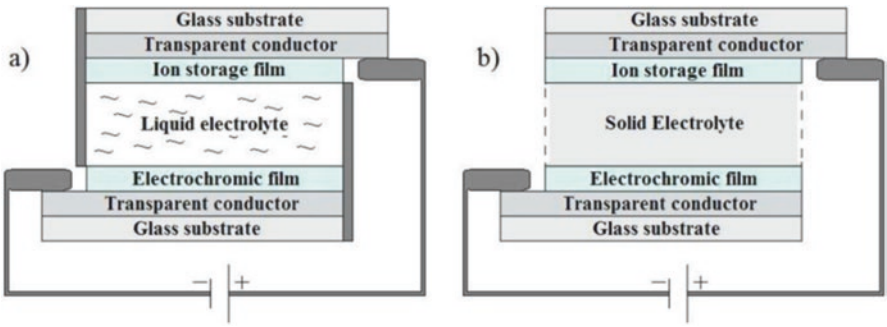

Fig. 9.5 The electrochromic device with (**a**) liquid and (**b**) solid electrolyte (Marszalek et al. 2012)

9.2.3 *Transparent Conductive Oxide*

Transparent conductive oxides (TCO) are semiconductors such as tin doped indium oxide, In_2O_3: Sn (ITO), fluorine doped tin oxide, SnO_2: F (FTO) and antimony doped tin oxide, SnO_2: Sb (ATO). They are known with high optical transparency in the visible region, good electrical conductivity, and high infrared reflectivity (Chuang 2010). These characteristics are found particularly useful as transparent thin-film conductors in applications like flat panel displays and solar cells, transparent heaters, heat mirrors, optoelectronic devices, and smart windows.

TCO materials suitable for transparent conductor thin films should have a carrier concentration on the order of 10^{20}–10^{21} cm^{-3} and band-gap energy above approximately 3 eV, that is, degenerated n-type or p-type semiconductors. Furthermore, TCO thin films that are in practical use as transparent conductors are polycrystalline or amorphous and exhibit a resistivity on the order of 10^{-3} Ω cm or less and an average transmittance above 80% in the visible range (Minami 2013). ITO is well-known in excellent optical and electrical properties. It is a highly degenerated n-type and wide band gap (e.g., 3.5–4.3 eV) semiconductor (Kim et al. 1999). Due to its relatively low electrical resistivity and high visible transmittance, this material has been used extensively as transparent conductors. ITO thin films can be obtained readily through various growth techniques including sputtering, evaporation, chemical vapor deposition, and sol-gel (Chuang 2010).

TCO thin films on glass substrate are located at outermost layer of smart windows as shown in Fig. 9.3. The excellent electrical and optical properties of TCO allow conduction of electricity between the transparent conductors without hinder transparency of a window. When voltage is applied to the transparent conductors, ions are transferred between the ion storage film and the EC film through the ion conductor layer at the centre. Depend on the voltage polarity, the electrons are then extracted from or injected into the transparent conductors that alter the optical absorption of the EC films. The original state can be easily restored by reversing the voltage.

9.3 Characterization of Electrochromic Materials

There are many different techniques to choose to deposit EC metal oxide thin films. EC thin films prepared by DC magnetron sputtering are specifically chosen in this work to elaborate various characterizations of EC materials. As mentioned earlier, sputtering is well understood in manufacturing. On top of that, sputtering has good reproducibility, good substrate adherence and the possibility of depositing many different types of materials with a variety of different compositions, layers, structures and stoichiometry. The general idea of sputtering is that a target (source) of certain raw material is bombarded by accelerating ions (typically Ar^+) impart a high kinetic energy to the expelled source atoms. These atoms transit through the

discharge and condense onto the substrate, thus providing the film growth. Then, a series of analyses on thickness, morphology, optic, etc. to identify the microstructure and composition of deposited thin films.

9.3.1 Physical Characterization

9.3.1.1 Film Thickness by Profilometry

Deposited EC thin films from sputtering are usually measured by contact surface profilometry. The surface profilometer measures the thickness by moving a diamond tip over the step between uncoated and coated sample areas. Multiple measurements from different positions along the step are always taken and averaged.

9.3.1.2 Crystal Structure by X-Ray Diffraction

In a crystalline structure the atoms form regularly repeating atomic planes separated by a certain distance, d, which varies with the material. If d is shorter than the X-ray wavelength λ, the X-rays are diffracted by the uniform atomic planes and an interference pattern is seen, as described by Bragg's law,

$$m\lambda = 2\mathrm{dsin}, \tag{9.4}$$

Where m is an integer and θ is the diffraction angle, i.e. the angle between the incident X-ray beam and the atomic plane. A spectrum with constructive inferences is obtained from scanning the diffracted beam. The peak distribution is directly related to the atomic distances. Hence, information about structure, phase composition and orientation of planes can be obtained by comparing the spectra with the database from JCDPS-International Centre for Diffraction Data (ICDD).

Non-crystalline materials with no long-range order, i.e. amorphous materials, do not show any diffraction peaks and cannot be examined by XRD. Polycrystalline materials are composed of many different crystalline grains of varying size and orientation. The size of the grains determines whether they will be detected. Crystalline samples show very distinct narrow peaks whereas the peaks from polycrystalline samples are broader. The width of the peak depends on the size of the grains, and the grain size, D, can be calculated by Scherrer's formula (Cullity and Stock 2001):

$$\mathrm{D} = \frac{k\lambda}{{}^{2}\cos,} \tag{9.5}$$

Where k is the shape factor, λ is the wavelength of X-ray, β is the full width at half maximum of the X-ray diffraction peak, and θ is the diffraction angle. Figure 9.6

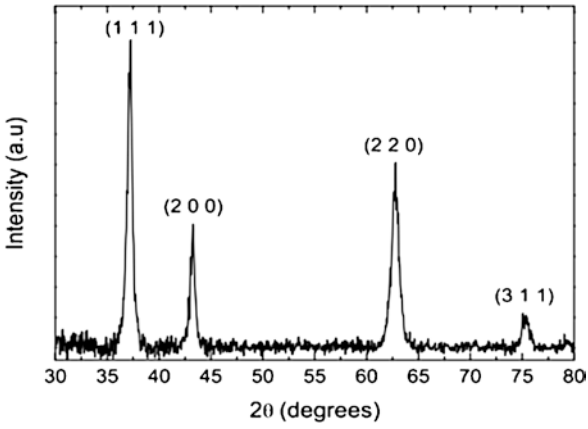

Fig. 9.6 XRD spectrum for polycrystalline NiO. The planes are assigned to the cubic phase of nickel (JCPDS-ICDD card number: 78–0429)

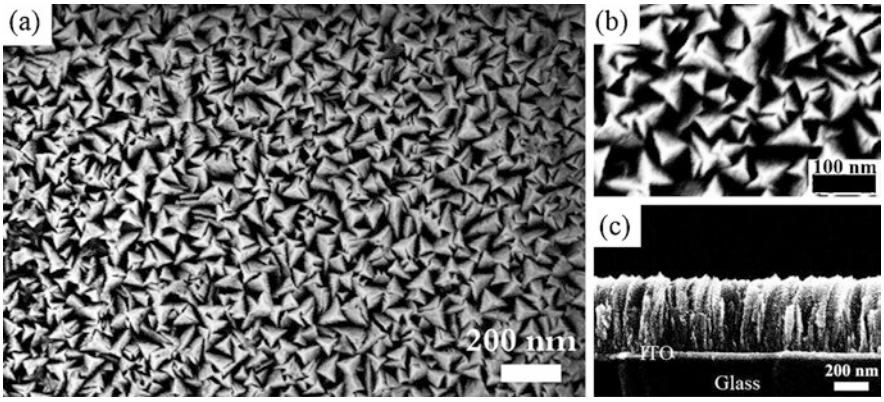

Fig. 9.7 SEM images of NiO thin film. (**a**) and (**b**) are top view at different magnifications, and (**c**) cross-sectional view of the film on an ITO-coated glass substrate (Wen et al. 2014)

shows an example of an XRD spectrum for polycrystalline NiO measured from Siemens D5000 diffractometer.

9.3.1.3 Surface and Cross-Sectional Morphology by Scanning Electron Microscopy

The scanning electron microscope (SEM) which uses electrons that are reflected or knocked off the near-surface region of a sample to create an image. Various signals are giving off when the electrons interact with the atoms on the surface of sample that contain information about the surface topography and composition of the sample. Figure 9.7 shows SEM image of a ~ 500 nm thick NiO film deposited on ITO-coated glass substrate. One can deduce that the film featured triangular morphology

with linear extents of ≤40 nm as shown in panel (a) and (b). The cross-sectional image in panel (c) indicates a columnar nanostructure of the deposited NiO film.

9.3.2 Electrochemical and Optical Characterization

Cyclic voltammetry (CV) test and optical transmittance measurement are usually conducted together to evaluate the CE in Eq. (9.3). Figure 9.8 displays an example of cyclic voltammograms of NiO-based films in KOH electrolyte for the first 15 cycles. Broad oxidation and reduction features are observed, which deduce that some minor evolution takes place during the initial cycles, but the properties are stabilized after a few cycles. Figure 9.9 presents in situ optical transmittance during the CV test as obtained in Fig. 9.8. Information obtained from these two graphical data enable the calculation of CE for this NiO films. The CE was evaluated and found to be 44±2 cm^2/C at wavelength of 550 nm (Wen et al. 2014).

9.4 Spectral Selective Nano Structured Thin Films

Plasmonic electrochromism is the current approach to isolate visible and infrared radiations from solar spectrum via modulated LSPR. Research team led by Milliron is spearheading in this field with notable publications (Garcia et al. 2013; Llordés

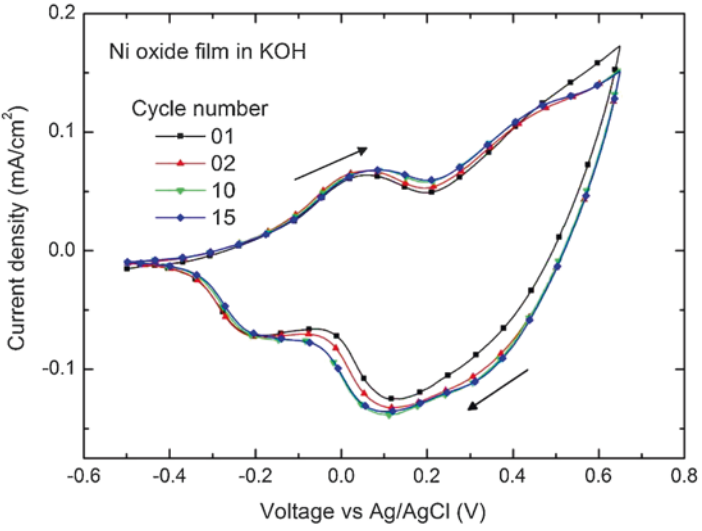

Fig. 9.8 Cyclic voltammograms for a ~ 500 nm thick NiO film in 1 M KOH; the voltage sweep rate was 10 mV/s and arrows indicate sweep direction (Wen et al. 2014)

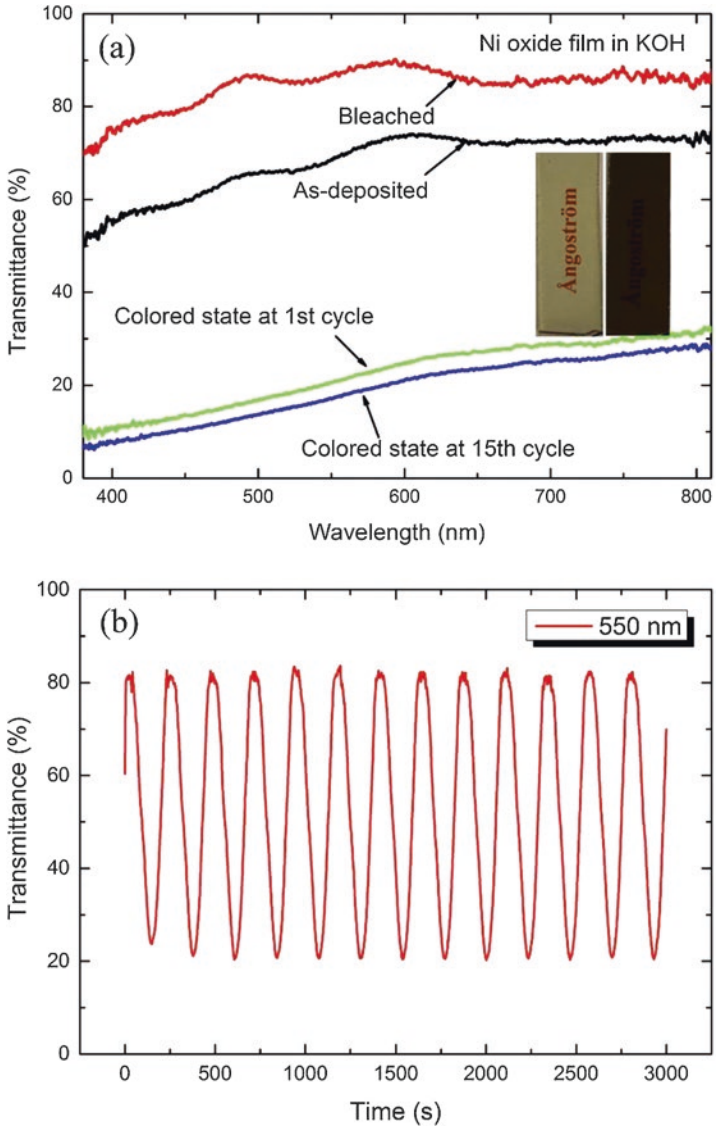

Fig. 9.9 (**a**) Spectra transmittance of a ~ 500 nm thick NiO film in 1 M KOH. Inserted images refer to NiO in fully bleached and coloured states respectively, and (**b**) corresponding optical transmittance modulation at wavelength of 550 nm (Wen et al. 2014)

et al. 2013; Runnerstrom et al. 2014). Figure 9.10 schematically illustrates this concept with two types of nanostructure designs of the EC thin films. As shown in Fig. 9.10 a, the nanocomposite electrolyte consists of polymer hosts and transparent conducting nanoparticles such as ITO, aluminium-doped zin oxide (AZO), and lanthanum hexaboride (LaB_6) (Bayrak Pehlivan et al. 2012). Electrochemical changes

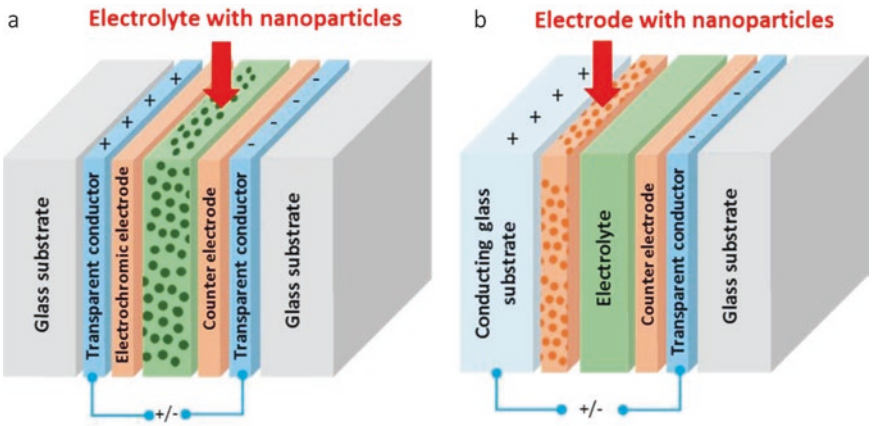

Fig. 9.10 (**a**) Structure of nanocomposite electrolyte with nanoparticles, and (**b**) ITO nanocrystal-NbO_x film (deposited ion a conducting glass substrate) as the working electrode in an EC structure (J. (Jialiang) Wang and Shi 2017)

under different electrical potential, which alter the LSPR absorption level and in turn the electron density. This alteration enables modulation of solar infrared absorption with minor effects on the visible region. In Fig. 9.10 b, development of the electrode based on deposition of ITO nanocrystals on niobium oxide (NbO_x) glass presents another approach (Llordés et al. 2013; Kim et al. 2015). Both ITO nanocrystals and NbO_x glass matrix exhibit distinctly different spectral EC responses, therefore each may independently yield modulation in the NIR (ITO nanocrystals) and visible region (NbO_x) (Llordés et al. 2013).

9.5 Other Implementation of Electrochromic Thin Films

In this work, we mainly talked about electrochromic oxides incorporate in smart windows and their sole purpose in filtering lights. However, researchers have come up with creative ideas by integrating electrochromism with other usability, such as energy storage (Yang et al. 2016). Moreover, the demand of bezel-less phone screen has pushed the smartphone manufacturers in developing new technology to hide the front cameras and sensors beneath the display, without compromising the display quality nor the camera capability (Byford 2019; Gartenberg 2019). Figure 9.11 showcase the working principle of under-display camera technology by Xiaomi. Judging from the illustration, we can conclude that it is a variant of EC devices because of the cathode and anode layers. The cameras and sensors beneath the display stay hidden until the user activates the front-facing camera as shown in the demo (Porter 2019).

Nonetheless, it is important to note that other than electrochromism, alternative materials that exhibit photochromism or thermochromism can also be used to

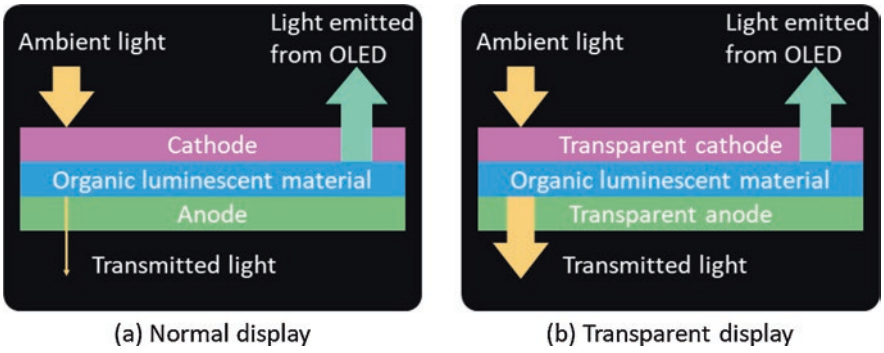

Fig. 9.11 (**a**) Normal display when front camera is inactive, and (**b**) Transparent display when front camera is active from "transparent display-in-a-display" for under-display camera technology by Xiaomi Corp (Gartenberg 2019)

fabricate smart windows. For example, perovskites are materials made of mix elements with a particular crystalline structure and they can be made into solar cells. By changing the perovskites' elemental components, their optical properties such as transparency can be altered. Researchers have successfully created modified perovskite solar window that combine all these features (Wheeler et al. 2017; Lin et al. 2018). For example, a lead-based perovskite solar window that switched from transparent to opaque when the temperature hit 60 °C while converting solar energy to electricity at the same time (Wheeler et al. 2017).

9.6 Conclusion

Electrochromism is one of the "green" nanotechnologies which are of large current interest (Smith and Granqvist 2011). The potential of saving energy from building sector by replacing conventional glass windows with EC smart windows is unmeasurable. This is the greatest importance for combating global warming as discussed in the beginning of this chapter. Smart windows also increased the aesthetics and comforts of modern buildings. Although tremendous research works have put into smart windows, the applicability is still far from large scale implementation. The major impediments for the installation of large-area EC windows remain fabrication cost and extended lifetime. One purposed solution is development of flexible EC devices that offer "retrofit installation" on existing glass windows to reduce overall cost. Finally, further researches on this field are necessary to realize this technology into every building and bring the concept of energy-efficient smart windows closer.

References

Avendaño E, Azens A, Niklasson GA, Granqvist CG (2005) Proton diffusion and electrochromism in hydrated NiO y and Ni1−x V x O y thin films. J Electrochem Soc 152(12):F203. https://doi.org/10.1149/1.2077308

Avendaño E, Rensmo H, Azens A, Sandell A, G. de M. Azevedo, Siegbahn H, Niklasson GA, Granqvist CG (2009) Coloration mechanism in proton-intercalated electrochromic hydrated NiO y and Ni1−x V x O y thin films. J Electrochem Soc 156(8):P132. https://doi.org/10.1149/1.3148327

Bayrak Pehlivan I, Runnerstrom EL, Li SY, Niklasson GA, Milliron DJ, Granqvist CG (2012) A polymer electrolyte with high luminous transmittance and low solar throughput: Polyethyleneimine-Lithium Bis(Trifluoromethylsulfonyl) imide with in 2O 3:Sn Nanocrystals. Appl Phys Lett 100(24):1–5. https://doi.org/10.1063/1.4728994

Byford S (2019) Oppo Unveils the World's First under-Screen Selfie Camera - The Verge. https://www.theverge.com/2019/6/26/18759380/under-display-selfie-camera-first-oppo-announcement

Chernova NA, Roppolo M, Dillon AC, Stanley Whittingham M (2009) Layered vanadium and molybdenum oxides: batteries and electrochromics. J Mater Chem 19(17):2526. https://doi.org/10.1039/b819629j

Chuang M (2010) ITO films prepared by long-throw magnetron sputtering without oxygen partial pressure. J Mater Sci Technol 26(7):577–583. https://doi.org/10.1016/S1005-0302(10)60088-6

Cullity BD, Stock SR (2001) Elements of X-ray diffraction, 3rd edn. Prentice Hall, Upper Saddle River NJ. https://www.worldcat.org/title/elements-of-x-ray-diffraction/oclc/46437243

Deb SK (2008) Opportunities and challenges in science and technology of WO3 for electrochromic and related applications. Sol Energy Mater Sol Cells 92(2):245–258. https://doi.org/10.1016/J.SOLMAT.2007.01.026

Drbohlavova J, Adam V, Kizek R, Hubalek J (2009) Quantum dots - characterization, preparation and usage in biological systems. Int J Mol Sci 10(2):656–673. https://doi.org/10.3390/ijms10020656

Estrada W, Andersson AM, Granqvist CG (1988) Electrochromic nickel-oxide-based coatings made by reactive dc magnetron sputtering: preparation and optical properties. J Appl Phys 64(7):3678–3683. https://doi.org/10.1063/1.341410

Garcia G, Buonsanti R, Llordes A, Runnerstrom EL, Bergerud A, Milliron DJ (2013) Near-infrared spectrally selective plasmonic electrochromic thin films. Adv Opt Mater 1(3):215–220. https://doi.org/10.1002/adom.201200051

Gartenberg C (2019) Xiaomi Explains More about How Its Under-Screen Camera Actually Works - The Verge. https://www.theverge.com/circuitbreaker/2019/6/5/18654365/xiaomi-camera-under-screen-no-notch-transparent-display-technology

Gillaspie DT, Tenent RC, Dillon AC (2010) Metal-oxide films for electrochromic applications: present technology and future directions. J Mater Chem 20(43):9585–9592. https://doi.org/10.1039/c0jm00604a

Girotto EM, Marco-A. Paoli (1999) Flexible electrochromic windows: a comparison using liquid and solid electrolytes. J Braz Chem Soc 10(5):394–400. https://doi.org/10.1590/S0103-50531999000500010

Goldner RB, Haas TE, Arntz FO, Slaven S, Wong KK, Wilkens B, Shepard C, Lanford W (1993) Nuclear reaction analysis profiling as direct evidence for Lithium ion mass transport in thin film "'rocking-chair'" structures. Appl Phys Lett 62(14):1699–1701. https://doi.org/10.1063/1.109580

Granqvist CG (1995) Handbook of inorganic electrochromic materials. Elsevier. https://doi.org/10.1016/B978-0-444-89930-9.X5000-4

Granqvist CG (2000) Electrochromic tungsten oxide films: review of progress 1993–1998. Sol Energy Mater Sol Cells 60(3):201–262. https://doi.org/10.1016/S0927-0248(99)00088-4

Granqvist CG (2014) Electrochromics for smart windows: oxide-based thin films and devices. Thin Solid Films 564:1–38. https://doi.org/10.1016/j.tsf.2014.02.002

Houghton JT, Jenkins GJ, Ephraums JJ (1990) Climate Change The IPCC Scientific Assessment. http://repositorio.cenpat-conicet.gob.ar:8081/xmlui/bitstream/handle/123456789/497/climateChange.pdf?sequence=1

Huovila P (2007) Management of Environmental Quality: An International Journal Buildings and Climate Change: Status, Challenges and Opportunities. United Nations Environment Programme. https://books.google.co.kr/books/about/Buildings_and_Climate_Change.html?id=-1gab8igWgcC&printsec=frontcover&source=kp_read_button&redir_esc=y#v=onepage&q&f=false

Kim H, Gilmore CM, Piqué A, Horwitz JS, Mattoussi H, Murata H, Kafafi ZH, Chrisey DB (1999) Electrical, optical, and structural properties of indium–tin–oxide thin films for organic light-emitting devices. J Appl Phys 86(11):6451–6461. https://doi.org/10.1063/1.371708

Kim J, Ong GK, Yang W, Leblanc G, Williams TE, Mattox TM, Helms BA, Milliron DJ (2015) Nanocomposite architecture for rapid, spectrally-selective electrochromic modulation of solar transmittance. Nano Lett 15(8):5574–5579. https://doi.org/10.1021/acs.nanolett.5b02197

Lin J, Lai M, Dou L, Kley CS, Chen H, Peng F, Sun J, Lu D, Hawks SA, Xie C, Fan C, Paul Alivisatos A, Limmer DT, Yang P (2018) Thermochromic halide perovskite solar cells. Nat Mater 17(3):261–267. https://doi.org/10.1038/s41563-017-0006-0

Litvin AP, Cherevkov SA, Dubavik A, Babaev AA, Parfenov PS, Simões Gamboa AL, Fedorov AV, Baranov AV (2018) Thin layer of semiconductor plasmonic nanocrystals for the enhancement of NIR fluorophores. J Phys Chem C 122(35):20469–20475. https://doi.org/10.1021/acs.jpcc.8b06059

Llordés A, Garcia G, Gazquez J, Milliron DJ (2013) Tunable near-infrared and visible-light transmittance in nanocrystal-in-glass composites. Nature 500(7462):323–326. https://doi.org/10.1038/nature12398

Marszalek KW, Swatowska B, Sobkow Z (2012) Ionic Conductor for Electrochromic Devices. (January). https://doi.org/10.13140/2.1.3705.2488

Minami T (2013) 88 semiconductors and semimetals transparent conductive oxides for transparent electrode applications, 1st edn. Elsevier Inc. https://doi.org/10.1016/B978-0-12-396489-2.00005-9

Mortimer RJ (2011) Electrochromic materials. Annu Rev Mater Res 41(1):241–268. https://doi.org/10.1146/annurev-matsci-062910-100344

Niklasson GA, Granqvist CG (2007) Electrochromics for smart windows: thin films of tungsten oxide and nickel oxide, and devices based on these. J Mater Chem 17(2):127–156. https://doi.org/10.1039/b612174h

Pastoriza-Santos I, Kinnear C, Pérez-Juste J, Mulvaney P, Liz-Marzán LM (2018) Plasmonic polymer nanocomposites. Nat Rev Mater 3(10):375–391. https://doi.org/10.1038/s41578-018-0050-7

Porter J (2019) Xiaomi Hits Back at Oppo with an "under-Display" Camera of Its Own - The Verge. https://www.theverge.com/2019/6/3/18650166/xiaomi-under-display-selfie-camera-weibo-teaser-mi-9-notch-hole-punch

Ren Y, Chim WK, Guo L, Tanoto H, Pan J, Chiam SY (2013) The coloration and degradation mechanisms of electrochromic nickel oxide. Sol Energy Mater Sol Cells 116:83–88. https://doi.org/10.1016/J.SOLMAT.2013.03.042

Richter B, Goldston D, Crabtree G, Glicksman L, Goldstein D, Greene D, Kammen D, Levine M, Lubell M, Savitz M, Sperling D, Schlachter F, Scofield J, Dawson J (2008) How America can look within to achieve energy security and reduce global warming. Rev Mod Phys 80(4). S1–109. https://doi.org/10.1103/RevModPhys.80.S1

Runnerstrom EL, Llordés A, Lounis SD, Milliron DJ (2014) Nanostructured Electrochromic smart windows: traditional materials and NIR-selective plasmonic nanocrystals. Chem Commun 50(73):10555–10572. https://doi.org/10.1039/c4cc03109a

Sims REH, Rogner HH, Gregory K (2003) Carbon emission and mitigation cost comparisons between fossil fuel, nuclear and renewable energy resources for electricity generation. Energy Policy 31(13):1315–1326. https://doi.org/10.1016/S0301-4215(02)00192-1

Smith GB, Granqvist CG (2011) Green nanotechnology : solutions for sustainability and energy in the built environment. CRC Press. https://www.crcpress.com/Green-Nanotechnology-Solutions-for-Sustainability-and-Energy-in-the-Built/Smith-Granqvist/p/book/9781420085327

Thakur VK, Ding G, Ma J, Lee PS, Lu X (2012) Hybrid materials and polymer electrolytes for electrochromic device applications. Adv Mater 24(30):4071–4096. https://doi.org/10.1002/adma.201200213

UNDESA (2019) World Population Prospects: Population Division Database. https://population.un.org/wpp/Graphs/Probabilistic/POP/TOT/900

Wang JM, Sun XW, Jiao Z (2010) Application of nanostructures in electrochromic materials and devices: recent Progress. Materials 3(12):5029–5053. https://doi.org/10.3390/ma3125029

Wang, Julian (Jialiang), and Donglu Shi (2017) Spectral selective and Photothermal Nano structured thin films for energy efficient windows. Appl Energy 208(August): 83–96. doi:https://doi.org/10.1016/j.apenergy.2017.10.066

Wen RT, Niklasson GA, Granqvist CG (2014) Electrochromic nickel oxide films and their compatibility with potassium hydroxide and Lithium perchlorate in propylene carbonate: optical, electrochemical and stress-related properties. Thin Solid Films 565:128–135. https://doi.org/10.1016/j.tsf.2014.07.004

Wheeler LM, Moore DT, Ihly R, Stanton NJ, Miller EM, Tenent RC, Blackburn JL, Neale NR (2017) Switchable photovoltaic windows enabled by reversible photothermal complex dissociation from methylammonium lead iodide. Nat Commun 8(1):1722. https://doi.org/10.1038/s41467-017-01842-4

Yang P, Sun P, Mai W (2016) Electrochromic energy storage devices. Mater Today 19(7):394–402. https://doi.org/10.1016/J.MATTOD.2015.11.007

Chapter 10
Graphitic Carbon Nitride/Metal Oxides Nanocomposites and Their Applications in Engineering

Faheem K. Butt, Sami Ullah, Junaid Ahmad, Sajid Ur Rehman, and Zeeshan Tariq

Abbreviations

CTL	Cataluminescence
CV	Cyclic voltammetry
DFT	Density functional theory
DPV	Differential pulse voltammetry
EDLC	Electrochemical double layer capacitor
FESEM	Field emission scanning electron microscopy
GCE	Glassy carbon electrode
HRTEM	High resolution transmission electron microscopy
LIBs	Lithium ion batteries
MB	Methylene Blue
MO	Metal Oxide
OER	Oxygen evolution reaction
ORR	Oxygen reduction reaction
PEC	Photoelectrocatalysis
PL	Photoluminescence
SAED	Selected area electron diffraction
SEI	Solid electrolyte interface
SEM	Scanning electron microscopy
TEM	Transmission electron microscopy
VLD	Visible light driven

F. K. Butt (✉) · S. Ullah · J. Ahmad
Department of Physics, Division of Science and Technology,
University of Education Lahore, Pakistan
e-mail: faheemk.butt@ue.edu.pk

S. U. Rehman · Z. Tariq
State Key Laboratory on Integrated Optoelectronics, Institute of Semiconductors,
Chinese Academy of Sciences, Beijing, China

S. Siddiquee et al. (eds.), *Composite Materials: Applications in Engineering, Biomedicine and Food Science*, https://doi.org/10.1007/978-3-030-45489-0_10

XPS X-ray photoelectron spectroscopy
XRD X-ray diffraction

10.1 Introduction

In the upcoming era of nanotechnology, there is a need to engineer nanocomposites in order to overcome two major concerns to mankind. First is environmental pollution and the second is energy shortage. Due to global warming and energy crises, researchers are trying to find out green, viable and proficient energy-conversion techniques to replace unsustainable energy sources i.e. fossil fuels. So, there is urgent need to introduce green, feasible, novel, and sustainable energy resources. In this regard, engineering of nanomaterials is one of the most critical areas of research in recent decade.

g-C_3N_4 is a fascinating 2D layered polymeric indirect bandgap semiconductor having high thermal as well as physiochemical stability. It holds a unique electronic structure and abundance on earth. Besides all this, it is a non-toxic and metal-free synthetic polymer which works like a visible-light-driven (VLD) photocatalyst. Moreover, it consists of only non-metal constituents, such as carbon, nitrogen, and some content of hydrogen that are earth abundant. Notably, the g-C_3N_4 possesses multifarious applications i.e. photocatalytic hydrogen production, organic pollutant decontamination from water, sensing, bio-imaging and energy conversion etc. (Wang et al. 2009, Gao et al. 2015, Hou et al. 2016). Figure 10.1 shows extraordinary characteristics and multifarious applications of g-C_3N_4.

10.1.1 Historical Backdrop and Structure of g-C_3N_4

History of C_3N_4 goes back to 1834 when scientist named Berzelius synthesized tris-triazine based linear polymer and was alluded to as "melon" by another scientist named Liebig (Wang et al. 2015b). For more than 1.5 century, scientific study on such material remained inactive up to 1989, when M. L. Cohen and A. Y. Liu predicted an ultra-hard covalent compound β-C_3N_4 having resemblance to β-Si_3N_4 (Liebig 1834). Franklin was first to portray the closer insights into these structures and familiarize the concept of C_3N_4 "carbonic nitride" in 1922. He proclaimed that C_3N_4 may be attained like the ultimate product of deammoniation of the series of ammono-carbonic acids (Franklin 1922). Inspired from a theoretical prediction about ultra-hardness (more than diamond) property of this material, Liu and Cohen successfully prepared β-C_3N_4 by using pulsed laser ablation in 1993. Moreover, β-C_3N_4 presented marvelous hardness, improved Si and Ni substrate's adhesion and great thermal stability (Liu and Cohen 1989). There exist many allotropic forms of C_3N_4 i.e. α-C_3N_4, β-C_3N_4, π-C_3N_4, pseudocubic C_3N_4, g-C_3N_4 having bandgaps of 5.5, 4.85, 4.3, 4.13, and 2.7 eV respectively (Niu and Lu 1993, Semencha and

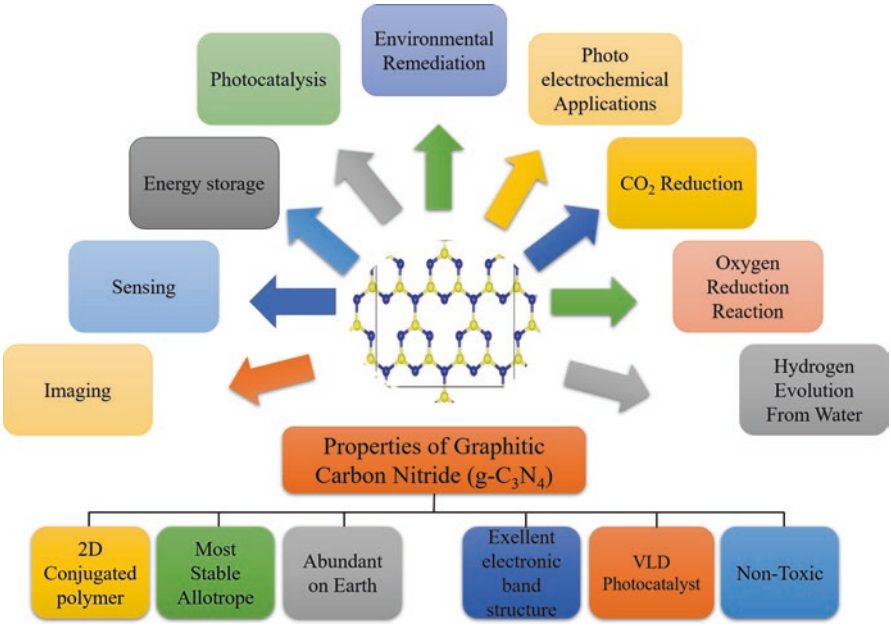

Fig. 10.1 Illustrating the noticeable properties and multifarious applications of g-C_3N_4

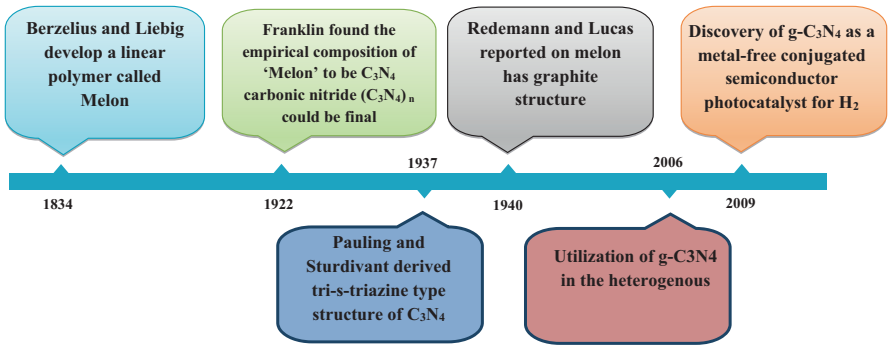

Fig. 10.2 Presenting the historical backdrop of graphitic carbon nitride (g-C_3N_4)

Blinov 2010). However, g-C_3N_4 is relatively more stable. The timeline development and history of carbon nitride is presented in Fig. 10.2.

The g-C_3N_4 exhibits yellow-colored polymers in powder form with exceptional physiochemical characteristics that can be prepared easily by thermal treatment of inexpensive feedstocks like melamine, thiourea, urea, cyanamide or dicyandiamide as shown in Fig. 10.3a (Dong et al. 2014, Kumar et al. 2014, Wang et al. 2015a, Mamba and Mishra 2016). Its electronic band structure and photocatalytic

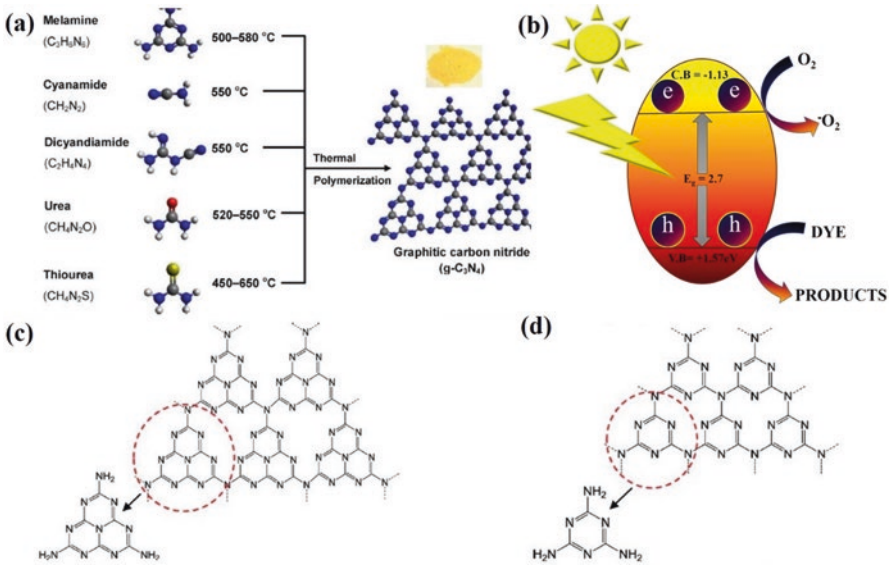

Fig. 10.3 **(a)** Diagrammatic depiction of the preparation routes (thermal polymerization) of g-C_3N_4. The white, red, black, yellow and blue spheres represent H, O, C, S and N atoms, respectively. Inset shows bulk g-C_3N_4 and **(b)** shows its charge transfer mechanism. **(c)** Illustrating the tri-s-triazine (heptazine) and **(d)** represents the triazine g-C_3N_4 structures. "(a) Reprinted with permission from ref. (Ong et al. 2016). Copyright 2016, American Chemical Society. (c and d) Reprinted with permission from ref. (Wang et al. 2012). Copyright 2012, American Chemical Society"

degradation mechanism is shown in Fig. 10.3b. It is usually accepted that condensed tri-s-triazine (C_6N_7 in Fig. 10.3c) is the primary subunit in the g-C_3N_4 formation. This type of possible structure is energetically favorable and more stable than another suggested s-triazine unit (C_3N_3 in Fig. 10.3d). g-C_3N_4 is stable (thermally) in air up to 600 °C because of aromatic C-N heterocycles. Moreover, in acidic, alkali or organic solvents, g-C_3N_4 cannot be dissolved that makes it an auspicious chemically stable robust material.

10.2 Motivation Behind the Composites

Immediate electron-hole (e^--h^+) pair recombination is generated by photon. Less ability to utilize visible spectrum of light effectively, large contact resistance, and low conductivity along with having small surface area of pure carbon nitride limits its photocatalytic efficiency. Because of the inimitable electronic structure with mild bandgap (2.7 eV), g-C_3N_4 is a promising nominee to make nanocomposites by combining with several functional materials in order to improve charge separation and to boost its performance.

10.3 Types of Composites

10.3.1 Carbon/g-C_3N_4 Composites

There are two significant reasons to introduce carbon into g-C_3N_4 (CN) framework: first is enhancement in electrical conductivity (which is due to the presence of delocalized π-bonds in the carbons that greatly improves the transfer of electrons) and second is the absorption enhancement in visible light spectrum due to narrow bandgap.

Dong et al. (2012) used the first-principles DFT calculations to show that the conductivity of g-C_3N_4 boosted by substitution of bridging nitrogen atoms with carbon atoms. This was due to delocalized π-bonds (giant) formation between the replaced hexatomic rings and C- atoms. Moreover, enhancement in visible light absorption takes place by C-doping in C-self-doped g-C_3N_4 as band-gap narrows. Therefore, they also prepared C-self-doped g-C_3N_4 via pretreatment of melamine with absolute ethanol. Obtained C-self-doped g-C_3N_4 exhibited boosted electrical conductivity, enhanced surface area and improved visible light absorption. Consequently, it shows an improved photocatalytic behavior. The obtained results were in agreement with the theoretical calculations (Dong et al. 2012). Ma et al. (2014) have reported the synthesis of efficient catalysts (O_2 evolution). They synthesized it via carbon nanotubes and g-C_3N_4 nanosheets (g-C_3N_4 NS–CNT) to form porous composites. Because of high content of nitrogen gas and excellent transformation of charge and mass, the highest oxygen evolution reaction (OER) activity was observed by the porous three-dimensional nanostructure among non-metal catalysts. Moreover, their results showed that g-C_3N_4@NS–CNT material was more durable and efficient than noble-metal catalysts (Ma et al. 2014).

Ma et al. (2017) used chemical solution process to synthesize core-shell of carbon sphere with g-C_3N_4 owing to the dual (polymerization-depolymerization) nature of g-C_3N_4 (Fig. 10.4(a, b)). Smooth surface display of homogeneously distributed uniform carbon spheres is shown in Fig. 10.4(c). The uniform dispersion of carbon spheres in the g-C_3N_4 gel is displayed in Fig. 10.4(d). The core-shell of carbon@g-C_3N_4 structure is achieved after calcinations of the carbon-protonated g-C_3N_4 (Fig. 10.4(e,f)). The nanospheres having diameter of about 200 nm is displayed by TEM Fig. 10.4g. About 3 nm thick layer of g-C_3N_4 was distinguished from core-shell structured carbon@g-C_3N_4 (Fig. 10.4h), which clearly verify the core-shell structures. The carbon@g-C_3N_4 is considered highly efficient metal-free VLD photocatalyst that can be used for large scale synthesis purpose. This material possesses expanded reachable surface area, boosted photocatalytic activity and improved charge separation (Ma et al. 2017).

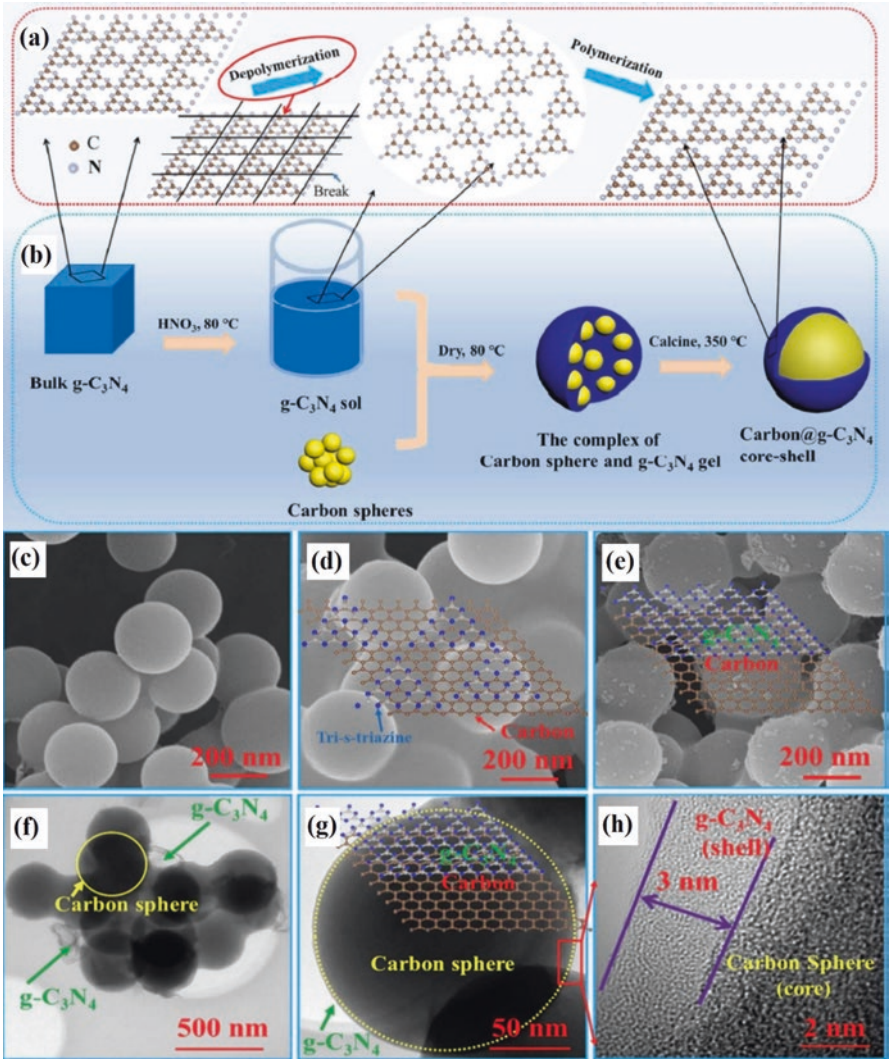

Fig. 10.4 Depolymerization-repolymerization mechanism for g-C_3N_4 **(a)**, carbon@g-C_3N_4 preparation (**b**). Spheres of carbon, carbon spheres complexes and gel, core-shell based C@g-C_3N_4 photocatalyst SEM images **(c, d, e respectively)**, TEM images **(f, g)** and (**h**) HR-TEM Image of core-shell catalyst based on C@g-C_3N_4. "Reprinted with permission from ref. (Ma et al. 2017). Copyright 2017, American Chemical Society"

10.3.2 Metals/g-C_3N_4 Composites

To increase chemical productivity of g-C_3N_4, which is limited by fast e^- and -h^+ recombination, different expensive noble metals including Pt, Au, Pd, Ag or Rh have be used as co-catalyst. Typically, these co-catalysts prevent recombination of

charge by acting as electrons traps which results the enhanced photocatalytic efficiency. However, their practical applications are restricted owing to their high cost.

Different methods such as photodeposition, reduction or impregnation methods are used to load Platinum (Pt) over g-C_3N_4 surface. e.g. Chen and co-workers used photo-deposition method in order to prepare g-C_3N_4 doped with Pt. They used H_2PtCl_4 and g-C_3N_4 as precursors (Chen et al. 2009). Zeng et al. (2005) have worked on the Pt catalyst preparation supported on C_3N_4 nanotubes via borohydride reduction method. Yu et al. (2014) successfully synthesized the Pt doped g-C_3N_4 nanocomposites, which showed the good performance for solar light photocatalysts for CO_2 reduction. g-C_3N_4 was prepared by thiourea thermolysis at 550 °C, after that Pt was deposited on g-C_3N_4 to make these nanocomposites. The nanoparticles (NPs) of Pt behaved like an efficient co-catalyst that greatly affected the product generation selectivity. In this way, photoactivity of g-C_3N_4 was improved. Their work not only indicated the selectivity and photoactivity of g-C_3N_4 for reduction of CO_2 due to incorporation of Pt NPs but also showed that CO_2 changed easily into hydrocarbon solar fuels (precious) i.e., HCHO, CH_3OH and CH_4 at ambient temperature and pressure (Yu et al. 2014).

Zhang et al. (2014) adopted photo-deposition method in order to prepare Rh-g-C_3N_4. They prepared controlled size Rh nanoparticles (4–9 nm) by using a caping agent such as polyvinyl pyrrolidone (PVP). Their results indicated that as prepared composite was found active for water splitting (photocatalytic) under visible light (Zhang et al. 2014). (Navlani-García et al. 2018) stated the construction of Ru/C/g-C_3N_4 through the standard impregnation method. In Fig. 10.5, TEM micrographs and their respective histograms of as-prepared catalysts are shown. Their results indicated that resulting samples are endowed with excellent stabilization of Ru nanoparticles. So, as prepared photocatalysts showed excellent catalytic results in the dehydrogenation chemical reaction of ammonia borane (Navlani-García et al. 2018).

Samanta et al. (2014) used deposition-participation method in order to prepare Au–g-C_3N_4. They used $HAuCl_4$, urea solution and g-C_3N_4 powder as precursors. Their results show that developed semiconductor material showed improved hydrogen production photocatalytic performance under visible light (Samanta et al. 2014).

Chang et al. (2014) adopted a simple citrate-reduction technique to synthesize Au–g-C_3N_4 nanocomposites. They used precursors like sodium citrate solution, g-C_3N_4 and $HAuCl_4$ in their work. Their results showed that as-prepared nanocomposites are efficient nominee for photoelectro-oxidation of small organic molecules and formic acid, as they are carbon-monoxide (CO) poisoning free, increase the oxidation current, and lowers the potential of oxidation (Chang et al. 2014).

Chang et al. (2013) reported the synthesis of polymer based on mesoporous graphitic carbon nitride modified with Pd (Pd/ mpg-C_3N_4). They got this polymer by strong magnetic stirring of the mixture of $PdCl_2$ solution in equal amount of mpg-C_3N_4. Potassium boron hydride (KBH_4) was added in the reaction mixture simultaneously. They have used the as-prepared polymer for the bisphenol A (BPA) decontamination. Moreover, it showed enhanced photocatalytic activity due to doping of Pd (Chang et al. 2013).

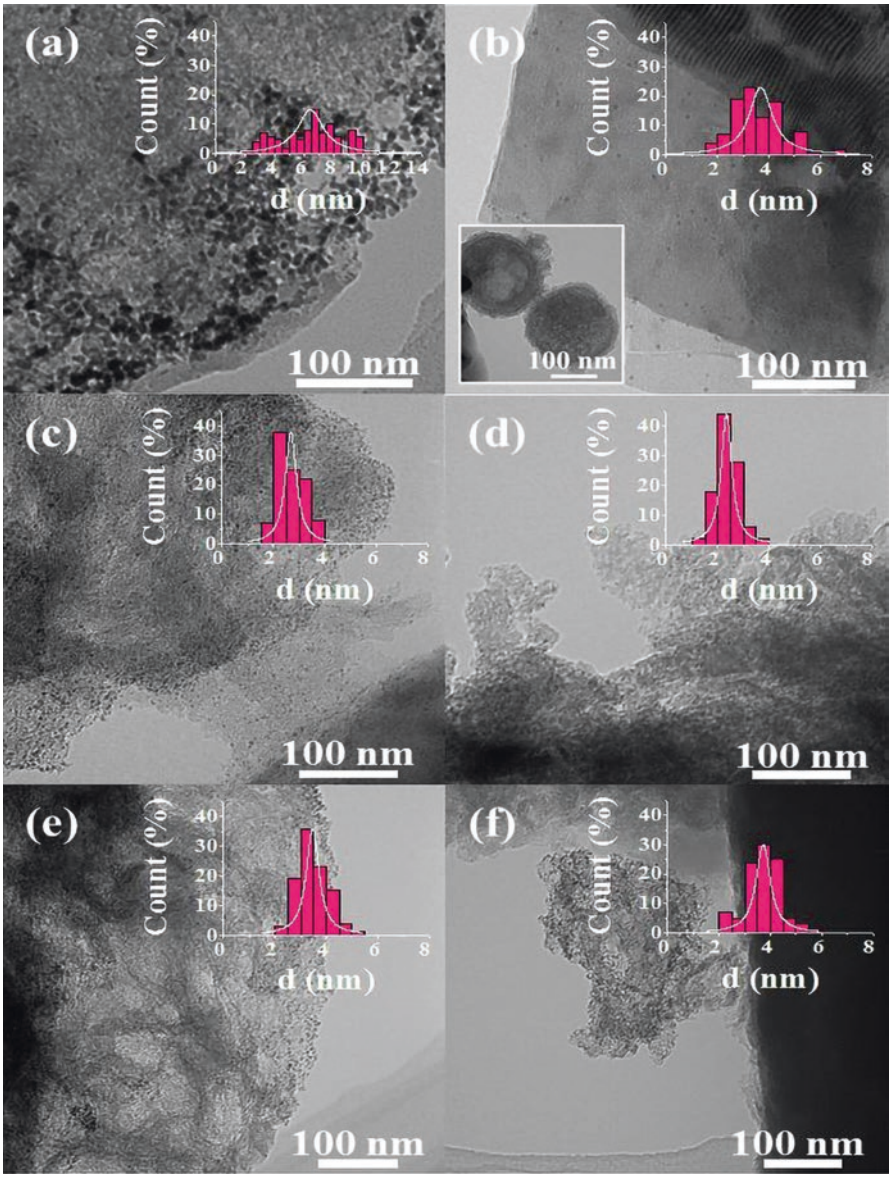

Fig. 10.5 TEM micro-graphs with the relevant distribution histogram (NP size) of Ru/g-C_3N_4 **(a)**, C(0.1) Ru/ g-C_3N_4 **(b)**, C(0.5)Ru/ g-C_3N_4 **(c)**, C(1.0)Ru/ g-C_3N_4 **(d)**, C(2.0) Ru/ g-C_3N_4 **(e)** and C(4.0) Ru/ g-C_3N_4 **(f)**. "Reprinted with permission from ref. (Navlani-García et al. 2018). Copyright 2017, Elsevier"

10.3.3 Metal Oxides/g-C_3N_4 Composites

This section focuses on coupling of different metal-oxides namely TiO_2, ZnO, WO_3, CuO, Fe_2O_3, MnO_2, NiO, etc. with g-C_3N_4 to make nanocomposites. Before opening the discussion on metal oxide/g-C_3N_4 composites, we first introduce two main types of heterojunctions that are mostly possessed by g-C_3N_4-based nanocomposites: (1) Type II heterojunction and (2) Z-scheme heterojunction system. These two systems of heterojunction have shown exceptional results for a cornucopia of CO_2 conversion for energy-bearing fuels, water splitting to H_2 and O_2, bacteria disinfection and pollutant decontamination. Therefore, the engineering of heterostructured composites based on g-C_3N_4 at distinct nanoscales will indubitably enrich the VLD photocatalysts family in a more rational way.

In a typical heterojunction of type-II, conduction-band and valence-band are higher for semiconductor A (SC A) as compared to semiconductor B (SC B). This can be seen in Fig. 10.6(a). Consequently, under the light irradiation, the photogenerated e^-'s will flow from CB of SC 'A' towards CB of SC 'B' due to the alignment of band. In the meantime, the photogenerated h^+'s from the VB of SC 'B' moves to VB of SC 'A'. Whereas, photogenerated e^-'s and h^+'s correspondingly a mass on SC 'B' and SC 'A'. So, e^-'s and h^+'s spatial separation can be achieved for increasing the photocatalytic activity with a photocatalyst having heterojunction of type-II. But there are some apparent issues that hamper the widespread application of photocatalysts with heterojunction of type-II. Such as, oxidation and reduction reactions in photocatalysts with heterojunction of type-II system, respectively, arise for SC 'A' with a low oxidation potential and SC 'B' with a low reduction potential.

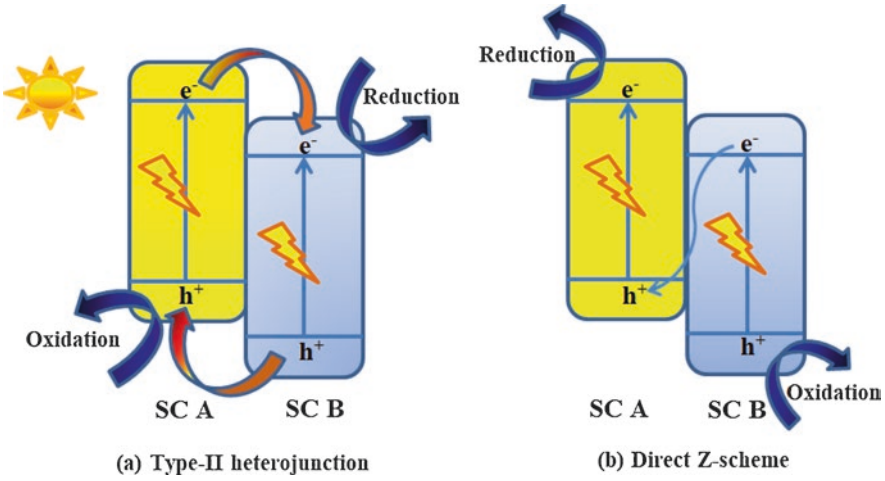

Fig. 10.6 Mechanism of charge migration and separation by two types of heterojunction systems; **(a)** Type-II and **(b)** Z-scheme (direct) constructed on two distinct semiconductors (SCs). "Reprinted with permission from ref. (Low et al. 2017). Copyright 2017, Elsevier"

Consequently, there will be great reduction in redox ability of photocatalysts with heterojunction of type-II system. Furthermore, hole–hole or due to electron–electron electrostatic repulsion, it is hard for e^-'s in SC 'A' and h^+'s in SC 'B' to respectively transfer to the electron-rich conduction band of SC 'B' and the hole-rich valence band of SC 'A'. So, there is need to develop photocatalytic systems with novel heterostructure to overwhelmed these issues (Low et al. 2017).

Specifically, a Z-scheme (direct) photocatalyst's structure is analogous to type-II heterojunction photocatalyst (Fig. 10.6). Nonetheless it has a slightly different charge-carrier transfer mechanism. In particular, the charge-carrier transfer pathway of a typical direct Z-scheme is similar to the alphabet "Z" (Fig. 10.6b). During photocatalysis, photogenerated e^-'s in SC 'B', with minor reduction capacity, recombine with photogenerated h^+'s in SC 'A' with minor oxidation capacity (Fig. 10.6b). Hence, photogenerated e^-'s in SC 'A' having high reduction ability can be maintained with photogenerated h^+'s in SC 'B' having high oxidation capacity. Consequently, it is possible to optimize the redox capacity of the Z-scheme (direct) photocatalyst. Moreover, for the direct Z-scheme photocatalyst charge-carrier migration should be more feasible physically as-compared to that of the photocatalysts with type-II heterojunction system. It is due to e^--h^+ electrostatic attraction that makes it more favorable to transfer photogenerated e^-'s from the conduction band (CB) of SC 'B' to the hole-rich (photogenerated) valence band (VB) of SC 'A' (Low et al. 2017).

Titania (TiO_2) is abundantly occurring metal oxide with bandgap of 3.2 eV acts as a UV-active photocatalyst. Owing to its properties, it is the most appropriate choice to couple with g-C_3N_4. For instance, Zhou et al. (2012) documented the formation of g-C_3N_4/TiO_2 nanotube array heterojunction via a simple electrochemical process, presenting highly effective visible-light performance as compared to both TiO_2 nanotube and bare g-C_3N_4 (Zhou et al. 2012).

In another report, Sridharan et al. (2013) presented the synthesis of g-C_3N_4/TiO_2 via a thermal transformation synthesis route. They used degradation of methylene blue and reduction of harmful Cr (VI) ions to assess the efficiency of the synthesized heterostructure (Sridharan et al. 2013). Yu et al. (2013) stated the process of Z-scheme g-C_3N_4 /TiO_2 heterostructure by means of one-step calcinations technique. For formaldehyde's decomposition in air, the prepared material showed effective photocatalytic response. Mechanism proposed for charge transfer and separation for as-prepared composites is demonstrated in Fig. 10.7. For pure TiO_2, the fast recombination of e^-'s and h^+'s limits the photocatalytic activity. The Z-scheme heterojunction structure is formed when surface of TiO_2 nanoparticles is partially covered by nanoparticles of g-C_3N_4 with an optimal content (U100 sample) Fig. 10.7(a, b). Notably the g-C_3N_4 content should be carefully controlled. When the g-C_3N_4 content surpass a specific amount, the surface of TiO_2 will be entirely sheltered by g-C_3N_4 (U200, U500 samples) as shown in Fig. 10.7c. Consequently, due to the shield effect of g-C_3N_4, the light intensity fall on the surface of TiO_2 particles will reduces. So, the photocatalytic efficiency will reduce due to reduction in photogenerated e^-'s and h^+'s. Moreover, photo-generated e^-'s may transfer to g-C_3N_4

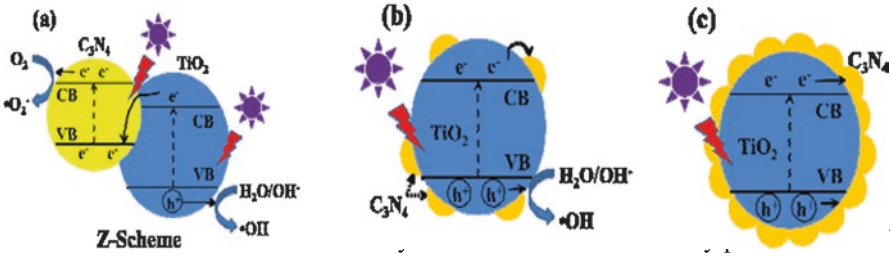

Fig. 10.7 Shows a separation of charges and migration in Z-scheme g-C_3N_4/TiO_2 heterostructure using UV light. "Reprinted with permission from ref. (Yu et al. 2013). Copyright 2013, Royal Society of Chemistry"

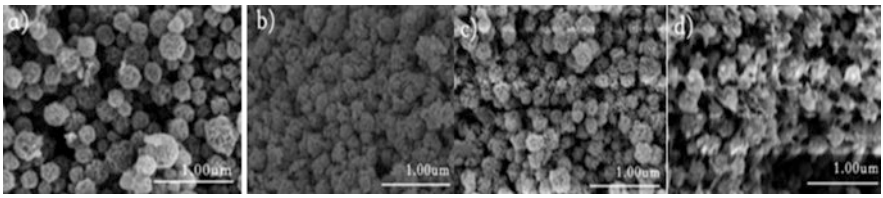

Fig. 10.8 **(a, b, c, d)** are SEM images of pure TiO_2, GCNTO1, GCNTO2 and GCNTO3 respectively. "Reprinted with permission from ref. (Li et al. 2019a). Copyright 2019, American Chemical Society"

FTCN, the as-synthesized material was further investigated to degrade two stable organic colors RhB and MB for small intervals compared to both foamed titanium (FT) and bare g-C_3N_4 (Shakeel et al. 2018).

Li et al. (2019a) used annealing process to synthesize g-C_3N_4@TiO_2 nanostructures with morphology of the hollow sphere, high crystalline quality, elevated surface area, and small grain size. They used TiO_2 hollow sphere and melamine as precursors in order to synthesize nanoheterojunction. SEM images of pure TiO_2 and different samples of g-C_3N_4@TiO_2 nanostructures are shown in Fig. 10.8. The prepared nanostructures showed efficient separation of charges and absorption of visible light which leads to enhanced photocatalytic water splitting activity (466.43 $\mu molg^{-1}\ h^{-1}$) during H_2 generation (Li et al. 2019a).

Besides TiO_2, Zinc oxide is an alternative eminent MO having bandgap approximately 3.2 eV. It is an n-type inorganic semiconductor with low cost, high quantum efficiency, good oxidation potential, environmentally benign property and appreciable photocatalytic activity as compared to TiO_2 towards several pollutants. However, ZnO in pure form shows few deficiencies including poor ability to utilize visible light, photocorrosion and high recombination rates of charge carriers. To enhance its photocatalytic performance, it appears acceptable to hybridize ZnO with g-C_3N_4.

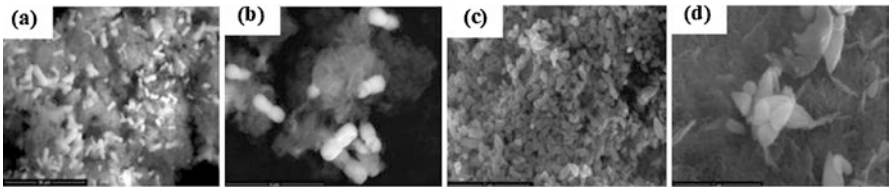

Fig. 10.9 FESEM images (**a** and **b**) of dumbbelled-shape g-C_3N_4/ZnO at low resolution and at high-resolution respectively. (**c** and **d**) FESEM images of cone-shaped g-C_3N_4/ZnO at low and high resolution respectively. "Reprinted with permission from ref. (Fageria et al. 2015). Copyright 2015, Royal Society of Chemistry"

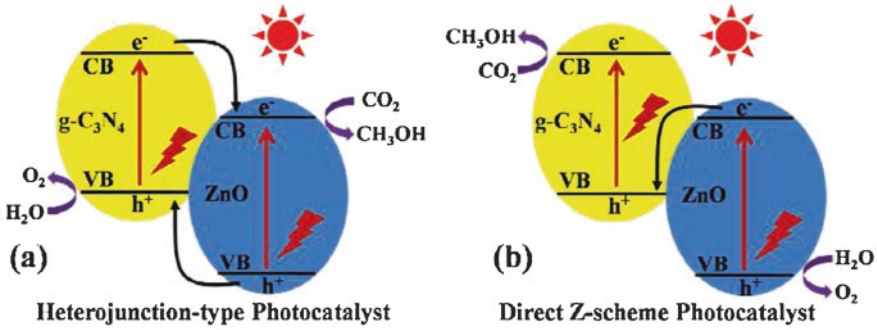

Fig. 10.10 Illustrating the charge two different charge separation mechanisms. **(a)** is conventional heterojunction while **(b)** is Z-scheme mechanism. "Reprinted with permission from ref.(Yu et al. 2015). Copyright 2015, Royal Society of Chemistry"

Under refluxing conditions, cone and dumbbell like shaped g-C_3N_4/ZnO was synthesized via facile wet-chemical approach (Fageria et al. 2015). FESEM images of as-synthesized heterostructures are shown in Fig. 10.9. They used degradation of phenol and MB to assess the photocatalytic capabilities of as-synthesized heterostructures. As compared to g-C_3N_4, boosted photocatalytic performance was shown by both heterostructures in degradation of phenol and MB. Both heterostructures took about 2.3 hours to degrade MB 99%. Dumbbell shaped g-C_3N_4/ZnO took 2.5 hours and cone shaped g-C_3N_4/ZnO took about 2.8 hour to degrade phenol 100%. Dumbbelled shape g-C_3N_4/ZnO showed higher photoactivity due to large surface area (45.35m^2/g) as-compared to conic shape g-C_3N_4/ZnO (23.67 m^2/g) (Fageria et al. 2015).

Yu et al. (2015) prepared g-C_3N_4@ZnO composite by one-step calcination technique. This direct Z-scheme heterostructure composite showed better photocatalytic performance for the reduction of CO_2 as related to both its components. They proposed that Z-scheme (direct) mechanism is responsible for boosted photoactivity performance. The difference between heterojunction of type-II and Z-scheme (direct) photocatalysts is shown in Fig. 10.10 (Yu et al. 2015).

Apart from UV-active titania (TiO_2) and zinc oxide (ZnO), 2D tungsten trioxide (WO_3) have attracted considerable interest because of its narrow bandgap (2.6–2.8 eV), resilience to photocorrosion and non-toxicity. Owing to these properties it is suitable material to use in solar applications. But its efficacy is hindered because of prompt recombination rate of charge carriers due to its lower conduction band (CB) edge potential. So, as to improve its photocatalytic performance, it is recommended to make couple with another semiconductor material. In this regard, coupling it with g-C_3N_4 is most promising technique (Yan et al. 2016, Chen et al. 2019).

WO_3/g-C_3N_4 composite was firstly synthesized by a quite simple calcination technique (Huang et al. 2013). Using visible light, they evaluated the photocatalytic performance of these composites and obtained better results for degradation of MB dye as compared to pristine graphitic carbon nitride. The boosted performance was attributed to synergistic effect due to both components and the fabrication of type-II heterojunction. Migration of photo-generated e^- s from g-C_3N_4 to tungsten oxide (WO_3) took place whereas the h^+ s was transferred from tungsten oxide (WO_3) to

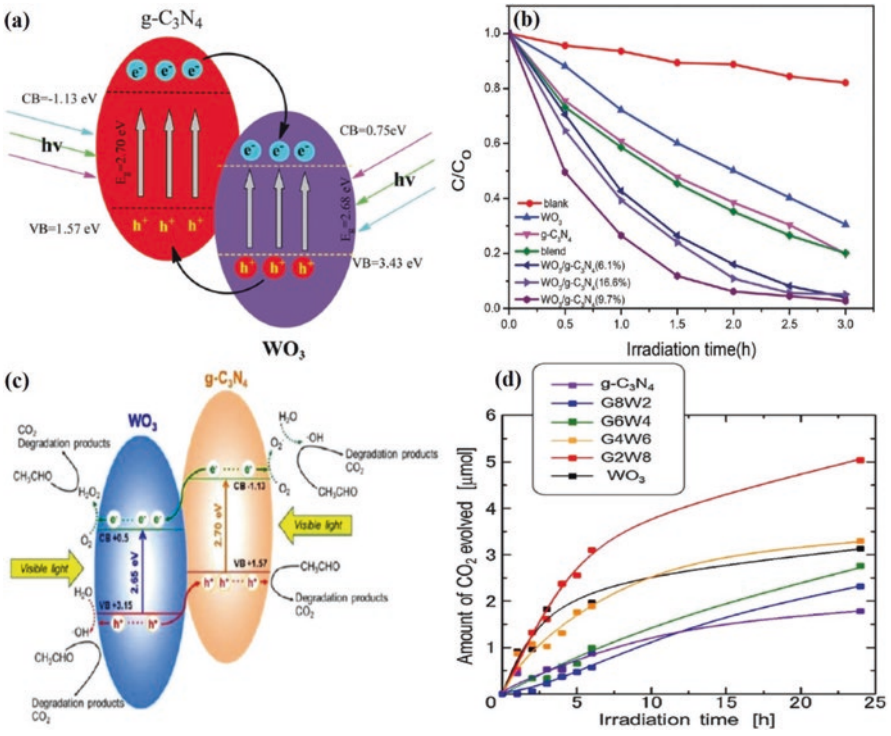

Fig. 10.11 **(a)** Suggested mechanism for the MB photodegradation on WO_3/g-C_3N_4; **(b)** Photocatalytic efficiency of MB degradation by WO_3; g-C_3N_4, blend and WO_3/g-C_3N_4 composites. **(c)** Probable acetaldehyde decontamination mechanism using WO_3/g-C_3N_4; **(d)** Shows graph of CO_2 concentration variation caused by acetaldehyde degradation verses irradiation time under visible light in the presence of WO_3, g-C_3N_4 and WO_3/g-C_3N_4 composites. "(a and b) Reprinted with permission from ref.(Huang et al. 2013). Copyright 2013, Royal Society of Chemistry, (c and d) "Reprinted with permission from ref.(Katsumata et al. 2013). Copyright 2013, Elsevier"

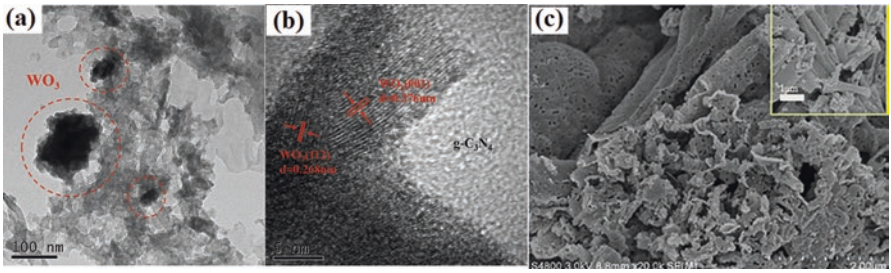

Fig. 10.12 Showing the TEM, HRTEM and SEM (along partial magnification inset) image of WO_3/g-C_3N_4 composite (**a**, **b** & **c** respectively). "Reprinted with permission from ref.(Chang et al. 2019). Copyright 2019, Elsevier"

g-C_3N_4. The heterojunction of Type-II helped to minimize the rate of charge carrier's recombination drastically as shown in Fig. 10.11 (a). Moreover, PL quenching by as-prepared composites was less than that of g-C_3N_4. MB degradation efficiency by various materials is shown in Fig. 10.11(b) (Huang et al. 2013).

Katsumata et al. (2013) documented the preparation of WO_3/g-C_3N_4 photocatalysts using mechanical mixing technique via an agate mortar. These VLD photocatalysts were used in decontamination of organic gas pollutants i.e. acetaldehyde. Figure 10.11(c) displays both semiconductors WO_3 and g-C_3N_4 have energy bandgaps of 2.65 and 2.70 eV respectively. This implies they are active under visible spectrum of light to generate photo-induced charge carriers (e^- and h^+'s). Valence band (VB) maximum and conduction band (CB) minimum corresponding to g-C_3N_4 were 1.57 and − 1.13 eV, respectively. While for WO_3 valence band maximum and conduction band minimum was 3.15 and 0.5 eV respectively. Subsequently CB potential 0.5 eV of WO_3 is higher than −1.13 eV of g-C_3N_4, so photo-excited e^-'s directly transferred from conduction band of g-C_3N_4 to conduction band of WO_3. Likewise, the VB edge +1.57 eV of g-C_3N_4 is lower than +3.15 eV of WO_3. So, photo-created h^+'s transferred directly from WO_3 VB to g-C_3N_4 VB. The relocation of e^-'s on one side of the junction and h^+'s on the other side significantly declines the recombination of e^- and h^+'s. Consequently, the photocatalytic output of WO_3/g-C_3N_4 was boosted due to promising structure of heterojunction, large surface area and the favorable band-edge positions. When acetaldehyde degraded, it transform into CO_2 (final product). In Fig. 10.11(d), the graph between change in CO_2 concentration caused by acetaldehyde degradation and irradiation time under visible light in the existence of as-synthesized samples has displayed (Katsumata et al. 2013).

Different binary composites of WO_3/g-C_3N_4 were synthesized using an easy calcination with one-step process and then systematically evaluated for physiochemical properties (Chang et al. 2019). TEM, HRTEM, and SEM images of as-prepared composites are presented in Fig. 10.12(a, b, c). Remarkably, the resulting composites displayed porous morphology along some tube-like structures. The formation of Z-heterojunction along with large specific surface area and enhanced absorption

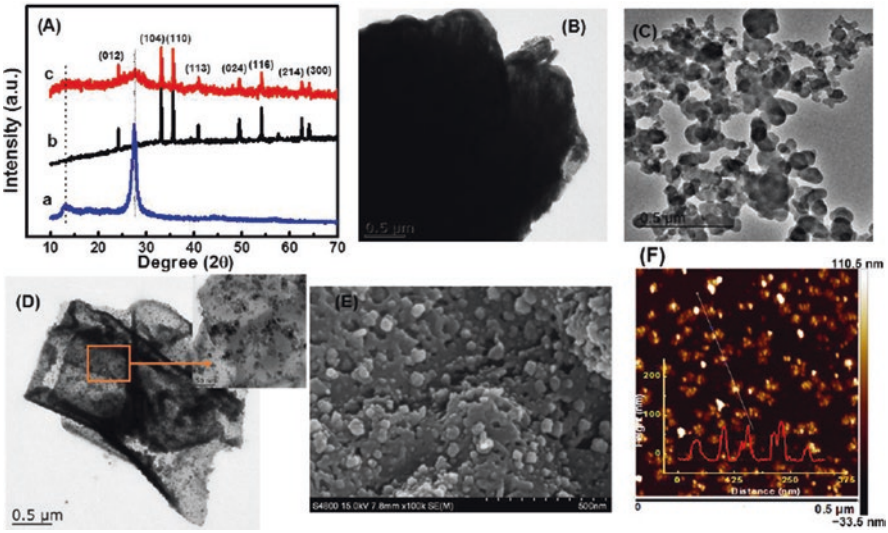

Fig. 10.13 **(a)** XRD Pattern of pristine g-C_3N_4 (x), α–Fe_2O_3 (y), the g-C_3N_4/α-Fe_2O_3 composites (z); the TEM images of g-C_3N_4 **(b)**, the α – Fe_2O_3 **(c)**, the g-C_3N_4/α-Fe_2O_3 heterostructure composites **(d)**; the SEM and AFM images of the g-C_3N_4/α-Fe_2O_3 composites (**e & f**). Reprinted with permission from ref.(Liu et al. 2016). Copyright 2016, Elsevier"

capacity of visible-light supported these composites to show strengthened photodegradation activity towards MB and RhB (Chang et al. 2019).

Duan et al. (2018) reported CuO/g-C_3N_4 nanosheets synthesized by novel one-pot method. Ammonium nitrate based thermal condensation of copper nitrate and melamine leads to form CuO/g-C_3N_4 catalysts. Performance of as-prepared catalysts was observed in the degradation of salicylic acid (SAL) under visible-light irradiation. Highest catalytic activity was shown by g-C_3N_4/CuO(1.0 wt%), more than 100% which is much greater than pure g-C_3N_4. The p-n heterojunctions formed between g-C_3N_4 and CuO caused the excellent separation of e^--h^+ pairs (photogenerated) and hence visible light absorption was increased, which ultimately boosted photocatalytic properties. Moreover, exceptional stability was shown by CuO/g-C_3N_4 composites (Duan 2018). Liu et al. (2016) have synthesized g-C_3N_4/α-Fe_2O_3 composites by pyrolysis of Prussian blue and melamine having the vast potential in sensors and energy storage applications. XRD patterns and TEM images of as-synthesized samples have shown in Fig. 10.13 (a-d). SEM and AFM images of the prepared heterostructure composite have also shown in Fig. 10.13 (e, f). The as-prepared composite exhibited a large specific surface area, presented high specific capacitance with good cyclic stability in the supercapacitor and outstanding electrocatalytic activity was shown. Moreover, for non-enzymatic detection of glucose (low detection limit), the composite based electrode was used extensively. Good anti-interference and stability performance was exhibited by as-prepared

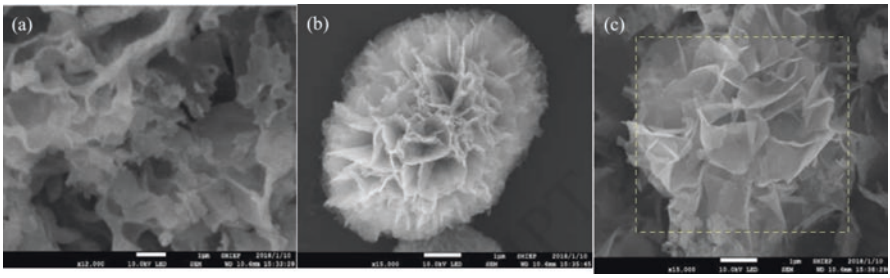

Fig. 10.14 Presenting the SEM images of g-C_3N_4 (**a**), Pure NiO (**b**) and NiO/g-C_3N_4 composite (**c**). "Reprinted with permission from ref.(Tang et al. 2018). Copyright 2018, Elsevier"

composites. Furthermore, its use in K-ion battery fabrication due to presence of K ions was also suggested (Liu et al. 2016).

Wang et al. (2017b) fabricated a novel 2D-2D heterojunction composite MnO_2/g-C_3N_4 for very first time in history. They reduced $KMnO_4$ and $MnSO_4{\cdot}H_2O$ (adsorbed on the surface of g-C_3N_4) via simple *in-situ* redox reaction. Synthesized composite showed well matched structure (band) and large specific surface area, which caused the separation of photo induced charge carriers and light-harvesting ability was increased which imparted the excellent photocatalytic activity for the prepared composite to reduce CO_2 (photo reduction) (Wang et al. 2017b). Tang et al. (2018) used method of hydrothermal deposition along with subsequent calcination route for fabrication of heterojunction composite NiO/g-C_3N_4. SEM images of g-C_3N_4, Pure NiO and NiO/g-C_3N_4 composite are shown in Fig. 10.14(a, b, c). As-prepared composite possessed excellent transfer of charge within the p-n junction and good band matching. Consequently, the as-prepared composites showed high specific surface area, good response towards visible light and enhanced photogenerated e^--h^+ pairs separation. Therefore, highly good photoreduction performance for CO_2 was observed by heterojunction composite (Tang et al. 2018).

10.4 Why Metal Oxides/g-C_3N_4 Composites?

Metals are refined form of ores, when they react with oxygen in the air. They produce respective metal oxides (MO). So, MO are indubitably ores and are basic in nature and neutralization takes place when they react with acids. Noble metals, however, are costly and can pollute the environment. The synthesis methods for attaining metal/g-C_3N_4 composites is also hard to regulate and can readily introduce impurities that can restrict their catalytic impact. Consequently, scientists should embrace inexpensive and environmentally benign materials to prepare g-C_3N_4 based composites in future studies. So, metal-oxides, in this regard are an exciting class of materials which display distinctive characteristics including mechanical stress tolerance, elevated optical transparency, outstanding carrier mobility etc. The synergistic effect of both g-C_3N_4 and MO results in enhanced stability, visible light usage, separation and transfer of charges and more effective oxidizing species formation.

Consequently, MO/g-C_3N_4 composites show boosted efficiency and overall performance.

10.5 Applications of g-C_3N_4

10.5.1 Batteries

In an electrochemical storage system, versatile batteries play a crucial role. Commonly, there are three types of batteries: rechargeable batteries, ultra-batteries, and flow batteries. The secondary battery is the other name of rechargeable battery because it has the ability to charge/discharge into a load and recharge repeatedly. Using distinct reversible electrochemical reactions, energy is accumulated and stored by these batteries. The features like a long lifetime and environmental friendliness make them promising candidate in large-scale applications. The large size and weight along with higher price are their few limitations. Ultra-battery is a hybrid device combining lead-acid battery technology with ultra-capacitor technology in one cell and a common electrolyte. So, it is another efficient alternative to store and transform intermittent energy. Flow batteries operate by moving a liquid solution across a membrane. Exchange of ions takes place on this membrane. With the help of the Nernst equation, their voltage can be determined. Fast response time and flexible layout are favorable features of these batteries, whereas their energy densities are lower than rechargeable batteries (Guo et al. 2018).

In 1991, rechargeable lithium ion batteries (LIBs) were first marketed to the public sector and were then used globally in portable electronic devices and electric vehicles. LIBs have steadily turned out to highly significant energy storage devices because of their light weight, high energy density and long cycle life. The main components of LIBs including: a solid-state electrolyte, separator, a cathode, and an anode. Lithium ions (Li^+) transfers from anode to cathode during charging and reverse movement during discharge take place in these batteries. There has been a lot of effort to optimize the materials of the electrode, particularly anodes.

The g-C_3N_4, being a 2D layered material has a great potential to use in LIBs as anode. However, low electrical conductivity, unstable SEI (solid electrolyte interphase) formation during lithiation/de-lithiation processes along with the pulverization and aggregation of electrodes are shortcomings still faced by it to store Li^+. To overcome these shortcomings, metal-oxides are expected to integrate with g- C_3N_4 to form composites (Veith et al. 2013).

Li et al. (2015) used productive low-temperature solution process to fabricate smart Zn_2GeO_4 /g-C_3N_4 composites. A synergistic effect was generated by the combination of both active elements in as-prepared hybrids. In LIBs, these smart composites act as anode material and showed improved electrochemical Li^+ storage. These anode materials showed remarkable rate capability (950 mA h g^{-1} at

2000 mA g^{-1}) and outstanding reversible capacity (1370 mA h g^{-1} at 200 mA g^{-1}) after 140 cycles (Li et al. 2015).

Senthil et al. (2017) reported the preparation of Titania nanoparticles coated by N-rich carbon nanosheets (TCNS) through self-assembly approach along with heat treatment. As-synthesized material used as anode in advanced LIBs. By optimized CNS loading resulting nanocomposite displayed high rate capability, specific capacity, and cycle stability. These capabilities credited to the combination of both pseudocapacitive and diffusion (intercalative) storages of TCNS core-shell playing at interfaces of NPs and over the nanosheet's surface. For first and second cycles the charge/discharge voltage profiles at 0.1C rate (1C = 335 mA/g) in 1.0–3.0 V voltage window is showed in Fig. 10.15a. In order to obtain further information about charge storage, differential capacity was evaluated and plotted at a particular current density of 35 mA/g for the first and second discharge-charge cycles Fig. 10.15b. The wide peak resided between 2.55 and 2.05 V during the initial cycle is ascribed to the electrolyte's surface reaction with CNS forming the solid electrolyte interphase layer. At 1.75 V another peak was noticed for the cathodic reaction caused by the insertion of lithium into the titania. A peak emerged in anodic scan at 1.98 V, which

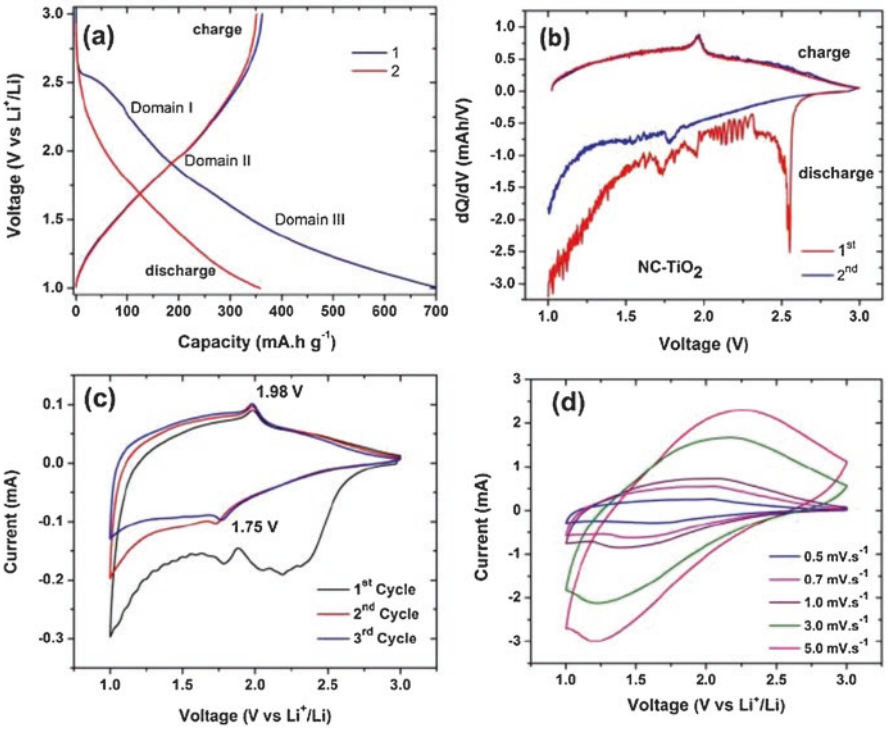

Fig. 10.15 (**a, b, c, d**) shows their charge-discharge sketches, differential capacity graph, cyclic voltammogram at 0.1 mV s^{-1} and 0.5–5 mV s^{-1} scan rates respectively. "Reprinted with permission from ref. (Senthil et al. 2017). Copyright 2017, Elsevier"

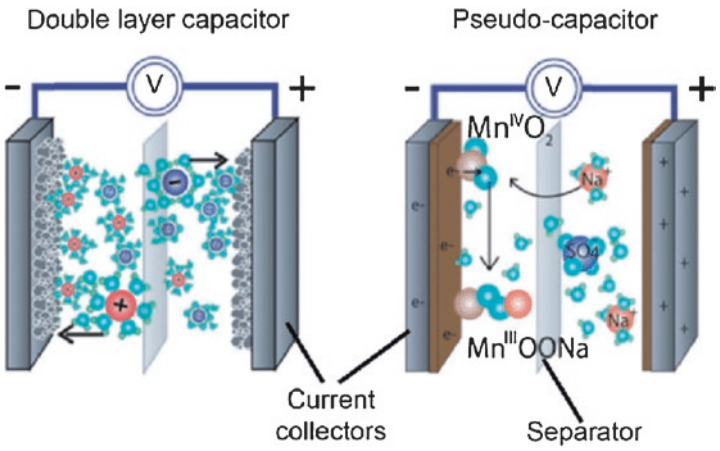

Fig. 10.16 Comparison of Double layer capacitor and Pseudo-Capacitor. "Reprinted with permission from ref. (Gulzar et al. 2016). Copyright 2016, Royal Society of Chemistry"

was almost same in the second cycle owing to Li^+ de-insertion. In the potential window of 1.0–3.0 V, the voltammogram curves were conducted at 0.1 $mV.s^{-1}$ scan rate (Fig. 10.15c). Storage mechanism and pseudocapacitive behavior of TCNS were further explained by using voltammogram curves recorded at distinct scanning rates 0.5 $mV.s^{-1}$- 5.0 $mV.s^{-1}$ (Fig. 10.15d). Cyclic Voltammetry (CV) results showed slight variation in peak current revealing a high stability and recyclability of the electrode. Moreover, TCNS anode delivered a remarkable capacity of 303 mA h g^{-1} over 125 cycles at current rate of 0.1C. It further shows an incredible rate capability (136 mA h g^{-1} after 500 cycles) at 5C (Senthil et al. 2017).

10.5.2 Supercapacitors

In recent decades, renewable energy demand of storage devices has gained much attention. Lithium Ion Batteries (LIBs) were successfully used for the renewable energy storage having elevated energy density. But, for the future generation hybrid vehicles, high power electronic devices and regenerative braking system energy storage devices should have large life cycle, low cost, high power density and high safety. Supercapacitors (SCs) are proposed candidates for the partial/complete replacement the LIBs. SCs have excellent cycle stability, safe charge storage mechanism, high power density, wide temperature range of performance and fast charging discharging (Periyat et al. 2018). The comparison between double layer capacitor and pseudo-capacitor is shown in Fig. 10.16 (Gulzar et al. 2016).

Recently, g-C_3N_4 has gained much consideration as an electrode material in EDLC due to its large surface area and good pore distribution. However, due to less chemical activity and very low conductivity of g-C_3N_4, its efficiency is not satisfactory. For the purpose of enhancing the efficiency of this material as electrode in SCs,

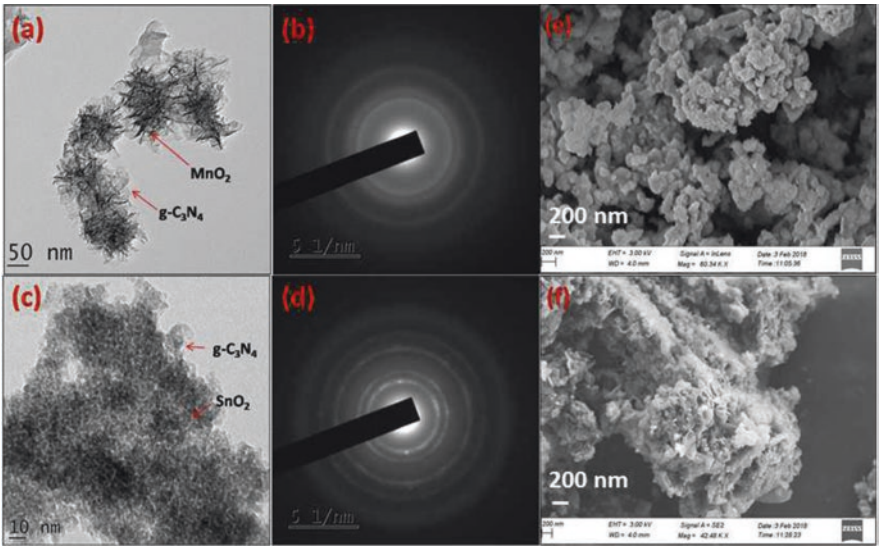

Fig. 10.17 Illustrating the TEM images of **(a)** g-C_3N_4/MnO_2 and **(c)** g-C_3N_4/SnO_2, (**e & f**) FESEM and (**b & d**) SAED patterns of the composites g-C_3N_4/MnO_2 and g-C_3N_4/SnO_2 respectively. "Reprinted with permission from ref. (Periyat et al. 2018). Copyright 2018, Royal Society of Chemistry"

attentions were paid towards fabrication of nano sized g-C_3N_4 and its composites with other compounds (Li et al. 2017). Metal oxides in pseudo-capacitors, upsurge the surface redox reactions and hence, specific capacitance was enhanced as electrode material. Liu et al. (2016) have found by their work that by combining the g-C_3N_4 along with MO (metal oxides), new doors for its applications could be opened i.e. energy storage devices and electrochemical sensors.

Periyat et al. (2018) used one pot method as well as reduction method to synthesize the nanocomposites of g-C_3N_4/SnO_2 and g-C_3N_4/MnO_2. FESEM and TEM analysis was done to investigate the morphology of microstructures. MnO_2 with flower like morphologies were uniformly distributed in the g-C_3N_4 matrix as presented in Fig. 10.17a. While growing MnO_2 phase on g-C_3N_4 sheets MnO_2 crystallize in nanoflakes morphology. Self-assembly of molecules is experienced by these nanoflakes exhibiting high energy of surface for the formation of more stable MnO_2 nanoflowers on the g-C_3N_4 sheets. Concentric rings in selected area electron diffraction (SAED) pattern reveals the fact that MnO_2 phases were observed in partially crystalline state and not in pure crystalline form as shown by XRD patterns. Precipitation of SnO_2 was done over the g-C_3N_4 phase in spherical morphology and they are more crystalline as compared to the phase of MnO_2 which can be observed in Fig. 10.17(b, d). TEM image of g-C_3N_4/SnO_2 is shown in Fig. 10.17c. FESEM images shown in Fig. 10.17(e, f) respectively were used to determine the constituent phases interaction and morphology of surface in the composites (g-C_3N_4/MnO_2 and

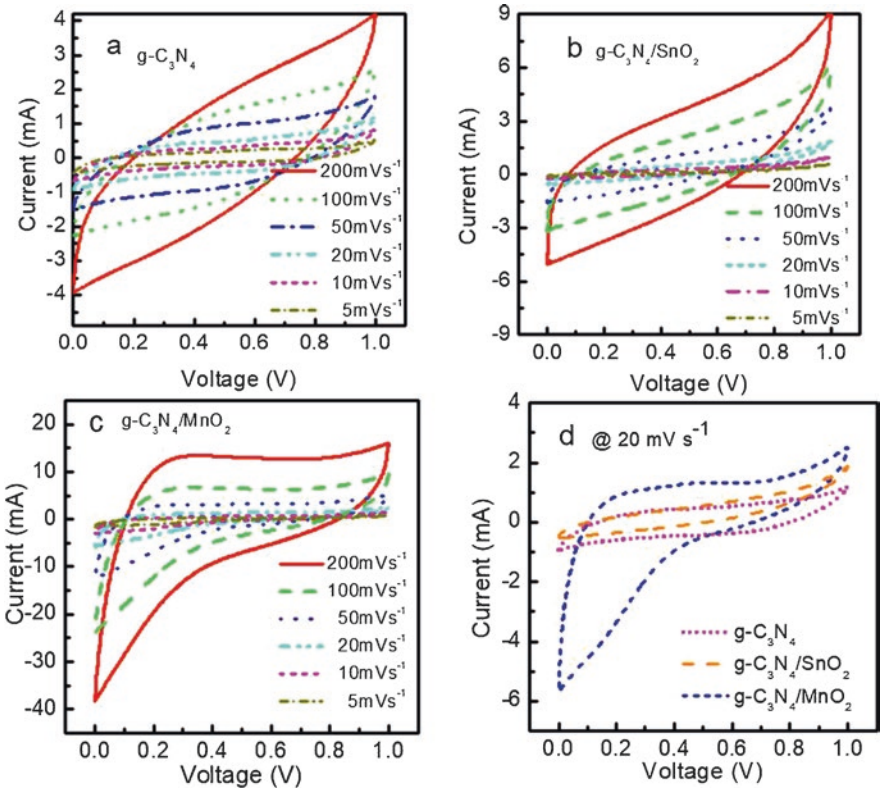

Fig. 10.18 Different scan rates cyclic voltammograms of **(a)** g-C3N4 **(b)** g-C_3N_4/MnO_2 **(c)** g-C_3N_4/SnO_2 **(d)** CV loops comparison of the various supercapacitor devices (scan rate of 20 mVs^{-1}). "Reprinted with permission from ref. (Periyat et al. 2018). Copyright 2018, Royal Society of Chemistry"

g-C_3N_4/SnO_2). Proper mixing of metal oxide nanostructure over g-C_3N_4 phase can be verified by using SEM images (Periyat et al. 2018).

The isotherms (Nitrogen adsorption-desorption) of different electrode samples were measured. The surface areas calculated from given isotherms were 70.2, 38.2 and 32.8 m^2g^{-1} for g-C_3N_4/MnO_2, g-C_3N_4/SnO_2 and g-C_3N_4 respectively. Due to large pore volume and increased surface area, g-C_3N_4 more efficiently interacts at large scale with the number of electrolytes for improving the electrochemical performance than that of g-C_3N_4/SnO_2. Fig. 10.18 (a, b, c) displays the CV curves at 5, 10, 20, 30, 50 and 200 mV/s for g-C_3N_4, g-C_3N_4/SnO_2, and g-C_3N_4/MnO_2 electrodes based supercapacitors respectively. At 20 mV/s scan rate, the comparison of CV loops of distinct supercapacitors prepared from different electrode materials have been displayed in Figure 10.18d (Periyat et al. 2018).

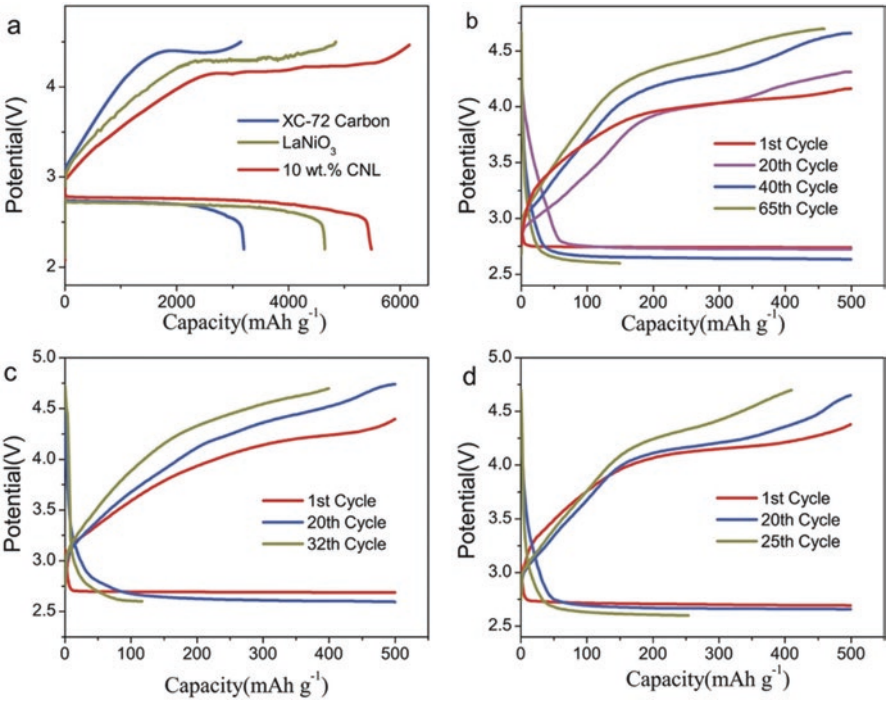

Fig. 10.19 **(a)** shows curve for first charge/discharge at 50 mA g^{-1} using air electrodes of $LaNiO_3$ XC-72 carbon and CNL 10%; **(b, c, d)** cells discharge/charge curve at 250 mA g^{-1} using air electrodes of CNL 10%, $LaNiO_3$ & XC-72 carbon respectively. "Reprinted with permission from ref. (Wu et al. 2016). Copyright 2016, Nature Publishing Group"

10.5.3 Electrocatalysis

The concept of a catalyst is defined as a substance that can change the velocity of a certain chemical reaction without any chemical change in itself. For electrocatalysis, this definition can be extrapolated directly. An electrode material that remains unchanged during a Faradaic reaction is called electrocatalyst. These are generally heterogeneous catalysts, which implies that reaction occur on the catalyst surfaces. Also, on the electrocatalyst surfaces there are steps of adsoprtion/desoprtion. At low potential, an excellent electrocatalyst should display elevated current density.

An efficient and low-cost g-C_3N_4-$LaNiO_3$ (CNL) composite was fabricated (Wu et al. 2016). For lithium-oxygen (Li-O_2) batteries, as-prepared material acted as bifunctional electrocatalyst. In an alkaline electrolyte, CNL catalysts display enhanced electrocatalytic rate for both ORR and OER, as-compared to its individual components. At a current density of 50 mA/g, the first charge and discharge profiles of 10 wt.% CNL, $LaNiO_3$ and XC-72 in the Li-air batteries were compared (Fig. 10.19a). Specifically, CNL displays the initial discharge capacity of 5500 mAh/g, superior to

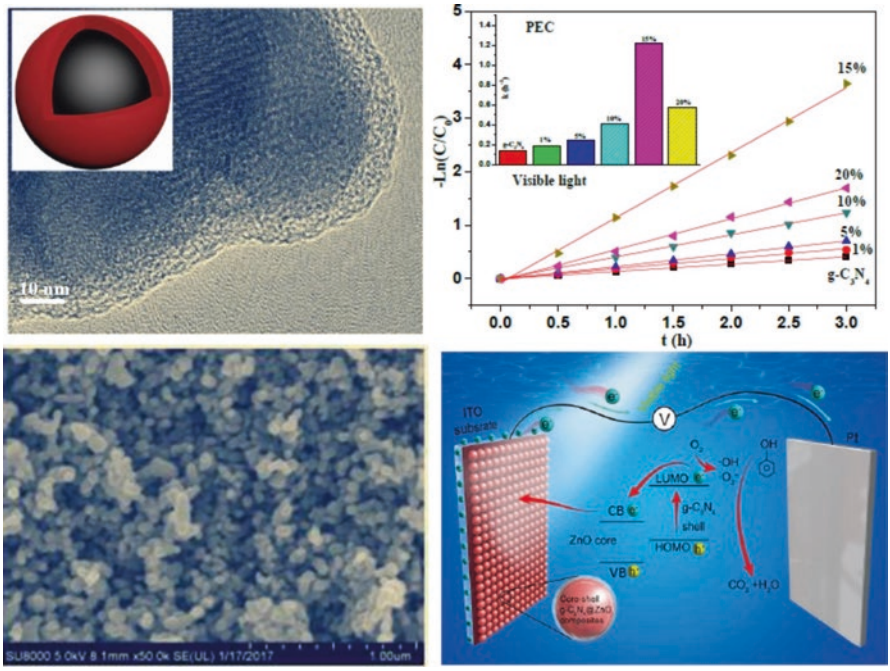

Fig. 10.20 (**a** and **c**) Illustrating the HRTEM and SEM images of ZnO@g-C_3N_4 composites. (**b**) Shows graph of PEC degradation rate of phenol and (**d**) schematic PEC mechanism of as-prepared composites. "Reprinted with permission from ref. (Wang et al. 2017a). Copyright 2017, Elsevier"

both XC-72 carbon (3600 mAh /g) and $LaNiO_3$ (4600 mAh /g). It is also evident that the CNL catalyst discharge voltage plateau was ~2.8 V, greater than the XC-72 carbon (~2.7 V) and $LaNiO_3$ (~2.7 V). For CNL charge voltage plateau was ~4.0 V, lower than XC-72 carbon (~4.4 V) and $LaNiO_3$ (~4.3 V). CNL's lower voltages suggest greater catalytic activity compared to XC-72 and $LaNiO_3$. Additionally, as shown in (Fig. 10.19b), CNL catalyst displayed 65 cycles between 2.6 V to 4.7 V voltage window. While the XC-72 carbon and $LaNiO_3$ catalyst output is only up to 25 and 32 cycles respectively. Moreover, in Li-O_2 batteries, CNL showed enhanced cycling stability, lower overpotential and round-trip efficiency. Their results recommended that in Li-O_2 batteries, CNL are favorable cathode catalyst (Wu et al. 2016).

Wang et al. (2017a) documented the synthesis of core-shell ZnO@g-C_3N_4 composites via reflux method. Figure 10.20 (a, c) displays HRTEM and SEM images of as-prepared composites with 15% g-C_3N_4 loading. The composites showed excellent performance as a photo-anode under visible light. Degradation of phenol was used to test PEC performance. At 1.5 V applied potential, PEC phenol degradation rate under visible light over pristine g-C_3N_4 and g-C_3N_4@ZnO photo-anodes is shown in Fig. 10.20b. Proposed mechanism for phenol degradation under visible light using photo-anode of 15% g-C_3N_4 @ ZnO and counter electrode of Pt is shown in Fig. 10.20d. Enhanced PEC phenol degradation was ascribed to electro-oxidation and distinct core-shell nanostructures (Wang et al. 2017a).

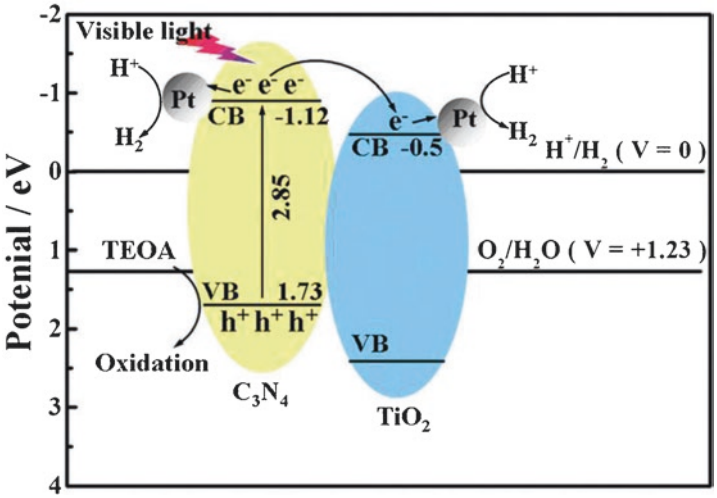

Fig. 10.21 Photocatalytic hydrogen generation mechanism. "Reprinted with permission from ref. (Chai et al. 2012). Copyright 2012, Royal Society of Chemistry"

10.5.4 Photocatalytic Hydrogen Generation

For the world, fossil fuels are considered most easy energy source but some issues like: air pollution and the emission of CO_2, make it less efficient and it contributes to the global warming and change of climate. Nowadays, the demands of energy are increasing day by day and the utilization of fossil fuels rapidly increases. The resources of fossil fuels are limited and hence we can face the crisis of energy to greater extent in future if don't find a substitute. Researchers think due to environment friendly nature, renewable source and abundance, fossil fuels can be replaced by solar energy in future to fulfill the needs for energy. It is observed that by utilizing the only 0.01% (one second) of the sunlight irradiation, energy usage of the world per year can be fulfilled (Fan et al. 2013, Gholipour et al. 2015). Yet, important thing is the practical utilization of this energy. It is suggested that to use hydrogen for energy carriers can solve the above said troubles, besides this, air pollution can be minimized to greater extent. Furthermore, during the consumption of hydrogen there is no emission of CO_2 (Chen et al. 2010, Gholipour et al. 2016).

In 1972, two scientists Honda and Fujishima discovered the splitting of water into its constituents like hydrogen and oxygen under UV light with help of TiO_2 and Pt (Fujishima and Honda 1972). After this, researches have concluded that the photocatalysts can generate hydrogen from water with the help of daylight. However, most of the sunlight includes the visible light (400–700 nm). Hence, the efficient photocatalysts should be activated in this region (Shen et al. 2011). Figure 10.21 illustrates the mechanism of photocatalytic hydrogen production by g-C_3N_4/TiO_2 composites (Chai et al. 2012).

Under visible light g-C_3N_4 is supposed to be the good photocatalyst (Zhao et al. 2015). It is observed by Wang et al. (2009) that hydrogen under visible light can be generated using g-C_3N_4 along with the addition of sacrificial reagent and water. In their experiment Pt was used as a cocatalyst and triethanolamine served as an electron scavenger (Wang et al. 2009). Later, researchers found new methodologies in order to enhance the effectiveness through synthesis of the composites with other elements.

Gholipour et al. (2016) fabricated the nanocomposites of TiO_2 and g-C_3N_4 for the enhancement of charge separation and particularly to increase the hydrogen production. Melamine heated at 550 °C to obtain graphitic carbon nitride (g-C_3N_4). Chu et al., (2014) also reported the same procedure in 2014 (Chu et al. 2014). After this g-C_3N_4 nanosheets were fabricated via gas template (one step) as reported earlier (Lu et al. 2014). Titanate nanodisks (TNDs) were synthesized by solvothermal technique. These nanoparticles (35 nm) can be used on the surface of g-C_3N_4 nanosheets. So that, g-C_3N_4 nanosheets and TNDs charge separation become more effective due to high g-C_3N_4/TNDs interface and extensively tiny range (Zhu et al. 2015).

10.5.5 Gas Sensors

Gas sensors gained much attention for the sake of public safety, air conditioning systems, environmental monitoring and domestic security (Kolmakov et al. 2005). Metal oxides-based gas sensors (semiconductor) are suitable for sensor system because of their important properties such as modifiable sizes and structures, easy operation, electronic circuit's simplified unification and being economical. Among all the metal oxides, hematite (α-Fe_2O_3) gained much attention for the gas-sensing applications because of its unique properties. It is naturally available, chemically stable, non-toxic and low priced. Due to stability issues in device, its effectiveness is restricted. α-Fe_2O_3 was combined with g-C_3N_4 to enhance the gas sensing efficiency (Comini 2006, Zeng et al. 2015, Zhang et al. 2016).

Recently, α-Fe_2O_3/g-C_3N_4 composites had been prepared by Zeng et al. (2015). They refluxed (in boiling water) the mixture of $FeCl_3$ solution and g-C_3N_4 suspension. The α-Fe_2O_3 NPs firmly hold the sheets of g-C_3N_4. During sensing of H_2S, the composite was utilized as a cataluminescence (CTL). Strong cataluminescence sensing emission was seen in the oxidation reaction of H_2S over the α-Fe_2O_3/g-C_3N_4 heterostructure composites. CTL intensity for different concentrations of α-Fe_2O_3/g-C_3N_4 has been illustrated in Fig. 10.22. The sintering of α-Fe_2O_3/g-C_3N_4 (0.05 g) was carried out and rod was inserted in quartz tube having length100 mm. They used air as carrier gas. Catalyst surface derived the H_2S gas which was oxidized by oxygen (from air) at normal temperature. BPCL ultra-weak luminescence analyzer was used to measure the CTL emission. Reaction temperature was controlled by achieving the transforming voltage from rod. Flow meter controlled the air flow rate while the α-Fe_2O_3/g-C_3N_4 heterostructure composites were used to determine their catalytic performance with the help of CTL with varying contents giving air flow

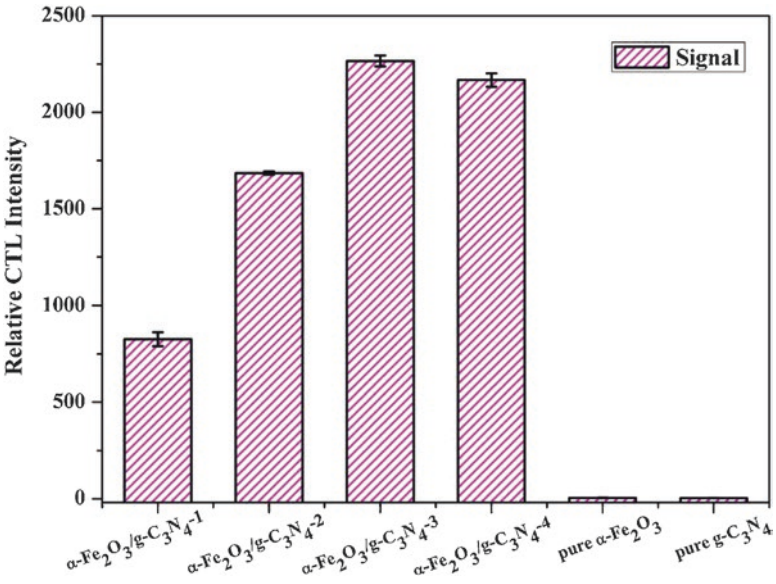

Fig. 10.22 CTL intensity for different concentrations of α-Fe_2O_3/g-C_3N_4. "Reprinted with permission from ref. (Zeng et al. 2015). Copyright 2015, Elsevier"

(300 mL min^{-1}), corresponding cataluminescence intensity responding to 4.38 μg mL^{-1} of H_2S, temperature 183 °C with 400 nm filter. Best sensitive CTL response was observed at loading of 5.97% of α-Fe_2O_3 (Zeng et al. 2015).

As compared to α-Fe_2O_3, CB of g-C_3N_4 is at lowest levels. Electron transportation across the interface is allowed efficiently. Besides this, electron carrying is also possible by g-C_3N_4 lamellar configuration. However, large number of reaction sites is offered by g-C_3N_4 as compared to other similar compounds. This is due to its high nitrogen content. Due to porous structure and the wide surface areas are delivered by α-Fe_2O_3/g-C_3N_4 nanocomposites. This enhances the charge transfer rate and greater number of molecules is transferred. Large lamellar structure and good permeability hence causes the rapid diffusion of gas towards the surface zone and internal zone. In this way, an efficient gas-sensing system can be developed by coupling of α-Fe_2O_3 with g-C_3N_4 (Mousavi et al. 2018).

Recently, Li et al. (2019b) presented the preparation of g-C_3N_4/ZnO (CNZ) hierarchical structures via precipitation-calcination method. Controlled amount of g-C_3N_4 nanosheets were anchored on flower-like ZnO. They used as-prepared materials as methane (CH_4) sensors. CH_4 sensing mechanisms by ZnO and CNZ composite is shown in Fig. 10.23 (a, b) and Fig. 10.23 (c, d) respectively. Figure 10.23(e) displays the preparation methodology of as-prepared materials schematically. Their results declared that the prepared CNZ based sensors are more efficient as-compared to bare-ZnO sensors. They also predicted that the formation of n-n junction by decoration of ZnO with 2D g-C_3N_4 is a useful technique to boost the gas sensing capabilities of ZnO (Li et al. 2019b).

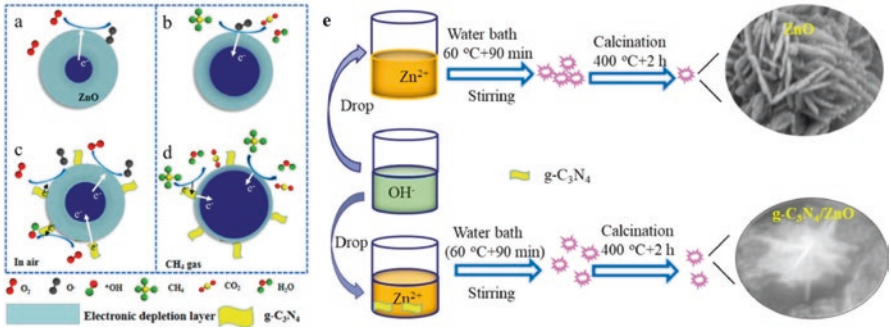

Fig. 10.23 Presenting CH_4 sensing process by ZnO (**a & b**) and CNZ (**c & d**); (**e**) shows diagram for the preparation of ZnO and CNZ composites. "Reprinted with permission from ref. (Li et al. 2019b). Copyright 2019, Nanomaterials"

10.5.6 Biomedical Applications

Antibiotics are the most commonly prescribed drugs that enter the aquatic system easily. Antibiotics are non-biodegradable and their persistence causes huge threat to the quality of natural sources of water. To remove antibiotics from wastewater different physico-chemical techniques like photocatalysis, chemical oxidation coagulation, aerobic biological and flocculation treatments have been used usually. Among all these techniques, photocatalysis shows outstanding possibility owing to successful usage of renewable sun light. Sudhaik et al. (2018) reported the preparation of magnetic photocatalyst GCN/$NiFe_2O_4$ for mineralization of oxytetracycline antibiotic under solar light. They used thermal condensation of urea to prepare GCN and then $NiFe_2O_4$ nanoparticles loaded over it to make the composite. The surface morphology of GCN and GCN/$NiFe_2O_4$ was analyzed by SEM images as-shown in Fig. 10.24(a-f). About 50–70 nm thick irregular and rough sheets of GCN were investigated by SEM images (Fig. 10.24(a-c)) and $NiFe_2O_4$ loading over GCN sheets was clearly seen in Fig. 10.24(d-f). Figure 10.24(g) shows A + P (adsorption + photocatalysis) and A-P (equilibrium adsorption followed by photodegradation) process for OTC degradation. Using GCN/$NiFe_2O_4$, 94% degradation of OTC took place in 1 hour during A + P process while during A-P only 65% OTC degraded in 65 min. It is clear that under solar light irradiation, the synergistic adsorption and photocatalytic process (A + P) showed boosted degradation of OTC. Moreover, having greater surface area and efficient charge separation, the as-prepared composites showed excellent photocatalytic activity and recyclability of ten catalytic cycles (Sudhaik et al. 2018).

Gong et al. (2016) used the thermal processing of melamine ($C_3H_6N_6$) and nickel chloride hexa-hydrate ($NiCl_2{\cdot}6H_2O$) in order to prepare Nickel oxide (NiO) and nickel (Ni) co-doped g-C_3N_4 (NiO/Ni/GCN) nanocomposites. As compared to pure GCN, NiO/Ni/GCN composites displayed higher catalytic activity for the oxidation of octylphenol (OP). OP is a type of endocrine disruptors (EDs) and phenolic environmental estrogens. EDs can interfere with the normal endocrine system and

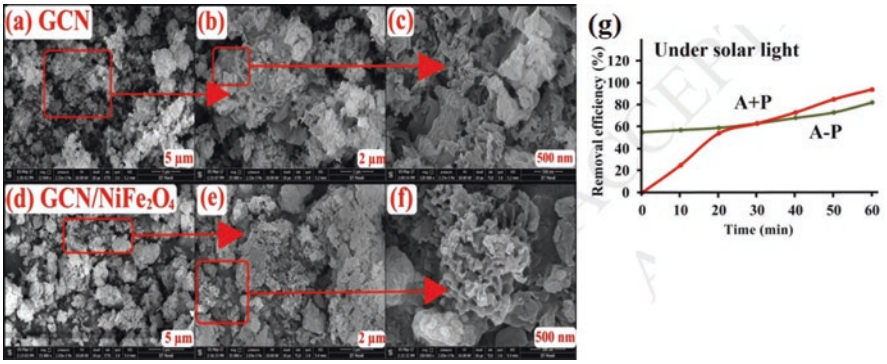

Fig. 10.24 SEM images of GCN (a-c) & (d-f) GCN/$NiFe_2O_4$. (g) OTC degradation under solar light by composites of GCN/$NiFe_2O_4$. "Reprinted with permission from ref. (Sudhaik et al. 2018). Copyright 2018, Elsevier"

hormonal regulations, resulting in humans and animals' health effects. It is of great importance to establish a rapid detection technique for OP to handle the level of this material in atmosphere because it can cause growth in human cancer cells and seriously affect the reproductive ability. So, there have been many complex, expensive and time-consuming analytical methods to detect OP. On the other hand, as prepared novel non-precious metal-polymer composites showed high selectivity and sensitivity for an OP electrochemical sensing (Gong et al. 2016).

Selvarajan et al. (2018) used a one-pot method synthesized electrochemically active and structurally uniform g-C_3N_4/NiO nanocomposite for electrocatalytic oxidation of quercetin (QR). QR a flavonoid of general existence in nature has been widely demonstrated in the literature due to its medicinal properties, especially the antioxidant capacity. To detect QR, capillary electrophoresis and high-performance liquid chromatography along with number of detection techniques like mass spectrometry, UV-spectrophotometry, electrochemical detection, UV photodiode array detection and chemiluminescence are used. As-mentioned techniques may deliver high assay selectivity, but also have certain disadvantages like consumption of reagent and time, operational complexity, high cost, etc. In this regard, nanocomposite (g-C_3N_4/NiO) modified glassy carbon electrode (GCE) based sensors prepared by S. Selvarajan et al. displayed high stability, repeatability and reproducibility. CV results in Fig. 10.25a shows the electrochemical behavior of QR (5 µM) on different electrodes investigated at scanning rate of 50 mV/s. The synthesized biosensor showed excellent electrochemical behavior due to synergistic effect. They also performed DPV to inspect the sensitivity of the prepared biosensor towards the detection of QR. Figure 10.25b indicates the DPV results of the prepared sensor for different concentrations of QR. They recorded DPV by sweeping the potential at amplitude of 0.05 V between −1.0 and 0.6 V, a step potential of 0.07 V, and at 20 mV s^{-1} scan rate. Figure 10.25b shows the stable and well-defined oxidation peak of anodic current for QR. These results also showed that the prepared sensor presents outstanding electrocatalytic activity for QR sensing. The inset of Fig. 10.25b

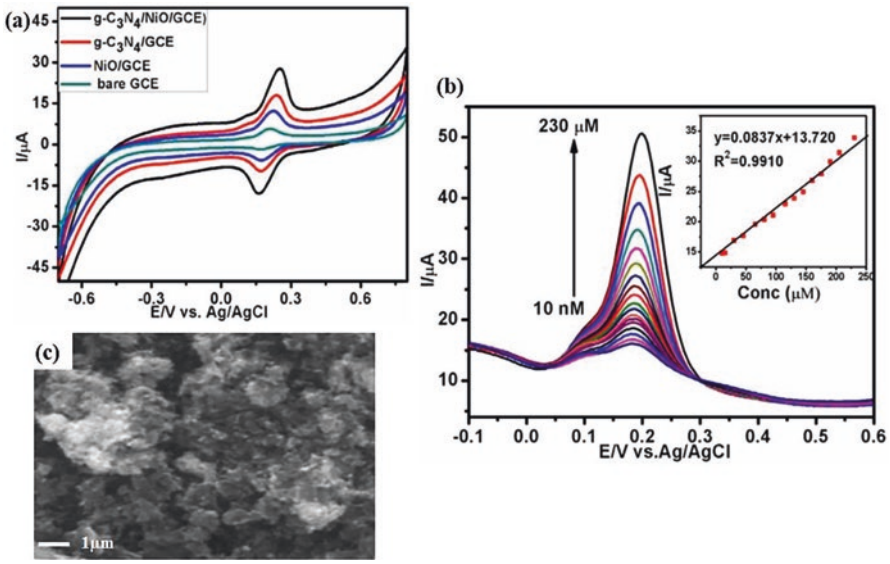

Fig. 10.25 Using 0.1 M phosphate buffer saline (PBS) having pH = 6.4, (**a**) shows cyclic voltammetry (CV) of bare GCE, g-C_3N_4/GCE, NiO/GCE, and g-C_3N_4/NiO/GCE; (**b**) shows differential pulse voltammograms (DPV) for several QR concentrations; (**c**) shows SEM images of g-C_3N_4/NiO/GCE. "Reprinted with permission from ref. (Selvarajan et al. 2018). Copyright 2018, Elsevier"

shows that there is a linear relation between DPVs current and QR concentration (0.01 μM - 250 μM) and limit of detection is 0.002 μM. SEM image of the prepared composite has also shown in Fig. 10.25c. As-fabricated sensor was proposed for detection of QR in several real models like green tea, apple and honeysuckle (Selvarajan et al. 2018).

Two-dimensional (2D) nanocomposites (g-C_3N_4/CuO) were prepared via pyrolysis of cupric acetate and melamine monohydrate precursors. As-synthesized nanocomposites act as a facile sensor used for dopamine (DA) electrochemical detection. DA molecules are important neurotransmitter for human central nervous system and hormones system in human they take park in various physiological processes where they are primarily involved in hormonal release and behavioral responses. The disease of Parkinson is a distinctive neurodegenerative disorder related with deficient DA levels in the serum of the patient. When DA is excessive, abnormalities like schizophrenia, euphoria and energy metabolism failure are often observed. To diagnosis prognosis and treatment of common disease like neurodegenerative, accurate and real-time detection of DA is desired and necessary. For sensing of DA, good electrochemical activity was shown by g-C_3N_4/CuO nanocomposites because of narrower band-gap and higher conductivity than pure graphitic carbon nitride (g-C_3N_4). Ultra-High sensitivity of this sensor was due to the process of surface transfer of electron, as density functional theory (DFT) calculations have confirmed that oxidized DA quinone functions behave like excellent electron acceptor while

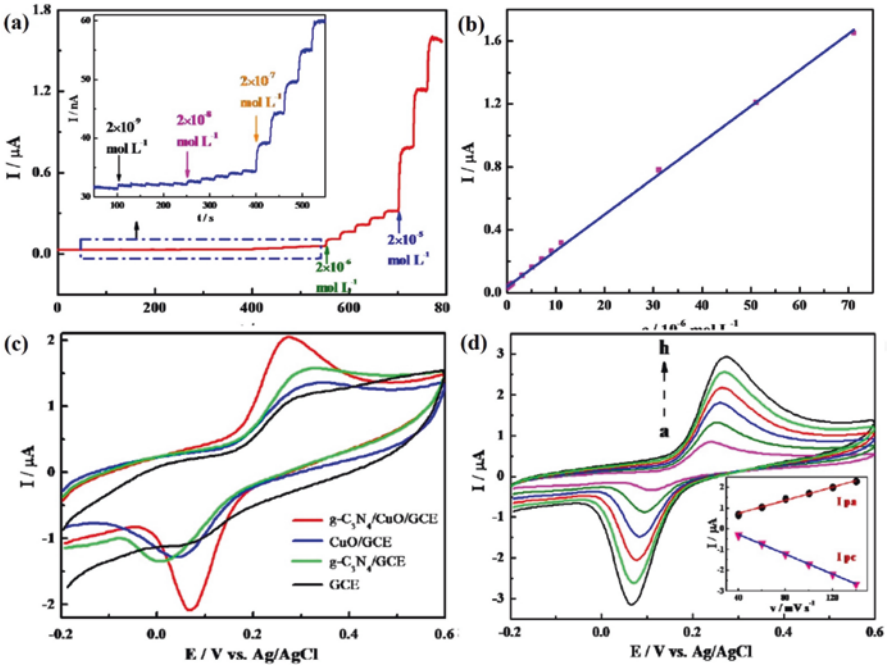

Fig. 10.26 Using Tris-HCl buffer solution (1.0×10^{-1} mol/L, pH = 7.2), (a) ampermetric responses shown by g-C_3N_4/CuO/GCE with DA successive addition from (2.0×10^{-9} mol/L - 2.0×10^{-5} mol/L); (**b**) At 0.28 V, Linear relationships between the DA concentrations and the oxidation peak currents; (**c**) At 100 mV/s (scan rate) CV by different electrodes in 1.0×10^{-5} mol/L DA; (d) g-C_3N_4/CuO/GCE CV curves at different scan rates i.e. 40, 60, 80, 100, 120 & 140 mV/s (**a-f**), plots b/w the redox peak and scan rate has displayed by the inset. "Reprinted with permission from ref. (Zou et al. 2018). Copyright 2018, Elsevier"

the 2D g-C_3N_4/CuO is observed as powerful electron donor. High selectivity was shown by sensor to DA over common biological (interfering) small molecules such as ascorbic acid, glucose and uric acid. This was due to lowest electron-injection-barrier b/w the 2-dimensional DA quinine and g-C_3N_4/CuO and also most positive electrostatic potential possessed by the DA quinine was the reason for this fact. Density functional theory (DFT) calculations also confirmed these reasons. They conducted a flow injection study with the detection of amperometer, an electrochemical method with greater current sensitivity, to examine the detection limit of DA using as-prepared g-C_3N_4/CuO modified g-C_3N_4/CuO/GCE sensor (Zou et al. 2018). Figure 10.26(a) demonstrates amperometric responses to applied potential of 0.28 V for consecutive injections of DA solution. The inset of Fig. 10.26(a) shows that even at a very low concentration (~ 2.0×10^{-7} mol /L), the performance of fabricated sensor is satisfactory. In the case of DA concentration C_{DA} varying from 2.00×10^{-9} to 7.11×10^{-5} mol/L, the response of current on the sensor increased linearly with increasing C_{DA} (Fig. 10.26(b)). Figure 10.26(c, d) shows that

as-prepared sensor showed well-defined redox peaks as-compared to other electrode materials. CV results clearly reveal the outstanding electrochemical performance of as-prepared sensor. In short, prepared innovative material (sensor) offers an electrochemical sensing method (ultra-sensitive) to sense DA trace in biological samples (Zou et al. 2018).

10.6 Conclusion

In recent years, dedicated efforts for nanocomposites based on g-C_3N_4 caused plenty of database and knowledge for smart engineering, features characterization, and useful applications related to energy and the environment. In the field of g-C_3N_4-based nanocomposites, the massive breakthroughs have absolutely witnessed unique promising properties along with ameliorated performance of photocatalysis. There are three major far-reaching criteria accredited for the improvement of photocatalytic efficiency of g-C_3N_4-based heterostructure nanocomposites, including (1) hampering the rate of recombination for photo-induced charge carriers (charge separation and migration), (2) enhancing the absorption of the visible-light (harvesting of visible-light), and (3) increasing the number of reactant species adsorbed on the surface of photocatalyst (surface reaction and adsorption).

The studies in this area are still in preliminary phases, despite some promising outcomes reported so far but future advances are obviously needed. Still, the works are suffering as related to low effectiveness and low hybrid stability of nanocomposites, that is far behind in context with the industrial needs. At this time, there are many problems that are required to be addressed in order to promise conversion of solar energy to fuel ahead of practical future commercial applications. Knowledge of efficient co-catalysts for water splitting and reduction of CO_2, for instance, is still rare and more research is required to improve the reaction's quantum efficiency.

This hotspot of booming research will offer an unlimited scope of opportunities and challenges in the future. We are assured that growing knowledge on fundamental features through more physical chemistry research escorted by the experimental results through mutual partnership between theory and experiment will results novel material science and technology findings in a positive way. This will undoubtedly continue to promote the growth of light harvesting nanocomposites based on g-C_3N_4 in the post-hype age. Thus, due to developments in engineering and materials science, the holdup of subjects related to energy and the environment can be addressed substantially. Subsequently, applications to convert solar energy will be improved with more real-world applications. As stated previously, joint initiatives from both sides, chemists (academia) and industrial technicians, are compulsory to provide the opportunities for practical use of g-C_3N_4-based nanostructures to give new ways to revolution in sustainable energy. Last but not the least, from collaboration of researchers of all the disciplines worldwide, encompassing physicists, chemists, and materials scientists on a single platform, it is greatly expected that the goals of achieving a cleaner environment and incapacitating the problem of depletion of

fossil fuel by producing alternative energy sources from green and environment friendly photocatalysis will be a reality along with sustainable future.

Acknowledgements Financial support from Higher Education Commission HEC, Pakistan, through grant number 7435/Punjab/NRPU/ R&D/HEC/2017 are acknowledged. The author F. K. Butt acknowledges financial support from the Alexander von Humboldt Foundation and Federal Ministry for Education and Research (BMBF).

References

Chai B, Peng T, Mao J, Li K, Zan L (2012) Graphitic carbon nitride (gC 3 N 4)–Pt-TiO 2 nanocomposite as an efficient photocatalyst for hydrogen production under visible light irradiation. Phys Chem Chem Phys 14(48):16745–16752

Chang C, Fu Y, Hu M, Wang C, Shan G, Zhu L (2013) Photodegradation of bisphenol a by highly stable palladium-doped mesoporous graphite carbon nitride (Pd/mpg-C3N4) under simulated solar light irradiation. Appl Catal B Environ 142:553–560

Chang S, Xie A, Chen S, Xiang J (2014) Enhanced photoelectrocatalytic oxidation of small organic molecules by gold nanoparticles supported on carbon nitride. J Electroanal Chem 719:86–91

Chang F, Zheng J, Wu F, Wang X, Deng B (2019) Binary composites WO3/g-C3N4 in porous morphology: facile construction, characterization, and reinforced visible light photocatalytic activity. Colloids Surf A Physicochem Eng Asp 563:11–21

Chen X, Jun Y-S, Takanabe K, Maeda K, Domen K, Fu X, Antonietti M, Wang X (2009) Ordered mesoporous SBA-15 type graphitic carbon nitride: a semiconductor host structure for photocatalytic hydrogen evolution with visible light. Chem Mater 21(18):4093–4095

Chen X, Shen S, Guo L, Mao SS (2010) Semiconductor-based photocatalytic hydrogen generation. Chem Rev 110(11):6503–6570

Chen G, Bian S, Guo C-Y, Wu X (2019) Insight into the Z-scheme heterostructure WO3/g-C3N4 for enhanced photocatalytic degradation of methyl orange. Mater Lett 236:596–599

Chu S, Wang C, Feng J, Wang Y, Zou Z (2014) Melem: a metal-free unit for photocatalytic hydrogen evolution. Int J Hydrog Energy 39(25):13519–13526

Comini E (2006) Metal oxide nano-crystals for gas sensing. Anal Chim Acta 568(1–2):28–40

Dong G, Zhao K, Zhang L (2012) Carbon self-doping induced high electronic conductivity and photoreactivity of gC 3 N 4. Chem Commun 48(49):6178–6180

Dong G, Zhang Y, Pan Q, Qiu J (2014) A fantastic graphitic carbon nitride (g-C3N4) material: electronic structure, photocatalytic and photoelectronic properties. J Photochem Photobiol C: Photochem Rev 20:33–50

Duan Y (2018) Facile preparation of CuO/g-C3N4 with enhanced photocatalytic degradation of salicylic acid. Mater Res Bull 105:68–74

Fageria P, Nazir R, Gangopadhyay S, Barshilia HC, Pande S (2015) Graphitic-carbon nitride support for the synthesis of shape-dependent ZnO and their application in visible light photocatalysts. RSC Adv 5(98):80397–80409

Fan W, Zhang Q, Wang Y (2013) Semiconductor-based nanocomposites for photocatalytic H 2 production and CO 2 conversion. Phys Chem Chem Phys 15(8):2632–2649

Franklin EC (1922) The ammono carbonic acids. J Am Chem Soc 44(3):486–509

Fujishima A, Honda K (1972) Electrochemical photolysis of water at a semiconductor electrode. Nature 238(5358):37

Gao X, Jiao X, Zhang L, Zhu W, Xu X, Ma H, Chen T (2015) Cosolvent-free nanocasting synthesis of ordered mesoporous gC 3 N 4 and its remarkable photocatalytic activity for methyl orange degradation. RSC Adv 5(94):76963–76972

Gholipour MR, Dinh C-T, Béland F, Do T-O (2015) Nanocomposite heterojunctions as sunlight-driven photocatalysts for hydrogen production from water splitting. Nanoscale 7(18):8187–8208

Gholipour MR, Béland F, Do T-O (2016) Graphitic carbon nitride-titanium dioxide nanocomposite for photocatalytic hydrogen production under visible light. Int J Chem React Eng 14(4):851–858

Gong W, Zou J, Zhang S, Zhou X, Jiang J (2016) Nickel oxide and nickel co-doped graphitic carbon nitride nanocomposites and its octylphenol sensing application. Electroanalysis 28(1):227–234

Gulzar U, Goriparti S, Miele E, Li T, Maidecchi G, Toma A, De Angelis F, Capiglia C Zaccaria RP (2016). Next-generation textiles: from embedded Supercapacitors to Lithium ion batteries

Guo X, Zhang G, Li Q, Xue H, Pang H (2018) Non-noble metal-transition metal oxide materials for electrochemical energy storage. Energy Storage Materials 15:171–201

Hou Y, Wen Z, Cui S, Feng X, Chen J (2016) Strongly coupled ternary hybrid aerogels of N-deficient porous graphitic-C3N4 nanosheets/N-doped graphene/NiFe-layered double hydroxide for solar-driven photoelectrochemical water oxidation. Nano Lett 16(4):2268–2277

Huang L, Xu H, Li Y, Li H, Cheng X, Xia J, Xu Y, Cai G (2013) Visible-light-induced WO 3/gC 3 N 4 composites with enhanced photocatalytic activity. Dalton Trans 42(24):8606–8616

Katsumata K-i, Motoyoshi R, Matsushita N, Okada K (2013) Preparation of graphitic carbon nitride (g-C3N4)/WO3 composites and enhanced visible-light-driven photodegradation of acetaldehyde gas. J Hazard Mater 260:475–482

Kolmakov A, Klenov D, Lilach Y, Stemmer S, Moskovits M (2005) Enhanced gas sensing by individual SnO2 nanowires and nanobelts functionalized with Pd catalyst particles. Nano Lett 5(4):667–673

Kumar S, Surendar T, Kumar B, Baruah A, Shanker V (2014) Synthesis of highly efficient and recyclable visible-light responsive mesoporous gC 3 N 4 photocatalyst via facile template-free sonochemical route. RSC Adv 4(16):8132–8137

Li X, Feng Y, Li M, Li W, Wei H, Song D (2015) Smart hybrids of Zn2GeO4 nanoparticles and ultrathin g-C3N4 layers: synergistic lithium storage and excellent electrochemical performance. Adv Funct Mater 25(44):6858–6866

Li L, Qin J, Bi H, Gai S, He F, Gao P, Dai Y, Zhang X, Yang D, Yang P (2017) Ni (OH) 2 nanosheets grown on porous hybrid gC 3 N 4/RGO network as high performance supercapacitor electrode. Sci Rep 7:43413

Li C, Lou Z, Yang Y, Wang Y, Lu Y, Ye Z, Zhu L (2019a) Hollowsphere Nanoheterojunction of g-C3N4@ TiO2 with high visible light Photocatalytic property. Langmuir 35(3):779–786

Li X, Li Y, Sun G, Luo N, Zhang B, Zhang Z (2019b) Synthesis of a flower-like g-C3N4/ZnO hierarchical structure with improved CH4 sensing properties. Nano 9(5):724

Liebig J v (1834) About some nitrogen compounds. Ann Pharm 10(10)

Liu AY, Cohen ML (1989) Prediction of new low compressibility solids. Science 245(4920):841–842

Liu L, Wang J, Wang C, Wang G (2016) Facile synthesis of graphitic carbon nitride/nanostructured α-Fe2O3 composites and their excellent electrochemical performance for supercapacitor and enzyme-free glucose detection applications. Appl Surf Sci 390:303–310

Low J, Jiang C, Cheng B, Wageh S, Al-Ghamdi AA, Yu J (2017) A review of direct Z-scheme photocatalysts. Small Methods 1(5):1700080

Lu X, Xu K, Chen P, Jia K, Liu S, Wu C (2014) Facile one step method realizing scalable production of gC 3 N 4 nanosheets and study of their photocatalytic H 2 evolution activity. J Mater Chem A 2(44):18924–18928

Ma TY, Dai S, Jaroniec M, Qiao SZ (2014) Graphitic carbon nitride nanosheet–carbon nanotube three-dimensional porous composites as high-performance oxygen evolution electrocatalysts. Angew Chem Int Ed 53(28):7281–7285

Ma L, Fan H, Fu K, Lei S, Hu Q, Huang H, He G (2017) Protonation of graphitic carbon nitride (g-C3N4) for an electrostatically self-assembling carbon@ g-C3N4 core–shell nanostructure toward high hydrogen evolution. ACS Sustain Chem Eng 5(8):7093–7103

Mamba G, Mishra A (2016) Graphitic carbon nitride (g-C3N4) nanocomposites: a new and exciting generation of visible light driven photocatalysts for environmental pollution remediation. Appl Catal B Environ 198:347–377

Mousavi M, Habibi-Yangjeh A, Pouran SR (2018) Review on magnetically separable graphitic carbon nitride-based nanocomposites as promising visible-light-driven photocatalysts. J Mater Sci Mater Electron 29(3):1719–1747

Navlani-García M, Verma P, Kuwahara Y, Kamegawa T, Mori K, Yamashita H (2018) Visible-light-enhanced catalytic activity of Ru nanoparticles over carbon modified g-C3N4. J Photochem Photobiol A Chem 358:327–333

Niu C, Lu Y (1993) Science 261:334

Ong W-J, Tan L-L, Ng YH, Yong S-T, Chai S-P (2016) Graphitic carbon nitride (g-C3N4)-based photocatalysts for artificial photosynthesis and environmental remediation: are we a step closer to achieving sustainability? Chem Rev 116(12):7159–7329

Periyat P, Kavil J, Rakhi R, Anjana P (2018) One-pot synthesis of g-C3N4/MnO2 and g-C3N4/SnO2 hybrid Nanocomposites for Supercapacitor applications

Samanta S, Martha S, Parida K (2014) Facile synthesis of Au/g-C3N4 nanocomposites: an inorganic/organic hybrid plasmonic photocatalyst with enhanced hydrogen gas evolution under visible-light irradiation. ChemCatChem 6(5):1453–1462

Selvarajan S, Suganthi A, Rajarajan M (2018) Fabrication of g-C3N4/NiO heterostructured nanocomposite modified glassy carbon electrode for quercetin biosensor. Ultrason Sonochem 41:651–660

Semencha A, Blinov L (2010) Theoretical prerequisites, problems, and practical approaches to the preparation of carbon nitride: a review. Glas Phys Chem 36(2):199–208

Senthil C, Kesavan T, Bhaumik A, Yoshio M, Sasidharan M (2017) Nitrogen rich carbon coated TiO2 nanoparticles as anode for high performance lithium-ion battery. Electrochim Acta 255:417–427

Shakeel M, Li B, Yasin G, Arif M, Rehman W, Khan HD (2018) In situ fabrication of foamed Titania carbon nitride nanocomposite and its synergetic visible-light Photocatalytic performance. Ind Eng Chem Res 57(24):8152–8159

Shen S, Shi J, Guo P, Guo L (2011) Visible-light-driven photocatalytic water splitting on nanostructured semiconducting materials. Int J Nanotechnol 8(6–7):523–591

Sridharan K, Jang E, Park TJ (2013) Novel visible light active graphitic C3N4–TiO2 composite photocatalyst: synergistic synthesis, growth and photocatalytic treatment of hazardous pollutants. Appl Catal B Environ 142:718–728

Sudhaik A, Raizada P, Shandilya P, Singh P (2018) Magnetically recoverable graphitic carbon nitride and NiFe2O4 based magnetic photocatalyst for degradation of oxytetracycline antibiotic in simulated wastewater under solar light. J Environ Chem Eng 6(4):3874–3883

Tang J-y, Guo R-t, Zhou W-g, Huang C-y, Pan W-g (2018) Ball-flower like NiO/g-C3N4 heterojunction for efficient visible light photocatalytic CO2 reduction. Appl Catal B Environ 237:802–810

Veith GM, Baggetto L, Adamczyk LA, Guo B, Brown SS, Sun X-G, Albert AA, Humble JR, Barnes CE, Bojdys MJ (2013) Electrochemical and solid-state lithiation of graphitic C3N4. Chem Mater 25(3):503–508

Wang X, Maeda K, Thomas A, Takanabe K, Xin G, Carlsson JM, Domen K, Antonietti M (2009) A metal-free polymeric photocatalyst for hydrogen production from water under visible light. Nat Mater 8(1):76

Wang X, Blechert S, Antonietti M (2012) Polymeric graphitic carbon nitride for heterogeneous photocatalysis. ACS Catal 2(8):1596–1606

Wang Y, Ibad MF, Kosslick H, Harloff J, Beweries T, Radnik J, Schulz A, Tschierlei S, Lochbrunner S, Guo X (2015a) Synthesis and comparative study of the photocatalytic performance of hierarchically porous polymeric carbon nitrides. Microporous Mesoporous Mater 211:182–191

Wang Y, Ou R, Wang H, Xu T (2015b) Graphene oxide modified graphitic carbon nitride as a modifier for thin film composite forward osmosis membrane. J Membr Sci 475:281–289

Wang J, Yang Z, Gao X, Yao W, Wei W, Chen X, Zong R, Zhu Y (2017a) Core-shell g-C3N4@ ZnO composites as photoanodes with double synergistic effects for enhanced visible-light photoelectrocatalytic activities. Appl Catal B Environ 217:169–180

Wang M, Shen M, Zhang L, Tian J, Jin X, Zhou Y, Shi J (2017b) 2D-2D MnO2/g-C3N4 heterojunction photocatalyst: in-situ synthesis and enhanced CO2 reduction activity. Carbon 120:23–31

Wu Y, Wang T, Zhang Y, Xin S, He X, Zhang D, Shui J (2016) Electrocatalytic performances of gC 3 N 4-LaNiO 3 composite as bi-functional catalysts for lithium-oxygen batteries. Sci Rep 6:24314

Yan M, Wu Y, Zhu F, Hua Y, Shi W (2016) The fabrication of a novel Ag 3 VO 4/WO 3 heterojunction with enhanced visible light efficiency in the photocatalytic degradation of TC. Phys Chem Chem Phys 18(4):3308–3315

Yu J, Wang S, Low J, Xiao W (2013) Enhanced photocatalytic performance of direct Z-scheme gC 3 N 4–TiO 2 photocatalysts for the decomposition of formaldehyde in air. Phys Chem Chem Phys 15(39):16883–16890

Yu J, Wang K, Xiao W, Cheng B (2014) Photocatalytic reduction of CO 2 into hydrocarbon solar fuels over gC 3 N 4–Pt nanocomposite photocatalysts. Phys Chem Chem Phys 16(23):11492–11501

Yu W, Xu D, Peng T (2015) Enhanced photocatalytic activity of gC 3 N 4 for selective CO 2 reduction to CH 3 OH via facile coupling of ZnO: a direct Z-scheme mechanism. J Mater Chem A 3(39):19936–19947

Zeng J, Lee JY (2005) Effects of preparation conditions on performance of carbon-supported nanosize Pt-co catalysts for methanol electro-oxidation under acidic conditions. J Power Sources 140(2):268–273

Zeng B, Zhang L, Wan X, Song H, Lv Y (2015) Fabrication of α-Fe2O3/g-C3N4 composites for cataluminescence sensing of H2S. Sensors Actuators B Chem 211:370–376

Zhang Y, Ligthart DM, Quek X-Y, Gao L, Hensen EJ (2014) Influence of Rh nanoparticle size and composition on the photocatalytic water splitting performance of Rh/graphitic carbon nitride. Int J Hydrog Energy 39(22):11537–11546

Zhang Y, Zhang D, Guo W, Chen S (2016) The α-Fe2O3/g-C3N4 heterostructural nanocomposites with enhanced ethanol gas sensing performance. J Alloys Compd 685:84–90

Zhao Z, Sun Y, Dong F (2015) Graphitic carbon nitride based nanocomposites: a review. Nanoscale 7(1):15–37

Zhou X, Jin B, Li L, Peng F, Wang H, Yu H, Fang Y (2012) A carbon nitride/TiO 2 nanotube array heterojunction visible-light photocatalyst: synthesis, characterization, and photoelectrochemical properties. J Mater Chem 22(34):17900–17905

Zhu B, Xia P, Ho W, Yu J (2015) Isoelectric point and adsorption activity of porous g-C3N4. Appl Surf Sci 344:188–195

Zou J, Wu S, Liu Y, Sun Y, Cao Y, Hsu J-P, Wee ATS, Jiang J (2018) An ultra-sensitive electrochemical sensor based on 2D g-C3N4/CuO nanocomposites for dopamine detection. Carbon 130:652–663

Part II
Book Chapter for Biomedical

Chapter 11
Application of Nanofiber-Based Composite: Progressive Health Impact

Norizah Abdul Rahman and Mohd Adib Tajuddin Ahmad

11.1 Nanofibers Composite

Nowadays, nanofiber-based composite has appeared as the one of the important advanced materials that attract the attention of many researchers. By definition, nanofibers are Fiber with diameter range of 100 nm or less (Nayak et al. 2011). The very small fiber diameter of the nanofibers produces very large surface area per unit of volume (nanofibers ratio can be as large as 10^3 times of microfibers) (Abdul Rahman et al. 2014), good flexibility in surface functionalities (Haghi and Zaikov 2011) and superior surface properties that act as a platform for the binding sites to cell receptors (Huang et al. 2003). The fiber with micro-scale and macro-scale have been shown less effective for molecular and cellular applications compared to nano-scale fibers (Huang et al. 2003). These excellent properties of nanofibers make them to be broadly used in many medical applications such as drug delivery (Kanafi et al., 2019), tissue engineering (Pompa-Monroy et al. 2018), cancer therapy (Qiu et al. 2013; Wei et al. 2014), cell therapy (Wolfe et al. 2011) and regenerative medicine (Abrigo et al. 2015).

Nanofiber-based composite is a subset of nanocomposites. Nanocomposite is a material comprising more than one phases/components and at least one dimension of the structural phase in nanometric range (Sahay et al. 2012). In composite, the combination of two materials/phases is to produce a new material with desirable physical, chemical and/or biological property, which are significantly different from any of the constituent materials/phases. However, by comparison with conventional composites, the structure of nanocomposites affects their macroscopic properties and gives a great function. There are one or more discontinuous phase in composite

N. A. Rahman (✉) · M. A. T. Ahmad
Department of Chemistry, Faculty of Science, Universiti Putra, Serdang, Selangor, Malaysia
e-mail: a_norizah@upm.edu.my

S. Siddiquee et al. (eds.), *Composite Materials: Applications in Engineering, Biomedicine and Food Science*, https://doi.org/10.1007/978-3-030-45489-0_11

that is called reinforcement and one continuous phase known as matrix (Shaohua et al. 2018). The reinforcing material can be fabricated of nanocomposite in zero, one or two-dimensional form (Mai and Yu 2006), which is usually stronger than the other material/phase as the name implies. Numerous studies have been done using the nanofiber-based composite and the results showed the mechanical properties and thermal/chemical stability that have been improved after incorporating nanofibers (Sahay et al. 2012; Paszkiewicz 2016; Komur et al. 2017; Pant et al. 2018; Park et al. 2019).

11.2 Classification of Nanofiber-Based Composite

Ramaligam and Ramakrishna (2017) classified nanofibers composite into three main categories according to matrix constituent, which are polymer matrix composites, ceramic matrix composites and metal matrix composites (Ramalingam and Ramakrishna 2017). The combination of a polymer matrix and a reinforcing matrix including carbon or glass is an example of polymer matrix composite (Ramalingam and Ramakrishna 2017). For instance, Xu et al. successfully synthesized PEO composite nanofiber mats using cellulose nanocrystals (CNCs) and cellulose nanofibers (CNFs) as reinforcement nanofillers (Xu et al. 2014). Ceramic matrix composite is a combination of ceramic matrix phase and a reinforcing ceramic phase (Ramalingam and Ramakrishna 2017). For example, highly environmental-resistant SiC/SiC composite has been strenuously performed using allylhydridopolycarbosilane (Li et al. 2012). The combination of metallic matrix phase with material other than metal such as ceramic or polymeric phase is known as the metal matrix composite (Ramalingam and Ramakrishna 2017). Biocompatible and antibacterial poly(ε-caprolactone)-nanosilver composite nanofibers scaffolds have been used for tissue engineering applications have a great potential in wound dressing applications (Sumitha et al. 2012).

11.3 Preparation Techniques

Nanofiber-based composite can be manufactured using various techniques such as electrospinning, template synthesis, self-assembly and phase separation. Electrospinning is considered as the most utilised method to produce polymer matrix composite nanofibers, possibly because it is a simple technique that can produce large-scale production of nanofibers, fast, can be applied to wide range of polymers besides the fiber diameter and pattern that are relatively easy to tune.

11.3.1 Electrospinning

Electrospinning is one of the most widely used techniques for polymer fibers. Polymer fibers can be produced by electrospinning technique with small diameter (Kong and Ziegler 2014) and uniform size of morphology (Dadvar et al. 2012). Nowadays, electrospinning technique has attracted much attention owing to its cost-effectiveness, appropriateness to a large variety of materials, goodness in controlling fiber morphology and its ability to be easily scaled. There are three important basic apparatus needed in electrospinning process, which are high voltage supply, collector and syringe pump (Fig. 11.1). To prepare polymer composite nanofibers, the polymer solution needs to be mixed with second materials until well dispersed. The metal needle fitted with syringe has to be filled with the solution on a syringe pump. The syringe pump slowly pumps out the solution; then, the needle is subjected into a high voltage. When the high voltage applied, the surface tension is reduced and the polymer droplet at the tip of metal needle transforms into a pointed shape. Increase in voltage supply will generate the Taylor cone formation and a jet from the tip of needle. When the solvent is jet travelled to the collector and form nanofibers, it will evaporate on the same time. To avoid the jet from turn into droplets (electrospraying), sufficient entanglement of polymer is required (Kong and Ziegler 2014).

Electrospinning is among the best techniques for nanofiber-based composite as it easily allows fabrication formation and can produce high yield of production (Ramalingam and Ramakrishna 2017). If the nanofiber-based composite involves paramagnetic, the magnetic nanoparticles will be directly mixed with polymer nanofibers. Surface treatment has been done in coating, salinization and grafting to avoid agglomeration to occur within matrices (Lee et al. 2015). For example, Fe_3O_4 nanoparticles can be directly mixed with polyvinylidene (PVdF) solution in dimethylacetamide (DMAc) and then, this mixed solution undergoes electrospinning to fabricate PVdF/Magnetite composite nanofibers composite (Russell and Venugopal

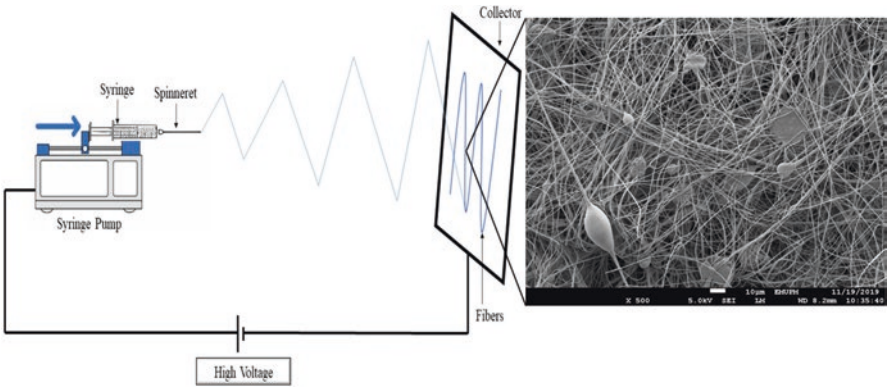

Fig. 11.1 Schematic diagram of electrospinning

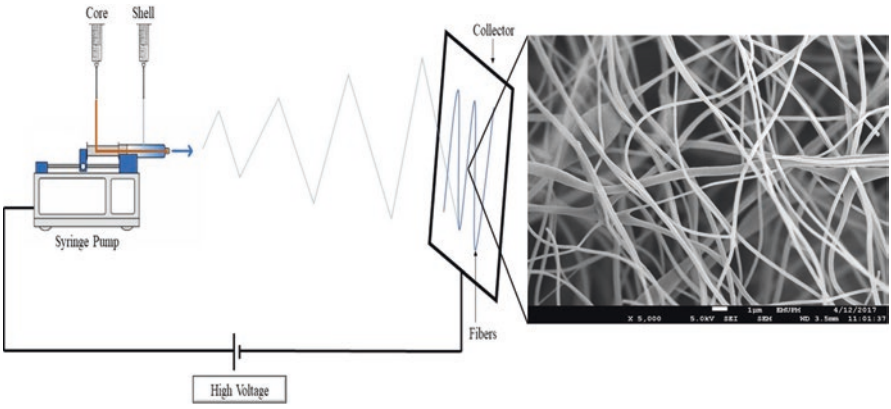

Fig. 11.2 Schematic diagram of coaxial electrospinning apparatus

2014). Electrospun ceramic composite fiber of aluminium acetate/polymer mixtures have been performed using electrospinning technique where the polymer used acted as a carrier for electrospinning purposes and was completely removed after the fiber was annealed at 1200 °C (Tuttle et al. 2008).

In advance technology, coaxial electrospinning has been used to fabricate the core shell nanofiber structures for particular applications. A schematic representation of coaxial electrospinning set up is shown in Fig. 11.2. Coaxial electrospinning is the extension and modification of electrospinning to produce polymer nanofibers with excellent core-sheath or hollow structures (Qu et al. 2013). The process of coaxial electrospinning and the electrospinning is almost the same; nevertheless, electrospinning process only use a single dispensing system to form a fiber on the collector, whereas two different dispensing methods are needed for coaxial electrospinning where the inner and outer fluids are fitted. This coaxial electrospinning technique is able to incorporate nonspinnable material into the phases of shell or core to turn into fiber form (Venugopal et al. 2010). In addition, the coaxial electrospinning can fabricate core-shell nanofiber (Ramalingam and Ramakrishna 2017). For instance, poly(ε-caprolactone) in a study has been dissolved in organic solvent 2,2,2-trifluoroethanol acting as shell solution while fluorescein isothiocyanate-conjugated bovine serum albumin was dissolved in deionised water and poly(ethylene glycol) act as core solution. After that, these shells outside the tube and core solution inside the tube were combined in electrospinning spinneret. It was then found that the nanostructure core-sheath composite nanofibers have achieved the desire product (Zhang et al. 2006) (Fig. 11.3). Nevertheless, electrospinning has some limitations including that it depends on high voltage power supply and low production rate (Abdal-hay et al. 2012a).

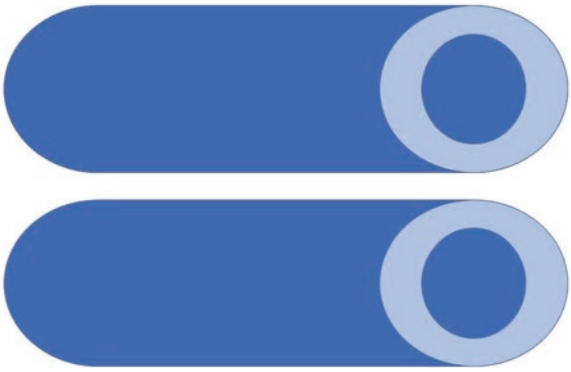

Fig. 11.3 Hollow composite nanofibers prepared by coaxial electrospinning technique

11.3.2 Air Jet Spinning

Air jet spinning is the one of the new techniques that can produce nanofibers with low cost, safe and ultra fast production rate. This technique is developed to overcome the problem from electrospinning technique. For air jet spinning technique, adjustment of the polymer concentration, distance between ground collector and the tip of nozzle are the factors controlling the diameter size of nanofibers. The air jet is invoked the surface tension of the polymer solution; thus, the solution of polymer is stretched into ultra thin fibers. At the same time, the solution vaporise from the product of nanofibers at the collector (Abdal-hay et al. 2012a). Polymer solution fed and pumped with air at high pressure is injected through an annular space around a small pipe. The ejection flow rate is controlled by needle. The polymer solution formed at the tip off the nozzle and the fast air jet stretch the polymer solution into nanofibers. The production of nanofibers takes place at the collector. The air jet spinning technique product is able to collect the nanofibers on solid or liquid collectors, which is similar with electrospinning technique, thus giving benefits to researchers for perform specific chemical or physical reaction on nanofibers product (Abdal-hay et al. 2012a).

This technique is excellent for producing all types of nanofiber composite as it is cheap to conformably and rapidly coat high yield on variety components. Extreme velocity is distributed by pressurised gas to form nanofibers at nozzle outlet and done until all fibers are deposited onto a substrate (Abdal-hay et al. 2012b). For example, nanohydroxyapatite/poly(lactic acid) (nHA/PLA) prepared by air jet spinning. Wet chemical precipitation method was used to synthesise the HA. Then, PLA solutions were dissolved in dichloromethane. Synthesized nHA was mixed with optimised PLA together to prepare suspension solution with continuous stirring followed by sonification of the colloids. Two colloidal solutions were prepared by nHA and PLA. These solutions were then deposited using custom design air brush spraying device. The operation was run at an optimised air pressure. The morphology was affected by variations of spraying distance. The samples were fabricated

and dried in vacuum. Hydroxyapatite/poly(lactic acid) hybrid nanocomposite membrane was then formed (Abdal-hay et al. 2013).

11.3.3 Centrifugal Spinning

Centrifugal spinning technique is another method to produce nanofibers with numerous materials at low price and high speed. It is a simple and fast fabrication of nanofibers for many applications. The important components of centrifugal spinning technique are rotating spinning head and nanofiber collecting system. At a high rotating speed, two liquid jets are generated by centrifugal force at the same time from the needles connected to the syringes. Nanofibers collecting system is used to collect nanofibers in different forms. In centrifugal spinning, rotating spinning head place for the spinning fluid, which is punctured with multiple nozzles around the sidewall. When critical value of rotating speed is reached, the surface tension is overcome by centrifugal force to flow out a liquid jet from the nozzle top of the spinning head. The air frictional force and centrifugal force elongate the jets and undergo a stretching process. The fabrication of nanofibers is formed and deposited on the collector. Other forces that could be involved in this centrifugal spinning is surface tension, gravitational force and rheological force. The most important thing about this centrifugal spinning is that the production rate is high and beneficial for industry (Zhang and Lu 2014).

Centrifugal spinning can be used to prepare metal, ceramic and other composite material nanofibers due to its low-cost, environmental friendly and high spinning efficiency (Zou et al. 2014). For example, recycled bottle-grade poly(ethylene terephthalate), polystyrene and polypropylene were spun into fiber by melting using a centrifugal spinning technique. All recycled bottles were grinded and then each of ground were prepared. These polymers were added to orifice opening per spinneret. The heat was exposed to melt the polymer. The collector consisted of bars in circular pattern with some working distance. Fibers were formed by rotating the spinneret on the surface of collector and fully drew out the polymer from the spinneret (Zander et al. 2017).

11.3.4 Template Synthesis

Template synthesis is a simple technique and easy procedure that can fabricate the nanofibers in almost any laboratory. It is the requiring access to the devices of metal sputtering and electrochemical deposition (Ugo and Moretto 2007). In this method, hollow channels of porous ceramic or polymer templates are the places for producing nanofibers (Wu and Bein 1994). For the first step, the monomers are filled in the porous template. Then, the monomers in the hollow channels of the porous template produce the chemical or electrochemical polymer nanofibers. When the template is

removed by dissolving or etching, the separated nanofibers are obtained. Most of nanofibers of template synthesis produced have a hollow structure because the synthesized polymer is prone to precipitate onto the inner surface of the hollow channels. The polymer solution can directly produce nanofibers and fed into hollow channel. The nanofibers are formed after the polymer solution is solidified, which removes the solvent. The diameter size of the nanofibers are larger compared to that of monomers preparation because polymer solution has high viscosity that will cause the hollow channel hard to be operated with small diameters. This technique can only produce a few micrometres long nanofibers. Membrane pore size is used to determine the diameter size of nanofibers (Zhang and Lu 2014). This technique is easy to utilise, which can adjust the particle size and morphology through template materials and is widely used for ceramic nanofibers composite as it has soft and hard templates; hard template can be used to synthesis the ceramic while the soft template is used to explore the combinations of inorganic and organic and propose a broad synthetic way (Xie et al. 2016).

11.3.5 Self-Assembly

Self-assembly technique is the method that produces nanofibers by holding small molecules together where the molecules arrange themselves into a structures or patterns using non-covalent forces such as hydrophobic forces, hydrogen bonding and electrostatic reaction (Beachley and Wen 2010). There are many mechanisms that can be employed to assemble nanofibers depending on the size of molecules. The most widely used mechanism on this technique is the formation of hydrogel that involves two interpenetrated phases, which are liquid phase and solid phase. Liquid phase usually uses water while solid phase is used in hydrogelator molecules to produce nanofibers (Yang and Xu 2007). Then, the liquid phase is removed from hydrogel and dried nanofibers are obtained. The disadvantage of this technique is that it is limited to small molecules that can self-assemble and arrange themselves under external stimulus. This technique also needs extremely long elaboration with low yield of production and cannot control fibers dimension (Li et al. 2007). For this technique, polymer nanofibers composite is widely utilised due to its clarity, high precision, cheap and high flexibility (Qi et al. 2018). Self-assemble technique can allow fast elaboration of nanocomposites that can integrated in sensors or films to modify microscopic properties. Firstly, silicon dioxide nanoparticles solution is dissolved in chloro-trimethyl-silane (CTS) and dried by solvent evaporation method known as salinization. Then, the nanoparticles bind on textiles where seven different solutions were used to bind with cotton textiles (Lopez-Barbosa and Osma 2017).

11.3.6 Phase Separation

The phase separation to produce nanofibers involves a few steps comprising polymer dissolution, drying, gelation, phase separation and solvent removal (Ma and Zhang 1999). For this preparation, the polymer needs to be dissolved to form homogenous solution at room or high temperature. The solution is kept at the gelation temperature until gel and phase separates are formed to form a nanofibrous matrix. The phases are separated because of the physical incompatibility. When the solvent is removed and the matrix is dried, the nanofibers are formed (Zhang and Lu 2014). The properties of nanofibers depend on polymer concentration; if the polymer concentration increase, the porosity of fibers decreases but with improved mechanical properties (Nune et al. 2017). Mechanical properties of nanofiber matrix can be changed by altering the concentration of the polymer (Ramakrishna et al. 2005). The disadvantage of using this technique is that the continuous fibers can be produced with short size, but not all polymers can use this technique as it needs gelation capability that is limited to only certain polymers (Alghoraibi 2018). The advantages are their porosity, charge density, hydrophilicity and thermal stability that may be adjusted by placing nanoparticles with definite elements and components on the surface or within the matrix of the polymer scaffold. The surface-located nanoparticles have excellent characteristics such as photocatalytic, adsorptive and antibacterial capabilities (Haase et al. 2017).

11.4 Application of Nanofiber-Based Composite in Biomedical Applications

Nowadays, nanofiber-based composite has been most widely used in biomedical applications including tissue engineering, drug delivery and gene delivery. The nanofiber composite offers many advantages and promising feature properties such as very high surface area per volume and designable flexibility in functionalisation of the fibers to form targeted product that can suit specific application.

11.4.1 Tissue Engineering

Biomimetic nanofiber scaffold mimicking with a great potential in the native extracellular matrix provides a good way to rebuild functions or achieve favourable responses for tissue regeneration. Nanofibers are now being used as scaffolds for cell infiltration and tissue growth. Electrospun nanofibrous scaffolds give promising achievement in cell attachment, penetration and proliferation (Goyal et al. 2013). In the tissue engineering field, the right choice of biomaterial as a substrate is very important for producing excellent scaffolds of fibrous materials. Among natural

biomaterials, gelatine, collagen and chitosan are commonly used for skin regeneration (Naves et al. 2017). There are many biomolecules that are involved in this field to improve fibers functional properties for biomedical application. Growth factor (GFs) are naturally occurring substances capable of binding cell surface receptors and directing cellular activities for a new tissue regeneration (Varkey et al. 2004). Localised delivery of exogenous GFs is effective for healing process and cellular components formation, thus making them as a promising aspect for tissue regeneration (Chen et al. 2010a). Polymeric nanofiber scaffolds give appropriate microenvironment by action from extracellular matrix and growth factors promoting cell growth and tissue generation. For instance, hydroxyapatite/poly(lactic-*co*-glycolic) nanofibers scaffolds have been used in drug delivery system to promote osteoblast growth, proliferation and differentiation (Haider et al. 2014). Metallic nanofiber-based composites have been used to make it durable and has high antibacterial activity (Zahedi et al. 2009). Due to its excellent morphology, it can be used as ideal wound healing material, which involves large surface area that increases the efficiency of antibacterial properties (Williams et al. 2012). The nanofiber composite is also utilised in bone tissue engineering. For example, in the study by Lui et al. (Liu et al. 2009), nanofibrous gelatine with diameter 150 nm over apatite composite was studied regarding its the biomimetic behaviour and compare it with that of commercial gelatine foam.

11.4.2 Drug Delivery

The main aim for producing drug delivery is to develop efficient transport of drug molecules into the target tissues, cells or organs in the body for a certain period of time (Ramalingam and Ramakrishna 2017). It is dynamic and futuristic way for transporting the drugs in the medical therapy, which is not yet commercial until now. This drug delivery perhaps alter the desired properties and proper manner (Mohanty and Geetha 2017). Drug delivery system (DDS) has the potential to improve the existed drug (Webster 2006). The promising of therapeutic efficiency involves drug specificity, efficiency, tolerability and therapeutic index. The benchmarks for promising drug delivery are slow delivery, controlled release and targeted delivery. To design an efficient DDS, some factors need to be considered in terms of targeting ability, duration delivery, mechanism, nature of drug carrier, administration route, bioavailability, biocompatibility and drug characteristics. The polymeric nanoparticles or nanofibers, hydrogels, micelles and microspheres have an excellent property for drug delivery system. The gains from using these materials are from their low toxicity, enhanced drug targeting, improved therapeutic adsorption rates and good self-defence against any degradation reaction in the body (Safari and Zarnegar 2014).

Electrospinning is widely used for producing drug-loaded nanofibers due to its low cost, ease of handling, high encapsulation efficiency, high loading capacity and concurrent delivery of diverse therapies (Zamani et al. 2013). Usually, the drug

molecules are delivered to target position by polymer nanofiber composites as candidate vehicle. Recently, nanofibers composite based titanium, which is a drug loaded nanofiber, has been studied for cancer chemotherapy. The titanium by the name of titanocene and PLLA nanofibers were studied to determine the efficiency of release system. The result of PLLA/titanocene composite fibers showed the best controlled release system for cancer chemotherapy (Chen et al. 2010b). In other study, Tran et al. (2015) demonstrated a controllable and switchable drug delivery of ibuprofen using poly(*N*-isopropylacryamide)(pNIPAM)/poly(ε-caprolactone) (PCL) depending on temperature responsive composite nanofibers. The ibuprofen was fabricated with three different types of nanofibers known as PCL, pNIPAM and pNIPAM/PCL composite nanofibers using electrospinning technique. Each nanofiber was tested on release rates at 22 °C and 34 °C. For PCL nanofibers, the ibuprofen was not affected with only 10% change in delivery rates while pNIPAM nanofibers were shown to quickly release the ibuprofen. Meanwhile, the pNIPAM/PCL nanofibers showed the best release rates of ibuprofen with linear and controlled release by 70% change in delivery at 22 °C and due to hydrophobicity of PCL and PNIPAM, this led to a lower release rates at 34 °C (Tran et al. 2015). Multiple drug delivery can be designed using nanofiber composite (Zhao et al. 2015). For instance, poly(ethylene glycol)(PEG)/poly($_{L}$-lactic acid)(PLA) nanofibers have been successfully loaded with two different drugs namely paclitaxel (PTX) and doxorubicin hydrochloride (DOX) for delivery system. The experiment was conducted to study their solubility properties and distribution in the nanofibers. The result showed DOX has a high release rate due to its high hydrophilicity that easily diffused into water, while PTX has low release rate due to its high hydrophobicity (Xu et al. 2009). A multi-layered electrospun nanofiber mesh is the time-engineered dual release system that is very useful in preparation when drug is release at different time. The drug to polymer ratio of every single mesh is designed as multilayer meshes. The control of release rate and duration of release of the drugs is depending on fiber diameter size and thickness of meshes (Wang et al. 2019).

11.4.3 Gene Delivery

Nanofiber-based composites are promising materials for emerging carrier system to deliver genes to the target sites. Gene delivery technologies can improve the functionalisation of the target. Appropriate carrier system, nontoxic, ability to overcome immune responses and ability to go through complicated reaction in the body to reach the target site are the important factor for gene delivery of clinically valuable cell types such as stem and cancer cells (Sung et al. 2003; Panyam and Labhasetwar 2003). Viral and nonviral vectors are categorised as gene delivery vehicles. It has been revealed that direct view of viral based vectors in the human body can cause immune responses to become bad. Thus, several studies have been done to fix gene delivery with biomaterial system (Jang et al. 2007). The gene delivery response to the target tissue relies on the delivery mechanisms such as receptor mediated

endocytosis, delivery mode and nanofiber material properties including biodegradability and bioavailability (Xiang et al. 2011).

The electrospun nanofiber composites is used as spatial templates to make it efficient in altering the functions of native extracellular matrix (Sill and von Recum 2008). Electrospinning and coaxial electrospinning are cost effective for producing nanofibers for gene delivery. Usually, nanofiber composites consist of ceramic or polymer. The genes also mix with polymer solution to embed themselves into nanofibers and immobilised into the target genes through nanofibers (Lakshmi Priya et al. 2017). For example, the electrospun poly(*L*-lactic acid)/collagen nanofiber composite has been used for bone morphogenetic protein plasmid DNA delivery and the result showed that the bone was greatly formed (Zhao et al. 2016). The DNA was successfully embedded into porous composite structures to utilise the encoded growth factors, signalling molecules and other bioactive molecules (Lee et al. 2014).

11.5 Conclusions and Future Remarks

Nanofiber composites are a new class of nanomaterials that have gained attention due to its outstanding structural and tunable physical properties, which is usually superior compared to their individual parent materials. Significant progress has been made by researchers to produce new nanofiber composite. New materials, systems, processes, and formulations are being developed to solve problems and to create new potential application of the nanofiber composite. Nanofiber composites prepared of biocompatible and biodegradable materials show great potential in biomedical applications such as wound healing, tissue engineering, cancer therapy, stem cells, and drug delivery. Although nanofiber composites were used effectively for the biomedical field, the applicability of the fibers could be enhanced. Nanofiber composites are expected to give big impact in wide range of biomedical applications, with great challenges and expectations ahead.

Acknowledgements The authors are grateful for the financial supports by the Research University Grant from Universiti Putra Malaysia (Grant code: GP-IPS/2018/9594900).

References

Abdal-hay A, Barakat N, Lim JK (2012a) Novel technique for polymeric nanofibers preparation: air jet spinning. Sci Adv 4:1268–1275

Abdal-hay A, Sheikh FA, Lim JK (2012b) Air jet spinning of hydroxyapatite/poly(lactic acid) hybrid nanocomposite membrane mats for bone tissue engineering. Colloids Surf B Biointerfaces 102C:635–643

Abdal-hay A, Sheikh FA, Lim JK (2013) Air jet spinning of hydroxyapatite/poly(lactic acid) hybrid nanocomposite membrane mats for bone tissue engineering. Colloids Surf B Biointerfaces 102:635–643

Abdul Rahman N, Srinivas ARG, Travas-Sejdic J (2014) Spontaneous stacking of electrospun conjugated polymer composite nanofibers producing highly porous fiber mats. Synth Met 191:151–160

Abrigo M, Kingshott P, McArthur S (2015) Electrospun polystyrene fiber diameter influences bacterial attachment, proliferation and growth. ACS Appl Mater Interfaces 7

Alghoraibi I Different methods for nanofibers design and fabrication. 2018

Beachley V, Wen X (2010) Polymer nanofibrous structures: fabrication, biofunctionalization, and cell interactions. Prog Polym Sci 35(7):868–892

Chen F-M, Zhang M, Wu Z-F (2010a) Toward delivery of multiple growth factors in tissue engineering. Biomaterials 31:6279–6308

Chen P et al 2010b A controlled release system of titanocene dichloride by electrospun fiber and its antitumor activity in vitro. European journal of pharmaceutics and biopharmaceutics: official journal of Arbeitsgemeinschaft für Pharmazeutische Verfahrenstechnik e.V, 76: p. 413–420

Dadvar S, Tavanai H, Morshed M (2012) Effect of embedding MgO and Al2O3 nanoparticles in the precursor on the pore characteristics of PAN based activated carbon nanofibers. J Anal Appl Pyrolysis 98:98–105

Goyal K, Rath AG, Garg T Nanotechnological approaches for genetic immunization. 2013. p. 67–120

Haase MF et al (2017) Multifunctional nanocomposite hollow fiber membranes by solvent transfer induced phase separation. Nat Commun 8(1):1234

Haghi AK, Zaikov GE (2011) Nano-scaled and smart materials. Nova Science Publishers. 1–163

Haider A, Chandra Gupta K, Kang I-K (2014) PLGA/HA hybrid nanofiber scaffold as a nanocargo carrier of insulin for accelerating bone tissue regeneration. 9:314

Huang Z-M et al (2003) A review on polymer nanofibers by electrospinning and their applications in nanocomposites. Compos Sci Technol 63(15):2223–2253

Jang J-H, Lim K-i, Schaffer D (2007) Library selection and directed evolution approaches to engineering targeted viral vectors. Biotechnol Bioeng 98:515–524

Kanafi N et al (2019) Hydrogel nanofibers from carboxymethyl sago pulp and its controlled release studies as a methylene blue drug carrier. Fibers 7:56

Komur B et al (2017) Starch/PCL composite nanofibers by co-axial electrospinning technique for biomedical applications. Biomed Eng 16(1):40–40

Kong L, Ziegler GR (2014) Fabrication of pure starch fibers by electrospinning. Food Hydrocoll 36:20–25

Lakshmi Priya M et al (2017) 10 - Nanofiber composites in gene delivery. In: Ramalingam M, Ramakrishna S (eds) Nanofiber composites for biomedical applications. Woodhead Publishing, pp 253–274

Lee S, Jin G, Jang J-H (2014) Electrospun nanofibers as versatile interfaces for efficient gene delivery. J Biol Eng 8(1):30

Lee H-J et al (2015) Biomedical applications of magnetically functionalized organic/inorganic hybrid nanofibers. Int J Mol 16:13661–13677

Li W-J, Shanti R, Tuan R Electrospinning technology for nanofibrous scaffolds in tissue engineering. 2007

Li Q et al (2012) Fabrication and properties of 3-D Cf/SiC–ZrC composites, using ZrC precursor and polycarbosilane. J Am Ceram Soc 95

Liu X et al (2009) Biomimetic nanofibrous gelatin/apatite composite scaffolds for bone tissue engineering. Biomaterials 30(12):2252–2258

Lopez-Barbosa N, Osma J (2017) Nanocomposites fabrication by self-assembly method to modify macroscopic properties. J Phys Conf Ser 786:012003

Ma PX, Zhang R (1999) Synthetic nano-scale fibrous extracellular matrix. J Biomed Mater Res 46(1):60–72

Mohanty S, Geetha M (2017) 4 - metallic nanofiber composites. In: Ramalingam M, Ramakrishna S (eds) Nanofiber composites for biomedical applications. Woodhead Publishing, pp 79–94

Naves LB, Almeida L, Rajamani L (2017) 11 - Nanofiber composites in skin tissue engineering. In: Ramalingam M, Ramakrishna S (eds) Nanofiber composites for biomedical applications. Woodhead Publishing, pp 275–300
Nayak R et al (2011) Recent advances in nanofibre fabrication techniques. Text Res J 82(2):129–147
Nune SK et al (2017) Chapter 11 - Electrospinning of collagen nanofiber scaffolds for tissue repair and regeneration. In: Ficai D, Grumezescu AM (eds) Nanostructures for novel therapy. Elsevier, pp 281–311
Pant B et al (2018) Electrospun salicylic acid/polyurethane composite nanofibers for biomedical applications. Int J Polym Mater 67(12):739–744
Panyam J, Labhasetwar V (2003) Biodegradable nanoparticles for drug and gene delivery to cells and tissue. Adv Drug Deliv Rev 55(3):329–347
Park Y et al (2019) Thermal conductivity enhancement in electrospun poly(vinyl alcohol) and poly(vinyl alcohol)/cellulose nanocrystal composite nanofibers. Sci Rep 9(1):3026
Paszkiewicz S (2016) Multifunctional polymer nanocomposites based on thermoplastic polyesters, pp 123–144
Mai Y-W, Yu Z-Z (2006) Polymer nanocomposites. Woodhead Publishing and Maney Publishing on behalf of The Institute of Materials, Minerals & Mining, Cambridge
Pompa-Monroy D et al Gelatin and collagen nanofiber scaffolds for tissue engineering. 2018
Qi W, Zhang X, Wang H (2018) Self-assembled polymer nanocomposites for biomedical application. Curr Opin Colloid Interface Sci 35:36–41
Qiu K et al (2013) Doxorubicin-loaded electrospun poly(L-lactic acid)/mesoporous silicananoparticles composite nanofibers for potential postsurgical cancer treatment. J Mater Chem B 1
Qu H, Wei S, Guo Z (2013) Coaxial electrospun nanostructures and their applications. J Mater Chem A 1
Ramakrishna S et al (2005) An introduction to electrospinning and nanofibers. World Scientific:396
Ramalingam M, Ramakrishna S (2017) 1 - introduction to nanofiber composites. In: Ramalingam M, Ramakrishna S (eds) Nanofiber composites for biomedical applications. Woodhead Publishing, pp 3–29
Russell S, Venugopal A (2014) Controlling dielectric and magnetic properties of PVdF/magnetite nanocomposite fibre webs. Int J Polym Sci 2014
Safari J, Zarnegar Z (2014) Advanced drug delivery systems: nanotechnology of health design a review. J Saudi Chem Soc 18(2):85–99
Sahay R et al Electrospun composite nanofibers and their multifaceted applications. 2012
Shaohua J et al (2018) Electrospun nanofiber reinforced composites: a review, vol 9
Sill TJ, von Recum HA (2008) Electrospinning: applications in drug delivery and tissue engineering. Biomaterials 29(13):1989–2006
Sumitha M et al (2012) Biocompatible and antibacterial nanofibrous poly(ϵ-caprolactone)-nanosilver composite scaffolds for tissue engineering applications. J Macromol Sci, Part A 49:131–138
Sung S-J et al (2003) Effect of polyethylene glycol on gene delivery of polyethylenimine. 26:492–500
Tran T et al (2015) Controllable and switchable drug delivery of ibuprofen from temperature responsive composite nanofibers. Nano Converg 2(1):15
Tuttle RW et al (2008) Electrospun ceramic fibers: composition, structure and the fate of precursors. Appl Surf Sci 254(16):4925–4929
Ugo P, Moretto LM (2007) 16.2 - template deposition of metals. In: Zoski CG (ed) Handbook of electrochemistry. Elsevier, Amsterdam, pp 678–709
Varkey M, Gittens SA, Uludag H (2004) Growth factor delivery for bone tissue repair: an update. Expert Opin Drug Del 1:19–36
Venugopal J et al (2010) Biomimetic hydroxyapatite-containing composite nanofibrous substrates for bone tissue engineering. Philos Trans A Math Phys Eng Sci 368(1917):2065–2081
Wang C et al (2019) Fabrication of electrospun polymer nanofibers with diverse morphologies. Molecules 24(5), p 834

Webster JG Encyclopedia of medical devices & instrumentation. 2006.; Available from: http://www.credoreference.com/book/wileymdi

Wei J et al (2014) Multiple drug-loaded electrospun PLGA/gelatin composite nanofibers encapsulated with mesoporous ZnO nanospheres for potential postsurgical cancer treatment. RSC Adv 4:28011

Williams GR et al (2012) Electrospun nanofibers in drug delivery: recent developments and perspectives. 3:515–533

Wolfe P et al (2011) The creation of electrospun nanofibers from platelet rich plasma. J Tissue Sci Eng 2

Wu C-G, Bein T (1994) Conducting polyaniline filaments in a mesoporous channel host. Science 264(5166):1757

Xiang S et al (2011) *Uptake mechanisms of non-viral gene delivery*. 158:371–378

Xie Y et al (2016) Review of research on template methods in preparation of nanomaterials. J Nanomater 2016:10

Xu X et al (2009) Ultrafine PEG–PLA fibers loaded with both paclitaxel and doxorubicin hydrochloride and their in vitro cytotoxicity. Eur J Pharm Biopharm 72(1):18–25

Xu X et al (2014) Comparison between cellulose nanocrystal and cellulose Nanofibril reinforced poly(ethylene oxide) nanofibers and their novel shish-kebab-like crystalline structures. Macromolecules 47:3409–3416

Yang Z, Xu B (2007) Supramolecular hydrogels based on biofunctional nanofibers of self-assembled small molecules. J Mater Chem 17(23):2385–2393

Zahedi P et al (2009) A review on wound dressing with an emphasis on electrospun nanofibrous polymeric bandages. 21:77–95

Zamani M, Prabhakaran MP, Ramakrishna S (2013) Advances in drug delivery via electrospun and electrosprayed nanomaterials. 8:2997–3017

Zander N, Gillan M, Sweetser D (2017) Composite fibers from recycled plastics using melt centrifugal spinning. 10

Zhang X, Lu Y (2014) Centrifugal spinning: an alternative approach to fabricate nanofibers at high speed and low cost. Polym Rev 54(4):677–701

Zhang Y et al (2006) Coaxial electrospinning of (fluorescein Isothiocyanate-conjugated bovine serum albumin)encapsulated poly(epsilon-caprolactone) nanofibers for sustained release. Biomacromolecules 7:1049–1057

Zhao X et al (2015) Self-coated interfacial layer at organic/inorganic phase for temporally controlling dual-drug delivery from electrospun fibers. Colloids Surf B Biointerfaces 130:1–9

Zhao X, Komatsu D, Hadjiargyrou M (2016) Delivery of rhBMP-2 plasmid DNA complexes via a PLLA/Collagen electrospun scaffold induces ectopic bone formation. J Biomed Nanotechnol 12:1285

Zou W et al (2014) Recent advances in centrifugal spinning preparation of nanofibers. 1015:170–176

Chapter 12
Polymer Based Nanocomposite: Recent Trend in Safety Assessment in Biomedical Application

Rabiatul Basria S. M. N. Mydin, Nor Hazliana Harun, Ku Nur Izzati Ku Mohamad Faudzi, and Nur Afiqah Amalina Romli

12.1 Introduction

The breakthrough and rapid developments of nanotechnologies has become one of the significant technological advances in every sector especially in biomedical sectors (Kim et al. 2018; Müller et al. 2017). Among these nanotechnologies, polymer-based nanocomposites (NCs) are the most famous one owing to the unique properties of nanomaterials. It can be defined as a mixture of two or more-phase materials forming solids where one or more dispersed phase is in nanoscale and a polymeric major phase (Müller et al. 2017). Polymer-based NCs could be synthesized with the combination of polymers and inorganic/organic nanoparticles which have obtained extensive research due of its distinctive physiochemical properties, outstanding mechanical strength and their high surface-to-volume ratio.

Rabiatul Basria S. M. N. Mydin (✉)
Oncological and Radiological Sciences Cluster, Advanced Medical and Dental Institute, Universiti Sains Malaysia, Kepala Batas, Pulau Pinang, Malaysia

Department of Biological Sciences, NUS Environmental Research Institutee, National University of Singapore, Singapore, Singapore
e-mail: rabiatulbasria@usm.my

N. H. Harun · N. A. A. Romli
Oncological and Radiological Sciences Cluster, Advanced Medical and Dental Institute, Universiti Sains Malaysia, Kepala Batas, Pulau Pinang, Malaysia

Ku Nur Izzati Ku Mohamad Faudzi
Oncological and Radiological Sciences Cluster, Advanced Medical and Dental Institute, Universiti Sains Malaysia, Kepala Batas, Malaysia

School of Materials and Mineral Resources Engineering, Engineering Campus, Universiti Sains Malaysia, Nibong Tebal, Pulau Pinang, Malaysia

S. Siddiquee et al. (eds.), *Composite Materials: Applications in Engineering, Biomedicine and Food Science*, https://doi.org/10.1007/978-3-030-45489-0_12

Synthesizing safe polymer-based NCs that have favourable compatibility and bioactivity has been targeted in the design of polymer-based NCs. The demand for environmental preservation has led to the evolution of greener and biodegradable polymers. In order to resolve potential risks of polymer materials, to create environmentally friendly products and sustaining ecological balance, biodegradable polymer materials are essential requirement (Sun et al. 2018; Tibolla et al. 2019).

One of the current challenges faced by hospital communities and society in biomedical arena arise from the infections associated with medical device. Medical device can be placed into human bodies either temporarily (short-term period); contact lenses, central venous catheters, mechanical heart valves, urinary catheters, or permanently; prosthetic hips and joints and intramedullary nails (Tran and Tran 2012). The introduction of medical devices by surgery or implantation with poor sterilization and disinfection practices to patient exposes to a high risk of nosocomial infections. This scenario also leads to the increment in mortality rates among immunocompromised patient.

In general, catheters will be inserted into a body cavity, blood vessel or duct to allow for the administration of liquids, medications, injection and urine drainage (Mandal 2019). Bacteremia causes by indwelling urethral catheter hold the highest rates of catheter urinary tract infections (80%) as compared to other types of nosocomial infections (CDC 2015; Nicolle 2014; Tambyah and Oon 2012). Asymptomatic bacteriuria and symptomatic urinary tract infection are another common adverse effect associated with indwelling urinary catheter after be placed for several weeks (Nicolle 2014). The insertion of catheter bypasses normal host defences leads to the entry of gram-positive and gram-negative pathogens such as *Staphylococcus aureus*, *Escherichia coli* and *Proteus mirabilis* into the bladder or blood vessel (Fisher et al. 2015; Tambyah 2004). Cases with bacterial contamination on implantable device such as prosthetic joint, ventricular assist devices, dental, orthopedic, pacemaker and vascular graft leading to device failure, chronic infection, increase patient postoperative morbidity and mortality rates (Darouiche 2004; Guggenbichler et al. 2011). Surgical site infections (SSIs), other types of nosocomial infection, occurred for most of 500,000 cases in each year with the rate of 2.8 per 100 operations (Whitehouse et al. 2002). It is most commonly related with bacterial biofilm colonization. Major challenges in treating biofilm development on implant device cause delivery of high dose antibiotics, however, repetitive exposure can develop resistance among organisms.

Thus, most researcher been urged to study alternative solution to prevent the current mentioned problems. Recently, most studies demonstrate the biomedical applications of polymer NCs could improve our health systems or vice versa. Hence, valid standards and protocols for measurements of both aspects; compatibility and bioactivity should be followed accordingly to prevent the possible damages.

12.2 Biocompatibility, Hemocompatibility and Bioactivity Assessment

The utilizing of the advantages and capabilities of those polymer -based NC in biomedical fields, relies heavily on three important aspects, which known as biocompatibility, hemocompatibility and bioactivity. The presented data in Tables 12.1, 12.2 and 12.3 particularly outlined the parameters been investigated to study the interaction of blood components responses to polymer-based NCs and direct surface reaction of polymer after being immersed in synthetic blood plasma. Whereas, Table 12.4 is summarized polymer-based NCs been synthesized to be used in biomedical fields in various purposes.

Table 12.1 Summary list of parameters under thrombosis, coagulation test and complement activation

Test group	Assays parameter	Instrument/Principle	References
Complement system	C3a, C5a, Bb, C4d, C5b-9	ELISA	Weber et al. (2018)
Coagulation and thrombosis	Factor XIIa, TAT, F1 + 2, free active thrombin, FPA, Apt	ELISA, Optical density, Viscoelasticity	Weber et al. (2018)
Thrombin generation (CAT assay)	Thrombin generation (TG) variables in the presence or absence of platelets: lag-time maximum thrombin concentration (Cmax) time required to reach Cmax (Tmax) endogenous thrombin potential (ETP)	Calibrated automated thrombogram (96-well plate fluorometer)	Tynngard et al. (2015)
Coagulation and fibrinolysis	Overall hemostasis potential (OHP) in plasma	–	Antovic (2010)

Table 12.2 Summary list of parameters under hemolysis assay

Assays parameter	Blood categories	Instrument / principle	Ref
ASTM E2524-08-2013	Whole blood	Spectrophotometer (Absorbance 540 nm)	Dobrovolskaia et al. (2008)
ASTM F-756-00	Whole blood	Spectrophotometer (Absorbance 540 nm)	Dobrovolskaia et al. (2008)
Amount of cyanmethemoglobin in the supernatant	Whole blood	Spectrophotometer (Absorbance 540 nm)	Neun et al. (2018)
Serum hemolytic activity	Serum	Spectrophotometer (Absorbance 414 nm)	Pham et al. (2014)

Table 12.3 Summary list of parameters under bioactivity assay

Assays parameter	Instrument / Principle	References
Surface changes and apatite formation	X-ray diffraction Field emission scanning electron microscope Quartz crystal microbalance method	Drouet (2013); Gyori et al. (2017); Juraski et al. (2017); Yoshida and Hayakawa (2017)
Ion release	Inductively coupled plasma mass spectrometry (ICP-MS) Graphite furnace atomic absorption	Ho et al. (2018)
Chemical properties	Fourier-transform infrared spectroscopy	Bollino et al. (2017)
Composition	Energy-dispersive X-ray spectroscopy	Wang et al. (2013)
pH changes	pH meter	Xu et al. (2016)

12.2.1 Biocompatibility Assay

One of the crucial features that must be measured in synthesizing polymer-based NCs for biomedical application is the biocompatibility reaction after being introduced to the host living cells (Hule and Pochan 2007). It is a sine qua non condition specifically for polymer-based NCs use. Biocompatibilities in polymer-based NCs are critical aspects in the performances of medical devices which rely entirely on the interactions between living cells and its microenvironment. However, the polymer-based NCs have to be considered as it serves as the active sites for cell adhesion and proliferation. Figure 12.1 provides an overview of biocompatibility definition and simplified different types of assays for this parameter.

Integrins are transmembrane protein that responsible for the interaction of cell adhesion to the biomaterial substrates and also involved in cell signalling, thereby controlling cellular behaviours such as shape, differentiation, motility and growth (Siebers et al. 2005). Understanding the mechanisms of cell responses to physicochemical and biological properties of biomaterial surfaces can enhance the development of novel bio-NCs with desired biological properties (Hule and Pochan 2007).

Polymer-based NCs have been widely reported in scientific literature regarding their commercial applications in many technological sectors and biomedical fields due to its outstanding properties of biodegradable and biocompatible of cell responses (Müller et al. 2017). However, toxicity of nano-structured materials on biological environment caused biocompatible issues, later could leads to some health problems. Biocompatibility testing of polymer-based NCs can be tested using in vitro cell culture, cell viability and *in vivo* animal tests. Nonetheless, *in vitro* studies are used for evaluating bioactivity of medical devices which not stimulate the real and complex conditions existing within living organisms. Therefore, *in vivo* studies are an accurate and precise testing for tissue responses to medical

Table 12.4 Summary of polymer-based nanocomposites been synthesized for biomedical application

Biomedical application	Nanoparticle	Types of polymer	Biocompatibility/Hemocompatibility Assays	References
Catheter	Zinc - doped copper oxide nanoparticles	Silicone	Under saline solution: leaching and HET-CAM test Under L929 growth medium: MTT test Under peripheral blood mononuclear cell (PBMC) growth medium: cytokine secretion assay	Shalom et al. (2017)
Multilumen catheters	Nitric Oxide (NO) Release from S-Nitroso-N-acetylpenicillamine (SNAP) composite filled lumen	Silicone	Catheter explant and evaluation of Hemocompatibility: Image collection of the exterior of the whole catheter and the interior of the vessel wall (camera and image J analysis)	Brisbois et al. (2016)
Extracorporeal circulation device	E2As with nitric oxide release PVC coating tubing loop	Polyvinyl chloride (PVC)	Rabbit thrombogenicity model protocol Platelet aggregometry Flow cytometry for P-selectin expression Determination of thrombus area	Handa et al. (2014)
Biomedical device	Titanium dioxide nanoparticles	Polytetrafluorethylene (PTFE)	Platelet adhesion measurement. Blood coagulation measurement	Xue et al. (2011)
Drug delivery	Silica and silk nanoparticles	–	Dose dependent effects of nanoparticles on coagulation and inflammation Nanoparticle uptake using whole and fractionated blood Shear flow incubation of nanoparticles with whole blood	Maitz et al. (2017)
Cardiovascular stents	Biofunctional coating composed of Type IV collagen (CoIV) and hyaluronan (HA) previously fabricated onto the titanium (Ti) substrate	–	Platelet adhesion Whole blood test	Li et al. (2016)

(continued)

Table 12.4 (continued)

Biomedical application	Nanoparticle	Types of polymer	Biocompatibility/Hemocompatibility Assays	References
Fluorescent labels	Hydrophilic copper indium sulphide/ Zinc sulphide quantum dots	Jeffamine	Whole blood test: Hemolysis Morphology and size distribution of blood cells and coagulation activation Extrinsic pathway (prothrombin time, PT assay) Intrinsic pathway (activated partial thromboplastin time, APTT assay)	Speranskava et al. (2016)
Drug delivery carriers/ biomedical implant	Halloysites nanotubes	–	Hemolysis rate test Plasma clotting activity assay Platelet activation	Liu et al. (2015)
Orthopedic device	Nanohydroxyapatite nanocomposites	Poly(methylmethacrylate)	Hemolysis rate test	Yilmaz et al. (2018)
Scaffold	–	Polycaprolactone films with Zwitterionic polymer	Platelet adhesion tests using PRP and human whole blood Hemolysis assay PRT assay	Jiang et al. (2011)
Cardiac patch	Nickel oxide (NiO)	Polyurethane (PU)	APTT assay PT assay Hemolysis studies	Jaganathan and Mani (2018)

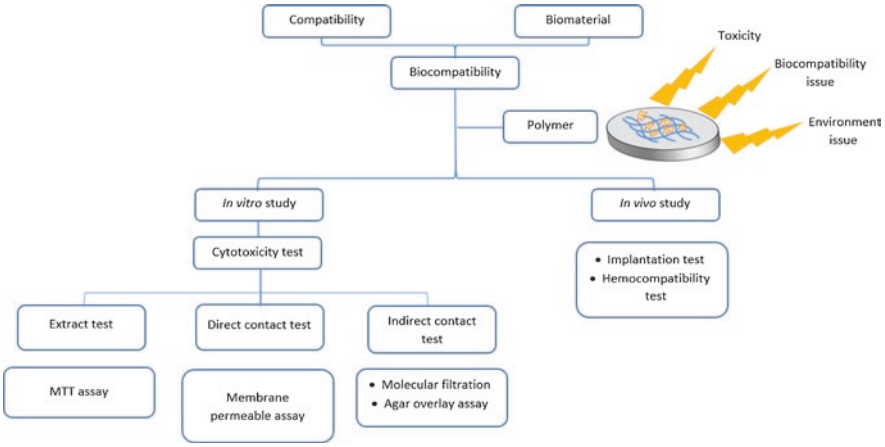

Fig. 12.1 Biocompatibility testing for *in vitro* and *in vivo* studies for cell-material interaction

devices. Biocompatibility problems are remaining challenges in the recent advances for polymeric NCs.

Therefore, the polymer-based NCs need to evaluate the overall safety of the material by performing three different biocompatibility tests which involved *in vitro* and *in vivo* studies such (i) *in vitro* cytotoxicity of the material, which follow standard cell culture procedures using both Hs680 (human tracheal fibroblast) and Saos-2 (human osteosarcoma), (ii) protein adsorption evaluation on the material surface to avoid body rejection towards material and (iii) test blood biocompatibility by comparing the haemoglobin concentration, red and white blood cell counts, and platelet count in the animal blood (Koo 2017).

An in vitro study conducted by Ziabka et al. (2018), the comparison between pure polymers (ABS-E and ABS-N) and polymers with composite materials (ABS-E, 0.5 Ag and ABS-N, 0.5 Ag) show polymers with composite materials possess good surface wettability (angle below 80°), compressible tensile strength and Young's modulus and good biocompatibility. Polymers with composite materials have enhance and promote cell adhesion and proliferation after 7 days of the experiment due to their influencing can modulate cell-material interaction thus, improving biocompatibility, e.g., osteoblast cell line. However, fibroblast lines cultured on the ABS-N group exhibit 9% increase in cytotoxicity after three days of cell culture while for the 7 days period, the cytotoxicity increased up to 14%. Based on cell morphology and viability, number of cells adhering to the polymers did not influence by the presence of silver nanoparticles.

An in vivo study performed by Ziabka et al. (2018), the implants made of the ABS and ABS modified with 0.1 Ag were used to investigate the implants biocompatibility on rats after 4, 12, 24 and 48 weeks of implantation. In this study, histochemical analysis shows the presence of inflammation and acute inflammatory infiltration around both types of implants which led to immunological reactions such as a low number of mast cells and eosinophiles. The C reactive Protein tests

(CRP) revealed no local inflammation and toxic effect happens as the composite materials were too small to cause a negative response in blood, consider that the concentration level of bioactive particles was safe. Furthermore, the implant instability may reason for the inflammation and irritation of muscle tissue caused by firmness and rigidness of the foreign body as well as the varied pattern of the implant.

12.2.2 Hemocompatibility Assay

Polymer-based NCs could have variety of components those possibly harmful or initiated body defense systems. It is very important to fulfill stringent safety-assessment requirement with respect to their capability causing harmful effect with blood element specifically known as hemocompatibility. Hemocompatibility testing may be defined as (Raghavendra et al. 2015);

> *hemocompatibility tests of in vivo examination evaluate the effects on blood and/or blood components by blood-contacting medical devices or materials. The five test categories indicated from the ISO standards perspective for hemocompatibility evaluation are thrombosis, coagulation, platelets, hematology, and immunology (complement and leukocytes).*

In this chapter, we had summarized list of tests and methods to create a standard platform for hemocompatibility assessment of polymer-based NCs before can be used in industries especially biomedical fields (Table 12.1). Good hemocompatibility was considered if the polymer-based NCs or their byproducts did not trigger any adverse effect such as inflammatory reaction, thrombogenicity response and blood components destruction once implanted. Currently, all biomedical devices have undergone hemocompatibility testing prior clinical application guided by International Standard Organization (ISO) 10,993 (Biological evaluation of medical devices) Part 4 (Selection of tests for interactions with blood).

In order to resolve the above issues, polymer-based NCs must be able to resist thrombosis and destruction from natural blood homeostasis mechanisms; procoagulant and anticoagulant systems. Key elements of the biomaterial/polymer-based NCs surfaces -blood interaction consists of interaction with platelets, the vascular endothelium, the coagulation cascade, and the fibrinolytic system (Harter et al. 2015). In normal condition, platelet aggregation and formation of platelet plug to the site of injury were activated when substances in contact with endothelium. Further, it also activates antithrombogenic endothelium by introducing the deposition of insoluble fibrin to strengthen the blood clot (Gale 2011). Artificial surfaces of the medical devices, for example, cardiovascular and wound healing implants and catheters usually initiated thrombus formation. It is well-known cause of failure for blood-contact medical devices, which initiated by the three main coagulating factors namely as Factor XII (hageman factor), Factor XI, and high molecular weight kininogen (HK) (Colman 2006).

Morbidity and mortality rates due to the infections associated with medical devices are still increasing even though various strategies be adapted among staffs. Sterilization and disinfection practices prior, during and after any of treatment

procedures are having difficulties due to the lack of constancy among staffs. Thus, alternative by using NCs incorporated into polymer was studied in order to resolve the above-mentioned problems. Nowadays, polymers were widely used in medical fields purposely for drug delivery, patches, implants, tube/loop and others. Surface properties and characterization of polymer-based NCs such as chemistry, availability of certain functional groups, domain structure, surface electrical charge, hydrophilicity/hydrophobicity, linker molecules, interfacial adaptability, or surface roughness played an important role for the adherence of platelets and coagulation activation.

12.2.2.1 Thrombosis, Coagulation Test and Complement Activation

Blood-contacting medical devices as be explained earlier are prone to thrombosis issues. The interaction of blood components with artificial surfaces associated thrombosis initially through protein adsorption activation. Thus, induces platelet adhesion, activation and aggregation (Jaffer et al. 2015). Protein adsorptions also trigger the adherence of platelets, leukocytes and red blood cells to be attached on surfaces. This can be related with a decrease in platelet count number and generation of fibrin network. Fibrinogen, fibronectin and von Willebrand factor (vWF) had been adsorb to the surface to mediate platelet adhesion. The three types of glycoproteins are replaced with coagulation and clotting components such as factor XII (Hageman factor), high molecular weight kininogen (HK) and kallikrein (Gorbet and Sefton 2004). In addition, it also activated complement pathways thus amplifies protein monolayer formation on the surfaces and local inflammatory responses. Both leukocytes and red blood cells also could adhere to adsorbed fibrinogen via CD11b/CD18, respectively for neutrophils. Leukocyte adhesion was promoted by platelet adherence via an interaction between P-selectin on activated surface of the activated platelets and leukocyte P-selectin glycoprotein ligand-1. However, red cells adherence activates platelets and cause erythrocyte hemolysis under high shear conditions (Jaffer et al. 2015). In Table 12.1, test categories for thrombosis, coagulation test and complement activation are summarized as followed (Weber et al. 2018; Tynngard et al. 2015; Antovic 2010);

12.2.2.2 Hemolysis Assay

One of the fundamental tests in determining the safety of blood-contacting medical materials is *via* evaluates red blood cells (RBCs) interaction (hemolytic potential) in vitro. Blood is a complex organ which comprising of 55% plasma, 44% red blood cells (RBC), and 1% leukocytes and platelets. RBC is bi-concave discoid cells filled with Hb and lack organelles (nucleus). Hemolysis refers to the RBCs destruction leading to the release of the iron-containing protein hemoglobin (Hb) into plasma, which lead to anemia, jaundice, hypertension, renal toxicity and other pathological condition (Rother et al. 2005). Hb is a protein, consists of a prosthetic heme

Table 12.5 Summary on toxicity of biodegradable polymer-based nanoparticles

Polymer	Nanoparticles	Findings	References
Poly(propylene fumarate)	Single-walled carbon nanotube	PPF/SWNTs nanocomposites were investigated for their in vitro cytotoxicity the unreacted components, the cross-linked networks, and the degradation products. The results indicating their potential for in vivo bone replacement therapies	Shi et al. (2008)
Polyurethanes	Montmorillonite	The PCL ester bonds of the materials were degraded and produced the mobility of lower mass chains and the ability to form crystalline structure. APRE-19 cells cultured with medium testing displayed viability proving their non-cytotoxic effect. It is a possible candidate for ophthalmological applications	Da Silva et al. (2010)
Polyurethane	Organophilic clay	*In vitro* assays performed with osteoblastic cells displayed no cytotoxicity associated with the synthesized nanocomposite. *In vivo* results after 29 days of implant proved that cells were able to penetrate through the porous structure to fully colonize the entire implant. It can be potentially useful in tissue engineering	Coeli Moreira Dias et al. (2010)
Guar gum	Silicon oxide	It can be used for removal of toxic anionic RB 4and CR dyes from aqueous solution. Hydrody-namic volume, higher surface area, uniform/ controlled growth of nanoscale silica fillers on g-GG matrix as well as multiple numbers of H-bonding sites of nanocomposites with dye molecules affects the major finding. The application is for dye contaminated wastewater treatment	Pal et al. (2015)
Polyamidoamine (PAMAM)	Gold/dendrimer nanocomposites	Modulating surface charge and composition were directly related with in vivo biodistribution characteristics and toxicology of the nanodevices. It demonstrated characteristics of potential materials for imaging and treatment of cancer	Khan et al. (2005)

(continued)

molecule [Fe II coordinated to a tetrapyrole ring (protoporphyrin IX)] joined to globin chains (Schechter 2008; Schechter 2012). The primary function of Hb is to sustain the energy requirements of cells, maintains cellular haemostasis, capture and release of oxygen facilitated by heme (with Fe II) which also enables the

Table 12.5 (continued)

Polymer	Nanoparticles	Findings	References
Polylactic acid or polylactide (PLLA) Cellulose	hydroxyapatite	Chemical and mechanical properties, crystallinity and porosity of the nanocomposites with the variation of weight ratio of MCC/PLLA and HA/PLLA were investigated Suitable candidate for bone repair applications	Eftekhari et al. (2014)
Collagen	hydroxyapatite	The animal tests displayed no toxicity and osteoclastic resorption with good osteoconductivity. It is proven that the resorption rate in vivo was decreased with no toxicity effects	Kikuchi et al. (2004)

reversible binding of carbon monoxide (CO) and NO. The damaging role of Hb under stress can be caused by Hb auto-oxidation within the RBC, extracellular release of Hb (outside RBC) to act as ROS source in the vasculature and tissues, Hb scavenging of NO and heme release from Hb (Quaye 2015). As polymer (NC) does generate ROS in the presence of cells and membrane damage by oxidative stress, numerous studies investigated NC/RBC interaction which lead to hemolysis. Various in vitro assays of sensitivity of the RBCs being applied to determined hemolytic properties (Table 12.2). Two existing practises known as Standard Practice for Assessment of Hemolytic Properties of Materials (ASTM F-756-00) and Standard Test Method for Analysis of Hemolytic Properties of Nanoparticles (ASTM E2524-08-2013) being used as standard in evaluating hemolytic properties in dilute human blood (Dobrovolskaia et al. 2008; ASTM 2000).

12.3 Bioactive Composite Materials in Biomedical Fields

Another importance aspect in evaluating artificial materials for biomedical use is by studying *in vivo* and *in vitro* methods in simulated body fluid (SBF) in order to evaluate their biocompatibility or bioactivity prior clinical settings. Moreover, these in vitro simulation methods can reduce the number of animals used and time effective. SBF is an organic-substance-free acellular solution and had similar ion concentrations but not exactly equal to human blood plasma, first reported by Kokubo et al. (1990). In this assay, the materials will be immersed in SBF solution for certain periods and been investigated for the ability of apatite formation on the surfaces. The apatite-forming ability (a hydroxylated form of calcium phosphate) of an implant in a physiological environment plays a vital role in cell response and bone integration, however dangerous for certain biomedical device, as example catheter tubing. According to Cox and Hukins (1989) and Stickler (2014), the crystalline biofilms coatings on catheters usually composed of two components known as

struvite (magnesium ammonium phosphate) and apatite. They usually develop large, coffin-shaped crystals and also appear as microcrystalline aggregations revealed by scanning electron microscopy. Accumulating crystalline deposits will block the flow of urine or blood through catheter inserted in patient's body, thus cause serious consequences. It is very important to have a proper method to investigate the biocompatibility and bioactivity in the aspect of surface behavior and hydroxyapatite formation ability. Ions release in the solution also important to ensure the materials does not release any component that could induce toxic or immune response. Here we tabulated the list of parameters being studied (Table 12.3).

12.4 The Toxicity of Biodegradable Polymer Based NCs

Biodegradable polymer can be defined as the materials which undergo decay and degradation process chemically and physically when encountered with microbes in aerobic and anaerobic processes (Abhilash and Thomas 2017). Biodegradable polymers are divided into two classes; synthetic or natural polymers. The polymers manufactured by using non-renewable resources is classified as synthetic while polymers from renewable resources (biological resources) categorized as natural (Vroman and Tighzert 2009; Abhilash and Thomas 2017). It is an alternative approach to enhance the properties of polymer NCs by combining NCs together with the polymer.

Though nanotechnology of biodegradable polymer has gained great interest from public in many fields, there is an increasing concern regarding infinite toxicological effects evaluation of nanoparticles but none of them come to a conclusive research findings associated with human, animal and environment (D and Rao 2011; Reidy et al. 2013; Arvidsson et al. 2013; Sanvicens and Marco 2008; Yah et al. 2012). One of the predominant concerns in biodegradable polymer-based NPs that have to be addressed is the toxic effect of nanomaterials on humans. Several factors including nanoparticles size, particle number, surface area, elemental composition, pH value, shape, surface coating, oxidation status, concentration, catalytic activity, bonded surface species, solubility, duration of their interaction with living matter, stability in biological system, degree of aggregation and degree of agglomeration may contribute to the effect of their toxicity (Mazumder et al. 2019; Sukhanova et al. 2018; Artiaga et al. 2015).

A lot of additional studies and researchers are needed to be done as there is limited information available until now in order to achieve conclusive research findings regarding polymer NCs toxicity has been summarized in Table 12.5.

12.5 Conclusion

The safety and environmental effects of polymer-based NCs have attracted wide attention as commercialisation of nanotechnologies grows in an extensive range of industries and markets especially in biomedical fields in the last few decades. Considering the biological effect and ecological risk of polymer-based NCs, this chapter reviewed three important aspects of safety assessment; compatibility, bioactivity and biodegradation prior been applied into healthcare industries. Therefore, by following these guidelines could help to improve synthesis characterization for each polymer-based NCs and ensure minimalization of adverse effects towards human usage and environments.

Acknowledgments The authors would like to acknowledge the Ministry of Education (MOE) Malaysia for funding this work under Transdisciplinary Research Grant Scheme (TRGS) grant no. 6769003 and Research in Undergraduate Institutions (RUI) grant 2019/2020.

References

Abhilash M, Thomas D (2017) Biopolymers for biocomposites and chemical sensor applications. In: Biopolymer composites in electronics. Elsevier, pp 405–435

Antovic A (2010, October). The overall hemostasis potential: a laboratory tool for the investigation of global hemostasis. In Seminars in thrombosis and hemostasis (Vol. 36, No. 07, pp. 772–779). © Thieme Medical Publishers

Artiaga G, Ramos K, Ramos L, Cámara C, Gómez-Gómez M (2015) Migration and characterisation of nanosilver from food containers by AF4-ICP-MS. Food Chem 166:76–85

Arvidsson R, Molander S, Sandén BA (2013) Review of potential environmental and health risks of the nanomaterial graphene. Hum Ecol Risk Assess 19(4):873–887

Bollino F, Armenia E, Tranquillo E (2017) Zirconia/hydroxyapatite composites synthesized via sol-gel: influence of hydroxyapatite content and heating on their biological properties. Materials 10(7):757

Brisbois EJ, Kim M, Wang X, Mohammed A, Major TC, Wu J, Brownstein J, Xi C, Handa H, Bartlett RH, Meyerhoff ME (2016) Improved hemocompatibility of multilumen catheters via nitric oxide (NO) release from S-Nitroso-N-acetylpenicillamine (SNAP) composite filled lumen. ACS Appl Mater Interfaces 8(43):29270–29279

Colman RW (ed) (2006) Hemostasis and thrombosis: basic principles and clinical practice. Lippincott Williams & Wilkins

Cox AJ, Hukins DW (1989) Morphology of mineral deposits on encrusted urinary catheters investigated by scanning electron microscopy. J Urol 142(5):1347–1350

Darouiche RO (2004) Treatment of infections associated with surgical implants. N Engl J Med 350(14):1422–1429

Dias RCM, Góes AM, Serakides R, Ayres E, Oréfice RL (2010) Porous biodegradable polyurethane nanocomposites: preparation, characterization, and biocompatibility tests. Mat Res 13(2):211–218

Drouet C (2013) Apatite formation: why it may not work as planned, and how to conclusively identify apatite compounds. Biomed Res Int 2013:12

Dobrovolskaia MA, Clogston JD, Neun BW, Hall JB, Patri AK, McNeil SE (2008) Method for analysis of nanoparticle hemolytic properties in vitro. Nano Lett 8(8):2180–2187

Eftekhari S, El Sawi I, Bagheri ZS, Turcotte G, Bougherara H (2014) Fabrication and characterization of novel biomimetic PLLA/cellulose/hydroxyapatite nanocomposite for bone repair applications. Mater Sci Eng C 39:120–125

Fisher LE, Hook AL, Ashraf W, Yousef A, Barrett DA, Scurr DJ, Chen X, Smith EF, Fay M, Parmenter CD, Parkinson R (2015) Biomaterial modification of urinary catheters with antimicrobials to give long-term broadspectrum antibiofilm activity. J Control Release 202:57–64

Fu PP, Xia Q, Hwang HM, Ray PC, Yu H (2014) Mechanisms of nanotoxicity: generation of reactive oxygen species. J Food Drug Anal 22(1):64–75

Gale AJ (2011) Continuing education course# 2: current understanding of hemostasis. Toxicol Pathol 39(1):273–280

Gorbet MB, Sefton MV (2004) Biomaterial-associated thrombosis: roles of coagulation factors, complement, platelets and leukocytes. In: The biomaterials: silver Jubilee compendium. Elsevier Science, pp 219–241

Guggenbichler JP, Assadian O, Boeswald M, Kramer A (2011) Incidence and clinical implication of nosocomial infections associated with implantable biomaterials–catheters, ventilator-associated pneumonia, urinary tract infections. GMS Krankenhhyg Interdiszip 6(1)

Győri E, Fábián I, Lázár I (2017) Effect of the chemical composition of simulated body fluids on aerogel-based bioactive composites. J Compos Sci 1(2):15

Handa H, Major TC, Brisbois EJ, Amoako KA, Meyerhoff ME, Bartlett RH (2014) Hemocompatibility comparison of biomedical grade polymers using rabbit thrombogenicity model for preparing nonthrombogenic nitric oxide releasing surfaces. J Mater Chem B 2(8):1059–1067

Harter K, Levine M, Henderson SO (2015) Anticoagulation drug therapy: a review. West J Emerg Med 16:11–17

Ho CC, Fang HY, Wang B, Huang TH, Shie MY (2018) The effects of biodentine/polycaprolactone three-dimensional-scaffold with odontogenesis properties on human dental pulp cells. Int Endod J 51:e291–e300

Hule RA, Pochan DJ (2007) Polymer nanocomposites for biomedical applications. MRS Bull 32(4):354–358

Jaffer IH, Fredenburgh JC, Hirsh J, Weitz JI (2015) Medical device-induced thrombosis: what causes it and how can we prevent it? J Thromb Haemost 13:S72–S81

Jaganathan SK, Mani MP (2018) Enriched mechanical, thermal, and blood compatibility of single stage electrospun polyurethane nickel oxide nanocomposite for cardiac tissue engineering. Polym Compos

Jiang H, Wang XB, Li CY, Li JS, Xu FJ, Mao C, Yang WT, Shen J (2011) Improvement of hemocompatibility of polycaprolactone film surfaces with zwitterionic polymer brushes. Langmuir 27(18):11575–11581

Juraski ADC, Rodas ACD, Elsayed H, Bernardo E, Soares VO, Daguano J (2017) The in vitro bioactivity, degradation, and cytotoxicity of polymer-derived wollastonite-diopside glass-ceramics. Materials 10(4):425

Khan MK, Nigavekar SS, Minc LD, Kariapper MS, Nair BM, Lesniak WG, Balogh LP (2005) In vivo biodistribution of dendrimers and dendrimer nanocomposites—implications for cancer imaging and therapy. Technol Cancer Res Treat 4(6):603–613

Kikuchi M, Matsumoto HN, Yamada T, Koyama Y, Takakuda K, Tanaka J (2004) Glutaraldehyde cross-linked hydroxyapatite/collagen self-organized nanocomposites. Biomaterials 25(1):63–69

Kim DY, Kadam A, Shinde S, Saratale RG, Patra J, Ghodake G (2018) Recent developments in nanotechnology transforming the agricultural sector: a transition replete with opportunities. J Sci Food Agric 98(3):849–864

Koo J (2017) Environmental and Health Impacts for Nanomaterials and Polymer Nanocomposites. Fundamentals, Properties, and Applications of Polymer Nanocomposites

Kokubo T, Kushitani H, Sakka S, Kitsugi T, Yamamuro T (1990) Solutions able to reproduce in vivo surface-structure changes in bioactive glass-ceramic A-W3. J Biomed Biomater Res, 24(6), pp.721–734

Lee SR, Park HM, Lim H, Kang T, Li X, Cho WJ, Ha CS (2002) Microstructure, tensile properties, and biodegradability of aliphatic polyester/clay nanocomposites. Polymer 43(8):2495–2500

Li J, Zhang K, Ma W, Wu F, Yang P, He Z, Huang N (2016) Investigation of enhanced hemocompatibility and tissue compatibility associated with multi-functional coating based on hyaluronic acid and type IV collagen. Regen Biomater 3(3):149–157

Liu HY, Du L, Zhao YT, Tian WQ (2015) In vitro hemocompatibility and cytotoxicity evaluation of halloysite nanotubes for biomedical application. J Nanomater 16(1):384

Maitz MF, Sperling C, Wongpinyochit T, Herklotz M, Werner C, Seib FP (2017) Biocompatibility assessment of silk nanoparticles: hemocompatibility and internalization by human blood cells. Nanomed-Nanotechnol 13(8):2633–2642

Mandal A (2019, Feb 26) Catheter uses. Retrieved from https://www.news-medical.net/health/Catheter-Uses.aspx

Mazumder B, Ray S, Pal P, Pathak Y (2019) Nanotechnology: therapeutic, nutraceutical, and cosmetic advances. CRC Press

Müller K, Bugnicourt E, Latorre M, Jorda M, Echegoyen Sanz Y, Lagaron J, Miesbauer O, Bianchin A, Hankin S, Bölz U, Pérez G (2017) Review on the processing and properties of polymer nanocomposites and nanocoatings and their applications in the packaging, automotive and solar energy fields. J Nanomater 7(4):74

Neun BW, Ilinskaya AN, Dobrovolskaia MA (2018) Updated method for in vitro analysis of nanoparticle hemolytic properties. In: Characterization of nanoparticles intended for drug delivery. Humana Press, New York, NY, pp 91–102

Nicolle LE (2014) Catheter associated urinary tract infections. Antimicrob Resist In 3(1):23

Pal S, Patra AS, Ghorai S, Sarkar AK, Mahato V, Sarkar S, Singh RP (2015) Efficient and rapid adsorption characteristics of templating modified guar gum and silica nanocomposite toward removal of toxic reactive blue and Congo red dyes. Bioresour Technol 191:291–299

Pham CT, Thomas DG, Beiser J, Mitchell LM, Huang JL, Senpan A, Hu G, Gordon M, Baker NA, Pan D, Lanza GM (2014) Application of a hemolysis assay for analysis of complement activation by perfluorocarbon nanoparticles. Nanomed-Nanotechnol 10(3):651–660

Quaye IK (2015) Extracellular hemoglobin: the case of a friend turned foe. Front Physiol 6:96

Ramakrishna D, Rao P (2011) Nanoparticles: is toxicity a concern? EJIFCC 22(4):92

Raghavendra GM, Varaprasad K, Jayaramudu T (2015) Biomaterials: design, development and biomedical applications. In: Nanotechnology applications for tissue engineering. William Andrew Publishing, pp 21–44

Reidy B, Haase A, Luch A, Dawson K, Lynch I (2013) Mechanisms of silver nanoparticle release, transformation and toxicity: a critical review of current knowledge and recommendations for future studies and applications. Materials 6(6):2295–2350

Rother RP, Bell L, Hillmen P, Gladwin MT (2005) The clinical sequelae of intravascular hemolysis and extracellular plasma hemoglobin: a novel mechanism of human disease. JAMA 293(13):1653–1662

Sanvicens N, Marco MP (2008) Multifunctional nanoparticles–properties and prospects for their use in human medicine. Trends Biotechnol 26(8):425–433

Schechter AN (2008) Hemoglobin research and the origins of molecular medicine. Blood 112(10):3927–3938

Schechter AN (2012) Introduction to the symposium on synthetic life. Perspect Biol Med 55(4):467–469

Shalom Y, Perelshtein I, Perkas N, Gedanken A, Banin E (2017) Catheters coated with Zn-doped CuO nanoparticles delay the onset of catheter-associated urinary tract infections. Nano Res 10(2):520–533

Shi X, Sitharaman B, Pham QP, Spicer PP, Hudson JL, Wilson LJ, Tour JM, Raphael RM, Mikos AG (2008) In vitro cytotoxicity of single-walled carbon nanotube/biodegradable polymer nanocomposites. J Biomed Mater Res A 86(3):813–823

Siebers MC, Ter Brugge PJ, Walboomers XF, Jansen JA (2005) Integrins as linker proteins between osteoblasts and bone replacing materials. A critical review. Biomaterials 26(2):137–146

da Silva GR, da Silva-Cunha Jr A, Behar-Cohen F, Ayres E, Oréfice RL (2010) Biodegradation of polyurethanes and nanocomposites to non-cytotoxic degradation products. Polym Degrad Stab 95(4):491–499

Speranskaya ES, Sevrin C, De Saeger S, Hens Z, Goryacheva IY, Grandfils C (2016) Synthesis of hydrophilic CuInS2/ZnS quantum dots with different polymeric shells and study of their cytotoxicity and hemocompatibility. ACS Appl Mater Interfaces 8(12):7613–7622

Standard practice for assessment of hemolytic properties of materials (2000) ASTM International: West Conshohocken, PA.

Stickler DJ (2014) Clinical complications of urinary catheters caused by crystalline biofilms: something needs to be done. J Intern Med 276(2):120–129

Sukhanova A, Bozrova S, Sokolov P, Berestovoy M, Karaulov A, Nabiev I (2018) Dependence of nanoparticle toxicity on their physical and chemical properties. Nanoscale Res Lett 13(1):44

Sun J, Shen J, Chen S, Cooper M, Fu H, Wu D, Yang Z (2018) Nanofiller reinforced biodegradable PLA/PHA composites: current status and future trends. Polymers 10(5):505

Tambyah PA (2004) Catheter-associated urinary tract infections: diagnosis and prophylaxis. Int J Antimicrob Agents 24:44–48

Tambyah PA, Oon J (2012) Catheter-associated urinary tract infection. Curr Opin Infect Dis 25(4):365–370

Tibolla H, Pelissari FM, Martins JT, Lanzoni EM, Vicente AA, Menegalli FC, Cunha RL (2019) Banana starch nanocomposite with cellulose nanofibers isolated from banana peel by enzymatic treatment: in vitro cytotoxicity assessment. Carbohydr Polym 207:169–179

Tran N, Tran PA (2012) Nanomaterial-based treatments for medical device-associated infections. ChemPhysChem 13(10):2481–2494

Tynngård N, Lindahl TL, Ramström S (2015) Assays of different aspects of haemostasis–what do they measure? ThrombJ 13(1):8

Vroman I, Tighzert L (2009) Biodegradable polymers. Materials 2(2):307–344

Wang B, Huang P, Ou C, Li K, Yan B, Lu W (2013) In vitro corrosion and cytocompatibility of ZK60 magnesium alloy coated with hydroxyapatite by a simple chemical conversion process for orthopedic applications. Int J Mol Sci 14(12):23614–23628

Weber M, Steinle H, Golombek S, Hann L, Schlensak C, Wendel HP, Avci-Adali M (2018) Blood-contacting biomaterials: in vitro evaluation of the hemocompatibility. Front Bioeng Biotech 6

Whitehouse JD, Friedman ND, Kirkland KB, Richardson WJ, Sexton DJ (2002) The impact of surgical-site infections following orthopedic surgery at a community hospital and a university hospital adverse quality of life, excess length of stay, and extra cost. Infect Cont Hosp Ep 23(4):183–189

Xue LL, Long P, Wei H, Liang Y (2011) Hemocompatibility of TiO2 nanoparticles composite PTFE coating for medical devices. In: Advanced materials research, vol 299. Trans Tech Publications, pp 600–603

Xu Z, Hodgson M, Cao P (2016) Effect of immersion in simulated body fluid on the mechanical properties and biocompatibility of sintered Fe–Mn-based alloys. Metals 6(12):309

Yah CS, Iyuke SE, Simate GS (2012) A review of nanoparticles toxicity and their routes of exposures. Iran J Pharm Sci 8(1):299–314

Yilmaz B, Doğan S, Çelikler Kasimoğullari S (2018) Hemocompatibility, cytotoxicity, and genotoxicity of poly (methylmethacrylate)/nanohydroxyapatite nanocomposites synthesized by melt blending method. Int J Polym Mater 67(6):351–360

Yoshida E, Hayakawa T (2017) Quantitative analysis of apatite formation on titanium and zirconia in a simulated body fluid solution using the quartz crystal microbalance method. Adv Mater Sci Eng 2017:9

Ziabka M, Dziadek M, Menaszek E (2018) Biocompatibility of poly(acrylonitrile-butadiene-styrene) nanocomposites modified with silver nanoparticles. Polymers 10(11):1–13

Chapter 13
Modern Approach of Hydroxyapatite Based Composite for Biomedical Applications

Che Azurahanim Che Abdullah, Eszarul Fahmi Esa, and Farinawati Yazid

13.1 Introduction

This chapter presents an overview related to the modern approach of hydroxyapatite (HA) based composite for biomedical applications. Composite refers to a heterogeneous combination made up of two or more materials having different composition, properties and morphology in order to produce new materials with specific physical, chemical and mechanical characteristics (Salernitano and Migliaresi 2003). Simply speaking, the composite contains at least two or more components known as matrix and reinforcement. Biocomposites, on the other hand, refers to the blends of different materials based on their biocompatibility for various applications. Different types of composites, already in use or currently investigated for various biomedical applications, are presented in this chapter. The focus will be on the types of HA based composite, synthesis and fabrication approaches, characterization, various biomedical applications, the cell-material interactions and its bioactivity and biocompatibility.

C. A. C. Abdullah (✉)
Department of Physics, Faculty of Science, Universiti Putra Malaysia, Serdang, Selangor, Malaysia

Material Synthesis and Characterization Laboratory, Institute of Advanced Technology, Universiti Putra Malaysia, Serdang, Selangor, Malaysia

Laboratory of Cancer Research UPM - MAKNA (CANRES), Institute of Bioscience, Universiti Putra Malaysia, Serdang, Selangor, Malaysia
e-mail: azurahanim@upm.edu.my

E. F. Esa
Department of Physics, Faculty of Science, Universiti Putra Malaysia, Serdang, Selangor, Malaysia

F. Yazid
Center of Family Oral Health, Faculty of Dentistry, Universiti Kebangsaan, Jalan Raja Muda Abdul Aziz, Kuala Lumpur, Malaysia

S. Siddiquee et al. (eds.), *Composite Materials: Applications in Engineering, Biomedicine and Food Science*, https://doi.org/10.1007/978-3-030-45489-0_13

HA based composite also known as bioceramics composite and been used for the past several years for various biomedical applications and recently its being used mainly in tissue engineering. Calcium phosphate or single-phase HA based composite have been widely used for the past thirty years. The advantages offer by the HA based composites consist of high compressive strength, comparative inertness towards body fluids, its attractive appearance, biodegradability, and high biocompatibility led to the use of bioceramics composite in dental and orthopaedic related biomedical applications. The structure of this chapter is organized as follows. In Sect. 13.2, classifications of the HA based composite materials are described. This is followed by a description of the modern synthesis or fabrication and characterization approaches (Sects. 13.3 and 13.4). Section 13.5 deals with current applications of HA based composite in biomedical focusing on the ideal properties and cell-material interaction. Concluding remarks are offered in the last Sect. 13.6.

13.2 Classification of Hydroxyapatite (HA) Based Composites

HA based composite used mainly in biomedical applications can be classified into various classifications. Herein, the main four classification consist of metal/metal oxide matrix HA based composite, polymer matrix HA based composite, carbonaceous HA based composite, and the hybrid HA based composite (Fig. 13.1). In terms of polymer matrix, HA based composite can be further divided into natural and synthetic polymer.

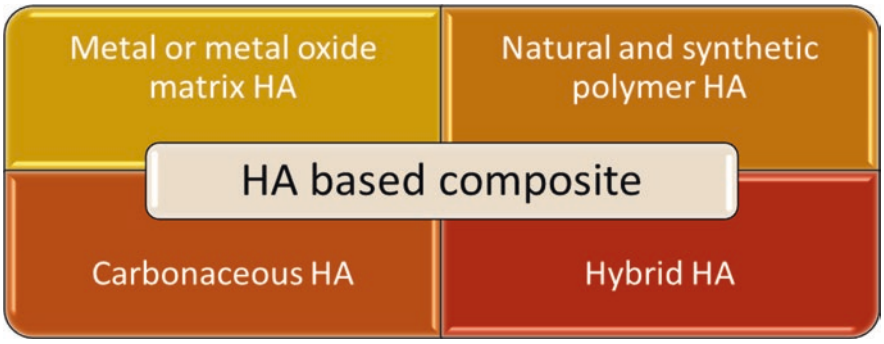

Fig. 13.1 Classification of hydroxyapatite (HA) composites

13.2.1 Metal Matrix Hydroxyapatite (HA) Based Composite

HA having component comparable to crystal structure of bone offers both bioactivity and compatibility. The major bottleneck related to the application of HA mainly due to their low fracture toughness and flexural strength. In order to enhance the mechanical properties of HA, metal and metal oxide such as magnesium, titanium dioxide, zirconia, alumina, and iron oxide usually incorporated in order to reinforce the prepared HA-based composites. The metal matrix HA based composite possess good tensile strength, high Young's modulus, high strength and highly resistance to corrosion. For biomedical application, the HA composite should be biodegradable and non-toxic (Bommala et al. 2018). Table 13.1 listed several types of metal and metal oxide previously used in preparing HA based composite for various biomedical application.

13.2.2 Polymer Matrix Hydroxyapatite (HA) Based Composite

Reinforcement can be achieved by incorporating HA with either natural or synthetic polymer the prepared HA-based composites (Fig. 13.2). Polymers provide various properties as a matrix for bone tissue engineering applications. Natural polymer-based composites received more attention than synthetic polymer composites owing to the biocompatible and biodegradable properties offered by natural polymers. Other advantages included biological recognition, good attachment to cells and having the ability to be degraded and resorbed by the body (Venugopal et al. 2010). Chitosan, chitin, collagen, gelatin and polylactic acid (PLA), hylauronic acid derivatives, starch, fibrin gels, silk and lignocelluloses are among popular natural polymer in preparing composites for medical application.

Table 13.1 Metal and metal oxide used in preparing HA based composite

Types of Metal or Metal Oxide	Applications	References
Titanium (Ti) / Titanium Dioxide (TiO_2)	Implant	Oleiwi et al. (2015); Lim et al. (2001)
Magnesium (Mg) / Magnesium Oxide (MgO)	Bone replacement	Khanra et al. (2010)
Zinc (Zn) / Zinc Oxide (ZnO)	Bone implant, Antibacterial Biomaterial	Begam et al. (2017); Suparto and Kurniawan (2019)
Lanthanum (La)	Bone replacement	Yang et al. (2007)
Zirconia (Zr) / Zirconia dioxide (ZrO_2)	Bone scaffold, Orthopaedic and Dental Prosthesis	An et al. (2012), Zhang et al. (2006), Matsumoto et al. (2011), Sung et al. (2007)
Iron Oxide (IO)	Bone cancer therapy	Sneha and Sundaram (2015)
Alumina (Al_2O_3)	Bone scaffold	Raj et al. (2018)

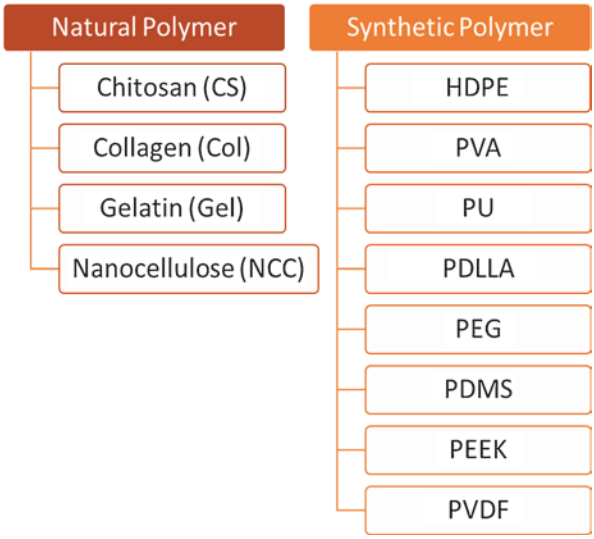

Fig. 13.2 Several examples of natural and synthetic polymer incorporated to produce HA-based polymer composites

Apart from biocompatible and biodegradable, antimicrobial and antioxidant properties of the prepared HA based composites widely expand their application in various fields ranging from food nutrition, biomedical engineering up to pharmaceutical. The composites also should mimic the behavior of the replaced tissue, providing an ideal when in contact with the tissue and capable to be degraded progressive as soon as the regeneration process ended. However, these naturally derived polymers have several drawbacks such as instability and immunogenicity from batch to batch. So, synthetic polymers with modifiable properties such as polyvinyl alcohol (PVA), polyurethane (PU), poly-d, l-lactic acid (PDLLA), polyethylene glycol (PEG), polydimethylsiloxane (PDMS), polyether ether ketone (PEEK) and thermoplastic polyvinylidene difluoride (PVDF) are among synthetic polymers usually used to create HA based composite as they offer exceptional applicability. The advantages offered by synthetic polymer consist of controlled mechanical properties, biodegradable, and reproducible for an extensive production.

13.2.3 Carbonaceous Hydroxyapatite (HA) Based Composite

Along with the excitement of nanoscience and the diverse applications of carbon-based nanomaterials, researchers worldwide started to utilise different carbonaceous materials to prepare nanocomposites either as a matrix material or as an additional reinforcing material. The carbonaceous materials reported to be bioactive for one or more purposes as it offers high competency for bone tissue engineering

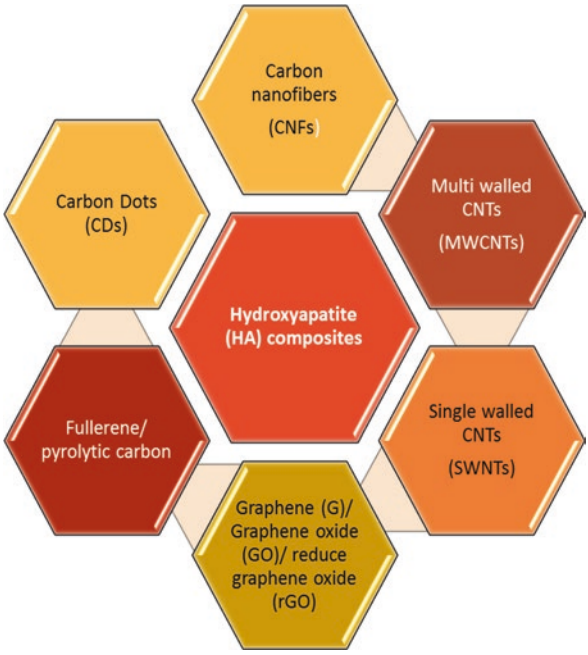

Fig. 13.3 Carbonaceous HA based composites

equipped with biocompatibility with native tissues and antibacterial activity. The incorporation of various carbonaceous materials with HA led to high biocompatibility and excellent structural properties of the prepared nanocomposite. The use of carbonaceous material such as glassy or pyrolytic carbon, fullerenes, carbon nanotubes (CNTs) graphene oxide (GO), carbon dots (CDs) and their derivatives and compositions are unique and innovative trend in creating HA based composites (see Fig. 13.3).

13.2.4 Hybrid Hydroxyapatite (HA) Based Composite

A major challenge in tissue engineering is the development of composite materials capable of promoting the desired cells and tissue behavior (Davis and Leach 2008). So, hybrid HA based composite biomaterials having the capability to synergize the beneficial properties of multiple materials into an outstanding matrix (Bencherif et al. 2013). The hybrid HA prepared by combination of various other materials such as metal or metal oxides with either natural or synthetic polymers or carbonaceous materials. The hybrid composites offer tuneable properties and providing enhancement in cellular and tissue interaction tissue. There are numerous hybrid HA based composite materials (as listed in Fig. 13.4) in order to promote the formation of cell proliferation for tissue engineering applications.

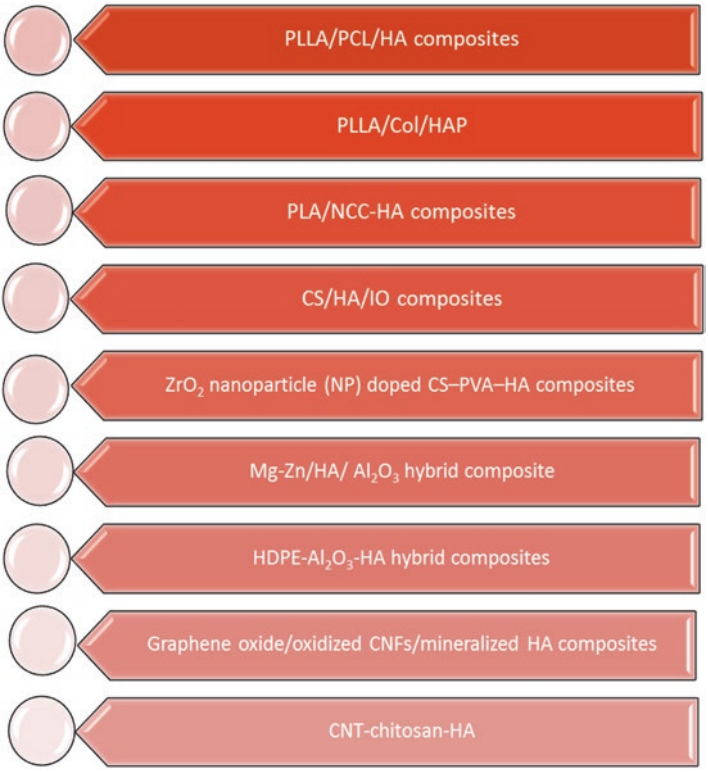

Fig. 13.4 Examples of hybrid HA based composite

13.3 Modern Synthesis and Fabrication Approaches

Owing to the importance of HA based composites in various biomedical applications not limited to tissue regeneration and drug delivery applications. So, various techniques (see Fig. 13.5) have been reported for the preparation of HA based composites (Haider et al. 2017). Two important factors when choosing the synthesis approach are particle size and morphology of the final product of HA. To date, many findings correlated the HA synthesis techniques with the particle size, but very few articles reported the fabrication method and the morphology control of HA based composites.

The commonly used techniques for the preparation of HA based composite including biometrics, freeze thawing, electronspinning, electrospraying, chemical precipitation, hydrothermal, solid state synthesis at high temperatures, microwave irradiation, surfactant-assisted precipitation, wet chemical synthesis, powder metallurgy, ultrasound cavitation, solvent casting, sol-gel method and green synthesis

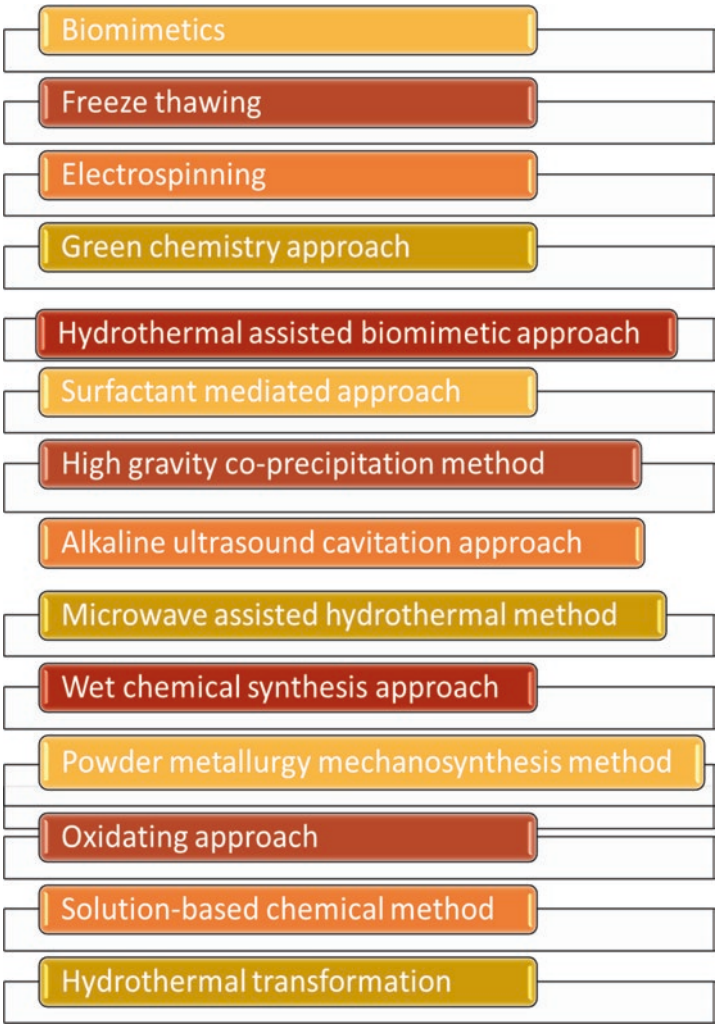

Fig. 13.5 Modern synthesis approaches in the fabrication of hydroxyapatite (HA) based composites

approach. Chemical precipitation, hydrothermal and sol–gel technique listed as the most frequently approach in the HA based nanocomposite fabrications. Table 13.2 summarized several common methods and the developed HA based composites. Until now researchers still are investigating for the method to prepare composites of HA with the right stoichiometry and having both high crystallinity and aspect ratio. So far, only conventional wet mechano-chemical methods have been reported to have the ability to control the stoichiometry of the final product.

Table 13.2 Several common methods and example of the developed hydroxyapatite (HA) based composites

Fabrication techniques of HA composites	Composites	References
Biomimetics	Col/HA, CNF/HA, PCL/HA	Lickorish et al. (2004); Wu et al. (2013); Lebourg et al. (2010)
Freeze thaw	PVA/HA, nHA@Fe_2O_3/PVA	Su et al. (2017); Hou et al. (2013)
Electronspinning	PLLA/MWNTs/HA, PLGA/HA, HA-PVP/PEO	Mei et al. (2007); Lao et al. (2011); Zhou et al. (2014)
Chemical precipitation	Nano-Al_2O_3 /HA	Zhang et al. (2016)
Hydrothermal	HA/Alumina and HA/MgO, SHA/rGO, GO/HA	Vijayalakshmi and Dhanasekaran (2017); Edwin et al. (2019); Rodríguez-González et al. (2018)
Microwave irradiation	PVOH/CNT/HA, Ag@Zn/HA, CS-HA	Lim (2018); Nedunchezhian et al. (2016); Sukhodub et al. (2018)
Sol-gel method	ZrO_2/Hap, TEOS/PDMS/HA, AMWCNT/HA	Bollino et al. (2017); Luo et al. (2015); Ji et al. (2015)
Solvent casting	P3HB/HA, p-PLLA/HA	Saadat et al. (2015); Dou et al. (2018)

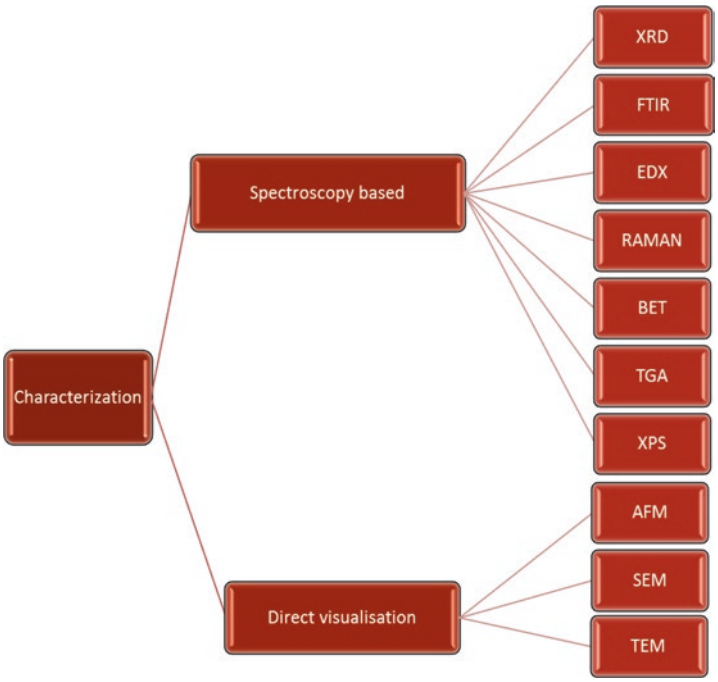

Fig. 13.6 Various characterization methods to evaluate the hydroxyapatite (HA) based composites

Table 13.3 Characterization methods and main findings of various HA based composites

X-Ray Diffraction Analysis (XRD) -degree of crystallinity -crystallite size	**Metal or metal oxide HA** - Diffraction peak of HA appeared in the composite at 2θ = 31.5°, 50° and 60° after samples dried at 100 °C (Bouiahya et al. 2019). - Crystallinity of the composite decreases and the crystallite size getting smaller when content of alumina increases (Bouiahya et al. 2019). - The intensity of diffraction peak of HA in Fe-HA became lower due to ion exchange between Fe^{3+} and Ca^{2+} ion. The increment of Fe^{3+} led to the crystallinity decreased (Pai and Yen 2013). - XRD peaks position for La-HA deviated slightly towards lower angle which may be due to distortion in crystal lattice following substitution of La in HA (Mathi et al. 2019)
	Natural or synthetic polymer HA - The addition of HA led to the reduction in terms of crystallinity degree of PCL as shown by the intensity peak of HA compared to PCL (Trakoolwannachai et al. 2019a, b). - Two notable sharp peaks for PEG noticeable at 2θ = 19.1° and 23.2° and peaks for HA is 2θ = 25.9° and 31.7°. As the positions does not overlapped, this indicated that there are no chemical interaction between PEG and HA (Wang et al. 2017). - HA peak in composite appeared at 2θ = 25.9° and growth took place at (002) crystal plane. The PPy diffraction peak disappear due to weak intensity and covered by the background of HA peaks (Huixia et al. 2016)
	Carbonaceous HA - Addition of fMWCNT into the HA found to have effect on the width at half maximum of the peak. As the width increases, it indicates that the crystallinity index decreased meanwhile crystallite size increased (Barabás et al. 2015). - XRD pattern of GO-HA consisted of HA peak at 2θ = 31.8° without any secondary phase. GO diffraction peak wasn't detectable in composite probably due to low concentration of GO or less crystallographic order (Karimi et al. 2019). - The XRD pattern obtained for HA/GO represented by the peaks at 25.87°, 31.42°, 32.11°, 32.52°, 39.62° and 49.42° with crystal plane (002), (211), (112), (300), (202), (310), (222), (213) and (004) was matched with the (JCPDS: No. 09–0432). The formation of well crystallized hexagonal phase of HA grown on two dimensional GO sheet was confirmed (Ramadas et al. 2017)
	Hybrid HA - Typical peak for GO disappear besides crystallinity of HA and PLA decreased in PLA/HA/GO composites due to good dispersion of GO and HA in PLA matrix (Gong et al. 2017). - Diffraction peaks at 38.2°, 44.3°, 64.5°, 77.3° corresponding to planes [1 1 1], [2 0 0], [2 2 0], [3 1 1] of fcc silver particles. The presence of peaks at 20° and 31.7° revealed the characteristic to the presence of crystalline chitosan and n-HA respectively (Saravanan et al. 2011). - Diffraction peak of Cs in composite revealed the semi crystalline nature as the peak was broad at 10°–20° meanwhile n-HA and $nZrO_2$ exhibited crystalline nature which is composite scaffold also corroborated as crystalline phase due to imparted by n-HA and $nZrO_2$ (Balagangadharan et al. 2018).

(continued)

Table 13.3 (continued)

Fourier Transform Infrared Spectroscopy (FTIR) -functional group	**Metal or metal oxide HA** - IR spectra for Al/HA displayed the stretching mode of PO_4 at 1100, 1050, 960 cm^{-1} and bending mode at 605 and 564 cm^{-1} (Bouiahya et al. 2019). - The stretching bond of phosphate observed at wavenumber of 962 cm^{-1} which indicate the formation of HA in composite (Valizadeh et al. 2014). - IR analysis for HA/Fe_3O_4 displays vibration peak of phosphate at wavenumber 569 cm^{-1}, 1044 cm^{-1}, and 1047 cm^{-1} (Vahdat et al. 2019)
	Natural or synthetic polymer HA - FTIR spectra of HA/PCL composites showed strong P-O stretching peak in the wavenumber range 1000–1100 cm^{-1} (Trakoolwannachai et al. 2019a, b). - N-H bending band for chitosan shift slightly due to hydrogen bond with HA and the P-O bending peak at wavenumber of 952 cm^{-1} (Trakoolwannachai et al. 2019a, b). - Specific bending vibration mode of PO_4 at wavenumber of 567 and 603 cm^{-1} while stretching mode vibration at wavenumber of 963, 1035 and 1101 cm^{-1}. Some peaks of HA and PPy in composite slightly shift due to interaction within composite (Huixia et al. 2016)
	Carbonaceous H - The peaks observed at 2920 and 2850 cm^{-1} attributed to ACH symmetric and asymmetric vibrations of GOs. The peak at 1642 cm^{-1} corresponds to the stretching vibration mode of carbonyl group present in the graphene. The bending vibration of phosphate display at wavenumber of 629, 600 and 564 cm^{-1} (Prabhu et al. 2016). - Phosphate absorption band at 610 cm^{-1}, 1037 cm^{-1} and 1091 cm^{-1} indicates the present of HA in composite and peak found at 1730 cm^{-1} related to GO (Karimi et al. 2019). - FTIR spectrum of HA/GO displayed bending vibration band of phosphate at 568 and 601 cm^{-1} meanwhile stretching vibration band were observed at 1099 and 1037 cm^{-1}. The band of C=C and C=O stretching of GO were 1622 and 1722 cm^{-1} respectively (Ramadas et al. 2017)
	Hybrid HA - CsAgHA composite exhibited different modes of phosphate band at 1035, 606, 517 cm^{-1}. Peak at 1610 cm^{-1} corresponds well to NH_2 absorption band in CS. Characteristic peak of C=O is shifted to 1635 cm^{-1} by the coordinative interaction between Ag ions and the NH_2 groups of CS (Yan et al. 2015). - Amine peak of CS displayed at wavenumber of 1656 cm^{-1}. Peak at 1634 cm^{-1}, 1070 cm^{-1} and 572 cm^{-1} correspond to n-HA in composite. Zr-O stretching vibration mode can be observed at wavenumber of 452 cm^{-1} and 416 cm^{-1} (Balagangadharan et al. 2018). - PLA/HA/GO composite displayed characteristic band of C=C vibration at ca. 1617 cm^{-1} indicates that GO successfully introduced in composite. Besides, the appearance of peaks at 1041, 605 and 566 cm^{-1} attributed to phosphate group of HA. Bands at 1184 cm^{-1} and 871 cm^{-1} are due to vibration of C-O-C and C-COO respectively besides bands at 2998 cm^{-1} and 2947 cm^{-1} are assigned to C-H stretching of PLA (Gong et al. 2017)

Table 13.3 (continued)

Scanning Electron microscopy (SEM) -morphology -particle size	**Metal or metal oxide HA** - Surface of La/HA was densely pack and the granules size are very small as well as high agglomeration (Mathi et al. 2019). - HA particle with elongated nanometric (irregular hexagonal) structure was agglomerated and contain silver nanoparticle in its interior (bright spot inside HA). The size of HA in range 100–150 nm long and 40–50 nm wide (Andrade et al. 2016) - Have irregular and porous structure as well as fine and spherical particles for HA/Fe_3O_4 (Vahdat et al. 2019)
	Natural or synthetic polymer HA - Small, irregular-shaped HA distributed homogenously on the surface and within PCL matrix as well as agglomeration occur which enhance its osteoinductive property (Trakoolwannachai et al. 2019a, b). - Scaffold composite showed interconnected pores and pore size within range 200–400 μm. Porosity slightly decreased when HA been incorporated with chitin due to interaction between polymer chains (Kumar et al. 2011). - nHA/CG scaffolds have a porous structure with interconnected pores. Agglomerated nHA particles discernible mostly on the surface of pore wall (Li et al. 2011)
	Carbonaceous HA - GO-nHA particles found to be bigger and having porous structure. However, after fluoride treatment, the particles become smaller and the porosity reduced as fluoride ion started to occupy the composite (Prabhu et al. 2016). - In GNs/HA, HA particles have a rod-like shaped with width around 50 nm and length in range of 100–200 nm (Pang et al. 2014). - C-HA in irregular shaped and rough surface was observed. Irregular surface may enhance the adsorption capacity. The plate-like nanocrystal might be the HA coating on the surface (Long et al. 2019)
	Hybrid HA - CS/n-HA/nAg scaffolds have rough surfaces and porous nature with size ca. 50–100 μm. Size of silver nanoparticles in range of 80–120 nm which distributed in the scaffolds. nHA particles ranging from 80 to 120 nm (Saravanan et al. 2011). - Cs/n-HA/nZrO_2 scaffold have interconnected pores which uniformly spread with size in the range of 55–65 μm. Interconnected porous structure significant in serving as template structure for cell attachment. Bone extracellular matrix formation and provide space for neovascularisation. (Balagangadharan et al. 2018). - PLA/HA/GO scaffold have rough surface with some joints and protuberances on that surface which suggested that GO and HA were attached to the surface of PLA (Gong et al. 2017

(continued)

Table 13.3 (continued)

Energy dispersive X-ray spectroscopy (EDX) -element present -Ca/P molar ratio	**Metal or metal oxide HA** - From EDX analysis concluded that when Al^{3+} ion from aluminium element increase, the Ca/P molar ratio of Al/HA became lower (Bouiahya et al. 2019)
	Natural or synthetic polymer HA - Ca/P molar ratio of nHA/PDLLA composite was 1.62 which is non- stoichiometric, calcium deficient and close to apatite in bone. The apatite mineralisation in surface of NHA/PDLLA is similar to animal bone in main composition (Deng et al. 2008)
	Carbonaceous HA - Ca/P Molar ratio of Go-HA are about 1.7. This result suggested that GO has positive effect on the mineralisation of HA with Ca/P molar ratio close to the pure HA (1.67) (Fathyunes and Khalil-alla 2017)
	Hybrid HA - C, P, O, Ca and Au element are traced in the EDX spectrum for PLA/HA/GO composite which clearly indicate the present of GO and HA in composite. Meanwhile, Au element came from the gold plate used to test sample using SEM measurement. The molar ratio of Ca and P for that composite obtained from EDX measurement is 1.64 which close to natural bone ratio (1.67) (Gong et al. 2017)
Thermogravimetric analysis (TGA) -thermal stability	**Metal or metal oxide HA** - TGA spectra of HA + GA displayed that 6.314% weight loss at 62.69 °C attribute to the presence of water content and 10.76% of weight loss correspond to the phosphate group. Besides, the weight loss of 8.574% at 433.56 °C due to presence of CaOOH. TGA spectra of HA + GA almost similar to HA but different in residual percentage due to presence of Ag metal in residual besides pure CaO. (Bharti et al. 2016). - TGA curve of Al_2O_3-BHA (alumina-bovine hydroxyapatite) display that at evaporation of solvent, adsorbed water and crystal water of boehmite phase (Al-OOH) occurred at ca. 150 °C and 450 °C. Then, transformation of boehmite to α-alumina which the only stable phase of alumina, can be observed at 500–1300 °C. Small amount of BHA converted into β-TCP at 1250–1300 °C (Yelten et al. 2012)
	Natural or synthetic polymer HA - PVAHA composite undergo continuous weight loss until 800 °C due to the degradation of PVA and dehydroxylation of HA. The weight loss due to water occurred up to 200 °C. Between 200 °C and 550 °C, the weight loss caused by degradation of PVA. 50% of PVA in HA has weight loss of 18.01% whereas 1% PVA in composite has weight loss of 7.05%. This finding indicated that the highest weight loss occurred on composite with highest percentage amount of PVA (Hussain et al. 2016). - Incorporation of nHA slightly enhanced the thermal stability of α-chitin. The thermogram of composite showed initial drop at 100 °C due to moisture loss and then it got straightened which indicates that no phase change in composite structure (Kumar et al. 2011)

Table 13.3 (continued)

	Carbonaceous HA - Two major weight loss when heating HA-CNT composite which takes place in air which is attributed to loss of amorphous carbon at 300–400 °C and CNT that typically above 400 °C (Kosma et al. 2013). - TGA curve of fMWCNT-HA composites show that the weight loss of 9.2% at 80–140 °C owing to the elimination of adsorbed water from the surface and pores. At 142–250 °C weight loss of 7.27% due to decomposition of NH_4NO_3 which was the by-product from the synthesis reaction. The composite has good thermal stability according to TGA measurement because of combustion of fMWCNT took place at higher temperature (510–609 °C). The TGA curve of fMWCNT-HA was a multi-stage process as without the formation of stable intermediates (Barabás et al. 2015)
	Hybrid HA - PLA/HA/GO showed the capability of the composite to remain stable without weight loss up to 200 °C. Major weight loss was observed between 240 and 400 °C. Based on the results, when the weight percentage of GO in composite increases, the maximum temperature decomposition become lower. Thermal stability of PLA revealed the enhancement by the addition of GO and HA may be due to interaction between HA, GO and PLA via hydrogen bond and van der Waals force. (Gong et al. 2017)
Brunauer–Emmett–Teller (BET) -pPorosity -specific surface area	**Metal or metal oxide HA** - The composite acted as mesoporous material. BET analysis showed that only moderate increase on specific surface area when high Al introduced to the composite. For lower content of Al, the mesoporosity became more obvious as the enlargement of hysteresis loop seen so obvious. The introduction of aluminium oxide to composite has specific surface area in range of 145 to 206 $m^2\ g^{-1}$, which clearly improve the specific surface area compared to pure HA (ca. $100 m^2 g^{-1}$) (Bouiahya et al. 2019)
	Natural or synthetic polymer HA - BET surface area of PVAHA composite was 41.3–63.7 m^2/g meanwhile for BET nitrogen adsorption/ desorption isotherms of composites showed type IV which a typical type for mesoporous material. (Hussain et al. 2016)
	Carbonaceous HA - BET nitrogen adsorption/desorption for GO-HA displayed type IV which similar to HA and having distinct hysteresis loop when P/P_0 over 0.5, which reveals the characteristic of mesoporous material (Fathyunes and Khalil-alla, 2017)
	Hybrid HA - BET analysis proved that there are mesopores in the GO/HA/CS based composite as from the nitrogen absorption/desorption, the composite has similar structure with that of Type IV isotherm with H3 hysteresis. Based on BJH calculation, that composite consist of large BET surface area and the mesoporous structure distributed at 3.71 nm (Yılmaz et al. 2019)

13.4 Characterization of HA Based Composites

Various characterization techniques have been used to characterize HA based composites. The characterization techniques can be divided into spectroscopic and direct visualization as listed in the Fig. 13.6. Table 13.3 concluded main findings of various HA based composites using both characterization techniques.

13.5 Current Application of Hydroxyapatite (HA) Based Composites

Hydroxyapatite based composites have various biomedical applications especially in tissue engineering. Tissue engineering or regenerative medicine is a field that involves in promoting new tissues or organs to restore defect, lost or damaged tissues and organs by engineered products. The current practice of using bone grafts for treating patients with bone defect resulted from trauma, pathology and congenital disease brings together a few disadvantages. The advancement of tissue engineering has shed a new light for both clinicians and patients involved. The triad of tissue engineering requires stem cells, growth factors and scaffold-based composites. HA based composite is one of the preferred scaffolds due to its similar composition and structure with the natural human bone (Roffi et al. 2017).

13.5.1 Bone Regeneration

Bone disorders due to trauma, congenital deformity and malignancy are one of the pathological areas that require transplantation of bone graft. Bone graft can either be autograft, allograft, xenograft or bone substitutes. However, each graft possesses different drawbacks that hinder optimal outcome after the surgery. Since the last few decades, the advancement in regenerative medicine has gradually being investigated to overcome the limitation of usual practice, including the bone tissue regeneration area. Even though it is difficult to mimic nature, recent scientific and technological findings show promising results to provide an alternative option to the current management. Scaffold, one of the important components in tissue engineering has received tremendous attention among researchers. The search for the right scaffold in bone tissue engineering since past few decades is still ongoing. The ideal scaffold for bone regeneration should have the following properties: biocompatible, bioresorbable, osteoconductive, osteoinductive and structurally similar to the native bone.

13.5.2 Ideal Properties of Scaffolds

Bioceramic such as HA, bioactive glass, zirconia and β-tricalcium phosphate (β-TCP) are mostly used for hard tissue regeneration (Huang et al., 2018; Lukić et al., 2011). HA based scaffolds have been reported to have good biocompatibility and osteoconductivity; suitable for bone regeneration (Hao et al., 2017). Owing to similar chemical composition with native bones HA has become the most common bioceramic used in bone tissue engineering (Mondal et al. 2019; Yang et al. 2019). Scaffolds chosen should mimic the actual microenvironment to allow cells to interact and behave at the optimum condition. Hence, scaffolds properties are essential in determining cellular response and fate (Loh and Choong 2013). There are few requirements for ideal scaffolds required in bone regeneration that include physical properties, biomaterial properties and mechanical properties (Tables 13.4 and 13.5).

Mechanical property of ideal scaffold in bone regeneration requires sufficient mechanical strength in order to maintain the cell integrity until formation of new bone. Newly bone regeneration should withstand loading to prevent shielding as compared to the surrounding native bone (Loh and Choong 2013).

Table 13.4 Physical properties of ideal HA based composite for scaffold in bone regeneration

Properties	Characteristics
Porosity	Pore size Minimum 100 μm in diameter for successful diffusion of nutrients and oxygen (Bose et al. 2012). More than 200 μm for better osteoconduction and up to 500 μm for vascularization (Khojasteh et al. 2016). More than 500 μm might wash away the cells that previously seeded during in vivo application
Interconnectivity	Important to enable proper diffusion of nutrients and metabolic waste into and from deeper part of scaffold for cell viability (Battistella et al. 2012). Important for cell penetration and angiogenesis of cell/scaffold co-culture (Ghassemi et al. 2018)
Porosity	Porous scaffolds will offer high surface area for scaffold-cell interaction; resulted in better cells infiltration and attachment (Loh & Choong 2013). Dense scaffold has excellent mechanical property and less susceptible to breakage, but it has slow dissolution rate

Table 13.5 Biomaterial property of ideal scaffold in bone regeneration

Properties	Characteristics
Biocompatibility	Biocompatible to the cells and environment (Ghassemi et al. 2018)
Osteoconductivity	Bone grows on a scaffold surface
Osteoinductive	Enhance osteogenesis
Bioresorbability	Ability to degrade in vivo, preferably at a controlled rate and eventually providing space for the new bone to grow

13.6 Conclusion and Future Remarks

This chapter reviewed modern approach used in the fabrication of HA based composite for various biomedical applications. Wide range of methods available for fabricating HA based composites have developed in the past few decades. Each of the fabrication methods has its own benefits and drawbacks. Factors need to be taken into consideration include the overall cost, easy and reliable procedures, the performance and characteristic of the end product. The HA composites prepared with either polymers, metals and metal oxide, carbonaceous and the hybrid mixtures have gain worldwide attention due to the outstanding biological properties on top of chemical resemblance to the bone tissues. It is important to consider the ideal properties of the biomaterial in designing the suitable HA based composite for biomedical applications. Future work will focus on the advancement and improvement in fabrication real bone like HA composites with improved mechanical, bioactivity, biocompatibility and osteoconductivity. The cell-material interaction, in vitro and in vivo studies will be the focus in the future.

References

An SH, Matsumoto T, Miyajima H, Nakahira A, Kim KH, Imazato S (2012) Porous zirconia/hydroxyapatite scaffolds for bone reconstruction. Dent Mater 28(12):1221–1231

Andrade FAC, de Oliveira Vercik LC, Monteiro FJ, da Silva Rigo EC (2016) Preparation, characterization and antibacterial properties of silver nanoparticles–hydroxyapatite composites by a simple and eco-friendly method. Ceram Int 42(2):2271–2280

Balagangadharan K, Chandran SV, Arumugam B, Saravanan S, Venkatasubbu GD, Selvamurugan N (2018) Chitosan/nano-hydroxyapatite/nano-zirconium dioxide scaffolds with miR-590-5p for bone regeneration. Int J Biol Macromol 111:953–958

Barabás R, Katona G, Bogya ES, Diudea MV, Szentes A, Zsirka B, Kovács J, Kékedy-Nagy L, Czikó M (2015) Preparation and characterization of carboxyl functionalized multiwall carbon nanotubes–hydroxyapatite composites. Ceram Int 41(10):12717–12727

Battistella E, Mele S, Foltran I, Lesci IG, Roveri N, Sabatino P, Ramondini L (2012) Cuttlefish bone scaffold for tissue engineering: a novel hydrothermal transformation, chemical-physical, and biological characterization. J Appl Biomater Func 10(2):99–106

Begam H, Nandi SK, Chanda A, Kundu B (2017) Effect of bone morphogenetic protein on Zn-HAp and Zn-HAp/collagen composite: a systematic in vivo study. Res Vet Sci 115:1–9

Bencherif SA, Braschler TM, Renaud P (2013) Advances in the design of macroporous polymer scaffolds for potential applications in dentistry. J Periodontal Implant Sci 43(6):251–261

Bharti A, Singh S, Meena VK, Goyal N (2016) Structural characterization of silver-hydroxyapatite nanocomposite: a bone repair biomaterial. Mater Today Proc 3(6):2113–2120

Bollino F, Armenia E, Tranquillo E (2017) Zirconia/hydroxyapatite composites synthesized via sol-gel: influence of hydroxyapatite content and heating on their biological properties. Materials 10(7):757

Bommala VK, Krishna MG, Rao CT (2018) Magnesium matrix composites for biomedical applications: a review. J Magnes Alloy

Bose S, Roy M, Bandyopadhyay A (2012) Recent advances in bone tissue engineering scaffolds. Trends Biotechnol 30(10):546–554

Bouiahya K, Es-saidi I, El Bekkali C, Laghzizil A, Robert D, Nunzi JM, Saoiabi A (2019) Synthesis and properties of alumina-hydroxyapatite composites from natural phosphate for phenol removal from water. Colloid Interfac Sci Commun 31:100188

Davis HE, Leach JK (2008) Hybrid and composite biomaterials in tissue engineering. Topics Multifunct Biomater and Dev 10:1–26

Deng C, Weng J, Lu X, Zhou SB, Wan JX, Qu SX, Feng B, Li XH (2008) Preparation and in vitro bioactivity of poly (D, L-lactide) composite containing hydroxyapatite nanocrystals. Mater Sci Eng C 28(8):1304–1310

Dou T, Jing N, Zhou B, Zhang P (2018) In vitro mineralization kinetics of poly (L-lactic acid)/hydroxyapatite nanocomposite material by attenuated total reflection Fourier transform infrared mapping coupled with principal component analysis. J Mater Sci 53(11):8009–8019

Edwin N, Saranya S, Wilson P (2019) Strontium incorporated hydroxyapatite/hydrothermally reduced graphene oxide nanocomposite as a cytocompatible material. Ceram Int 45(5):5475–5485

Fathyunes L, Khalil-Allafi J (2017) Characterization and corrosion behavior of graphene oxide-hydroxyapatite composite coating applied by ultrasound-assisted pulse electrodeposition. Ceram Int 43(16):13885–13894

Ghassemi T, Shahroodi A, Ebrahimzadeh MH, Mousavian A, Movaffagh J (2018) Current concepts in scaffolding for bone tissue engineering. Archi Bone Joint Surg 6(2):90–99

Gong M, Zhao Q, Dai L, Li Y, Jiang T (2017) Fabrication of polylactic acid/hydroxyapatite/graphene oxide composite and their thermal stability, hydrophobic and mechanical properties. J Asian Ceramic Soc 5(2):160–168

Haider A, Haider S, Han SS, Kang IK (2017) Recent advances in the synthesis, functionalization and biomedical applications of hydroxyapatite: a review. RSC Adv 7(13):7442–7458

Hao Z, Song Z, Huang J, Huang K, Panetta A, Gu Z, Wu J (2017) Scaffold microenvironment for stem cell based bone tissue engineering. Biomater Sci 5(8):1382–1392

Hou R, Zhang G, Du G, Zhan D, Cong Y, Cheng Y, Fu J (2013) Magnetic nanohydroxyapatite/PVA composite hydrogels for promoted osteoblast adhesion and proliferation. Colloids Surf B: Biointerfaces 103:318–325

Huang B, Caetano G, Vyas C, Blaker JJ, Diver C, Bártolo P (2018) Polymer-ceramic composite scaffolds: the effect of hydroxyapatite and β-tri-calcium phosphate. Materials 11(129):2–13

Huixia L, Yong L, Lanlan L, Yanni T, Qing Z, Kun L (2016) Development of ammonia sensors by using conductive polymer/hydroxyapatite composite materials. Mater Sci Eng C 59:438–444

Hussain R, Tabassum S, Gilani MA, Ahmed E, Sharif A, Manzoor F, Shah AT, Asif A, Sharif F, Iqbal F, Siddiqi SA (2016) In situ synthesis of mesoporous polyvinyl alcohol/hydroxyapatite composites for better biomedical coating adhesion. Appl Surf Sci 364:117–123

Ji L, Wang W, Stevens MM, Zhou S, Zhu A, Liang J (2015) A general strategy for the preparation of aligned multiwalled carbon nanotube/inorganic nanocomposites and aligned nanostructures. Mater Res Bull 61:453–458

Karimi N, Kharaziha M, Raeissi K (2019) Electrophoretic deposition of chitosan reinforced graphene oxide-hydroxyapatite on the anodized titanium to improve biological and electrochemical characteristics. Mater Sci Eng C 98:140–152

Khanra AK, Jung HC, Yu SH, Hong KS, Shin KS (2010) Microstructure and mechanical properties of Mg-HAP composites. Bull Mater Sci 33(1):43–47

Khojasteh A, Fahimipour F, Eslaminejad MB, Jafarian M, Jahangir S, Bastami F, Tahriri M, Karkhaneh A, Tayebi L (2016) Development of PLGA-coated β-TCP scaffolds containing VEGF for bone tissue engineering. Mater Sci Eng C 69:780–788

Kosma V, Tsoufis T, Koliou T, Kazantzis A, Beltsios K, De Hosson JTM, Gournis D (2013) Fibrous hydroxyapatite–carbon nanotube composites by chemical vapor deposition: in situ fabrication, structural and morphological characterization. Mater Sci Eng B 178(7):457–464

Kumar PS, Srinivasan S, Lakshmanan VK, Tamura H, Nair SV, Jayakumar R (2011) β-Chitin hydrogel/nano hydroxyapatite composite scaffolds for tissue engineering applications. Carbohydr Polym 85(3):584–591

Lao L, Wang Y, Zhu Y, Zhang Y, Gao C (2011) Poly (lactide-co-glycolide)/hydroxyapatite nanofibrous scaffolds fabricated by electrospinning for bone tissue engineering. J Mater Sci Mater Med 22(8):1873–1884

Lebourg M, Anton JS, Ribelles JG (2010) Hybrid structure in PCL-HAp scaffold resulting from biomimetic apatite growth. J Mater Sci Mater Med 21(1):33–44

Li J, Sun H, Sun D, Yao Y, Yao F, Yao K (2011) Biomimetic multicomponent polysaccharide/nano-hydroxyapatite composites for bone tissue engineering. Carbohydr Polym 85(4):885–894

Lickorish D, Ramshaw JA, Werkmeister JA, Glattauer V, Howlett CR (2004) Collagen–hydroxyapatite composite prepared by biomimetic process. Journal of Biomedical Materials Research Part A: An Official Journal of The Society for Biomaterials, The Japanese Society for Biomaterials, and The Australian Society for Biomaterials and the Korean Society for Biomaterials 68(1):19–27

Lim LS (2018) *Effects of Microwave Radiation on Properties of Polyvinyl Alcohol-Carbon Nanotube-Hydroxyapatite Blends* (Doctoral dissertation, UTAR)

Lim YM, Hwang KS, Park YJ (2001) Sol-gel derived functionally graded TiO2/HAP films on Ti-6Al-4V implants. J Sol-Gel Sci Technol 21(1–2):123–128

Loh QL, Choong C (2013) Three-dimensional scaffolds for tissue engineering: role of porosity and pore size. Tissue Eng Part B Rev 19(6)

Long Y, Jiang J, Hu J, Hu X, Yang Q, Zhou S (2019) Removal of Pb (II) from aqueous solution by hydroxyapatite/carbon composite: preparation and adsorption behavior. In: *Colloids and surfaces A: physicochemical and engineering aspects*

Lukić MJ, Stanković A, Veselinović L, Škapin SD, Bračko I, Marković S, Uskoković D (2011) Chemical precipitation synthesis and characterization of Zr-doped hydroxyapatite nanopowders. In: The thirteenth annual conference YUCOMAT 2011: programme and the book of abstracts. Materials Research Society of Serbia, Belgrade, pp 89–89

Luo Y, Xiao L, Zhang X (2015) Characterization of TEOS/PDMS/HA nanocomposites for application as consolidant/hydrophobic products on sandstones. J Cult Herit 16(4):470–478

Mathi DB, Gopi D, Kavitha L (2019) Implication of lanthanum substituted hydroxyapatite/poly (n-methyl pyrrole) bilayer coating on titanium for orthopedic applications. *Materials today: proceedings*

Matsumoto TJ, An SH, Ishimoto T, Nakano T, Matsumoto T, Imazato S (2011) Zirconia–hydroxyapatite composite material with micro porous structure. Dent Mater 27(11):e205–e212

Mei F, Zhong J, Yang X, Ouyang X, Zhang S, Hu X, Ma Q, Lu J, Ryu S, Deng X (2007) Improved biological characteristics of poly (L-lactic acid) electrospun membrane by incorporation of multiwalled carbon nanotubes/hydroxyapatite nanoparticles. Biomacromolecules 8(12):3729–3735

Mondal S, Hoang G, Manivasagan P, Moorthy MS, Kim HH, Vy Phan TT, Oh J (2019) Comparative characterization of biogenic and chemical synthesized hydroxyapatite biomaterials for potential biomedical application. Mater Chem Phys

Nedunchezhian G, Anburaj DB, Gokulakumar B, Jeyakumar SJ (2016) Microwave assisted synthesis and charecterization of silver and zinc doped hydroxyapatite nanorods from mussel shell (MOLLUSK). Rom J Biophys 26(1)

Oleiwi APDJK, Anaee APDRA, Muhsin LSA (2015) Fabrication, characterization and physical properties of functionally graded Ti/HAP bioimplants. Wulfenia J 22(7):336–348

Pai NS, Yen SK (2013) Preparation and characterization of platinum/iron contained hydroxyapatite/carbon black composites. Int J Hydrog Energy 38(30):13249–13259

Pang P, Liu Y, Zhang Y, Gao Y, Hu Q (2014) Electrochemical determination of luteolin in peanut hulls using graphene and hydroxyapatite nanocomposite modified electrode. Sensors Actuators B Chem 194:397–403

Prabhu SM, Elanchezhiyan SS, Lee G, Khan A, Meenakshi S (2016) Assembly of nano-sized hydroxyapatite onto graphene oxide sheets via in-situ fabrication method and its prospective application for defluoridation studies. Chem Eng J 300:334–342

Raj SV, Rajkumar M, Sundaram NM, Kandaswamy A (2018) Synthesis and characterization of hydroxyapatite/alumina ceramic nanocomposites for biomedical applications. Bull Mater Sci 41(4):93

Ramadas M, Bharath G, Ponpandian N, Ballamurugan AM (2017) Investigation on biophysical properties of hydroxyapatite/Graphene oxide (HAp/GO) based binary nanocomposite for biomedical applications. Mater Chem Phys 199:179–184

Rodríguez-González C, Salas P, López-Marín LM, Millán-Chiu B, De La Rosa E (2018) Hydrothermal synthesis of graphene oxide/multiform hydroxyapatite nanocomposite: its influence on cell cytotoxicity. Mater Res Express 5(12):125023

Roffi A, Krishnakumar GS, Gostynska N, Kon E, Candrian C, Filardo G (2017) The role of three-dimensional scaffolds in treating long bone defects: evidence from preclinical and clinical literature- a systematic review. Biomed Res Int

Saadat A, Karbasi S, Ghader AB, Khodaei M (2015) Characterization of biodegradable P3HB/HA nanocomposite scaffold for bone tissue engineering. Procedia Mater Sci 11:217–223

Salernitano E, Migliaresi C (2003) Composite materials for biomedical applications: a review. J Appl Biomater Biomech 1(1):3–18

Saravanan S, Nethala S, Pattnaik S, Tripathi A, Moorthi A, Selvamurugan N (2011) Preparation, characterization and antimicrobial activity of a bio-composite scaffold containing chitosan/nano-hydroxyapatite/nano-silver for bone tissue engineering. Int J Biol Macromol 49(2):188–193

Sneha M, Sundaram NM (2015) Preparation and characterization of an iron oxide-hydroxyapatite nanocomposite for potential bone cancer therapy. Int J Nanomedicine 10(Suppl 1):99

Su C, Su Y, Li Z, Haq MA, Zhou Y, Wang D (2017) In situ synthesis of bilayered gradient poly (vinyl alcohol)/hydroxyapatite composite hydrogel by directional freezing-thawing and electrophoresis method. Mater Sci Eng C 77:76–83

Sukhodub LB, Kumeda MO, Gapon VI, Sukhodub LF (2018, September) Microwave assisted formation of the chitosan/hydroxyapatite scaffold for bone tissue regeneration. In: *2018 IEEE 8th international conference nanomaterials: application & properties (NAP)*. IEEE, pp 1–4

Sung YM, Shin YK, Ryu JJ (2007) Preparation of hydroxyapatite/zirconia bioceramic nanocomposites for orthopaedic and dental prosthesis applications. Nanotechnology 18(6):065602

Suparto IH, Kurniawan E (2019, August) Synthesis and Characterization of Hydroxyapatite-Zinc Oxide (HAp-ZnO) as Antibacterial Biomaterial. In *IOP conference series: materials science and engineering* (Vol. 599, No. 1, p. 012011). IOP Publishing

Trakoolwannachai V, Kheolamai P, Ummartyotin S (2019a) Characterization of hydroxyapatite from eggshell waste and polycaprolactone (PCL) composite for scaffold material. Compos Part B:106974

Trakoolwannachai V, Kheolamai P, Ummartyotin S (2019b) Development of hydroxyapatite from eggshell waste and a chitosan-based composite: in vitro behavior of human osteoblast-like cell (Saos-2) cultures. Int J Biol Macromol 134:557–564

Vahdat A, Ghasemi B, Yousefpour M (2019) Synthesis of hydroxyapatite and hydroxyapatite/Fe3O4 nanocomposite for removal of heavy metals. Environ Nanotechnol Monit Manage 12:100233

Valizadeh S, Rasoulifard MH, Dorraji MS (2014) Modified Fe3O4-hydroxyapatite nanocomposites as heterogeneous catalysts in three UV, Vis and Fenton like degradation systems. Appl Surf Sci 319:358–366

Venugopal J, Prabhakaran MP, Zhang Y, Low S, Choon AT, Ramakrishna S (2010) Biomimetic hydroxyapatite-containing composite nanofibrous substrates for bone tissue engineering. Philos Trans R Soc A Math Phys Eng Sci 368(1917):2065–2081

Vijayalakshmi V, Dhanasekaran P (2017) Synthesis and structural properties characterization of HA/alumina and HA/MgO Nanocomposite for biomedical applications. Open Access J Trans Med Res 1(4):00020

Wang Y, Liang D, Liu F, Zhang W, Di X, Wang C (2017) A polyethylene glycol/hydroxyapatite composite phase change material for thermal energy storage. Appl Therm Eng 113:1475–1482

Wu M, Wang Q, Liu X, Liu H (2013) Biomimetic synthesis and characterization of carbon nanofiber/hydroxyapatite composite scaffolds. Carbon 51:335–345

Yan Y, Zhang X, Li C, Huang Y, Ding Q, Pang X (2015) Preparation and characterization of chitosan-silver/hydroxyapatite composite coatings onTiO2 nanotube for biomedical applications. Appl Surf Sci 332:62–69

Yang H, Zhang L, Xu KW (2007) The microstructure and specific properties of La/HAP composite powder and its coating. Appl Surf Sci 254(2):425–430

Yang W, Zhou W, Li N, Huang Y, Cheng X, Shua B, Wen B (2019) A clinical study of early intervention with coralline hydroxyapatite on fresh extraction sockets. J Nanosci Nanotechnol 19(11):6956–6960

Yelten A, Yilmaz S, Oktar FN (2012) Sol–gel derived alumina–hydroxyapatite–tricalcium phosphate porous composite powders. Ceram Int 38(4):2659–2665

Yılmaz P, Elif öztürk Er, Bakırdere S (2019) Application of supercritical gel drying method on fabrication of mechanically improved and biologically safe three-component scaffold composed of graphene oxide/chitosan/hydroxyapatite and characterization studies. J Mater Res Technol

Zhang C, Zhang X, Liu C, Sun K, Yuan J (2016) Nano-alumina/hydroxyapatite composite powders prepared by in-situ chemical precipitation. Ceram Int 42(1):279–285

Zhang J, Iwasa M, Kotobuki N, Tanaka T, Hirose M, Ohgushi H, Jiang D (2006) Fabrication of hydroxyapatite–zirconia composites for orthopedic applications. J Am Ceram Soc 89(11):3348–3355

Zhou Y, Qi P, Zhao Z, Liu Q, Li Z (2014) Fabrication and characterization of fibrous HAP/PVP/PEO composites prepared by sol-electrospinning. RSC Adv 4(32):16731–16738

Chapter 14
Hybrid Composite for Orthopedic Applications

Yanny Marliana Baba Ismail and Yvonne Reinwald

14.1 Introduction

Various biomaterials have been explored for designing engineered bone tissue, ranging from natural to materials synthetic materials as well as the combination of the two employing numerous fabrication techniques. These materials are expected to resemble the chemical composition and architecture of the natural human bone as well as providing sufficient biomechanical properties to withstand load once implanted in the patient's body. In order to mimic the complex bone structure, a novel engineered bone material could be designed by combining two or more materials, forming a hybrid composite material. Ideally, this hybrid composite material should be biocompatible, bioresorbable/ biodegradable over time, osteoinductive and osteoconductive. Furthermore, the hybrid composite material should enable the fabrication of 3D porous structures with sufficient porosity and interconnected pores to allow cell ingrowth, transport of nutrients and metabolic waste throughout and most importantly promoting vascularization. In order to fabricate a suitable hybrid composite for bone regeneration, one should firstly understand the natural bone formation and remodelling, bone-health problems, as well as limitations of current treatments and current approaches to accelerate bone remodelling. This chapter will provide an insight into these aaspects to enable the right selection of

Y. M. Baba Ismail (✉)
School of Materials & Mineral Resources Engineering, Engineering Campus, Universiti Sains Malaysia, Nibong Tebal, Penang, Malaysia
e-mail: yannymarliana@usm.my

Y. Reinwald
Department of Engineering, School of Science and Technology, Nottingham Trent University, Nottingham, UK
e-mail: yvonne.reinwald@ntu.ac.uk

S. Siddiquee et al. (eds.), *Composite Materials: Applications in Engineering, Biomedicine and Food Science*, https://doi.org/10.1007/978-3-030-45489-0_14

materials for the fabrication of functional hybrid composite materials for bone regeneration.

14.2 Brief Insights into Bone Biology

Bone is a dynamic and highly vascularized tissue which undergoes remodelling throughout the lifetime of an individual (Salgado et al. 2004; Stevens 2008a). Basically, bone tissue is comprised of two main components; (i) the inorganic mineralized phase, which forms 65–70% of the bone tissue and consists of carbonated hydroxyapatite (CHA), and (ii) non-mineralized organic phase, which forms 30–35% of bone tissue and is predominantly collagen type I and other organic proteins. The inorganic mineralized phase increases the stiffness and the compressive strength of the bone while, the tensile strength and flexibility of bone are provided by the organic non-mineralized phase (Viguet-Carrin et al. 2006; Balint and Cartmell 2012). Each of the bone components plays an important role in allowing bone (1) to protect vital internal organs, (2) to support locomotion by providing support and site of muscle attachment, (3) to ensure that the skeleton has sufficient load-bearing capacity, (4) to promote the generation of red and white blood cells for oxygenation and immunological protection of other tissues and (5) to act as mineral reservoir for calcium, phosphate, and other important ions.

In adult skeleton, bone tissue can be divided into two architectural forms namely, the cortical also known as compact or dense bone (around 80% of total skeleton) and trabecular also called cancelleous or spongy bone (around 20% of total skeleton). Cortical bone is the denser bone, consisting of parallel cylindrical units with 5–10% porosity. Cortical bone is primarily found in the shaft of long bones such as femur, tibia, fibula; and forms the outer shell around the cancellous bone at the end of joints and the vertebrae. In contrast, the cancellous bone acquires sponge-like honeycomb morphology, comprising of branching bars, plates, and rods of various sizes called trabeculae. The mechanical properties of cancellous bone are greatly dependent on its porosity and internal porous structure. Its porosity ranges from 50 to 90%, making its ultimate compressive strength and modulus of elasticity 10 times inferior compared to cortical bone. Besides that, the pores also perform other physiological functions and contain the marrow. Cancellous bone is normally found at the end of the long bones in vertebrate and in flat bones like the pelvis (Salgado et al. 2004; Stevens 2008a).

The formation, maintenance and resorption of bone tissue results from the interaction of bone cells, namely osteoblasts, osteocytes and osteoclasts. Osteoblasts are responsible for the production and mineralization of the bony matrix whereas, osteoclasts are responsible for bone resorption during remodelling, the repair of micro-damage and the adaptation to mechanical loading. Osteocytes are the most abundant cells in bone which are characterized by stellate shape and possess fewer organelles than the osteoblasts. Osteocytes reside in the lacunae within the mineralized matrix and act as the mechanosensor cells of bone (Balint and Cartmell 2012;

Kini and Nandeesh 2012). Bone development and repair are finely coordinated through the balance between bone matrix resorption and formation orchestrated by osteoclasts and osteoblasts, respectively. Together, they form multicellular units, present in the vicinity of the vascular spaces and bone surfaces, responsible for bone remodelling. Fundamentally, the bone remodelling process involves six stages, namely (1) quiescence, (2) activation, (3) resorption, (4) reversal, (5) formation and (6) mineralization (Kohli et al. 2018). The understanding of the physiological process involved in bone remodelling is of critical importance with regards to the design and development of a biomaterial for it to completely reconstruct the damaged tissue. The next section of this review will discuss the need of biomaterial intervention in accelerating bone remodelling followed by the sequence of events that take place upon biomaterial implantation.

14.3 Clinical Needs for Bone Regeneration

Bone loss or dysfunction due to disease, trauma or infection can dramatically alter one's body equilibrium and quality of life (Salgado et al. 2004; Balint and Cartmell 2012). It is considered as one of the major public health problems, which could result in huge socioeconomic implications. For younger people who generally have higher regenerative capacity, most fractures will possibly heal without the need of any intervention (Stevens 2008a). However, it is not the same scenario for elderly people. The growing elderly population is one of the major factors contributing to the increase in bone-related degenerative diseases such as osteoporosis, which is due to hormonal changes and oxidative stress related to aging. Proximal femur, proximal humerus or the vertebral body are the typical locations of such commuted fractures for these patients. The reconstruction of fractured bones remains a critical challenge in the field of orthopaedic surgery. According to the National Health Service's (NHS) records, more than 300,000 people receive hospital treatment for fragility fractures every year as a result of osteoporosis in the United Kingdom, thus resulting in enormous economic burden for the NHS. For instance, hip fractures alone cost the UK an estimated £5 million per day- that is approximately £2 billion pounds per year.

In other parts of the world, particularly in Asia, the largest bone-related are due to the high rate of road accidents (Muhammad et al. 2012). For instance, in Malaysia alone, annually there are over 400,000 road accidents with approximately 7000 fatal cases and over 10,000 serious and minor injuries. In 2014, it was reported that Malaysian roads were considered the 17th most dangerous roads in the world with road accidents leading to serious trauma and fractures. In addition to trauma the loss or resection of bone due to tumour or infection can cause critical-size defects (CSD). Bone-health problems do not only restrict the physical movement of the patients but indirectly also affect the psychological condition and quality of life of an individual (Balint and Cartmell 2012).

Historically, bone defects are treated autografts or allografts. Transplanting autologous bone has been considered as gold standard in clinic as it integrates

reliably with the host bone and avoids immune- and disease-related complications (Athanasiou et al. 1996). Allografts, on the other hand, are bone donated from other patients. However, numerous drawbacks of this treatment have been reported such as short supply, high cost, and donor site morbidity as associated with the harvest and potential risk of disease transmission. The limitations associated with the use of autografts and allografts have driven the development of various engineered bone biomaterials. The use of these biomaterials could reduce the risk of disease transmission, the number of surgical procedures, cost, pain and immunogenicity as well as eliminate the issue regarding the shortage of supply (Kohli et al. 2018; Fernandez de Grado et al. 2018). Various materials such as natural or synthetic biomaterials mostly based on calcium phosphates bioceramics, polymer-based substitutes and biological products such as growth factors have been developed for bone tissue engineering (BTE) applications. To date, no adequate bone substitute has been developed to meet the clinical needs; hence, bone-health problems remain unresolved. The search of new bone regeneration strategies is therefore a key priority fuelled by the debilitating pain associated with bone damage, particularly in managing large bone defects. For these particular defects, not only is the bone tissue damaged, but the surrounding vascular network is often markedly disrupted as well, which can consequently affect the repair response of the tissue. Bone regeneration is a complex process as it involves not only bone cells, vascular network but also the surrounding immune responses. Developing porous synthetic materials such as 3D hybrid composite biomaterials, which can ultimately act as bone scaffolds exhibiting bone like composition and architecture is crucial. These bone scaffolds are able to support faster bone regeneration and inclusion of functional vascular networks within their structure.

14.4 Approaches to Accelerate Bone Regeneration

With a long history of development, Calcium orthophosphates (CaPs) have been accepted as main inorganic components of hard tissues of vertebrates. The mineral phase of bone and teeth is a basic calcium phosphate, which is assimilated to synthetic hydroxyapatite (HA) with a chemical formula of $Ca_{10}(PO_4)_6(OH)_2$. Besides its strong affinity for the mineral constituents of bones, HA also has good bioactivity, osteoconductivity, and biocompatibility with the human bone tissue. These properties provide a rationale for its use as bone substitute material in orthopaedic and dental applications. However, biological apatites differ from stoichiometric HA in several respects, including non-stoichiometry, small crystal dimensions and poor crystallinity (i.e. low degree of structural order) (Boanini et al. 2010; Malhotra and Habibovic 2016; Baba Ismail et al. 2017). Biological apatites are uniquely similar in that they all comprise carbonate (CO_3) in varying amounts of 2–8 wt %, preferentially substituting the PO_4 site (B-type) compared with OH (A-type) ions in the apatite lattice. The composition of CO_3 depends on bone age, site, sex, and health of the individual (Zhou et al. 2008; Landi et al. 2003).

For the past few decades, much research has demonstrated that a variety of trace elements such as carbonate, magnesium, zinc, strontium, and cobalt can be incorporated into the HA lattice to improve its properties by producing a mineral composition more akin to that of mineral native bone tissue. Not only the chemical composition of the biomaterials plays a major role, but also the ability to encourage rapid osteogenesis coupled with angiogenesis. These processes are intricately linked and osteogenesis would not be possible without angiogenesis (Grellier et al. 2009; Bose et al. 2013). A common way to promote osteoinductivity and agiogenesis in CaPs scaffolds is by incorporating growth factors such as recombinant human bone morphogentic protein-2 (rhBMP-2), transforming growth factor (TGF-β), insulin growth factor (IGF), vascular endothelial growth factor (VEGF) and a variety of bisphosphates (BPs)(Hankenson et al. 2011; Portal-Núñez et al. 2012). However, recent concerns over their safety has lead to increased resistance of their use through the Food and Drug Administration (FDA). The major concerns have related to ectopic or unwanted bone formation, which in certain situations can lead to very serious side effects (Boraiah et al. 2009; Luca et al. 2010). An alternative and potentially safer strategy has been the addition of multi-doping ions into the HA lattice as it has been reported that the addition of trace elements can lead to controlled resorbability, improve mechanical strength and positively influence the biological response (Bose et al. 2013; Bandyopadhyay et al. 2006). The roles of these trace elements and their mechanisms of action are summarized in Table 14.1.

14.5 Materials for Bone Scaffolds

Given the demanding clinical need, it is not surprising that the market for biomaterial-based orthopedic treatments is evolving at a rapid rate. While materials intended for the implantation in the classical approach were in the past designed to be bioinert, material scientists have now shifted toward the use of bioactive materials. These bioactive materials are supposed to integrate with the host and regenerate damaged. For BTE applications, these bioactive materials should preferably be osteoinductive, osteoconductive and osseointegrative. The terms osteoinductive, osteoconductive and osseointegrative are repeatedly used in many orthopaedic papers, but not always correctly defined. Thus, the suggested definitions of these terms are shown in Table 14.2.

The selection of the most appropriate material for the fabrication of a scaffold is very important, as its properties will influence the scaffold properties to a great extent. A number of materials such as metals, ceramics and polymers have been proposed but most metals and ceramics are non-biodegradable, which leaves the researcher's choice to limited small number of ceramics and biodegradable polymers.

Table 14.1 Roles of trace elements and their mechanisms of action

Trace elements	Role	Mechanism of action
CO_3^{2-}	Major substituent in bone	The presence of B-carbonate in the apatite lattice causes a decrease in crystallinity and increase in solubility in both *in vitro* and *in vivo* tests (Landi et al. 2003; Murugan and Ramakrishna 2006). The higher the carbonate content, the higher the metabolic activity of the tissue (Landi et al. 2010)
Sr^{2+}	Osteogenesis	Strontium stimulates osteoblasts activity and simultaneously inhibits sthe activity and differentiation of osteoclast cells (Aina et al. 2012; Chandran et al. 2016)
Co^{2+}	Angiogenesis	Cobalt ions can induce hypoxia on the cellular level. Cells compensate for this hypoxic environment by expressing genes (such as VEGF) that promote neovascularization and angiogenesis (Pacary et al. 2006; Kim et al. 2006a). In large doses, CO^{2+} can also induce toxicity. Increased soluble CO^{2+} ion levels might cause serious adverse reactions to the surrounding tissues as well as systematic toxicity (Simonsen et al. 2012).
Zn^{2+}	Osteogenesis	Zinc ions have a positive effect on bone metabolism. In the cellular microenvironment, Zn^{2+} are thought to promote osteoblastic bone formation and inhibit osteoclastic bone resorption *in vitro* (Bose et al. 2013; Dasgupta et al. 2010)
Mg^{2+}	Angiogenesis	Magnesium induces nitric oxide production in endothelial cells which is essentially the same function as VEGF uses to induce angiogenesis (Cooke 2002; Maier et al. 2004)

Table 14.2 Definitions of osteoinductive, osteoconductive and osseointegrative

Terms	Definitions
Osteoinductive	Capable to stimulate the differentiation of progenitor cells towards osteoblastic lineage
Osteoconductive	Permits bone growth on its surface and supports the ingrowth of surrounding bone
Osseointegrative	Ability to integrate into surrounding bone which forms a direct contact between host bones and implant

14.5.1 Bioactive Ceramics

Bioactive ceramic materials have similar composition to the inorganic mineral phase of bone, and hence hydroxyapatite (HA) and tricalcium phosphate (TCP) are of clinical interest (Best et al. 2008; Stevens 2008b). The rationale of using these calcium phosphate (CaP) based materials stems from the fact that CaP is the major component of biological apatite and that it shows promises of biocompatibility, osteoconductivity and biodegradability.

Synthetic HA has been used as coatings on metallic implants, fillers in polymer matrices and scaffolds for maxillofacial reconstruction, treatment of bone defects, total joint replacement and revision surgery for the last 20–30 years (Best et al. 2008). However, previous studies have reported that pure HA shows negligible

resorption even years after implantation. Besides, it was found that biological apatites differ chemically from stoichiometric HA in that they contain a number of additional trace elements substituted into the HA lattice (Boanini et al. 2010; Gibson and Bonfield 2002; David et al. 2013).

Back in 1960s, Raquel LeGeros (1969) first started the work on the characterization of carbonated HA (CHA) for biomedical application. Since then, synthetic CHA has been extensively studied, as carbonate is the most abundant substitution in bone mineral (2–8 wt%). Its amount depends on bone age, site, animal species and individual. Thus, biological apatite is more accurately described as carbonated HA rather than HA alone (Landi et al. 2003; Best et al. 2008; Merry et al. 1998; Tadic et al. 2002). There are three types of carbonate substitution; (i) the substitution of carbonate for hydroxyl ions (A-type), (ii) carbonate substitution for phosphate site (B-type) and (iii) both hydroxyl and phosphate groups substituted by carbonate (AB-type) (Landi et al. 2010; LeGeros et al. 1969; Shepherd et al 2012). Previous studies have shown that the presence of B-carbonate in the apatite lattice causes a decrease in crystallinity and increase in solubility in both *in vitro* and *in vivo* tests. The increase in solubility has considerably enhanced the bioactivity of CHA. This has been shown by greater bone apposition found around dense CHA compared to pure HA. Besides CHA, various other trace elements have been incorporated into the hydroxyapatite structure with the aim to either improve the osteogenesis (bone formation) or angiogenesis (vascular network formation). Among the trace elements that have been investigated and incorporated into the apatite structure are Sr^{2+}, Co^{2+}, Zn^{2+} and Mg^{2+}. Their roles are described in Table 14.1.

For all the aforementioned reasons, the development of synthetic HA powders with fully complete and controlled levels of ionic substitutions into the HA lattice seem promising candidates for the fabrication of ideal bone scaffold materials. These materials have the potential to become the new "gold standard", mimicking the composition of the natural human bone mineralized matrix (Sprio et al. 2008).

14.5.2 Biodegradable Polymers

There are two types of biodegradable polymers, i.e. natural and synthetic polymers (Chen et al. 2002; Rezwan et al. 2006). Natural polymers, such as collagen and hyaluronic acid are among the potential candidates for bone substitute materials which would provide essential biological guidance to cells, supporting cell attachment and promoting chemotactic responses. Collagen is the major component of extracellular matrix (ECM) which is responsible for cellular adhesion and proliferation (Kim et al. 2010; Zhao et al. 2014). It occurs in many places throughout our body. For instance, it is found in bone (Type I), cartilage (Type II), blood vessel walls (Type III), cell basement membrane (Type IV) and cell surfaces (Type V). Collagen type I is a popular choice of material for the scaffold preparation for bone regeneration since it offers excellent biocompatibility, degrades easily and is resorbed by the body. It also promotes cell attachment, but its mechanical properties

however, are much lower than that of the native bone (Wahl and Czernuszka 2006; Jones et al. 2010).

On the other hand, hyaluronic acid is the major non-collagenous component present in the ECM and the synovial fluid (Zhao et al. 2014; Zhang et al. 2005). Therefore, hyaluronic acid and collagen, have been incorporated into 3D scaffolds for bone regeneration (Holtorf et al. 2005; Yu et al. 2012). Hyaluronic acid and collagen type I have been used as coating materials for PLLA films to enhance cell-material interaction. These coatings may improve the bioactivity of PLLA films, for potential BTE applications (Zhao et al. 2014).

The most often utilized biodegradable synthetic polymers for 3D scaffolds in BTE are saturated poly-α-hydroxyl esters such as poly (lactic acid) (PLA), poly (glycolic acid) (PLGA), as well as poly (lactic-co-glycolide) (PLGA) copolyers (Athanasiou et al. 1996; El-amin et al. 2003; Li et al. 2010). These polymers have been approved by the FDA for certain human clinical use, such as surgical sutures and some implantable devices (Chen et al. 2001). The chemical properties of these polymers allow hydrolytic degradation through de-esterfication. The degradation by-products can be removed by the body through natural metabolic pathways as lactic and glycolic acids. The degradtion rate, physical and mechanical propeties of these polymers can be easily tailored over a wide range by using various molecular weights and copolymers. However, these polymers undergo bulk erosion process, where a massive release of the acidic by-products could cause local inflammatory reactions in vivo. Consequently, this can cause the scaffold to fail prematurely. Another drawback of these synthetic polymers is related to their hydrophobicity and lack of physiological activity (Kim et al. 2006b). It has been shown that PLA does not provide a favorable surface for cell attachment and proliferation due to lack of specific cell recognition sites. Modification of the outermost part of the material is seen to be sufficient as to tailor their biocompatibility, while the bulk properties of the materials are maintained.

14.5.3 Composites

Composite or hybrid materials can be generated via the combination of functional polymers with inorganic nanostructured compounds. Inorganic-organic composites aiming to closely mirror the composite nature of real bone by combining the toughness of a polymer phase with the compressive strength of a ceramic phase has been shown to improve both the degradation and mechanical properties of these hybrid scaffolds (Stevens 2008b). For instance, tissue-engineered HA-Collagen nanocomposite systems are developing rapidly and showing promise (Wahl and Czernuszka 2006; Jones et al. 2010). Comparing ceramic scaffolds and ceramic composite scaffolds, it was shown that HA-Collagen composite have better osteoinductive capacity compared to single HA or TCP. Several approaches have been developed to create the inorganic-organic polymer composites including blending, sol-gel and emulsion polymerization. The main challenge in synthesizing composite materials

to recreate the organization of native organic and inorganic components at the nanoscale as found in vivo. However, mechanical properties of these composites is still low compared to the native bone (Stevens 2008b).

14.6 Engineered Scaffolds for Bone Tissue Engineering

In seeking to meet the current challenges of hard tissue augmentation through mimicking the native bone, clinically viable three-dimensional multi-functional scaffolds can be incorporated as matrices for the regeneration of new tissue. Scaffolds can be used either as permanent or temporary template to restore organ functionality. To facilitate tissue repair, scaffolds should meet certain criteria, which might vary slightly between types of tissues. Nevertheless, the following properties have been identified as essential scaffold criteria for BTE applications:

(a) Scaffolds should be biocompatible, which suggests that they should be well integrated in the host's tissue without inducing any adverse response (Salgado et al. 2004; Rezwan et al. 2006). Scaffold should also be osteoconductive in order to guide the formation of new bone tissue along their surfaces (Leong et al. 2003).
(b) Scaffolds should be biodegradable/ bioresorbable. The scaffold should allowed tissues/cells to adhere, proliferate, and differentiate to form healthy tissues and help tissue recovers to the original shape and strength. Subsequently, the scaffold would then degrade while the tissue regenerates (Hutmacher 2000).
(c) Scaffolds should be osteoinductive to promote bone tissue regeneration in large bone defects. Natural osteoinduction in combination with a biodegradable scaffold may not be enough to facilitate bone healing (Albrektsson and Johansson 2001).
(d) Surface properties both chemical and topographical of a scaffold are primarily important to regulate cell activities, such as for adhesion, differentiation, proliferation and thus promote tissue growth (Oh et al. 2006).
(e) Scaffolds should possess sufficient amount of porosity (40–90% depends on the nature of biomaterials used) to allow cell ingrowth as well as flow of nutrients and metabolic waste throughout the entire scaffold (Hutmacher 2000).
(f) The pore size of a scaffold should be large enough to allow cell penetration. It is well recommended that for BTE application, the pore size should be in the range of 200–900 μm (Mikos and Temenoff 2000).
(g) Scaffolds should demonstrate adequate mechanical strength so that they do not collapse during handling and during the patient's daily activities. *In vitro*, the scaffolds should have sufficient strength to withstand the mechanical stimuli applied when cultured in dynamic 3D culture environments such as bioreators (Leong et al. 2003).

(h) Biomaterials should also be reproducible and processable into 3D scaffolds with various shapes and sizes (Leong et al. 2003; Hutmacher 2000). The fabrication process should be controllable and cost-effective (Hutmacher et al. 2004).
(i) As the scaffolds will be in direct contact with the biological environment, they should be easily sterilizable to prevent infection (Rezwan et al. 2006).
(j) Suitable substrate stiffness is also important because it has been shown to affect cell responses including proliferation, differentiation, migration and apoptosis while cells are being attached to a scaffold. It has a huge influence on cell migration, proliferation and apoptosis (Pelham and Wang 1998; Wang et al. 2000).

14.7 Conclusion and Future Direction

Key requirements for engineering a functional hybrid composite for bone regeneration are depending on the selection materials to be used, the appropriate ratio of inorganic and organic materials as well as the architectural design of the hybrid composite scaffolds. These influence the properties of the hybrid composite to a great extent. It is critically important to ensure the produced hybrid composite closely resembles the composition and architecture of natural human bone, and reaches a balance between mechanical and biological performance to assure successful bone regeneration.

Acknowledgements The authors would like to thank Arthritis Research United Kingdom-Tissue Engineering Centre (ARUK-TEC) and the Ministry of Higher Education Malaysia (MOHE) for supporting part of this work. The research leading to these results has also received funding from the Fundamental Research Grant Scheme (FRGS): 6071380 and Nottingham Trent University.

References

Aina V et al (2012) Magnesium- and strontium-co-substituted hydroxyapatite: the effects of doped-ions on the structure and chemico-physical properties. J Mater Sci Mater Med 23:2867–2879

Albrektsson T, Johansson C (2001) Osteoinduction, osteoconduction and osseointegration. Eur Spine J 10:S96–S101

Athanasiou KA, Niederauer GG, Agrawal CM (1996) Biocompatibility and clinical applications of polylactic acid / polyglycolic acid copolymers. 17

Baba Ismail YM, Wimpenny I, Bretcanu O, Dalgarno K, El Haj AJ (2017) Development of multisubstituted hydroxyapatite nanopowders as biomedical materials for bone tissue engineering applications. J Biomed Mater Res – Part A 105:1775–1785

Balint R, Cartmell SH (2012) Osteoblasts and their applications in bone tissue engineering. Cell Health and Cytoskeleton 4:49–61

Bandyopadhyay A, Bernard S, Xue W, Böse S (2006) Calcium phosphate-based resorbable ceramics: influence of MgO, ZnO, and SiO 2 dopants. J Am Ceram Soc 89:2675–2688

Best SM, Porter AE, Thian ES, Huang J (2008) Bioceramics: Past, present and for the future. *J. Eur. Ceram. Soc* 28:1319–1327

Boanini E, Gazzano M, Bigi A (2010) Ionic substitutions in calcium phosphates synthesized at low temperature. Acta Biomater 6:1882–1894

Boraiah S, Paul O, Hawkes D, Wickham M, Lorich DG (2009) Complications of recombinant human BMP-2 for treating complex tibial plateau fractures: a preliminary report. Clin Orthop Relat Res 467:3257–3262

Bose S, Fielding G, Tarafder S, Bandyopadhyay A (2013) Understanding of dopant-induced osteogenesis and angiogenesis in calcium phosphate ceramics. Trends Biotechnol 31:594–605

Chandran S, Suresh Babu S, Hari Krishnan VS, Varma HK, John A (2016) Osteogenic efficacy of strontium hydroxyapatite micro-granules in osteoporotic rat model. J Biomater Appl 31:499–509

Chen G, Ushida T, Tateishi T (2001) Development of biodegradable porous scaffolds for tissue engineering. Mater Sci Eng C 17(1–2):63–69

Chen, G., Ushida, T., Tetsuya, T. Scaffold Design for Tissue Engineering. (2002)

Cooke JP (2002) Nitric Oxide and Angiogenesis. *Circulation* 105:2133–2135

Dasgupta S, Banerjee SS, Bandyopadhyay A, Bose S (2010) Zn- and Mg-doped hydroxyapatite nanoparticles for controlled release of protein. Langmuir 26:4958–4964

David M et al (2013) Physico-chemical characterization and in vitro biological evaluation of pure SiHA for bone tissue engineering application. 530:351–356

El-amin SF et al (2003) Extracellular matrix production by human osteoblasts cultured on biodegradable polymers applicable for tissue engineering. 24:1213–1221

Fernandez de Grado G, Keller L, Idoux-Gillet Y, Wagner Q, Musset AM, Benkirane-Jessel N, Bornert F, Offner D (2018) Bone substitutes: a review of their characteristics, clinical use, and perspectives for large bone defects management. *J. Tissue Eng.* 9. https://doi.org/10.1177/2041731418776819

Gibson IR, Bonfield W (2002) Novel synthesis and characterization of an AB-type carbonate-substituted hydroxyapatite. J Biomed Mater Res 59:697–708

Grellier M, Bordenave L, Amédée J (2009) Cell-to-cell communication between osteogenic and endothelial lineages: implications for tissue engineering. Trends Biotechnol 27:562–571

Hankenson KD, Dishowitz M, Gray C, Schenker M (2011) Angiogenesis in bone regeneration. Injury 42:556–561

Holtorf HL, Sikavitsas VI, Jansen JA (2005) Effect of bone extracellular matrix synthesized in vitro on the osteoblastic differentiation of marrow stromal cells. 26:971–977

Hutmacher DW (2000) Scaffolds in tissue engineering bone and cartilage. Biomaterials 21:2529–2543

Hutmacher DW, Sittinger M, Risbud MV (2004) Scaffold-based tissue engineering: rationale for computer added design and solid free-form fabrication systems. 2

Jones GL et al (2010) Primary human osteoblast culture on 3D porous collagen-hydroxyapatite scaffolds:1244–1250. https://doi.org/10.1002/jbm.a.32805

Kim KS, Rajagopal V, Gonsalves C, Johnson C, Kalra VK (2006a) A novel role of hypoxia-inducible factor in cobalt chloride- and hypoxia-mediated expression of IL-8 chemokine in human endothelial cells. J Immunol 177:7211–7224

Kim S-S, Park MS, Jeon O, Choi CY, Kim BS (2006b) Poly(lactide-co-glycolide)/hydroxyapatite composite scaffolds for bone tissue engineering. Scanning 27:1399–1409

Kim TG, Park S-H, Chung HJ, Yang D-Y, Park TG (2010) Microstructured scaffold coated with hydroxyapatite/collagen nanocomposite multilayer for enhanced osteogenic induction of human mesenchymal stem cells. J Mater Chem 20:8927

Kini U, Nandeesh BN (2012) Radionuclide and hybrid bone imaging. Radionucl Hybrid Bone Imaging 9783642024**,** 1–1046

Kohli N et al (2018) Bone remodelling in vitro : Where are we headed ? -A review on the current understanding of physiological bone remodelling and in fl ammation and the strategies for testing biomaterials in vitro. 110**,** 38–46

Landi E, Celotti G, Logroscino G, Tampieri A (2003) Carbonated hydroxyapatite as bone substitute. J Eur Ceram Soc 23:2931–2937

Landi E, Uggeri J, Sprio S, Tampieri A, Guizzardi S (2010) Human osteoblast behavior on as-synthesized SiO(4) and B-CO(3) co-substituted apatite. J Biomed Mater Res A 94:59–70
LeGeros RZ, Trautz OR, Klein E, LeGeros JP (1969) Two types of carbonate substitution in the apatite structure. Experientia 25:5–7
Leong KF, Cheah CM, Chua CK (2003) Solid freeform fabrication of three-dimensional scaffolds for engineering replacement tissues and organs. Biomaterials 24:2363–2378
Li J et al (2010) A one-step method to fabricate PLLA scaffolds with deposition of bioactive hydroxyapatite and collagen using ice-based microporogens. Acta Biomater 6:2013–2019
Luca L, Rougemont AL, Walpoth BH, Gurny R, Jordan O (2010) The effects of carrier nature and pH on rhBMP-2-induced ectopic bone formation. J Control Release 147:38–44
Maier JAM, Bernardini D, Rayssiguier Y, Mazur A (2004) High concentrations of magnesium modulate vascular endothelial cell behaviour in vitro. Biochim Biophys Acta Mol basis Dis 1689:6–12
Malhotra A, Habibovic P (2016) Calcium phosphates and angiogenesis: implications and advances for bone regeneration. Trends Biotechnol 34:983–992
Merry JC, Gibson IR, Best SM, Bonfield W (1998) Synthesis and characterization of carbonate hydroxyapatite. J Mater Sci Mater Med 9:779–783
Mikos AG, Temenoff JS (2000) Formation of highly porous biodegradable scaffolds for tissue engineering 3:1995–2000
Muhammad H, Khairuddin NA, Zakaria AR, NNN Y, Wan Mustafa WM (2012) Facial fractures presenting to a tertiary referral centre in Malaysia: A 9-year study. *Malays. Dent. J.* 34:10–15
Murugan R, Ramakrishna S (2006) Production of ultra-fine bioresorbable carbonated hydroxyapatite. Acta Biomater. 2:201–206
Oh S, Oh N, Appleford M, Ong JL (2006) Bioceramics for tissue engineering applications – a review. Am J Biochem Biotechnol 2:49–56
Pacary E et al (2006) Synergistic effects of CoCl(2) and ROCK inhibition on mesenchymal stem cell differentiation into neuron-like cells. J Cell Sci 119:2667–2678
Pelham RJ, Wang YL (1998) Cell locomotion and focal adhesion are regulated by substrate flexibility. Proceeding National Academy of Sciences USA, 94:13661–13665
Portal-Núñez S, Lozano D, Esbrit P (2012) Role of angiogenesis on bone formation. Histol Histopathol 27:559–566
Rezwan K, Chen QZ, Blaker JJ, Roberto A (2006) Biodegradable and bioactive porous polymer / inorganic composite scaffolds for bone tissue engineering. 27:3413–3431
Salgado J, Coutinho OP, Reis RL (2004) Bone tissue engineering: state of the art and future trends. Macromol Biosci 4(8):743–765
Shepherd JH, Shepherd DV, Best SM (2012) Substituted hydroxyapatites for bone repair:2335–2347. https://doi.org/10.1007/s10856-012-4598-2
Simonsen LO, Harbak H, Bennekou P (2012) Cobalt metabolism and toxicology-a brief update. Sci Total Environ 432:210–215
Sprio S et al (2008) Physico-chemical properties and solubility behaviour of multi-substituted hydroxyapatite powders containing silicon. 28:179–187
Stevens MM (2008a) Biomaterials for bone materials tissue engineering. Mater Today 11:18–25
Stevens MM (2008b) Biomaterials for bone Materials that enhance bone regeneration have a wealth of potential. 11:18–25
Tadic D, Peters F, Epple M (2002) Continuous synthesis of amorphous carbonated apatites. 23:2553–2559
Viguet-Carrin S, Garnero P, Delmas PD (2006) The role of collagen in bone strength. Osteoporos Int 17:319–336
Wahl DA, Czernuszka JT (2006) Collagen-Hydroxyapatite composites for hard tissue repair. 11:43–56
Wang HB et al (2000) Substrate flexibility regulates growth and apoptosis of normal but not transformed cells. Am J Physiol Cell Physiol 279:C1345–C1350

Yu B et al (2012) Effect of calcium source on structure and properties of sol − gel derived bioactive glasses.
Zhang J et al (2005) Natural polyelectrolyte films based on layer-by layer deposition of collagen and hyaluronic acid. Biomaterials 26:3353–3361
Zhao MY, Li LH, Li B, Zhou CR (2014) LBL coating of type I collagen and hyaluronic acid on aminolyzed PLLA to enhance the cell-material interaction. 8:322–335
Zhou WY, Wang M, Cheung WL, Guo BC, Jia DM (2008) Synthesis of carbonated hydroxyapatite nanospheres through nanoemulsion. J Mater Sci Mater Med 19:103–110

Chapter 15
Polymer-Based Composite in Biomedical Applications

Rabiatul Basria S. M. N. Mydin, Ku Nur Izzati Ku Mohamad Faudzi, Nor Hazliana Harun, Wan Nuramiera Faznie Wan Eddis Effendy, Nur Afiqah Amalina Romli, and Amirah Mohd Gazzali

15.1 Introduction

Polymer-based composites with significant features and properties have attracted researchers worldwide owing to their numerous opportunities in processing, fabrication, design, properties and bio application that can lead to the development of high performance and biocompatible materials. The discovery of advanced polymer-based composite plays a key role in the development of nanocomposites for biomedical applications. This chapter will briefly describe information about four main applications of polymer based nanocomposite in biomedical science field; healthcare-associated infection (HAIs), drug delivery, medical implants and biomedical applications.

Rabiatul Basria S. M. N. Mydin (✉)
Oncological and Radiological Sciences Cluster, Advanced Medical & Dental Institute, Universiti Sains Malaysia, Bertam, Kepala Batas, Pulau Pinanag, Malaysia

Department of Biological Sciences, NUS Environmental Research Institute, National University of Singapore, Singapore, Republic of Singapore
e-mail: rabiatulbasria@usm.my

N. H. Harun · Wan Nuramiera Faznie Wan Eddis Effendy · N. A. A. Romli
Oncological and Radiological Sciences Cluster, Advanced Medical and Dental Institute, Universiti Sains Malaysia, Kepala Batas, Pulau Pinang, Malaysia

Ku Nur Izzati Ku Mohamad Faudzi
Oncological and Radiological Sciences Cluster, Advanced Medical and Dental Institute, Universiti Sains Malaysia, Kepala Batas, Pulau Pinang, Malaysia

School of Materials & Mineral Resources Engineering, Universiti Sains Malaysia, Engineering Campus, Nibong Tebal, Pulau Pinang, Malaysia

A. M. Gazzali
School of Pharmaceutical Sciences, Universiti Sains Malaysia, Gelugor, Pulau Pinang, Malaysia

S. Siddiquee et al. (eds.), *Composite Materials: Applications in Engineering, Biomedicine and Food Science*, https://doi.org/10.1007/978-3-030-45489-0_15

15.2 Healthcare-Associated Infection (HAIs)

Since few decades ago, the healthcare systems confronted spreading of pathogens that associated with healthcare-associated infections (HAIs) risk. This type of infection lead to public health challenge as endanger patient's safety, extend length of hospital stay, increase treatment costs and high mortality and morbidity rates (Olar et al. 2010; Apisarnthanarak et al. 2017). It can be acquired in two possible ways commonly by a patient itself and also can be acquired from healthcare workers in a healthcare facility in which develop after 48 hours of admissions (WHO 2011; Ducel et al. 2002). Based on the survey done by Ling et al. (2015), they had estimated about 25% of hospitalized HAIs patients and have been 2–20 times HAIs risk's infections higher than in developed countries among Asian-Pacific countries.

HAIs can be specifically classified into four main types of infections includes central line-associated bloodstream infections (CLABSIs), catheter-associated UTIs (CAUTI), ventilator-associated pneumonia (VAP) and surgical sites infections (SSIs) (Haque et al. 2018). There are wide range of microorganisms can be as causative organisms for HAIs (Table 15.1). This table summarized groups of microorganisms responsible for each type of HAIs.

To date, various types of preventive actions had been outlined by government to overcome HAIs risks (WHO 2002; Fernando et al. 2017). Prevention of HAIs is the responsibility of all individuals includes patients itself, visitors and healthcare staffs which providing the services. Hospital environmental cleaning, disinfection and sterilization are the key components in controlling the transmission of HAIs pathogen to patients. Implementation of proper hand hygiene and proper personal protective equipment (PPE) also been fully optimized in every healthcare setting. However, the weakness lies in the consistency which is not easier to achieve the fully success of the series of measures (Li and Webster 2018). For instance, a dramatic increase in the emergence of antibiotic resistant bacterial strains had urged researchers to find alternative solution to reduce HAI's risks at a faster pace (Li and Webster 2018).

15.3 Antimicrobial Polymer Composites with Metal-Oxide Nanoparticles

In the past decade, metal oxide nanoparticle (MNPs) had been considered as an outstanding antibacterial agent material. Two important elements; metal and oxygen were combined together with nanoparticles to form MNPs. Recently, MNPs played a significant role in the novel as antibacterial agents. Synthesized MNPs had been identified to have capability in inactivated and killing wide variety of microorganisms includes gram-positive, gram-negative and fungi (See in Table 15.2) (Kadiyala et al. 2018; Wang et al. 2017). In addition, polymer also showed antibacterial properties and have been reviewed in several publications (Alvarez-Paino et al. 2017; Huang et al. 2016; Santos et al. 2016). It has a great advantage as it exhibit

Table 15.1 Causative microorganisms responsible for HAIs

Group of pathogens	List of pathogens	Types of HAIs	Reference
Gram-positive	*Staphylococcus aureus*	CLABSI,SSI, VAP	Haddadin and Regunath (2017); Li et al. (2017); Alexiou et al. (2017); Adwan et al. (2016); Chi et al. (2012)
	Coagulase-negative staphylococci	CLABSI, SSI	Haddadin and Regunath (2017); Li et al. (2017); See et al. (2016); Alexiou et al. (2017)
	Enterococci (Enterococcus faecium)	CLABSI, CAUTI, SSI	Haddadin and Regunath (2017); Li et al. (2017); Nicolle (2014); Alexiou et al. (2017)
Gram-negative	*Klebsiella pneumoniae*	CLABSI, CAUTI, SSI, VAP	Haddadin and Regunath. (2017); Li et al. (2017); Nicolle (2014); Adwan et al. (2016); Chi et al. (2012)
	Enterobacter	CLABSI, SSI	Haddadin and Regunath (2017); Li et al. (2017); Adwan et al. (2016)
	Pseudomonas aeruginosa	CLABSI, CAUTI, VAP	Haddadin and Regunath (2017); Li et al. (2017); Cole et al. (2014); Adwan et al. (2016); Chi et al. (2012)
	Escherichia coli	CLABSI, CAUTI, SSI	Haddadin and Regunath (2017); Li et al. (2017); Nicolle (2014); Cortese et al. (2018); Alexiou et al. (2017); Adwan et al. (2016)
	Acinetobacter baumanii	CLABSI, VAP	Haddadin and Regunath (2017); Li et al. (2017); Chi et al. (2012)
	Proteus mirabilis	CLABSI, CAUTI, SSI	Haddadin and Regunath (2017); Li et al. (2017); Nicolle (2014); Cortese et al. (2018); Adwan et al. (2016)
	Serratia marcescens	CLABSI, VAP	Haddadin and Regunath (2017); Li et al. (2017); Chi et al. (2012)
	Stenotrophomonas maltophilia	VAP	Chi et al. (2012)
	Citrobacter spp.	CLABSI, SSI	Haddadin and Regunath (2017); Li et al. (2017); Adwan et al. (2016)
	Achromobacter spp.	CLABSI	Haddadin and Regunath. (2017); Li et al. (2017)

(continued)

Table 15.1 (continued)

Group of pathogens	List of pathogens	Types of HAIs	Reference
	Stenotrophomonas maltophilia	CLABSI	Haddadin and Regunath (2017); Li et al. (2017)
Fungi	*Candida species (Candida albicans, Candida glabrata, Candida krusei, Candida parapsilosis, Candida tropicalis)*	CLABSI, CAUTI, SSI	Haddadin and Regunath (2017); Li et al. (2017); Nicolle (2014);

long-term antibacterial activity as compared with antibiotics, nonvolatile, stable, less toxic and most importantly does not permeate into skin of living organisms (Alvarez-Paino et al. 2017). Both polymers and MNPs had highly desirable characteristics such as have a high surface area-to-volume ratio, stiff, tough, high resistance to corrosion, lack of conductivity and less expensive make it suitable to be applied in biomedical fields. MNPs fillers are known as excellent candidate to be embed into polymers owning their ability to generate reactive oxygen species (ROS), metallic ions and electrostatic close interaction that could alter or destroy the bacterial cell membrane by itself, thus lead to the cell death (Raghunath and Perumal 2017).

15.4 Diverse Polymer-Based Composite for Medical Devices

Across the medical industry, various biomedical implants and devices have been explored and continuously invented for diverse used in human body by towards achieving the main goal which able to improve the quality and preventing of human lives (Teo et al. 2016). The placement and positions of this implants and devices in human body has a different set of criteria in terms of functionality, design and materials use which needs to be fulfil before approved by U.S. Food and Drug Administration (FDA). FDA stated that a medical device is "an instrument, apparatus, implement, machine, contrivance, implant, in vitro reagent or other similar or related article which is used in the diagnosis, cure, mitigation, treatment or prevention of a disease, or intended to affect the structure of any function of the body which does not achieve its primary intended purpose through chemical action within or on the body" (U.S. Food and Drug Administration 2018). On forward, these applications are expected to growth in demand due to its stabilizing capabilities within the biological environment and improving functionality of human body system.

Advanced polymeric biomaterial with nanocomposite may contribute to the successful of medical implants operation in the various aspects such as in medical disposable materials, prosthetic materials, dental materials, implants, dressings, polymeric drug delivery systems, tissue engineering products, metal and ceramics substituent (Rebelo et al. 2017). Figure 15.1 demonstrate the potential of advanced

Table 15.2 Antimicrobial polymer composites with metal oxides nanoparticles

Polymer	MNPs	Synthesis/Method	Target	Types of polymer	Findings	Reference
Polyethylene glycol (PEG)	Zinc oxide NPs	Sol-gel	*Staphylococcus aureus, Escherichia coli*	Synthetic	A shorter reaction time of PEG capped ZnO NPs have a higher antibacterial activity. Discrete antibacterial mechanisms via the generation of ROS and hydrogen peroxide (H_2O_2) from ZnO NPs	Meshram et al. (2018)
	Silver NPs	Aqueous solutions	*Staphylococcus aureus* (ATCC 2592), *Escherichia coli* (ATCC 25922), *Candida albican* (ATCC 10261)	Synthetic	Addition of Ag NPs loaded on PEG layer plays a vital role of the antibacterial properties	Zomorodian et al. (2018)
	Copper oxide NPs	Chemical precipitation	*Staphylococcus aureus* (NCIM 2901), *Bacillus subtilis* (NCIM 2063), *Proteus vulgaris* (NCIM 2027), *Escherichia coli* (NCIM 2256), *Vibrio cholarae* (ATCC 14033)	Synthetic	CuO:PEG showed lower MIC concentration. Generation of ROS via deposition of CuO NPs on the surface of bacteria were purpose responsible for antibacterial activity	Hemalatha and Akilandeswari, (2016).
Polyaniline (PANI)	Zinc oxide NPs	Chemical oxidative polymerization	*Staphylococcus aureus, Escherichia coli*	Synthetic	Antibacterial activity solely depends on the concentration of ZnO NPs capped with PANI which inhibit the growth of bacteria due to photocatalytic efficiencies	Mohsen et al. (2019)

(continued)

Table 15.2 (continued)

Polymer	MNPs	Synthesis/Method	Target	Types of polymer	Findings	Reference
Ecoflex	Zinc oxide NPs		*Staphylococcus aureus* (ATCC 25923), *Escherichia coli* (ATCC 25922)	Semi-synthetic	The lesser inhibition average halo values for the *E. coli* (0.67 cm) as compared with *S.aureus* (1.13 cm) due to difference in structure membrane after be treated with ZnO NPs. Polymer ZnO NPs (1%) did showed great reduction (0.5% of survived *S.aureus* colonies) after be treated for 24 hours	Capelezzo et al. (2018)
Linear low-density polyethylene (LLDPE)	Titanium oxide NPs, zinc oxide NPs	Sol-gel	*Staphylococcus aureus* (ATCC 25923), *Escherichia coli* (ATCC 25922)	Synthetic	LLDPE nanocomposites with higher ratio of ZnO NPs did showed remarkable efficacy against both pathogens. Two primary mechanisms played a significant role for bacteriostatic effect; generation of ROS and release off zinc ions	Saharuddin et al. (2018)
	Cuprous oxide NPs	Co-extrusion, thermal adhesion, and attachment with ethyl cyanoacrylate, trimethoxyvinylsilane, and epoxy resin. The	*Staphylococcus aureus* (ATCC 25923), *Escherichia coli* (ATCC 10798)	Synthetic	Composite demonstrated the highest of antibacterial activity against both pathogens through thermal adhesion to the polymer with zero copper leaching. The bactericidal activity was purpose due to direct contact with polymer surface	Gurianov et al. (2019)

Polymer	MNPs	Synthesis/Method	Target	Types of polymer	Findings	Reference
Chitosan	Iron oxide NPs	Coprecipitation and surface coating	*Escherichia coli, Bacillus subtilis, Candida albicans, Aspergillus Niger, Fusarium solani*	Natural	Fe3O4 showed a diameter of inhibition (14.0 mm) against both *E. coli* and *B. subtilis*	Nehra et al. (2018)
Cellulose	Silver NPs, titanium dioxide NPs	Sol-gel	*Escherichia coli*	Natural	The incorporation of Ag with TiO_2/cellulose composite films did enhance antibacterial performance under UV condition. Under UV irradiation, the generation ROS from TiO_2 nanocrystals and co-doping of Ag promoted the antibacterial activity. In addition, direct transfer from the chemisorbed silver ions in composite films onto bacterial surface also increase bactericidal effect	Li et al. (2018)

polymeric biomaterial with nanocomposite applications in the medical aspects. These polymeric implants mimic to biological tissue which preferable to stay in the body to serve their function and responsibility thus, they faded without the need of a second surgical intervention (Maitz 2015). In this chapter we are focusing on biopolymers which are commonly used in medical fields for biomedical applications.

15.5 General Guidelines for Polymeric Biomaterial

The polymeric biomaterial for implant or medical device must be followed in order to avoid any undesirable experience of side effect in the human body or severe complication lead to death (Table 15.3).

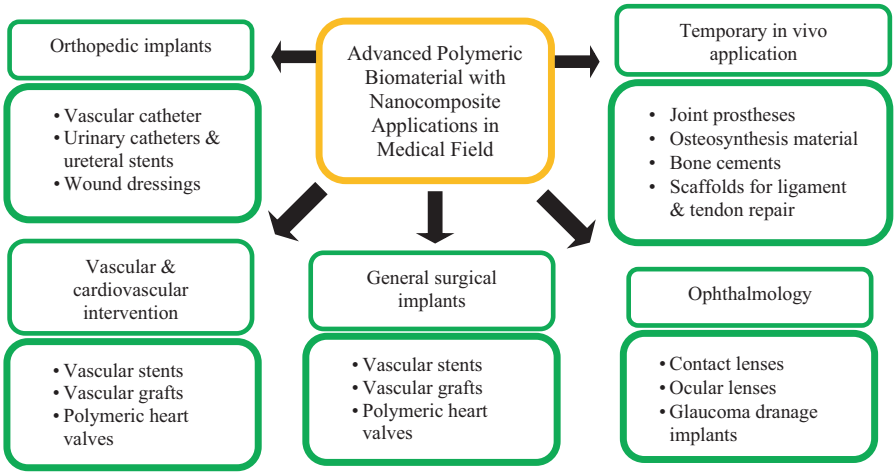

Fig. 15.1 Potential applications of synthetic polymers in clinical applications

Table 15.3 Criteria for polymeric biomaterials as implants

Properties	Description
Compatibility	Non-carcinogenesis, non-pyrogenicity, non-toxicity, non-allergic
Sterilizability	Autoclave, dry heating, ethylene oxide gas, and radiation
Physical properties	Strength, elasticity,and durability
Manufacturability	Machining, molding, extruding, and fiber forming

15.6 General Types of Synthetic Polymers in Medical Implants Applications

On the medical line, biodegradable polymeric biomaterials also have been widely used for drug delivery and tissue engineering applications especially for dental or craniofacial implantation. Besides biocompatibility, the critical aspects in these applications are to prevent any immunologic response and modulates rate of biodegradation (Tamariz and Rios-Ramrez 2013). Importantly, the diversity of polymeric biomaterials must meet the specific biodegradable characteristics in order to regulate drug release, to develop resorbable devices and to enhance cell integration. Table 15.4 illustrate the utilization of biodegradable polymers in medical implants which make body to accept these materials as non-foreign substances (no rejection) in the biological system.

15.7 Polymer for Drug Delivery

Drug delivery is defined as a method or process to safely administer a pharmaceutical active compound into the body, in order to achieve the desired therapeutic effects (Tiwari et al. 2012). This concept was first described by Paul Ehrilich in the early twentieth century, who proposed the 'magic bullet' theory, in which defined as 'compounds which would have specific attraction to disease-causing microorganism by seeking them out and destroying them whilst avoiding other organisms and having minimal undesired/harmful effects on the patient' (Josefsen and Boyle 2012).This theory was further expanded through extensive research works which gave rise to the different drug delivery materials and methods available today.

Drug delivery system starts from administration of drug into the body until excretion of drug from the body. The presence of side effects after administration of drug can caused from the direct interaction of drug like inflammation and swelling or after effect of the drug such as nausea, headaches, heart burn and faint (Babu et al. 2017; NIBIB 2016). Administration of drug through swallowing mostly caused damage of the drug by immunology reaction against foreign substances. Most effective route of administration of the treatment is intravenous in which the medicine will directly achieve the blood vessel thus will not be eliminated or destroy by immune system. One of the interventions to overcome hurdle in drug delivery is by adding polymer to applied drug (Liechty et al. 2012).

Polymer uses in drug delivery had attract attention due to bioactive properties in which other than to improve drug administration, the polymer also has antimicrobial, able to promote adhesion of the cell and biodegradable (Sallem et al. 2017). Synthetic and natural type of polymer is exhibited variety in the function regarding mechanical properties, biocompatibility and shape. Generally, the natural polymer has better compatibility in cellular level compare to synthetic however synthetic ones has better mechanical strength for medical devices design (Boni et al. 2018).

Table 15.4 Applications of polymers as implants (Teo et al. 2016)

Synthetic Polymer	Application	Field
Polyethylene Polytetrafluoroethylene Polyamide	Epidural catheters	Anesthesiology
Polypropylene Polyethylene Polytetrafluoroethylene Polyamide Polyethyleneterephthalate Polydimethylsiloxane Polyhydroxyalkanoates	Pacemaker Implantable cardioverter/defobrillaotr Left ventricular assist device Mechanical heart valves Artificial blood vessels Catheters	Cardiovascular
Polymethylmethacrylate	Dentures Dental implants	Dental
Polypropylene Polyethyleneterephthalate Polytetrafluoroethylene Silicone Polydimethylsiloxane	Synthetic blood vessels Breast implants Cheek, jaw and chin implants Lip implant Titanium surgical implants Hip implant	General and plastic surgery
Polyethylene Polytetrafluoroethylene Polyamide	Central venous access device Peripherally inserted central catheter	Hematology and pathology
Silicone Polyurethane Polypropylene	Intrauterine Device (IUD) Intravaginal rings Etonogestrel-releasing contraceptive implant Urogynecologic surgical mesh implants Fetal micro-pacemaker	Obstetric and gynecologic
Polymethylmetacrylate Polyethylene Polytetrafluoroethylene Polyamide	Dexamethasone Intravitreal implant Retinal prosthesis Artificial intraocular lens Glaucoma valve Fluocinolone Opthalmic Implnt Orbital implant Catheters	Ophthalmic
Polyethylene Polyether ether ketone Polyhydroxyalkanoates	Orthopaedic implants	Orthopaedic

Uses of polymer in drug delivery is to control the drug release from the substrate by interaction of hydrophobic and hydrophilic material such as acrylic polymer (Liechty et al. 2012; Babu et al. 2017) Research by Aw et al. (2011); Werengowska-Ciećwierz et al. (2014) and Wang et al. (2017) on drug delivery with polymer coating showed that presence of polymer can prolong the release of drug hence suitable for long term treatment without repeated administration (Min et al. 2019; Wang et al. 2017). Drug delivery had been widely studied due to rejection of drug, accumulation of the drug in plasma and side effect of high concentration of the drug delivered especially to the neighboring cell (Babu et al. 2017).

Chitosan, PLGA, hyaluronic acid, calcium phosphate and hydroxyapatite (HA) are the most frequently studied biopolymer in drug release due to high biocompatibility at cellular stage (Min et al. 2019; Mohan et al. 2016; Misra 2014; Liechty et al. 2012). Most importantly, these polymers also exhibited other characteristic hemocompatibility, excellent biodegradability and ability to response to the changes of the body system due to pH, temperature and presence ultrasonic wave which are helpful in ensuring the effectiveness of the treatment (Bi et al. 2017). In addition, these polymers could also accommodate various drugs such as chemotherapeutic drug; paclitaxel (Babu et al. 2017), antibiotics; amoxicillin and ciprofloxacin (Venkatasubbu et al. 2018) and protein; bone morphogenetic protein-2 (Min et al. 2019) without causing any damage or changing the drug. Table 15.5 below listed the characteristic, and the recent findings for each of the aforementioned polymer in drug delivery.

15.8 Polymer-Based Composite in Biomedical Field

Significant interest towards polymer matrix based nanocomposites has aroused and attracted wide attention due to their excellent potential in diverse areas especially in biomedical applications like diagnostic magnetic resonance imaging (MRI), thermal therapy, artificial blood vessels, biosensors, cancer therapy, antimicrobial agents, wound dressing and drug delivery (Boccaccini et al. 2010; Sarkar et al. 2012). Numerous opportunities in processing, fabrication, design, properties and bio application can lead to the development of high performance and biocompatible materials. The modification and combination of both polymer nanocomposites can produce desirable and enhance properties of the materials. Despite the benefits of polymer nanocomposites such as low cost, ease manufacturing, superior mechanical properties, structural and thermal stabilities, good electrical conductivity and corrosion resistance, polymer nanocomposites also has some limitations including inadequate stability, non-uniform distribution, high viscosity and formation agglomeration (Tanahashi 2010; Puggal et al. 2016; Zare and Shabani 2016; Müller et al. 2017; Zagho et al. 2018; 'Fundamentals of Nanomaterials and Polymer Nanocomposites 2019; Huang et al. 2019). Ongoing research studies have done to investigate, synthesize and analyse their properties to maximize the potential for future used. Varieties of polymer nanoparticles in biomedical fields are summarized in Table 15.6.

15.9 Summary and Future Advancement

This book chapter discussed potential of Polymer-based Composite in healthcare setting, drug delivery, medical devices and other biomedical field. Development polymer-based composite have been extensively used for biomedical applications

Table 15.5 Common use polymer in drug delivery with special characteristics and current stages of the polymer

Polymer	Special characteristic/s	Important research finding	Reference
Chitosan	Natural polymer from shellfish and *crustacean*. Biodegradable, non-cytotoxic, exhibits antifungal, antitumor and antibacterial properties. Can be tailored for certain function and shape such as beads, membranes, gel, scaffold and sponges	(i) Chitosan hydrogel had been recognized to exhibit cell adhesion and promote cell survival besides promoting neurite outgrowth in neural tissue engineering. (ii) Chitosan has shown a good potential in regenerative medicine for central nervous system and peripheral nervous system. (iii) *In vitro* study of chitosan with other polymers such as PVA, PCL and PLGA showed successful proliferation of the studied cell line	Min et al. (2019); Boni et al. (2018)
Poly lactic co-glycolic acid (PLGA)	Has tunable mechanical properties, biodegradable and also has a variable dissolution time	(i) Most common polymer used in drug delivery applications study. (ii) FDA approves the use of PLGA in drug formulation and medical devices	Srivastava et al. (2015); Misra (2014)
Hyaluronic acid (HA)	Exhibit mucoadhesive ability. It does not stimulate immunology response. Has ability to identify overexpression of receptors on tumor cells	(i) *In vitro* study of HA showed the ability of this polymer to control the release of a model drug (α- chymotrypsin) up to 28 days. (ii) Another study showed the erythropoietin (EPO), was slowly released into the blood in the duration of one week	Huang and Huang (2018); Vimalson et al. (2016)
Calcium phosphate (CaP)	Promote better bone osseointegration by interacting with rhbFGF and rhIGF-1	The study is still under investigation and has partly conventional opinion	Meng et al. (2016)
Hydroxyapatite	Has ability to circulate in wet environment Has antibacterial characteristic by damaging the cell membrane of the bacteria	(i) Long term prognosis is still controversial. Not susceptible to degradation or dissolution under long term loading	Pan et al. (2018)

due to its great characteristics which award an excellent impact in various medical employment. Interfacing between bio-based polymers and composite especially nanocomposite have shown better performance and achievement in various field. The future outcomes for bio-based polymers in biomedical industry are expected to receive wide attention as it becomes global emphasis in healthcare industry. Up

Table 15.6 Summary applications of polymer nanoparticles in biomedical fields

Applications	Types of Polymer	Types of composite	References
Drug delivery	Polycaprolactone (PCL)	Hydroxyapatite	Kim et al. (2004)
	Chitosan	Graphene oxide	Rana et al. (2011)
	Chitosan	Rectorite	Wang et al. (2007)
	Poly(N-isopropylacrylamide)	Graphene	Pan et al. (2011)
	Chitosan	Calcium phosphate	Zhang and Zhang (2002)
	Chitosan	Graphene oxide	Bao et al. (2011)
Artificial blood vessels	Poly(ethylene terephthalate)	Hydroxyapatite	Furuzono et al. (2006)
	Polyurethane	Gelatin	Detta et al. (2010)
	Polycaprolactone	Gelatin	Jiang et al. (2017)
Biosensors	Polytetrafluoroethylene (PTFE) / Teflon	Carbon nanotube	Wang and Musameh (2003)
	Nafion	Silicate	Kim and Lee (2003)
	Polyaniline	Carbon nanotube tin oxide	Dhand et al. (2008)
Cancer therapy	Polylactic acid or polylactide (PLA)	Magnetite (Fe_3O_4)	Hu et al. (2006)
	Polyaniline	Magnetite (Fe_3O_4)	Zhao et al. (2006)
	Collagen	Gold	Xing et al. (2016)
Magnetic resonance imaging (MRI)	Chitosan	Iron oxide	Yuk et al. (2011)
	Poly (lactide-co-glycolide)	Cellulose	Nkansah et al. (2011)
	Polyethylenimine	Iron oxide	Masotti et al. (2009)
Antimicrobial agents	Polypropylene	Silver composites	Radheshkumar and Münstedt (2006)
	Polypropylene	Copper metal or copper oxide nanoparticles	Delgado et al. (2011)
Wound dressing	Polyester	Cellulose	Liu et al. (2012)
	Chitosan	Zinc oxide	Sudheesh Kumar et al. (2012)
	Chitin	Nanosilver composite	Madhumathi et al. (2010)
Thermal therapy	Polyethylene glycol	Iron oxide	Wydra et al. (2013)
	Epoxy	Graphite	Yu et al. (2007)

until now, researches on natural and synthetic polymers are still on going in order to invent advance functionality for medical usage. Ultimately, research advances in the past few decades have led researchers to break through the challenges in biomedical field.

Acknowledgement The authors would like to acknowledge the Ministry of Education (MOE) Malaysia for funding this work under Transdisciplinary Research Grant Scheme (TRGS) grant no. 6769003 and Research in Undergraduate Institutions (RUI) grant 2019/2020.

References

Adwan G, Abu Hasan N, Sabra I, Sabra D, Al-butmah S, Odeh S et al (2016) Detection of bacterial pathogens in surgical site infections and their antibiotic sensitivity profile. Int J Med Res Health Sci 5(5):75–82. https://doi.org/10.1007/s12663-013-0575-7

Alexiou K, Drikos I, Terzopoulou M, Sikalias N, Ioannidis A, Economou N (2017) A prospective randomised trial of isolated pathogens of surgical site infections (SSI). Annals of medicine and surgery 21:25–29. https://doi.org/10.1016/j.amsu.2017.07.045

Álvarez-Paino M, Muñoz-Bonilla A, Fernández-García M (2017) Antimicrobial polymers in the nano-world. Nano 7(2):48. https://doi.org/10.3390/nano7020048

Aw MS, Gulati K, Losic D (2011) Controlling drug release from titania nanotube arrays using polymer nanocarriers and biopolymer coating. J Biomater Nanobiotechnol 2(05):477. https://doi.org/10.4236/jbnb.2011.225058

Babu A, Amreddy N, Muralidharan R, Pathuri G, Gali H, Chen A, Zhao YD, Munshi A, Ramesh R (2017) Chemodrug delivery using integrin-targeted PLGA-chitosan nanoparticle for lung cancer therapy. Sci Rep 7(1):14674. https://doi.org/10.1038/s41598-017-15012-5

Bao H, Pan Y, Ping Y, Sahoo NG, Wu T, Li L, Li J, Gan LH (2011) Chitosan-functionalized graphene oxide as a nanocarrier for drug and gene delivery. Small 7(11):1569–1578. https://doi.org/10.1002/smll.201100191

Bi S, Bao Z, Bai X, Hu S, Cheng X, Chen X (2017) Tough chitosan hydrogel based on purified regeneration and alkaline solvent as biomaterials for tissue engineering applications. Int J Biol Macromol 104:224–231. https://doi.org/10.1016/j.ijbiomac.2017.06.017

Boni R, Ali A, Shavandi A, Clarkson AN (2018) Current and novel polymeric biomaterials for neural tissue engineering. J Biomed Sci 25(1):90. https://doi.org/10.1186/s12929-018-0491-8

Capelezzo AP, Mohr LC, Godoy JS, Bellei AS, Silva LL, Martins MAPM et al (2018) Addition of zinc oxide nanoparticles in biodegradable polymer and evaluation of its antimicrobial activity. In: Materials science forum, vol 930. Trans Tech Publications, pp 230–235. https://doi.org/10.4028/www.scientific.net/MSF.930.230

Chi SY, Kim TO, Park CW, Yu JY, Lee B, Lee HS et al (2012) Bacterial pathogens of ventilator associated pneumonia in a tertiary referral hospital. Tuberculosis and respiratory diseases 73(1):32–37. https://doi.org/10.4046/trd.2012.73.1.32

Cole SJ, Records AR, Orr MW, Linden SB, Lee VT (2014) Catheter-associated urinary tract infection by Pseudomonas aeruginosa is mediated by exopolysaccharide-independent biofilms. Infect Immun 82(5):2048–2058. https://doi.org/10.1128/IAI.01652-14

Cortese YJ, Wagner VE, Tierney M, Devine D, Fogarty A (2018) Review of catheter-associated urinary tract infections and in vitro urinary tract models. Journal of healthcare engineering:2018. https://doi.org/10.1155/2018/2986742

Delgado K, Quijada R, Palma R, Palza H (2011) Polypropylene with embedded copper metal or copper oxide nanoparticles as a novel plastic antimicrobial agent. Lett Appl Microbiol 53(1):50–54. https://doi.org/10.1111/j.1472-765X.2011.03069.x

Detta N, Errico C, Dinucci D, Puppi D, Clarke DA, Reilly GC, Chiellini F (2010) Novel electrospun polyurethane/gelatin composite meshes for vascular grafts. J Mater Sci Mater Med 21(5):1761–1769. https://doi.org/10.1007/s10856-010-4006-8

Dhand C, Arya SK, Datta M, Malhotra BD (2008) Polyaniline–carbon nanotube composite film for cholesterol biosensor. Anal Biochem 383(2):194–199. https://doi.org/10.1016/j.ab.2008.08.039

Ducel G, Fabry J, Nicolle L (2002) Prevention of hospital acquired infections: a practical guide. Prevention of hospital acquired infections: a practical guide., (Ed. 2). https://doi.org/10.1016/S0377-1237(04)80079-0

Fernando SA, Gray TJ, Gottlieb T (2017) Healthcare-acquired infections: prevention strategies. Intern Med J 47(12):1341–1351. https://doi.org/10.1111/imj.13642

Furuzono T, Masuda M, Okada M, Yasuda S, Kadono H, Tanaka R, Miyatake K (2006) Increase in cell adhesiveness on a poly (ethylene terephthalate) fabric by sintered hydroxyapatite nanocrystal coating in the development of an artificial blood vessel. ASAIO J 52(3):315–320. https://doi.org/10.1097/01.mat.0000214860.08820.f9

Gurianov Y, Nakonechny F, Albo Y, Nisnevitch M (2019) Antibacterial composites of cuprous oxide nanoparticles and polyethylene. Int J Mol Sci 20(2):439. https://doi.org/10.3390/ijms20020439

Haddadin Y, Regunath H (2017) Central line associated blood stream infections (CLABSI). In: In StatPearls [internet]. Publishing, StatPearls

Haque M, Sartelli M, McKimm J, Bakar MA (2018) Health care-associated infections–an overview. Infect Drug Resist 11:2321. https://doi.org/10.2147/IDR.S177247

Hemalatha T, Akilandeswari S (2016) Effect of poly ethylene glycol on CuO nanoparticles and its antibacterial application. International Letters of Chemistry, Physics and Astronomy 63:111. https://doi.org/10.18052/www.scipress.com/ILCPA.63.111

Hu FX, Neoh KG, Kang ET (2006) Synthesis and in vitro anti-cancer evaluation of tamoxifen-loaded magnetite/PLLA composite nanoparticles. Biomaterials 27(33):5725–5733. https://doi.org/10.1016/j.biomaterials.2006.07.014

Huang G, Huang H (2018) Application of hyaluronic acid as carriers in drug delivery. Drug Deliv 25(1):766–772. https://doi.org/10.1080/10717544.2018.1450910

Huang KS, Yang CH, Huang SL, Chen CY, Lu YY, Lin YS (2016) Recent advances in antimicrobial polymers: a mini-review. Int J Mol Sci 17(9):1578. https://doi.org/10.3390/ijms17091578

Huang Y, Kormakov S, He X, Gao X, Zheng X, Liu Y, Sun J, Wu D (2019) Conductive polymer composites from renewable resources: an overview of preparation, properties, and applications. Polymers 11(2):187. https://doi.org/10.3390/polym11020187

Jiang YC, Jiang L, Huang A, Wang XF, Li Q, Turng LS (2017) Electrospun polycaprolactone/gelatin composites with enhanced cell–matrix interactions as blood vessel endothelial layer scaffolds. Mater Sci Eng C 71:901–908. https://doi.org/10.1016/j.msec.2016.10.083

Josefsen LB, Boyle RW (2012) Unique diagnostic and therapeutic roles of porphyrins and phthalocyanines in photodynamic therapy, imaging and theranostics. Theranostics 2(9):916

Boccaccini AR, Erol M, Stark WJ, Mohn D, Hong Z, Mano JF (2010) Polymer/bioactive glass nanocomposites for biomedical applications: a review. Compos Sci Technol 70(13):1764–1776. https://doi.org/10.1016/j.compscitech.2010.06.002

Kadiyala U, Kotov NA, VanEpps JS (2018) Antibacterial metal oxide nanoparticles: challenges in interpreting the literature. Curr Pharm Des 24(8):896–903. https://doi.org/10.2174/1381612824666180219130659

Kim HW, Knowles JC, Kim HE (2004) Hydroxyapatite/poly (ε-caprolactone) composite coatings on hydroxyapatite porous bone scaffold for drug delivery. Biomaterials 25(7–8):1279–1287. https://doi.org/10.1016/j.biomaterials.2003.07.003

Kim MA, Lee WY (2003) Amperometric phenol biosensor based on sol–gel silicate/Nafion composite film. Anal Chim Acta 479(2):143–150. https://doi.org/10.1016/S0003-2670(02)01538-6

Li B, Webster TJ (2018) Bacteria antibiotic resistance: new challenges and opportunities for implant-associated orthopedic infections. J Orthop Res 36(1):22–32. https://doi.org/10.1002/jor.23656

Li Y, Tian J, Yang C, Hsiao B (2018) Nanocomposite film containing fibrous cellulose scaffold and Ag/TiO2 nanoparticles and its antibacterial activity. Polymers 10(10):1052. https://doi.org/10.3390/polym10101052

Liu X, Lin T, Gao Y, Xu Z, Huang C, Yao G, Jiang L, Tang Y, Wang X (2012) Antimicrobial electrospun nanofibers of cellulose acetate and polyester urethane composite for wound dressing. J Biomed Mater Res B Appl Biomater 100(6):1556–1565. https://doi.org/10.1002/jbm.b.32724

Madhumathi K, Kumar PS, Abhilash S, Sreeja V, Tamura H, Manzoor K, Nair SV, Jayakumar R (2010) Development of novel chitin/nanosilver composite scaffolds for wound dressing applications. J Mater Sci Mater Med 21(2):807–813. https://doi.org/10.1007/s10856-009-3877-z

Maitz MF (2015) Applications of synthetic polymers in clinical medicine. Biosurface and Biotribology 1(3):161–176. https://doi.org/10.1016/j.bsbt.2015.08.002

Masotti A, Pitta A, Ortaggi G, Corti M, Innocenti C, Lascialfari A, Marinone M, Marzola P, Daducci A, Sbarbati A, Micotti E (2009) Synthesis and characterization of polyethyleniminebased iron oxide composites as novel contrast agents for MRI. MAGMA 22(2):77–87. https://doi.org/10.1007/s10334-008-0147-x

Meng HW, Chien EY, Chien HH (2016) Dental implant bioactive surface modifications and their effects on osseointegration: a review. Biomarker research 4(1):24. https://doi.org/10.1186/s40364-016-0078-z

Meshram JV, Koli VB, Kumbhar SG, Borde LC, Phadatare MR, Pawar SH (2018) Structural, spectroscopic and anti-microbial inspection of PEG capped ZnO nanoparticles for biomedical applications. Materials Research Express 5(4):045016. https://doi.org/10.1088/2053-1591/aab917

Min Q, Yu X, Liu J, Wu J, Wan Y (2019) Chitosan-based hydrogels embedded with hyaluronic acid complex nanoparticles for controlled delivery of bone morphogenetic Protein-2. Pharmaceutics 11(5):214. https://doi.org/10.3390/pharmaceutics11050214

Misra, A. 2014. Applications of polymers in drug delivery. Smithers Rapra

Mohan L, Anandan C, Rajendran N (2016) Drug release characteristics of quercetin-loaded TiO2 nanotubes coated with chitosan. Int J Biol Macromol 93:1633–1638. https://doi.org/10.1016/j.ijbiomac.2016.04.034

Mohsen RM, Morsi SM, Selim MM, Ghoneim AM, El-Sherif HM (2019) Electrical, thermal, morphological, and antibacterial studies of synthesized polyaniline/zinc oxide nanocomposites. Polym Bull 76(1):1–21. https://doi.org/10.1007/s00289-018-2348-4

Müller K, Bugnicourt E, Latorre M, Jorda M, Echegoyen Sanz Y, Lagaron J, Miesbauer O, Bianchin A, Hankin S, Bölz U, Pérez G (2017) Review on the processing and properties of polymer nanocomposites and nanocoatings and their applications in the packaging, automotive and solar energy fields. Nano 7(4):74. https://doi.org/10.3390/nano7040074

Nehra P, Chauhan RP, Garg N, Verma K (2018) Antibacterial and antifungal activity of chitosan coated iron oxide nanoparticles. Br J Biomed Sci 75(1):13–18. https://doi.org/10.1080/09674845.2017.1347362

Nicolle LE (2014) Catheter associated urinary tract infections. Antimicrob Resist Infect Control 3(1):23. https://doi.org/10.1186/2047-2994-3-23

Nkansah MK, Thakral D, Shapiro EM (2011) Magnetic poly (lactide-co-glycolide) and cellulose particles for MRI-based cell tracking. Magn Reson Med 65(6):1776–1785. https://doi.org/10.1002/mrm.22765

Pan C, Zhou Z, Yu X (2018) Coatings as the useful drug delivery system for the prevention of implant-related infections. J Orthop Surg Res 13(1):220. https://doi.org/10.1186/s13018-018-0930-y

Pan Y, Bao H, Sahoo NG, Wu T, Li L (2011) Water-soluble poly (N-isopropylacrylamide) –graphene sheets synthesized via click chemistry for drug delivery. Adv Funct Mater 21(14):2754–2763. https://doi.org/10.1002/adfm.201100078

Puggal S, Dhall N, Singh N, Litt MS (2016) A review on polymer nanocomposites: synthesis, characterization and mechanical properties. Ind J Sci Technol 9:1–6. https://doi.org/10.17485/ijst/2016/v9i4/81100

Olar R, Badea M, Marinescu D, Chifiriuc CM, Bleotu C, Grecu MN, Iorgulescu EE, Bucur M, Lazar V, Finaru A (2010) Prospects for new antimicrobials based on N, N-dimethylbiguanide complexes as effective agents on both planktonic and adhered microbial strains. Eur J Med Chem:2868–2875. https://doi.org/10.1016/j.ejmech.2010.03.009

Radheshkumar C, Münstedt H (2006) Antimicrobial polymers from polypropylene/silver composites—Ag+ release measured by anode stripping voltammetry. React Funct Polym 66(7):780–788. https://doi.org/10.1016/j.reactfunctpolym.2005.11.005

Raghunath A, Perumal E (2017) Metal oxide nanoparticles as antimicrobial agents: a promise for the future. Int J Antimicrob Agents 49(2):137–152. https://doi.org/10.1016/j.ijantimicag.2016.11.011

Rana VK, Choi MC, Kong JY, Kim GY, Kim MJ, Kim SH, Mishra S, Singh RP, Ha CS (2011) Synthesis and drug-delivery behavior of chitosan-functionalized graphene oxide hybrid nanosheets. Macromol Mater Eng 296(2):131–140. https://doi.org/10.1002/mame.201000307

Saharudin K, Sreekantan S, Basiron N, Khor Y, Harun N, Mydin SMN et al (2018) Bacteriostatic activity of LLDPE Nanocomposite embedded with sol–gel synthesized TiO2/ZnO coupled oxides at various ratios. Polymers 10(8):878. https://doi.org/10.3390/polym10080878

Sallem F, Boudon J, Heintz O, Séverin I, Megriche A, Millot N (2017) Synthesis and characterization of chitosan-coated titanate nanotubes: towards a new safe nanocarrier. Dalton Trans 46(44):15386–15398. https://doi.org/10.1039/c7dt03029k

Santos M, Fonseca A, Mendonça P, Branco R, Serra A, Morais P, Coelho J (2016) Recent developments in antimicrobial polymers: a review. Materials 9(7):599. https://doi.org/10.3390/ma9070599

See I, Freifeld AG, Magill SS (2016) Causative organisms and associated antimicrobial resistance in healthcare-associated, central line–associated bloodstream infections from oncology settings, 2009–2012. Clin Infect Dis 62(10):1203–1209. https://doi.org/10.1093/cid/ciw113

Srivastava A, Yadav T, Sharma S, Nayak A, Kumari A, Mishra N (2015) Polymers in drug delivery. JBM 4:69–84. https://doi.org/10.4236/jbm.2016.41009

Sudheesh Kumar PT, Lakshmanan VK, Anilkumar TV, Ramya C, Reshmi P, Unnikrishnan AG, Nair SV, Jayakumar R (2012) Flexible and microporous chitosan hydrogel/nano ZnO composite bandages for wound dressing: in vitro and in vivo evaluation. ACS Appl Mater Interfaces 4(5):2618–2629. https://doi.org/10.1021/am300292v

Teo AJT, Mishra A, Park I, Kim YJ, Park WT, Yoon YJ (2016) Polymeric biomaterials for medical implants and devices. ACS Biomaterials Science and Engineering 2(4):454–472. https://doi.org/10.1021/acsbiomaterials.5b00429

Tiwari G, Tiwari R, Sriwastawa B, Bhati L, Pandey S, Pandey P, Bannerjee SK (2012) Drug delivery systems: An updated review. Int J Pharm Investig 2(1):2. https://doi.org/10.4103/2230-973X.96920

U.S. Food and Drug Administration (2018). Is the product a medical device? Retrieved on June 17th, 2019 from https://www.fda.gov/medical-devices/classify-your-medical-device/product-medical-device

Vimalson, D.C., Parimalakrishnan, S., Jeganathan, N.S. & Anbazhagan, S. (2016). Techniques to enhance solubility of hydrophobic drugs: an overview. Asian Journal of Pharmaceutics. Suppl 10 (2) page 67–75. doi:https://doi.org/10.22377/ajp.v10i2.625

Wang J, Musameh M (2003) Carbon nanotube/teflon composite electrochemical sensors and biosensors. Anal Chem 75(9):2075–2079. https://doi.org/10.1021/ac030007

Wang T, Weng Z, Liu X, Yeung KW, Pan H, Wu S (2017b) Controlled release and biocompatibility of polymer/titania nanotube array system on titanium implants. Bioactive materials 2(1):44–50. https://doi.org/10.1016/j.bioactmat.2017.02.001

Wang X, Du Y, Luo J, Lin B, Kennedy JF (2007) Chitosan/organic rectorite nanocomposite films: structure, characteristic and drug delivery behaviour. Carbohydr Polym 69(1):41–49. https://doi.org/10.1016/j.carbpol.2006.08.025

Werengowska-Ciećwierz K, Wiśniewski M, Terzyk AP, Gurtowska N, Olkowska J, Kloskowski T, Drewa TA, Kiełkowska U, Drużyński S (2014) Nanotube-mediated efficiency of cisplatin anticancer therapy. Carbon 70:46–58. https://doi.org/10.1016/j.carbon.2013.12.060

Wydra RJ, Kruse AM, Bae Y, Anderson KW, Hilt JZ (2013) Synthesis and characterization of PEG-iron oxide core-shell composite nanoparticles for thermal therapy. Mater Sci Eng C 33(8):4660–4666. https://doi.org/10.1016/j.msec.2013.07.019

Xing R, Liu K, Jiao T, Zhang N, Ma K, Zhang R, Zou Q, Ma G, Yan X (2016) An injectable self-assembling collagen–gold hybrid hydrogel for combinatorial antitumor photothermal/photodynamic therapy. Adv Mater 28(19):3669–3676. https://doi.org/10.1002/adma.201600284

Yu A, Ramesh P, Itkis ME, Bekyarova E, Haddon RC (2007) Graphite nanoplatelet− epoxy composite thermal interface materials. J Phys Chem C 111(21):7565–7569. https://doi.org/10.1021/jp071761s

Yuk SH, Oh KS, Cho SH, Lee BS, Kim SY, Kwak BK, Kim K, Kwon IC (2011) Glycol chitosan/heparin immobilized iron oxide nanoparticles with a tumor-targeting characteristic for magnetic resonance imaging. Biomacromolecules 12(6):2335–2343. https://doi.org/10.1021/bm200413a

Zhang Y, Zhang M (2002) Calcium phosphate/chitosan composite scaffolds for controlled in vitro antibiotic drug release. Journal of Biomedical Materials Research: An Official Journal of The Society for Biomaterials, The Japanese Society for Biomaterials, and The Australian Society for Biomaterials and the Korean Society for Biomaterials 62(3):378–386. https://doi.org/10.1002/jbm.10312

Zhao DL, Zhang HL, Zeng XW, Xia QS, Tang JT (2006) Inductive heat property of Fe3O4/polymer composite nanoparticles in an ac magnetic field for localized hyperthermia. Biomed Mater 1(4):198. https://doi.org/10.1088/1748-6041/1/4/004

Zomorodian K, Veisi H, Mousavi SM, Ataabadi MS, Yazdanpanah S, Bagheri J, Mehr AP, Hemmati S, Veisi H (2018) Modified magnetic nanoparticles by PEG-400-immobilized Ag nanoparticles (Fe3O4@ PEG–Ag) as a core/shell nanocomposite and evaluation of its antimicrobial activity. Int J Nanomedicine 13:3965. https://doi.org/10.2147/IJN.S161002

Chapter 16
Components of All-Solid-State Ion-Selective Electrodes (AS-ISEs)

Abdelmohsen M. Benoudjit, Ihda Uswatun Shalihah Shohibuddin, Mamoun Mohamad Bader, and Wan Wardatul Amani Wan Salim

16.1 Introduction

An electrochemical sensor is a qualitative and quantitative device that converts a chemical signal to a measurable electrical signal (Yogeswaran and Shen-Ming 2008). Electrochemical sensors can be divided into three classes: potentiometric, amperometric, and conductometric (Stradiotto et al. 2003). A potentiometric sensor measures an electrical potential when no current is present, while an amperometric sensor produces current when a potential is applied between two electrodes. A conductometric sensor assesses conductivity by measuring the electrical resistance of a sample solution. Ion-selective electrodes (ISEs) are potentiometric ion sensors and a subgroup of electrochemical sensors; they are widely used in various fields of biomedical, environmental, and chemical analysis, and physiological sensing (Bobacka et al. 2003; Bakker et al. 2008; Hu et al. 2016). ISEs are classified into three groups, depending on the nature of the membrane material: glass, polymeric or liquid, and crystal or solid (Fig. 16.1) (Faridbod et al. 2007).

All-solid-state ion-selective electrodes (AS-ISEs) are solid-based selective membrane electrodes that convert the activity of a specific ion to a measurable electrical signal without an internal filling solution – a liquid electrolyte that separates the sensing membrane from the inner reference electrode (Bobacka 2006; Bratovčić et al. 2009; Faridbod et al. 2008). Measuring voltage potential requires two electrodes: a reference electrode and a sensing electrode. The reference electrode

A. M. Benoudjit · I. U. S. Shohibuddin · Wan Wardatul Amani Wan Salim (✉)
Department of Biotechnology Engineering, Faculty of Engineering, International Islamic University Malaysia, Selangor, Kuala Lumpur, Malaysia
e-mail: asalim@iium.edu.my

M. M. Bader
Department of Chemistry, College of Science and General Studies, Alfaisal University, Riyadh, Kingdom of Saudi Arabia

S. Siddiquee et al. (eds.), *Composite Materials: Applications in Engineering, Biomedicine and Food Science*, https://doi.org/10.1007/978-3-030-45489-0_16

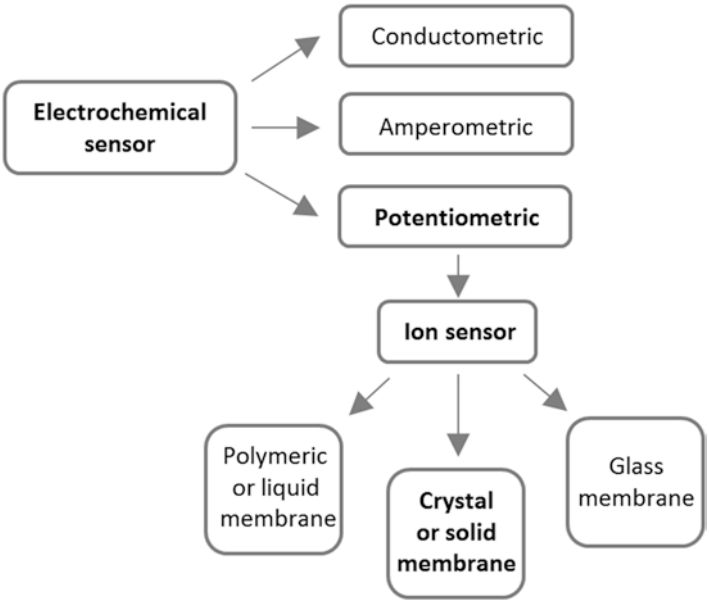

Fig. 16.1 Classification of an electrochemical sensor

potential is constant, and the sensing-electrode potential varies with the concentration of the target ions (Bratovčić et al. 2009). The potential being measured is equal to the difference in potential at the reference electrode and the sensing electrodes.

Key components of AS-ISEs are an ion-selective membrane (ISM) and a transducer or solid contact deposited on a conductive electrode made from carbon, platinum, or gold (Fig. 16.2) (Faridbod et al. 2008; Hu et al. 2016).The role of the ISM is to recognize and select the target ion, while the transducer converts the target-ion concentration to an electrical signal that can be measured against a reference electrode. A silver/silver chloride (Ag/AgCl, Cl^-) electrode is usually used as the reference electrode in ISEs owing to its environmental compatibility, biocompatibility, stable potential, and redox capability (Michalska 2012). A saturated calomel (Hg/Hg_2Cl_2, Cl^-) reference electrode has the advantage of stable potential and is not influenced by light, but is applicable only up to temperatures of about 80 °C. The aforementioned electrodes are currently commercially available; two others, the thallium chloride (Tl (Hg)/TlCl, Cl^-) and the Thalamid™ electrodes are no longer used as reference electrodes owing to toxicity (Guth et al. 2009).

Polymers have been utilized as homogeneous membrane matrices in ISMs owing to good elasticity and mechanical stability (Faridbod et al. 2008). Conductive polymers are often applied as ion-to-electron transducers because of the ohmic properties integrated to a polymer that is flexible and biocompatible (Bobacka et al. 2008). Furthermore, carbon-based materials like carbon nanotubes (CNTs), graphene, and graphene derivatives (e.g., graphene oxide and reduced graphene oxide) have been

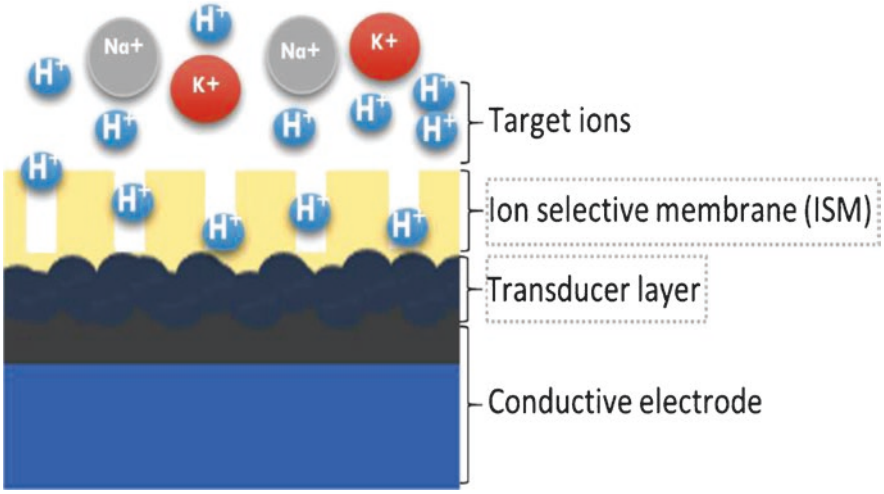

Fig. 16.2 Key components of all-solid-state ion-selective electrodes (AS-ISEs): conductive electrode, solid contact or transducer, and ion-selective membrane

used as transducers in AS-ISEs as their physical, electrical, mechanical, optical, thermal, and chemical properties make them suitable for such use (Yan et al. 2016).

This chapter will introduce readers to the materials in ion-selective membranes and all-solid-state transducers for AS-ISEs. The components of ISMs include a polymeric matrix, ionophores, plasticizers, and ionic additives, while commonly used all-solid-state transducers are conductive polymers of polypyrrole (PPy), polyaniline (PANI), and polythiophene (PT), or carbon-based materials such as carbon nanotubes and graphene.

16.2 Components of an Ion-Selective Membrane

An ion-selective membrane (ISM) cocktail consists of four components: a polymeric matrix, an ionophore as a recognition material, a membrane solvent or plasticizer, and ionic additives. The amount of each component can influence the physical and chemical characteristics of an ISM. Typical composition of an ISM is approximately 33% (w/w) polymeric matrix, 66% (w/w) plasticizer, 1% (w/w) ionophore, and 0.5% (w/w) ionic additives; each component of the ISM depends on the target ion (Faridbod et al. 2008).

16.2.1 Polymeric Matrix Materials

Polymers function as homogeneous membrane matrices for ISMs where their glass transition temperature (Tg) value should be below room temperature (Jadhav et al. 2009). The polymer membrane should be fluid enough under ambient conditions to allow for diffusion of other ISM components. Besides Tg, ISM biocompatibility is especially important for clinical applications; polyvinyl chloride (PVC) is the most commonly used polymer in ISM preparation (Fig. 16.3). Furthermore, acrylate and acrylate derivatives as well as polystyrene have been approved as polymeric matrices for biomedical applications (Faridbod et al. 2008).

16.2.2 Ionophores as Membrane–Active Recognition Components for Ion Carrier and Selectivity

Ionophores provide selectivity towards a target ion owing to their chemical and structural properties. The chemical property involves chemical bond strength and types of molecular interaction, while the structural property includes recognition of size and physical shape of molecular analytes. These specific characteristics influence ISEs selectivity in recognizing the target ions (Ganjali et al. 2006).

Studies have been conducted to understand how the chemical properties of ionophores lead to highly selective ISEs. Wilson et al. (2010) discovered that thioureas – compounds with N-C(S)-N functionality – will significantly improve the selectivity of ISEs towards different metal ions. The presence of intra-molecular interactions, the particular effects by conformational isomerism, and the existence of S and N atoms which act as donor sites make the thiourea derivatives as ligands more versatile (Wilson et al. 2010). Furthermore, the existence of a carbonyl group bonded to the thiourea will result in a heterocyclic compound that provides strong bonding potential as a ligand. The carbonyl group can interact with heavy metal ions such as

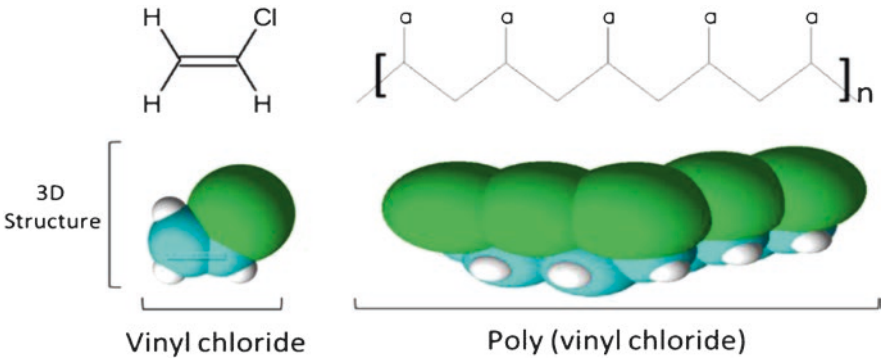

Fig. 16.3 Chemical structure of vinyl chloride and poly (vinyl chloride) (PVC)

Cu(II), Ni(II), and Hg(II) (Saeed et al. 2014). Therefore, thioureas have proved to be attractive ionophores for selective detection of heavy metal ions (Jumal et al. 2012; Ying et al. 2018).

In addition to chemical properties, the structure of an ionophore plays an important role in selectivity towards target ions. The internal cavity of an ionophore whose inner diameter is equivalent to the diameter of the target ions – but not to that of other interfering ions – makes ionophores very selective for ions of interest. In fact, the ionophore is one of the most vital components of the membrane because it is responsible for making the ISEs selective (Pięk et al. 2018).

16.2.3 Plasticizers as Membrane Solvent

A plasticizer is an additive in which the components of the ISM are dissolved; the plasticizer increases the plasticity and fluidity of the material to which it is added. In order to ensure high mobility of the ISM components, a 2:1 weight ratio of plasticizer to polymer is required; the ideal composition of ISMs is 60–66% (w/w) plasticizer and 30–33% polymer matrix. Tables 16.1 and 16.2 summarize the potassium-ion (K^+) and calcium-ion (Ca^{2+}) composition of an ISM, respectively. As can be seen from the tables, both K^+ and Ca^{2+} ISMs have the same components with only a difference in the ionophores. For instance, valinomycin acts as the K^+ ionophore (He et al. 2016; Vanamo and Bobacka 2014; Zhang and Zhang 2013), whereas ETH 129 (Zhao et al. 2019; Park et al. 2017; Ping et al. 2012), and ETH 5234 (ul Haque et al. 2007) act as Ca^{2+} ionophores. The rest of the ISM composition consists of ionic additives, plasticizers, polymer matrix, and solvent. Previous studies have used potassium tetrakis (4-chlorophenyl) borate (KTCPB) (Park et al. 2017; ul Haque et al. 2007; Shiwaku et al. 2018; Guzinski et al. 2017; Vázquez et al. 2002), potassium tetrakis[(3,5-bis[trifluoro methyl]phenyl) borate (KTFPB) (Vanamo and Bobacka 2014; Zhao et al. 2019; Ping et al. 2012), or sodium tetrakis(3,5bis[trifluoromethyl]phenyl) borate (NaTFPB) (Liu et al. 2019) as the ionic additives. The plasticizers are a membrane solvent such as bis(2-ethylhexyl) sebacate (DOS) (He et al. 2016; Guzinski et al. 2017), 2-nitrophenyl octyl ether (2-NPOE) (Ping et al. 2012; ul Haque et al. 2007; Liu et al. 2019), or bis(1-butylpentyl) adipate (BBPA) (Vázquez et al. 2002). Polyvinylchloride (PVC) has been used as the polymer matrix of the membrane (Vanamo and Bobacka 2014; Zhang and Zhang 2013; Liu et al. 2019). Looking into the weight ratio of plasticizer to polymer for K^+-ISMs, Shiwaku et al. used 64.7% DOS plasticizer and 32.7% PVC (Shiwaku et al. 2018), while Vanamo and Bobacka used 62.5% and 33.3% for DOS plasticizer and PVC (Vanamo and Bobacka 2014), respectively. For Ca^{2+}-ISMs, Zhao et al. used 65.6% 2-NPOE plasticizer and 32.8% PVC (Zhao et al. 2019), while Park et al. used 63.5% 2-NPOE plasticizer and 31.7% PVC (Park et al. 2017); both ISM cocktails follow similar ratio of plasticizer to polymer, mainly to ensure high mobility of ISM components.

Table 16.1 Summary of ion-selective membrane composition for K^+

No.	Types of component	Chemical components	Abbreviation	Components amount (% w/w)					
1	Ionophore	Valinomycin		2.0%	1.0%	2.05%	1.0%	1.0%	1.16%
2	Ionic additives	Potassium tetrakis (4-chlorophenyl) borate	KTCPB	0.5%		0.45%			0.32%
3		Potassium tetrakis (3,5-bis [trifluoromethyl] phenyl) borate	KTFPB		0.4%		0.5%	0.2%	
4	Plasticizers	Bis(2-ethylhexyl) sebacate	DOS	64.7%	65. 7%	65.0%	62.5%		
5		2-nitro phenyl octyl ether	2-NPOE					66.0%	
6		Bis (1-butylpentyl) adipate	BBPA						66.4%
8	Polymer matrix	Polyvinylchloride	PVC	32.7%	32.9%	32.5%	33.3%	32.8%	32. 1%
9	Solvent	Tetrahydrofuran	THF	350 µL	1 mL	1.5 mL	-ns-	-ns-	-ns-
References				Shiwaku et al. (2018)	He et al. (2016)	Guzinski et al. (2017)	Vanamo and Bobacka (2014)	Zhang and Zhang (2013)	Vázquez et al. (2002)

ns: not specified.

Table 16.2 Summary of ion-selective membrane composition for Ca^{2+}

No.	Types of component	Chemical components	Abbreviation	Components amount (% w/w)				
1	Ionophore	Calcium ionophore II	ETH 129	1.0%	3.0%		1.0%	0.49%
2		Calcium ionophore IV	ETH 5234			1.0%		
3	Ionic additives	Potassium tetrakis (4-chlorophenyl) borate	KTCPB		1.8%	0.7%		
4		Potassium tetrakis (3,5-bis [trifluoromethyl] phenyl) borate	KTFPB	0.6%			0.2%	
5		Sodium tetrakis(3,5-bis[trifluoromethyl] phenyl)borate	NaTFPB					0.46%
6	Plasticizers	Bis(2-ethylhexyl) sebacate	DOS					
7		2-nitrophenyl octyl ether	2-NPOE	65.6%	63.5%	65.3%	65.8%	66.03%
9	Polymer matrix	Polyvinylchloride	PVC	32.8%	31.7%	33.0%	33.0%	33.02%
10	Solvent	Tetrahydrofuran	THF	1.5 mL		4 mL	-ns-	3.6 mL
11		Cyclohexane			-ns-			
References				Zhao et al. (2019)	Park et al. (2017)	ul Haque et al. (2007)	Ping et al. (2012)	Liu et al. (2019)

ns: not specified.

16.2.4 Ionic Additives as Lipophilic Salts

Ionic additives, also called as lipophilic salts, provide two advantages for the ISMs: increase selectivity towards the target ion and reduce membrane ionic resistance (Morf et al. 2005). With respect to selectivity for divalent cations, a lipophilic anion improves preference for divalent over interfering monovalent cations, and at the same time reduces interference from anionic molecules (Eugster et al. 1991). Therefore, a lipophilic anion will ultimately increase the overall selectivity of ISEs for target divalent cations. Furthermore, the inclusion of ionic additives can act as an ion exchanger, which can improve selectivity when insufficient ionophore is present (Faridbod et al. 2008).

Another advantage of ionic additives is the lowering of ISM ionic resistance, easing the movement of target ions from sample solution into the membrane. Therefore, ionic additives enhance the interfacial ion-exchange kinetics and ultimately reduce the response time of ISEs (Gehrig et al. 1990). Overall, the four

components of ISMs complement each other in terms of selectivity, response time, ion-exchange kinetics, fluidity and plasticity of the ISMs. The next section will discuss another important component of an ISE, the transducer.

16.3 Transducer Materials for AS-ISEs

Conductive polymers and nanomaterials as ion-to-electron transducers improve the performance of AS-ISEs in terms of detection limit, sensitivity, selectivity, and chemical stability (Bobacka 2006); these materials enable the miniaturization of ISEs (Hu et al. 2016). Commonly used conductive polymers are polypyrrole (PPy), polyaniline (PANI), and polythiophene (PT) (Fig. 16.4). Commonly used

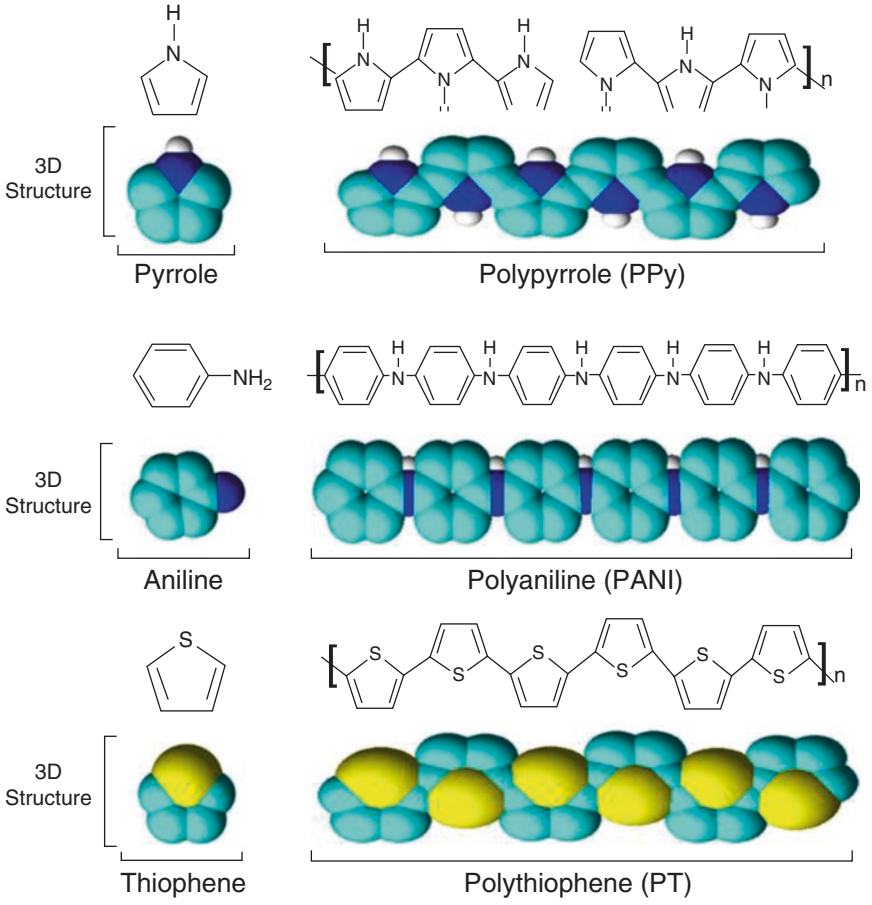

Fig. 16.4 Chemical structure of monomer and polymer units of conducting polymers that have been applied as ion-to-electron transducers in all-solid-state ion-selective electrodes

nanomaterials are three dimensionally–ordered macroporous (3DOM) carbon, colloid-imprinted mesoporous (CIM) carbon, carbon nanotubes (CNTs), graphene, fullerene, nanoclusters and gold nanoparticles (Liu et al. 2019).

16.3.1 Conductive Polymers

Conductive polymers of PPy, PANI, and PT have some key features that make them useful as ion-to-electron transducers (Bobacka 2006; Faridbod et al. 2008; Bobacka et al. 2008). First, conducting polymers can provide ohmic contact with high work function like noble metals and carbon materials. Second, conductive polymers can be deposited from solution onto the conductive electrodes either by electrochemical polymerization or by drop-casting. Third, conductive polymers electroactive property as a result of combinatory effect of electronic and ionic conductivity allows for ion to electron transduction (Faridbod et al. 2008; Bobacka et al. 2008). These are the features that make conducting polymers suitable as solid contact transducers for AS-ISEs.

i. Polypyrrole (PPy)

Polypyrrole has been used as an ion-to-electron transducer in solid-contact ISEs since the beginning of the 1990s and is still used today (Bobacka et al. 2003). PPy as a solid contact enhances the performance of AS-ISEs in terms of Nernstian behavior, linear range, detection limit, and response time (Table 16.3). For example, PPy doped with Titan yellow dye (PPy/TY) as solid contact resulted in a magnesium-selective ISE (Mg^{+2}-ISE); the solid-state electrode has a Nernstian behavior almost equivalent to that of a typical glass electrode (Gupta et al. 2004; Mosayebzadeh et al. 2014). The calibration slope and concentration range for polypyrrole- and non-polypyrrole–based solid contacts were 28.27 ± 0.40 mV per decade within the concentration range of $1.0 \times 10^{-5} - 5.0 \times 10^{-2}$ M, and 29.2 ± 0.4 mV per decade within the concentration range of 9.4×10^{-6} to 1.0×10^{-1} M, respectively (Gupta et al. 2004; Mosayebzadeh et al. 2014). The detection limits of PPy-based and non-PPy-based solid contacts were 6.28×10^{-6} M and 9.4×10^{-6}, respectively, showing not much difference in performance. However, the potentiometric response of PPy-based solid-contact electrodes toward Mg^{+2} was found to be independent of pH from 4.5–8.0, while non–PPy–based solid contacts were independent of pH from 3.5–7.8 (Gupta et al. 2004; Mosayebzadeh et al. 2014). Polypyrrole-based Mg^{+2}-ISEs showed fast response time compare to non-PPy-based Mg^{+2}-ISEs, < 10 s and 13 s, respectively (Mosayebzadeh et al. 2014). The results show that a PPy solid contact is comparable to a non-solid state one.

ii. Polyaniline (PANI)

Polyaniline (PANI) is utilized in ISEs fabrication owing to its stable potential, easy preparation, and low cost (Shishkanova et al. 2005). PANI has been used as a solid contact (Jiang et al. 2019), or as a component of an ion-selective membrane

Table 16.3 Linear range, detection limit, and response time of polypyrrole as solid contact in AS-ISEs

Transducer	Target ion	Application	Linear range	Detection limit	Response time	Reference
GCE/PPy-rGO	Nitrate ion (NO_3^-)	Agricultural	10^{-5} to 10^{-1} M	$10^{-5.2 \pm 0.1}$ M	≤15 s	Pan et al. (2016)
CSPE/PPy	Iron ion (Fe^{2+})	Biological, industrial, environmental	1×10^{-6} to 1×01^{-1} M	8.78×10^{-7} M	–	(Gholami et al. (2015)
PGE/PPy-TY	Magnesium ion (Mg^{2+})	Medical	1.0×10^{-5} to5.0×10^{-2} M	6.28×10^{-6} M	<10 s	(Mosayebzadeh et al. (2014)
PGE/PPy	Arsenate ion (AsO^{3-})	Environmental	5.0×10^{-5} to 1.0×10^{-1} M	2.8×10^{-5} M	≤10 s	(Ansari et al. (2013)
PGE/PPy	Uranyl ion (UO^{2+})	Environmental	1.0×10^{-6} to 1.0×10^{-2} M	6.30×10^{-7} M	≤12 s	(Ansari and Mosayebzadeh (2013)
PGE/PPy	Zinc ion (Zn^{2+})	Environmental	1.0×10^{-5} to 1.0×10^{-1} M	8.0×10^{-6} M	–	(Ansari et al. (2012)

PGE: Pencil graphite electrode
rGO: Reduce graphene oxide
TY: Titanium yellow
PPy: Polypyrrole
GCE: Glass carbon electrode
CSPE: Screen-printed carbon electrode

(Aytaç et al. 2004). In addition, PANI can exist as either film, microfiber, or nanoparticle; PANI in microfiber form enhances ISE performance owing to its hydrophobicity, which minimizes water intake into the ISM (Jiang et al. 2019). As an example, electrospun PANI-polystyrene microfiber film (e-PANI-PS) was used as a transducer in solid-contact ISEs to sense lead ion (Pb^{2+}). The Pb^{2+}-ISEs based on e-PANI-PS exhibited a wide linear detection range (10^{-8} to 10^{-3} mol/L), a low detection limit (~5×10^{-9} mol/ L), a Nernstian slope of 29.1 mV/decade, and a fast response time (< 10 s) (Jiang et al., 2019). Moreover, the fabricated ISEs demonstrated a lower detection limit for Pb^{2+} and better potential stability compared to ISEs fabricated using drop-cast PANI-PS films. The analytical performance of the e-PANI-PS microfiber transducer for Pb^{2+} detection is a result of the high hydrophobicity that minimizes water uptake. Furthermore, e-PANI-PS has higher capacitance and lower impedance than the drop-cast PANI-PS, which promoted fast ion-to-electron transfer at the electrode-solution interface (Jiang et al. 2019). These features make PANI one of the most used conductive polymers as a transducer for AS-ISE fabrication.

iii. Polythiophene (PT)

The first polythiophene used as a solid contact in ISEs was poly(3-octylthiophene) (POT) (Bobacka et al. 2008). Poly(3,4-ethylene-dioxythiophene) (PEDOT) in its p-doped form is highly electroactive and possesses good environmental stability (less sensitive to O_2 and CO_2) compared to transducers based on PPy as solid contact (Bobacka 2006). Therefore, water-dispersible PEDOT with poly(styrenesulfonate) (PEDOT:PSS) (Fig. 16.5) was used as an ion-to-electron transducer in solid-contact ISEs for detection of certain ions: potassium (K^+), silver (Ag^+), sodium (Na^+), cesium (Cs^+), calcium (Ca^{2+}), and some aromatic cations (e.g., N-methylpyridinium, bupivacaine) (Bobacka et al. 2008). However, few research

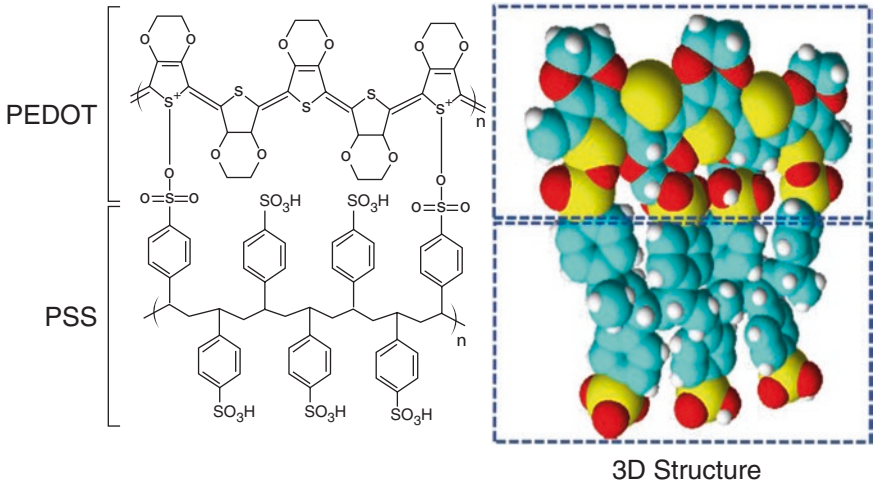

Fig. 16.5 Chemical structure of poly (3,4-ethylenedioxythiophene) poly(styrenesulfonate) (PEDOT:PSS)

reports on PEDOT:PSS use as an electrochemical sensor owing to poor adhesion of PEDOT:PSS on conductive electrode surfaces. In aqueous solution, PSS can result in swelling of PEDOT:PSS and the film can be removed from the electrode surface (Wang et al. 2014; Benoudjit et al. 2018), limiting PEDOT:PSS use as a transducer for AS-ISEs. Therefore, some studies focus on enhancing the adhesion of PEDOT:PSS on electrode surface by using polyvinyl alcohol (PVA) (Wang et al. 2014) and sodium carboxymethyl cellulose (Na-CMC) (Zhang et al. 2015) binders, or depositing PEDOT:PSS with electro-polymerization instead of by drop-casting (Benoudjit et al. 2018). The resulting improvement allows PEDOT:PSS to be an effective transducer for AS-ISEs.

16.3.2 Nanomaterials

Recently, nanomaterials have been suggested as transducer materials for AS-ISEs (Liu et al. 2019). Three-dimensionally ordered macroporous (3DOM) carbon (Lai et al. 2007), colloid-imprinted mesoporous (CIM) carbon (Hu et al. 2014), carbon nanotubes (CNTs) (Ganjali et al. 2010; Crespo et al. 2008), graphene (Ping et al. 2011), fullerene (Fouskaki and Chaniotakis 2008), nanoclusters (Zhou et al. 2012), and gold nanoparticles (Jaworska et al. 2011) are commonly used nanomaterials as a result of their high surface area, intrinsic hydrophobicity, and electric conductivity. Furthermore, these nanomaterial-based ISEs exhibit high potential stability and have shown more excellent resistance to O_2, CO_2, light, and redox interferences than do the classical conducting polymers (Liu et al. 2019). These features make these nanomaterials suitable as transducer materials for AS-ISE fabrication. Generally, nanomaterial-based solid contacts are prepared layer by layer using drop-casting methods. However, it should be noted that nanomaterials can easily detach from an electrode surface owing to poor adhesion (Liu et al. 2019). Although PVC has been successfully used as a facile and effective binder to fabricate nanomaterial-based solid contact (Hu et al. 2014), the electrical conductivity of nanomaterials might be reduced by the poor conductivity of PVC.

More recently, we utilized PEDOT:PSS with reduced graphene oxide (rGO) nanomaterial as solid contact for biosensors because the composite showed good adhesion to the electrode surface while retaining good conductivity (Ismail et al. 2019). From electrochemical analyses by cyclic voltammetry (CV), the transducer showed a high effective surface area of 0.219 mm^2 and a high peak current of 0.793 mA. The high conductivity is further confirmed with electrical impedance spectroscopy (EIS), showing the composite to have low charge-transfer resistance (R_{ct}) of 200.7 Ω (Ismail et al. 2019). The CV and EIS results suggest that rGO-PEDOT:PSS composite has the potential to be used as solid contacts for AS-ISEs.

16.4 Summary

This chapter introduces the materials used for fabricating the components of AS-ISEs: the ion-selective membrane (ISM) and the all-solid-state transducer. The role of an ISM is to recognize and select the target io; the ISM consists of four components: polymeric matrix, plasticizer, ionophore, and ionic additives. The physical and chemical characteristics of AS-ISEs can be influenced by the amount of each component, and the typical cocktail mix for an ISM is polymeric matrix 33% (w/w), plasticizer 66% (w/w), and ionophore 1% (w/w). Polyvinyl chloride (PVC) functions as a homogeneous membrane matrix for the other ISM components. Ionophores provide selectivity towards a target ion, which is also known as membrane-active recognition; selection of ionophore depends on the target ion. Plasticizers are responsible for controlling the physical property (plasticity or fluidity) of ISMs. Ionic additives are ion exchangers that ensure the permselectivity of the ISMs if no or insufficient ionophore is present. The solid-state transducer converts the target-ion concentration to an electrical signal that can be measured. Materials used as solid-state transducers are conductive polymers and nanomaterials. Common conductive polymers used in AS-ISEs are polypyrrole, polythiophene, and polyaniline, owing to their intrinsic characteristics. Nanomaterials such as Three-dimensionally-ordered macroporous carbon, colloid-imprinted mesoporous carbon, carbon nanotubes, graphene, fullerene, nanoclusters, and gold nanoparticles are good solid contacts for AS-ISEs owing to their ion-to-electron transduction. Reduced graphene oxide can be combined with PEDOT:PSS to serve as a solid contact for AS-ISEs.

References

Ansari R, Mosayebzadeh Z (2013) Construction of a new solid-state U (VI) ion-selective electrode based on polypyrrole conducting polymer. vi

Ansari R, Delavar AF, Mohammad-Khah A (2012) Solid-state ion selective electrode based on polypyrrole conducting polymer nanofilm as a new potentiometric sensor for Zn 2+ ion. J Solid State Electrochem 16(10):3315–3322

Ansari R, Mosayebzadeh Z, Mohammad-khah A (2013) Fabrication of a solid-state ion selective electrode based on polypyrrole conducting polymer for As (V) ion. Int J Env Anal Chem:37–41

Aytaç A, Kabasakaloğlu M, Sarı B, Talu M (2004) Ion-selective electrodes prepared with polyaniline membranes. Russ J Electrochem 40(7):732–735

Bakker E, Bhakthavatsalam V, Gemene KL (2008) Beyond potentiometry: robust electrochemical ion sensor concepts in view of remote chemical sensing. Talanta 75(3):629–635

Benoudjit A, Bader MM, Wan Salim WWA (2018) Study of electropolymerized PEDOT:PSS transducers for application as electrochemical sensors in aqueous media. Sens Bio-Sensing Res 17:18–24

Bobacka J (2006) Conducting polymer-based solid-state ion-selective electrodes. Electroanalysis 18(1):7–18

Bobacka J, Ivaska A, Lewenstam A (2003) Potentiometric ion sensors based on conducting polymers. Electroanalysis 15(5–6):366–374

Bobacka J, Ivaska A, Lewenstam A (2008) Potentiometric ion sensors. Chem Rev 108(2):329–351

Bratovčić A, Odobašić A, Ćatić S (2009) The advantages of the use of ion-selective potentiometry in relation to UV / VIS spectroscopy. Agric Conspec Sci Cus 74(3):139–142

Crespo GA, Macho S, Rius FX (2008) Ion-selective electrodes using carbon nanotubes as ion-to-electron transducers. Anal Chem 80(4):1316–1322

Eugster R, Gehrig PM, Morf WE, Spichiger UE, Simon W (1991) Selectivity-modifying influence of anionic sites in neutral-carrier-based membrane electrodes. Anal Chem 63(20):2285–2289

Faridbod F, Ganjali MR, Dinarvand R, Norouzi P (2007) The fabrication of potentiometric membrane sensors and their applications. African J Biotechnol 6(25):2960–2987

Faridbod F, Ganjali MR, Dinarvand R, Norouzi P (2008) Developments in the field of conducting and non-conducting polymer based potentiometric membrane sensors for ions over the past decade. Sensors 8(4):2331–2412

Fouskaki M, Chaniotakis N (2008) Fullerene-based electrochemical buffer layer for ion-selective electrodes. Analyst 133(8):1072–1075

Ganjali MR, Norouzi P, Rezapour M, Faridbod F, Pourjavid MR (2006) Supramolecular based membrane sensors. Sensors 6(8):1018–1086

Ganjali MR, Motakef-Kazami N, Faridbod F, Khoee S, Norouzi P (2010) Determination of Pb2+ ions by a modified carbon paste electrode based on multi-walled carbon nanotubes (MWCNTs) and nanosilica. J Hazard Mater 173(1–3):415–419

Gehrig P, Morf WE, Welti M, Pretsch E, Simon W (1990) Catalysis of ion transfer by tetraphenylborates in neutral carrier-based ion-selective electrodes. Helv Chim Acta 73(1):203–212

Gholami M, Rezayi M, Moozarm Nia P, Yusoff I, Alias Y (2015) A novel method for fabricating Fe2+ ion selective sensor using polypyrrole and sodium dodecyl sulfate based on carbon screen-printed electrode. Meas J Int Meas Confed 69:115–125

Gupta VK, Prasad R, Kumar A (2004) Magnesium-tetrazaporphyrin incorporated PVC matrix as a new material for fabrication of Mg2+ selective potentiometric sensor. Talanta 63(4):1027–1033

Guth U, Gerlach F, Decker M, Oelßner W, Vonau W (2009) Solid-state reference electrodes for potentiometric sensors. J Solid State Electrochem 13(1):27–39

Guzinski M et al (2017) PEDOT(PSS) as solid contact for ion-selective electrodes: the influence of the PEDOT(PSS) film thickness on the equilibration times. Anal Chem 89(6):3508–3516

He N, Gyurcsányi RE, Lindfors T (2016) Electropolymerized hydrophobic polyazulene as solid-contacts in potassium-selective electrodes. Analyst 141(10):2990–2997

Hu J, Zou XU, Stein A, Bühlmann P (2014) Ion-selective electrodes with colloid-imprinted mesoporous carbon as solid contact. Anal Chem 86(14):7111–7118

Hu J, Stein A, Bühlmann P (2016) Rational design of all-solid-state ion-selective electrodes and reference electrodes. Trends Anal Chem 76:102–114

Ismail NAB, Abd-Wahab F, Wan Salim WWA(2019) Cyclic voltammetry and electrochemical impedance spectroscopy of partially reduced graphene oxide PEDOT:PSS transducer for biochemical sensing, in *IEEE EMBS Conference on Biomedical Engineering and Sciences, IECBES 2018 Proceedings*, cv: 330–335

Jadhav NR, Gaikwad VL, Nair KJ, Kadam HM (2009) Glass transition temperature: basics and application in pharmaceutical sector. Asian J Pharm 3(2):82–89

Jaworska E, Wójcik M, Kisiel A, Mieczkowski J, Michalska A (2011) Gold nanoparticles solid contact for ion-selective electrodes of highly stable potential readings. Talanta 85(4):1986–1989

Jiang W, Liu C, Zhao Y, Waterhouse GIN, Zhang Z, Yu L (2019) A solid-contact Pb 2+ −selective electrode based on a hydrophobic polyaniline microfiber film as the ion-to-electron transducer. Synth Met 248:94–101

Jumal J, Yamin BM, Ahmad M, Heng LY (2012) Mercury ion-selective electrode with self-plasticizing poly(n–butylacrylate) membrane based on 1,2-bis-(N'–benzoylthioureido)cyclohexane as ionophore. APCBEE Procedia 3:116–123

Lai CZ, Fierke MA, Stein A, Bühlmann P (2007) Ion-selective electrodes with three-dimensionally ordered macroporous carbon as the solid contact. Anal Chem 79(12):4621–4626

Liu K, Jiang X, Song Y, Liang R (2019) Robust fabrication of nanomaterial-based all-solid-state ion-selective electrodes. RSC Adv 9(29):16713–16717

Michalska A (2012) All-solid-state ion selective and all-solid-state reference electrodes. Electroanalysis 24(6):1253–1265

Morf WE, De Rooij NF, Pretsch E (2005) Influence of cationic and anionic additives on the electrical properties of ionophore-based ion-selective membranes. J Electroanal Chem 581(2):265–274

Mosayebzadeh Z, Ansari R, Arvand M (2014) Preparation of a solid-state ion-selective electrode based on polypyrrole conducting polymer for magnesium ion. J Iran Chem Soc 11(2):447–456

Pan P et al (2016) Preparation and evaluation of a stable solid state ion selective electrode of polypyrrole/electrochemically reduced graphene/glassy carbon substrate for soil nitrate sensing. Int J Electrochem Sci 11(6):779–4793

Park J et al (2017) An autonomous lab on a chip for space flight calibration of gravity-induced transcellular calcium polarization in single-cell fern spores. Lab Chip 17(6):1095–1103

Pięk M, Paczosa-Bator B, Smajdor J, Piech R (2018) Molecular organic materials intermediate layers modified with carbon black in potentiometric sensors for chloride determination. Electrochim Acta 283:1753–1762

Ping J, Wang Y, Wu J, Ying Y (2011) Development of an all-solid-state potassium ion-selective electrode using grapheme as the solid-contact transducer. Electrochem Commun 13(12):1529–1532

Ping J, Wang Y, Ying Y, Wu J (2012) Application of electrochemically reduced graphene oxide on screen-printed ion-selective electrode. Anal Chem 84(7):3473–3479

Saeed A, Flörke U, Erben MF (2014) A review on the chemistry, coordination, structure and biological properties of 1-(acyl/aroyl)-3-(substituted) thioureas. J Sulfur Chem 35(3):318–355

Shishkanova TV, Sapurina I, Stejskal J, Král V, Volf R (2005) Ion-selective electrodes: Polyaniline modification and anion recognition. Anal Chim Acta 553(1–2):160–168

Shiwaku R et al (2018) A printed organic amplification system for wearable potentiometric electrochemical sensors. Sci Rep 8(1):1–8

Stradiotto NR, Yamanaka H, Zanoni MVB (2003) Electrochemical sensors: a powerful tool in analytical chemistry. J Braz Chem Soc 14(2):159–173

ul Haque A et al (2007) A MEMS fabricated cell electrophysiology biochip for in silico calcium measurements. Sensors Actuators B Chem 123(1):391–399

Vanamo U, Bobacka J (2014) Electrochemical control of the standard potential of solid-contact ion-selective electrodes having a conducting polymer as ion-to-electron transducer. Electrochim Acta 122:316–321

Vázquez M, Bobacka J, Ivaska A, Lewenstam A (2002) Influence of oxygen and carbon dioxide on the electrochemical stability of poly(3,4-ethylenedioxythiophene) used as ion-to-electron transducer in all-solid-state ion-selective electrodes. Sensors Actuators B Chem 82(1):7–13

Wang Z et al (2014) Facile preparation of highly water-stable and flexible PEDOT:PSS organic/inorganic composite materials and their application in electrochemical sensors. Sensors Actuators B Chem 196:357–369

Wilson D, de los Ángeles Arada M, Alegret S, del Valle M (2010) Lead(II) ion selective electrodes with PVC membranes based on two bis-thioureas as ionophores: 1, 3-bis(N'-benzoylthioureido)benzene and 1, 3-bis(N'-furoylthioureido)benzene. J Hazard Mater 181(1–3):140–146

Yan R, Qiu S, Tong L, Qian Y (2016) Review of progresses on clinical applications of ion selective electrodes for electrolytic ion tests: from conventional ISEs to graphene-based ISEs. Chem Speciat Bioavailab 28(1–4):72–77

Ying KS, Heng LY, Hassan NI, Hasbullah SA (2018) A new copper ionophore N^1, N^3 -bis [[3,5-bis(trifluoromethyl)phenyl] carbamothioyl] isophtalamide for potentiometric sensor. Sains Malays 47(11):2657–2666

Yogeswaran U, Shen-Ming C (2008) A review on the electrochemical sensors and biosensors composed of nanogaps as sensing material. J Optoelectron Adv Mater 12(8):290–313

Zhang L, Zhang M (2013) Screening of pretreatment parameters for novel solid-state ISE-based soil extractable potassium detection, in *Proceedings of 2013 IEEE 11th International Conference on Electronic Measurement and Instruments, ICEMI 2013*. 2: 947–953

Zhang H, Xu J, Wen Y, Wang Z, Zhang J, Ding W (2015) Conducting poly(3,4-ethylenedioxythi ophene):poly(styrene- sulfonate) film electrode with superior long-term electrode stability in

water and synergistically enhanced electrocatalytic ability for application in electrochemical sensors. Synth Met 204:39–47
Zhao L et al (2019) In vivo measurement of calcium ion with solid-state ion-selective electrode by using shelled hollow carbon nanospheres as a transducing layer. Anal Chem 91(7):4421–4428
Zhou M et al (2012) Effective solid contact for ion-selective electrodes: Tetrakis(4-chlorophenyl) borate (TB^-) anions doped nanocluster films. Anal Chem 84(7):3480–3483

Part III
Book Chapter for Food

Chapter 17
Nanocellulose and Nanocellulose-Based Composites for Food Applications

Suryani Saallah, Mailin Misson, Shafiquzzaman Siddiquee, Jumardi Roslan, M. Nazli Naim, Noor Fitrah Abu Bakar, and I. Wuled Lenggoro

17.1 Introduction

Increasing global demand for energy, depletion of petroleum sources, and concern over global climate change has led to the resurgence in the development of renewable and sustainable resources as an alternative to fossil fuel or petroleum-based materials (Chen et al. 2019a, b). In response, extensive research and development in nanocellulose production, a green, bio-based and renewable bio-material have been initiated and currently a subject of immense interest as a prominent candidate to replace the petroleum-based materials (Chen et al. 2017) as reflected in the rapid growing of scientific publications related to nanocellulose over the past two decades (Fig. 17.1).

Cellulose is the most abundant and ubiquitous renewable natural biopolymer in the biosphere with an estimated annual production of 75 to 100 billion tonnes (Xie

S. Saallah (✉) · M. Misson · S. Siddiquee
Biotechnology Research Institute, Universiti Malaysia Sabah,
Kota Kinabalu, Sabah, Malaysia
e-mail: suryani@ums.edu.my

J. Roslan
Faculty of Food Science and Nutrition, Universiti Malaysia Sabah,
Kota Kinabalu, Sabah, Malaysia

M. N. Naim
Department of Process and Food Engineering, Faculty of Engineering, Universiti Putra Malaysia, Serdang, Selangor, Malaysia

N. F. A. Bakar
Faculty of Chemical Engineering, Universiti Teknologi MARA,
Shah Alam, Selangor, Malaysia

I. W. Lenggoro
Institute of Engineering, Tokyo University of Agriculture and Technology, Koganei, Japan

S. Siddiquee et al. (eds.), *Composite Materials: Applications in Engineering, Biomedicine and Food Science*, https://doi.org/10.1007/978-3-030-45489-0_17

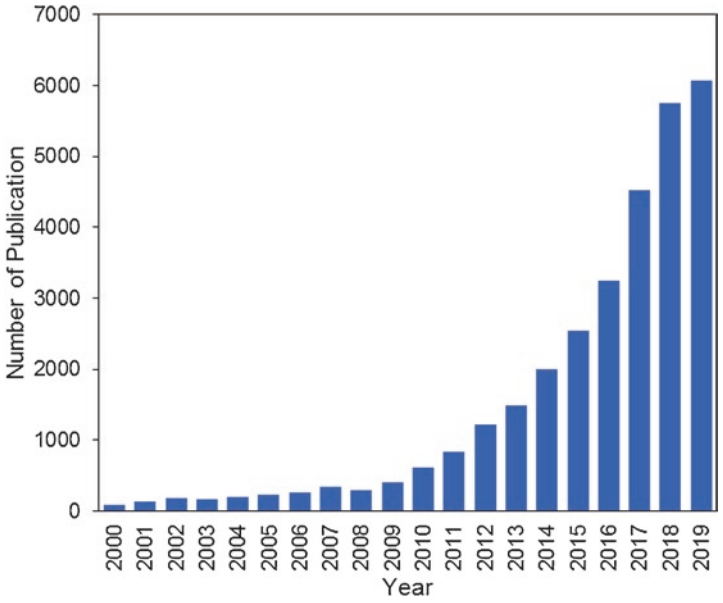

Fig. 17.1 Number of publications related to nanocellulose as analyzed by Scholar Plot[R] using data from Google Scholar (Data analysis was extracted from Scholar Plot[R] on 5 November 2019)

et al. 2016). Fibers generated from cellulosic material have long been used as lumber, textile and cordage. The extraction of nanocellulose from cellulosic materials through various chemical, biochemical, and mechanical means has enabled the emerging utilization of cellulose for much more sophisticated applications (Thomas et al. 2017). This include as synthetic reinforcement materials used in the composites and polymer matrixes, as stabilizers in food products and cosmetics, drug delivery excipient, scaffold for enzyme immobilization, tissue engineering, and biosensors, biodegradable packaging, air and water filtration, among others (Camacho et al. 2017; Tibolla et al. 2018).

According to a recent report by Global Market Insights, Inc. (2019), the global nanocellulose market in 2016 was USD 87.5 million and is forecasted to exceed USD 1 billion by 2024 by an outstanding compound annual growth rate (CAGR) of 33.8%. The growing market demand for nanocellulose is mainly attributed to its low-density, non-toxic and biodegradability in combination with its unsurpassed quintessential nano-dimensional properties including high aspect ratio and specific surface area, a high degree of crystallinity and transparency, tuneable self-assembly in aqueous media as well as its exceptional mechanical strength. Nanocellulose also holds a unique rheological behavior, good barrier properties and oxygen permeability which are desirable for food applications such as packaging, coating and as additives in food products (Kargarzadeh et al. 2017; Lee et al. 2017; Thomas et al. 2017).

In this chapter, we present the applications of nanocellulose and its composites in the food sector, one of the major growth enablers for the nanocellulose market.

Particularly, we highlight the function of nanocellulose as additives and ingredients in food products and the applications of nanocellulose-based composites in the development of active food packaging and edible coatings. Beforehand, sources, chemical and structural compositions of cellulose followed by nanocellulose and its classification are described.

17.2 Cellulose

17.2.1 Sources of Cellulose

As the most abundant biopolymer on the earth, cellulose has been used for centuries in highly diverse applications, even before its polymeric nature was recognized and well understood. It is a major component of lignocellulosic biomass, which mostly refers to plants or plant-based materials and widely distributed in wood of higher plants, forest and agricultural residues (Torabi et al. 2016).

Based on Fig. 17.2, conventional sources such as wood and cotton are ranked as the primary source of cellulose followed by forestry residues which consist of branches, leaves, bark, and other portions of wood and agricultural residues including palm oil empty fruit bunch, rice straw, rice husk, wheat straw, corn cob, banana rachis, and coconut husk which are mostly left on the fields as post-harvests residue. Industrial waste is the processed waste produced mainly by the food industries such as sugar cane bagasse, vegetable peels (i.e potato, carrot, tomato) and fruit peels (orange, apple, pear, banana), which is another source of cellulose emerging recently

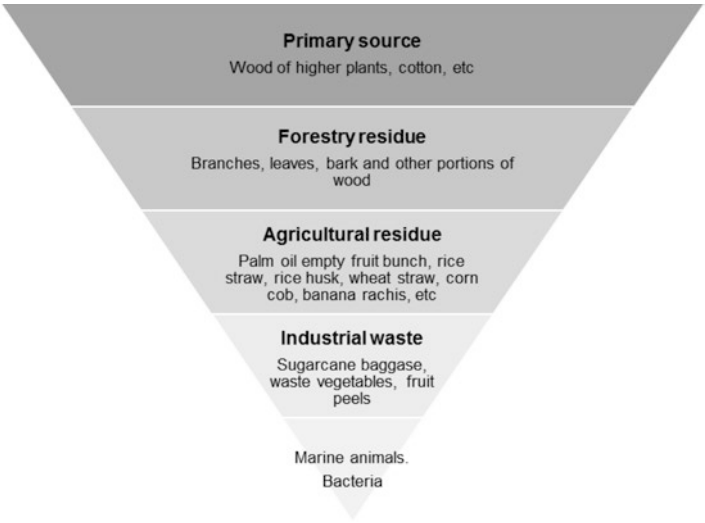

Fig. 17.2 Hierarchy of cellulose from different sources (Source: Torabi et al. 2016)

Table 17.1 Composition of lignocellulosic biomass from different sources (g/100 g of dry matter)

Source	Composition (%)			References
	Cellulose	Hemicellulose	Lignin	
Sugarcane bagasse	51.52	19.07	29.03	Huang et al. (2017)
Banana peel	35.27	19.51	6.68	Tiwari et al. (2019)
Banana peel	12.10	10.20	2.90	Tibolla et al. (2018)
Sugarcane bagasse	47.35	17.86	24.41	Moreno et al. (2018)
Banana rachis	49.12	18.57	20.23	Moreno et al. (2018)
Pineapple leaf	45.32	17.43	25.63	Moreno et al. (2018)
Bamboo	41.72	22.86	20.91	Xie et al. (2016)
Pear peel	38.50	23.60	28.10	Chen et al. (2019a, b)
Rice straw	36.50	38.00	22.00	Oun and Rhim (2018)
Orange bagasse	11.85	15.58	1.67	Mariño et al. (2018)
Unwoven cotton waste	58.72	6.20	15.99	Maciel et al. (2019)

(Rajinipriya et al. 2018). These vary in cellulose content and composition as described in Table 17.1. In addition to its plant origins, cellulose can also be obtained from several marine animals such as tunicate and algae. It is also secreted extracellularly by numerous bacterial species such as Acetobacter, Agrobacterium, Alcaligenes, Pseudomonas, Rhizobium and Sarcina.

17.2.2 Plant Cellulose

Plant fibers are the main natural sources of cellulose. Their hierarchical structure is essential not only for most living plants but also for several industries that take advantage of the outstanding features of natural fibers. Plant fiber wall structure is composed of cellulose molecules, elementary fibril, microfibril, macrofibril and lamellar membrane (Fig. 17.3). It was reported that the elementary fibrils are having a width of around 1.53.5 nm. These elementary fibrils were bundled to form microfibrils, which form the core structural units of the plant cell wall as a mechanism to reduce the free energy of the surface. Each microfibril might contain up to 40 cellulose chains and are 10–30 nm in width. The bundling of microfibrils formed a macrofibril, larger than 100 nm in width (Lee et al. 2017).

Plant cell wall is a complex, heterogeneous network of several components, mainly cellulose, hemicellulose and lignin, and a trace amount of proteins and extractives. Cellulose represents about 35–50% of lignocellulosic biomass dry weight while the remaining 20–35% and 10–25% were accounted for hemicellulose and lignin, respectively (Phanthong et al. 2018). The composition of these three major components is species-, types- and sources-dependent. Lignin keeps the water in fibers which confers the stiffness, strength, and protection to the cell wall and acts as a binder that holds the cellulose and hemicellulose complex. Hemicellulose, which adheres to the cellulose fibrils through hydrogen bonds and

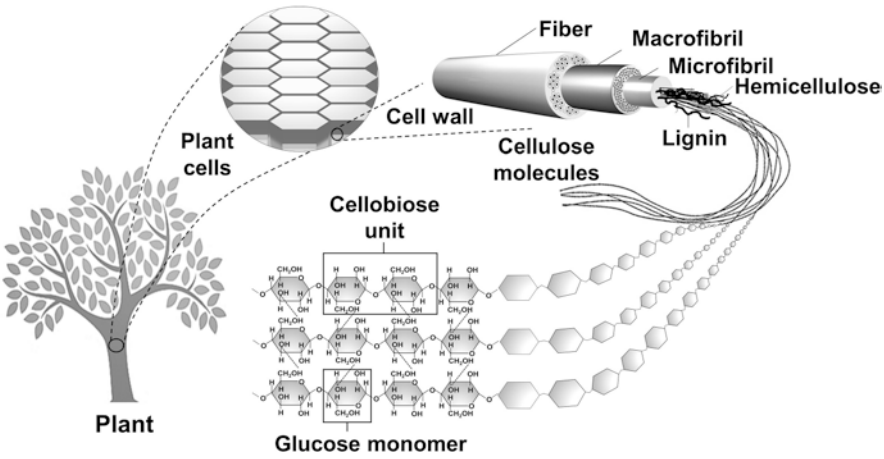

Fig. 17.3 Hierarchical structure of plant fibre. This figure was originally drawn by the author

Van der Waal's interactions and cross-linked with lignin, serves as a compatibilizer between cellulose and lignin (Halib et al. 2017; Kargarzadeh et al. 2017).

17.3 Chemical and Structural Composition of Cellulose

Since its discovery and isolation by a French chemist, Anselme Payen in 1838, the structure and properties of cellulose have been widely studied and highlighted in the literature. As the production of nanocellulose involves a breakdown of cellulose into smaller polymer branches in the nanoscale, it is necessary to comprehend the cellulose chemical and structural composition to give better insight on nanocellulose production (Chen et al. 2019a, b).

Cellulose is a structural polysaccharide, composed of repeating units of two anhydroglucose linked by a β-1,4-glycosidic bond, known as cellobiose. The anhydroglucose unit (AGU) consists of three hydroxyl groups in the equatorial position, responsible for the formation intra- and inter-molecular hydrogen bonding with the adjacent glucose unit in the same chain as well as with the different chains. These strong and tightly packed hydrogen bonding networks in the crystalline part of cellulose fibrils form a stable three-dimensional structure which makes them highly ordered and rigid, insoluble in water and highly resistant to most organic solvents (Kargarzadeh et al. 2017; Phanthong et al. 2018). The internal hydrogen bonds are also responsible for cellulose stiffness (Lee et al. 2017). On the other hand, very weak hydrogen bonds in non-crystalline amorphous domains contribute to the increased hydrophilicity and accessibility of cellulose materials (Kargarzadeh et al.

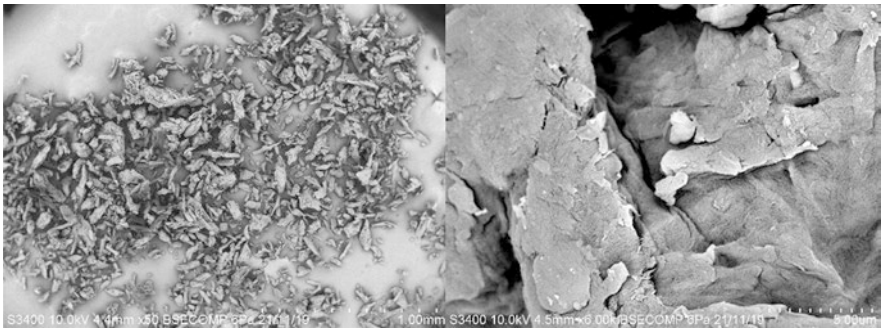

Fig. 17.4 Scanning Electron Microscope (SEM) images of microcrystalline cellulose with different magnifications. The strong and tightly packed hydrogen bonding networks of cellulose fibrils form a stable three-dimensional structure which makes them highly ordered and rigid. This figure is the author's own figure and has not been previously used or published

2017). The morphological structure of microcrystalline cellulose viewed under an electron microscope is shown in Fig. 17.4.

The wide orientation of glucose molecules and hydrogen bonding networks in cellulose producing different allomorphs which can be categorized into cellulose types I, II, III, and IV. Cellulose derived from plant, referred to as native cellulose is mainly found in two crystalline forms, known as cellulose type I and II. For cellulose type I, the hydrogen-bond network is packed in parallel. Chemical regeneration of cellulose type I by acid or alkaline treatment resulted in different arrangements of antiparallel packing of the hydrogen-bond network, known as cellulose type II. Treatment of cellulose type I or II with ammonia resulted in cellulose type III and heating of cellulose type III generates cellulose type IV. Among the four allomorphs, cellulose type I is thermodynamically less stable while cellulose type II has the most stable structure (Lavanya et al. 2011; Phanthong et al. 2018).

Functional groups of cellulose can be identified by using Fourier Transform Infrared (FTIR) spectroscopy. As lignocellulosic materials consist of a combination of cellulose, lignin, hemicellulose, and other constituents, this information is particularly important to determine the cellulose purity prior to nanocellulose isolation. FTIR band assignments for the main constituents in lignocellulosic materials are listed in Table 17.2 (Hospodarova et al. 2018; Sulaiman et al. 2015).

For pure cellulose, the characteristic peaks were located at 3325 cm^{-1}, 2891 cm^{-1} and 1159 cm^{-1}, corresponding to -OH stretching, -CH stretching and -COC stretching absorptions, respectively (Fig. 17.5). The broad -OH stretching vibration band in the 3700–3000 cm^{-1} region gives considerable information regarding inter- and intra-molecular hydrogen bond vibrations. The peaks located at ~1650 cm^{-1} correspond to the vibration of water molecules absorbed in cellulose. The absorption bands at 1426, 1364, 1159, 1027 and 896 cm^{-1} are associated with stretching and bending vibrations of -CH_2 and -CH, -CH and -CO, -COC, and glycosidic bond, respectively. The band at around 1420–1430 cm^{-1} is related to the cellulose crystalline structure, while the band at 897 cm^{-1} is assigned to the amorphous region in cellulose (Hospodarova et al. 2018).

Table 17.2 FTIR band assignments of main components in lignocellulosic materials

Wavenumber (cm^{-1})	Vibration	Component
3400–3300	-OH stretching	Cellulose
2900–2800	-CH symmetrical stretching	Lignin, cellulose
1800–1700	-C=O stretching	Lignin, hemicellulose
1650–1630	Adsorbed water	Water
1505	-C=C aromatic symmetrical stretching	Lignin
1435–1425	-CH_2 symmetrical bending -C=C stretching in aromatic groups	Pectin, Lignin, Hemicellulose
1380–1320	-CH, -CO, aromatic ring	Polysaccharides and cellulose
1240–1230	-CO stretching	Lignin
1162–1159	-COC asymmetrical stretching	Cellulose, hemicellulose
899–895	Glycosidic bond	Polysaccharide
670	-CH out of plane bending	Cellulose

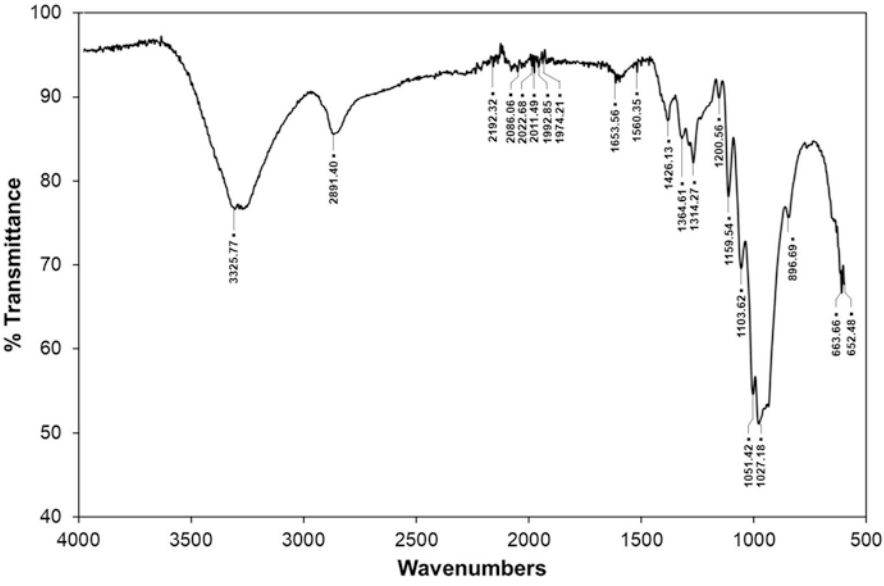

Fig. 17.5 FTIR spectra of pure cellulose (Avicel PH-101)

17.3.1 Nanocellulose

Nanocelluloses refer to cellulosic materials with at least one dimension in the nanoscale. A combination of inherent desirable cellulose properties and fascinating features of nanomaterials have made nanocellulose a promising alternative to replace the conventional materials made from non-renewable resources. Thanks to its biodegradability, lightweight, low density (1.6 g/cm^3), and outstanding mechanical

strength, nanocellulose is currently in high demand worldwide for a wide range of applications. Specifically, nanocellulose has an elastic modulus of up to 220 GPa, greater than Kevlar, tensile strength of up to 10 GPa comparable to cast iron and eight times higher weight to strength ratio than stainless steel (Phanthong et al. 2018). Additionally, nanocellulose offers unprecedented opportunities for surface functionalization due to their abundance reactive surface of hydroxyl groups.

Extraction of nanocellulose from lignocellulosic matters can be performed through chemical, mechanical, biological or combination of two (or more) approaches. Details description of these approaches can be found in Thomas et al. (2017) and Tan et al. (2019). Depending on the sources and extraction methods, nanocellulose can be categorized into three main groups; cellulose nanofibrils (CNFs), cellulose nanocrystal (CNCs) and bacterial nanocellulose (BC) (Table 17.3) (Lee et al. 2017). Although all types of nanocellulose are having similar chemical composition, their morphology, dimension, crystallinity and some other properties are different those largely determine their role in later applications.

17.3.2 Cellulose Nanofibrils (CNF)

Currently the nanocellulose markets are dominated by cellulose nanofibrils (CNF), accounted for more than 50% of market share in 2016 (Transparency Market Research). Several pilot facilities have been developed for CNFs production especially in Japan including Nippon Paper, Oji Paper, and Daicel as well as in other countries such as Finland (VTT), Sweden (Innventia), Canada (Kruger), among

Table 17.3 Terminology and description of different type of nanocellulose (Source: Lee et al. 2017)

Type of Nanocellulose	Other terminology	Description
Cellulose nanofibrils (CNFs)	– Cellulose microfibrils – Microfibrillated cellulose – Nanofibrillated cellulose – Cellulose nanofibers	Diameter: <100 nm Length: up to several microns Isolation process: Top-down (mechanical disintegration, enzymatic hydrolysis)
Cellulose nanocrystals (CNCs)	– Nanocrystalline cellulose – Cellulose nanowhiskers	Diameter: 5–70 nm Length: 100–250 nm (plant); 100 nm to several microns (tunicates, algae, bacteria) Isolation process: Top-down (acid hydrolysis)
Bacterial nanocellulose (BNC)	– Bacterial cellulose – Microbial cellulose – Biocellulose	Diameter: 20–100 nm Length: up to several microns Isolation process Bottom-up approach by bacterial synthesis

others. CNFs are viewed as important advanced biomaterials solutions in the packaging and composites market (Gómez et al. 2016; Tan et al. 2019).

Cellulose nanofibrils are a flexible nano-scale fiber consisting of bundles of elementary nanofibrils that are constructed from alternating crystalline and amorphous domains. As indicated in Table 17.3, CNFs are sometimes referred to as cellulose microfibrils (CMFs), microfibrillated cellulose, nanofibrillated cellulose or cellulose nanofibers. The width of CNFs can vary between 20 to 50 nm and length from 500 nm up to several microns. Isolation of CNFs from lignocellulosic materials can be performed through top-down approach (Fig. 17.6) employing mechanical disintegrations including high-pressure homogenization, cryo-crushing, ball-milling, microfluidization and high-intensity ultrasonication (Thomas et al. 2017).

Large-scale production of CNFs is hampered by the high energy required for the mechanical disintegration of lignocellulosic materials into CNFs. Hence, chemical pre-treatment with acid and/or alkali, or biological pre-treatment with enzymes, are often required to loosen the lignocellulosic structure (Tibolla et al. 2017). It is worth to highlight that CNFs have certain negative properties such as poor compatibility with hydrophobic polymers, which limit their application, especially in the development of composite materials. In this case, chemical modification is necessary to reduce the CNFs hydrophilicity (Kargarzadeh et al. 2017).

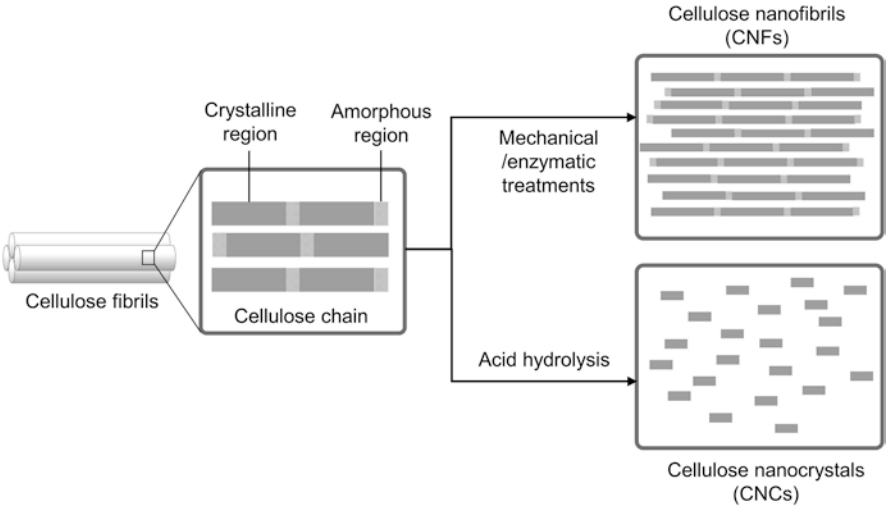

Fig. 17.6 Isolation of nanocellulose by top-down approaches. This figure was originally drawn by the author

17.3.3 Cellulose Nanocrystals (CNCs)

Needle-like nanocellulose, or also known as cellulose nanocrystals (CNCs), nanocrystalline cellulose and cellulose nanowhiskers have a width ranging from 5 to 70 nm. Depending on the sources, the length can vary between 100 to 250 nm for plants, and 100 nm up to several microns for tunicate, algae, and bacteria (Börjesson and Westman 2016).

Isolation of CNCs from cellulosic materials is commonly performed via hydrolysis with strong acid. With simpler procedures and shorter reaction time, sulfuric acid is usually the reagent of choice in comparison with other types of acids such as hydrochloric (HCl), hydrobromic (HBr), and phosphoric (H_3PO_4). CNCs have produced through this process consists of functionalized surface, high crystallinity and good colloidal stability in water. Unfortunately, acid hydrolysis is corrosive, the high tendency of cellulose over-degradation, low yield, requires a large amount of water and generates a huge amount of waste which eventually cause environmental pollution (Chen et al. 2017; Harini et al. 2018; Chen et al. 2019a, b). Given these drawbacks, diluted or organic acids have been suggested to provide milder reaction conditions, but with compromised efficiency. This drawback could be overcome by the addition of metal salt catalysts such as Chromium (III) Nitrate $Cr(NO_3)_3$ as reported by Chen et al. (2019a, b). This co-catalyst promotes complete solubilization of cellulose, hemicellulose and lignocellulosic into water-soluble chemicals and fuels.

17.3.4 Bacterial Nanocellulose (BNC)

Bacterial nanocellulose (BNC) is another kind of nanocellulose. Unlike CNCs and CNFs where the nanocelluloses were isolated through a top-down approach, BNC is synthesized by bacteria through the bottom-up process. Synthesis of BNC involves building up of low molecular weight of sugars by bacteria mainly by *Gluconacetobacter* for a few days up to two weeks. Nanocellulose synthesized by bacteria is free from other typical components in lignocellulosic biomass such as lignin and hemicellulose. BNC has extensive network structure due to the random motion of bacteria, with width ranging from 20 to 100 nm and length from 500 nm up to several microns. (Corral et al. 2017; Kargarzadeh et al. 2017; Sharma et al. 2019)

17.4 Applications

History of cellulose in food application can be traced back to the 1980s when Turbak and his group developed a series of food products using nanocellulose as the stabilizer owing to its exceptional wettability to water over oil, or as an additive in whipped cream, salad dressing and sauces. However, the progress has been stagnant, and this product was not commercially exploited mainly due to the high production costs (Tan et al. 2019). In the 2000s, with the rapid development of nanotechnology, the production and utilization of nanocellulose have received considerable attention, driven by the development of more cost-effective extraction technology and the availability of advanced analytical instruments for nanocellulose characterization. Today, the application of nanocellulose in food industries has grown tremendously especially as food additives, functional food ingredients, active packaging, and edible coating.

17.4.1 Food Additives and Stabilizers

Nowadays, a new generation of food products which combined the health benefits and excellent sensory quality is in high demand. In the development of food products, additives such as enzymes, emulsifiers, oxidants, and hydrocolloids are usually used to facilitate processing, improving microstructure for elevated mouth-feel and preserve the freshness of food products (Tan et al. 2019). With the distinctive rheological behavior in combination with the multifaceted advantages of nano-scale materials, nanocellulose-based additives are of great interest to be used as an emulsifying and stabilizing agent of food products such as salad dressings, foams, puddings, among others (Camacho et al. 2017; Gómez et al. 2016).

The potential use of bacterial nanocellulose as an additive in bread-making has been studied through thermo-rheological and dynamic oscillatory experiments by Corral et al. (2017). The addition of BNC has resulted in improved bread quality, reducing browning index, increasing the specific volume, porosity, luminosity, and moisture content. Moreover, the bread produced was more tenders and have less firm crumb than the control formulation without BNC, which make it more acceptable to the consumer. Based on these promising findings, in 2017, Marchetti and co-workers have employed BNC as an additive for the development of low-lipid and low-sodium meat sausages. The sausages show improvement in water-binding properties, hardness, cohesiveness, and chewiness with the addition of up to 0.267 g of dry BNC/100 g of batter was added. Besides act as fat mimetic and at the same time, the BNC could maintain the quality of the sausage with shelf-life of 45 days under vacuum refrigerated storage. Very recently, Marchetti et al. (2019) have investigated the rheological behavior of BNC-formulated gluten-free muffin. Low concentration of dry BNC (0.12 to 0.18 g/100 g) in the raw batter could produce batter with high elasticity, low specific gravity, and low flow indexes. The high viscosity

of the batter due to the addition of BNC could entrap more air and ultimately improve the volume of the baked product.

Besides improving the food products characteristic, many efforts have been devoted to the development of additives as a low-calorie fat replacer. This is due to the growing concern over the adverse health effect of foods with a high content of fat (Franco 2018). Removing fat from a food product is a possible and easiest solution, but the desirable properties such as flavor, aroma, and texture are compromised. Therefore, the addition of the so-called ''fat replacer' is a promising alternative. In general, fat replacers can be obtained from protein and carbohydrates. In most cases, a combination of several fat replacers is necessary to obtain fat-mimicking properties (Aaen et al. 2019).

Nanocellulose-based materials have recently been proposed as a low-calorie fat replacer for food products due to their availability and excellent viscosifying and gel-forming abilities. However, the interaction between the charged nanocellulose and other food components such as electrolytes and additives might affect their rheological behavior. With this view in mind, Aaen and co-workers (2019) have studied the rheological interactions of TEMPO-oxidized CNFs with pure water, electrolyte solutions and xantham gum, the commonly used food additives. Their findings suggest the applicability of CNFs as fat replacers in food products, even at low concentrations. The presence of salt in food could reduce the amount of CNFs required to obtain the desired storage modulus even further. It is worth noted that the interaction of highly charged CNFs with high salt content may promote aggregation of the CNFs component.

Nanocellulose has also been used as a food stabilizer owing to its well-dispersibility in water and self-assembled properties. The electrostatic interaction among the hydroxyl groups leading to the formation of a sol-gel structure and promoting stabilization of oil in water emulsion by the formation of a steric barrier at the oil and water interface. The addition of nanocellulose in the range of 0.10 to 0.30 wt% has shown to improve the stability of ice cream based on the melting and falling time. Besides significant improvement in stability, the addition of a small amount of nanocellulose could eliminate the need to change the composition of the ice-cream mix, thus the good flavor and texture of the frozen dessert could be maintained (Gómez et al. 2016).

17.4.2 Functional Food Ingredients

According to Functional Food Centre (FFC), functional food is defined as "Natural or processed foods or food ingredients that contains known or unknown biologically-active compounds; which in defined amounts provide a clinically proven and documented health benefit for the prevention, management, or treatment of chronic disease" (Gómez et al. 2016). Based on this definition, nanocellulose, especially in the form of nanofibrils (CNFs) could be considered as a potential functional food

ingredient owing to their dietary fiber characteristics that able to give positive health effects especially gastrointestinal related diseases.

As mentioned previously, CNFs have distinctive properties when compared to other sources of food fibers. For example, CNFs of approximately 18 nm in width and high aspect ratio derived from Parenchyma cells of pears and apples by one-time fibrillation using grinding apparatus is expected to improve the nutritional and technological properties of foods. Moreover, with their high viscosity and good dispersibility in water, the CNFs produced could be a good candidate in the formulation of functional foods (Ifuku et al. (2011).

While various studies have proved the potential of nanocellulose to be used as food ingredients based on the quality attributes, limited information is available on their effectiveness with regard to the improvement of human health, safety aspects, and possible side effects. Thus, biological, biochemical and histological tests on mice supplemented with an increasing amount of CNFs have been conducted by Andrade et al. (2015) to find the effect of the addition of CNFs on their health condition. Accordingly, no significant changes in the blood sugar level, lipid profile, and mineral nutrients were observed within the range of CNFs concentration studied. More importantly, the CNFs did not cause an adverse effect on the animals' hepatic system and metabolism.

The health benefits of nanocellulose-supplemented food products such as milk, soy protein isolate, whey protein isolate, and starch have been reported by Liu and co-workers in a series of studies utilizing three types of nanocellulose; CNFs, CNCs, and TEMPO-CNFs. Overall, the presence of the nano-scale dietary fiber could improve gastrointestinal health, glucose tolerance, insulin response, promotes satiation, thus benefiting weight loss. The positive correlation between nanocellulose and gastrointestinal health is further supported by a recent study conducted by Chen et al. (2019a, b). Oral consumption of CNFs by Western diets (WD)-fed mice at a sub-chronic concentration of 30 mg/kg body weight could decrease fat absorption in the jejunum and protected the liver from a high-fat burden.

17.4.3 Active Packaging

The importance of packaging in the protection, communication, convenience and containment of goods is undisputable. However, these basic functions are no longer sufficient as society demand for a new generation of packaging with improved functionalities to prolong the shelf-life and reduce the growth rate of microorganism in food products. Hence, research and development in the field of 'active' packaging have increased tremendously in the last few years (Gómez et al. 2016).

Active packaging is the new generation of packaging materials designed to deliver protective agents such as antimicrobial agents, preservatives, antioxidants, and oxygen and moisture barrier. Polycarbonate- and polyethylene-based packaging with antimicrobial agents such as copper, zinc and phenolic substances have been widely reported (Lee et al. 2017). With the increasing concern over the

environmental impact of petroleum-based packaging, trends have now shifted towards the use of green, sustainable and biodegradable polymers from natural resources particularly cellulose-based materials (Rajinipriya et al. 2018; Tan et al. 2019).

While cellulose can form strong and stiff packages, the barrier properties are not comparable to those of the synthetic polymers. The breakings down of cellulosic materials have produced nanocellulose with promising properties for active packaging applications. Films made from nanocellulose have a high air and oxygen barrier. It has been reported that the oxygen permeability of nanocellulose films with thickness of 21 ± 1 mm was 17 ± 1 ml m^{-2} day^{-1}, competitive with those made from synthetic polymers such as ethylene-vinyl alcohol (EVOH) (3–5 ml m^{-2} day^{-1}) and polyvinylidene chloride (PVdC) films (9–15 ml m^{-2} day^{-1}) of roughly the same thickness. The excellent barrier properties of nanocellulose film are mainly contributed by its high crystallinity, tight fiber network; entangle structure and dense fiber packing (Gómez et al. 2016).

Despite this outstanding feature, the oxygen permeability of nanocellulose films is strongly influenced by relative humidity. At high humidity, the interaction of nanocellulose with water molecules caused the film to swell and increasing the oxygen permeability. Several modifications have been implemented to overcome this drawback. One such example is by developing a nanocellulose composite film. Active packaging made from nanocellulose-based composite such as CNFs/PPy/PVA (Bideau et al. 2017), poly(sulfobetaine methacrylate) (PSBMA)/BNC (Vilela et al. 2019) and clove oil/chitosan/β-cyclodextrin citrate/CNFs (Adel et al. 2019), have shown improved hydrophobicity and mechanical properties as well as combines the biodegradability, antibacterial and antioxidant properties for active packaging.

17.4.4 Edible Coating

The edible coating is usually made from starch due to its high transparency, odorless, tasteless and semi-permeability. However, starch-based films exhibit poor water resistance and mechanical strength. Incorporation of nanomaterials in starch films could be an effective strategy to overcome these limitations. Jeevahan and coworkers (2019) have shown that nanocellulose obtained from banana pseudostems has improved film properties of rice starch-based edible films. This work was further extended to other types of starch including wheat, maize, and potato, and similar findings were observed. Besides improving the mechanical and barrier properties, nanocellulose can also act as an antimicrobial agent and oxygen scavenger.

Another example of the application of nanocellulose in edible food coating in the development of agar-based edible film (Wang et al. 2018). Crystallinity, thermal stability and tensile strength of the edible film were improved with the addition of bacterial nanocellulose with concentration ranging between 3 to 10 wt%. Significantly decreased moisture content, water solubility, and water permeability

was also observed. This indicates that nanocellulose has high potential to be used as reinforcing material in edible food coating.

17.5 Conclusion and Outlook

Nanocellulose is an inexhaustible and sustainable material derived from lignocellulosic biomass with ground-breaking applications in the food industry. The fundamental characteristics that make nanocellulose a fascinating material are the fact that it combines the inherent properties of cellulose (low-density, biodegradability, non-toxicity) and nano-dimensional characteristics including high surface area, high aspect ratio, and extensive hydrogen bonding ability. These features contribute to high crystallinity and excellent mechanical strength of nanocellulose. For food applications, its unique rheological behavior, good barrier properties, and oxygen permeability are particularly attractive. It should be noted that while the role of nanocellulose in improving food quality attributes is indubitable, information on the safety aspects and possible side effects of nanocellulose is still limited, which calls for more and in-depth investigation. Moreover, as the current extraction processes mainly rely on acid hydrolysis, more environmentally friendly approaches are highly sought.

Acknowledgements This project is funded by Universiti Malaysia Sabah (PHD0020-2019) and Ministry of Education, Malaysia (RACER/1/2019/TK10/UMS//1).

References

Aaen R, Simon S, Wernersson Brodin F, Syverud K (2019) The potential of TEMPO-oxidized cellulose nanofibrils as rheology modifiers in food systems. Cellulose 26(9):5483–5496. https://doi.org/10.1007/s10570-019-02448-3

Adel AM, Ibrahim AA, El-Shafei AM, Al-Shemy MT (2019) Inclusion complex of clove oil with chitosan/β-cyclodextrin citrate/oxidized nanocellulose biocomposite for active food packaging. Food Packag Shelf Life 20(December 2018):100307. https://doi.org/10.1016/j.fpsl.2019.100307

Andrade DRM, Mendonça MH, Helm CV, Magalhães WLE, de Muniz GIB, Kestur SG (2015) Assessment of nano cellulose from peach palm residue as potential food additive: Part II: Preliminary Studies. J Food Sci Technol 52(9):5641–5650. https://doi.org/10.1007/s13197-014-1684-0

Bideau B, Bras J, Adoui N, Loranger E, Daneault C (2017) Polypyrrole/nanocellulose composite for food preservation: barrier and antioxidant characterization. Food Packag Shelf Life 12:1–8. https://doi.org/10.1016/j.fpsl.2017.01.007

Börjesson M, Westman G (2016) Crystalline Nanocellulose — preparation, modification, and properties. In: Cellulose fundamental aspects and current trends the, p 13. https://doi.org/10.5772/57353

Camacho M, Ureña YRC, Lopretti M, Carballo LB, Moreno G, Alfaro B, Vega Baudrit JR (2017) Synthesis and characterization of nanocrystalline cellulose derived from pineapple peel residues. J Renew Mater 5(3–4):271–279. https://doi.org/10.7569/JRM.2017.634117

Chen YW, Tan TH, Lee HV, Hamid SBA (2017) Easy fabrication of highly thermal-stable cellulose nanocrystals using Cr(NO3)3 catalytic hydrolysis system: a feasibility study from macroto nano-dimensions. Materials 10(1). https://doi.org/10.3390/ma10010042

Chen Y, Lin YJ, Nagy T, Kong F, Guo TL (2019a) Subchronic exposure to cellulose nanofibrils induces nutritional risk by non-specifically reducing the intestinal absorption. Carbohydr Polym (June):115536. https://doi.org/10.1016/j.carbpol.2019.115536

Chen YW, Hasanulbasori MA, Chiat PF, Lee HV (2019b) Pyrus pyrifolia fruit peel as sustainable source for spherical and porous network based nanocellulose synthesis via one-pot hydrolysis system. Int J Biol Macromol 123:1305–1319. https://doi.org/10.1016/j.ijbiomac.2018.10.013

Corral ML, Cerrutti P, Vázquez A, Califano A (2017) Bacterial nanocellulose as a potential additive for wheat bread. Food Hydrocoll 67:189–196. https://doi.org/10.1016/j.foodhyd.2016.11.037

Franco TS (2018) Nanocellulose in food science and technology - potential, advantages and gaps of research. Nov Tech Nutr Food Sci 1(3):2016–2017. https://doi.org/10.31031/ntnf.2018.01.000514

Global Market Insights. Inc (2019). https://www.gminsights.com/pressrelease/nanocellulose-market

Gómez HC, Serpa A, Velásquez-Cock J, Gañán P, Castro C, Vélez L, Zuluaga R (2016) Vegetable nanocellulose in food science: a review. Food Hydrocoll 57:178–186. https://doi.org/10.1016/j.foodhyd.2016.01.023

Halib N, Perrone F, Cemazar M, Dapas B, Farra R, Abrami M et al (2017) Potential applications of nanocellulose-containing materials in the biomedical field. Materials 10(8):1–31. https://doi.org/10.3390/ma10080977

Harini K, Ramya K, Sukumar M (2018) Extraction of nano cellulose fibers from the banana peel and bract for production of acetyl and lauroyl cellulose. Carbohydr Polym 201(June):329–339. https://doi.org/10.1016/j.carbpol.2018.08.081

Hospodarova V, Singovszka E, Stevulova N (2018) Characterization of cellulosic fibers by FTIR spectroscopy for their further implementation to building materials. Am J Anal Chem 09(06):303–310. https://doi.org/10.4236/ajac.2018.96023

Huang J, Liu Y, Sun B, Shang Z (2017) Microwave-assisted alkali extraction of bagasse hemicellulose enhanced by an enzymatic pretreatment process. J Bioresour Bioprod 2(3):105–109. https://doi.org/10.21967/jbb.v2i3.117

Ifuku S, Adachi M, Morimoto M, Saimoto H (2011) Fabrication of cellulose nanofibers from parenchyma cells of pears and apples. J Fiber Sci Technol 67(4):86–90. https://doi.org/10.2115/fiber.67.86

Jeevahan JMC (2019) Influence of nanocellulose additive on the film properties of native rice starch based edible films for food packaging. Recent Pat Nanotechnol. https://doi.org/10.2174/1872210513666190925161302

Kargarzadeh H, Ioelovich M, Ahmad I, Thomas S, Dufresne A (2017) Methods for extraction of Nanocellulose from various sources. In: Handbook of Nanocellulose and Cellulose Nanocomposites, pp 1–49. https://doi.org/10.1002/9783527689972.ch1

Lavanya D, Kulkarni PK, Dixit M, Raavi PK, Krishna LNV (2011) Sources of cellulose and their applications – a review. Int J Drug Formul Res 2(6):19–38

Lee H, Sundaram J, Mani S (2017) Production of cellulose nanofibrils and their application to food: a review. In: Nanotechnology: food and environmental paradigm, pp 1–344. https://doi.org/10.1007/978-981-10-4678-0

Maciel MMÁD, Benini KCC d C, Voorwald HJC, Cioffi MOH (2019) Obtainment and characterization of nanocellulose from an unwoven industrial textile cotton waste: effect of acid hydrolysis conditions. Int J Biol Macromol 126:496–506. https://doi.org/10.1016/j.ijbiomac.2018.12.202

Marchetti L, Muzzio B, Cerrutti P, Andrés SC, Califano AN (2017) Bacterial nanocellulose as novel additive in low-lipid low-sodium meat sausages: Effect on quality and stability. Food Struct 14(March), 52–59. https://doi.org/10.1016/j.foostr.2017.06.004

Mariño MA, Rezende CA, Tasic L (2018) A multistep mild process for preparation of nanocellulose from orange bagasse. Cellulose 25(10):5739–5750. https://doi.org/10.1007/s10570-018-1977-y

Moreno G, Ramirez K, Esquivel M, Jimenez G (2018) Isolation and characterization of nanocellulose obtained from industrial crop waste resources by using mild acid hydrolysis. J Renew Mater 6(4):362–369. https://doi.org/10.7569/JRM.2017.634167

Oun AA, Rhim JW (2018) Isolation of oxidized nanocellulose from rice straw using the ammonium persulfate method. Cellulose 25(4):2143–2149. https://doi.org/10.1007/s10570-018-1730-6

Phanthong P, Reubroycharoen P, Hao X, Xu G, Abudula A, Guan G (2018) Nanocellulose: extraction and application. Carbon Resour Convers 1(1):32–43. https://doi.org/10.1016/j.crcon.2018.05.004

Rajinipriya M, Nagalakshmaiah M, Robert M, Elkoun S (2018) Importance of agricultural and industrial waste in the field of nanocellulose and recent industrial developments of wood based nanocellulose: a review. ACS Sustain Chem Eng 6(3):2807–2828. https://doi.org/10.1021/acssuschemeng.7b03437

Sharma A, Thakur M, Bhattacharya M, Mandal T, Goswami S (2019) Commercial application of cellulose nano-composites – a review. Biotechnol Rep 21(2018):e00316. https://doi.org/10.1016/j.btre.2019.e00316

Sulaiman S, Mokhtar MN, Naim MN, Baharuddin AS, Salleh MAM, Sulaiman A (2015) Study on the preparation of cellulose nanofibre (CNF) from Kenaf Bast fibre for enzyme immobilization application. Sains Malaysiana 44(11):1541–1550

Tan KW, Heo SK, Foo ML, Chew IML, Yoo CK (2019) An insight into nanocellulose as soft condensed matter: challenge and future prospective toward environmental sustainability. Sci Total Environ 650:1309–1326. https://doi.org/10.1016/j.scitotenv.2018.08.402

Thomas B, Raj MC, Athira KB, Rubiyah MH, Joy J, Moores A, Drisko GL (2017) Nanocellulose, a versatile green platform : from biosources to materials and their applications. Chem Rev. https://doi.org/10.1021/acs.chemrev.7b00627

Tibolla H, Pelissari FM, Rodrigues MI, Menegalli FC (2017) Cellulose nanofibers produced from banana peel by enzymatic treatment: study of process conditions. Ind Crop Prod 95:664–674. https://doi.org/10.1016/j.indcrop.2016.11.035

Tibolla H, Pelissari FM, Martins JT, Vicente AA, Menegalli FC (2018) Cellulose nanofibers produced from banana peel by chemical and mechanical treatments: characterization and cytotoxicity assessment. Food Hydrocoll 75:192–201. https://doi.org/10.1016/j.foodhyd.2017.08.027

Tiwari G, Sharma A, Kumar A, Sharma S (2019) Assessment of microwave-assisted alkali pretreatment for the production of sugars from banana fruit peel waste. Biofuels 10(1):3–10. https://doi.org/10.1080/17597269.2018.1442665

Torabi M, Drahansky M, Paridah M , Moradbak A, Mohamed A , Owolabi F abdulwahab taiwo, … Abdul Khalid SH (2016) We are IntechOpen, the world ' s leading publisher of Open Access books Built by scientists, for scientists TOP 1%. *Intech*, *i*(tourism), 13. https://doi.org/10.5772/57353

Vilela C, Moreirinha C, Domingues EM, Figueiredo FML, Almeida A, Freire CSR (2019) Antimicrobial and conductive nanocellulose-based films for active and intelligent food packaging. Nano 9(7):1–16. https://doi.org/10.3390/nano9070980

Wang X, Guo C, Hao W, Ullah N, Chen L, Li Z, Feng X (2018) Development and characterization of agar-based edible films reinforced with nano-bacterial cellulose. Int J Biol Macromol 118:722–730. https://doi.org/10.1016/j.ijbiomac.2018.06.089

Xie J, Hse CY, De Hoop CF, Hu T, Qi J, Shupe TF (2016) Isolation and characterization of cellulose nanofibers from bamboo using microwave liquefaction combined with chemical treatment and ultrasonication. Carbohydr Polym 151:725–734. https://doi.org/10.1016/j.carbpol.2016.06.011

Chapter 18
Nanocomposite Materials in Food Packaging: Opportunities, Challenges and Safety Assessment

Ku Nur Izzati Ku Mohamad Faudzi, Srimala Sreekantan, Rabiatul Basria S. M. N. Mydin, and Nur Afiqah Amalina Romli

18.1 Introduction

Nanotechnology by using nanocomposite is a promising future in food packaging applications in the global market. The capabilities of nanocomposite to improve mechanical, thermal, barrier and other properties has urged the researchers to explore more on this area. The common applications are used for food packaging such as active packaging, intelligent packaging, surface biocides, nanocoating, nano sensors, nutrition and nutraceuticals and bioplastics. However, the challenges occur when the unknown potential risks to human health is questioned by the society including ability of nanoparticles to migrate and the leaching mechanisms of nanoparticles leaching. This chapter discussed how nanocomposite plays an important role in food industry especially in food packaging. The opportunities, challenges and safety assessment were explained clearly to give overview to the reader the importance of nanotechnology.

Ku Nur Izzati Ku Mohamad Faudzi
School of Materials and Mineral Resources Engineering, Engineering Campus, Universiti Sains Malaysia, Nibong Tebal, Pulau Pinang, Malaysia

Oncological and Radiological Sciences Cluster, Advanced Medical & Dental Institute, Universiti Sains Malaysia, Kepala Batas, Malaysia

S. Sreekantan (✉)
School of Materials and Mineral Resources Engineering, Engineering Campus, Universiti Sains Malaysia, Nibong Tebal, Pulau Pinang, Malaysia
e-mail: srimala@usm.my

Rabiatul Basria S. M. N. Mydin (✉) · N. A. A. Romli
Oncological and Radiological Sciences Cluster, Advanced Medical and Dental Institute, Universiti Sains Malaysia, Kepala Batas, Pulau Pinang, Malaysia
e-mail: rabiatulbasria@usm.my

S. Siddiquee et al. (eds.), *Composite Materials: Applications in Engineering, Biomedicine and Food Science*, https://doi.org/10.1007/978-3-030-45489-0_18

The breakthrough and rapid developments of nanotechnologies has become one of the significant technological advances in every sector and areas including agricultural, electronics, food processing, forestry, environmental problems, water industry, energy production, waste resources, packaging materials, solar energy, automotive and biomedical uses (Kim et al. 2018; Müller et al. 2017). Recent technological developments have enabled the researchers to develop high performance food packaging that prolongs food quality, food safety, shelf life and expanding their marketing potential. The problems with food packaging nowadays include solid waste problem, lack of recyclability, poor mechanical strength, thermal instability, poor barrier properties, brittleness, high water vapour and oxygen permeability (Peelman et al. 2013; Othman 2014; Han et al. 2018). As one of the emerging materials, nanocomposite materials had been used as an alternative approach to overcome these issues. In 1950, the invention by Carter, Hendricks and Bolley brought the discovery of novel reinforced elastomer where the modified clay was mixed thoroughly with latex of elastomeric material thus resulting in increment of hardness, modulus and tensile strength, respectively. This finding is the starting point for the development of integrating nanoparticles with polymer matrix up until now. The utilisation of nanotechnology in the food packaging applications may contribute to the significant impact on the food industry in the near future.

Nanocomposite can be defined as a multiphases solid material matrix where nanosized particles have been added with dimensions of less than 100 nanometres (nm) in order to enhance any particular properties of the materials (De Azeredo et al. 2011). Nanoparticles (NPs) can offer larger surface area which favours filler-matrix interactions, properties and performance of the resulting materials. They can increase barrier properties, increased mechanical strength and enhance heat resistance. Previous studies have reported the incorporation of nanoparticles inside the matrices will improve the barrier, mechanical, thermal and biodegradable properties (Moura et al. 2009; Honarvar et al. 2016; Jawaid et al. 2017). A study demonstrated the usage of nanosized montmorillonite clay together with nylon were able to boost the mechanical properties of the materials. The nylon 6-organoclay nanocomposites which prepared by direct melt compounding had a well dispersion composition with significant increment of mechanical properties. The tensile strength of Nylon 6 (N6) without nanoparticles was 64.2 ± 0.8 MPa, N6/montmorillonite was 75.4 ± 0.3 MPa and N6/organoclay was 83.4 ± 0.7 MPa. These results indicated the addition of NPs increased the strength of N6 in overall (Cho and Paul 2001). Luis Feijoo et al. 2006 discovered mixing of poly(lactic acid) (aPLA), poly- caprolactone (PCL) and clay enhanced mechanical, thermal and gas barrier properties of the materials. Based on this finding, there is an enhancement on mechanical properties and thermal stability while maintaining the barrier properties. From TGA mass loss curves, there is an increment in the temperature of the maximum weight loss rate from the mixture of aPLA with PCL.

According to Moura et al. (2009), hydroxypropyl methylcellulose (HPMC) with chitosan/tripolyphosphate nanoparticles improved the mechanical and film barrier properties. The vacant inside HPMC matrix were filled with chitosan nanoparticles contributing to their compact and dense structure. The presence of nanoparticles in

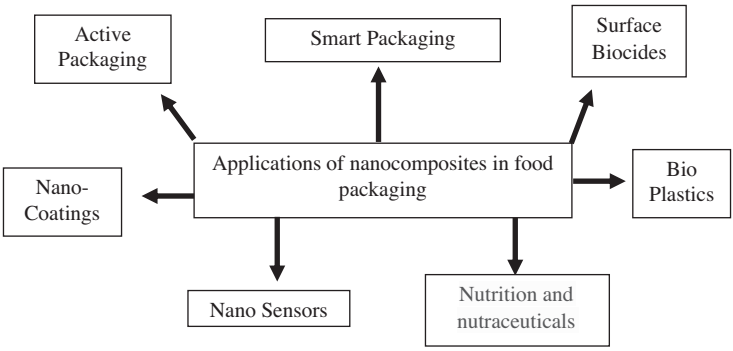

Fig. 18.1 Applications of nanocomposites in food packaging (Source: Vasile 2018)

the films raised the thermal stability from 232 °C to 271 °C as shown by two-way ANOVA. For tensile properties, the tensile strength of HPMC matrix without NPs value change from 28.3 ± 1.0 MPa rising to 62.6 ± 1.0 MPa when the particle size is 85 nm. The existence of NPs in the films reduced the water vapour permeability of the HPMC films because of the formation of hydrogen bonding between chitosan and HPMC film matrix. Other study done by Casariego et al. (2009) showed chitosan/clay films water vapor barrier properties and tensile strength upgraded significantly. After MNC was dispersed in the film matrix, the water vapour barrier property improved and the best value was found when the films have the lowest concentrations of chitosan. The tensile strength increased ($p < 0.05$) with increasing chitosan concentration.

In terms of food packaging, polymers commonly used either as matrices or substrates are low density and high density polyethylene (LDPE and HDPE), polypropylene (PP), polyethylene terephthalate (PET), ethylene vinyl alcohol (EVOH) copolymer, polyamide (PA), polystyrene (PS), polyhydroxyalkanoates (polyhydroxybutyrate (PHB), poly(hydroxybutyrate-co-hydroxyvalerate) (PHBV)), poly (lactic acid) (PLA), polycaprolactone (PCL), polyvinyl chloride (PVC), polyethylene terephthalate (PET) and polyvinyl alcohol (PVOH). Another examples of nanoparticles particularly used for food packaging; zinc oxide (ZnO), silver (Ag), copper (Cu), chitosan, talc, zein, titanium oxide (TiO_2), chitin and cellulose (Chang et al. 2010; De Lima et al. 2010; Espitia et al. 2012; Longano et al. 2012; Tankhiwale and Bajpai 2012; Abdollahi et al. 2013; Othman et al. 2014; López et al. 2015; Carbone et al. 2016; Oymaci and Altinkaya 2016). Figure 18.1 summarised applications of nanocomposites in food packaging.

The aims and objectives of using nanotechnology in polymer nanotechnology is basically to enhance principle features of conventional packaging system like ease of transportation and handling; convenience, protection, preservation and marketing. The well-known applications of food packaging include (1) active packaging: nanoparticles will correspond to the food and environment contributing to food preservation; (2) intelligent packaging: nanodevices will sense biochemical or microbial changes in the food or environment, (3) surface biocides: nanoparticles

with antimicrobial properties is used on the surface of packaging material, (4) nanocoatings, (5) nanosensors, (6) nutrition and nutraceuticals and (7) bioplastics (Vasile 2018).

18.2 Opportunities

18.2.1 Barrier Resistance

Numerous types of food and plastics bottle that used plastic wrapping exploit nanomaterials to modify the barrier properties of the materials. The problem with standard packaging films made from plastic is they can be easily penetrable and permeable gases (oxygen, carbon doxide and others), water vapour which resulting in food spoilage (Fig. 18.2) (Siracusa 2012). The coating from metal or glass is somewhere unacceptable due to their impracticality in terms of reducing flexibility and high cost. Thus, this is where nanotechnology becomes useful.

Polymer nanocomposite provide outstanding barrier properties as they have highly dispersed nanofillers with large aspect ratios in polymer matrix impermeable to water molecules and increase the diffusion path (Shankar and Rhim 2016). Nano sensors based on conducting polymers like gas sensors have been developed by researchers to evaluate, identify and/or quantify microbes based on their gas release (Pereda et al. 2018). The nanoparticles are embedded inside polymer matrix to enable gas detection from the microorganisms. Some examples of nanoparticles used for nano sensors are gold, ZnO and TiO_2 nanoparticles (Chellaram et al. 2014).

18.2.2 Traceability and Authenticity

On the other hand, nano sensors also have the ability to trace and track microbes, toxins, and contaminants that occur before or after food processing by controlling internal and external conditions of the food. Previous study has reported nano sensors also can function as 'Active Transport Tracking Devices' to monitor process of

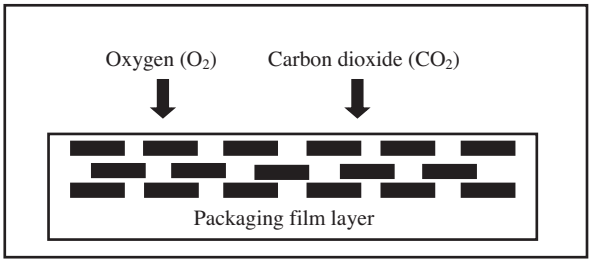

Fig. 18.2 Gases penetrating (O_2, CO_2 and others gases) through packaging film layer in standard packaging films. (Source: Siracusa 2012)

transportation and proper handling conditions of food. Other than that, it also can identify damage such as sudden shocks or seal damage (Lu and Bowles 2013).

18.2.3 Preservation or Shelf-Life

The food products in stores usually has short shelf-life as they are exposed to varying conditions and factors that affect the food condition. It is vital to preserve the quality of food because consumers demand for safe and fresh food. Food packaging can conserve the food throughout the distribution chain from being contaminated by physical, chemical and biological contaminants (Guilbert et al. 1996). The ability of nanocomposite for nanoencapsulation to extend longer shelf-life is done by prevent or deceleration degradation processes.

18.3 Challenges

In the last few years, the fast development of novel processing methods for food preservation of a number of products have marketed in order to improve safety, quality and shelf life of packaged foods gave place to crucial challenges of knowledge that must be filled in the area of suitable packaging materials. Most of food nanotechnology or nanocomposite food packaging applications shall be undergo process of permission before being approved for legal utilization in industry.

The most challenging concerns about nanotechnology use for food packaging regarding their reduced particle size, because it reveal discrete chemical and physical characteristics which quite different from their macroscale chemical counterparts (Huang, Li and Zhou 2015). According to Munro et al. (2009), this issues concerning about their findings of toxicity studies on conventional form of large particles may be different due to their very small sizes for determining their toxicity profiles. The decisions and approval by GRAS or generally known as safe is the troublesome part because the conclusion have been made without any consideration of the size or the nanoscale safety evaluations (Huang et al. 2015). Lack of bioavailability and toxicokinetic of nanomaterials are the limiting factors in conducting risk assessments with the reported cases stated that this engineered nanomaterials are potentially harmful to human health. However, there is insufficient evidence to apply the precautionary principle to all applications, especially in the food industry. The considerations on the nanomaterials type and their claimed added value for the product is important for initiate and organize any regulation in this field. Sufficient new scientific knowledge could provide consistent and comprehensive screening and protection for consumers.

An Institute of Food Science and Technology (IFST) report by recommending nanomaterials serve as new and as potentially harmful materials before their safety is proved to be used for consumer due to lessen their possible effects on human

health (Huang et al. 2015). Furthermore, the European Food Safety Authority (EFSA) stated that a prudent, case-by-case risk assessment is required for substances deliberately engineered to particle size which exhibit functional, physical and chemical properties that significantly differ from those at a larger scale until more information is available about nanoscience and nanotechnologies (Network et al. 2010). Based on Llorens et al. (2012), the requirement on *in vitro* and *in vivo* studies are needed if it failed to demonstrate that there is no nanomaterial migration after formulation and also changes of nanomaterial neither before nor during digestion.

The Food and drug Administration (FDA) formed the Nanotechnology Task Force to ensure the safety and efficacy of nanoscale products (Thostenson et al. 2005) and being evaluated case-by-case according to approved standard (Sandoval 2009). The challenges face by FDA is the complexities of nanotechnologies since there is no labeling prerequisites for such products that state whether nanotechnology has been used in their production to assess their safety (Sandoval 2009). The expectations exist between consumers and commercial developments about regulating nanotechnologies because most manufacturers thought that approval by FDA regulation is sufficient for marketing the nano-based products. Currently, the legislation show the nano-based products and those made by ordinary manufacturing approaches are treated-like similar causes the specific or overall migration limits into food contact with nanomaterials have been not evaluated and their safety is not guarantee (Busolo and Lagaron 2012).

18.4 Safety Assessment

The utilization of biodegradable or natural polymers in food packaging is controllable due to their weak barrier and mechanical properties (Honarvar et al. 2016). Nanocomposite materials markedly promote packaging characteristics due to their nanometer size dispersion by improving modulus and strength, decrease gas permeability, and increase water resistance (Youssef 2013). However, enhancement in general performances of food packaging modification can be reached by incorporating of even low percentages of nanofillers, such as clay into these biopolymers which believed can preserve the food against external factors and increase the food's stability through antimicrobial properties and/or responding to environmental changes. Despite of several benefits of nano-materials in food packaging, it may cause safety issues to human health since they show different physicochemical properties from their macro-scale chemical counterparts (Honarvar et al. 2016) (Table 18.1).

The selection of proper choice of packaging materials are crucial for obtaining a suitable shelf life with convenient physical protection which provide the good physicochemical conditions for every products (Youssef 2013). The packaging system enrich with appropriate gas (O_2, CO_2) and water vapour barrier and mechanical properties, possessing good physicochemical or biological factors can avoid

Table 18.1 Nanomaterials utilized in food packaging related to safety assessment

Nanomaterials	Physical, chemical and biological activity	Applications in food system	Safety assessment
Silver-based nanoparticles	Improved barrier and mechanical performances Low transparency Thermal stability Good anti-microbial activity inhibiting both gram-positive and gram-negative bacteria Higher anti-oxidant activity of the biosynthesized from persimmon byproducts	**Nuts**: extending the shelf-life of nuts with the highest shelf-life of hazelnuts, almonds, pistachios and walnuts extended to 18, 19, 20 and 18 months respectively (Tavakoli et al. 2017) **Chicken meat**: control the pathogenic and spoilage bacteria (Ahmed et al. 2018)	Gallocchio et al. (2016) ***Study:*** Evaluation of silver migration from a commercially available food packaging containing AgNPs into chicken meatballs under plausible domestic storage conditions, and tested the contribution of this packaging to restrict food spoilage bacteria proliferation. ***Result:*** The migration was slow and no significant difference in the analyzed bacteria levels between meatballs stored in AgNPs plastic bags and control bags. Tiimob et al. (2017) ***Study:*** Evaluated the release of eggshell-silver tailored copolyester polymer blend film exposed to water and food samples by atomic absorption spectroscopy (AAS) analysis. ***Results:*** AgNPs was not released in chicken breast or distilled water until 168 and 72 h, respectively.
Zinc oxide nanoparticles	Strong antimicrobial agent Exhibited diverse morphologies Showed robust inhibition against growth of broad-spectrum bacterial species Increase mechanical properties with increasing of ZnO-NPs content Increase tensile strength and Young's modulus Decrease the duration of material break	**Soft white cheese**: enhance the shelf-life with good antibacterial activity against gram positive (*Staphylococcus aureus*), gram negative (*Pseudomonas aeruginosa, Escherichia coli*) bacteria and fungi (*Candidia albicans*) (Youssef et al. 2016). **Fresh-cut apple**: provided a better retention of firmness, total phenolic content, color and sensory quality (Li et al. 2017). **Pork meat**: help retain the quality of meat during cold storage by increasing the occurrence of microorganism injury (Suo et al. 2017)	Zhang et al. (2016) ***Study:*** Evaluated the fate of the packaging material of ZnO-NPs on the coating layer incorporated into PLA-coated paper entering into paper recycling processes. ***Results:*** The mass balance indicated that 86–91% ZnO-NPs ended up in the material stream, mostly incorporated into the polymer coating; however, 7–16% nanoparticles completed in the desired material stream. Furthermore, the nano-coating showed positive impacts on the quality of recovered fibre. Chia and Leong (2016) ***Study:*** Surface modification by silica coating was used to reduce the toxicity of ZnO-NPs by significantly reducing the dissolution of the core ZnO NPs. ***Results:*** Silica coating showed a significant decrease on the dissolution of ZnO-NPs and offered a possible solution to enhance the biocompatibility of ZnO-NPs, which could broaden the applications such as antibacterial agent in food packaging.

(continued)

Table 18.1 (continued)

Nanomaterials	Physical, chemical and biological activity	Applications in food system	Safety assessment
Copper-based nanoparticles	CuO-NPs properties depends on the synthesis method Antimicrobial activity	**Coconut oil:** enhance the thermal stability and increased the antimicrobial activity of heat-treated nanocomposite (Gautam and Mishra 2017). **Soy protein**: improved elongation at break and tensile strength, and higher water contact angle and degradation temperature and decreased water vapour permeation (Li et al. 2017). **Peda (Indian sweet dairy product)**: showed extended shelf life with strong microbial activity and barrier properties (Lomate et al. 2018)	There is little known on the toxicity of copper-based nanocomposites and more attentions have been concentrated in CuO-NPs (Tamayo et al. 2016)
TiO_2 nanoparticles	Antimicrobial activity Enhanced the optical transparency, increased the tensile strength and contact angle and declined the water vapour permeability properties Decreased the elongation at break of the film Increased hydrophobicity	**Cellulose-based papers for bread packaging**: The efficiency in the bread storage was compared in terms of nutritional parameters (proteins, total fat and carbohydrates), acidity, and change of molds and yeasts (Mihaly-Cozmuta et al. 2017) **Strawberry fruits**: Nano-TiO_2-low-density polyethylene (NTLDPE) promoted ROS scavenging and related to antioxidant enzyme activities (Li et al. 2017)	Salarbashi et al. (2018) ***Study:*** Evaluated biodegradable soluble soybean polysaccharides (SSPS) nanocomposites consisting of varying ratios of SSPS and TiO2-NPs, and found that TiO2-NPs existed in plasma membranes of epithelial cell lines after a 10-day exposure to a number of free nanomaterials. ***Results***: SSPS/TiO_2 nanocomposites showed excellent antimicrobial activity against *Staphylococcus aureus.* However, anti-cancerous and pro-cancerous activities were not determined because this nanomaterial denoted their neutrality in regards to cancer inhibition or promotion in gastrointestinal tracts. Jo et al. (2016) ***Study*:** Evaluated the interactions between TiO2-NPs and biomolecules including albumin and glucose with altered the physical and chemical properties as well as the consequence regarding TiO2-NPs under physiological conditions. ***Results***: Oral absorption of food grade TiO2-NPs was slightly higher compared to general grade TiO2-NPs; however, these nanoparticles were excreted through the feces. Besides, the biokinetics of food grade TiO2-NPs were extremely relied on their interaction with biomolecules.

product decay or degrade over time and able to controls the overall quality during storage and handling. In a realistic time period, these material types of food packaging will not causing environmental waste issues. Nanocomposites-based packaging materials have properties that can improve food quality and extending the shelf-life through minimizing microbial growth in the product. Moreover, they also responsible as carriers of some active substances in spite of as barrier to moisture, water vapour gases and solutes.

18.5 Conclusions

The impact of utilizing the usage of nanotechnology has contributed to the development of some novel materials with interesting properties in a wide range application especially in food packaging. The use of polymer alone is restricted due to their poor properties thus resulting in limited performances. By introducing nanocomposite as filler, a considerable improvement in general performance can be achieved especially in terms of mechanical, thermal and barrier properties. It has a great potential to improve food quality, food safety but at the same time reduce manufacturing costs. Although the effect of nanoparticles on human health is still in debate and unknown, extensive studies and research need to be done in future.

Acknowledgments The authors would like to acknowledge the Ministry of Education (MOE) Malaysia for funding this work under Transdisciplinary Research Grant Scheme (TRGS) grant no. 6769003 and MRUN (USM- MCUN/MTUN) Translational Research Grant no. 656206.K145.

References

Abdollahi M, Alboofetileh M, Behrooz R, Rezaei M, Miraki R (2013) Reducing water sensitivity of alginate bio-nanocomposite film using cellulose nanoparticles. Int J Biol Macromol 54:166–173

Ahmed J, Arfat YA, Bher A, Mulla M, Jacob H, Auras R (2018) Active chicken meat packaging based on polylactide films and bimetallic Ag–cu nanoparticles and essential oil. J Food Sci 83(5):1299–1310

Busolo MA, Lagaron JM (2012) Oxygen scavenging polyolefin nanocomposite films containing an iron modified kaolinite of interest in active food packaging applications. Innov Food Sci Emerg Technol 16:211–217

Carbone M, Donia DT, Sabbatella G, Antiochia R (2016) Silver nanoparticles in polymeric matrices for fresh food packaging. J King Saud Univ Sci 28(4):273–279

Carter LW, Hendricks JG, Bolley DS (1950) U.S. Patent No. 2,531,396. Washington, DC: U.S. Patent and Trademark Office

Casariego A, Souza BWS, Cerqueira MA, Teixeira JA, Cruz L, Díaz R, Vicente AA (2009) Chitosan/clay films' properties as affected by biopolymer and clay micro/nanoparticles' concentrations. Food Hydrocoll 23(7):1895–1902

Chang PR, Jian R, Yu J, Ma X (2010) Starch-based composites reinforced with novel chitin nanoparticles. Carbohydr Polym 80(2):420–425

Chellaram C, Murugaboopathi G, John AA, Sivakumar R, Ganesan S, Krithika S, Priya G (2014) Significance of nanotechnology in food industry. APCBEE Procedia 8:109–113

Chia SL, Leong DT (2016) Reducing ZnO nanoparticles toxicity through silica coating. Heliyon 2(10):e00177
Cho JW, Paul DR (2001) Nylon 6 nanocomposites by melt compounding. Polymer 42(3):1083–1094
de Azeredo HMC, Mattoso LHC, McHugh TH (2011) Nanocomposites in food packaging–a review. Advances in diverse industrial applications of nanocomposites, 57–78
De Lima R, Feitosa L, Pereira ADES, De Moura MR, Aouada FA, Mattoso LHC, Fraceto LF (2010) Evaluation of the genotoxicity of chitosan nanoparticles for use in food packaging films. J Food Sci 75(6):N89–N96
Espitia PJP, Soares NDFF, dos Reis Coimbra JS, de Andrade NJ, Cruz RS, Medeiros EAA (2012) Zinc oxide nanoparticles: synthesis, antimicrobial activity and food packaging applications. Food Bioproc Tech 5(5):1447–1464
Gallocchio F, Cibin V, Biancotto G, Roccato A, Muzzolon O, Carmen L, Ricci A (2016) Testing nano-silver food packaging to evaluate silver migration and food spoilage bacteria on chicken meat. Food Additives & Contaminants: Part A 33(6):1063–1071
Gautam G, Mishra P (2017) Development and characterization of copper nanocomposite containing bilayer film for coconut oil packaging. J Food Process Pres 41(6):e13243
Guilbert S, Gontard N, Gorris LG (1996) Prolongation of the shelf-life of perishable food products using biodegradable films and coatings. LWT-Food Sci Technol 29(1–2):10–17
Han JW, Ruiz-Garcia L, Qian JP, Yang XT (2018) Food packaging: a comprehensive review and future trends. Compr Rev Food Sci Food Saf 17(4):860–877
Honarvar Z, Hadian Z, Mashayekh M (2016) Nanocomposites in food packaging applications and their risk assessment for health. Electron Physician 8(6):2531
Huang JY, Li X, Zhou W (2015) Safety assessment of nanocomposite for food packaging application. Trends Food Sci Technol 45(2):187–199. https://doi.org/10.1016/j.tifs.2015.07.002
Jawaid M, Tahir PM, Saba N (2017) Lignocellulosic fibre and biomass-based composite materials: processing, properties and applications. Woodhead Publishing
Jo MR, Yu J, Kim HJ, Song JH, Kim KM, Oh JM, Choi SJ (2016) Titanium dioxide nanoparticle-biomolecule interactions influence oral absorption. Nano 6(12):225
Kim J, Waliser DE, Cesana GV, Jiang X, L'Ecuyer T, Neena JM (2018) Cloud and radiative heating profiles associated with the boreal summer intraseasonal oscillation. Clim Dyn 50(5–6):1485–1494, https://doi.org/10.1007/s00382-017-3700-3
Llorens A, Lloret E, Picouet PA, Trbojevich R, Fernandez A (2012) Metallic-based micro and nanocomposites in food contact materials and active food packaging. Trends Food Sci Technol 24(1):19–29
Lomate GB, Dandi B, Mishra S (2018) Development of antimicrobial LDPE/cu nanocomposite food packaging film for extended shelf life of peda. Food Packag Shelf Life 16:211–219
Longano D, Ditaranto N, Cioffi N, Di Niso F, Sibillano T, Ancona A, Conte A, Del Nobile MA, Sabbatini L, Torsi L (2012) Analytical characterization of laser-generated copper nanoparticles for antibacterial composite food packaging. Anal Bioanal Chem 403(4):1179–1186
López OV, Castillo LA, Garcia MA, Villar MA, Barbosa SE (2015) Food packaging bags based on thermoplastic corn starch reinforced with talc nanoparticles. Food Hydrocoll 43:18–24
Lu J, Bowles M (2013) How will nanotechnology affect agricultural supply chains? Int Food Agribus Man 16(1030–2016-82815):21–42
Luis Feijoo J, Lagarón JM, Pilar Villanueva M, Giménez E, Cabedo L (2006) Optimization of biodegradable nanocomposites based on aPLA/PCL blends for food packaging applications. Macromol Symp 233(1):191–197
Mihaly-Cozmuta A, Peter A, Craciun G, Falup A, Mihaly-Cozmuta L, Nicula C, Baia M (2017) Preparation and characterization of active cellulose-based papers modified with TiO2, Ag and zeolite nanocomposites for bread packaging application. Cellulose 24(9):3911–3928
Moura M, Aouada F, Avena-Bustillos R, Mchugh TM, Krochta J, Mattoso HCL (2009) Improved barrier and mechanical properties of novel hydroxypropyl methylcellulose edible films with chitosan/tripolyphosphate nanoparticles. J Food Eng 92:448–453
Müller C, Elliott J, Chryssanthacopoulos J, Arneth A, Balkovič J, Ciais P, Deryng D, Folberth C, Glotter M, Hoek S, Iizumi T, Izaurralde RC, Jones C, Khabarov N, Lawrence P, Liu W, Olin S, Pugh TAM, Ray D, Reddy A, Rosenzweig C, Ruane, G. Sakurai AC, Schmid E,

Skalsky R, Song CX, Wang X, de Wit A, Yang H (2017) Global gridded crop model evaluation: Benchmarking, skills, deficiencies and implications. Geosci Model Dev 10:1403–1422, https://doi.org/10.5194/gmd-10-1403-2017

Munro IC, Haighton LA, Lynch BS, Tafazoli S (2009) Technological challenges of addressing new and more complex migrating products from novel food packaging materials. Food Addit Contam Part A Chem Anal Control Expo Risk Assess 26(12):1534–1546

Network S, Risk FOR, Nanotechnologies OF, Food IN (2010) Scientific network for risk assessment of nanotechnologies in food and feed b, (January 2002), 2–5

Othman SH (2014) Bio-nanocomposite materials for food packaging applications: types of biopolymer and Nano-sized filler. Agriculture and Agricultural Science Procedia 2:296–303

Othman SH, Salam A, Raudhah N, Zainal N, Kadir Basha R, Talib RA (2014) Antimicrobial activity of TiO2 nanoparticle-coated film for potential food packaging applications. Int J Photoenergy 2014:6

Oymaci P, Altinkaya SA (2016) Improvement of barrier and mechanical properties of whey protein isolate based food packaging films by incorporation of zein nanoparticles as a novel bionanocomposite. Food Hydrocoll 54:1–9

Peelman N, Ragaert P, De Meulenaer B, Adons D, Peeters R, Cardon L, Van Impe F, Devlieghere F (2013) Application of bioplastics for food packaging. Trends Food Sci Technol:128–141

Pereda M, Marcovich N, Ansorena MR (2018) Nanotechnology in food packaging applications: barrier materials, antimicrobial agents, sensors, and safety assessment. In: Martínez LMT, Kharissova OV, Kharisov BI (eds) Handbook of ecomaterials. Springer International Publishing, Cham, pp 1–22

Salarbashi D, Tafaghodi M, Bazzaz BSF (2018) Soluble soybean polysaccharide/TiO2 bionanocomposite film for food application. Carbohydr Polym 186:384–393

Sandoval B (2009) Perspectives on FDA's regulation of nanotechnology: emerging challenges and potential solutions. Compr Rev Food Sci Food Saf 8(4):375–393

Shankar S, Rhim JW (2016) Polymer nanocomposites for food packaging applications. Functional and physical properties of polymer nanocomposites, 29

Siracusa V (2012) Food packaging permeability behaviour: a report. Int J Polym Sci 2012:11

Suo B, Li H, Wang Y, Li Z, Pan Z, Ai Z (2017) Effects of ZnO nanoparticle-coated packaging film on pork meat quality during cold storage. J Sci Food Agric 97(7):2023–2029

Tamayo L, Azócar M, Kogan M, Riveros A, Páez M (2016) Copper-polymer nanocomposites: an excellent and cost-effective biocide for use on antibacterial surfaces. Mater Sci Eng C 69:1391–1409

Tankhiwale R, Bajpai SK (2012) Preparation, characterization and antibacterial applications of ZnO-nanoparticles coated polyethylene films for food packaging. Colloids Surf B Biointerfaces 90:16–20

Tavakoli H, Rastegar H, Taherian M, Samadi M, Rostami H (2017) The effect of nano-silver packaging in increasing the shelf life of nuts: an in vitro model. Ital J Food Saf 6(4)

Thostenson ET, Li C, Chou TW (2005) Nanocomposites in context. Compos Sci Technol 65(3–4):491–516

Tiimob BJ, Mwinyelle G, Abdela W, Samuel T, Jeelani S, Rangari VK (2017) Nanoengineered eggshell-silver tailored Copolyester polymer blend film with antimicrobial properties. J Agric Food Chem 65(9):1967–1976

Vasile C (2018) 'Polymeric nanocomposites and nanocoatings for Food packaging: a review', materials (Basel, Switzerland). MDPI 11(10):1834

Youssef AM (2013) Polymer Nanocomposites as a new trend for packaging applications. Polym Plast Technol Eng 52(7):635–660

Youssef AM, El-Sayed SM, El-Sayed HS, Salama HH, Dufresne A (2016) Enhancement of Egyptian soft white cheese shelf life using a novel chitosan/carboxymethyl cellulose/zinc oxide bionanocomposite film. Carbohydr Polym 151:9–19

Zhang H, Bussini D, Hortal M, Elegir G, Mendes J, Jordá Beneyto M (2016) PLA coated paper containing active inorganic nanoparticles: material characterization and fate of nanoparticles in the paper recycling process. Waste Manag 52:339–345

Chapter 19
Biodegradability and Composite Coatings: Past, Present and Future Prospects

Mizanur Rahman, Sajib Paul, Farhan Mahbub, and Rezwan-Us-Saleheen

19.1 Introduction

The consideration of Bio-based polymers is raised due to the environmental concerns and the apprehension of global petroleum belongings. Biodegradable polymers are polymers which rupture down after its planned use. The formation of natural byproducts like oxygen, nitrogen, carbon dioxide, water, biomass, and inorganic salts are the result of squalor of polymer. Normally biodegradable polymers which are studied could be naturally and synthetically derived. Their backbone could possess ester, amide, and ether functional groups. As well as their properties and the manner of their degradation is determined by their structure. There are many examples and applications of biodegradable polymers. Biodegradable polymers could be polyesters, polyamides, polyanhydrides, polycarbonates, polysaccharides, etc. Polysaccharides are biodegradable polymers of a kind of monosaccharide which is more than one kind of monosaccharide. They are usually originated in living organisms such as plants and animals. The plant origin of polysaccharides is such as starch, cellulose, hemicellulose, hyaluronic, alginate, guar gums and etc. and the animal origin polysaccharides are chitin and chondroitin. Polysaccharides play different types of roles in nature (Janarthanan and Veeramachineni 2016).

Recently, synthetic plastic turn as a sovereign pollutants on the earth. It is used for daily life like covering materials, carry bags, manufacturing of different types of equipment etc. Therefore an alternate is needed to be developed as a replacement of synthetic plastic which can take part for lessening the rising environmental pollutions. This environmental harmful synthetic plastic can be replaced with the bio plastics such as Polyhydroxyalkanoates (PHAs) and Polyhydroxybutyrate (PHB).

M. Rahman (✉) · S. Paul · F. Mahbub · Rezwan-Us-Saleheen
Department of Mechatronics Engineering, World University of Bangladesh, Dhaka, Bangladesh
e-mail: mizanur.rahman@mte.wub.edu.bd

S. Siddiquee et al. (eds.), *Composite Materials: Applications in Engineering, Biomedicine and Food Science*, https://doi.org/10.1007/978-3-030-45489-0_19

These are biodegradable thermoplastic recently recognized because of its biodegradable nature (Singh et al. 2019). The biological origin of PHB is similar to synthetic plastics stereo-specific and biodegradable. Therefore, to achieve sustainability it can be used as an appropriate option. Several bacterial genuses like Actinobacillus, Azotobacter, Agrobacterium, Rhodobacter and Sphaerotilius have been under focus for their aptitude of converting organic desecrate to bacterial PHA. The progress of inventive biopolymer materials has been developing for a number of years, and continues to be an area of interest for many scientists. In 1996, the Canadian Plastic Industry increased by 10.6% from 1995 levels, to $9.1 billion (Kolybaba et al. 2003). Fomin (2001) has been reported that the end of the twentieth century, worldwide manufacture of synthetic plastics reaches approximately 130million tons per year, while the demand for biodegradable plastics is reported to be growing by 30% each year. The usage of 100 kg of plastic per person per year has been reported in European countries (Kolybaba et al. 2003).

Synthetic plastics are rebellious to degradation, and therefore their discarding is fuelling an international drive for the growth of biodegradable polymers. Many industries all over the world must find novel applications for the expansion of these materials. Final mode of biodegradation is dependent on the composition. For efficient use, recycle, and dispose of biopolymer materials an integrated waste management system may introduce (Abdel-Shafy and Mansour 2018; Subramanian 2000). To extend an effective waste management system, reduction in consumption of sources, reuse of existing materials, and recycling of unnecessary materials must all be measured. Polymer resources are solid, non-metallic compounds of high molecular weights (Callister 1999).They are comprised of repeating macromolecules, and have varying characteristics depending upon their composition. Each macromolecule that comprises a polymeric material is known as a mer unit. A single mer is called a monomer, while repeating mer units are known as polymers. For modern plastic materials an assortment of materials (both renewable and non-renewable) is engaged as feedstock sources. Plastics that are formed from non-renewable feedstock's are generally petroleum-based, and toughened by glass or carbon fibers (Williams and Wool 2000). Renewable resource feedstocks include microbially-grown polymers and those extracted from starch. It is possible to strength such materials with natural fibers, from plants such as flax, jute, hemp, and other cellulose sources (Bismarck et al. 2002).

For the use of sustainable materials and processes an increasing environmental concern has been developed in the last decades. In that sense, biopolymers such as PA11 and biodegradable polymers like starch or polycaprolactone were introduced (Imre and Pukánszky 2013). Recently, the higher cost of those polymers, the production of biocomposite materials and biodegradable composites has gained interest. Poly(lactic acid) (PLA) is polyester obtained from the ring-opening polymerization of lactide (Thomas 2010). The properties of Poly(lactic acid) depend on the hilarity of the monomers used, but in general terms it has a tensile strength about 50–60 MPa and stiffness close to 3.5 GPa. Those properties, together with its biodegradability, have made it an attractive polymer for some applications, especially in the packaging sector. The production prediction for 2020 is four times

higher than the 2014 one, exceeding the amount of seven million tons per year. However, in spite of all these advantages, its range of application is still limited by its high production cost, its brittleness and its low thermal stability (Espinach et al. 2018).

The use of composites reinforced with lignocellulosic bio-fibres has rapidly expanded and is stirring from a niche market to a mass production scale, namely in the building, automobile and packaging industries (Espinach et al. 2018). This growing interest is driven by the attributes of cellulosic fibres properties namely low cost, lightweight, renewable character, high specific strength and modulus, availability in a variety of forms throughout the world, reactive surface, and biodegradability. This later property makes them especially attractive for processing with biodegradable polymers such as PLA polymers to elaborate totally biodegradable composite materials. The biodegradable polymer matrix is expected to cost effectiveness of natural cellulosic fibres and their high stiffness balance. For instance, the addition of those reinforcements may influence on other thermal properties such as crystallinity, thermal conductivity, or the thermal expansion coefficient has been previously observed in other composites. Composites based on PLA and lignocellulosic filler such as jute fibre, flax fibres, kenaf, coir, bamboo, wood fibresand cellulose fibres were extensively investigated (Yusoff et al. 2016; Espinach et al. 2018; Faruk et al. 2012). Although, there is not a consensus regarding the effect of lignocellulosic filler on the strength, impact and others mechanical properties of PLA composites, therefore, the addition of cellulose filler improved the stiffness, the heat deflection temperature (HDT) and the crystallization extent (Bledzki et al. 2009; Bledzki and Jaszkiewicz 2010).

This literature review is intended to provide information regarding progress made in the development of biodegradable polymer materials. Biodegradable Polymers for Controlled Drug Delivery, Biodegradable composites and packaging films, applications, methods of biodegradation and environmental and economic implications of such materials will be examined. Finally, information regarding the future direction for biodegradable polymers will be objectively discussed.

19.2 Biodegradability of Polymers

Polymers has special chemical structure under specific environmental conditions that can easily breaks down with the bacterial decomposition process and produce gases, water, biomass and inorganic salts. Therefore, the changes result in a loss of physical and mechanical properties, as measured by standard methods. Biodegradable plastics undergo degradation from the action of naturally occurring microorganisms such as bacteria, fungi, and algae. Plastics may also be designated as photodegradable, oxidatively degradable, hydrolytically degradable, or those which may be composted. During the time period between October 1990 and June1992, confusion is raised to define “biodegradable polymer”as a resultled to lawsuits regarding aenvironmental advertising which wasmisleading and deceitful (Kumar et al. 2011).

The international standard organization ASTM and ISO already developed a common testing methods and protocols for degradable polymer or biodegradable plastics. Three types of polymer materials (thermoplastics, thermosets and elastomers) are available where material scientists and researcher are now focusing on. The biodegradable plastics or polymer is developed base on its thermal properties. The polymer materials are easy to get in the market usually referred as a general class of plastics by the consumers and the industry. Their design is often that of a combined, where a polymer matrix (plastic material) forms a primary phase around filler material. In order to raise mechanical properties the filler is used in the biodegradable plastics, as well as reduce the material costs (Shivam 2016).

19.3 Materials & Methods

19.3.1 Materials

The materials of biodegradable matrix Ingeosed by PLA Biopolymer which is one of the polymers based on PLA. A commercial bleached Kraft soft wood (BKSW) pulp derived from *Pinusradiata*was used as fibrous reinforcement. Diglycol methyl ether isalso known as diglyme and used in order to diminish the interaction between fibres and thus forming aggregates (Sharif and Hoque 2019; Espinach et al. 2018; Gandini 2008).

19.3.2 Fibre Preparation

The commercial bleached Kraft soft wood (BKSW) was composed by cellulose fibres without lignin. For Morfi measurement Morphological characterization was indicated by arithmetical length and width about 2.4 mm and 20 μm, respectively. In addition, the observations of SEM were also showed flattened fibres with close width (Espinach et al. 2018; Chung et al. 2018; Khan et al. 2017). For the fiber preparation there few steps are involved at first the selected fiber are poised and washed to take away impurities and foreign particles from the outside. Depending on the nature of the fiber it kept into the water for softening for two weeks product. In the next steps fibers are removed from the water cut into small pieces about 2 to 3 mm in size. In order to apply PLA the small size fiber washed with chemical (acetone) layer as well to remove impurities from fiber. This process is also help to improve the compatibility between the matrix and the fibers. According to the standard the mechanical and physical properties of the fiber is measured and compared.

19.3.3 Composite Preparation

The BKSW and the PLA were dried at 70 to 80 °C before mixing. The BKSW was dried during 24 hours and the PLA for 3 hours. To adjust the moisture BKSW and PLA is dried in the fiber materials. It is important to make sure that the BKSW has very low water content before started the next step. 15 to 35% Composites with fibre content from were prepared by kinetic mixing using a Gelimatmultikinetic mixer. The speed was increased up to 2500 rpm when the PLA-fibre mixture was fed at 300 rpm to heat them and proceed to the melting of the matrix and the wetting of the fiber (Delgado-Aguilar et al. 2018). During the processing the volatiles were allowed to be removed from the concoction. The composite blends were granulated in a blade mill (Agrimsa) equipped with a strainer of 10 mm nominal size. By using an injection-molding machine the pelletized materials were molded (Meteor 40) using a steel mould complying with ASTM: D3641 standard specifications (Alizadeh et al. 2019; Delgado-Aguilar et al. 2018; Laxmeshwar et al. 2012;).

19.3.4 Sample Obtaining

Biodegradable polymer was injected to prepare 3 × 13 × 130 mm standard samples to use in a Meteor-40 injection machine. To establish the coefficient of expansion the biodegradable polymer two types of samples were cut into 3 × 3 × 5 mm, and 3 × 13 × 65 mm for DMA. The samples were also obtained for the TGA and DSC, which is milled injected samples. Therefore the resources or biodegradable polymer samples passed through the analogous thermal processes for all the tests (Espinach et al. 2018).

19.3.5 Scanning Electron Microscopy (SEM)

For visualization in material science scanning electron microscopy (SEM) is one of the very powerful tools. Polymer sciences field is also included SEM technology for further inspection. Before mixing scanning electron microscopy (SEM) is used for the observation, and of the broken surface of the tensile samples was run in order to get information about the effect of the processing in the fibers, as well as of the interface quality generated between BKSW fibers and the PLA matrix. Samples were coated in gold, and the electronic microscope was used (Rydz et al. 2019; Bootz et al. 2004).

19.3.6 Determination of the Fibers' Morphology

To measure the length and diameter of the fibers Morfi equipment can be used. According to the international standard ISO/FDIS 160652, total 25 mg of fibre were added with one litre of distilled water. The suspension of the fiber is located at the bottom of the equipment. To determinate the morphology distribution of the fibers an optical measurement instrument is used (Sencadas et al. 2012; Espinach et al. 2018).

19.3.7 Thermogravimetric Analysis (TGA)

To determine the weight losses of a sample during heating Thermogravimetry (TGA) is a well-established standard technique, cooling and maintains a constant temperature. The aim of this analysis is to characterize the sample materials with respect to its composition. Thermo balance was used to determine the weight loss during heating. The samples were heated from 30 to 700 °C with a heating rate of 10 °C/min. The test was performed in an inert atmosphere with a nitrogen flow rate of 40 ml/min (Espinach et al. 2018).

19.3.8 Differential Scanning Calorimetry (DSC)

To determine the amount of heat required to increase sample temperature differential scanning calorimetry (DSC) is an established international standard thermoanalytical technique. In order to evaluate the influence of the fibers on the thermal transitions biodegradable polymer DSC was performed with a Mettler Toledo DSC822e calorimeter and on the matrix crystallinity degree according international standardmethod ASTM E 1269.01. According to the standard procedure, during heating and cooling processes, the samples were heated and cooled at 10 °C/min. Once the sample cooled at 30 °C then the samples were heated between 30 to 220 °C. The heating results shown in this work correspond to this second heating, as the thermal history was removed. A flow rate of 40 ml/min of nitrogen was used for testing the samples in an inert atmosphere (Espinach et al. 2018).

19.4 Biodegradable Polymers for Controlled Drug Delivery

For drug delivery system Research interests on using biodegradable polymers are becoming increasingly important. As binders in tablets, viscosity enhancer in liquids or emulsions natural biodegradable polymers is being used. Polymers are also

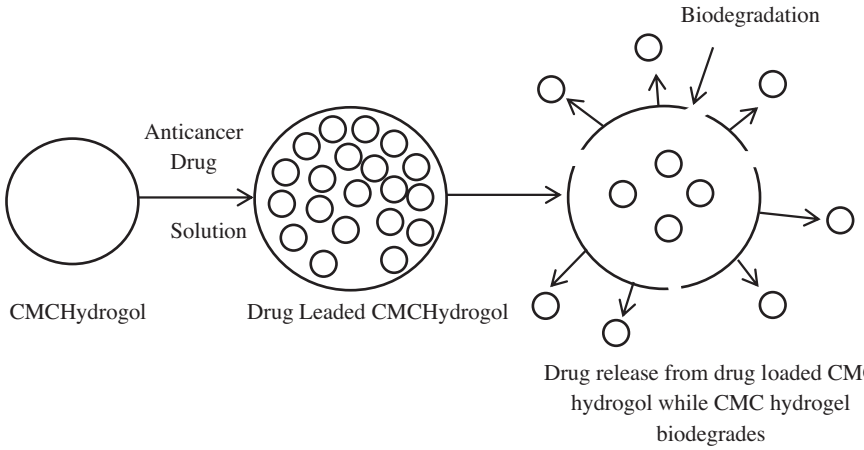

Fig. 19.1 Drug release from the cross-linked polysaccharide by biodegradation

being used as a coating agent to eliminate the unpleasant taste of a drug and to progress drug stability and to modify the amount and liberate rate of the drug. The short half-life of the drugs leads to multiple dosing .Multiple dosages has tendency to lift the aspect effects and price of the medication. To beat these issues, perishable polymers area unit anticipated to enhance technique of providing drug to the patients. The drug encapsulated within the cross connected perishable polymers may unharnessed the drug in sustained or controlled manner as shown in Fig. 19.1.

To the concentration of the cross-linking compound the rate of drug unharness relies upon the cross linking extent of the compound wherever the upper concentrations leading to larger cross-linking and so slower drug release (Boppana et al. 2010).The drug may be loaded into colloidal gel like carboxymethylcellulose(CMC) hydrogels that Consists of the many pores and formed into beads/tablets that disintegrates by biodegradation to free the drug (Pushpamalar et al. 2013).

19.5 Application for Perishable Polymers

To introduce the utilization of perishable compound materials Research and development is barely some of the work that's tired. The look of such materials sometimes begins with an abstract application. It should be expected to interchange Associate in nursing existing material, or to enhance one. Sectors wherever applications for biopolymers have introduced embrace (but aren't restricted to) drugs, packaging, agriculture, and therefore the automotive business. Several materials are urbanised and commercialised area unit applied in additional than one in every of these classes.

For the other application Biopolymers which will be used in packaging still receive additional attention. For the widespread application all levels of state,

notably in China (Chau and Yu 1999) and European country (Bastioli 1998) area unit endorsing of perishable packaging materials so as to cut back the amount of inert materials presently being willing of in landfills, occupying scarce out there house. It's calculable that forty first of plastics area unit utilized in packaging, which virtually half that volume is employed to package food product. For the development of perishable plastics BASF, a world leader within the chemical and plastic business, is functioning based mostly upon polyester and starch (Kasirajan and Ngouajio 2012). In 2001 Ecoflex could be a totally perishable plastic material that was introduced to customers by BASF. The fabric is proof against water and grease, creating it appropriate to be used as a sanitary throwaway wrapping, suited decomposes in traditional composting systems. Consequently, Ecoflex has found variety of applications as a packaging wrap. Moreover Environmental Polymers has developed a perishable plastic material called Depart, the polyvinyl alcohol product is proposed for extrusion, injection molding, and blow molding. Depart options user-controlled solubility in water that is set by the formulation used. Dissolution happens at a predetermined temperature, permitting the utilization of Depart during a sort of applications. Examples embrace hospital laundry luggage that area unit "washed away" permitting healthful washing of flyblown laundry, also as applications as disposable food service things, agricultural product, and tube luggage. For innovative uses in packaging the renewable and perishable characteristics of biopolymers area units are appealing. The top use of such product varies wide. As an example, perishable plastic films are also used as garbage luggage, disposable cutlery and plates, food packaging, and shipping materials. From starch gallinaceous bird and Hanna documented a perishable loose-fill packaging materials are also developed. The starch material is treated by Associate in Nursing acylation method, chemical treatments, and post-extrusion steaming. Mechanical properties of the fabric area unit adequate and true biodegradability are achieved. The biopolymer resources fitted to packaging area unit typically utilized in agricultural product. Ecoflex, specifically, sees use in each area. Young plants that area unit notably liable to frost is also lined with a skinny Ecoflex film. The film may be worked into the soil, wherever it'll be diminished by the days. Therefore, plastic films that begin to degrade in average soil conditions after approximately one month are ideal candidates as crop mulches (Kolybaba et al. 2003).

Agricultural applications for biopolymers are not limited to film covers. Containers such as biodegradable plant pots and disposable composting containers and bags are areas of interest. The pots are seeded directly into the soil, and breakdown as the plant begins to grow. Scientists have examined that Fertilizer and chemical storage bags which are biodegradable. From an agricultural standpoint, biopolymers which are compostable are important, as they may supplement the current nutrient cycle in the soils where the remnants are added.

The medical world is continually dynamic, and consequently the materials utilized by it conjointly see repeated changes. The biopolymers utilized in medical applications should be compatible with the tissue they're found in, and will or might

not be expected to interrupt down once a given period. Mukhopadhyay (2002) reported that researchers operating in tissue engineering try to develop organs from chemical compound materials, that area unit fit transplantation into humans. The plastics would need injections with growth factors so as to encourage cell and vessel growth within the new organ. Work completed during this break includes the event of biopolymers with adhesion sites that act as cell hosts in giving shapes that mimic completely different organs. Not all biopolymer applications within the field of drugs area.

Artificial organs are most significant biopolymer applications within the field of drugs area unit. All biopolymers used for medical applications are included by the umbrella classification of bioactive materials. One example is artificial bone material that adheres and integrates onto bone within the figure. The term Bioglass seems to be the foremost normally utilized substance during this space (Kokubo et al. 2003). The bioactive material releases medication at a rate determined by its protein degradation which is another common biopolymers application for controlled release of medicines (Sakiyama-Elbert and Hubbell 2001). PLA materials were developed for medical devices like restorable screws, sutures, and pins. These materials scale back the danger of tissue reactions to the devices, shorten recovery times, and reduce the necessity of experts required by patients for the maintenance of implantable medical devices (Janarthanan and Veeramachineni 2016).

The automotive sector is responding to societal and governmental demands for environmental responsibility. Bio-based cars are lighter, making them a more economical choice for consumers, as fuel costs are reduced. Glass fibers are replaced by natural fibers as reinforcement materials in plastic elements of vehicles (Lammers and Kromer 2002). Degeneration of waste product is an extra advantage of exploitation perishable compound materials. Natural fibers (from flax or hemp) are typically applied in shaped interior elements. The parts don't want load bearing capacities, however dimensional stability is vital. Analysis and development during this space continues to be popular, particularly in European countries.

There are varieties of novel applications for biopolymers. One such example is that the use of biopolymer systems to switch food textures. As an example, biopolymer starch (gelatin-based) fat replacers possess fat-like characteristics of swish, short plastic textures that stay extremely viscous once melting. Analysis expanded to control biopolymers into food product in order to improved physical characteristics like foaming, gelling, and water- or fat-binding talents (Ledward 1993). Recently Biopolymer materials are incorporated into adhesives, paints, engine lubricants, and construction materials (Fomin and Guzeev 2001). Biodegradable golf tees and fishing hooks (Canadian Patent # 2198680–1997) have additionally been made-up. Biopolymers along with those areas are their derivation from renewable sources, swiftness the depletion of restricted fuel stores (Kolybaba et al. 2003).

19.6 Biodegradable Composites and Casing Films

Normally hydrocolloids and lipids are worn in diversity for the preparation of biodegradable wrapping components. Independently they have deficiency of structural fidelity and characteristic functionality. Here, hydrocolloids are deprived of moisture barriers. Which is a property remunerated by the addition of lipids, which carries good moisture barriers. Composite films are basically a composition of sea and other ingredients in varying proportions. This proportions will determinate their barrier (H_2O, O_2, CO_2 and Aroma compounds) and other mechanical properties. Sometimes composite film formulation can be customized in order to meet the necessity of a septic commodity or farm produce. For example, oranges having a thick peel are prone to anaerobic conditions. This condition leads to an untimely sense scene and spoilage if the composite film is rich in lipids. Phase separation encountered during the training of composites is overcome by using emulsifying agents. Plasticizers such as glycerin, ethylene glycol, sorbitol etc. can be used in the film formulations or composites for conveying pliability and flexibility. This will improve handling (Garcia et al. 2000). The brittleness of the film can be reduced by using plasticizers interfering the chemical element bonding between the lipid and substance molecules. The involvement of wax coating of fruits by immersing is one of the antique strategies that were common in the early twelfth century (Krochta et al. 1994). This strategy was used in China in order to reduce water transpiration losses in lemon and oranges. Later fat coating of food merchandise, which was referred as "larding", was introduced in European Nations. Uses of sausage casing are very common these days are nothing however a cloth derived from a macromolecule supply (gelatin). Typically a movie thickness of 22.5 millimeter is utilized, and coating is completed by many strategies. Films square measure preformed skinny membranous structures, that square measure used when being shaped one by one, whereas in coatings the skinny film is created directly on the trade goods. Dip technique coating is that the usually used technique for fruits, vegetables and meat merchandise. In here the trade goods is directly unfit into the composite coating formulations (in liquid medium), removed and allowed to air dry, whereby a skinny membranous film is created over the trade goods surface.

Continuous submerging builds up decay organisms, soil and trash within the dipping resolution that has to be removed for better performance. The coating can even be done by a foam application technique, which generally applied in Emulsions square measure. Here the depth tumbling action is critical to break onward for uniform distribution of the coating resolution over the trade goods surface. Most of the cases coating by spraying is that the standard technique normally used. For a stronger coverage high (60–80 psi) less coating resolution is needed to allow. Programmable spray systems square measure accessible for automation throughout such operations. Biodegradable packaging films square measure typically ready by wet casting of the solution on marginal base material and later drying. Selection of the bottom material is essential to get films, which might be removed with none tearing and wrinkling. By accelerating the drying method Infrared drying chambers

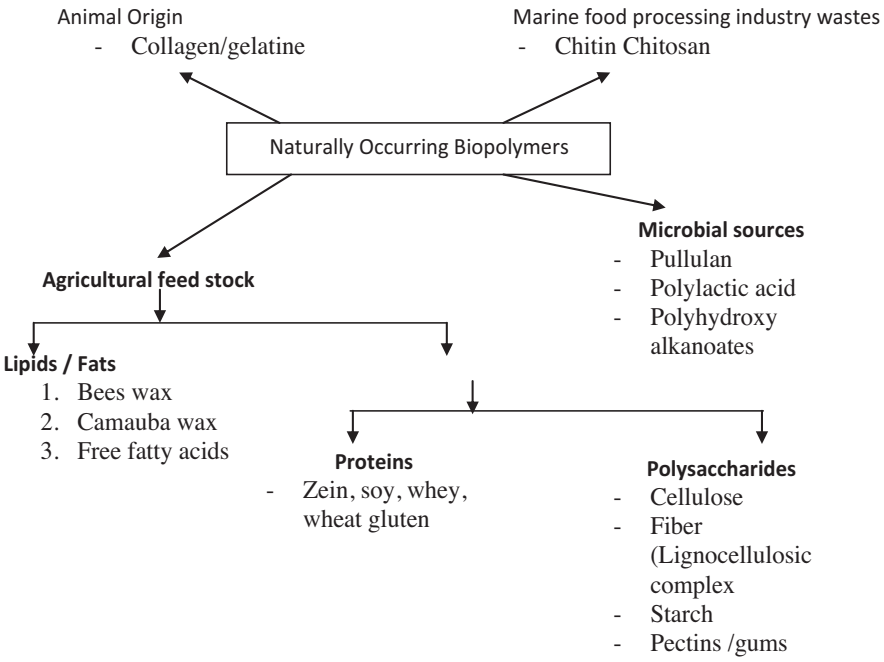

Fig. 19.2 Naturally occurring biopolymers of use in biodegradable packaging films and composites

square measure may privileged (Tharanathan 2003) optimum wet content (5–8%) is fascinating within the dried film for their straightforward strips aloof from one fringe of the bottom material. The mixture in biopolymeric materials may use in composite film creating and coating formulations square measure shown in Fig. 19.2.

Coating composites supported such biomolecules have brought a rolling of latest forms of packaging materials into use. These biomolecules square measure are consistent amongst themselves and with alternative hydrocolloids, surfactants and additives. And their liquid solutions square measure typically stable at acidic and neutral pH. The composite solutions square measure conserved repeated use by adding carboxylic acid, carboxylic acid or their sodium salts. Polysaccharides are known for their structural complexity and functional mixture (Tharanathan 2003).

19.7 Environmental Impacts of Biopolymers

Now a day's Engineers are considering ecological concerns during the material selection processes, in order to act in response to an increased responsiveness of environmental protection. The use of renewable resources in the production of

polymer materials achieves this in two ways. First, the feedstock's being engaged can be replaced, either through natural cycles or through intentional involvement by humans. The biodegradable nature of the end products are second environmental advantage of using renewable feedstock's for biopolymer development, thereby preventing likely pollution from the disposal of the corresponding amount of conformist plastics. At the end of their useful period, biopolymer materials are normally sent to landfills or composted.

Recycling of plastic materials makes an attempt at increasing environment safety efforts are but effective. Within the U. S., presently but 100% of plastic product area unit recycled at the tip of their helpful life (Chiellini et al. 2001). Practice should be recognized as a disposal technique, not a final goal for material development. A useful angle concerning exercise processes ignores the actual fact that advanced infrastructure is necessary to properly house exercise. In the underdeveloped countries the outcome on investment for recycling plastic materials is positive in their economic state of affairs. This seems to be positive at the onset; however the open systems by that the plastics area unit recycled enable the emission of harmful gases at crucial levels.

A useful solution scale back pollution and environmental harm seems to recycle once it had been introduced as a waste reduction technique. However, currently it's obvious that the engagement of plastics supported renewable feed stocks that area unit biodegraded could be a lot of good selection than exercise standard plastics. Because the finish product area unit organic matter, and harmful emissions area unit is avoided. Therefore, growth of plastics that area unit compostable or simply degraded should be encouraged.

Recently a couple of perceived garbage crisis has full-grown. Landfills have reached capability, and sites for brand spanking new landfills area unit tough to seek out. Once biopolymers area unit disposed in lowland environments, the required microorganisms are additional advantages. Unless the soil is inoculated with them, this could not continuously be the case. As reported by carrots are found to stay orange, and grass clippings inexperienced, once years in very lowland. Increasing biopolymer breakdown at intervals soil using Immunization with bacterium, fungi, and actionmycetales is effective. However, if the suitable microorganisms area unit gift, the disposal (and eventful breakdown) of perishable (or partly biodegradable) plastic materials can result in a rise of accessible area in current landfills because the volume of waste is reduced through biodegradation.

19.8 Economic Impacts of Biopolymers

In trade perspective, low price of mistreatment biopolymers derived from renewable feed stocks is their best advantage. Primarily biopolymers seem to be a win-win chance for the economy and therefore the atmosphere. However, despite of the scenario with environmental problems, a more in-depth look into the cost-performance

magnitude relation of biopolymers should be taken to create sound economic selections (Kolybaba et al. 2003).

According to Leaversuch (2002), the price could be an obstacle for synthetically derived biodegradable plastic materials once they area unit directly compared with their typical counterparts. For any new material, makers should expect a minimum of 2 years of losses before a profit is came back. Migrant such additionally indicated that a key issue restraining growth of biopolymer industries is that the development of infrastructure for sorting and composting organic waste is very slow against the expectation. Many reports paint an additional optimistic image for the economic promise of biopolymers. According to As Salmoral et al. (2000), variety of major chemical firm's area unit gaining interest in developing biopolymer technologies conventional manufacture product from renewable resources.

Tharanathan (2003) states artificial plastics can ne'er be entirely replaced by perishable materials. However, he believes that in niche markets wherever the event is possible, there is a chance for makers to search out a considerable profit margin. The utilization of biopolymer materials is a major sector within which economic advantages exist within the automotive trade. Comparing with fiber reinforcements wide utilized ancient glass fibers area unit abrasive and quickly deals with process instrumentation. The feel of flax fibers is a smaller amount coarse, prolonging the lifetime of process instrumentation (Stamboulis et al. 2000). Williams and Pool (2000) found that natural fibers have unit advantage over artificial ones as a result of their less costly and additional without delay out there. In Canada the enlargement of flax fiber incorporation into automobile components could be a significant development for agriculture trade in its diversification efforts.

Recently China has developed another application of fiber reinforcement, uses of China reed fiber to bolster transport pallets. This was associate economically sound call, because the China reed pallets area unit as automatically stable as typical pallets, however they're less costly to form, and wish a shorter lifetime for price recovery. Logistically, the China reed pallets have additional economic advantage than the traditional kind for their lighter mass needs less fuel for transport (Corbiere-Nicollier et al. 2000). Work continues within the development of the biopolymer trade to a satisfactory degree wherever it's economically competitive with the traditional plastic trade. Normally the foremost half biopolymers area unit created on a little scale whereas artificial plastics area unit created on an oversized scale. Researcher and Industry officials are encouraged for further development of these processes due to the cheap nature of the natural resources feedstocks. Along with the expansion of biopolymers production, so too will the services associated with it. For example, facilities where flax straw is decorticated and processed into fibers are useful for further expansion of flax fiber incorporation as material reinforcements (Lammers and Kromer 2002). While for microbially-grown polymers, large fermentation and separation facilities are needed for the further use of such materials. Hence, it may be stated that time will lead to greater economic strength for the incorporation of biopolymer materials into society (Kolybaba et al. 2003).

19.9 The Future Outlook for Perishable Plastics

Perishable plastic trade needs to evolve and flourish in several areas (Chau and Yu 1999). Approximately plastic waste generation can grow by V-J Day each year for successive decade. CO_2 emissions from the formation and disposal of typical plastics square measure reaching epic levels. A balanced CO_2 level can be obtained in environment by substituting the whole petroleum-based feedstock plastics by renewable resource-based feedstock ones (Dahlke et al. 1998). However, instead of full replacement of typical polymers by their perishable counterparts, the enlargement of specific niche markets appears to be the foremost applicable and achievable choice (Kolybaba et al. 2003).

Researchers worldwide are encouraging to work within the space of biopolymer development now a day. The German government has stricken their laws in situ relating to acceptable emission levels. In 1990, the German government printed a need analysis and development of perishable thermoplastics (Grigat et al. 1998; Simon et al. 1998). Due to this, several German material scientists and engineers have centered their work on environmentally stable perishable plastics. Followed by these researches numerous materials are created, as well as the aspirin BAK line that was initiated in extrusion and injection moulding grades in 1996. The Mater-Bi line was introduced by Novamont, associate degree Italian company, for similar reasons. Queen Mary University in London, European nation organizes a plastics department that is actively conducting biocomposite development (Hogg 2001). EU packaging directives are expected to be followed by all European nations square measure combine that expects a cloth recovery of packaging waste. Organic recovery (composting spent materials) is that the simplest waste reduction technique applied (Schroeter 1998). European nations are expected to comprise V-J Day w/w of recycled plastics into the manufacture of packaging materials. European country aimed to achieve a predetermined goal in 2001 for incorporation of recycled plastics into new packaging materials (Fomin and Guzeev. 2001). Despite of spectacular biological process undergoing in different geographical areas, European nations square measure the front runners of biopolymer analysis. Due to oversized population on low land base, the Chinese government starts preservation of house and reasonable disposal of waste square measure earnestly. Hence Chinese researchers' square measure absorption on processing of microbially created PHA (Chau and Yu 1999). North yankee researchers along with the University of Canadian province researchers, are interested about biopolymer development due to the agricultural trade that can enjoy the potential worth more process. The reduction in the uses of fuel feedstocks and a rise in the use of natural resources is a requirement of the metropolis granted by the government of North American country. These requirements can be fulfilled by biodegradable plastics because the biopolymer trade rises, problems with production are going to be figured out. There square measure some square measure as of concern that researchers are awake to, and square measure consequently involvement on. Multilayer films having starch and/or natural fibers tend to possess adhesion issues (Frisoni et al. 2001; Martin et al. 2001). Hence the exploration of a process to avoid this drawback continues during this regard.

Verhoogt et al. (1995) have gone through the advance starch content in thermoplastic blends will gives rise in flexibility, however decreases mechanical strength. The biopolymer trade encompasses a positive future, driven chiefly by the environmental advantages of mistreatment natural resource feedstock sources. Development of a cloth with optimum technical performance, and full biodegradability is the final word goal for this work.

19.10 Conclusion

Management of Environmental balance is a rapidly increasing concern for both consumers and industry. This obligation is a key advantage for those who produce biodegradable plastic materials. Biopolymers restrict carbon dioxide emissions during creation and degenerate to organic matter after disposal. Despite of being more economically feasible, more consumers will choose biodegradable plastics instead of synthetic plastics because of their availability and environment friendly characteristics. The engagement of renewable resource feedstocks is the most promising aspect for further development of biopolymer materials. Biodegradable plastics containing starch and/or cellulose fibers seems to be the most reasonable to experience continual advancement in usage. However being microbial grown plastics are scientifically sound and a novel idea, their use is still expensive. Hence the infrastructure needed to be commercially expanded so that Biodegradable plastic can convenient to for further development.

References

Abdel-Shafy HI, Mansour MS (2018) Solid waste issue: sources, composition, disposal, recycling, and valorization. Egypt J Pet 27(4):1275–1290

Alizadeh-Osgouei M, Li Y, Wen C (2019) A comprehensive review of biodegradable synthetic polymer-ceramic composites and their manufacture for biomedical applications. Bioact Mater 4(1):22–36

Bastioli C (1998) Properties and applications of mater-bi starch-based materials. Polym Degrad Stab 59(1–3):263–272

Bismarck A, Aranberri-Askargorta I, Springer J, Lampke T, Wielage B, Samboulis A, Shenderovick I, Limbach H (2002) Surface characterization of flax, hemp, andcellulose fibers, surface properties and the water uptake behavior. Polym Compos 23(5):872–894

Bledzki AK, Jaszkiewicz A (2010) Mechanical performance of biocomposites based on PLA and PHBV reinforced with natural fibres–a comparative study to PP. Compos Sci Technol 70(12):1687–1696

Bledzki AK, Jaszkiewicz A, Scherzer D (2009) Mechanical properties of PLA composites with man-made cellulose and abaca fibres. Compos Part A Appl Sci Manuf 40(4):404–412

Bootz A, Vogel V, Schubert D, Kreuter J (2004) Comparison of scanning electron microscopy, dynamic light scattering and analytical ultracentrifugation for the sizing of poly (butyl cyanoacrylate) nanoparticles. Eur J Pharm Biopharm 57(2):369–375

Boppana R, Kulkarni RV, Mutalik SS, Setty CM, Sa B (2010) Interpenetrating network hydrogel beads of carboxymethylcellulose and egg albumin for controlled release of lipid lowering drug. J Microencapsul 27(4):337–344

Callister WD (1999) Materials science and engineering: an introduction. Wiley, New York
Chau H, Yu P (1999) Production of biodegradable plastics from chemical wastewater–a novel method to resolve excess activated sludge generates from industrial wastewater treatment. Water Sci Technol 39(10–11):273–280
Chiellini E, Cinelli P, Imam SH, Mao L (2001) Composite films based on biorelated agro-industrial waste and poly (vinyl alcohol). Preparation and mechanical properties characterization. Biomacromolecules 2(3):1029–1037
Chung TJ, Park JW, Lee HJ, Kwon HJ, Kim HJ, Lee YK, Tai Yin Tze W (2018) The improvement of mechanical properties, thermal stability, and water absorption resistance of an eco-friendly PLA/kenafbiocomposite using acetylation. Appl Sci 8(3):376
Corbiere-Nicollier T, Gfeller Laban G, Lundquist L, Letterier Y, Manson J, Jolliet O (2000) Life cycle assessment of biofibers replacing glass fibers as reinforcement in plastics. Resources, Conservation, and Recycling. 33:267–287
Dahlke B, Larbig H, Scherzer HD, Poltrock R (1998) Natural fiber reinforced foams based on renewable resources for automotive interior applications. J Cell Plast 34(4):361–379
Delgado-Aguilar M, Reixach R, Tarrés Q, Espinach FX, Mutjé P, Méndez JA (2018) Bleached Kraft eucalyptus fibers as reinforcement of poly (lactic acid) for the development of high-performance biocomposites. Polym 10(7):699
Espinach FX, Boufi S, Delgado-Aguilar M, Julián F, Mutjé P, Méndez JA (2018) Composites from poly (lactic acid) and bleached chemical fibres: thermal properties. Compos Part B Eng 134:169–176
Faruk O, Bledzki AK, Fink HP, Sain M (2012) Biocomposites reinforced with natural fibers: 2000–2010. Prog Polym Sci 37(11):1552–1596
Fomin VA (2001) Biodegradable polymers, their present state and future prospects. Prog Rubber Plast Re 17(3):186–204
Fomin VA, Guzeev VV (2001) Biodegradable polymers, their present state and future prospects. Int Polym Sci Technol 28(11):76–84
Frisoni G, Baiardo M, Scandola M (2001) Natural cellulose fibers: heterogeneous acetylation kinetics and biodegradation behavior. Biomacromolecules 2:476–482
Gandini A (2008) Polymers from renewable resources: a challenge for the future of macromolecular materials. Macromolecules 41(24):9491–9504
García MA, Martino MN, Zaritzky NE (2000) Microstructural characterization of plasticized starch-based films. Stärke 52(4):118–124
Grigat E, Kock R, Timmermann R (1998) Thermoplastic and biodegradable polymers of cellulose. Polym Degrad Stab 59(1–3):223–226
Hogg P (2001) Plastics, rubber, and composites at queen Mary. Plast Rubber Compos 30(5):193–194
Imre B, Pukánszky B (2013) Compatibilization in bio-based and biodegradable polymer blends. Eur Polym J 49(6):1215–1233
Janarthanan P, Veeramachineni AK (2016) Biodegradable Polysaccharides, In book Reference Module in Materials Science and Materials Engineering. Polymer Science: A Comprehensive Reference 5(2012):333–361
Kasirajan S, Ngouajio M (2012) Polyethylene and biodegradable mulches for agricultural applications: a review. Agron Sustain Dev 32(2):501–529
Khan RA, Salem HJ, Korehei R, Martinez DM, Olson JA (2017) Application of fractionated bleached pulp fibres on sodium alginate films. Can J Chem Eng 95(1):33–38
Kokubo T, Kim HM, Kawashita M (2003) Novel bioactive materials with different mechanical properties. Biomaterials 24(13):2161–2175
Kolybaba M., L.G. Tabil, S. Panigrahi, W.J. Crerar, T. Powell, B. Wang (2003) Biodegradable polymers: past, present, and future., An ASAE Meeting Presentation
Krochta JM, Baldwin EA, Nisperos-Carriedo MO (1994) Edible coatings and films to improve food quality. Technomic Publ Co
Kumar A, Karthick K, Arumugan KP (2011) Biodegradable polymers and its applications. IJBBB 1(3). September 2011

Lammers PS, Kromer KH (2002) Competitive natural fibre used in composite materials for automotive parts. In: 2002 ASAE Annual Meeting. American Society of Agricultural and Biological Engineers, p 1

Laxmeshwar SS, Madhu Kumar DJ, Viveka S, Nagaraja GK (2012) Preparation and properties of biodegradable film composites using modified cellulose fibre-reinforced with PVA. ISRN Polymer Science 2012

Leaversuch R (2002) Biodegradable polyesters: packaging goes green. Plast Technol 48(9):66–79

Ledward DA (1993) Creating textures from mixed biopolymer systems. Trends Food Sci Technol 4(12):402–405

Martin O, Schwach E, Averous L, Couturier Y (2001) Properties of biodegradable multilayer films based on plasticized wheat starch. Starch 53(8):372–380

Mukhopadhyay P (2002) Emerging trends in plastics technology. Plast Eng 58(9):28–28

Pushpamalar J, Langford SJ, Ahmad M, Hashim K, Lim YY (2013) Absorption characterization of Ca 2+, Na+, and K+ on irradiation crosslinked carboxymethylsago pulp hydrogel. J Appl Polym Sci 128(3):1828–1833

Rydz J, Šišková A, Andicsová Eckstein A (2019) Scanning Electron microscopy and atomic force microscopy: topographic and dynamical surface studies of blends, composites, and hybrid functional materials for sustainable future. Adv Mater Sci Eng 2019

Sakiyama-Elbert SE, Hubbell JA (2001) Functional biomaterials: design of novel biomaterials. Annu Rev Mater Res 31(1):183–201

Salmoral EM, Gonzalez ME, Mariscal MP (2000) Biodegradable plastic made from bean products. Ind Crop Prod 11:217–225

Schroeter J (1998) Creating a framework for the widespread use of biodegradable polymers. Polym Degrad Stab 59(1–3):377–381

Sencadas V, Correia DM, Areias A, Botelho G, Fonseca AM, Neves IC, Mendez SL (2012) Determination of the parameters affecting electrospun chitosan fiber size distribution and morphology. Carbohydr Polym 87(2):1295–1301

Sharif A, Hoque ME (2019) Renewable resource-based polymers. In: Bio-based polymers and nanocomposites. Springer, Cham, pp 1–28

Shivam P (2016) Recent developments on biodegradable polymers and their future trends. IRJSE 4:17–26

Simon J, Müller HP, Koch R, Müller V (1998) Thermoplastic and biodegradable polymers of cellulose. Polym Degrad Stab 59(1–3):107–115

Singh MK, Rai PK, Rai A, Singh S, Singh JS (2019) Poly-β-Hydroxybutyrate production by the cyanobacterium ScytonemageitleriBharadwaja under varying environmental conditions. Biomol Ther 9(5):198

Stamboulis A, Baille C, Garkhail S, Van Melick H, Peijs T (2000) Environmental durabilityof flax fibers and their composites based on polypropylene matrix. Appl Compos Mater 7(5–6):273–294

Subramanian PM (2000) Plastics recycling and waste management in the US. Resour Conserv Recycl 28(3–4). February 2000:253–263

Tharanathan RN (2003) Biodegradable films and composite coatings: past, present, and future. Trends Food Sci Technol 14:71–78

Thomas CM (2010) Stereocontrolled ring-opening polymerization of cyclic esters: synthesis of new polyester microstructures. Chem Soc Rev 39(1):165–173

Verhoogt H, Truchon F, Favis B, St-Pierre N, Ramsay B (1995) Morphology and mechanical properties of blends containing thermoplastic starch and PHB. Annual Technical Conference – ANTEC 95 (53rd). Boston, Mass

Williams G, Pool R (2000) Composites from natural fibers and soy oil resins. Appl Compos Mater 7(5–6):421–432

Williams GI, Wool RP (2000) Composites from natural fibers and soy oil resins. Appl Compos Mater 7(5–6):421–432

Yusoff RB, Takagi H, Nakagaito AN (2016) Tensile and flexural properties of polylactic acid-based hybrid green composites reinforced by kenaf, bamboo and coir fibers. Ind Crop Prod 94:562–573

Chapter 20
Nanocomposite Film for Food Packaging: Opening Doors to Future Applications

Norfatehah Basiron, Srimala Sreekantan, Rabiatul Basria S. M. N. Mydin, and Khairul Arifah Saharudin

20.1 Polymer in Daily Life

Since many years, polymers are widely used to replace metals, glass, paper, wood, brick and other traditional materials in various applications, due to their strength, light weight properties, along with low cost. To date, the importance of polymer has been highlighted because of their application in different dominions of science, technology and industry such as horticulture, consumer goods, packaging, building & construction, medical, packaging, automotive, transportation, food industry, and electronics and communication.

The word polymer is derived from classical Greek *poly* meaning "many" and *meres* meaning "parts" (Emmanuel et al. 2014). Thus, polymers are high weight molecules made of reposted chemical units called monomer. Theoretically, polymers are obtained through polymerization process whereby the monomer molecules undergo chemical reaction to form polymer chain. The property and quality of polymer depends upon the interaction bonds, additives, and length of polymer chain.

Polymers are consists of two types: natural and synthetic polymers. Examples of natural polymers are proteins, cellulose and rubber whereas synthetic polymers are derived from petroleum oil or plants and made by scientist and engineers. Other than that, polymers can be classified as organic, inorganic and hybrid polymers. Typically, in global market, polymer is classified into thermosetting, elastomers,

N. Basiron · S. Sreekantan (✉) · K. A. Saharudin
School of Materials and Mineral Resources Engineering, Engineering Campus, Universiti Sains Malaysia, Nibong Tebal, Pulau Pinang, Malaysia
e-mail: srimala@usm.my

Rabiatul Basria S. M. N. Mydin (✉)
Oncological and Radiological Sciences Cluster, Advanced Medical and Dental Institute, Universiti Sains Malaysia, Kepala Batas, Penang, Malaysia
e-mail: rabiatulbasria@usm.my

S. Siddiquee et al. (eds.), *Composite Materials: Applications in Engineering, Biomedicine and Food Science*, https://doi.org/10.1007/978-3-030-45489-0_20

and thermoplastics. Due to the flexibility design, the polymer market is expected to grow at an exponential rate. As reported by Plastics Europe (PEMRG) / Consultic / ECEBD, from 2012 to 2017, there is a steady increase in demand for plastic products about 3.7% per year with a total world plastics production of about 300 M tonne in 2013. In United States, the thermoplastics industry is the third largest manufacturing industry which worth of 10.9 billion dollars. Among all the industrial plastics, plastics for food packaging comprises almost one fifth of the net revenue of the plastic industry (Chin 2010). Based on Malaysia Plastics Manufacturers Association (MPMA), the plastics industry registered a total sales turnover of RM24.77 billion in 2015 from RM19.46 billion in 2014 with the actual growth of 5% to 6%.

20.1.1 Polymer Applications

Thermoplastics are used in various manufacturing sectors such as food, beverages, chemicals, electronic packaging, automotive, household products, medical and health care. Examples of thermoplastics polymers normally used are polyethylene (PE) such as high density polyethylene (HDPE) and low density polyethylene (LDPE), polypropylene (PP) polyethylene terephthalate (PET), polystyrene (PS) and polyvinyl chloride (PVC). For other applications such as paint, coating, sealants, automotive industry (dashboard, seating and headliners), thermoset polymers including polyurethane (PU), epoxy and phenolic have been utilized. Each of the polymers has their pros and cons and the characteristics are summarized in Table 20.1.

20.1.2 Polymer Composite Evolution

Even though, there is demand for plastic due to the growth of end-user market, there are also certain limitations that need to be addressed. The limitations of polymers are: low strength relative to metals and ceramics, low modulus of elasticity (stiffness), the service temperature are limited to only few hundred degrees, low viscoelastic properties which can be a distinct limitation in load bearing applications. Some polymers will restructure when subjected to sunlight and other form of radiation. These limitations will affect the performance in certain application and probably possess harmful impact on human health, environment and ecosystem (Bratovčić et al. 2015). Other than that, these limitations also have negative impact to economic prospect.

Polymer also are extensively used in packaging application to keep the food fresh by preventing its deterioration (Bratovčić et al. 2015) and protecting from foodborne pathogens (Carbone et al. 2016). This reduces the risks of various food poisoning outbreaks and illness. Therefore, offering polymer nanocomposites with

Table 20.1 Characteristics and application of polymers

Type of plastic	Characteristics	Application or usage	References
PET	Clear, strong, good barrier to gases and moisture, resistant to heat, mineral oils, solvents and acids	Plastics bottles for carbonated drinks	Bratovčić et al. (2015)
PP	Strong, excellent chemical resistance and low density	Packaging film	Bratovčić et al. (2015)
LDPE	Very low cost, inert, large stretch ability, heat sealable, odour free and shrinks when heated, good moisture barrier but relatively permeable to oxygen	Plastic bags and containers for general purposes, for coating papers or boards and as a component in laminates	Bratovčić et al. (2015) Allahvaisi (2012) Chin (2010)
HDPE	Cheap, stronger, thicker, less flexible and more brittle than LDPE and has a better barrier to gases and moisture	Clouded containers or bottles for foods such as milk where strength is required but not clarity	Allahvaisi (2012) Chin (2010)
PS	Rigid, heat resistance	Styrofoam food containers and cups as well as meat and egg trays	Chin (2010)
PVC	Cheap and capable of stretching	Packaging films, containers and structural containers	Chin (2010) Bratovčić et al. (2015)

improved gas barrier properties, thermal stability, and strength, are of great importance for packaging materials (Bratovčić et al. 2015). Polymer nanocomposites are blends of different polymer matrices with nanosized functional particles. The properties of such nanocomposites are remarkably different compared to conventionally filled polymers. The incorporation of only a few percent of nanosized particles allows dramatic property change. Polymer materials reinforced with nanoscale components are therefore adding new dimensions to composite materials and major improvements in functional and structural properties.

20.2 Emerging of Nanocomposites in Food Packaging

In food industry, conventional materials faces various problems such as contamination by microorganisms (Manohar et al. 2017), biofilm formation, and adherence of fungi and viruses on packaging walls (Tamayo et al. 2016) . These problems may lead to the propagation of serious infections among humans. Foodborne pathogen are major contributor to human illness, hospitalization and deaths per year. An estimated that the costs of foodborne illness in the United States is $152 billion dolars per year for acute medical care and long term health related costs (Tamayo et al. 2016). According to the Centers for Disease Control and Prevention, in the United State alone, some 48 million illnesses and 3000 deaths are caused

annually by bacterially contaminated foods. *Salmonella spp*., *Listeria monocytogenes*, *Campylobacter spp*., *Staphylococcus aureus* and *Toxoplasma gondii* are among the top pathogens causing foodborne illness and death . Other than that, recall of food due to microbial contamination has lost millions of dollars annually in food industry.

As the polymer nanocomposite technology in favored to resolve the microbiological contaminants, food packaging materials has undergone a radical change in recent years. From passive packaging, which acts as a simple container and/or insulating barrier from the outside environment, to active packaging that absorbs substances interacting with food has been explored to increase the shelf life and quality of food products. However, the demand of polymer nanocomposites as active packaging for food industry has emerged tremendously because it offers several benefits over standard passive packaging materials. Polymer nanocomposites ensure the food freshness and storage stability since it extends the lag phase and reduce growth phase of microorganisms (Reesha et al. 2015). Therefore, polymer nanocomposite incorporated with antimicrobial agent nanoparticles is now widely introduced as an active packaging technology by food manufacturers and packaging industry to combat food borne illnesses outbreak. There has been much interest in the use of metals/metal oxides as antimicrobial agent in polymer composites. Among the metals have been studied and applied for centuries nanoparticles such as silver (Ag) (Zapata et al. 2016), silver oxide (Ag_2O) (Zapata et al. 2016), gold (Au) (Zare and Shabani 2016), titanium dioxide (TiO_2) (Joost et al. 2015), copper (Cu) (Wu et al. 2014), copper oxide (CuO) (Dizaj et al. 2014) and zinc oxide (ZnO) (Li et al. 2010, Youssef and El-Sayed 2018, de Azeredo et al. 2011). Furthermore, these nanoparticles have received great attention for their potential antimicrobial applications due to their desirable varying physical and chemical properties such as surface modification, phase, crystals, shape and size of antimicrobial agent, which could be easily modified using different synthesis and processing method. Therefore, in the subsequent section the desirable physical and chemical properties of the particles and their killing mechanism are elaborated in detail.

20.3 Mechanism of Antimicrobial Activity

There are various killing mechanism proposed for the antimicrobial activity of polymer composites. It differs and depends on different type of antimicrobial agents. In general, it has been reported that the killing mechanisms of nanoparticles towards different microbes differs and depends on Reactive Oxygen Species (ROS) generated on the surface of particles, metal ions release, protein oxidation, disruption of membrane/ cell wall and DNA damage as illustrated in Fig. 20.1 (Gold et al. 2018). Nevertheless, the actual killing mechanisms of inorganic oxides in polymer inhibiting bacterial growth remain unanswered.

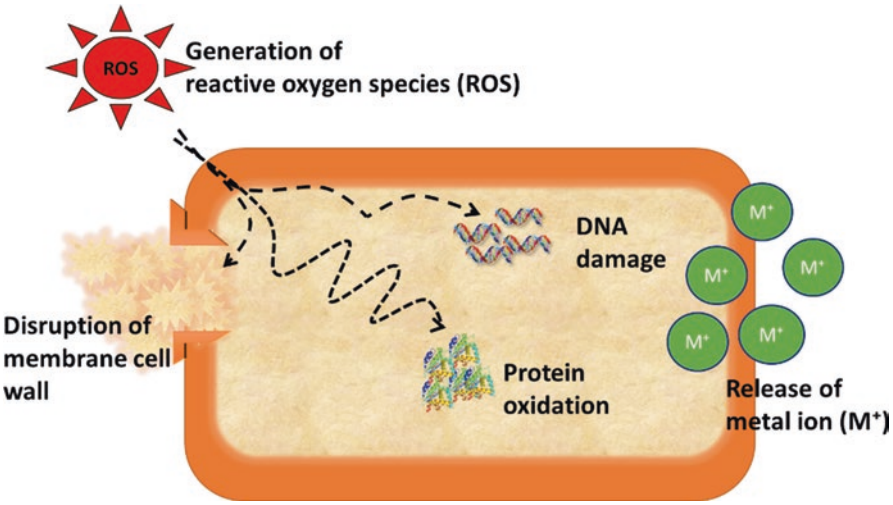

Fig. 20.1 Illustration on the mechanism of antimicrobial activity (Emamifar 2011)

20.3.1 Ag/Ag Nanoparticles

The most common antimicrobial agents that have been employed since ancient time is Ag nanoparticles. It was demonstrated that, the Ag nanoparticles have the most effective bactericidal properties against a wide range of pathogenic microorganism, including bacteria, yeasts, fungi and viruses (Carbone et al. 2016). On the other hand, Ag exhibit low volatility and stability at high temperature (Youssef and Abdel-Aziz 2013). Thus, Ag can be incorporate in different matrices such as polymers and stabilizing agents (citrates and long chain alcohols) (Kang et al. 2019), through different technology such as coating, adsorption and impregnation into the system (Carbone et al. 2016).

The mechanism of Ag nanoparticles and Ag_2O is based on the release of Ag^+ ion and its ability to formed complex with bacterial protein including enzyme, which can lead to a loss function and cell death (Palza 2015). As recognized, Gram-positive and Gram negative bacteria have different cell membrane cell structures and their surface is negatively charge. Gram-positive bacteria have a thick cell walls composed of techoic and lipoteichoic acids lying on the plasma membrane and covalently bonded with peptidoglycan (Salton and Kim 1996). The cell structure of teichoic acids is negatively charged and water soluble in nature due to the present of phosphate, carboxyl and amino group. However, Ag nanoparticles has difficulty to penetrate the Gram-positive bacteria as reported by Hasim, et al. *P. fluorescens* is more sensitive towards LDPE/Ag composites compared to *S.aureus*, because of the differences thickness of the cell walls. Thus, it will be difficult to penetrate Gram-positive's cell walls, which restricts the ability of Ag^+ ion.

In contrast, different antimicrobial effects are observed on Gram-negative bacteria. This is because Gram-negative bacteria have an external lipopolysaccharide followed by a thin layer of peptidoglycan and plasma membrane. The inner core region of polysaccharide contains heptose residues which are often substituted by phosphate, pyrophosphate or diphosphoethano-lamine. Hence, as indicated the outer cell layer of *E.coli* composed of lipid A-containing lipopolysaccharide and glycerophospholipid. Lipid A contains two phosphate groups in each glycosaminoglycan (Azlin-Hasim et al. 2016). Therefore, Ag^+ ion are attracted towards negatively charged cell membranes through electrostatic interactions. This deactivates cellular enzymes, causing disruption in membrane integrity. Furthermore, Ag^+ ion can interact with thiol groups in protein, promoting the release of ROS and this causes damage to proteins and DNA, resulting in cell death (Chandana et al. 2018). In general, Ag^+ ions are more active and effective against Gram-negative bacteria than Gram-positive bacteria since Gram-negative bacteria have thin cell wall layer and contains a higher proportion of negatively charged phosphate groups.

20.3.2 Au Nanoparticles

Au is another type of inorganic antimicrobial agent has been used during ancient times. It was believe that, the Au application was introduced by Michael Faraday to scientific community through his lecture entitled "Experimental Relations of Gold (and other Metals) to Light in 1857 (Carnovale et al. 2016). Unlike Ag, Au is more inert and highly stable metal that cannot be easily dissociated. Similar with Ag, Au nanoparticles antimicrobial properties are depended on its size, shape and concentration (Zhang et al. 2015). Penders and group has investigated the inhibition of *S. aureus* on effect of various gold shape such as nanoflower, nanosphere and nanostar. It was found the nanoflower has highest inhibition growth because the surface composed of high area, pillar and spikes that induced high local stress to the bacteria and led to membrane ruptured (Penders et al. 2017). Nevertheless, Au nanoparticle antimicrobial efficacy is low compare to Ag nanoparticle unless used in very high concentrations or ionic complex (Zhang et al. 2015).

Many studies have been conducted to understand the antimicrobial activity of Au towards pathogen. Au has a strong affinity to sulphur atom and this enhanced the interaction between Au nanoparticles and thiol groups that originated from the bacterial proteins (Zhang et al. 2015). Various literatures have reported the antimicrobial activity of Au nanoparticle is through generation of ROS due to their catalytic activity, analogous to glucose oxidase generating H_2O_2 (Tay et al. 2014). In order to investigated the killing mechanism, Zheng et al. reported the antimicrobial activity on variety of bacteria species, both Gram-positive and Gram-negative (Zheng et al. 2017). In this study, Au nanoparticle were available to kill *Staphylococcus epidermis*, *Bacillus Subtilis*, *E.coli* and *Pseumodonas aeruginosa*. However, the mechanism is favourable towards Gram-positive bacteria. Using microarray gene expression profiling, Au nanoparticle treatment created a metabolic imbalance,

upregulating oxidative enzymes and downregulating reductive enzymes, leading to an accumulation of intracellular ROS. Excess ROS generation results in cellular stress and impairs basic cell function, and led to cell death. Au provides a tunable system based on the size and surface chemistry, therefore it provides a method to govern fundamental antibacterial parameters like cell death, metabolism and ROS generation. This permits modulation of Au nanoparticle to be use in variety of application.

20.3.3 ZnO Nanoparticles

ZnO is one of the common metal oxides that has gained attention as an antimicrobial agent. ZnO nanoparticles have emerged as very efficient tool to prevent microbial proliferation on food product and increasing the shelf life of the product due to their activity against a wide range of microorganism. In fact, ZnO is listed as a General Recognized as Safe (GRAS) materials by the U.S food drug and administration (21CFR182.8991) (Sewalt et al. 2016). Although commercially used, the toxicity mechanism of ZnO is still not well understand, It is believe ZnO interact with bacteria through electrostatic interactions that alter the prokaryotic cell wall, enzyme and DNA pathways through release of Zn^{2+} ion and ROS production (Khatami et al. 2018).

ZnO is a semiconductor with a wide bandgap (3.37 eV) and high binding energy of 60 meV that shows multiple semiconductor properties and piezoelectric effect (Li et al. 2015). Upon the light exposure that higher/equal ZnO bandgap, an electron in the valence band is excited to the conduction band, and left a hole in the valence band (Eq. 20.1). These photogenerated electron-hole pair can either recombine (Eq. 20.2) or interact separately with other molecules such as adsorbed O_2 (Eq. 20.3) to form superoxide radical anion ($\cdot O_2^-$). The holes in valence band react with water or hydroxide ion on the surface of ZnO to form highly reactive hydroxyl radicals (·OH) (Eq. 20.4). O_2^- from Eq. (20.3) may form organic peroxides or H_2O_2 in the presence of organic scavenger (Eqs. 20.5 and 20.6). These ROS are powerful oxidizing agent and can enter the prokaryotic cell and destroy various organelles. In the meantime, lipid peroxidation can happen on the bacterial membrane, weakening the integrity of membrane and promoting cell lysis. The reaction are summarized as below (Kaur et al. 2013)

$$ZnO + hv \rightarrow h^+ + e \tag{20.1}$$

$$h^+ + e \rightarrow heat \tag{20.2}$$

$$e + O_2 \rightarrow \cdot O_2 \tag{20.3}$$

$$h^+ + OH \rightarrow \cdot OH \tag{20.4}$$

$$\cdot O_2 + H_2O + H^+ \rightarrow H_2O_2 + O_2 \tag{20.5}$$

$$\cdot O_2 + organic\ species \rightarrow organic\ species \cdot OO \tag{20.6}$$

$$\cdot OH + organic\ species \rightarrow oxidized\ product\left(CO_2 + H_2O\right) \tag{20.7}$$

Other than that, another commonly proposed mechanism is release of Zn^{2+} ion upon the water adsorption on the ZnO surface. Zn^{2+} ions from the ZnO surface, strongly bind to thiol groups of bacterial proteins and lead to cell death. The electrostatic interactions between ZnO nanoparticles and cell walls resulting in the destruction of bacterial cell integrity. The antibacterial properties of ZnO is also dependent on the bacterial species. Some authors have reported that this tendency may be connected with differences in the polarity and charge of microorganisms' outer membranes between Gram-positive and Gram-negative bacteria.

Arakha et al. reported that ZnO nanoparticles (60 nm) showed ability to inhibit the growth of both Gram-negative (*E.coli*, *S.Flexneri* and *P.vulgaris*) and Gram-positive (*B. subtilis*, *S.aureus* and *B.thuringiensis*) in a concentration of 250 μg/ml. Although ZnO nanoparticles show ability inhibit for both Gram-positive and Gram-negative bacteria, this materials shows higher susceptibility and increased sensitivity to opposite charge of the surface ZnO nanoparticles. As p-ZnO is positive, charged surface ZnO is more susceptible toward *E.Coli* and n-ZnO is prone to *B.subtilis*. The outer membrane of *B. subtilis*, which is a Gram-positive bacteria have a membrane and cell wall composed of peptidoglycans, techoic acid and lipoteichoic acid that is easier for ROS to penetrate.

20.3.4 Copper Nanoparticles

Due to the similar electron configuration of copper with silver (Cu [Kr] $3d^{10}$ $4s^1$; Ag: [Kr] $4d^{10}$ $5s^1$), Cu can be considered as an outstanding material for the development of antimicrobial materials. Cu nanoparticles can easily be oxidized to form copper oxides. CuO is a useful metal oxide that has many applications in different fields such as gas sensors, magnetic storage media, batteries, diodes, solar energy transformation, nanofluids, semiconductors, and heterogeneous catalysis (Tamayo et al. 2016). CuO is a p-type semiconductor that has monoclinic structure, narrow band gap (Eg = 1.2 eV), black color, and partial transparency in the visible range.

Cu compounds (Cu and CuO nanoparticles) exerts its antimicrobial properties by suppressing the bacterial growth. The electrostatic attraction between positively charge Cu^{2+} and negatively charged cell membranes of the microorganism is a vital step in Cu compounds antibacterial activity (Gurianov et al. 2019). The released Cu^{2+} ion has ability to penetrate through cell wall and strongly bind to molecules likes protein, DNA and RNA. This obstruct the functional group of cell, thus

leading to cell wall disruptions (Thokala et al. 2017). Other possible antibacterial mechanism is generation of ROS that causes oxidative stress. ROS damage the membrane and cause loss of structural integrity, alteration to the conformational structure of proteins as well as degradation of the cellular DNA and/or RNA (Kredl et al. 2016). Applerot et al. have demonstrated that Gram-negative bacteria are more susceptible to the action of CuO nanoparticles than Gram-positive bacteria. This is due to the presence of golden carotenoid pigments in Gram-positive bacteria, which provide integrity to the cell membrane and promote a more powerful oxidation resistance. When the bacterial defense mechanisms are overwhelmed by the generated ROS, the Programmed Cell death (PCD) genetic module is triggered as reported by (Applerot et al. 2012), which in turn stimulates an outbreak of oxidative stress, and it is this burst of radicals that is lethal to the cells. It is noteworthy that Cu^{2+} ions may interact with phosphorus and sulfur-containing biomolecules such as DNA and protein, distorting their structures and disrupting biochemical processes (Tamayo et al. 2016).

20.3.5 TiO_2 Nanoparticles

Titanium dioxide (TiO_2) nanoparticles have been investigated in recent years because of their unique properties such as, high thermal stability, bactericidal effect, inexpensive price and nontoxic materials (Noori Hashemabad et al. 2017). American Food and Drug Administration (FDA) has approved TiO_2 for use in human food, drugs, cosmetic, and food contact materials (Othman et al. 2012). Due to its photocatalytic activity, TiO_2 in anatase form can degrade different organic compound including microorganism such as bacteria, fungi, viruses and yeast (Zare and Shabani 2016). Thus, TiO_2 nanoparticles have been used as antimicrobial agents for both Gram-positive bacteria and Gram-negative bacteria.

The antimicrobial mechanism of TiO_2 is correlated to production of hydroxyl radical and generation of ROS that can breaking the covalent bond in peptidoglycan layer and destroy the cell wall by disturb the stability of the cell (Tallósy et al. 2016). Schematic diagram of proposed antibacterial mechanism is shown in Fig. 20.2 and almost similar to ZnO. Once the TiO_2 received sufficient light the electron from valence electron (e^-_{VB}) will excite to conduction band (e^-_{CB}) and left valence band hole (h^+_{VB}). These photogenerated electrons (e^-_{CB}) can reduce adsorbed oxygen to produce superoxide radicals ($\cdot O_2^-$). Further, h^+_{VB} can react with water to produce hydroxyl radicals ($\cdot OH$) and hydrogen peroxide (H_2O_2). The radicals will oxidize the organic compounds and decompose into harmless organic compound such as CO_2 and H_2O, thus kill and decompose the bacteria (Podporska-Carroll et al. 2015). This properties permits the use of TiO_2 in sterilization of medical devices, air-conditioning, water treatment and textile applications (Gold et al. 2018).

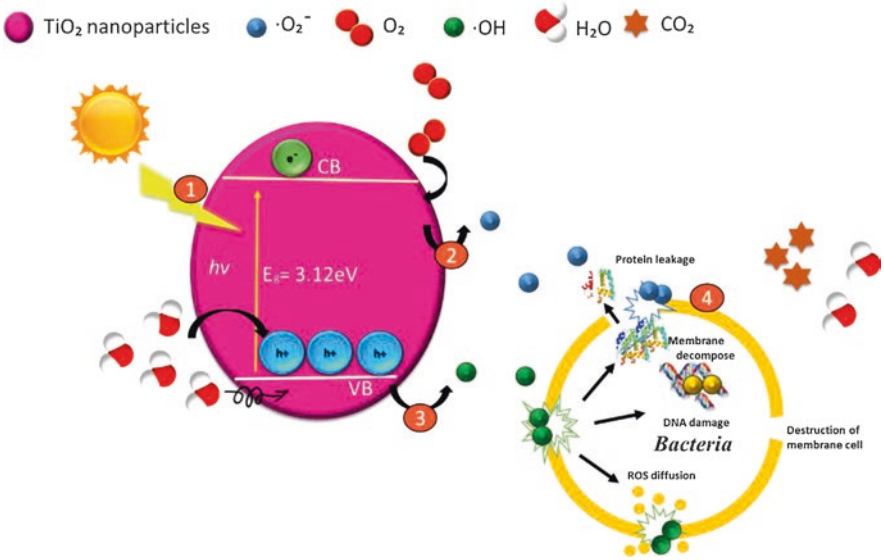

Fig. 20.2 Schematic diagram of proposed killing mechanism of TiO_2 nanoparticles. First, electron excitement from valence band to conduction band, labelled as 1. Electrons (at conduction band reduce adsorbed oxygen to produce superoxide radicals ($\cdot O_2^-$), labeled as 2. h^+ at valence band react with water to produce hydroxyl radicals (·OH), labeled as 3. The radicals will oxidize the bacteria and decompose into harmful organic compound, labeled as 4

20.4 Challenges and Conclusion

As discussed above, the killing mechanism of the nanoparticles is depended not only on material chemistry, but influenced with their physical properties, such as shape, size, solubility, agglomeration and surface charge. One of the drawbacks that nanoparticles face is inadequate stability and obvious tendency for aggregation due nanoparticle has large surface area to volume. This phenomenon dictates the behaviour and toxicity of nanoparticles. In this case, the agglomerated nanoparticles do not have the capability to enter a cell or produce significant amount of ROS. Thus, embedding nanoparticles into polymer matrices is one of the most efficient strategies to avoid aggregation of nanoparticles and conserve their properties. However, the interfacial/interphase are between polymer matrices and nanoparticles facilitates the achievement of significant desired properties. Generally, the properties of polymer nanocomposites are strongly influenced by type of polymer matrix, nature, size, contents and dispersion level of metal nanoparticles incorporated in polymer.

There is also a concern for safety risks of polymer nanocomposites for food industry applications. Hence, the toxicological studies on nano-systems are compulsory for improved characterization and reliable toxicity valuations. Therefore, screening analyses are required to understand the chemical and physical properties of nanocomposites. As we concern, for in vitro method, the mechanisms for adverse

effects of metal nanoparticles have not been understood yet, because it is a difficult to relate the reports on one type of nanoparticles to other types, due to the intrinsic differences in physical properties of metal nanoparticles such as particle size and shape, chemical properties such as surface chemistry and hydrophobicity and methods of preparation as well as biological targets including cells, organs and tissues. Moreover, deploying these materials for in vivo studies has even more challenges.

In conclusion, the advent of new technologies has been addressed by the food industry to reduce the risks to consumer health and fulfil consumer requirements. In particular, substantial progress in food packaging has been achieved using antimicrobial polymers. Polymer nanocomposites promise a new crop of stronger, more heat resistant, and high barrier materials new potential to create new and innovative bio-nanocomposite materials with improved properties and performance. However, the area of polymer nanocomposites as packaging materials still need scientific research and improvement in order to develop the shelf life, quality and marketability of diverse packaging materials. Also, the production of polymer/metal nanocomposites in industrial scale assuming the economic aspects can provide numerous advantages for people and community.

Acknowledgements The authors are thankful to the Ministry of Education (MOE) Malaysia for funding this work under MRUN (USM- MCUN/MTUN) Translational Research Grant grant no. 656206.K145.

References

Allahvaisi S (2012) Polypropylene in the industry of food packaging. INTECH Open Access Publisher

Applerot G, Lellouche J, Lipovsky A, Nitzan Y, Lubart R, Gedanken A, Banin E (2012) Understanding the antibacterial mechanism of CuO nanoparticles: revealing the route of induced oxidative stress. Small 8:3326–3337

Azlin-Hasim S, Cruz-Romero MC, Cummins E, Kerry JP, Morris MA (2016) The potential use of a layer-by-layer strategy to develop LDPE antimicrobial films coated with silver nanoparticles for packaging applications. J Colloid Interface Sci 461:239–248

Bratovčić A, Odobašić A, Ćatić S, Šestan I (2015) Application of polymer nanocomposite materials in food packaging. Croat J Food Sci Technol 7:86–94

Carbone M, Donia DT, Sabbatella G, Antiochia R (2016) Silver nanoparticles in polymeric matrices for fresh food packaging. Journal of King Saud University Science 28:273–279

Carnovale C, Bryant G, Shukla R, Bansal V (2016) Size, shape and surface chemistry of nano-gold dictate its cellular interactions, uptake and toxicity. Prog Mater Sci 83:152–190

Chandana L, Ghosal P, Shashidhar T, Subrahmanyam C (2018) Enhanced photocatalytic and antibacterial activity of plasma-reduced silver nanoparticles. RSC Adv 8:24827–24835

Chin AW (2010) Polymers for innovative food packaging. Worcester Polytechnic Institute, Massachusetts

De Azeredo HMC, Mattoso LHC, Mchugh TH (2011) Nanocomposites in food packaging–a review. Advances in diverse industrial applications of nanocomposites:57–78

Dizaj SM, Lotfipour F, Barzegar-Jalali M, Zarrintan MH, Adibkia K (2014) Antimicrobial activity of the metals and metal oxide nanoparticles. Mater Sci Eng C Mater Biol Appl 44:278–284

Emamifar A (2011) Applications of antimicrobial polymer nanocomposites in food packaging. Advances in nanocomposite technology, InTech

Emmanuel, A., Aziz, S. & Serwan, G. 2014. Polymer Nanocomposites

Gold K, Slay B, Knackstedt M, Gaharwar AK (2018) Antimicrobial activity of metal and metal-oxide based nanoparticles. Advanced Therapeutics 1:1700033

Gurianov Y, Nakonechny F, Albo Y, Nisnevitch M (2019) Antibacterial composites of cuprous oxide nanoparticles and polyethylene. Int J Mol Sci 20:439

Joost U, Juganson K, Visnapuu M, Mortimer M, Kahru A, Nommiste E, Joost U, Kisand V, Ivask A (2015) Photocatalytic antibacterial activity of nano-TiO_2 (anatase)-based thin films: effects on Escherichia coli cells and fatty acids. J Photochem Photobiol B 142:178–185

Kang H, Buchman JT, Rodriguez RS, Ring HL, He J, Bantz KC, Haynes CL (2019) Stabilization of silver and gold nanoparticles: preservation and improvement of plasmonic functionalities. Chem Rev 119:664–699

Kaur J, Bansal S, Singhal S (2013) Photocatalytic degradation of methyl orange using ZnO nanopowders synthesized via thermal decomposition of oxalate precursor method. Phys B Condens Matter 416:33–38

Khatami M, Alijani HQ, Heli H, Sharifi I (2018) Rectangular shaped zinc oxide nanoparticles: green synthesis by Stevia and its biomedical efficiency. Ceram Int 44:15596–15602

Kredl J, Kolb JF, Schnabel U, Polak M, Weltmann KD, Fricke K (2016) Deposition of antimicrobial copper-rich coatings on polymers by atmospheric pressure jet plasmas. Materials (Basel) 9

Li M, Li G, Jiang J, Zhang Z, Dai X, Mai K (2015) Ultraviolet resistance and antimicrobial properties of ZnO in the polypropylene materials: a review. J Mater Sci Technol 31:331–339

Li S-C, Li B, Qin Z-J (2010) The effect of the Nano-ZnO concentration on the mechanical, antibacterial and melt rheological properties of LLDPE/modified Nano-ZnO composite films. Polym-Plast Technol Eng 49:1334–1338

Manohar CM, Kundgar SD, Doble M (2017) Betanin immobilized LDPE as antimicrobial food wrapper. LWT Food Sci Technol 80:131–135

Noori Hashemabad Z, Shabanpour B, Azizi H, Ojagh SM, Alishahi A (2017) Effect of TiO_2 nanoparticles on the antibacterial and physical properties of low-density polyethylene film. Polym-Plast Technol Eng 56:1516–1527

Othman SH, Rashid SA, Ghazi TIM, Abdullah N (2012) Dispersion and stabilization of photocatalytic TiO_2 nanoparticles in aqueous suspension for coatings applications. J Nanomater 2012:2

Palza H (2015) Antimicrobial polymers with metal nanoparticles. Int J Mol Sci 16:2099

Penders J, Stolzoff M, Hickey DJ, Andersson M, Webster TJ (2017) Shape-dependent antibacterial effects of non-cytotoxic gold nanoparticles. Int J Nanomedicine 12:2457–2468

Podporska-Carroll J, Panaitescu E, Quilty B, Wang L, Menon L, Pillai SC (2015) Antimicrobial properties of highly efficient photocatalytic TiO_2 nanotubes. Appl Catal B Environ 176-177:70–75

Reesha KV, Panda SK, Bindu J, Varghese TO (2015) Development and characterization of an LDPE/chitosan composite antimicrobial film for chilled fish storage. Int J Biol Macromol 79:934–942

Salton MRJ, Kim K-S (1996) Chapter 2 Structure. In: Baron S (ed) Medical microbiology, 4th edn. University Of Texas Medical Branch at Galveston, Galveston (TX)

Sewalt V, ShanahaN D, Gregg L, La Marta J, Carrillo R (2016) The generally recognized as safe (GRAS) process for industrial microbial enzymes. Ind Biotechnol 12:295–302

Tallósy SP, Janovák L, Nagy E, Deák Á, Juhász Á, Csapó E, Buzás N, Dékány I (2016) Adhesion and inactivation of gram-negative and gram-positive bacteria on photoreactive TiO_2/polymer and Ag–TiO_2/polymer nanohybrid films. Appl Surf Sci 371:139–150

Tamayo L, Azocar M, Kogan M, Riveros A, Paez M (2016) Copper-polymer nanocomposites: an excellent and cost-effective biocide for use on antibacterial surfaces. Mater Sci Eng C Mater Biol Appl 69:1391–1409

Tay CY, Yu Y, Setyawati MI, Xie J, Leong DT (2014) Presentation matters: identity of gold nanocluster capping agent governs intracellular uptake and cell metabolism. Nano Res 7:805–815

Thokala N, Kealey C, Kennedy J, Brady DB, Farrell JB (2017) Characterisation of polyamide 11/copper antimicrobial composites for medical device applications. Mater Sci Eng C Mater Biol Appl 78:1179–1186

Wu H, Zhang X, Geng Z, Yin Y, Hang R, Huang X, Yao X, Tang B (2014) Preparation, antibacterial effects and corrosion resistant of porous Cu–TiO_2 coatings. Appl Surf Sci 308:43–49

Youssef AM, Abdel-Aziz MS (2013) Preparation of polystyrene nanocomposites based on silver nanoparticles using marine bacterium for packaging. Polym-Plast Technol Eng 52:607–613

Youssef AM, El-Sayed SM (2018) Bionanocomposites materials for food packaging applications: concepts and future outlook. Carbohydr Polym 193:19–27

Zapata PA, Larrea M, Tamayo L, Rabagliati FM, Azócar MI, Páez M (2016) Polyethylene/silver-nanofiber composites: a material for antibacterial films. Mater Sci Eng C 69:1282–1289

Zare Y, Shabani I (2016) Polymer/metal nanocomposites for biomedical applications. Mater Sci Eng C Mater Biol Appl 60:195–203

Zhang Y, Shareena Dasari TP, Deng H, Yu H (2015) Antimicrobial activity of gold nanoparticles and ionic gold. J Environ Sci Health C 33:286–327

Zheng K, Setyawati MI, Leong DT, Xie J (2017) Antimicrobial gold nanoclusters. ACS Nano 11:6904–6910

Chapter 21
Functional Chitosan-Based Composites for Potential Application in Food Industry

Joon Fatt Wong, Jia Xin Chan, Azman Hassan, Zurina Mohamad, and Norhayani Othman

21.1 Introduction

Chitosan is a linear semi-crystalline polysaccharide prepared by purification and deacetylation of chitin, which shown as Fig. 21.1. Chitin or poly (β(1–4)-N-acetyl-D-glucosamine) is one of the most abundant polysaccharides from natural sources which can be found in the exoskeleton of crustaceans and insects and in the cell walls of most fungi and some algae (Ma et al. 2017; Muxika et al. 2017). To purify chitin from the shells of crustaceans, the shells are ground, processed with hydrochloric acid (HCl) to achieve demineralization and boiled in dilute sodium hydroxide (NaOH) to remove proteins (Puvvada et al. 2012; Arbia et al. 2013; Kumari et al. 2015). Deacetylation of chitin is achieved through alkaline treatment at more than 80 °C. The degree of deacetylation is dependent on the reaction condition. Treatment with 12.5 mol/L NaOH at 95 to 100 °C deacetylates chitin within 2 hours, yielding chitosan with a degree of deacetylation of 87 to 90% and an average molecular weight of 160 to 1600 kDa (Puvvada et al. 2012).

Chitosan has three functional groups, which are primary and secondary hydroxyl groups and amine groups, that allow the chitosan to undergo chemical modifications (Dutta et al. 2004). It is soluble in nearly all diluted acid (pH < 6.5), but insoluble in sulfuric acid and water (Helander et al. 2001; Ambore et al. 2013). Chitosan is classified as biocompatible material, as it is one of the natural biopolymer which is biodegradable, safe and non-toxic to human and environments (Dutta et al. 2004). Due to the availability of chitosan for chemical modification, chitosan can be used as a versatile biomaterial for the wastewater treatment application (Poon et al. 2014). Besides that, chitosan has notable performance in its antioxidant,

J. F. Wong · J. X. Chan · A. Hassan (✉) · Z. Mohamad · N. Othman
School of Chemical and Energy Engineering, Faculty of Engineering, Universiti Teknologi Malaysia, Skudai, Johor, Malaysia
e-mail: azmanh@cheme.utm.my

S. Siddiquee et al. (eds.), *Composite Materials: Applications in Engineering, Biomedicine and Food Science*, https://doi.org/10.1007/978-3-030-45489-0_21

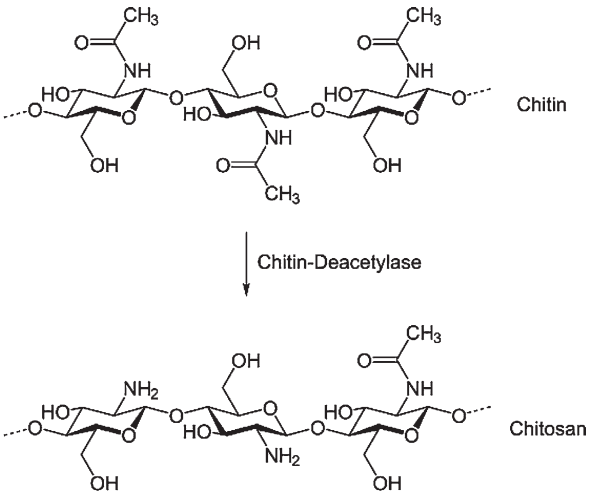

Fig. 21.1 Forming chitosan by partial deacetylation of chitin

antimicrobial, antifungal and anticancer properties (Elsabee and Abdou 2013; Mujtaba et al. 2019). It is found out that chitosan can be used as biopesticide for the agriculture application, as it is able to significantly reduce the infestation of root knot worm and suppress the growth of fungal (Dutta et al. 2004). In biomedical application, chitosan possesses acceleratory effect on wound healing, thus it is used as the coating on normal biomedical materials, such as bandages, to act as antibacterial agent besides of reducing the wound bleeding (Dutta et al. 2004; Mujtaba et al. 2019). Chitosan also widely used in food application, as dietary ingredient, emulsifying agent, and food preservatives (Ambore et al. 2013). Nowadays, chitosan is attaining huge attention from the industrialists and researchers in the field of food packaging application, as an environmentally friendly material, potentially replacing the use of petroleum-based packaging material.

21.2 Chitosan in Food Packaging Application

Chitosan presents high potential as films with tough, flexible, and durable to extension characteristics. Chitosan films show a great property, for instance, outstanding film-forming also at dry condition chitosan has shown gas and aroma barrier activities that appropriate to apply to food packaging (Dutta et al. 2009). The properties of the film rely on its physical characteristics, including molecular weight, degree of N-acetylation, evaporation of the solvent, and free amine regenerating mechanism (Casariego et al. 2009).

The chitosan films can be used for edible food packaging due to great barrier properties of oxygen and carbon dioxide, besides having remarkable antimicrobial

activities. However, is soluble in aqueous medium of an organic acid such as acetic acid, which makes the films not appropriate for some applications. Chitosan films are also sensitive to humidity that decrease the efficiency of physicochemical of the films (Mujtaba et al. 2019).

Several researchers attempt to overcome this drawback by using surface modification techniques or combine them with other polymers and active substance such as a moisture-resistant polymer, plasticizers, and/or active ingredient. Combining chitosan film with another polymer can improve the stability of films by lessens melting temperature or increase the temperature of glass transition. In addition, adding active substance such as essential oil, antimicrobial agent, or antioxidant agent can be assembled advantages of each component to improve the antimicrobial and/or antioxidant properties of the films.

Chitosan-based materials have been widely investigated and reported as a potential material for food packaging due to its biological and physical properties of biocompatibility, biodegradability, antimicrobial ability, and easy film-forming ability. However, chitosan is poor in physicochemical properties that necessary to meet industry standards such as mechanical, thermal and barrier properties. Chitosan films need to be improved in order to make chitosan-based wrapping ingredients reasonable, moderate, economical in contrast to petroleum-based synthetic materials.

Different chitosan-based films have been fabricated and applied in the field of food packaging, by preventing the decline in contents of ascorbic acid, anthocyanins and total polyphenols in various fruits and vegetables during the storage of post-harvest (Kerch 2015). Acetic acid and hydrochloric acid are solvent that can dissolve chitosan, which makes film-forming possible. Wang et al. (2018) have reported various methods of chitosan film-forming, including casting, coating and layer-by-layer assembly as can be summarized in Fig. 21.2. Direct casting is often used for film preparation due to the simplicity, whereas coating is usually applied for protection. Dipping or immersing is similar to coating, but the uniform films will be able to develop. Layer-by-layer assembly is targeted to control the properties and functionality of the material. Meanwhile, extrusion is used to prepare material formulations with different compositions or blended with other materials. Mujtaba et al. (2019) reported the current advancements in chitosan-based film production for food technology and focused on the incorporation of plant extracts and blending with other polymers to enhance the biological (mainly antimicrobial and antioxidant) and physiological (mainly mechanical, thermal and barrier) attributes of the chitosan-based films.

The functionalization of chitosan has been conducted to modify the characteristics of chitosan, such as antimicrobial activity, barrier property, antioxidant activity, mechanical property, optical property, sensing/indicating capacity, and thermal stability. In this article, the recent advances in the strategies to functionalize the chitosan-based packaging materials such as grafting, cross-linking, the addition of nanofillers, incorporation of additives and their effect on the parameters of chitosan films were comprehensively reviewed.

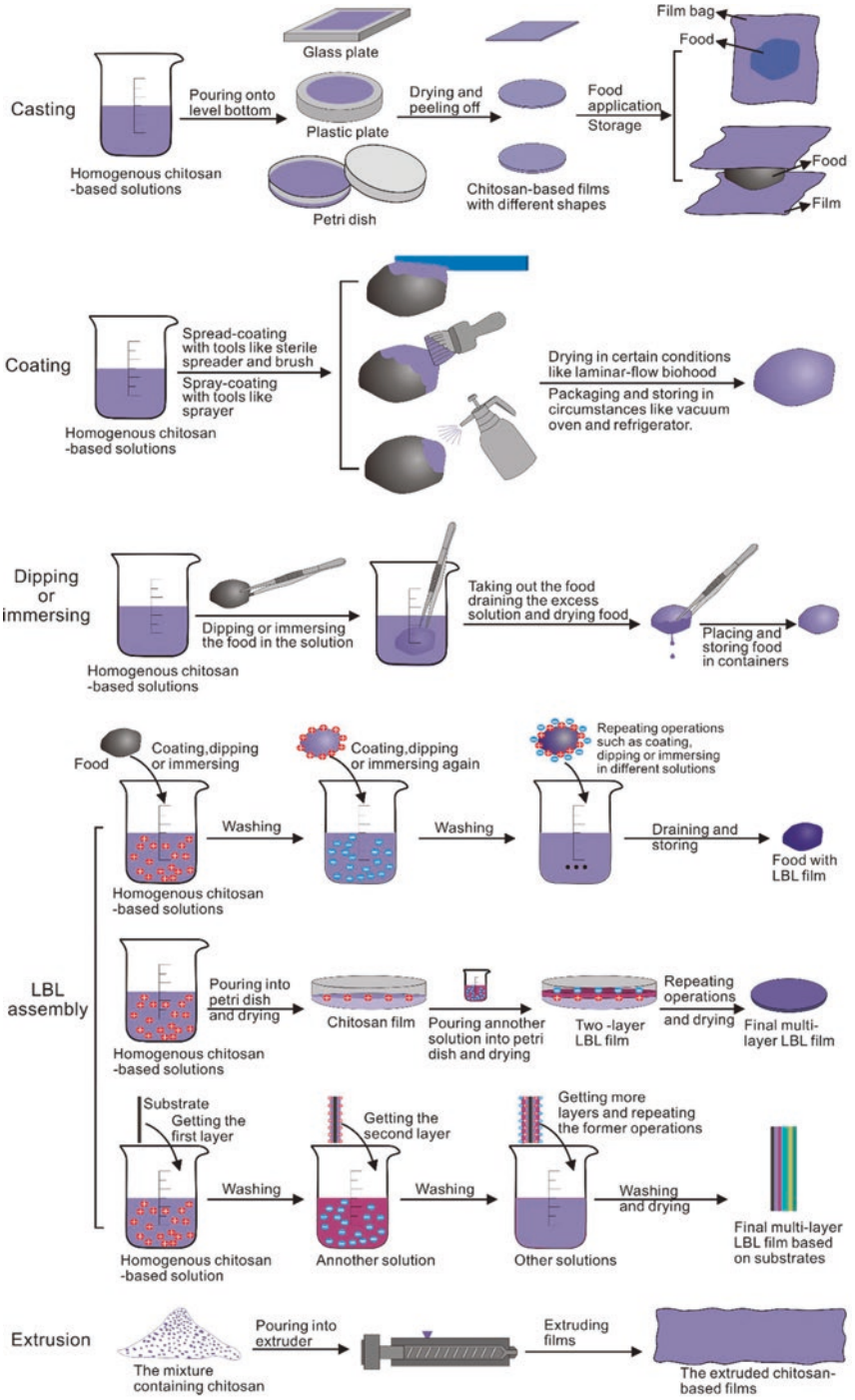

Fig. 21.2 Different methods to fabricate the chitosan-based films. ("Reprinted (adapted) with permission taken from Wang et al. (2018)

21.3 Chitosan Functionalization

Chitosan functionalization which are grafting and crosslinking are necessary to overcome the limitations of chitosan-based films which will allow them to be used in food packaging application. Besides that, blending with other natural polymers and the incorporation of other ingredients such as essential oil and clay are also used together with grafting and crosslinking.

21.3.1 Grafting

Chitosan has been grafted with several grafting agents such as gallic acid (Zhang et al. 2019a), acrylonitrile and acrylamide (Kumar et al. 2018), 4-hexyloxyphenol (Liu et al. 2018), phenyllatic acid (Li et al. 2017) and etc. It is mainly for the enhancement of properties such as antimicrobial and antioxidant of chitosan film, hydrophobic properties and physical properties of chitosan films. Natural antioxidants were added into chitosan-based films to delay the lipid oxidation that leads to food spoilage and this can be done through grafting method (Ganiari et al. 2017). The total phenolic content and antiradical activity was increased and the oxidation of fish and meat products was slowed down, when the extracts from several herbs (rosemary, oregano, tea), berries and plant by-products were added into the chitosan-based films. The incorporation of natural antioxidants into chitosan-based films improved the barrier properties due to the interactions between the matrix and the active groups of additives, such as polyphenols. In a study that added aqueous green tea extract into the chitosan-based films, the water vapour permeability of the composite films is reduced, whereas the polyphenolic content and antioxidant activity, as well as mechanical properties are improved (Siripatrawan and Harte 2010). The incorporation of grape pomace extracts into the chitosan-based films also showed that the films have lower water solubility but higher antioxidant capacity in organic medium (Ferreira et al. 2014). Therefore, these natural antioxidants become the promising ingredients to be incorporated into chitosan-based films, which is worth investigating for the usage in the application of active packaging. Besides of natural antioxidants, the incorporation of various types of oil (rosemary, sunflower, lavender, olive, carp) into chitosan-based films are also able to improve the barrier properties, as well as the mechanical properties (Kerch 2015).

Gallic-acid which is one of the natural antioxidants was grafted into chitosan with different grafting ratios, where the antioxidant properties and water solubility of gallic acid-g-chitosan films were studied (Cho et al. 2011). All gallic acid-g-chitosan films have improved antioxidant capacities, cytocompatibility and inhibition of the formation of intracellular reactive oxygen species. Besides, it is found out that film with the highest gallic acid content has highest scavenging activity against 2,2-diphenyl-1-picrylhydrazyl (DPPH) and hydrogen peroxide up to 92.26% and 93.15% respectively. In another study by Zhang et al. (2019a), the physical

property and antioxidant potential of gallic acid-g-chitosan films fabricated using different grafting methods were studied. Three grafting methods were used, namely: free radical initiation, carbodiimide coupling and tyrosinase catalysis. Carbodiimide coupling method gave the highest grafting efficiency, whereas enzyme catalyzed grafting method had the lowest grafting ratio. Therefore, gallic acid-g-chitosan films obtained through carbodiimide coupling method showed the highest water vapor barrier property, tensile strength, thermal stability and DPPH radical scavenging ability. This indicated that gallic acid-g-chitosan film prepared by carbodiimide coupling method could be further developed as antioxidant active packaging film.

Besides gallic acid, caffeic acid, phenolic acid, phenyllactic acid and protocatechuic acid were also grafted into chitosan-based films for development of potential active packaging materials; to improve food quality, safety and shelf life. The grafting of caffeic acid above 5% into chitosan has higher grafting efficiency with lower molecular weight of chitosan, without causing the loss of antioxidant activity (Aytekin et al. 2011), whereas the grafting of phenolic acid into chitosan has improved the bioactivity of chitosan (Liu et al. 2017b). Besides that, it has the potential as coating agent, encapsulation agent and bio-adsorbent in many applications. There are a number of properties which have improved after grafting the chitosan with phenolic acid; antioxidant, antimicrobial, antitumor, anti-allergic, anti-inflammatory, anti-diabetic and acetylcholinesterase inhibitory activities.

Another successful preparation of antimicrobial and antioxidant chitosan derivatives with grafted phenyllactic acid was recently reported by Li et al. (2017). The proposed reaction schemes are shown as Fig. 21.3. The grafting ratio increased from 5.72% to 11.83% when the phenyllactic acid to chitosan molar ratio increase from 1:1 to 3:1. A greater grafting ratio corresponded to a higher activity of scavenging DPPH radicals and greater inhibition to growth of Gram-positive *Staphylococcus*

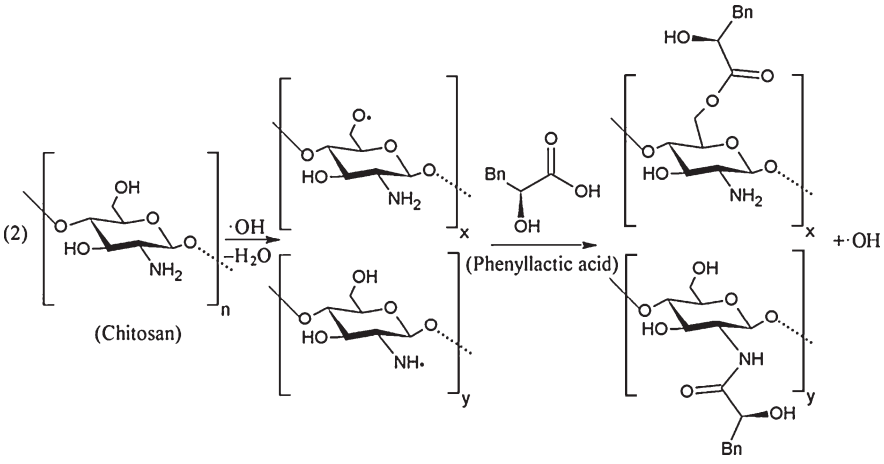

Fig. 21.3 Proposed reaction schemes of grafting phenyllactic acid to chitosan. (Source: Li et al. 2017)

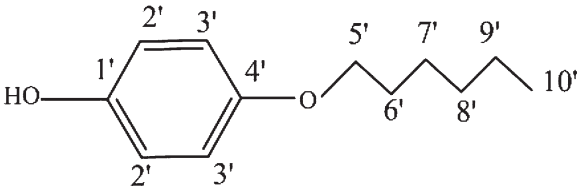

Fig. 21.4 Structure of 4-hexyloxyphenol. (Source: Liu et al. 2018)

aureus and *Listeria monocytogenes*, Gram-negative *Escherichia coli* and *Salmonella enterica*, and fungi *Saccharomyces cerevisiae* and *Penicillium expansum* ($P < 0.05$).

Natural phenolic antioxidant of protocatechuic acid grafted chitosan-based films was developed by Liu et al. (2017a). The results showed that the properties of chitosan-based films; moisture content, water solubility, ultraviolet (UV) light absorbing ability, colour, opacity, tensile strength, elongation at break, thermal stability, microstructure and antioxidant activity can be described as a function of grafting ratio. From the study, it was concluded that protocatechuic acid grafted chitosan-based films can be effectively used as antioxidant food packaging materials.

Hydrogels composed of chitosan grafted with eugenol monomer were studied by Jung et al. (2006). Although eugenol side chains disturbed the crystalline arrangement of chitosan, the hydrophobicity of eugenol reduced the equilibrium water content, particularly when the graft yield increased. After being grafted with eugenol, the hydrogels exhibited lower pH sensitivity and higher scavenging activity which results the improvement in antioxidant activity. Flavonoids, such as flavanols, flavonols, flavone, flavanone, and isoflavone also can be grafted into chitosan to improve the antioxidant and antimicrobial activity of the material, where some of them particularly against *Bacillus subtills* and *Pseudomonas aeruginosa*. (Sousa et al. 2009).

The grafting of α,β-dipeptoids-carrying benzyloxyethyl side chains into chitosan films was reported by Elchinger et al. (2017). It is found out that the low cost chitosan originated from waste of shellfish factories displayed an enhancement of antioxidant activity up to 90%, when grafted with these short length peptoid oligomers. In another study by Moreno-Vasquez et al. (2017), the epigallocatechin gallate (EGCG)-functionalized chitosan was thermally stable at temperature higher than 150 °C. Meanwhile, the antioxidant and antibacterial activity of the EGCG-g-chitosan against *S. aureus* and *Pseudomonas sp.* ($p < 0.05$) was improved. In addition, 4-hexyloxyphenol, shown as Fig. 21.4, also can be used to functionalize the chitosan, to improve the thermal stability, significantly enhance 2,2-azino-bis(3-ethylbenzothiazoline-6-sulphonic acid) (ABTS) and DPPH radicals scavenging capacity, hydrophobicity property and antioxidant characteristics, as compared to pure chitosan (Liu et al. 2018).

Preparation of a novel binary grafted chitosan film with satisfactory antimicrobial activity and biodegradable nature for potential application in food packaging was reported, by grafting of acrylonitrile and acrylamide into chitosan via microwave-initiated graft copolymerization (Kumar et al. 2018). The mechanism of the grafting is shown as Fig. 21.5. Compared to pure chitosan, the binary grafted chitosan film is more thermally stable at elevated temperature, also it possessed efficient

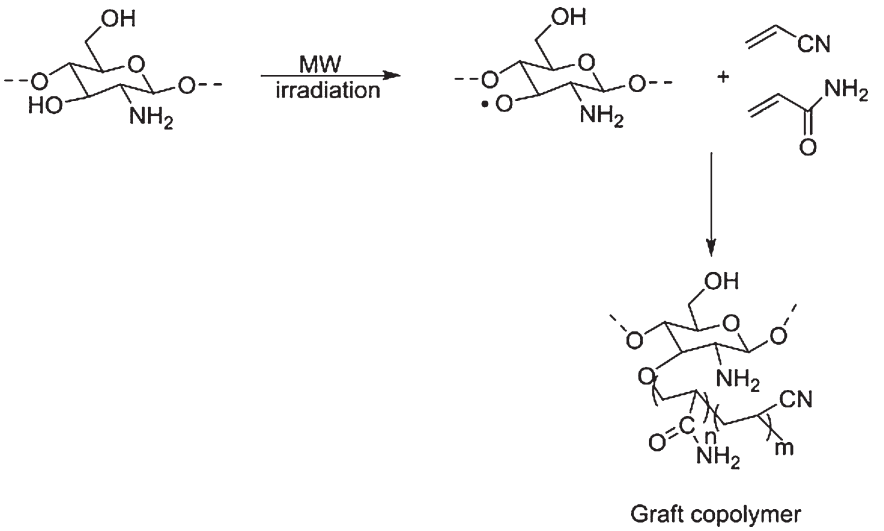

Fig. 21.5 Grafting mechanism of acrylonitrile and acrylamide into chitosan via microwave-initiated graft copolymerization. (Source: Kumar et al. 2018)

antimicrobial activity against three tested strains, namely *Escherichia coli*, *Staphylococcus aureus* and *Pseudomonas aeruginosa*. Therefore, the newly prepared packaging film in this study successfully protected apple and guava from microbial infection and extended their shelf life besides being biodegradable in nature.

Despite of the surface-properties and biodegradability, the high sensitivity of chitosan towards water limited its application as a promising green packaging material. Thus, Lepoittevin et al. (2019) proposed the fluorinated polymer brushes grafted chitosan films with enhanced stability in wet environment. The contact angle measurements and surface energy calculations revealed that the grafted chitosan films have hydrophobic and oleophobic surfaces properties with low surface energy. Hence, these new hydrophobic grafted chitosan films have great potential in food packaging application.

Furthermore, there are studies that blend or hybrid the grafted chitosan with other materials, to produce better materials for food packaging application and hard tissue engineering application. The starch-chitosan blend films were incorporated with ferulic acid for investigation on the potential to be used as an edible film or coating (Mathew and Abraham, 2008). It is found out that the incorporation of the oxidized ferulic acid is able to enhance considerably the barrier properties of the films, and reduce the formation of lipid peroxide, thus preserving the food for longer shelf life.

Table 21.1 shows the recent studies that have chitosan-based materials grafted with other ingredients to achieve the desired properties for the food packaging applications.

Table 21.1 Recent studies of grafted chitosan-based materials

Grafting compounds	Effects of grafting	References
Gallic acid	Improved water vapour barrier property Improved tensile strength Improved thermal stability Improved antioxidant property	Zhang et al. (2019a)
Acrylonitrile and acrylamide	Improved thermal stability Improved antimicrobial activity	Kumar et al. (2018)
4-hexyloxyphenol	Improved thermal stability Improved ABTS and DPPH radicals scavenging capacity Improved antioxidant characteristics Improved hydrophobicity Reduced tensile strength	Liu et al. (2018)
Phenyllactic acid	Reduced thermal stability Improved antioxidant and antimicrobial properties	Li et al. (2017)
α,β-dipeptoids-carrying benzyloxyethyl side chains	Improved antioxidant activity	Elchinger et al. (2017)
Epigallocatechin gallate (EGCG)	Improved thermal stability Improved antibacterial and antioxidant activity	Moreno-Vasquez et al. (2017)
Protocatechuic acid	Lowered moisture content and water vapor permeability Increased water solubility Improved tensile strength and elongation at break Improved UV light barrier	Liu et al. (2017a)
Fluorinated polymer brushes	Increased hydrophobicity Improved stability in wet environment	Lepoittevin et al. (2019)

21.3.2 Crosslinking

Crosslinking of chitosan matrix is another method for functionalization to enhance the chitosan film properties. Glutaraldehyde (GL), a dialdehyde with high affinity due to the free primary amine groups of amino acids, is one of the earliest crosslinking agent studied for chitosan films (Cheung et al. 1985). In 1999, Monteiro and Airoldi reported a study on crosslinking chitosan-GL interaction in a homogeneous system. Chitosan which was dissolved in acetic acid reacted with GL solution, ranging in concentration from 0.10 to 25.0 × 10^{-2} mol/dm^3. The data from ^{13}C NMR, infrared and Raman spectroscopies provided the evidence of the formation of an ethylenic double bond in the chitosan–GL interaction. The results suggest that free pendant amine groups of chitosan polymer interact with the aldehydic group of the GL to form stable imine bonds, due to the resonance established with adjacent double ethylenic bonds.

In a recent study on GL crosslinked chitosan-based films, the use of NaOH as alkaline post-treatment was reported (Frick et al. 2018). The swelling degree of films decreased while the fragility of films increased due to the crosslinking effect by GL and the post-treatment by NaOH. Based on the result of water vapour permeability, it is found out that post-treatment with NaOH is necessary to enable the films to be used in food packaging application. This is because the NaOH post-treatment increased the film water stability without compromise greatly with the barrier properties of films. Besides, the films also experienced higher tensile strength with lower elongation at break after the GL crosslinking and alkaline post-treatment. Instead of using NaOH post-treatment, the development of bioactive composite films from chitosan and carboxymethyl cellulose (CMC) using GL as crosslinker and cinnamon essential oil (CEO) as additive was recently investigated (Valizadeh et al. 2019). The outcome of this study showed that the crosslinking of GL significantly gave higher mechanical strength and lower water vapor permeability, which is similar to the study by Frick et al. (2018). The simultaneous incorporation of CEO increased the antibacterial and antioxidant properties of composite films. Therefore, the composite films prepared in the study are good candidates for improving perishable foods shelf life.

Genipin is a chemical compound that can be derived from the geniposide which found in Gardenia jasminoides fruits, via hydrolysis with β-glucosidase (Nunes et al. 2018). Due the safety of the materials used, genipin was the preferred crosslinking agent compared to GL. This is because genipin has low cytotoxicity as compared to GL and is able to demonstrate good biological properties such as anti-inflammatory, lipid peroxidation inhibition, nitric oxide production inhibition and anti-angiogenesis (Koo et al. 2004). Thus, genipin are safe and non-cytotoxic to animal and human cells (Muzzarelli 2009). It is found out that genipin as a water-soluble bi-functional crosslinking reagent, is able to react quickly with chitosan to produce blue-coloured fluorescent complexes, via the nucleophilic attack on genipin by primary amine group that led to the linkage between the heterocyclic compound of genipin formed and glucosamine residue in chitosan, followed by the nucleophilic substitution of the genipin's ester group that able to form a secondary amide link with chitosan (Butler et al. 2003), shown as Fig. 21.6. Besides of food packaging application, genipin also become an alternative to replace GL in the biomedical and pharmaceutical applications due to its better stability and biocompatibility, also easier manipulation and quality assessment (Muzzarelli 2009). Several studies were reported on the crosslinking of genipin as an effective cross-linking agent for chitosan.

The effect of pH on the cross-linking between chitosan and genipin to form chitosan-based polymeric network was documented (Mi et al. 2005). It is found out that the crosslink bridges were consisted of long crosslink units of genipin at the basic conditions; but short chains of heterocyclic amines bridges formed when under neutral and acidic conditions. Under pH condition of 9, the network segments of chitosan were consisting of both short crosslink units of cyclic bridges and long crosslink unit of polymerized genipin. The results showed that the crosslinking mode, crosslink bridges length and the crosslinking extent were significantly dependent on the crosslinking pH value, where shown as Fig. 21.7. These were then

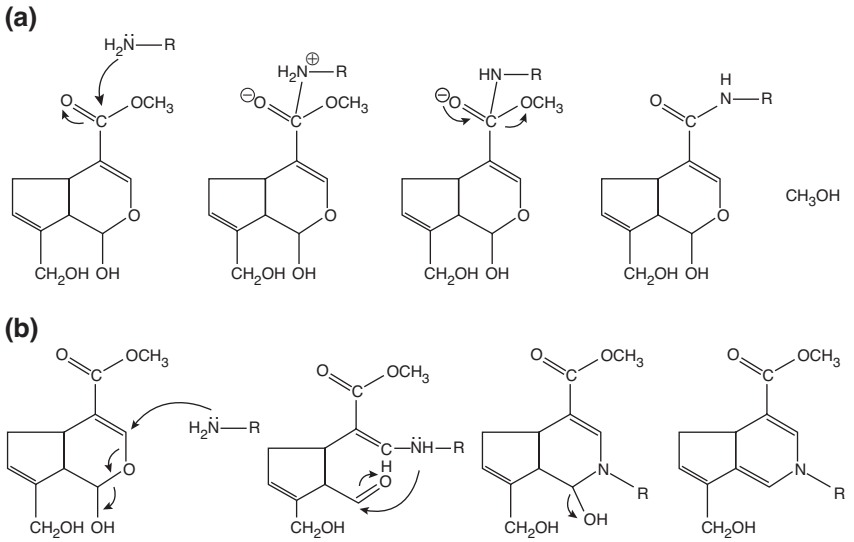

Fig. 21.6 Crosslinking reactions involving genipin: (**a**) reaction Scheme 1 (**b**) reaction Scheme 2. (Source: Butler et al. 2003)

affecting the swelling capability and resistance against enzymatic hydrolysis of the chitosan polymeric network.

Besides, the chitosan-genipin films were suggested for sustainable wine preservation instead of the addition of sulphur dioxide as preservative during the wine production (Nunes et al. 2016). The films were produced from shrimp by-products, which have similar mechanical and chemical properties as fungi-based films, also showing negative Immunoglobulin E (IgE) reaction against shellfish allergenic compounds. Moreover, it is found out that the wines showed lower metal availability, susceptibility to browning, lesser oxidation reactions, microbial growth inhibited with comparable organoleptic and volatile characteristics.

` Besides genipin, aglycone geniposidic acid (aGSA) was also used to crosslink chitosan-based films (Mi et al. 2006). This naturally occurring crosslinking agent is produced from the fruits of *Gardenia jasminoides*. It is found out that aGSA-crosslinked chitosan films with an increasing aGSA concentration up to 0.8 mM significantly increased the ultimate tensile strength but reduced the strain at fracture and swelling ratio of the films. The antimicrobial capability of the cross-linked chitosan films showed no significant difference compared to their fresh counterpart. However, compared to the GL-crosslinked counterpart, aGSA-crosslinked chitosan film showed lower cytotoxicity, slower degradation rate, and relatively lower water vapor permeability. These results proposed the newly developed aGSA-cross-linked chitosan film to be used as an edible film.

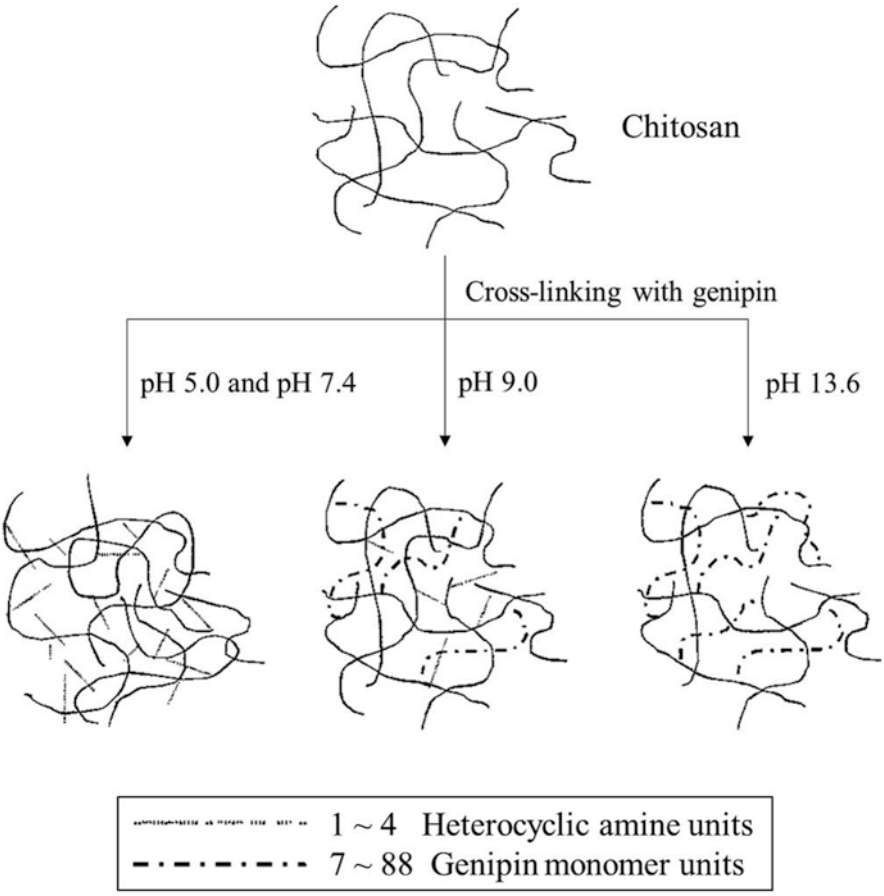

Fig. 21.7 Conformations of the network segments of genipin-crosslinked chitosan under different pH conditions. (Source; Mi et al. 2005)

In recent studies, *Lepidium sativum* seedcake phenolic extract (LSE) and *Nigella sativa* seedcake phenolic extract (NSE) can be incorporated into the chitosan-based films respectively (Kadam and Lele 2018; Kadam et al. 2018). The water vapour permeability and crystallinity decreased when incorporated LSE into the chitosan-based films (Kadam and Lele 2018), and the incorporation of NSE gave similar outcome as well (Kadam et al. 2018). Compared to another crosslinker, tannic acid, the incorporation of LSE is able to enhance both tensile strength and elongation at break; whereas the incorporation of NSE only improved the elongation at break. Based on the study of Kadam and Lele (2018), the oxidation reaction of the food that packaged within the crosslinked films were prevented, which may be attributed to the antioxidant activity of the films in terms of DPPH and Ferric Reducing Antioxidant Power (FRAP) activity that have the similar pattern in both aqueous

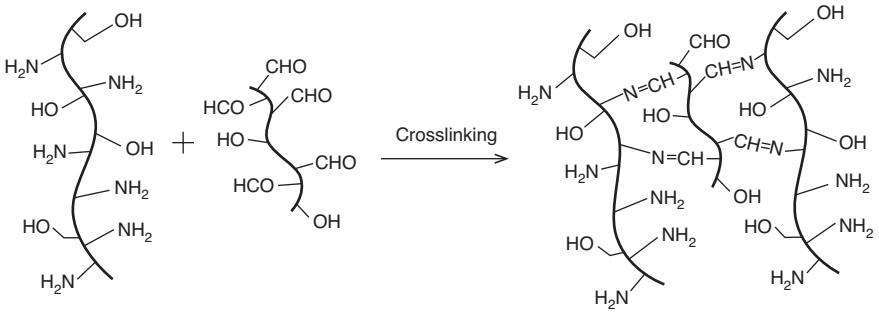

Fig. 21.8 Schematic crosslinking reaction between DAC and chitosan. (Source: Tian and Jiang 2018)

and fatty food simulants. Meanwhile, the incorporation of NSE into chitosan-based films triggered the release of polyphenols and subsequent antioxidant activity in both water and ethanol medium (Kadam et al. 2018). Hence, both chitosan/LSE composite films and chitosan/NSE composite films are worth to be investigated and developed as a novel and potential bioactive and biodegradable active packaging materials, particularly in the aspect of food preservation.

The water soluble 2,3-dialdehyde cellulose (DAC) was used as crosslinker for chitosan-based films (Tian and Jiang 2018), and the schematic crosslinking reaction between DAC and chitosan is shown as Fig. 21.8. The crosslinked chitosan films have enhanced acid resistance and tensile strength compared to the neat chitosan films. These improvements are attributed to the good compatibility between DAC and chitosan. In addition, chitosan can be crosslinked with ε-polylysine (ε-PL) to produce bionanocomposite films by using sodium tripolyphosphate (TPP) as the cross-linking agent (Wu et al. 2019b). The proposed formation mechanism of chitosan/ε-PL bionanocomposite films shown as Fig. 21.9. The films exhibited excellent antimicrobial efficacy against both *Escherichia coli* and *Staphylococcus aureus* by the increasing ratio of ε-PL.

In addition, there are number of studies that incorporated crosslinked chitosan-based films with other ingredients or blended with biopolymer, to overcome the limitation possessed by chitosan itself. Tannic acid used as crosslinker and glycerol used as plasticizer in the chitosan-based films (Rivero et al. 2010). It is found out that the addition of tannic acid together with glycerol in the chitosan-based films have synergic effect, which provided higher tensile strength, lower water vapour permeability and more stable structure of films. In another study by Priyadarshi et al. (2018), citric acid is used instead of tannic acid in the chitosan-based films with glycerol as plasticizer. Citric acid improved the stability of the films, whereas glycerol improved the flexibility of the films. The crosslinking mechanism between citric acid and chitosan is shown as Fig. 21.10. Besides, the barrier properties were improved by reducing the water vapour permeability, and it is found out that these films exhibited enhanced antioxidant properties, where they are able to extend the shelf life of green chilli and believed to be able on working for other fresh products.

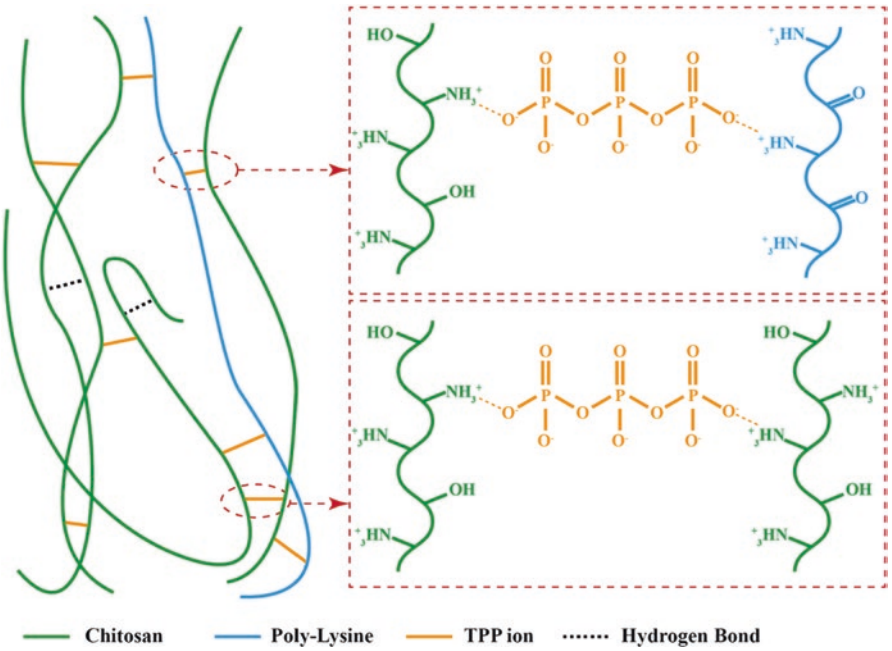

Fig. 21.9 Proposed formation mechanism of chitosan/ε-PL bionanocomposite films. (Source: Wu et al. 2019b)

Composite films consist of sodium alginate and chitosan were firstly prepared, followed by crosslinking of CMC with the crosslinking agent, calcium chloride ($CaCl_2$) (Lan et al. 2018). The composite films have advantageous properties on the inhibition of the growth and reproduction of microorganisms with the antibacterial rate against *Escherichia coli* and *Staphylococcus aureus* is up to 95.7% and 93.4% respectively. Besides, the mechanical strength and ductility of the composite films are able to meet the requirements for food packaging application. Furthermore, another composite films were prepared by loading the carvacrol nanoemulsions (CA-NEs) into the carboxymethyl chitosan films that were self-crosslinked (Lei et al. 2019). CA-NEs/carboxymethyl chitosan composite films are potential materials for active packaging, as the films are able to extend the shelf life of wheat bread, besides of having good antibacterial activity against *Staphylococcus aureus* and *Escherichia coli*, as well as antioxidant activity.

The crosslinked chitosan-based films can also blend with biopolymers. Genipin-crosslinked chitosan was blended with poly(ethylene oxide) (PEO) to produce films that have improved stability and mechanical properties, including elasticity (Jin et al. 2004). Besides, the films were insoluble in acidic and alkaline solutions. It is also found out that the swelling characteristics of the films in these aqueous media were pH and temperature dependence. As compared to the uncrosslinked chitosan/PEO films, the crosslinking of genipin allowed the films to be more hydrophobic. In

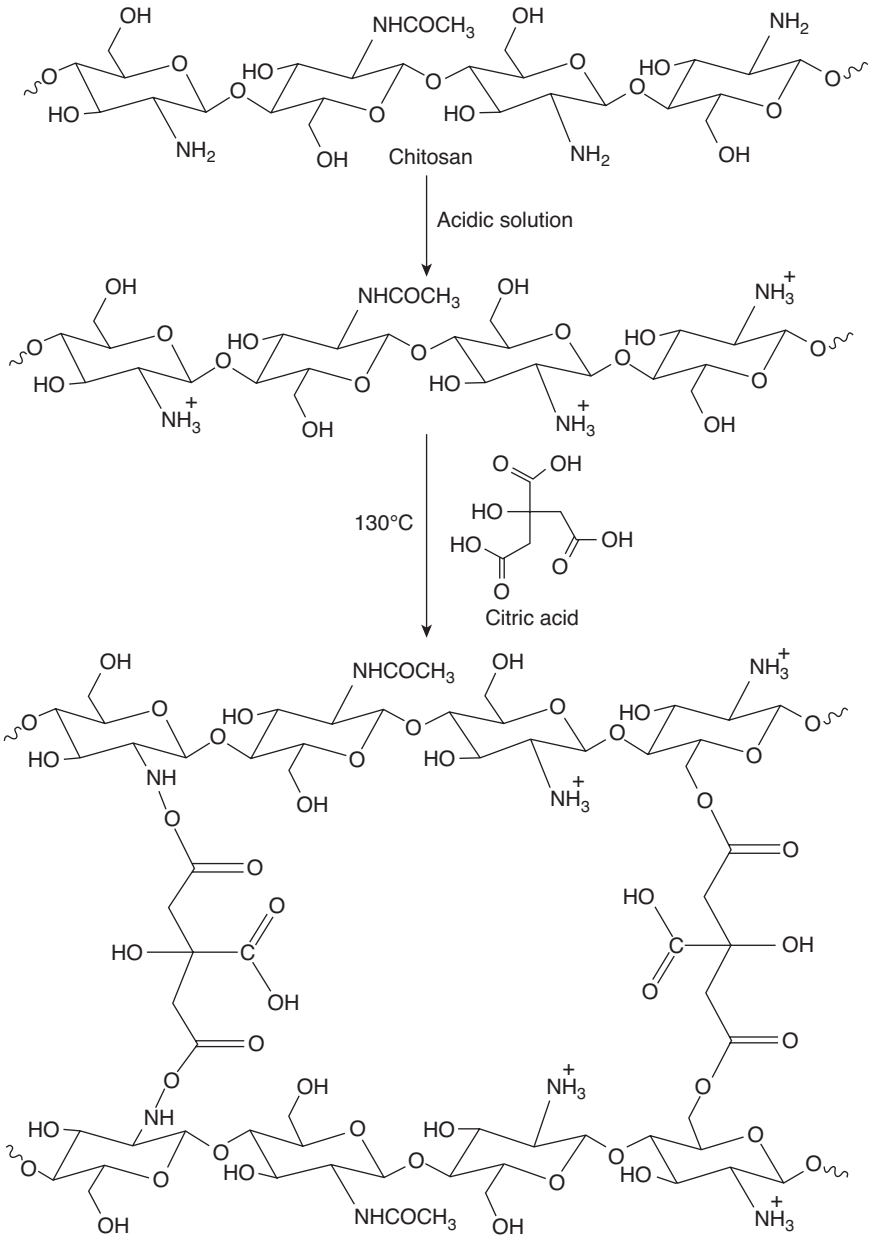

Fig. 21.10 Schematic crosslinking between citric acid and chitosan. (Source: Priyadarshi et al. 2018)

another study, the pH and temperature also affecting the swelling characteristics of the genipin-crosslinked chitosan films that blended with poly(vinyl pyrrolidone) (PVP) (Khurma et al. 2005). Poly(vinyl alcohol) (PVA) is another biopolymer that blended with chitosan-based films to produce potential materials for food packaging application (Wu et al. 2018). It is found out that the physical crosslinking occurred through the interchain hydrogen bonding between the carbonyl group of chitosan and hydroxyl group of PVA, which had high compatibility. The optimum composition of chitosan and PVA is 60 wt% chitosan and 40 wt% PVA, where the blending with this composition are able to against the bacterial adhesion and inhibit the biofilm formation against *Pseudomonas aeruginosa* PAO1. Thus, chitosan/PVA blended films can become the potential food packaging materials due to the antimicrobial and biofilm inhibiting properties.

There are also studies that involved both grafting and crosslinking method to produce chitosan-based films with desired properties for food packaging application. In order to overcome the limitations of chitosan films in terms of antioxidant activity and stability in acidic media, chitosan-based films were grafted with caffeic acid and crosslinked with genipin (Nunes et al. 2013). Compared to the pristine film, genipin-crosslinked-caffeic acid-g-chitosan films exhibited higher antioxidant activity up to 80%, and the films have higher stability in acidic condition as the total mass loss after seven days immersion was only 11%. Meanwhile, the surface wettability, mechanical properties and thermal stability of the films were maintained after grafting and crosslinking. Genipin resulted in decreasing of solubility in acidic medium, while caffeic acid improved the antioxidant activity (Coimbra et al. 2012). Besides of caffeic acid, the genipin-crosslinked chitosan-based films were grafted with the phenolic compounds from red wine (Nunes et al. 2015). The phenolic compounds found in red wine are anthocyanins, proanthocyanidins, monomeric catechins, and phenolic acids, which they have strong antioxidant properties generally. Similar to the previous studies, the addition of genipin as crosslinking agent is able to increase the film stability in wide range of pH. Hence, these films are potential active packaging material for food preservation and enhance the shelf life of food products.

Furthermore, a novel active blend films were prepared, by firstly grafted the chitosan-based films with gallic acid, then crosslinked with PVA and incorporated citric acid as plastisizer (Yoon et al. 2017). It is found out that light-emitting diode-ultraviolet (LED-UV) irradiation able to strengthen the cross-linkage between gallic acid-g-chitosan and PVA, which led to higher tensile strength, but lower elongation at break, degree of solubility and swelling behaviour as compared to the films without LED-UV irradiation exposure. However, the water vapour absorption increased because of the changes of pore volume and roughness of surface. The optimum gallic acid-g-chitosan to PVA mass ratio is 1:1 in the blend films for the highest antimicrobial activity against Gram-negative bacteria (*Escherichia coli* and *Salmonella typhimurium*) and Gram-positive bacteria (*Staphylococcus aureus* and *Bacillus cereus*). Table 21.2 shows the recent studies of chitosan-based materials that are crosslinked to achieve the desired properties for the food packaging applications.

Table 21.2 Recent studies of crosslinked chitosan-based materials

Crosslinking agents	Other ingredients (Additives, Biopolymers etc.)	The effects of crosslinking	References
Sodium tripolyphosphate (TPP)	ε-polylysine	Improve tensile strength Reduced water solubility, water vapour permeability, surface wettability	Wu et al. (2019b)
Poly(vinyl alcohol) (PVA)		Reduced tensile strength Reduced light transmittance Improved antimicrobial activity	Wu et al. (2018)
Lepidium sativum seedcake phenolic extract (LSE)		Improved tensile strength and elongation Reduced water vapour permeability Improved antioxidant activity	Kadam and Lele (2018)
Nigella sativa seedcake phenolic extract (NSE)		Improved tensile strength Improved elongation Reduced water vapour permeability Improved antioxidant activity	Kadam et al. (2018)
Glutaraldehyde (GL)		Reduced swelling degree Increased rigidity and fragility Improved tensile strength Reduced elongation at break	Frick et al. (2018)
Dialdehyde cellulose (DAC)		Improved acid resistance Improved tensile strength Reduced elongation at break	Tian and Jiang (2018)
Glutaraldehyde (GL)	Cinnamon essential oil (CEO)	Effect of GL crosslinking Improved mechanical strength Lowered solubility and water vapour permeability Effect of CEO Improved antioxidant activity and antimicrobial properties	Valizadeh et al. (2019)

Calcium ion (Ca^{2+})	Carvacrol nanoemulsions (CA-NEs)	Improved stability in water Improved antioxidant and antibacterial activity	Lei et al. (2019)
Citric acid	Glycerol as plasticizer	Improved moisture barrier and water resistance Increased solubility Increased flexibility Reduced tensile strength and Young's modulus Improved thermal properties Improved antioxidant properties	Priyadarshi et al. (2018)
Calcium chloride ($CaCl_2$)	Carboxymethyl cellulose and sodium alginate	Improved tensile strength and elongation after fracture Improved water vapour transmission rate Improved antibacterial properties	Lan et al. (2018)
LED-UV irradiation	Citric acid as plasticizer, poly(vinyl alcohol) (PVA) for blending, gallic acid for chitosan grafting	Increased tensile strength Reduced elongation at break Reduced solubility and swelling behavior Increased water vapour adsorption Improved antimicrobial activities	Yoon et al. (2017)

21.4 Addition of Nanofillers

Besides grafting and crosslinking, chitosan has been incorporated with different nanofillers to obtain modified packaging materials with improved mechanical and barrier properties. Nanometric materials such as nanoclay (Bourakadi et al. 2019; Dias et al. 2019), titanium dioxide (TiO_2) nanoparticle (Zhang et al. 2019b), graphene oxide (Barra et al. 2019), carbon nanotubes (Bibi et al. 2018), nanocellulose and metal nanoparticles have been successfully incorporated in biopolymer-based films, resulting in packaging materials with good mechanical properties and advanced characteristics. Table 21.3 presents some recent studies on the impact of nanofillers on functional properties of chitosan films. The inorganic fillers improved the rigidity, dimensional stability and thermal stability of the film. In order to extend the functionality of chitosan film, organic or inorganic materials were also added together with the reinforcement fillers.

Montmorillonite (MMT) is among the most often used nanoclay because of its natural abundance and low cost. The unique properties such as good adsorption ability, high cation exchange capacity, swelling capacity and large specific surface area attracted the use of nanoclay in active and smart packaging application. The Young's modulus and tensile strength of chitosan film increased from 66.98 to 143.43 MPa and from 24.95 to 34.65 MPa, respectively with incorporation of 5 phr modified MMT with thiabendazolium surfactants into the chitosan/PVA matrix (Bourakadi et al. 2019). The enhancement in mechanical properties were due to the strong interaction and good dispersion of thiabendazolium-MMT within the polymer chains. Dias et al. (2019) reported that the incorporation of MMT resulted in water vapour transmission rate reduction and provided a controlled release of tocopherol to inhibit oxidation reactions of salmon until 8 days. Mesoporous silica nanoparticle reported to be effective in controlling the release of curcumin (Wu et al. 2019a). The bio-nanocomposites film exhibited sustained release behaviour of curcumin and demonstrated efficient antimicrobial activity against *Staphylococcus aureus* and *Escherichia coli*.

Cellulose is the most abundant biopolymer on earth that can be found in plant or produced by bacteria, algae and marine tunicates. Salari et al. (2018) obtained cellulose nanocrystals from bacterial synthesized by *Gluconacetobacter xylinus* in the molasses medium. It was found that the incorporation of bacterial cellulose nanocrystals and silver nanoparticles into chitosan films significantly influenced the apparent colour and transparency of the films. In addition, sensibility to water, water vapor permeability and mechanical properties were also greatly improved with the incorporation of the fillers.

Numerous researches reported on modification of cellulose nanocrystals and nanoparticles with addition of active ingredients to extend the functionality of chitosan film (Xu, et al. 2019; Zhang et al. 2019; Qin et al. 2019). Xylooligosaccharides, N-Halamine, anthocyanin-rich purple corn extract and anthocyanin-rich black plum peel extract are amongst that were incorporated together with nanofillers to provide prebiotic, antimicrobial and antioxidant properties.

Table 21.3 The effects of nanofiller addition on chitosan films

Nanofiller	Modification/extend functionality	The effects of nanofillers addition	References
(MMT) Montmorillonite	Thiabendazolium surfactants	Improvement of Young's modulus and tensile strength Improvement of antimicrobial activity against *P. eruginosa, S. aureus* and *E. coli*	Bourakadi et al. (2019)
(MMT) Montmorillonite	α-tocopherol	Reduction in water vapour transmission rate Controlled release of tocopherol	Dias et al. (2019)
Halloysite	Clove essential oil	Improvement of water vapor barrier property of the films Incorporation of clove essential oil decreased the elongation of the film, whereas the HNT particles dispersed in the film matrix mitigated this effect.	Lee et al. (2018)
Silica nanoparticles	Curcumin	Improvement of mechanical properties Antimicrobial activity against *Staphylococcus aureus* and *Escherichia coli* Controlled release of curcumin	Wu et al. (2019a)
Cellulose nanofiber	Xylooligosaccharide	Tensile strength of chitosan film increased by 2.5 times with adding 5 wt% CNF Addition of xylooligosaccharide tensile strength (42.7–50.7 MPa) and lower oxygen permeability	Xu et al. (2019)
Cellulose nanocrystal	N-halamine	Improvement of tensile strength Excellent antibacterial property against *Staphylococcus aureus* and *Escherichia coli*	Zhang et al. (2019)

Nanofiller	Modification/extend functionality	The effects of nanofillers addition	References
Wood auto-hydrolysates (WAH)	–	Improvement of tensile strength, light transmittances and thermal stability Improvement of oxygen transfer rate and water vapor permeability	Xu et al. (2018)
Bacterial cellulose nanocrystal and silver nanoparticles	–	Improvement of water vapor permeability and mechanical properties Antibacterial activity against food borne pathogens	Salari et al. (2018)
Silver nanoparticles	Anthocyanin-rich purple corn extract	Improvement of light and water vapor barrier ability Improvement of mechanical strength Antioxidant and antimicrobial properties of chitosan film Able to change colors in different pH buffers due to anthocyanin in the purple corn	Qin et al. (2019)
Titanium dioxide (TiO_2) nanoparticles	Anthocyanin-rich black plum peel extract	Improvement of barrier properties against water vapor and UV–vis light, and better mechanical strength Antioxidant, ethylene scavenging, antimicrobial and pH-sensitive	Zhang et al. (2019b)

Table 21.4 The properties of chitosan filled carbon-based nanofillers

Nanofillers	Biological properties	Mechanical properties	Other Physical properties	References
Graphene oxide (GO)	High antioxidant properties	Increase tensile strength	Improve electrical conductivity, reduced water solubility	Barra et al. (2019)
Graphene oxide (GO)	Superior antimicrobials properties	Improve mechanical and thermal properties		Grande et al. (2017)
Graphene oxide (GO)	Improve antimicrobial properties	Increase tensile properties until 3% GO content Improve thermal properties		Zhang et al. (2018).
Multi-walled carbon nanotube		Improvement of thermal stability		Mallakpour and Ezhieh (2017)
Carbon nanotubes		Enhancement of tensile strength (by up to ~131%), elongation at break (by up to ~18%) and toughness (by up to 125%) Improvement of thermal stability	Reduction of dielectric properties	Bibi et al. (2018)

Carbon-based nanofillers have gained attention due to their properties which include excellent mechanical properties and substantial electron mobility. Graphene, in comparison to other carbon-based nanomaterials, is characterized by a larger surface area that could facilitate interactions with the polymer matrix. Graphene oxide (GO) is the most promising nanofiller because it has lower tendency to agglomerate than pristine graphene. The chemical functionalization of (GO) leads to its modification and thus has very good mechanical, physical, electrical, and thermal properties, which makes it an attractive nanofiller in biopolymer films.

Recently there have been few reports on the incorporation of carbon-based nanofiller with chitosan for food packaging application (Barra et al. 2019; Grande et al. 2017; Zhang et al. 2018). Table 21.4 summarizes the properties of chitosan filled carbon-based nanofiller. The effect of carbon-based nanofillers on the chitosan matrix or film has been highlighted. Barra et al. (2019) highlighted that the eco-friendly bio-nanocomposite films from (GO) and chitosan present remarkable high antioxidant properties, good electrical and mechanical properties, making the material suitable to be used in several applications, including food packaging. Grande et al. (2017) also reported that the incorporation of (GO) with chitosan has enhanced the mechanical and antimicrobial properties of the bio-nanocomposite films.

The performance of other carbon-based chitosan nanocomposite films was also reported. The use of carbon nanotube in chitosan has shown the improvement in mechanical, thermal and electrical properties (Bibi et al. 2018). Mallakpour and

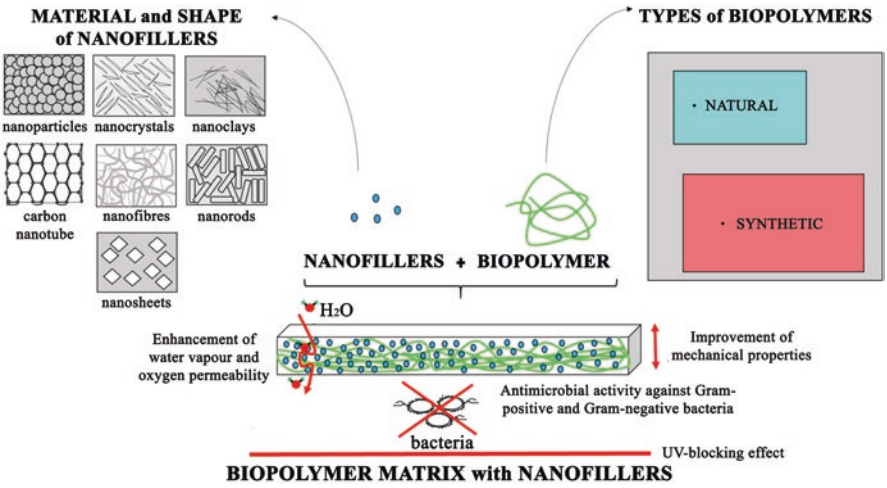

Fig. 21.11 Schematic preparation of nanocomposite films and their functional properties. (Source: Jamróz et al. 2019)

Ezhieh (2017) also reported the improvement in thermal properties of chitosan film when multiwall carbon nanotubes were added into the chitosan matrix. The graphical illustration of nanofillers within the biopolymer matrix along with their functional properties is presented in Fig. 21.11.

21.5 Conclusions and Future Perspectives

Chitosan is a natural biopolymer with several outstanding properties including nontoxic, biodegradable, antioxidant, antimicrobial and has film-forming ability. However, the industrial use of chitosan, particularly in food packaging applications, was limited by their poor mechanical and water or gas vapour barrier properties. Thus, functionalised chitosan films and chitosan-based composites have received much attention to enhance the properties of chitosan-based films, hoping this natural biodegradable polymer can replace conventional petroleum-based food packaging materials and overcome the environmental issues. The amine functional groups in chitosan allows molecular entities modifications through cross-linking, grafting and nanofillers. Crosslinking of chitosan films using cross-linkers, such as genipin, capable in overcoming the weak physical properties of chitosan, namely swelling features, mechanical properties, stability in acidic and alkaline solutions, and water or gas permeability. On the other hand, grafting of chitosan with phenolic compounds, hydrophobic agent or essential oils mainly enhanced the barrier properties, antioxidant and antibacterial activity of the films. Incorporation of nanofillers in chitosan films not only improved the mechanical and barrier properties, but also added electrical conductivity to the films for the use in *in pack* sterilization.

The addition property of chitosan-based composite films extended its applications as active and intelligent food packaging materials.

To ensure the development of chitosan-based materials in food packaging applications, mechanical strength, gas and water barrier properties, as well as antimicrobial and antioxidant properties, ability to extend shelf life of food need to be further enhanced. Therefore, investigations on more chitosan derivatives and functional materials are necessary to meet the requirements of food packaging application. It is believed that nanotechnology will be able to play this role and the incorporation of different types of nanofillers (e.g. cellulose nanowhiskers, chitin nanowhiskers, synthetic wollastonite nanofibre) into the chitosan-based materials will be worth investigating. Besides incorporating nanofillers into the chitosan-based materials, blending with other biodegradable polymers (e.g. polyhydroxybutyrate, polycaprolactone) is also an option to produce new materials with desired properties for practical usage in food packaging applications.

Furthermore, the study on the toxicity of chitosan-based materials need to be performed to ensure safety while in contact with food, for further practical usage in food packaging application. The impacts of these materials toward the environment in the aspect of degradation should also be further investigated, to guarantee they are harmless to our environment. In addition, the mass production of chitosan-based materials at a more competitive cost is one of the issues that is yet to be resolved. With the modifications, chitosan-based materials will have a bright future in food packaging applications, replacing petroleum-based packaging materials.

References

Ambore S, Sangameshwar K, Mukesh G, Chandrakant R, Avinash D, Ambore M, Pharm M (2013) A brief overview on chitosan applications. Indo Am J Pharm Res 20133:2231–6876

Arbia W, Arbia L, Adour L, Amrane A (2013) Chitin extraction from crustacean shells using biological methods - a review. Food Technol Biotechnol 51

Aytekin AO, Morimura S, Kida K (2011) Synthesis of chitosan–caffeic acid derivatives and evaluation of their antioxidant activities. J Biosci Bioeng 111(2):212–216. https://doi.org/10.1016/j.jbiosc.2010.09.018

Barra A, Ferreira NM, Martins MA, Lazar O, Pantazi A, Jderu AA, Neumayer SM, Rodriguez BJ, Enăchesc M, Ferreira P, Nunes C (2019) Eco-friendly preparation of electrically conductive chitosan - reduced graphene oxide flexible bionanocomposites for food packaging and biological applications. Compos Sci Technol 173:53–60. https://doi.org/10.1016/j.compscitech.2019.01.027

Bibi S, Jamil A, Yasin T, Rafiq MA, Nawaz M, Price GJ (2018) Ultrasound promoted synthesis and properties of chitosan nanocomposites containing carbon nanotubes and silver nanoparticles. Eur Polym J 105:297–303. https://doi.org/10.1016/j.eurpolymj.2018.06.004

Bourakadi KE, Merghoub N, Fardioui M, Mekhzoum MEM, Kadmiri IM, Essassi EM, El Kacem QA, Bouhfid R (2019) Chitosan/polyvinyl alcohol/thiabendazoluim-montmorillonite bionanocomposite films: mechanical, morphological and antimicrobial properties. Compos Part B 172:103–110. https://doi.org/10.1016/j.compositesb.2019.05.042

Butler MF, Ng YF, Pudney PDA (2003) Mechanism and kinetics of the crosslinking reaction between biopolymers containing primary amine groups and genipin. J Polym Sci A Polym Chem 41(24):3941–3953. https://doi.org/10.1002/pola.10960

Casariego A, Souza BWS, Cerqueira MA, Teixeira JA, Cruz L, Díaz R, Vicente AA (2009) Chitosan/clay films' properties as affected by biopolymer and clay micro/nanoparticles' concentrations. Food Hydrocoll 23(7):1895–1902. https://doi.org/10.1016/j.foodhyd.2009.02.007

Cheung DT, Perelman N, Ko EC, Nimni ME (1985) Mechanism of crosslining of proteins by glutaraldehyde III. Reaction with collagen in tissue. Connect Tissue Res 13(2):109–115

Cho YS, Kim SK, Ahn CB, Je JY (2011) Preparation, characterization, and antioxidant properties of gallic acid-grafted-chitosans. Carbohydr Polym 83(4):1617–1622. https://doi.org/10.1016/j.carbpol.2010.10.019

Coimbra MA, Nunes C, Maricato E, Cunha A, Mendo S, da Silva JAL (2012) Winemaking method without the admixture ofsulphur dioxide using chitosan-based films. US Patent 2014/0328974A1, 2 Nov 2012

Dias MV, Azevedo VM, Santos TA, Pola CC, Lara BRB, Borges SV, Soares NFF, Medeiros ÉAA, Sarantópoulous C (2019) Effect of active films incorporated with montmorillonite clay and α-tocopherol: potential of nanoparticle migration and reduction of lipid oxidation in salmon. Packag Technol Sci 32(1):39–47. https://doi.org/10.1002/pts.2415

Dutta P, Duta JD, Tripathi VS (2004) Chitin and chitosan: chemistry, properties and applications. J Sci Ind Res 63(1):20–31. https://doi.org/10.1016/j.foodhyd.2010.08.008

Dutta PK, Tripathi S, Mehrotra GK, Dutta J (2009) Perspectives for chitosan based antimicrobial films in food applications. Food Chem 114(4):1173–1182. https://doi.org/10.1016/j.foodchem.2008.11.047

Elchinger PH, Delattre C, Faure S, Roy O, Badel S, Bernardi T, Michaud P, Taillefumier C (2017) Antioxidant activities of Peptoid-grafted chitosan films. Appl Biochem Biotechnol 181(1):283–293. https://doi.org/10.1007/s12010-016-2212-7

Elsabee MZ, Abdou ES (2013) Chitosan based edible films and coatings: a review. Mater Sci Eng C 33(4):1819–1841. https://doi.org/10.1016/j.msec.2013.01.010

Ferreira AS, Nunes C, Castro A, Ferreira P, Coimbra MA (2014) Influence of grape pomace extract incorporation on chitosan films properties. Carbohydr Polym 113:490–499. https://doi.org/10.1016/j.carbpol.2014.07.032

Frick JM, Ambrosi A, Pollo LD, Tessaro IC (2018) Influence of glutaraldehyde crosslinking and alkaline post-treatment on the properties of chitosan-based films. J Polym Environ 26(7):2748–2757. https://doi.org/10.1007/s10924-017-1166-3

Ganiari S, Choulitoudi E, Oreopoulou V (2017) Edible and active films and coatings as carriers of natural antioxidants for lipid food. Trends Food Sci Technol 68:70–82. https://doi.org/10.1016/j.tifs.2017.08.009

Grande CD, Mangadlao J, Fan J, De Leon A, Delgado-Ospina J, Rojas JG, Rodrigues DF, Advincula R (2017) Chitosan cross-linked graphene oxide Nanocomposite films with antimicrobial activity for application in food industry. Macromol Symp 374(1):1–8. https://doi.org/10.1002/masy.201600114

Helander IM, Nurmiaho-Lassila EL, Ahvenainen R, Rhoades J, Roller S (2001) Chitosan disrupts the barrier properties of the outer membrane of gram-negative bacteria. Int J Food Microbiol 71(2):235–244. https://doi.org/10.1016/S0168-1605(01)00609-2

Jamróz E, Kulawik P, Kopel P (2019) The effect of Nanofillers on the functional properties of biopolymer-based films: a review. Polymers 11(4):675–716. https://doi.org/10.3390/polym11040675

Jin J, Song M, Hourston DJ (2004) Novel chitosan-based films cross-linked by Genipin with improved physical properties. Biomacromolecules 5(1):162–168. https://doi.org/10.1021/bm034286m

Jung BO, Chung SJ, Lee SB (2006) Preparation and characterization of eugenol-grafted chitosan hydrogels and their antioxidant activities. J Appl Polym Sci 99(6):3500–3506. https://doi.org/10.1002/app.22974

Kadam D, Lele SS (2018) Cross-linking effect of polyphenolic extracts of Lepidium sativum seedcake on physicochemical properties of chitosan films. Int J Biol Macromol 114:1240–1247. https://doi.org/10.1016/j.ijbiomac.2018.04.018

Kadam D, Shah N, Palamthodi S, Lele SS (2018) An investigation on the effect of polyphenolic extracts of Nigella sativa seedcake on physicochemical properties of chitosan-based films. Carbohydr Polym 192:347–355. https://doi.org/10.1016/j.carbpol.2018.03.052

Kerch G (2015) Chitosan films and coatings prevent losses of fresh fruit nutritional quality: a review. Trends Food Sci Technol 46(2):159–166. https://doi.org/10.1016/j.tifs.2015.10.010

Khurma JR, Rohindra DR, Nand AV (2005) Swelling and thermal characteristics of Genipin Crosslinked chitosan and poly(vinyl pyrrolidone) hydrogels. Polym Bull 54(3):195–204. https://doi.org/10.1007/s00289-005-0375-4

Koo HJ, Seon Song Y, Kim HJ, Lee YH, Hong SM, Kim SJ, Kim BC, Jin C, Lim CJ, Park EH (2004) Antiinflammatory effects of genipin, an active principle of gardenia. Eur J Pharmacol 495:201–208. https://doi.org/10.1016/j.ejphar.2004.05.031

Kumar D, Kumar P, Pandey J (2018) Binary grafted chitosan film: synthesis, characterization, antibacterial activity and prospects for food packaging. Int J Biol Macromol 115(2017):341–348. https://doi.org/10.1016/j.ijbiomac.2018.04.084

Kumari S, Rath P, Kumar ASH, Tiwari TN (2015) Extraction and characterization of chitin and chitosan from fishery waste by chemical method. Environ Technol Inno 3:77–85. https://doi.org/10.1016/j.eti.2015.01.002

Lan W, He L, Liu Y (2018) Preparation and properties of sodium Carboxymethyl cellulose/sodium alginate/chitosan composite film. Coatings 8(8):291–370. https://doi.org/10.3390/coatings8080291

Lee MH, Kim SY, Park HJ (2018) Effect of halloysite nanoclay on the physical, mechanical, and antioxidant properties of chitosan films incorporated with clove essential oil. Food Hydrocoll 84:58–67. https://doi.org/10.1016/j.foodhyd.2018.05.048

Lei K, Wang X, Li X, Wang L (2019) The innovative fabrication and applications of carvacrol nanoemulsions, carboxymethyl chitosan microgels and their composite films. Colloids Surf B: Biointerfaces 175:688–696. https://doi.org/10.1016/j.colsurfb.2018.12.054

Lepoittevin B, Elzein T, Dragoe D, Bejjani A, Lemée F, Levillain J, Bazin P, Roger P, Dez I (2019) Hydrophobization of chitosan films by surface grafting with fluorinated polymer brushes. Carbohydr Polym 205:437–446. https://doi.org/10.1016/j.carbpol.2018.10.044

Li R, Sun X, Xu Y, Zhong Q, Wang D (2017) Novel antimicrobial and antioxidant chitosan derivatives prepared by green grafting with Phenyllactic acid. Food Biophysics 12(4):470–478. https://doi.org/10.1007/s11483-017-9503-6

Liu J, Meng CG, Liu S, Kan J, Jin CH (2017a) Preparation and characterization of protocatechuic acid grafted chitosan films with antioxidant activity. Food Hydrocoll 63:457–466. https://doi.org/10.1016/j.foodhyd.2016.09.035

Liu J, Pu H, Liu S, Kan J, Jin C (2017b) Synthesis, characterization, bioactivity and potential application of phenolic acid grafted chitosan: a review. Carbohydr Polym 174:999–1017. https://doi.org/10.1016/j.carbpol.2017.07.014

Liu N, Ni S, Ragauskas AJ, Meng X, Hao N, Fu Y (2018) Laccase-mediated functionalization of chitosan with 4-hexyloxyphenol enhances antioxidant and hydrophobic properties of copolymer. J Biotechnol 269:8–15. https://doi.org/10.1016/j.jbiotec.2018.01.015

Ma Z, Garrido-Maestu A, Jeong KC (2017) Application, mode of action, and in vivo activity of chitosan and its micro- and nanoparticles as antimicrobial agents: a review. Carbohydr Polym 176:257–265. https://doi.org/10.1016/j.carbpol.2017.08.082

Mallakpour S, Ezhieh AN (2017) Preparation and characterization of chitosan-poly(vinyl alcohol) nanocomposite films embedded with functionalized multi-walled carbon nanotube. Carbohydr Polym 166:377–386. https://doi.org/10.1016/j.carbpol.2017.02.086

Mathew S, Abraham TE (2008) Characterisation of ferulic acid incorporated starch–chitosan blend films. Food Hydrocoll 22(5):826–835. https://doi.org/10.1016/j.foodhyd.2007.03.012

Mi FL, Huang CT, Liang HF, Chen MC, Chiu YL, Chen CH, Sung HW (2006) Physicochemical, antimicrobial, and cytotoxic characteristics of a chitosan film cross-linked by a naturally occurring cross-linking agent, aglycone geniposidic acid. J Agric Food Chem 54(9):3290–3296. https://doi.org/10.1021/jf0529868

Mi FL, Shyu SS, Peng CK (2005) Characterization of ring-opening polymerization of genipin and pH-dependent cross-linking reactions between chitosan and genipin. J Polym Sci A Polym Chem 43(10):1985–2000. https://doi.org/10.1002/pola.20669

Monteiro OAC, Airoldi C (1999) Some studies of crosslinking chitosan-glutaraldehyde interaction in a homogeneous system. Int J Biol Macromol 26(2–3):119–128. https://doi.org/10.1016/s0141-8130(99)00068-9

Moreno-Vásquez MJ, Buitimea-Valenzuela EL, Plascencia-Jatomea M, Encinas-Encinas JC, Rodríguez-Félix F, Sánchez-Valdes S, Rosas-Burgos EC, Ocaño-Higuera VM, Graciano-Verdugo AZ (2017) Functionalization of chitosan by a free radical reaction: characterization, antioxidant and antibacterial potential. Carbohydr Polym 155:117–127. https://doi.org/10.1016/j.carbpol.2016.08.056

Mujtaba M, Morsi RE, Kerch G, Elsabee MZ, KayaM LJ, Khawar KM (2019) Current advancements in chitosan-based film production for food technology; a review. Int J Biol Macromol 121:889–904. https://doi.org/10.1016/j.ijbiomac.2018.10.109

Muxika A, Etxeberria A, Uranga J, Guerrero P, la Caba K (2017) Chitosan as a bioactive polymer: processing, properties and applications. Int J Biol Macromol 105:1358–1368. https://doi.org/10.1016/j.ijbiomac.2017.07.087

Muzzarelli RAA (2009) Genipin-crosslinked chitosan hydrogels as biomedical and pharmaceutical aids. Carbohydr Polym 77(1):1–9. https://doi.org/10.1016/j.carbpol.2009.01.016

Nunes C, Maricato É, Cunha Â, Nunes A, da Silva JAL, Coimbra MA (2013) Chitosan–caffeic acid–genipin films presenting enhanced antioxidant activity and stability in acidic media. Carbohydr Polym 91(1):236–243. https://doi.org/10.1016/j.carbpol.2012.08.033

Nunes C, Maricato É, Gonçalves FJ, da Silva JAL, Rocha SM, Coimbra MA (2015) Properties of chitosan-Genipin films grafted with phenolic compounds from red wine. Trends Carbohydr Res 7(1):25–32

Nunes C, Maricato É, Cunha Ã, Rocha MS, Santos S, Ferreira P, Martins MA, Rodrigues A, Amado O, Coimbra M (2016) Chitosan-genipin film, a sustainable methodology for wine preservation. Green Chem 18(19):5331–5341. https://doi.org/10.1039/C6GC01621A

Nunes C, Coimbra MA, Ferreira P (2018) Tailoring functional chitosan-based composites for food applications. Chem Rec 18(7–8):1138–1149. https://doi.org/10.1002/tcr.201700112

Poon L, Wilson LD, Headley JV (2014) Chitosan-glutaraldehyde copolymers and their sorption properties. Carbohydr Polym 109:92–101. https://doi.org/10.1016/j.carbpol.2014.02.086

Priyadarshi R, Sauraj Kumar B, Negi YS (2018) Chitosan film incorporated with citric acid and glycerol as an active packaging material for extension of green chilli shelf life. Carbohydr Polym 195:329–338. https://doi.org/10.1016/j.carbpol.2018.04.089

Puvvada Y, Vankayalapati S, Sukhavasi S (2012) Extraction of chitin and chitosan from exoskeleton of shrimp for application in the pharmaceutical industry. Int Curr Pharm J 1(9):258–263. https://doi.org/10.3329/icpj.v1i9.11616

Qin Y, Liu Y, Yuan L, Yong H, Liu J (2019) Preparation and characterization of antioxidant, antimicrobial and pH-sensitive films based on chitosan, silver nanoparticles and purple corn extract. Food Hydrocoll 96:102–111. https://doi.org/10.1016/j.foodhyd.2019.05.017

Rivero S, García MA, Pinotti A (2010) Crosslinking capacity of tannic acid in plasticized chitosan films. Carbohydr Polym 82(2):270–276. https://doi.org/10.1016/j.carbpol.2010.04.048

Salari M, Khiabani MS, Mokarram RR, Ghanbarzadeh B, Kafil HS (2018) Development and evaluation of chitosan based active nanocomposite films containing bacterial cellulose nanocrystals and silver nanoparticles. Food Hydrocoll 84:414–423. https://doi.org/10.1016/j.foodhyd.2018.05.037

Siripatrawan U, Harte BR (2010) Physical properties and antioxidant activity of an active film from chitosan incorporated with green tea extract. Food Hydrocoll 24(8):770–775. https://doi.org/10.1016/j.foodhyd.2010.04.003

Sousa F, Guebitz GM, Kokol V (2009) Antimicrobial and antioxidant properties of chitosan enzymatically functionalized with flavonoids. Process Biochem 44(7):749–756. https://doi.org/10.1016/j.procbio.2009.03.009

Tian X, Jiang X (2018) Preparing water-soluble 2, 3-dialdehyde cellulose as a bio-origin cross-linker of chitosan. Cellulose 25(2):987–998. https://doi.org/10.1007/s10570-017-1607-0

Valizadeh S, Naseri M, Babaei S, Hosseini SMH, Imani A (2019) Development of bioactive composite films from chitosan and carboxymethyl cellulose using glutaraldehyde, cinnamon essential oil and oleic acid. Int J Biol Macromol 134:604–612. https://doi.org/10.1016/j.ijbiomac.2019.05.071

Wang H, Qian J, Ding F (2018) Emerging chitosan-based films for food packaging applications. J Agric Food Chem 66:395–413. https://doi.org/10.1021/acs.jafc.7b04528

Wu C, Zhu Y, Wu T, Wang L, Yuan Y, Chen J, Hu Y, Pang J (2019a) Enhanced functional properties of biopolymer film incorporated with curcurmin-loaded mesoporous silica nanoparticles for food packaging. Food Chem 288:139–145. https://doi.org/10.1016/j.foodchem.2019.03.010

Wu C, Sun J, Lu Y, Wu T, Pang J, Hu Y (2019b) In situ self-assembly chitosan/ε-polylysine bionanocomposite film with enhanced antimicrobial properties for food packaging. Int J Biol Macromol 132:385–392. https://doi.org/10.1016/j.ijbiomac.2019.03.133

Wu Y, Ying Y, Liu Y, Zhang H, Huang J (2018) Preparation of chitosan/poly vinyl alcohol films and their inhibition of biofilm formation against Pseudomonas aeruginosa PAO1. Int J Biol Macromol 118:2131–2137. https://doi.org/10.1016/j.ijbiomac.2018.07.061

Xu JD, Niu YS, Yue PP, Hu YJ, Bian J, Li MF, Peng F, Sun RC (2018) Composite film based on pulping industry waste and chitosan for food packaging. Materials 11:2264–2274. https://doi.org/10.3390/ma11112264

Xu J, Xia R, Yuan T, Sun R (2019) Use of xylooligosaccharides (XOS) in hemicelluloses/chitosan-based films reinforced by cellulose nanofiber: effect on physicochemical properties. Food Chem 298:125041–125047. https://doi.org/10.1016/j.foodchem.2019.125041

Yoon SD, Kim YM, Kim BI, Je JY (2017) Preparation and antibacterial activities of chitosan-gallic acid/polyvinyl alcohol blend film by LED-UV irradiation. J Photochem Photobiol B Biol 176:145–149. https://doi.org/10.1016/j.jphotobiol.2017.09.024

Zhang D, Yang S, Chen Y, Liu S, Zhao H, Gu J (2018) 60Co γ-ray irradiation crosslinking of chitosan/Graphene oxide composite film: swelling, thermal stability, mechanical, and antibacterial properties. Polymers 10:294–307. https://doi.org/10.3390/polym10030294

Zhang X, Liu J, Qian C, Kan J, Jin C (2019a) Effect of grafting method on the physical property and antioxidant potential of chitosan film functionalized with gallic acid. Food Hydrocoll 89:1–10. https://doi.org/10.1016/j.foodhyd.2018.10.023

Zhang X, Liu Y, Yong H, Qin Y, Liu J, Liu J (2019b) Development of multifunctional food packaging films based on chitosan, TiO2 nanoparticles and anthocyanin-rich black plum peel extract. Food Hydrocoll 94:80–92. https://doi.org/10.1016/j.foodhyd.2019.03.009

Zhang Y, Liu Y, Li R, Ren X, Huang TS (2019) Preparation and characterization of antimicrobial films based on nanocrystalline cellulose. J Appl Polym Sci 136(8):47101. https://doi.org/10.1002/app.47101

Chapter 22
Metal-Insulator-Metal as a Biosensing Platfrom

Amir Syahir Amir Hamzah

22.1 Introduction

Since late 50's theoretical works concerning nanotechnology had begun to seed, however, it wasn't until two decades later that the technology started to bloom out. This is due to the availability of sophisticated machinery studying nano-sized mater, like scanning tunneling microscope and atomic force microscopy. Today, more than half a century later, many versatile applications of nanobio-devices like sensors, plasmonic nanomaterials, meta-materials, and chemically or biologically controllable nano-structure, flooded the scientific communications. Underpinning the discoveries and innovations is the advances in nanofabrication methodologies, which are the key for growth in many areas of nanobio- and bionano- science and technology. Therefore, substantial researches focus on constructing novel functioning nanobio-sensor devices were made possible during recent decades. It is more so for biosensors that function best in nanostructure to quantify biomolecular abundance and interactions.

In the late 1960's Economou published fundamental concept for electromagnetic wave penetrating multilayer thin films of metal-insulator-metal (MIM) (Economou 1969). In the metal surface where free electrons are readily mobile called surface plasmon, the oscillations are shown to match the motion quantity of an incoming photon from a free space (illuminated light) towards the MIM. In contrast with what is known as Kretschmann configuration, where the match of resonant oscillation is found at only critical angle, the MIM can achieve resonance at even a normal incidence angle. Such finding was sitting in dormancy until the advancement in nanofabrication has developed, thus sparked a series of applications such as in biosensing

A. S. A. Hamzah (✉)
Department of Biochemistry, Faculty of Biotechnology and Molecular Biosciences, Universiti Putra Malaysia, Serdang, Selangor, Malaysia
e-mail: amirsyahir@upm.edu.my

S. Siddiquee et al. (eds.), *Composite Materials: Applications in Engineering, Biomedicine and Food Science*, https://doi.org/10.1007/978-3-030-45489-0_22

technology, metamaterials; superlenses, optoelectronic; nanometer circuits, and also in plasmonic devices (Ogawa and Kimata 2018; Jiang et al. 2019; Kong et al. 2017).

22.2 The Metal-Insulator-Metal (MIM) Nanostructure

In the MIM, only by changing a simple parameter of the nanostructure like the thickness of the sandwiched insulator layer, one can control surface plasmon that is excited in the MIM waveguides. The MIM surface plasmon can be excited with propagating light without using ATR geometry. Hence, unlike the attenuated total reflection ATR-based SPR, the resonance condition can be achieved in a simple reflection geometry even at normal incidence. Such properties have been applied to the enhancement of photoemission from the insulator layer. Besides, the MIM geometry exhibits less-propagated surface plasmon that would be a suitable condition for preparing a highly condensed label-free detection method such as in a biochip format (Syahir et al. 2012; Syahir et al. 2010). The thickness of sandwiched insulator (dielectric layer) is adjustable to produce the optimum phase of light to maximize the detection signal. This is because SP modes in MIM structures are radiative and tunable. Therefore, externally incident light can transmit through the structure and the transmitted light can be tuned by altering the thickness or the refractive index of the insulator layer, or by changing the illumination angle.

We demonstrate theoretical consideration of a metal-insulator-metal nanosandwich geometry to be utilized as a biosensing platform. Although we previously report the anomalous reflection (AR) of gold that required a semi-infinite gold thin layer (>150 nm) as practical label-free biosensing platform, we considered the used of alternative coinage materials other than gold (ex. Ag, Al and Cu). The calculations involve a simple transfer matrix technique consisting 5 layer; (1) ambient, (2) biolayer, (3) Top MIM layer, (4) middle MIM layer, and (5) bottom MIM layer. Total reflection coefficient, r, is calculated as - T_{21}/T_{22} from the components of matrix T.

$$T = \frac{1}{t_{54}}\begin{pmatrix} 1 & r_{54} \\ r_{54} & 1 \end{pmatrix}\begin{pmatrix} \phi_4 & 1 \\ 1 & \frac{1}{\phi_4} \end{pmatrix}\frac{1}{t_{43}}\begin{pmatrix} 1 & r_{43} \\ r_{43} & 1 \end{pmatrix}\begin{pmatrix} \phi_3 & 1 \\ 1 & \frac{1}{\phi_3} \end{pmatrix}\frac{1}{t_{32}}\begin{pmatrix} 1 & r_{32} \\ r_{32} & 1 \end{pmatrix}\begin{pmatrix} \phi_2 & 1 \\ 1 & \frac{1}{\phi_2} \end{pmatrix}\frac{1}{t_{21}}\begin{pmatrix} 1 & r_{21} \\ r_{21} & 1 \end{pmatrix}$$

Here, t_{ij} and r_{ij} are the transmission and reflection coefficient of light radiation from layer i to layer j, and ϕ_i is phase in layer i. From the calculations, optimization of the materials and thicknesses that can be used in actual biosensing assembly can be done. Alternative materials other than gold for a biosensor platform reduce the

preparation cost drastically. Previously we had reduced the amount of gold used in anomalous reflection (AR) of gold technique, from 300 nm thinlayer to 30 nm thinlayer when using metal-insulator-metal (MIM) geometry (Syahir et al. 2016; Syahir et al. 2009; Watanabe et al. 2007; Watanabe et al. 2005). We decided to change the semi-infinite material layer 5; 150 nm of Au to other coinage metals (Ag, Cu, or Al). Changing metals in MIM-based biosensor will cause major effect in the optical behavior, however, the whole MIM system can be tuned back by changing the thickness of the insulator and the top-layer metal. It is important that the top layer of Au (30 nm) in MIM stays as it is, because of chemical stability and the established surface chemistry knowledge of Au compare to other metals.

The MIM structures in the format of; top layer metal---insulator---bottom layer metal listed below are considered; The calculated results were depicted into two form, (i) a 3-dimensional topography graph, and (ii) a contour plot graph. Upon 1 nm biomolecular layer formation, ΔR, R_0, and R_0 - R_1 values (z-axis in 3-dimensional graph, and shown in tone color with a border-marker in contour plot graph) are plotted in percentage. For Au-PMMA-Au structure, Fig. 22.1(b) clearly shows improvement of the MIM detection signal, ΔR from less than 2% at (0, 0) coordinate that is gold only thinlayer, to more than 8% when using the MIM structure. The improvement is originated from the altered light phase that was produced as light passing through the top layer Au and the mid-layer insulator. In the results shown in Fig. 22.1(c) and 22.1(d), one can see that by lowering the R_0 of the substrate (in c), from around 40% to 10%, R_0 - R_1 decreases just scarcely (from 0.6% to 0.2%). This made the signal larger as $\Delta R = R_0 - R_1 / R_0$. Here, one must not decreases the R_0 - R_1 into too close to 0%, because it will increase detection noise or even eliminate the detection signal.

Interestingly, if one changes the bottom layer of Au to other metals (Ag, Cu, Al), the enhancement effect can be found somewhere in the range of 50–80 nm insulator and 10–20 nm Au (top layer). In comparison to Au-MIM structure, the Ag-MIM, Cu-MIM, and Al-MIM require thicker Au (top layer, layer 3) thickness. The required thickness is 5–10 nm thicker than that of Au-MIM structure, in the manner of Ag-MIM > Al-MIM > Cu-MIM > Au-MIM. They can be compared at (b) section of Figs. 22.1, 22.2, 22.3, 22.4. As for the insulator layer (mid-layer, layer 4), the required thickness shifted about 10–20 nm thicker for Ag-MIM (Fig. 22.2) and Al-MIM (Fig. 22.3), compared to Au-MIM (Fig. 22.1) and Cu-MIM (Fig. 22.4) structures that require almost the same thickness.

The ΔR, R_0, and R_1/R_0 profiles can be calculated for both in air ($n_1 = 1.0$), and in water ($n_1 = 1.33$) with the whole visible wavelength spectrum. In this case, the thickness parameters of d_2 (Au) and d_3 (insulator) are fixed after optimization is found. For example, the calculated $R0$, sensitivity, s, and mass resolution, σ_m, for d_2 (Au) = 15, 20, 25, and 30 nm are summarized in Table 22.1 for in-air calculation. The sensitivity is defined as a decreasing rate in reflectivity with respect to $R0$ upon adsorption of a biomolecular layer as layer 1 (1 nm thick and dielectric constant of 2.25), namely $s = 1\text{-}R_1/R_0$. The mass resolution is calculated by $\sigma m = \sigma/s$, assuming unity mass density of layer 1. Among samples tabulated in Table 22.1, Ag-MIM (25,

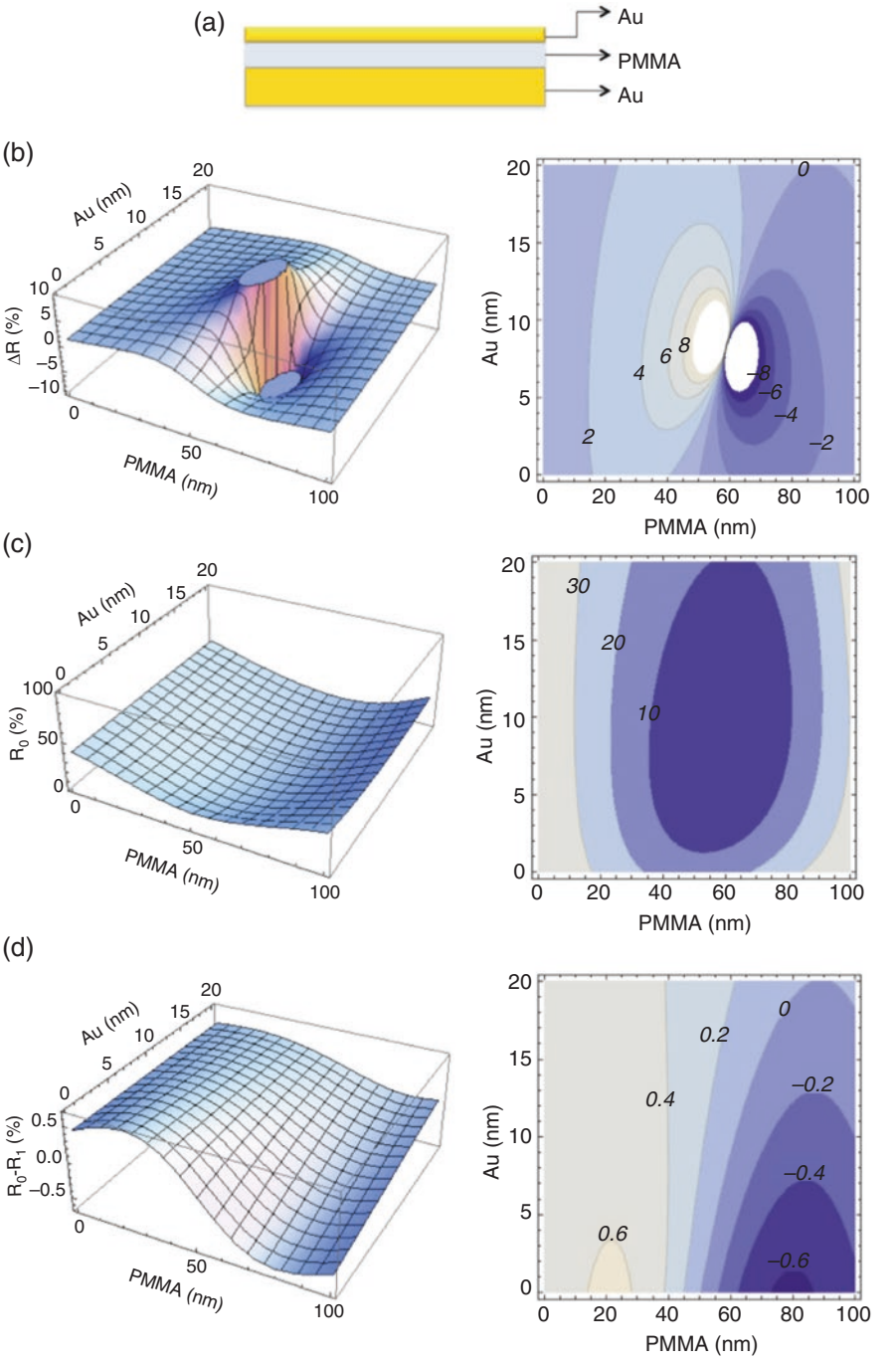

Fig. 22.1 The schematic drawing of the Au-MIM structure consists of Au (top layer, layer 3), insulator (mid-layer, layer 4) and a semi-infinite Au thinlayer (bottom layer, layer 5). A 3-dimesional graph with a contour plot of the MIM detection signal ΔR (b), bare substrate reflectivity R_0 (c), and R_0 minus the reflectivity when 1 nm bio-layer (n = 1.5) exist on the substrate surface R_0 - R_1 (d) are shown here. Values at the boundary are shown in %, while lamda = 470 nm

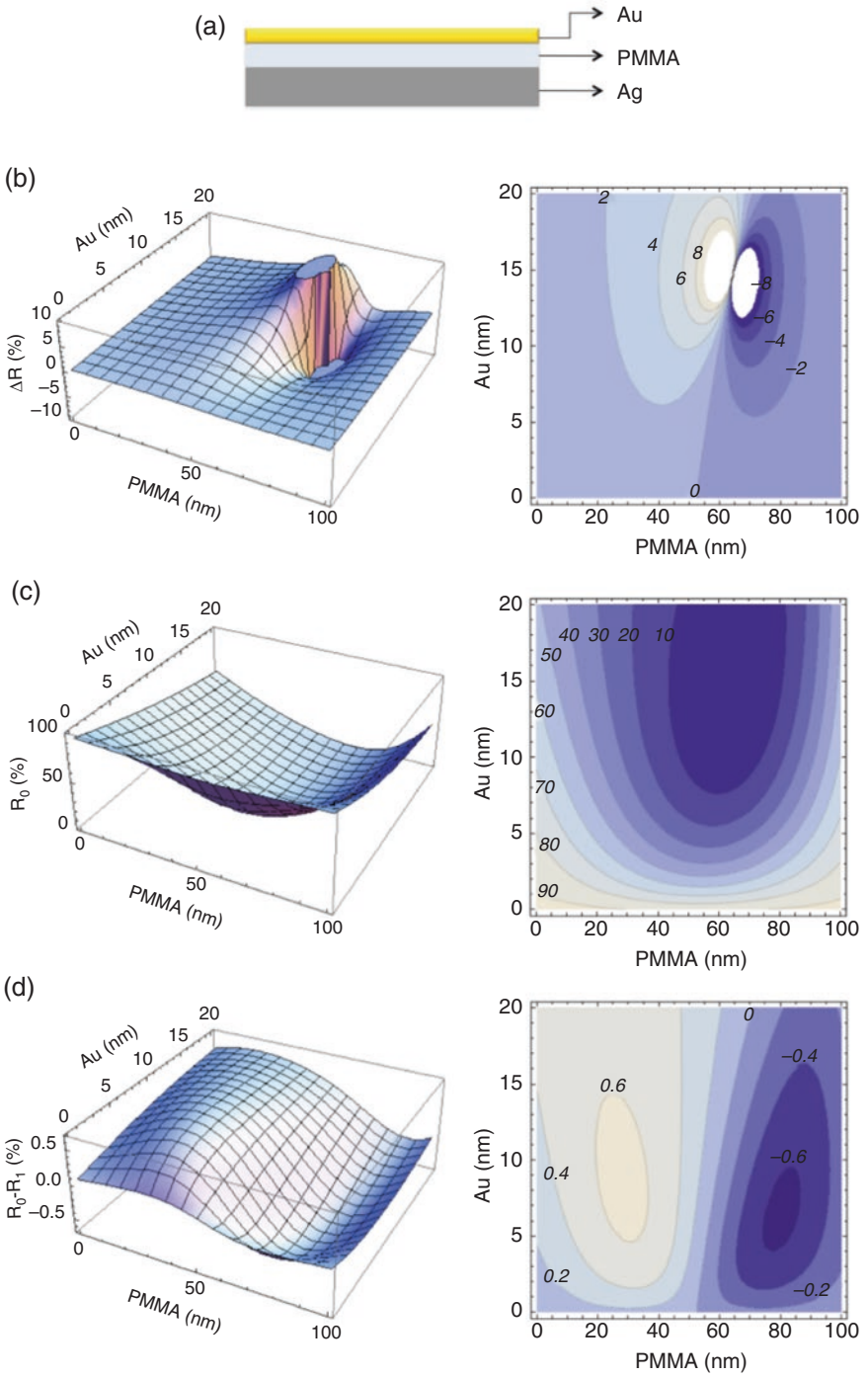

Fig. 22.2 The schematic drawing of the Ag-MIM structure consists of Au (top layer, layer 3), insulator (mid-layer, layer 4) and a semi-infinite Ag thinlayer (bottom layer, layer 5). A 3-dimesional graph with a contour plot of the MIM detection signal ΔR (b), bare substrate reflectivity R_0 (c), and R_0 minus the reflectivity when 1 nm bio-layer (n = 1.5) exist on the substrate surface R_0 - R_1 (d) are shown here. Values at the boundary are shown in %, while lamda = 470 nm

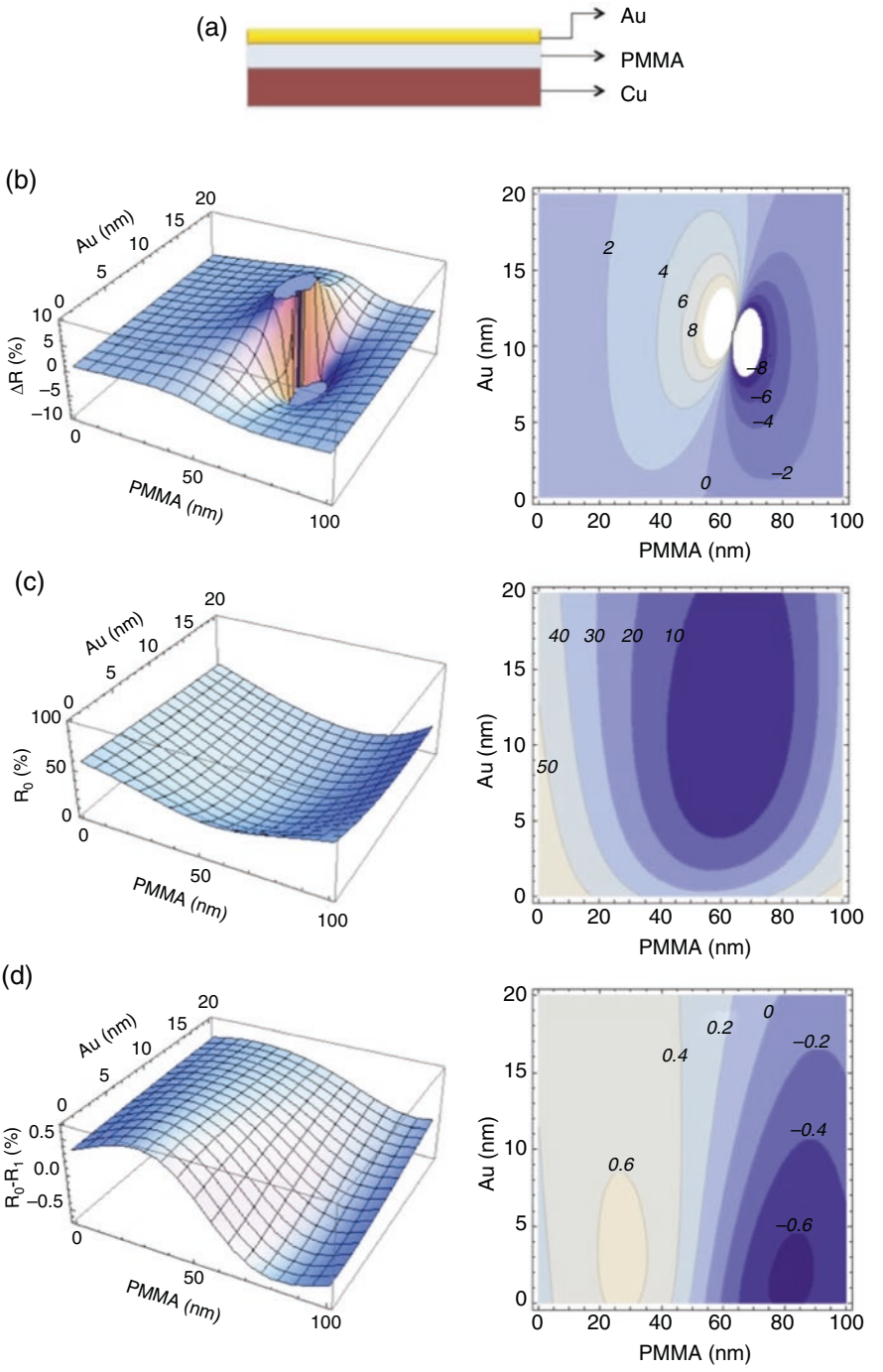

Fig. 22.3 The schematic drawing of the Cu-MIM structure consists of Au (top layer, layer 3), insulator (mid-layer, layer 4) and a semi-infinite Cu thinlayer (bottom layer, layer 5). A 3-dimesional graph with a contour plot of the MIM detection signal ΔR (b), bare substrate reflectivity R_0 (c), and R_0 minus the reflectivity when 1 nm bio-layer (n = 1.5) exist on the substrate surface R_0 - R_1 (d) are shown here. Values at the boundary are shown in %, while lamda = 470 nm

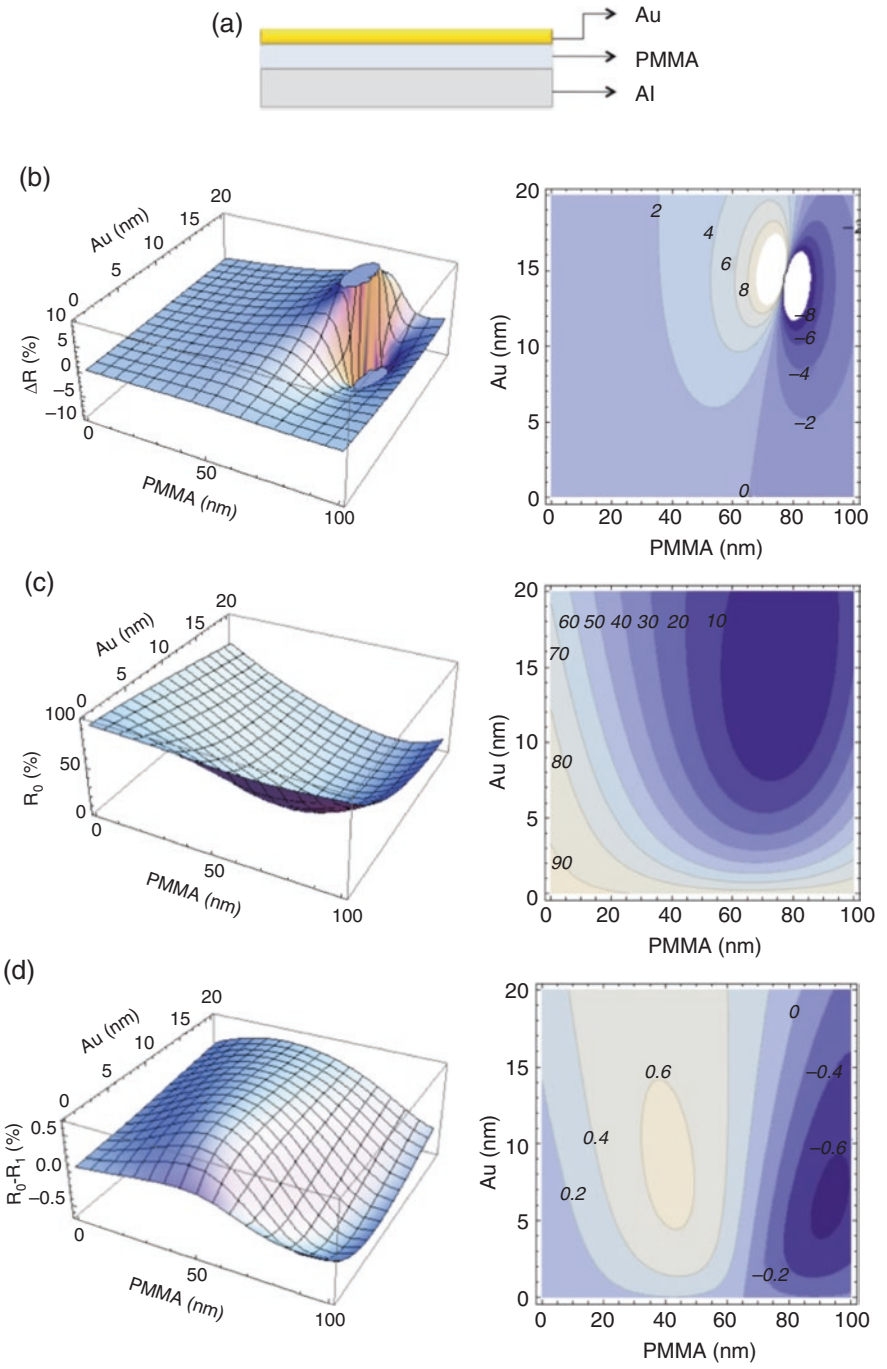

Fig. 22.4 The schematic drawing of the Al-MIM structure consists of Au (top layer, layer 3), insulator (mid-layer, layer 4) and a semi-infinite Al thinlayer (bottom layer, layer 5). A 3-dimesional graph with a contour plot of the MIM detection signal ΔR (b), bare substrate reflectivity R_0 (c), and R_0 minus the reflectivity when 1 nm bio-layer (n = 1.5) exist on the substrate surface R_0 - R_1 (d) are shown here. Values at the boundary are shown in %, while lamda = 470 nm

Table 22.1 Theoretical reflectivity R_0, calculated sensitivity s, measured error σ, and calculated mass resolution σ_m, of Ag-MIM substrate at their sensitive wavelength λ, in air

d_2(nm)	d_3(nm)	R_0(%)	s (% nm^{-1})	σ(%)	σ_m (pg mm^{-2})	λ(nm)
10	30	6.3	7.3	0.015	2.1	380
10	50	0	13.0	—	—	415
a10	70	5.0	-6.5	0.017	-2.6	455
a10	90	26.3	-2.2	0.012	-5.5	500
10	120	50.2	-0.8	0.010	-12.5	580
15	30	10.0	-19.0	0.013	-0.7	380
15	50	3.2	5.0	0.020	4.0	440
15	70	0	4.9	—	—	490
15	90	7.6	-4.5	0.014	-3.1	505
15	120	28.0	-1.8	0.012	-6.7	565
20	30	16.0	3.0	0.013	4.3	420
20	50	9.3	4.2	0.013	3.1	470
20	70	1.0	11.5	0.025	2.2	490
20	90	0.4	-14.9	0.050	-3.4	505
20	120	12.2	-2.8	0.013	-4.6	560
25	30	22.5	2.0	0.012	6.0	470
25	50	14.8	3.3	0.013	3.9	480
a25	70	5.1	5.4	0.017	3.1	495
a25	90	0.2	18.0	0.055	3.1	510
25	120	3.9	-6.0	0.018	-3.0	560
30	30	26.3	1.6	0.012	7.5	480
30	50	17.6	2.4	0.013	5.4	485
a30	70	10.2	3.2	0.013	4.1	495
a30	90	3.9	5.9	0.018	3.1	510
30	120	0	14.3	—	—	555

70), Ag-MIM (25, 90), Ag-MIM (30, 70), Ag-MIM (30, 90), are among those that have good mass resolution. Then, we had experimentally prepared the Ag-MIM substrates as described in experiment procedure below.

22.3 Biomolecules Immobilization

The MIM substrate is used as a solid support for protein/biomolecule detection platform. The use of Au thinlayer as the top layer for the MIM substrate made it easy to use the well-established gold surface chemistry to immobilized capturing agent or biomolecule of interest. There are several kinds of surface chemistry that could be utilized. One the most common methods using a self-assembled monolayer (SAM) molecules (Love et al. 2005). SAM can act as a biocompatible interface as it typically has a long hydrocarbon chain ($-C_nH_{n+1}$, which n = 6 to 18)

anchored with an active sulfide. The Au-S covalent bond formation is expected due to strong affinity (48 kcal/mol) of thiol group (-SH) towards gold surface. SAM molecule can have variety of ω-functional group that could be of interest to the researchers, depending on the immobilization purposes. As example maleimide functional group is used to anchor a cysteine ended designed peptide.

The measured signal in MIM measurement can be directly converted into a dry mass (mass that does not take hydration into account). For example, the height of SAM is typically not more than 2 nm thinfilm, but it can vary depending on the SAM molecules. In a MIM measurement involving SAM, one can assume the 100% coverage of the molecule. Therefore the surface density (number of molecule / mm^2) can be calculated using the equation $\Delta R_{MIM} \bullet d$ / (5.7•Mw). Here, the density of the adsorbates, d, is set at 1 ng $nm^{-1} \bullet mm^2$ for the convenience of the calculation process. In the case that 100% coverage assumption is not valid, e.g. protein adsorption, a maximum coverage has to be estimated first. The maximum amount of protein per unit surface area, M, (ng•mm^{-2}) can be estimated by using the eq. $M = 10^{14}/(\pi \cdot r^2)/(10^9 N_A/Mw)$, where r, Mw, and N_A denote the radius (in Å), molecular weight of a molecule, and Avogadro's number, respectively. The radius of a protein, r, can be estimated using $r = 10^8(3Mw/4\pi d N_A)$, where d corresponds to the density, which is a function of molecular weight and calculated to be 1.41–1.52 g•cm^{-3}. It is understood that 90% surface coverage of protein is considered as a full coverage of the two-dimensional surface area, considering a honeycomb-like arrangement model (Lahiri et al. 1999; Heyman et al. 2009).

22.4 Important Criteria for the Development of Biosensor

For development of the next generation biochip, certain criteria have to be met;

i. *Sensitivity*: A biochip with label-free detection format is about how to visualize the target molecule, but without a visible label. In other word, the development in this particular field requires a highly sensitive method, so that it can distinguish a sub nm to nm order of molecular adsorption. Thus, it is not surprising that the most cited figure of merit for any biosensor is the *sensitivity*. However, there are several opinions that is universally acceptable to define sensitivity of biosensor. In includes limit of detection (LOD), resolution, and signal-to-noise (S/N) ratio. In most literatures, sensitivity is often associated with the LOD. The LOD can be determined by measuring the sensor response to a dilution series. It is defined as the smallest concentration at which the sensor response is clearly distinguishable (before the response reaches undistinguishable signal) (Haes et al. 2005). Nevertheless, many researchers calculate a limit of detection as three times of standard deviation of the blank response, without actually demonstrating reproducible detection at the stated concentration. Therefore it is necessary for a particular author to clarify the definition used. On the other hand, another factor that should be given attention to is the sensor resolution.

Resolution is the smallest detectable change of a particular biosensor, defined as irreducible measurement noise divided by the slope of the response curve.

ii. *Linear dynamic range*: The dynamic range is the ratio of the largest measurable target concentration and the limit of detection. If the sensor is to be used to quantify the target protein being immobilized, the linearity between sensor response and the range of measurable layer thickness is important.

iii. *Practicality*: Practicality of a biosensor includes less sophisticated system, so that it is suitable for various conditions, and less labor needed. It also includes the issue of low in fabrication cost.

22.5 Conclusion and Future Remarks

The tracking of protein structural changes is a vital aspect towards understanding the fundamental of a molecular event. It is important that the measurement (if possible) be done under a label-free condition, in which the target protein is in a native state without any label attached to it. This is extremely challenging because label molecules are needed to access the molecular depth and therefore convey out the structural information. To this end, above presented the MIM biosensing platform is capable to measure changes at near-surface resulting molecular interactions, which have been observed using such technique. Moreover, the MIM nanosandwich structure has the potential to provide Fano resonance condition, which is a favorable for measuring sub-nm changes at near-surface with unprecedented spatial resolution, and broader dynamic range. This phenomenon arose from the interference of subradiant and superradiant plasmon modes. In the near future, this can be further manipulated using structural symmetry breaking to produce molecular ruler. This will help to open new avenues towards understanding many protein biophysical features.

Acknowledgement The author thanks Universiti Putra Malaysia for supporting this study with Putra Berimpak Research Grant UPM/700-2/1/GBP/2017/9551200.

References

Economou EN (1969) Surface Plasmons in thin films. Phys Rev 182(2):539–554. https://doi.org/10.1103/PhysRev.182.539

Haes AJ, Chang L, Klein WL, Van Duyne RP (2005) Detection of a biomarker for Alzheimer's disease from synthetic and clinical samples using a Nanoscale optical biosensor. J Am Chem Soc 127(7):2264–2271. https://doi.org/10.1021/ja044087q

Heyman A, Medalsy I, Dgany O, Porath D, Markovich G, Shoseyov O (2009) Float and compress: honeycomb-like array of a highly stable protein scaffold. Langmuir 25(9):5226–5229. https://doi.org/10.1021/la804132z

Jiang Z, Luo H, Guo S, Wang L (2019) 40 nm thick photoresist-compatible plasmonic nanolithography using a bowtie aperture combined with a metal-insulator-metal structure. Opt Lett 44(4):783–786. https://doi.org/10.1364/OL.44.000783

Kong Y, Wei Q, Liu C, Wang S (2017) Nanoscale temperature sensor based on fano resonance in metal–insulator–metal waveguide. Opt Commun 384:85–88. https://doi.org/10.1016/j.optcom.2016.09.041

Lahiri J, Isaacs L, Tien J, Whitesides GM (1999) A strategy for the generation of surfaces presenting ligands for studies of binding based on an active ester as a common reactive intermediate: a surface plasmon resonance study. Anal Chem 71(4):777–790. https://doi.org/10.1021/ac980959t

Love JC, Estroff LA, Kriebel JK, Nuzzo RG, Whitesides GM (2005) Self-assembled monolayers of thiolates on metals as a form of nanotechnology. Chem Rev 105(4):1103–1170. https://doi.org/10.1021/cr0300789

Ogawa S, Kimata M (2018) Metal-insulator-metal-based plasmonic metamaterial absorbers at visible and infrared wavelengths: a review. Materials 11(3):458. https://doi.org/10.3390/ma11030458

Syahir A, Tomizaki K, Kajikawa K, Mihara H (2009) Poly(amidoamine)-Dendrimer-modified gold surfaces for anomalous reflection of gold to detect biomolecular interactions. Langmuir 25(6):3667–3674. https://doi.org/10.1021/la8028275

Syahir A, Mihara H, Kajikawa K (2010) A new optical label-free biosensing platform based on a metal−insulator−metal structure. Langmuir 26(8):6053–6057. https://doi.org/10.1021/la903794b

Syahir A, Kajikawa K, Mihara H (2012) Sensitive detection of small molecule–protein interactions on a metal–insulator–metal label-free biosensing platform. Chem Asian J 7(8):1867–1874. https://doi.org/10.1002/asia.201200138

Syahir A, Tomizaki K, Kajikawa K, Mihara H (2016) Anomalous reflection of gold: a novel platform for biochips. Methods Mol Biol Clifton NJ 1352:97–110. https://doi.org/10.1007/978-1-4939-3037-1_8

Watanabe S, Usui K, Tomizaki K, Kajikawa K, Mihara H (2005) Anomalous reflection of gold applicable for a practical protein-detecting Chip platform. Mol BioSyst 1(5–6):363–365. https://doi.org/10.1039/B513075C

Watanabe S, Tomizaki K, Takahashi T, Usui K, Kajikawa K, Mihara H (2007) Interactions between peptides containing nucleobase amino acids and T7 phages displaying S. Proteins. *Pept Sci* 88(2):131–140. https://doi.org/10.1002/bip.20662

Index

S. Siddiquee et al. (eds.), *Composite Materials: Applications in Engineering, Biomedicine and Food Science*, https://doi.org/10.1007/978-3-030-45489-0